

2013-07-17

# Understanding the Influence of Confinement on the Excited State Properties of Small Organic Molecules

Shipra Gupta

University of Miami, shreesr9@yahoo.co.in

Follow this and additional works at: [https://scholarlyrepository.miami.edu/oa\\_dissertations](https://scholarlyrepository.miami.edu/oa_dissertations)

---

## Recommended Citation

Gupta, Shipra, "Understanding the Influence of Confinement on the Excited State Properties of Small Organic Molecules" (2013). *Open Access Dissertations*. 1055.

[https://scholarlyrepository.miami.edu/oa\\_dissertations/1055](https://scholarlyrepository.miami.edu/oa_dissertations/1055)

This Embargoed is brought to you for free and open access by the Electronic Theses and Dissertations at Scholarly Repository. It has been accepted for inclusion in Open Access Dissertations by an authorized administrator of Scholarly Repository. For more information, please contact [repository.library@miami.edu](mailto:repository.library@miami.edu).

UNIVERSITY OF MIAMI

UNDERSTANDING THE INFLUENCE OF CONFINEMENT  
ON THE EXCITED STATE PROPERTIES OF  
SMALL ORGANIC MOLECULES

By

Shipra Gupta

A DISSERTATION

Submitted to the Faculty  
of the University of Miami  
in partial fulfillment of the requirements for  
the degree of Doctor of Philosophy

Coral Gables, Florida

August 2013

©2013  
Shipra Gupta  
All Rights Reserved

UNIVERSITY OF MIAMI

A dissertation submitted in partial fulfillment of  
the requirements for the degree of  
Doctor of Philosophy

UNDERSTANDING THE INFLUENCE OF CONFINEMENT  
ON THE EXCITED STATE PROPERTIES OF  
SMALL ORGANIC MOLECULES

Shipra Gupta

Approved:

\_\_\_\_\_  
Vaidhyanathan Ramamurthy, Ph. D.  
Professor of Chemistry

\_\_\_\_\_  
M. Brian Blake, Ph.D.  
Dean of the Graduate School

\_\_\_\_\_  
Rajeev Prabhakar, Ph.D.  
Assistant Professor of Chemistry

\_\_\_\_\_  
Jamie D. Walls, Ph.D.  
Assistant Professor of Chemistry

\_\_\_\_\_  
Anna D. Gudmundsdottir, Ph.D.  
Professor of Chemistry  
University of Cincinnati

GUPTA, SHIPRA

(Ph.D., Chemistry)

Understanding the Influence of Confinement on  
the Excited State Properties of Small Organic Molecules.

(August 2013)

Abstract of a dissertation at the University of Miami.

Dissertation supervised by Professor Vaidhyanathan Ramamurthy.  
No. of pages in text. (337)

This research work is an attempt towards understanding the role of supramolecular organic hosts in altering the photochemical and photophysical properties of small organic molecules. The two most important aspects of this study are: use of “*light*” to provide the activation energy for the desired chemical changes and exploitation of water soluble supramolecular organic hosts. An organic molecule undergoes chemical changes from an excited state. This excited state can be reached in two ways: (i) in tiny steps, traversing through closely spaced vibrational and rotational levels (heat energy) or, (ii) hopping directly and discreetly to the excited state by absorbing quanta of light energy. In this thesis we focus on the latter means. Most of the chemical reactions carried out in various organic solvents, lack the feature of product selectivity. In this work we exploited water soluble organic hosts like cavitand Octa Acid (OA), Cucurbiturils (CB) and dendrimers to firstly solubilize the otherwise insoluble organic molecules in aqueous medium and then carry out their photolysis in a confined space to achieve product selectivity.

We have tried to control and stabilize the highly reactive intermediate species like carbenes, nitrenes and hydroperoxides generated as a result of “ene” reaction with singlet

oxygen by encapsulating their precursors in various host systems. Remarkable product selectivity has been witnessed in most of the cases. For instance, carbene precursors-aziadamantane derivatives gives more than 90% of 1, 3- inner molecular insertion products when encapsulated inside CB [7] and CB[8], which is produced only in traces in organic solvents. Similarly nitrene generated by the photolysis of azidoadamantanes encapsulated inside OA, can be used to achieve modified OA derivative. It has been investigated in detail how the size and the spatial orientation of the guest molecules confined in a host, govern the photochemical outcome. For example, due to the restricted space, formation of *cis*-stilbene is preferred inside the hydrophobic pockets of the dendrimers, in a photoinduced *cis-trans* isomerization reaction.

Most part of this work focuses on understanding the role of weak, non-covalent interactions like: van der Waals forces, columbic ion-pair interactions, hydrophobic forces, etc. in organizing a host and guest complex. By investigating the change in the aggregation behavior of positively charged organic dye molecules, in presence of different hosts, we observed that columbic ion-pair interactions win over hydrophobic interactions. We utilized this observation in designing a FRET donor-acceptor pair, in which the donor being uncharged occupies the hydrophobic cavity of the cavitand OA and the positively charged acceptor is attached to its anionic exterior. The donor-acceptor distance  $R_{DA}$ , thus obtained matches closely with the dimensions of host cavitand OA, confirming our hypothesis. We expect this work to be a small contribution towards enhancing our knowledge on the vast field of organic supramolecular photochemistry.

*This Thesis is dedicated to Lord Krishna  
and Rahul, for their enduring love  
and unconditional support.*

*“What you get by achieving your goals is not as important as what you become by achieving them.”*

*Henry David Thoreau*



## Acknowledgements

Towards the edge of this crucial phase of my life it would be my heartfelt pleasure to acknowledge all those who have been an integral part of it. I start with simply bowing to my Lord Krishna, whose have always blessed me with the best things in life and have been my “light” in the darkest moments.

I am immensely grateful to Dr. Ramamurthy, for being my *guru* for all this time and hopefully in future too. I am sincerely thankful to him for his constant encouragement, inspiration and novel scientific ideas which transformed me from an amateur to a budding scientist. Christopher Pike says-- “A true teacher would never tell you what to do. But he would give you the knowledge with which you could decide what would be best for you to do.” That is how I would like to define the mentorship of Dr. Ramamurthy. I am greatly obliged to him for his liberal attitude and confidence in me, which kept me going on and on despite many obstacles. The most appreciable qualities he infused in me are: being well organized, poised and try being meticulous. In addition to the scientific knowledge, he has taught us to be presentable and humble to admit our mistakes. This research work is a consequence of his intelligent guidance and my efforts in following it. I would like to thank Raji Ma’am for being our “*gurumata*” and making us feel at home, being away from home.

My sincere gratitude extends to my committee members Dr. T.K. Harris, Dr. J. Walls and Dr. Anna, for evaluating and appreciating my hard work in various exams. Their constructive suggestions have always encouraged me to perform better. And their easy, yet smart manner of interaction during the discussions has taught me to be confident during a scientific presentation, which I think is a valuable aspect of a young

scientist's life. I am also thankful to Dr. Kankan Bhattacharya, Dr. Udo Brinker, Dr. N. Jayaraman and Dr. A. Gudmundottir for their precious support in various collaborative research projects carried out towards the completion of this thesis.

I would like to mention two people, who have been the most important part of my academic enrichment- Dr. Nithyanandhan and Dr. Mintu Porel Sadukhan. From synthesis to interpreting data...Dr. Nithyanandhan has taught me everything. All the credit goes to him for carving my present skills set. He has been my most severe critic and made me strive hard to achieve perfection. I cannot forget the night he stayed in the lab till 3:00 a.m. to assist me in the final step of tedious dendrimer synthesis. His eyes were wet when we realized the product yield was better than what he had reported- a true mark of a sincere teacher. Next, I am grateful to Mintu for being my best friend. I am delighted to disclose that she has been my secret inspiration. She has been extremely successful as a Ph.D. student. Some people would say it's simply a matter of luck, though I would say that I have learned from her how to being "lucky". I am also thankful to Sushobhan for making us feel like a family.

I am greatly thankful to my lab seniors- Dr. Murthy V. S. N. Maddipatla, Dr. Arunkumar Sundaresan, Dr. Anand Parthasarathy, Dr. S. Annalakshmi, Dr. Bala KrishnaBhogala, Dr. Raja Kaliappan, and especially Dr. Yaopeng Zhao, for offering me help in all the instants and sharing their invaluable scientific experiences with me. I would like to thank my colleagues: Shampa, Revathy and Rajib for lending some tints and tones in my life. I am very thankful to Elam, Pradeep, Barnali, Ashwini, Naresh, Giri Babu, and Mohanraj for making my stay in this lab a memorable one. And I am glad to

possess a great friend, Dr. Aniruddh Adhikari, on whom I can rely doubtlessly for all scientific advice.

“Faith makes all things possible and love makes all things easy.” I fall short of words when it comes to acknowledge my best ally and the “center” of my life, my husband Rahul. It is he who has inspired me and helped me to apply for a Ph. D. program at the first place. And he stood by me in all thick and thin. He has sacrificed his own professional growth and endured the painful absence of his wife’s company all these five long years. At this moment I feel complete because I am blessed with both- true love and bright career, all credit goes to Rahul. My sincere thanks go to my parents in law for being the best parents in the world and for their broad mindedness. I am thankful to my father for imbibing in me an honest and progressive character, and to my mother, for lending me a sweetness of character. I am also very proud to fulfill my grandpa’s dream of becoming a doctor. I know he would be smiling fondly at me, in this moment. I would like to thank my brother Prashant and my sister and brother in laws (Didi and Jijaji), for loving and supporting me unconditionally. And the youngest person to appear in this list is my ten months old darling son “Krishna”. He (five months old) would sit patiently in my lap and observe me writing my thesis. And this little baby allowed his Mommy to leave him for two whole months to travel to thousands of miles away in order to defend her thesis. I would be always indebted to him for his remarkable cooperation.

At last I would like to extend my thanks to the Department of Chemistry, University of Miami for providing me the instrumental and official assistance that was necessary to carry out my research work.

## TABLE OF CONTENTS

<b>LIST OF FIGURES</b> .....	<b>xiv</b>
<b>LIST OF SCHEMES</b> .....	<b>xxix</b>
<b>LIST OF TABLES</b> .....	<b>xxxii</b>
<b>CHAPTER 1: Introduction to Supramolecular Photochemistry</b> .....	<b>1</b>
1.1 Photochemistry.....	2
1.2 Supramolecular Photochemistry.....	5
1.3 Leading examples of photochemistry and photophysics in host/guest chemistry..	7
1.3.1 Vision.....	7
1.3.2 Photosynthesis.....	8
1.3.3 “Taming” of cyclobutadiene in a carcerand.....	9
1.3.4 Achieving high enantio-selectivity inside Cyclodextrins.....	9
1.3.5 Selective photodimerization of acenaphthylene inside Palladium Nanocage.....	10
1.3.6 High product selectivity in “ene” reaction when substrate is encapsulated in Octa Acid.....	11
1.3.7 Phosphorescence of the triplet state is rarely observed in fluid solution...	12
1.3.8 Role of Cyclodextrins in achieving phosphorescence of Aromatic Hydrocarbons (AH).....	12
1.3.9 Enhancement of phosphorescence of AH in zeolites due to heavy atom effect .....	13
1.4 Brief description of supramolecular hosts used in this thesis.....	14
1.4.1 Octa Acid (OA).....	15
1.4.2 Cucurbiturils (CB[n]).....	20
1.4.3 Cyclodextrins (CD).....	21

1.4.4 Calixarenes (CA).....	23
1.4.5 Palladium Nanocage (PdNC).....	24
1.4.6 Dendrimers.....	27
1.5 Instruments and techniques used in this research work.....	28
1.5.1 UV-Visible Spectroscopy.....	28
1.5.2 Fluorescence Spectroscopy.....	29
1.5.3 Time-Resolved Emission Spectroscopy.....	30
1.5.4 Nuclear Magnetic Resonance Spectroscopy.....	30
1.5.5 Gas Chromatography /GC-Mass Spectrometry.....	33
1.5.6 Electronic Paramagnetic Resonance Spectroscopy (EPR).....	35
1.6 Scope and aim of this thesis.....	35
<b>CHAPTER 2: Photochemical Generation and Reactivity of Carbenes in Various Nanoenvironments.....</b>	<b>39</b>
2.1 Overview.....	40
2.2 Results and discussion.....	42
2.2.1 Encapsulation of carbene precursors 1a-d in OA as studied by <sup>1</sup> H NMR...42	
2.2.2 Photolysis of carbene precursors 1a-d@OA and 1a-d@OA on silica Surface.....	52
2.2.3 Encapsulation of carbene precursors 1a-d in CB[7] and CB[8] as studied by <sup>1</sup> H NMR.....	55
2.2.4 Photolysis of carbene precursors 1a-d@CB[7] and 1a-d@CB[8].....	60
2.2.5 Encapsulation of carbene precursors 1a-d in PdNC as studied by <sup>1</sup> H NMR.....	63
2.2.6 Photolysis of carbene precursors 1a-d@PdNC.....	65
2.2.7 Comparison of the products obtained in the case of different hosts.....	67

2.2.8 Observations supported by ITC and Computational Studies.....	72
2.3 Conclusion.....	77
2.4 Experimental Section.....	78
<b>CHAPTER 3: Encapsulation and Photoreactions of Nitrene Precursors within Various Host Systems.....</b>	<b>84</b>
3.1 Overview.....	85
3.2 Results and discussion.....	88
3.2.1 Encapsulation and photoreaction of 1-azidoadamantane@OA.....	88
3.2.2 Encapsulation and photoreaction of 1-azidoadamantane@CB[7].....	94
3.2.3 Encapsulation and photoreaction of 1-azidoadamantane@PdNC.....	97
3.2.4 Encapsulation and photoreaction of 2-azidoadamantane@OA.....	100
3.2.5 Encapsulation and photoreaction of 2-azidoadamantane@CB[7].....	104
3.2.6 Encapsulation and photoreaction of 2-azidoadamantane@PdNC.....	106
3.2.7 Comparative studies of 1- and 2-azidoadamantanes included in various hosts.....	108
3.2.8 Mass spectrometry, ITC and Computational experiments done to support the above studies.....	111
3.3 Conclusion.....	118
3.4 Experimental Section.....	120
<b>CHAPTER 4: Photolysis Studies of Triplet Nitrene Precursors Encapsulated inside Octa Acid Cavitand.....</b>	<b>124</b>
4.1 Overview.....	125
4.2 Results and discussion.....	127
4.2.1 Encapsulation and photochemistry of $\alpha$ -Azide@OA.....	127
4.2.2 Encapsulation and photochemistry of $\beta$ -Azide@OA .....	129

4.2.3 Encapsulation and photochemistry of $\gamma$ -Azide@OA.....	134
4.2.4 Encapsulation and photochemistry of $\delta$ -Azide@OA.....	139
4.2.5 Encapsulation and photochemistry of $\varepsilon$ -Azide@OA.....	141
4.3 Conclusion.....	146
4.4 Experimental Section.....	147
<b>CHAPTER 5: Photo-oxygenation of Alkylcyclohexenes by Singlet Oxygen in Solution and inside Confined Media.....</b>	<b>150</b>
5.1 Overview.....	151
5.2 Results and discussions.....	155
5.2.1 Encapsulation and “ene” reaction of 1-alkylcycloalkenes inside Host OA.....	155
5.2.2 Encapsulation and “ene” reaction of 1-alkyl-4-methylcycloalkenes inside OA.....	176
5.2.3 Encapsulation and “ene” reaction of four cycloalkene guests of similar molecular length inside host OA.....	179
5.2.4 Encapsulation studies of guest molecules ( $G_3$ , 4-Me- $G_2$ and 4-Et $G_1$ ) of intermediate size.....	186
5.3 Conclusion.....	188
5.4 Experimental Section.....	189
<b>CHAPTER 6: Ultrafast FRET between the Donor Encapsulated inside and Acceptor Non-covalently Attached to the Walls of Nano Cavitand OA.....</b>	<b>193</b>
6.1 Overview.....	194
6.2 Results and discussion.....	197
6.2.1 Encapsulation of donor within OA.....	197
6.2.2 Association of acceptor Rhodamine 6G to the capsule’s exterior.....	201

6.2.3 Confirmation of spectral overlap between the donor emission and acceptor absorption.....	203
6.2.4 Steady-state emission studies.....	204
6.2.5 Time-Resolved emission studies.....	206
6.2.6 Comparison of parameters involved in calculation of $R_{DA}$ .....	208
6.3 Diminishing FRET between donor@OA and acceptor-OA by introducing other hosts.....	211
6.3.1 Steady-state emission studies.....	211
6.3.2 Time Resolved emission studies.....	213
6.4 Conclusion.....	214
6.4 Experimental Section.....	215

**CHAPTER 7: Study of the Hydrophobic and Columbic Association of Dyes with Various Organic Supramolecular Hosts.....218**

7.1 Overview.....	219
7.2 Results and discussion.....	225
7.2.1 Interaction of Azure B and Thionin Acetate with OA.....	225
7.2.2 Interaction of Thionin Acetate with CB[7] and CB[8].....	229
7.2.3 Comparative studies of OA vs. CB[8] and OA vs. CB[7] for Thionin Acetate.....	234
7.2.4 Basic experiments done with various cationic dyes to support above observations and inferences.....	239
7.2.5 Comparative binding studies for the dyes Thionin Acetate and Cresyl Violet Perchlorate between the hosts-Cyclodextrin, Dendrimers, Calixarene vs. Octa Acid.....	243
7.3 Conclusion.....	254
7.4 Experimental Section.....	256



<b>CHAPTER 8: Characterization and Use of Dendrimers as Micro and Nano-Molecular Reactors.....</b>	<b>258</b>
8.1 Overview.....	259
8.2 Results and discussion.....	263
8.2.1 Probing the microenvironment of phenolic end group dendrimers ( $C_nGO$ ) with fluorescence probes.....	263
8.2.2 Probing the microenvironment of phenolic end group dendrimers ( $C_nGO$ ) by Solvation Dynamics.....	270
8.2.3 Phenolic end group dendrimers ( $C_nGO$ ) as reaction media for photolysis of 1-Phenyl-3-p-tolyl-propane-2-one.....	276
8.2.4 Photochemical isomerizations of Stilbenes inside phenolic end group dendrimers ( $C_nGO$ ).....	278
8.2.5 Characterization of poly alkyl aryl dendrimers ending with carboxylic acid group ( $C_5G1A-C_5G3A$ ) with UV-visible and Fluorescence Spectroscopies.....	283
8.2.6 Characterization of poly alkyl aryl dendrimers ending with carboxylic acid group ( $C_5G1A-C_5G3A$ ) with EPR Spectroscopy.....	286
8.2.7 Photochemical isomerizations of Stilbenes inside carboxylic acid end group dendrimers ( $C_nGA$ ).....	297
8.3 Conclusion.....	302
8.4 Experimental Section.....	304
<b>REFERENCES.....</b>	<b>310</b>

## LIST OF FIGURES

<b>Figure 1.1</b> Pictorial depiction of photochemistry and photobiology of <i>vision</i> .....	7
<b>Figure 1.2</b> Pictorial depiction of photochemistry and photobiology of <i>photosynthesis</i> .....	8
<b>Figure 1.3</b> Highly reactive cyclobutadiene stabilized in a carcerand.....	9
<b>Figure 1.4</b> Enantioselective photoconversion of benzaldehyde and dependence of host-guest conformation on the cavity size of CD.....	10
<b>Figure 1.5</b> Self-assembled coordination cage 1 (left) and <sup>1</sup> H NMR spectroscopic analysis (D <sub>2</sub> O, r.t.) of the photodimerization of 2 within 1 (a: before irradiation, b: after irradiation for 0.5 h, c: after extraction with CDCl <sub>3</sub> ) (right). ....	10
<b>Figure 1.6</b> High Product selectivity in “ene” reaction when cycloalkene@OA.....	11
<b>Figure 1.7</b> Luminescence of naphthalene@SDS and naphthalene@TIDS.....	12
<b>Figure 1.8</b> Luminescence of phenanthrene@CD in solution in the absence (solid line) and presence of CH <sub>2</sub> Br <sub>2</sub> (dashed line).....	13
<b>Figure 1.9</b> Luminescence of naphthalene in FAU zeolites MX as a function of M.....	13
<b>Figure 1.10</b> (a) Chemical structure of OA with labeled protons A-J, (b) <sup>1</sup> H NMR of 1mM OA in buffered D <sub>2</sub> O, dimensions of the host cavity as calculated by Spartan, (c) Side view, (d) Top view.....	15
<b>Figure 1.11</b> Partial <sup>1</sup> H NMR spectra (500 MHz) of (a) 4-hydroxy aziadamantane@OA in buffered D <sub>2</sub> O, (b) 4-hydroxy adamantine in buffered D <sub>2</sub> O.....	16
<b>Figure 1.12</b> Pictorial representation of possible host-guest stoichiometries for host OA.....	18
<b>Figure 1.13</b> Pictorial representation of the types of rotation possible for a guest@OA <sub>2</sub> .....	19
<b>Figure 1.14</b> (a) Chemical structure of CB[n], (b) Calculated structure, (c) pictorial representation of CB[n]- pumpkin like shape.....	20
<b>Figure 1.15</b> Chemical structures of α-, β-, γ-cyclodextrins and their dimensions.....	22
<b>Figure 1.16</b> Chemical structure of most basic Calixarene [4].....	24

<b>Figure 1.17</b> (a) Chemical structure of Palladium Nanocage (PdNC) and (b) Cartoon representation of PdNC.....	25
<b>Figure 1.18</b> Pictorial representation of :(a) various structural units, (b) whole dendrimer.....	27
<b>Figure 2.1</b> Structures of hosts OA, cucurbiturils CB[7], CB[8], palladium nano cage (PdNC), and guest molecules carbene precursors and its derivatives.....	42
<b>Figure 2.2</b> <sup>1</sup> H NMR spectra of (a) OA in buffered D <sub>2</sub> O, (b) <b>1a<sub>2</sub>@OA<sub>2</sub></b> in buffered D <sub>2</sub> O, (c) <b>1c@OA</b> in buffered D <sub>2</sub> O, (d) <b>1d@OA</b> in buffered D <sub>2</sub> O, (e) <b>1b@OA</b> in buffered D <sub>2</sub> O. Buffer: 10 mM sodium tetra borate solution in D <sub>2</sub> O.....	43
<b>Figure 2.3</b> Partial <sup>1</sup> H NMR spectra of (a) <b>1a</b> in buffered D <sub>2</sub> O, (b) <b>1a<sub>2</sub>@OA<sub>2</sub></b> in buffered D <sub>2</sub> O, (c) <b>1b</b> in buffered D <sub>2</sub> O, (d) <b>1b@OA</b> in buffered D <sub>2</sub> O, (e) <b>1c</b> in buffered D <sub>2</sub> O, (f) <b>1c@OA</b> in buffered D <sub>2</sub> O, (g) <b>1d</b> in buffered D <sub>2</sub> O, (h) <b>1d@OA</b> in buffered D <sub>2</sub> O. Buffer: 10 mM sodium tetra borate solution in D <sub>2</sub> O.....	45
<b>Figure 2.4</b> <sup>1</sup> H NMR Titration of <b>1a</b> against 1mM OA in 10 mM buffered D <sub>2</sub> O.....	46
<b>Figure 2.5</b> 2D DOSY NMR spectra of (a) <b>1a<sub>2</sub>@OA<sub>2</sub></b> , (b) <b>1b@OA</b> , (c) <b>1c@OA</b> , (d) <b>1d@OA</b> .....	48
<b>Figure 2.6 (a)</b> 2D COSY NMR spectra of <b>1b@OA</b> .....	50
<b>Figure 2.6 (b)</b> 2D NOESY NMR spectra of <b>1b@OA</b> .....	50
<b>Figure 2.7 (a)</b> 2D COSY NMR spectra of <b>1c@OA</b> .....	51
<b>Figure 2.7 (b)</b> 2D NOESY NMR spectra of <b>1c@OA</b> .....	51
<b>Figure 2.8</b> <sup>1</sup> H NMR spectra of (a) <b>1a@OA</b> before irradiation, (b) Products@OA after irradiation, (c) OA after extraction of products, (d) control experiment.....	55
<b>Figure 2.9</b> <sup>1</sup> H NMR spectra of (a) <b>1a</b> in D <sub>2</sub> O, (b) <b>1a@CB[7]</b> in D <sub>2</sub> O, (c) <b>1b</b> in D <sub>2</sub> O, (d) <b>1b@CB[7]</b> in D <sub>2</sub> O, (e) <b>1c</b> in D <sub>2</sub> O, (f) <b>1c@CB[7]</b> in D <sub>2</sub> O, (g) <b>1d</b> in D <sub>2</sub> O, (h) <b>1d@CB[7]</b> in D <sub>2</sub> O.....	56
<b>Figure 2.10</b> <sup>1</sup> H NMR spectra of (a) 1mM of CB[7] in D <sub>2</sub> O, (b)-(e) 1 mM CB[7] + 0.2, 0.6, 0.8, 1.0 equivalent of <b>1a</b> respectively in D <sub>2</sub> O, (f) 1mM of <b>1a</b> in D <sub>2</sub> O.....	57
<b>Figure 2.11</b> <sup>1</sup> H NMR spectra of (a) <b>1a</b> in D <sub>2</sub> O, (b) <b>1a@CB[8]</b> in D <sub>2</sub> O, (c) <b>1b</b> in D <sub>2</sub> O, (d) <b>1b@CB[8]</b> in D <sub>2</sub> O, (e) <b>1c</b> in D <sub>2</sub> O, (f) <b>1c@CB[8]</b> in D <sub>2</sub> O, (g) <b>1d</b> in D <sub>2</sub> O, (h) <b>1d@CB[8]</b> in D <sub>2</sub> O.....	59

<b>Figure 2.12</b> $^1\text{H}$ NMR spectra of (a) 1mM of <b>1a</b> in $\text{D}_2\text{O}$ , (b)-(d) $\sim 1$ mM CB[8] + $\sim 0.2, 0.4, 1.0$ equivalent of <b>1a</b> respectively in $\text{D}_2\text{O}$ , (e) $\sim 1\text{mM}$ of CB[8] in $\text{D}_2\text{O}$ .....	60
<b>Figure 2.13</b> (a) $^1\text{H}$ NMR spectra of <b>1a</b> @CB[7] before irradiation, (b) $^1\text{H}$ NMR spectra of Products@CB[7] after irradiation.....	62
<b>Figure 2.14</b> (a) $^1\text{H}$ NMR spectra of <b>1a</b> @CB[8] before irradiation, (b) $^1\text{H}$ NMR spectra of Products@CB[8] after irradiation.....	63
<b>Figure 2.15</b> $^1\text{H}$ NMR (500 MHz, $\text{D}_2\text{O}$ )spectra of (a) <b>1a</b> @PdNC, (b) <b>1a</b> in $\text{D}_2\text{O}$ , (c) <b>1b</b> @PdNC, (d) <b>1b</b> in $\text{D}_2\text{O}$ , (e) <b>1c</b> @PdNC, (f) <b>1c</b> in $\text{D}_2\text{O}$ , (g) <b>1d</b> @PdNC, (h) <b>1d</b> in $\text{D}_2\text{O}$ .....	64
<b>Figure 2.16</b> $^1\text{H}$ NMR spectra of (a) 1mM of PdNC in $\text{D}_2\text{O}$ , (b)-(f) 1 mM PdNC + 0.6, 1.2, 1.8, 2.4 and 3.0 equivalents of <b>1a</b> respectively in $\text{D}_2\text{O}$ , (g) 1mM of <b>1a</b> in $\text{D}_2\text{O}$ .....	65
<b>Figure 2.17</b> (a) $^1\text{H}$ NMR spectra of <b>1a</b> @PdNC before irradiation, (b) $^1\text{H}$ NMR spectra of Products@PdNC after irradiation.....	67
<b>Figure 2.18</b> Orientation of the adamantanediazirines in (a) <b>1b</b> @OA, (b) <b>1c</b> @OA, and (c) <b>1d</b> @OA based on molecular dynamics simulations (GROMACS, OPLS-AA force-field). Color code for atoms:C, gray;N, blue; O, red; Cl, green; Br, dark red; H, white.....	75
<b>Figure 2.19</b> BLYP/6-311G (d, p) energy-minimized structures of aziadamantanes within CB[7].....	76
<b>Figure 3.1</b> Example of a nitrene precursor reacting with the host cavitand.....	87
<b>Figure 3.2</b> Hosts employed to study the photoreactions of nitrene precursors 1- and 2-azidoadamantanes.....	87
<b>Figure 3.3</b> $^1\text{H}$ NMR spectra of (a) 1-azidoadamantane in buffered $\text{D}_2\text{O}$ , (b) 1-azidoadamantane@OA, (c) only 1mM OA in buffered $\text{D}_2\text{O}$ .....	89
<b>Figure 3.4</b> $^1\text{H}$ NMR titration spectra of 1-azidoadamantane with host OA.....	90
<b>Figure 3.5</b> 2D DOSY NMR spectrum of 1-azidoadamantane@OA.....	90
<b>Figure 3.6</b> $^1\text{H}$ NMR spectra of (a) <b>1</b> @OA before irradiation, (b) photoproducts of <b>1</b> @OA after 40 min of irradiation and (c) photoproducts of <b>1</b> @OA after extraction by $\text{CHCl}_3$ ...92	92
<b>Figure 3.7</b> Partial 2D COSY NMR (500 MHz, $\text{D}_2\text{O}$ ) spectrum of <b>1</b> @OA. [OA] = 5.0 mM, [ <b>1</b> ] = 5 mM in 50 mM sodium tetraborate buffer. * indicates residual water signal.....	93

<b>Figure 3.8</b> Partial 2D NOESY NMR (500 MHz, D <sub>2</sub> O) spectrum of <b>1@OA</b> . [OA] = 5.0 mM, [ <b>1</b> ] = 5 mM in 50 mM sodium tetraborate buffer.....	94
<b>Figure 3.9</b> <sup>1</sup> H NMR spectra of (a) 1-azidoadamantane in buffered D <sub>2</sub> O, (b) <b>1@CB[7]</b> in D <sub>2</sub> O, and (c) 1 mM CB[7] in D <sub>2</sub> O without any guest.....	95
<b>Figure 3.10</b> <sup>1</sup> H NMR titration spectra of 1-azidoadamantane with CB[7].....	95
<b>Figure 3.11</b> <sup>1</sup> H NMR spectra of (a) <b>1@CB[7]</b> in D <sub>2</sub> O before irradiation, (b) photoproducts of <b>1@CB[7]</b> after the reaction was complete, and (c) photoproducts of <b>1@CB[7]</b> after the solution was washed three times with CDCl <sub>3</sub> to extract the soluble photoproducts.....	96
<b>Figure 3.12</b> <sup>1</sup> H NMR spectra of (a) 1-azidoadamantane in buffered D <sub>2</sub> O, (b) <b>1@PdNC</b> in D <sub>2</sub> O, and (c) 1 mM PdNC in D <sub>2</sub> O.....	98
<b>Figure 3.13</b> <sup>1</sup> H NMR titration of 1-azidoadamantane with 1mM PdNC in D <sub>2</sub> O.....	99
<b>Figure 3.14</b> <sup>1</sup> H NMR spectra of (a) <b>1@PdNC</b> in D <sub>2</sub> O before irradiation, (b) photoproducts of <b>1@PdNC</b> after the reaction was complete, and (c) PdNC after the solution was washed three times with CDCl <sub>3</sub> to extract the soluble photoproducts.....	100
<b>Figure 3.15</b> <sup>1</sup> H NMR spectra (500 MHz) of (a) 2-azidoadamantane in buffered D <sub>2</sub> O, (b) only 1mM OA in buffered D <sub>2</sub> O, (c) <b>2@OA</b> .....	101
<b>Figure 3.16</b> <sup>1</sup> H NMR titration spectra of 2-azidoadamantane with 1mM OA.....	102
<b>Figure 3.17</b> 2D DOSY NMR (500 MHz, room temperature) spectrum of <b>2@OA</b> .....	103
<b>Figure 3.18</b> <sup>1</sup> H NMR spectra of (a) <b>2@OA</b> before irradiation, (b) photoproducts of <b>2@OA</b> after 40 min of irradiation and (c) photoproducts of <b>2@OA</b> after extraction by CDCl <sub>3</sub> .....	104
<b>Figure 3.19</b> <sup>1</sup> H NMR spectra (500 MHz) of (a) 2-azidoadamantane in buffered D <sub>2</sub> O, (b) only 1mM CB[7] in D <sub>2</sub> O, (c) <b>2@CB[7]</b> .....	105
<b>Figure 3.20</b> <sup>1</sup> H NMR titration spectra of 2-azidoadamantane with 1 mM CB[7] in D <sub>2</sub> O.....	105
<b>Figure 3.21</b> <sup>1</sup> H NMR spectra (500 MHz) of (a) 2-azidoadamantane in buffered D <sub>2</sub> O, (b) 1mM PdNC in D <sub>2</sub> O and (c) <b>2@PdNC</b> in D <sub>2</sub> O.....	106
<b>Figure 3.22</b> <sup>1</sup> H NMR titration spectra of 2-azidoadamantane with 1 mM of PdNC.....	107

- Figure 3.23** Partial  $^1\text{H}$  NMR spectra of (a) host PdNC before irradiation, (b) host PdNC after 40 min of irradiation and (c) host PdNC after extraction of photoproducts by  $\text{CDCl}_3$ .....108
- Figure 3.24** Orientations of the azidoadamantanes in (a) **1@OA** and (b) **2@OA** based on molecular docking experiment (AutoDock Vina). Color code for atoms: C, gray; N, blue; O, red; H, white.....113
- Figure 3.25** ESI-MS of an aqueous solution of **1@OA** complexes in the presence of  $\text{NH}_3$  (1  $\mu\text{L}/\text{mL}$ ): (a) full scan spectrum; (b) fragmentation ( $\text{MS}^2$ ) of  $m/z$  952.6 (**1@OA**). The arrow indicates the fragmented peak. Assignments:  $m/z$  863.6 [ $\text{OA} - 2\text{H}$ ] $^{2-}$ ; 952.6 [ $\text{OA} - 2\text{H} + 1$ ] $^{2-}$ .....114
- Figure 3.26** ESI-MS spectra of an aqueous solution of **2@OA** complexes in the presence of  $\text{NH}_3$  (1  $\mu\text{L}/1$  mL). (a) Full scan spectrum and (b) fragmentation ( $\text{MS}^2$ ) of  $m/z$  952.6 (**2@OA**) The arrow indicates the fragmented peak. Assignments:  $m/z$  863.6 [ $\text{OA}-2\text{H}$ ] $^{2-}$ ; 952.6 [**2@OA**-2H] $^{2-}$ .....115
- Figure 3.27** ESI-MS spectra (full scans) of (a) photolyzed **1@OA** in the negative polarity, (b) photolyzed **1@OA** in the positive polarity. Assignments:  $m/z$  863.6 [ $\text{OA} - 2\text{H}$ ] $^{2-}$ ; 938.2 [ $5 - 2\text{H}$ ] $^{2-}$ ; 1747.4 [ $\text{OA} + \text{NH}_3 + \text{H}$ ] $^+$ ; 1879.6 [ $5 + \text{H}$ ] $^+$ .....116
- Figure 3.28** ESI-MS spectra of (a) photoproduct **2e** ( $m/z$  1879.6) in the positive polarity (full scan) and (b) fragmentation ( $\text{MS}^2$ ) of  $m/z$  1879.6. The arrow indicates the fragmented peak.....117
- Figure 3.29** ESI-MS spectra (full scans) of (a) photoproduct of **1@CB7** and (b) photoproduct of **1@CB7** in the presence of dimethylviologen $^{2+}$ . Assignments:  $m/z$  604.4 [ $\text{CB}[7] + 2\text{Na}$ ] $^{2+}$ ; 674.4 [ $\text{Dimethylviologen@CB}[7]$ ] $^{2+}$ ; 1163.4 [ $\text{CB}[7] + \text{H}$ ] $^+$ ; 1185.4 [ $\text{CB}[7] + \text{Na}$ ] $^+$ ; 1201.4 [ $\text{CB}[7] + \text{K}$ ] $^+$ ; 1330.6 [ $\text{CB}[7] + 6 + \text{H}$ ] $^+$ .....118
- Figure 4.1**  $^1\text{H}$  NMR spectra (500 MHz,  $\text{D}_2\text{O}$ ) of (a)  $\alpha$ -azide in buffered  $\text{D}_2\text{O}$ , (b)  $\alpha$ -azide@OA, (c) 1mM OA alone.....128
- Figure 4.2**  $^1\text{H}$  NMR Titration of  $\alpha$ -azide against 1mM OA in 10 mM buffered  $\text{D}_2\text{O}$ ....128
- Figure 4.3**  $^1\text{H}$  NMR spectra (500 MHz,  $\text{D}_2\text{O}$ ) of (a)  $\beta$ -azide in buffered  $\text{D}_2\text{O}$ , (b)  $\beta$ -azide@OA, (c) 1mM OA alone.....129
- Figure 4.4**  $^1\text{H}$  NMR Titration of  $\beta$ -azide against 1mM OA in 10 mM buffered  $\text{D}_2\text{O}$ ....130
- Figure 4.5** 2D DOSY NMR spectra of  $\beta$ -azide@OA $_2$ .....130
- Figure 4.6**  $^1\text{H}$  NMR spectra (500 MHz,  $\text{D}_2\text{O}$ ) of (a)  $\gamma$ -azide in buffered  $\text{D}_2\text{O}$ , (b)  $\gamma$ -azide@OA, (c) 1mM OA alone.....134

<b>Figure 4.7</b> $^1\text{H}$ NMR Titration of $\gamma$ -azide against 1mM OA in 10 mM buffered $\text{D}_2\text{O}$ ...	135
<b>Figure 4.8</b> 2-D DOSY NMR spectra of $\gamma$ -azide@OA <sub>2</sub> .....	135
<b>Figure 4.9</b> $^1\text{H}$ NMR spectra of (a) $\gamma$ -azide@OA <sub>2</sub> before irradiation, (b) Products@OA after irradiation, (c) OA after extraction of products.....	139
<b>Figure 4.10</b> $^1\text{H}$ NMR spectra (500 MHz, $\text{D}_2\text{O}$ ) of: (a) only OA 1mM, (b) 1mM $\delta$ -Azide in buffered $\text{D}_2\text{O}$ , (c) 1mM OA +0.1 eqt. $\delta$ -Azide, (d) 1mM OA +0.2 eqt. $\delta$ -Azide, (e) 1mM OA +0.3 eqt. $\delta$ -Azide, (f) 1mM OA +0.4 eqt. $\delta$ -Azide, (g) 1mM OA +0.5 eqt. $\delta$ -Azide.....	140
<b>Figure 4.11</b> $^1\text{H}$ NMR spectra (500 MHz, $\text{D}_2\text{O}$ ) of (a) $\varepsilon$ -azide in buffered $\text{D}_2\text{O}$ , (b) $\varepsilon$ -azide@OA, (c) 1mM OA alone.....	142
<b>Figure 4.11</b> $^1\text{H}$ NMR Titration of $\varepsilon$ -azide against 1mM OA in 10 mM buffered $\text{D}_2\text{O}$ ...	143
<b>Figure 4.12</b> 2D DOSY NMR spectra of $\varepsilon$ -azide@OA.....	143
<b>Figure 4.13</b> $^1\text{H}$ NMR spectra of $\varepsilon$ -azide@OA <sub>2</sub> before irradiation and OA after extraction of products.....	145
<b>Figure 5.1 (a)</b> The chemical structure of the host cavitand Octa Acid and the $^1\text{H}$ NMR assignment A-J. <b>(b)</b> The formation of capsule.....	152
<b>Figure 5.2</b> Partial $^1\text{H}$ NMR spectra of G <sub>10</sub> in CD <sub>3</sub> CN and in OA.....	156
<b>Figure 5.3</b> Various guest@host complexes in $\text{D}_2\text{O}$ and the stoichiometric ratio of complexes; 500 MHz, 25 ° C.....	157
<b>Figure 5.4</b> $^1\text{H}$ NMR titration spectra of G <sub>10</sub> @OA [G <sub>10</sub> ] = 0.25 -0.75 mM, [OA] = 1mM. Spectra recorded in 500 MHz NMR and at room temperature.....	158
<b>Figure 5.5</b> $^1\text{H}$ NMR titration spectra of G <sub>2</sub> @OA [G <sub>10</sub> ] = 0.10 -1.0 mM, [OA] = 1mM. Spectra recorded in 500 MHz NMR and at room temperature.....	158
<b>Figure 5.6</b> The formation of (2:1), (2:2) and both the complexes simultaneously in presence of various guests.....	159
<b>Figure 5.7</b> The dimensions of the host cavity, as calculated by Spartan.....	160
<b>Figure 5.8</b> The expanded $^1\text{H}$ NMR upfield region (depicting the guest protons) for G <sub>2</sub> @OA and G <sub>3</sub> @OA. The guest protons have been assigned on the basis of 2D COSY NMR experiments for the above complexes.....	161

<b>Figure 5.9</b> The expanded $^1\text{H}$ NMR upfield region (depicting the guest protons) for $\text{G}_4@OA$ , $\text{G}_6@OA$ , $\text{G}_8@OA$ , $\text{G}_{10}@OA$ and $\text{G}_{12}@OA$ . The guest protons have been assigned on the basis of 2D COSY NMR experiments for the above complexes.....	163
<b>Figure 5.10</b> 2D NOESY NMR spectrum of $\text{G}_8@OA$ . Spectrum recorded in 500 MHz NMR and at room temperature.....	165
<b>Figure 5.11</b> 2D NOESY NMR spectrum of $\text{G}_{10}@OA$ . Spectra recorded in 500 MHz NMR and at room temperature.....	166
<b>Figure 5.12</b> 2D NOESY NMR spectrum of $\text{G}_{12}@OA$ . Spectra recorded in 500 MHz NMR and at room temperature.....	167
<b>Figure 5.13</b> Expanded upfield region of 2D NOESY NMR, (depicting intermolecular guest-guest proton correlations) spectrum of $\text{G}_8@OA$ . Spectra recorded in 500 MHz NMR and at room temperature.....	168
<b>Figure 5.14</b> Expanded upfield region of 2D NOESY NMR, (depicting intermolecular guest-guest proton correlations) spectrum of $\text{G}_{10}@OA$ . Spectra recorded in 500 MHz NMR and at room temperature.....	169
<b>Figure 5.15</b> Expanded upfield region of 2D NOESY NMR, (depicting intermolecular guest-guest proton correlations) spectrum of $\text{G}_{12}@OA$ . Spectra recorded in 500 MHz NMR and at room temperature.....	170
<b>Figure 5.16</b> The aromatic host region, shows $^1\text{H}$ signal “c” shift of the host, upon forming various complexes.....	171
<b>Figure 5.17</b> Possible axes of rotation for the guest inside host.....	172
<b>Figure 5.18</b> Sensitization of singlet oxygen by Rose Bengal.....	173
<b>Figure 5.19</b> Graph showing the relative percentages of the product of “ene” reaction inside OA.....	175
<b>Figure 5.20</b> The $^1\text{H}$ NMR spectra showing the complexation of $4\text{-MeGs}@OA$ , in $\text{D}_2\text{O}$ , at $25^\circ\text{C}$ , 500 MHz.....	177
<b>Figure 5.21</b> The expanded guest region, assignment of two methyl peaks on the basis of multiplicity.....	177
<b>Figure 5.22</b> $^1\text{H}$ NMR spectra showing the complexation of $\text{G}_6@OA$ , $4\text{-MeG}_5@OA$ , $4\text{-EtG}_4@OA$ and $4\text{-PrG}_3@OA$ , respectively, in $\text{D}_2\text{O}$ , at $25^\circ\text{C}$ , 500 MHz.....	180
<b>Figure 5.23</b> Partial $^1\text{H}$ NMR of (a) $\text{G}_6@OA_2$ (b) $4\text{-Me-G}_5@OA_2$ (c) $4\text{-Et-G}_4@OA_2$ (d) $4\text{-Pr-G}_3@OA_2$ .....	182



**Figure 5.24** Probable position of guest@OA<sub>2</sub>.....183

**Figure 5.25** Partial 2D NOESY NMR (depicting guest-guest through space interactions) spectra of 4-EtG<sub>4</sub>@OA and 4-PrG<sub>3</sub>@OA.....186

**Figure 5.26 (a)** Pictorial representation, **(b)** expansion of the guest region of the <sup>1</sup>H NMR spectra of G<sub>3</sub>@OA showing first the formation of (1:2) complex, followed by both complexes and eventually only (2:2) G<sub>3</sub>@OA complex. \* Represents the peaks from (2:2) complex and represents peaks from (2:1) complex.....187

**Figure 5.27** Expansion of the guest region of the <sup>1</sup>H NMR spectra of 4-MeG<sub>2</sub>@OA showing first the formation of (1:2) complex, followed by both complexes and eventually only (2:2) G<sub>3</sub>@OA complex. \* Represents the peaks from (2:2) complex and represents peaks from (2:1) complex.....188

**Figure 6.1** Pictorial Representation of FRET occurring through dipole-dipole interaction.....194

**Figure 6.2** <sup>1</sup>H NMR (500 MHz, D<sub>2</sub>O) spectra of (i) OA (1mM, in buffered D<sub>2</sub>O), (ii) C1@OA<sub>2</sub> (0.5mM: 1mM in buffered D<sub>2</sub>O), (iii) C480@OA<sub>2</sub> (0.5mM: 1mM in buffered D<sub>2</sub>O), (iv) C153@OA<sub>2</sub> (0.5mM: 1mM in buffered D<sub>2</sub>O). Signals marked A-J in represent uncomplexed OA protons; signals marked a,a'-j,j' represent complexed OA protons; and signals marked \* represent the guest alkyl proton signals.....198

**Figure 6.3** <sup>1</sup>H NMR (500 MHz, D<sub>2</sub>O), spectra of (i) OA (1mM) alone in sodium borate buffered D<sub>2</sub>O, (ii) C1@OA (1:8), (iii) C1@OA (1:4), (iv) C1@OA (1:2). Signals marked A-J in represent uncomplexed OA protons; signals marked a,a'-j,j' represent complexed OA protons; and signals marked \* represent the guest alkyl proton signals.....199

**Figure 6.4** DOSY NMR(500 MHz, D<sub>2</sub>O) spectra of C1@OA<sub>2</sub> (1:2) complex. [OA] = 1 mM in 10 mM buffered D<sub>2</sub>O and [C1] = 0.5 mM.....199

**Figure 6.5** Fluorescence spectra of (a) C480 (10 μM) in water (black line) and in the presence of OA (80 μM in 0.8 mM borate buffer) (red line), λ<sub>ex</sub>= 370 nm; (b) C1 (20 μM) in water (black line) and in the presence of OA (120 μM in 1.2 mM borate buffer) (red line), λ<sub>ex</sub>= 360 nm; (c) C153 (16 μM) in water (black line) and in the presence of OA (80 μM in 0.8 mM borate buffer) (red line), λ<sub>ex</sub>= 400 nm (a.u. = arbitrary units).....200

**Figure 6.6** Emission spectra of C1 (20 μM) in water and on gradual increase of OA (0-120 μM). Increasing OA concentration stepwise. Concentration of stock solution of OA = 10 mM in 100 mM buffered H<sub>2</sub>O. λ<sub>ex</sub>= 360 nm (a. u. = arbitrary units).....201

**Figure 6.7** <sup>1</sup>H NMR (500 MHz, D<sub>2</sub>O) spectra of (i) 0.5mM R6G alone in D<sub>2</sub>O, (ii) 0.5mM OA and 0.5mM R6G in 5mM sodium borate buffered D<sub>2</sub>O, and (iii) 0.5mM OA

alone in 5 mM sodium borate buffered D<sub>2</sub>O. Signals due to R6G protons are marked with a symbol \*.....202

**Figure 6.8** (a) Absorption and (b) emission spectra of 50  $\mu\text{M}$  of R6G in the absence (black line) and in the presence (red line) of 150  $\mu\text{M}$  of OA in 1.5 mM sodium borate buffered water,  $\lambda_{\text{ex}} = 525 \text{ nm}$ . (The abbreviations O.D. = optical density and a.u. = arbitrary unit.).....203

**Figure 6.9** Representations of spectral overlap between (a) the emission of C480@OA (black line) and the absorption of R6G in the presence of OA (red line); (b) the emission of C1@OA (black line) and the absorption of R6G in the presence of OA (red line); and (c) the emission of C153@OA (black line) and the absorption of R6G in the presence of OA (red line). Excitation wavelength ( $\lambda_{\text{ex}}$ ) in all cases is 375 nm.....204

**Figure 6.10** Steady-state fluorescence spectra demonstrating FRET between donor coumarins and acceptor R6G. (a) C480@OA and R6G; (b) C1@OA and R6G; and (c) C153@OA and R6G. The black line represents emission by the donor alone in the absence of the acceptor R6G, and the red line represents the emission in the presence of the acceptor. In this case, both donor and acceptor emissions are seen. Conditions for the spectra: (a) C480 at 10  $\mu\text{M}$ , OA at 80  $\mu\text{M}$ , R6G at 30  $\mu\text{M}$  in 0.8mM buffered water;  $\lambda_{\text{ex}} = 370 \text{ nm}$ ; (b) C1 at 20  $\mu\text{M}$ , OA at 120  $\mu\text{M}$ , R6G at 50  $\mu\text{M}$  in 1.2mM buffered water;  $\lambda_{\text{ex}} = 360 \text{ nm}$ ; and (c) C153 at 16  $\mu\text{M}$ , OA at 80  $\mu\text{M}$ , R6G at 48  $\mu\text{M}$  in 0.8mM buffered water;  $\lambda_{\text{ex}} = 400 \text{ nm}$ .....205

**Figure 6.11** Steady state fluorescence spectra demonstrating FRET between C1 (20  $\mu\text{M}$ )@OA (120  $\mu\text{M}$  in 1.2 mM buffered water) only (red line) and on addition of R6G (0-50  $\mu\text{M}$ ) (black lines),  $\lambda_{\text{ex}} = 360 \text{ nm}$ . In this case donor@OA concentration is kept constant and acceptor R6G is increased stepwise. (a. u. = arbitrary units).....206

**Figure 6.12** Femtosecond transient decays of donor coumarins: (a) C480 (10  $\mu\text{M}$ )@OA (80  $\mu\text{M}$  in 0.8 mM buffered water) alone (black dots), and on addition of R6G (30  $\mu\text{M}$ ) (red dots),  $\lambda_{\text{ex}} = 375 \text{ nm}$ ,  $\lambda_{\text{em}} = 440 \text{ nm}$ ; (b) C1 (20  $\mu\text{M}$ )@OA (120  $\mu\text{M}$  in 1.2 mM buffered water) alone (black dots) and on addition of R6G (50  $\mu\text{M}$ ) (red dots),  $\lambda_{\text{ex}} = 375 \text{ nm}$ ,  $\lambda_{\text{em}} = 420 \text{ nm}$ ; (c) C153 (16  $\mu\text{M}$ )@OA (80  $\mu\text{M}$  in 0.8 mM buffered water) alone (black dots) and on addition of R6G (48  $\mu\text{M}$ ) (red dots),  $\lambda_{\text{ex}} = 375 \text{ nm}$ ,  $\lambda_{\text{em}} = 470 \text{ nm}$ . Transient decays were recorded by monitoring the donor emission. The black line indicates the fit line to the recorded femtosecond transients.....207

**Figure 6.13** Femtosecond transient decays of: (a) R6G (30  $\mu\text{M}$ ) alone (black dots) and on addition of C480 (10  $\mu\text{M}$ )@OA (80  $\mu\text{M}$  in 0.8 mM buffered water) (red dots) and  $\lambda_{\text{ex}} = 375 \text{ nm}$ ,  $\lambda_{\text{em}} = 560 \text{ nm}$ ; (b) R6G (50  $\mu\text{M}$ ) alone (black dots) and on addition of C1 (20  $\mu\text{M}$ )@OA (120  $\mu\text{M}$  in 1.2 mM buffered water) (red dots) and  $\lambda_{\text{ex}} = 375 \text{ nm}$ ,  $\lambda_{\text{em}} = 570 \text{ nm}$ ; (c) R6G (48  $\mu\text{M}$ ) alone (black dots) and on addition of C153 (16  $\mu\text{M}$ )@OA (80  $\mu\text{M}$  in 0.8mM buffered water) (red dots) and  $\lambda_{\text{ex}} = 375 \text{ nm}$ ,  $\lambda_{\text{em}} = 570 \text{ nm}$ . The black line indicates the fit line to the recorded femtosecond transients.....208

**Figure 6.14** Femtosecond decay of C480 (10  $\mu\text{M}$ ) in presence of OA (80  $\mu\text{M}$  in 0.8 mM buffered water),  $\lambda_{\text{ex}}= 375 \text{ nm}$   $\lambda_{\text{em}}= 530 \text{ nm}$  (red end of C480 emission spectrum).....210

**Figure 6.15** Steady state fluorescence spectra of C1 (20  $\mu\text{M}$ )@OA (120  $\mu\text{M}$  in 1.2 mM buffered water) only (blue line); on addition of R6G (50  $\mu\text{M}$ ) (red line), and on addition of G3A (40  $\mu\text{M}$ ) (green line)  $\lambda_{\text{ex}}= 360 \text{ nm}$ . The blue arrow indicates the decrease in emission intensity of donor on addition of the acceptor and red arrow indicates the regain in the emission intensity of the donor on addition of another host G3A into the above solution. (a. u. = arbitrary units).....212

**Figure 6.16** Steady state fluorescence spectra of C1 (20  $\mu\text{M}$ )@OA (120  $\mu\text{M}$  in 1.2 mM buffered water) only (blue line); on addition of R6G (50  $\mu\text{M}$ ) (red line), and on addition of CB[7] (30  $\mu\text{M}$ ) (green line)  $\lambda_{\text{ex}}= 360 \text{ nm}$ . The blue arrow indicates the decrease in emission intensity of donor on addition of the acceptor and red arrow indicates the regain in the emission intensity of the donor on addition of another host CB[7] into the above solution. (a. u. = arbitrary units).....212

**Figure 6.17** Pictorial representation of ultrafast FRET taking between the donor@OA and acceptor-OA.....215

**Figure 7.1** Pictorial representation of J- and H-aggregates.....219

**Figure 7.2** Energy graphs for the dye dimers of H- and J-type types according to a molecular exciton theory.  $\Psi^+$ -directions of the transition moments are parallel, and the transition is non-zero.  $\Psi^-$ - directions of the transition moments are anti-parallel, and the transition is zero.....220

**Figure 7.3** Pictorial representation of the location of H- and J-aggregates on UV-visible absorption spectra.....221

**Figure 7.4** UV-visible spectra of Thionin Acetate (Th) titrated with OA at room temperature. Lighter color lines represent the increase of [OA] to  $2.3 \times 10^{-6} \text{ M}$  and the darker shade lines represent the increase in [OA] from  $2.3 \times 10^{-6} \text{ M}$  to  $2.0 \times 10^{-4} \text{ M}$ . Wavelength measured in nanometers.....226

**Figure 7.5** Fluorescence spectra of Thionin Acetate (Th) titrated with OA at room temperature. Lighter color lines represent the increase of [OA] to  $2.3 \times 10^{-6} \text{ M}$  and the darker shade lines represent the increase in [OA] from  $2.3 \times 10^{-6} \text{ M}$  to  $2.0 \times 10^{-4} \text{ M}$ . Wavelength in nanometer.....227

**Figure 7.6** UV-visible spectra of Azure B (AB) titrated with OA at room temperature. Lighter color lines represent the increase of [OA] to  $1.3 \times 10^{-6} \text{ M}$  and the darker shade lines represent the increase in [OA] from  $1.3 \times 10^{-6} \text{ M}$  to  $4.6 \times 10^{-5} \text{ M}$ . Wavelength measured in nanometers.....227

<b>Figure 7.7</b> Fluorescence spectra of Azure B (AB) titrated with OA at room temperature. Lighter color lines represent the increase of [OA] to $1.3 \times 10^{-6}$ M and the darker shade lines represent the increase in [OA] from $1.3 \times 10^{-6}$ M to $4.6 \times 10^{-5}$ M. Wavelength measured in nanometers.....	228
<b>Figure 7.8</b> Cartoon representations of the probable mechanism of formation of dimer followed by monomer of the cationic dyes due the interaction with the anionic exterior of the host OA.....	229
<b>Figure 7.9</b> UV-Visible spectra of Thionin Acetate (Th) titrated with CB[8] at room temperature. [Th] = $1.5 \times 10^{-5}$ M and CB[8] = 0 to $12 \times 10^{-6}$ M. Wavelength is measured in nanometers.....	230
<b>Figure 7.10</b> Fluorescence spectra of Thionin Acetate (Th) titrated with CB[8] at room temperature. [Th] = $1.5 \times 10^{-5}$ M and CB[8] = 0 to $12 \times 10^{-6}$ M. Wavelength is measured in nanometers.....	231
<b>Figure 7.11</b> Cartoon representations of the probable mechanism of the formation of the dimer in presence of host CB[8].....	232
<b>Figure 7.12</b> UV-Visible spectra of Thionin Acetate (Th) titrated with CB[7] at room temperature. [Th] = $1.5 \times 10^{-5}$ M and CB[7] = 0 to $6.6 \times 10^{-5}$ M. Wavelength is measured in nanometers.....	233
<b>Figure 7.13</b> Fluorescence spectra of Thionin Acetate (Th) titrated with CB[7] at room temperature. [Th] = $1.5 \times 10^{-5}$ M and CB[7] = 0 to $6.6 \times 10^{-5}$ M. Wavelength is measured in nanometers.....	233
<b>Figure 7.14</b> Cartoon representations of the probable mechanism of the formation of the dimer followed in presence of host CB[8].....	234
<b>Figure 7.15</b> UV-Visible spectra of Thionin Acetate (Th) first titrated with CB[8] (0- $12 \times 10^{-6}$ M) followed by OA (0- $3.63 \times 10^{-4}$ M) at room temperature. Initial concentration of Th = $1.5 \times 10^{-5}$ M. Wavelength is measured in nanometers.....	236
<b>Figure 7.16</b> Fluorescence spectra of Thionin Acetate (Th) first titrated with CB[8] (0- $12 \times 10^{-6}$ M) followed by OA (0- $3.63 \times 10^{-4}$ M) at room temperature. Initial concentration of Th = $1.5 \times 10^{-5}$ M. Wavelength is measured in nanometers.....	236
<b>Figure 7.17</b> Cartoon representations of the probable mechanism of the formation of the dimer in CB[8] followed by formation of monomer in presence of host OA.....	237
<b>Figure 7.18</b> UV-Visible spectra of Thionin Acetate (Th) first titrated with CB[7] (0- $6.66 \times 10^{-5}$ M) followed by OA (0- $5.0 \times 10^{-4}$ M) at room temperature. Initial concentration of Th = $1.5 \times 10^{-5}$ M. Wavelength is measured in nanometers.....	238

- Figure 7.19** Fluorescence spectra of Thionin Acetate (Th) first titrated with CB[7] ( $0-6.66 \times 10^{-5}$  M) followed by OA ( $0-5.0 \times 10^{-4}$  M) at room temperature. Initial concentration of Th =  $1.5 \times 10^{-5}$  M. Wavelength is measured in nanometers.....238
- Figure 7.20** Cartoon representations of the probable mechanism of the formation of the dimer in CB[8] followed by formation of monomer in presence of host OA.....239
- Figure 7.21** The absorption spectra of dyes in neutral aqueous (black lines) and borate buffer (red lines) ( $\geq 6$  mM) solution at room temperature.....240
- Figure 7.22** Absorption spectra of CVP ( $1.07 \times 10^{-5}$  M) titrated with aq. solution of DHAS@OA<sub>2</sub> capsular ( $0-2.2 \times 10^{-5}$  M).....243
- Figure 7.23** UV-Visible spectra of Thionin Acetate (TA) titrated with  $\gamma$ -CD ( $0-1.17 \times 10^{-2}$  M) Initial concentration of TA =  $1.5 \times 10^{-5}$  M. Wavelength is measured in nanometers.....244
- Figure 7.24** Fluorescence spectra of Thionin Acetate (TA) titrated with  $\gamma$ -CD ( $0-1.17 \times 10^{-2}$  M) Initial concentration of TA =  $1.5 \times 10^{-5}$  M. Wavelength is measured in nanometers.....245
- Figure 7.25** UV-Visible spectra of Thionin Acetate (TA) first titrated with  $\gamma$ -CD ( $0-1.17 \times 10^{-2}$  M), followed by OA ( $0-0.16 \times 10^{-6}$  M solid black lines) ( $0.16 \times 10^{-6}$  M -  $5.0 \times 10^{-4}$  M dotted red lines). Initial concentration of TA =  $1.5 \times 10^{-5}$  M. Wavelength is measured in nanometers.....245
- Figure 7.26** Fluorescence spectra of Thionin Acetate (TA) first titrated with  $\gamma$ -CD ( $0-1.17 \times 10^{-2}$  M), followed by OA ( $0-0.16 \times 10^{-6}$  M solid black lines) ( $0.16 \times 10^{-6}$  M -  $5.0 \times 10^{-4}$  M dotted red lines). Initial concentration of TA =  $1.5 \times 10^{-5}$  M. Wavelength is measured in nanometers.....246
- Figure 7.27** UV-Visible spectra of Thionin Acetate (TA) titrated with G<sub>3</sub>A ( $0-1.2 \times 10^{-6}$  M, solid black lines) and ( $1.2 \times 10^{-6}$  M –  $2.0 \times 10^{-4}$  M, red dotted lines) Initial concentration of TA =  $1.5 \times 10^{-5}$  M. Wavelength is measured in nanometers.....247
- Figure 7.28** Fluorescence spectra of Thionin Acetate (TA) titrated with G<sub>3</sub>A ( $0-1.2 \times 10^{-6}$  M, solid black lines) and ( $1.2 \times 10^{-6}$  M –  $2.0 \times 10^{-4}$  M, red dotted lines) Initial concentration of TA =  $1.5 \times 10^{-5}$  M. Wavelength is measured in nanometers.....248
- Figure 7.29** UV-Visible spectra of Thionin Acetate (TA) first titrated with G<sub>3</sub>A ( $0-2.4 \times 10^{-4}$  M), followed by OA ( $0-6.0 \times 10^{-3}$  M). Initial concentration of TA =  $1.5 \times 10^{-5}$  M. Wavelength is measured in nanometers.....249

<b>Figure 7.30</b> Fluorescence spectra of Thionin Acetate (TA) first titrated with G <sub>3</sub> A (0- 2.0 x 10 <sup>-4</sup> M), followed by OA (0- 6.0 x 10 <sup>-3</sup> M). Initial concentration of TA = 1.5 x 10 <sup>-5</sup> M. Wavelength is measured in nanometers.....	250
<b>Figure 7.31</b> UV-Visible spectra of Thionin Acetate (TA) titrated with Cal [8] (0- 1.9 x 10 <sup>-6</sup> M, solid black lines); (1.9 x 10 <sup>-6</sup> M – 2.7 x 10 <sup>-6</sup> M, red dotted lines) and (2.7 x 10 <sup>-6</sup> M – 2.3 x 10 <sup>-5</sup> M, dotted green lines). Initial concentration of TA = 1.5 x 10 <sup>-5</sup> M. Wavelength is measured in nanometers.....	251
<b>Figure 7.32</b> Fluorescence spectra of Thionin Acetate (TA) titrated with Cal [8] (0- 2.3 x 10 <sup>-5</sup> M). Initial concentration of TA = 1.5 x 10 <sup>-5</sup> M. Wavelength is measured in nanometers.....	252
<b>Figure 7.33</b> UV-Visible spectra of Thionin Acetate (TA) first titrated with Cal [8] (0- 2.3 x 10 <sup>-5</sup> M), followed by OA (0- 6.0 x 10 <sup>-4</sup> M). Initial concentration of TA = 1.5 x 10 <sup>-5</sup> M. Wavelength is measured in nanometers.....	253
<b>Figure 7.34</b> Fluorescence spectra of Thionin Acetate (TA) first titrated with Cal [8] (0- 2.3 x 10 <sup>-5</sup> M), followed by OA (0- 6.0 x 10 <sup>-4</sup> M). Initial concentration of TA = 1.5 x 10 <sup>-5</sup> M. Wavelength is measured in nanometers.....	253
<b>Figure 8.1</b> Emission spectra of pyrene in the presence of dendrimers. [pyrene] = 0.01 mM and [dendrimer] = 0.2 mM in aq. NaOH (0.1 M), excitation wavelength = 335 nm.....	264
<b>Figure 8.2</b> Emission spectra of pyrene in the presence of first generation dendrimers C <sub>2</sub> G1O-C <sub>5</sub> G1O in aq alkaline medium (0.2mM), λ <sub>ex</sub> =335 nm.....	265
<b>Figure 8.3</b> Molecular structures of coumarins used as fluorescent probes.....	266
<b>Figure 8.4</b> Emission spectra of C153 in the presence of various generation dendrimers (C <sub>n</sub> G1 O -C <sub>n</sub> G3 O, n = 2, 3, 4, 5) [C <sub>n</sub> G1O] = 0.8mM in 0.1M aq NaOH; [C <sub>n</sub> G2 O] and [C <sub>n</sub> G3 O] = 0.6 mM in 0.1 M aq NaOH; [C153] = 0.04 mM; λ <sub>ex</sub> = 400 nm and λ <sub>em</sub> for C153 in water = 550 nm.....	270
<b>Figure 8.5</b> Rearrangement of solvent molecules around the excited probe molecule....	271
<b>Figure 8.6</b> Processes of Solvation Dynamics.....	272
<b>Figure 8.7</b> Schematic illustration of the potential energy surfaces involved in the solvation dynamics of water. (Reproduced from Pal et al, <i>J. Phys. Chem. B</i> , <b>2002</b> , 106, 12376-12395).....	273
<b>Figure 8.8</b> Picosecond time-resolved experiments for the probe C480 and C <sub>5</sub> G3O dendrimer.....	274

<b>Figure 8.9</b> Femtosecond time-resolved experiments for the probe C480 and C <sub>5</sub> G3O dendrimer.....	275
<b>Figure 8.10</b> Picosecond time-resolved experiments for the probe C153 and C <sub>5</sub> G3O dendrimer.....	276
<b>Figure 8.11</b> Absorption spectra of <i>cis</i> -, <i>trans</i> -stilbenes, C <sub>5</sub> G3O, CVP, and 380 nm filter.....	281
<b>Figure 8.12</b> Fluorescence studies of CVP in presence of various (a–d) (C <sub>2</sub> G3O–C <sub>5</sub> G3O) dendrimers respectively. [CVP] = 3 × 10 <sup>-5</sup> M in water. [C <sub>n</sub> G3] = 0.33 × 10 <sup>-6</sup> M to 1.7 × 10 <sup>-4</sup> M. λ <sub>ex</sub> = 580 nm.....	283
<b>Figure 8.13</b> UV-visible spectra of first, second and third generation dendrimers along with the peripheral molecule.....	284
<b>Figure 8.14</b> Fluorescence spectra of first, second and third generation dendrimers along with the peripheral molecule.....	285
<b>Figure 8.15</b> UV-visible spectra of third generation dendrimer ending with ester group along with the trimethoxybenzene (representing the core of the dendrimer).....	286
<b>Figure 8.16</b> EPR spectra of CAT-1 in (a) buffer solution, (b) C <sub>5</sub> G1A, (c) C <sub>5</sub> G2A, (d) C <sub>5</sub> G3A. [CAT-1] = 0.1 mM, [C <sub>5</sub> G1-3A] = 1 mM, [buffer]= 10 mM. Spectra recorded at room temperature.....	290
<b>Figure 8.17</b> EPR spectra of TEMPO in (a) buffer solution, (b) C <sub>5</sub> G1A, (c) C <sub>5</sub> G2A, (d) C <sub>5</sub> G3A. [TEMPO] = 0.1 mM, [C <sub>5</sub> G1-3A] = 1 mM, [buffer]= 10 mM. Spectra recorded at room temperature.....	291
<b>Figure 8.18</b> EPR spectra of 4-carboxy-TEMPO in (a) buffer solution, (b) C <sub>5</sub> G1A, (c) C <sub>5</sub> G2A, (d) C <sub>5</sub> G3A. [4-carboxy-TEMPO] = 0.1 mM, [C <sub>5</sub> G1-3A] = 1 mM, [buffer]= 10 mM. Spectra recorded at room temperature.....	293
<b>Figure 8.19</b> EPR spectra, hyperfine coupling constants and rotational correlation time of (a) CAT-1 in C <sub>5</sub> G3A, (b) CAT-1 in buffer, (c) CAT-8 in C <sub>5</sub> G3A, (d) CAT-8 in buffer. [CAT-1] = 0.01 mM, [CAT-8]= 0.01 mM, [C <sub>5</sub> G1-3A] = 1 mM, [buffer]= 10 mM. EPR spectra recorded at room temperature.....	294
<b>Figure 8.20</b> EPR spectra, hyperfine coupling constants and rotational correlation time of (a) CAT-10 in C <sub>5</sub> G3A, (b) CAT-10 in buffer, (c) CAT-12 in C <sub>5</sub> G3A, (d) CAT-12 in buffer. [CAT-1] = 0.01 mM, [CAT-8]= 0.01 mM, [C <sub>5</sub> G1-3A] = 1 mM, [buffer]= 10 mM. EPR spectra recorded at room temperature.....	296
<b>Figure 8.21</b> Interaction of carboxylic acid functionalized third generation dendrimer with Dicynoanthracene and <i>trans</i> -stilbene.....	298

<b>Figure 8.22</b> Interaction of carboxylic acid functionalized third generation dendrimer with N-methyl acridinium Iodide (NMA) and trans-stilbene.....	300
<b>Figure 8.23</b> Quenching of Fluorescence of NMA upon addition of dendrimer.....	301
<b>Figure 8.24</b> Graph of fluorescence intensity vs. dendrimer concentration to calculate the quenching. ....	301



## LIST OF SCHEMES

<b>Scheme 2.1</b> Photolysis of Carbene Precursors and Possible Products.....	40
<b>Scheme 2.2</b> Cartoon representation of the complexation modes of the guest of various size and shape with the host OA.....	47
<b>Scheme 3.1</b> Photoreaction and possible products from photo-irradiation of 1-azidoadamantane.....	85
<b>Scheme 3.2</b> Photoreaction and possible products from photo-irradiation of 2-azidoadamantane.....	86
<b>Scheme 4.1</b> Chemical structures of the azido aryl ketones, used as guests in this study.....	126
<b>Scheme 4.2</b> Chemical structure and <sup>1</sup> H NMR peak assignment of host Octa Acid.....	127
<b>Scheme 4.3</b> Photolysis reactions $\beta$ -azide undergoes in (a) solution and (b) crystals.....	132
<b>Scheme 4.4</b> Proposed Reaction mechanism for the photolysis of $\beta$ -azide.....	133
<b>Scheme 4.5</b> Products obtained from the photolysis of $\gamma$ -azide under various experimental conditions.....	136
<b>Scheme 4.6</b> Proposed Reaction mechanism for the photolysis of $\gamma$ -azide in Toluene (Ar).....	137
<b>Scheme 4.7</b> Proposed Reaction mechanism for the photolysis of $\gamma$ -azide in Toluene (O <sub>2</sub> ).....	138
<b>Scheme 4.8</b> Products obtained upon photolysis of $\delta$ -Azide under various experimental conditions.....	141
<b>Scheme 4.9</b> Products obtained upon photolysis of $\epsilon$ -Azide under various experimental conditions.....	144
<b>Scheme 4.10</b> Probable mechanism for the formation of nitro products from the photolysis of $\epsilon$ -azide in presence of molecular O <sub>2</sub> .....	144
<b>Scheme 5.1</b> The products of the “ene” reaction, when alkylcycloalkenes are used as substrates.....	151

<b>Scheme 5.2</b> Two sets of guests 1-alkylcyclohexene studied for the “ene” reactions.....	153
<b>Scheme 5.3</b> Two sets of guests 1-alkyl-4-methylcyclohexene studied for the “ene” reactions.....	154
<b>Scheme 5.4</b> Chemical structure of guests cycloalkenes with almost similar molecular length.....	154
<b>Scheme 5.5</b> Chemical structure of guests cycloalkenes with intermediate molecular size.....	154
<b>Scheme 5.6</b> Possible products of “ene” reaction in solution.....	174
<b>Scheme 5.7</b> Possible “ene” reaction products in case of 4-Me-1-alkylcyclohexene guests.....	178
<b>Scheme 5.8</b> Synthetic reactions for the formation of 1-substituted cyclohexene.....	189
<b>Scheme 6.1</b> Chemical Structures of hosts – OA with Proton Signals Assigned from A-J, CB[7], G3A and Structures of Donors C480, C1, and C153 and Acceptor R6G.....	196
<b>Scheme 7.1</b> Chemical structures of the cationic dyes used for these studies.....	223
<b>Scheme 7.2</b> Chemical structures of the hosts Octa Acid and Cucurbiturils.....	223
<b>Scheme 7.3</b> Chemical structures of the other hosts involved in this study.....	224
<b>Scheme 7.4</b> Chemical structures of cationic dyes used for the studies- Cresyl Violet Perchlorate (CVP), Oxazine 170 (O170), Oxazine 1 Perchlorate (O1P), Acridine Orange (AO), Thionin Acetate (TA), Methylene Blue (MB), Azure B (AB), and Toluidine Blue (TBO).....	240
<b>Scheme 7.5</b> Capsular complex of DHAS@OA <sub>2</sub> .....	242
<b>Scheme 8.1</b> Cartoon representation of the topological parts of a dendrimer.....	260
<b>Scheme 8.2</b> Chemical structures of poly (aryl alkyl ether) dendrimers with phenolic (C <sub>n</sub> GO) and carboxylic acid (C <sub>n</sub> GA) peripheral group.....	262
<b>Scheme 8.3</b> Photolysis of Dibenzylketone inside Aqueous Basic Solutions of Dendrimers.....	277
<b>Scheme 8.4</b> Photoisomerization of <i>trans</i> -Stilbene@(C <sub>5</sub> -C <sub>2</sub> )G3O Dendrimers in the Presence of CVP as Electron-Transfer Sensitizer.....	281

<b>Scheme 8.5</b> Chemical structures of Peripheral Molecule and TMB.....	284
<b>Scheme 8.6</b> Nitroxide radical probes used for the characterization of dendrimers using EPR.....	287

## LIST OF TABLES

<b>Table 2.1</b> The diffusion constants for various guest@host complexes.....	47
<b>Table 2.2</b> Relative percentages of the products upon the photolysis of the guests <b>1a-d@OA</b> , <b>1a-d@OA</b> on silica surface and in D <sub>2</sub> O.....	54
<b>Table 2.3</b> Relative percentages of the products upon the photolysis of the guests on silica without any host.....	55
<b>Table 2.4</b> Relative percentages of the products upon the photolysis of guests <b>1a-d@CB[7]</b> , <b>1a-d@CB[8]</b> and in D <sub>2</sub> O.....	62
<b>Table 2.5</b> Relative percentages of the products upon the photolysis of the guests <b>1a-d@PdNC</b> and in D <sub>2</sub> O.....	66
<b>Table 2.6</b> Relative percentages of the products upon the photolysis of the guests <b>1a-d@hosts</b> as mentioned in the literature.....	68
<b>Table 2.7</b> Relative percentages of the products upon the photolysis of the guests <b>1a-d@hosts</b> .....	71
<b>Table 2.8</b> Binding Constants (K) and Relevant Thermodynamic Parameters for Complexation of Adamantanediazirines with OA at 298 K.....	73
<b>Table 2.9</b> Binding Constants (K) and Relevant Thermodynamic Parameters for Complexation of Carbene Precursors with CB[7] at 298 K.....	74
<b>Table 3.1</b> Diffusion constant of free OA and <b>1@OA</b> as obtained by 2D DOSY NMR....	91
<b>Table 3.2</b> Ratio of the photoproducts after the photolysis of <b>1@OA</b> .....	91
<b>Table 3.3</b> Ratio of the photoproducts after the photolysis of <b>1@CB[7]</b> .....	97
<b>Table 3.4</b> Ratio of the photoproducts after the photolysis of <b>1@PdNC</b> .....	100
<b>Table 3.5</b> Diffusion Constants for free OA and <b>2@OA</b> , as obtained by 2D DOSY experiments.....	103
<b>Table 3.6</b> Ratio of the photoproducts after the photolysis of <b>2@OA</b> .....	103
<b>Table 3.7</b> Ratio of the photoproducts obtained after the irradiation of <b>2@CB[7]</b> .....	106

<b>Table 3.8</b> Ratio of the photoproducts obtained after the irradiation of 2@PdNC.....	108
<b>Table 3.9</b> Ratio of the photoproducts of 1-azidoadamantane irradiated in various media.....	109
<b>Table 3.10</b> Ratio of the photoproducts of 2-azidoadamantane irradiated in various media.....	111
<b>Table 3.11</b> Binding constants (K) and relevant thermodynamic parameters for complexation of 1- and 2-azidoadamantanes with OA at 25 °C.....	113
<b>Table 4.1</b> Relative Percentages of the products obtained upon irradiation of $\beta$ -azide in solution and in OA.....	133
<b>Table 4.2</b> Relative Percentages of the products obtained upon irradiation of $\gamma$ -azide in solution and in OA.....	138
<b>Table 4.3</b> Relative Percentages of the products obtained upon irradiation of $\delta$ -azide in solution and in OA.....	141
<b>Table 4.4</b> Relative Percentages of the products obtained upon irradiation of $\epsilon$ -azide in solution and in OA.....	145
<b>Table 5.1</b> The length and volume for each guest molecule. Spartan has been utilized and the energy is minimized for each structure. The guest molecule is taken in linear conformation.....	160
<b>Table 5.2</b> The diffusion constants for various guest@host complexes.....	173
<b>Table 5.3</b> Product ratio for “ene” reaction in solution and inside OA.....	174
<b>Table 5.4</b> Product ratio for “ene” reaction in solution and inside OA* .....	179
<b>Table 5.5</b> Product ratio for “ene” reaction in solution and inside OA* .....	185
<b>Table 6.1</b> Femtosecond Decay Parameters of the Acceptor in the Presence and Absence of the Donors.....	209
<b>Table 6.2</b> Comparison of Parameters for Calculating $R_{DA}$ .....	210
<b>Table 6.3</b> Picosecond Decay Parameters of C480-R6G-OA systems + G3A/ CB[7].....	213
<b>Table 6.4</b> Femtosecond Decay Parameters of C480-R6G-OA systems + G3A/ CB[7]..	214
<b>Table 6.5</b> Calculated Donor-Acceptor distances.....	214
<b>Table 7.1</b> Red shift observed for the $\lambda_{max}$ of the cationic dyes in presence of host OA..	241

<b>Table 8.1</b> Relative $I_3/I_1$ Fluorescence Band Intensity of Pyrene in Aqueous Basic Solutions of Dendrimers.....	265
<b>Table 8.2</b> Blue shift in emission $\lambda_{\max}$ and $E_T$ 30 value of Coumarin 480 in various dendrimer solutions.....	267
<b>Table 8.3</b> Blue shift in emission $\lambda_{\max}$ and $E_T$ 30 value of Coumarin 1 in various dendrimer solutions.....	268
<b>Table 8.4</b> Blue shift in emission $\lambda_{\max}$ and $E_T$ 30 value of Coumarin 153 in various dendrimer solutions.....	269
<b>Table 8.5</b> Photolysis of 1-Phenyl-3-p-tolyl-propan-2-one in Aqueous Basic Dendrimer Solutions.....	278
<b>Table 8.6</b> Isomerization of <i>trans</i> -Stilbene in Aqueous Dendrimer Solutions and in EtOH.....	280
<b>Table 8.7</b> Photo-isomerization of <i>trans</i> -Stilbene Encapsulated within C <sub>2</sub> G3O-C <sub>5</sub> G3O Dendrimers, in the Presence of CVP as Electron-Transfer Sensitizer Dye, Using a 380 nm Filter and Irradiation for 2 h.....	282
<b>Table 8.8</b> Hyperfine coupling constant and rotational correlation time for CAT-1 in different media.....	290
<b>Table 8.9</b> Hyperfine coupling constant and rotational correlation time for TEMPO in different media.....	292
<b>Table 8.10</b> Hyperfine coupling constant and rotational correlation time for 4-carboxy TEMPO in different media.....	293
<b>Table 8.11</b> Isomerization of <i>trans</i> -Stilbene in Aqueous Dendrimer Solutions and in CH <sub>3</sub> CN.....	298

# **CHAPTER 1**

## **Introduction to Supramolecular Photochemistry**

## 1.1 Photochemistry

Ancient civilizations recognized the importance of *light* for the maintenance and sustenance of life on earth. The sun, the ultimate source of light that provides the energy that drives life as we know it, has been an object of worship since antiquity. Use of *light*, is the basic foundation of this research work, hence it is befitting to initiate this presentation with appreciating the instrumental role of light energy.

A number of folk medicines which date back hundreds of years suggests that exposure of the patient to sunlight was an integral part of medical treatments. However, orderly investigations of the connection between the absorption of light by matter and its chemical and physical consequences were not reported in the scientific literature until about the turn of this century, when systematic efforts revealed that exposure of matter to sunlight led to a rich range of transformations that are now termed photochemical reactions. Hence the scientific field of “Photochemistry” was born. During this period many photoreactions that are still the object of investigation and practical use today were discovered: dimerization of cinnamic acids, styrene derivatives, quinones, and anthracenes; photoreduction, intramolecular cycloaddition, and cleavage reactions of carbonyl compounds; photoreduction of aromatic nitro compounds; photoisomerization of olefins; etc.<sup>1</sup>

Below are presented few of the innumerable examples<sup>2,3</sup> of applications of the Photochemistry, which have large impact on our lives today:

(a) An instructive example for the technical exploitation of fluorescence phenomena is the development of optical brighteners.<sup>4</sup> The current annual production of optical brighteners is about 65000—70000 tons with a value of about \$350 million. More than



half is consumed by the detergents industry, and one-quarter is used for optical bleaching of paper.

(b) Fluorescent or phosphorescent stamps are used for automatic sorting of letters and postcards. Another lucrative application for phosphorescent or luminous paints is marking dials and light switches.

(c) Production of sunscreen lotions in cosmetics industry. The function of a sunscreen cosmetic is to filter solar radiation.<sup>5</sup> It utilizes photoactive chemicals which can inhibit the rays that are most responsible for erythema, i.e. those between 290 and 320 nm, and allow those that tan direct, i.e. those between 320 and 390 nm.

(d) There are innumerable applications for photoconductors in photography, reprography and electronics. An economically interesting application for energy transfer in the gas phase is modern high-wattage lamps for illuminating streets, sporting events and greenhouses.<sup>6</sup>

(e) The ene-reaction with singlet oxygen is being used by two perfumery manufacturers, Dragoco (West Germany) and Firmenich (Switzerland), for the production of rose oxide.<sup>7</sup>

(f) Application of two important photochemical isomerization reactions are an electrocyclic ring opening in the vitamin D synthesis and a thermo-reversible hydrogen shift in the ultra-violet stabilization of plastics.

(g) The dimerization of cinnamic acid has found practical use in U.V.-curable coatings.

(h) Photopolymeric printing plates and photoresists are other important, or perhaps the most important, technical fields of applications for coatings that are cured by light.<sup>8</sup>

Some biomedical applications include:

(a) PDT in oncology: Photo Dynamic Therapy (PDT) is a treatment modality using photosensitizer and light and the subsequent photochemical reactions to kill cancer cells. PDT has been developed as an alternative cancer treatment for more than 40 years and is the most well known and established biomedical application of photochemistry.

(b) Gene regulation study in molecular biology: Photochemical cross-linking has been used as a powerful method for studying protein–nucleic acid interactions in the field of molecular biology.<sup>9</sup>

(c) Photochemical tissue bonding in bio-surgery: Photochemical tissue bonding (PTB) presents another biomedical application of photochemistry and focuses on the surgical modalities of tissue repair, aiming to bond tissue edges or surfaces together.

(d) Photochemical crosslinking and polymerization in tissue engineering: Comparing with chemical and physical crosslinking, photochemical crosslinking possesses several important advantages like, controllable parameters such as laser energy, power density, influence, and photosensitizer concentration, selectivity in where to crosslink and moreover it is a rapid and efficient process.

(e) Controlled release drug delivery: Many photopolymerizable hydrogels such as PEG methacrylate derivatives, polyvinyl alcohol derivatives, and dextran methacrylate are by default controlled release drug delivery systems<sup>10,11</sup> because many parameters, including the light factors, the material factors, and the drug factors, can be controlled so as to achieve controlled release.

Hence, Photochemistry is proved to be an important branch of science, and holds promising future in the solution of global problems from the energy crisis (solar energy

storage and conversion) to environmental protection (waste-water treatment, destruction of chemical wastes, etc.).

Photochemistry underwent the advancement from the “molecular” level to the “supramolecular” level in terms of external environments in late 1980’s. The ability of the "environment" to influence the course of photoreactions opened new fields of photoreactions in "micro-heterogeneous media", in "constrained spaces", on "interfaces", and so forth. This advancement was triggered by understanding the involvement of photochemical events in processes such as vision, photosynthesis, photoimaging, optical recording, office copying, nonlinear optics, the ozone hole problem, and the greenhouse effect. Hence, modern supramolecular photochemistry has become to some extent a connecting link between various branches of chemistry (organic, inorganic, analytical, biological and physical chemistry and materials science).

So by now, we are able to appreciate the role of light energy in our lives. We have seen how photochemistry has numerous applications. We also, understood how and why photochemistry evolved into “Supramolecular Organic Photochemistry.” The following section, brings forth a brief account of “Supramolecular Photochemistry”, and showcase some examples which highlight its significance and which are our motivation for undertaking this research work.

## **1.2 Supramolecular Photochemistry**

In nature, chemical conversions take place in a confined environment and are closely geared to each other such that the product of one reaction is the substrate or catalyst of the subsequent one. Nature realizes this control and fine-tuning of the products, by using well-defined reaction environments, which vary from nanometer-sized

and relatively simple systems, such as enzymes, to micrometer-sized and extremely complex assemblies, such as cells. Indeed, efforts to understand the driving forces for these fundamental biological processes has led to the development of a new genre of chemical research collectively termed “supramolecular chemistry”.<sup>12</sup>

Supramolecular chemistry generally encompasses chemistry of the noncovalent bond for the assembly of large “supermolecules” from smaller molecular subunits,<sup>12-14</sup> and as such it relies heavily on weak intermolecular forces such as hydrogen bonding, aromatic  $\pi$ - $\pi$  stacking, ion-pair and van der Waals interactions. Additionally, the resultant macromolecules possess structural features and chemical properties that are distinct from the original constituents from which they were constructed.<sup>15</sup> A part of supramolecular chemistry is “**host-guest chemistry**”, wherein a host compound spatially accommodates a guest molecule or ion. The primary properties of host guest systems are to alter the reactivity of one or more of its components or to perform a specific function. For example host-guest systems have been designed to function as sensors<sup>16,17</sup>, as catalysts<sup>18</sup>, preferential solubilization<sup>19</sup>, for delivery of drugs<sup>20</sup>, or for photoinduced charge separation<sup>21</sup>.

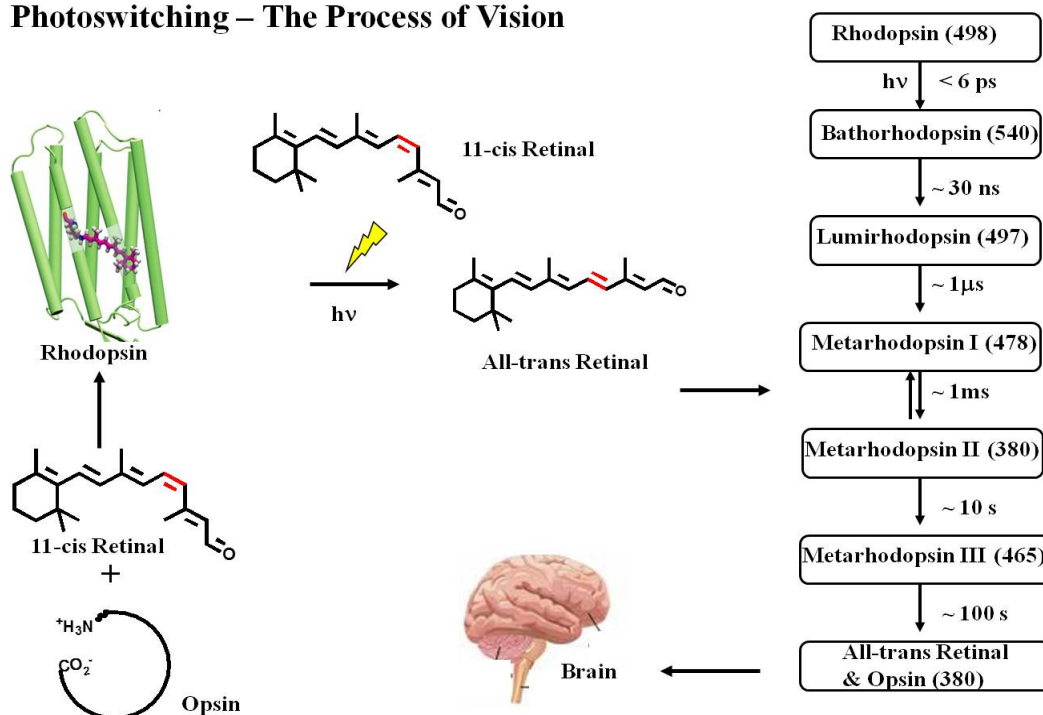
Efforts in this area have focused on creating macromolecular capsules, which can totally encapsulate guest molecules both reversibly and irreversibly<sup>22-24</sup>. Numerous examples of structurally defined, container-like molecules with interesting host-guest binding properties have been reported in the past decade. These include Rebek’s glycouril-based spheres and cavitands,<sup>24b,25,26</sup> dimeric cyclocholates,<sup>27</sup> cucurbituril,<sup>28</sup> cyclodextrins,<sup>29</sup> and calixarenes-based dimers and oligomers.<sup>30,31</sup> Some of these host systems, which have been used in this research work are covered in **Section 1.4**, briefly.

### 1.3 Leading Examples of Photochemistry and Photophysics in Host – Guest Chemistry

Below are presented some examples to highlight the features, uses and significance of “Supramolecular Photochemistry”. The first two examples show how supramolecular photochemistry is involved in two most important biological processes, namely- *photosynthesis*, and *vision*. Following it are the examples of exploitation of host-guest chemistry to alter the photochemical and photophysical pathways of a chemical reaction:

**1.3.1 Vision:** The retina, in the eye, contains the molecules that undergo a chemical change upon absorbing light. These molecules are located in the light-sensitive cells known as rods and cones or photoreceptors. Specifically, 11-*cis* retinal combines with a protein called “opsin” to make rhodopsin, this acts as the reaction cavity for photoisomerization of 11-*cis*-retinal to all *trans* retinal.

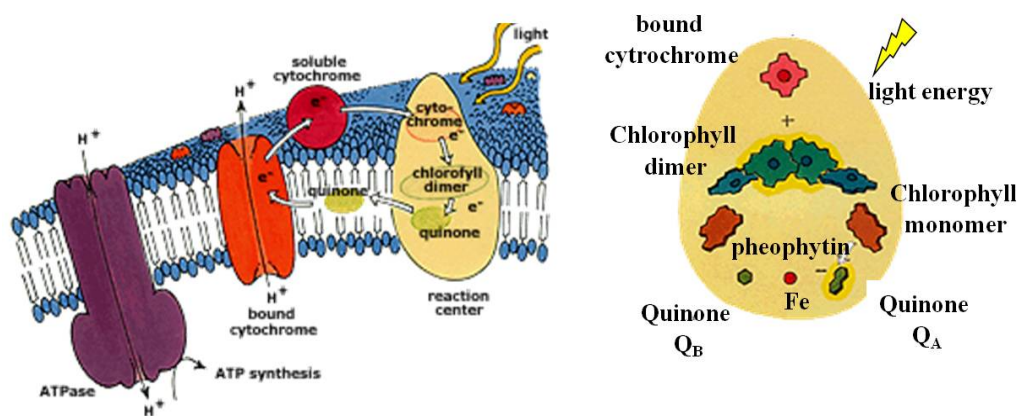
#### Photoswitching – The Process of Vision



**Figure 1.1** Pictorial depiction of photochemistry and photobiology of *vision*.

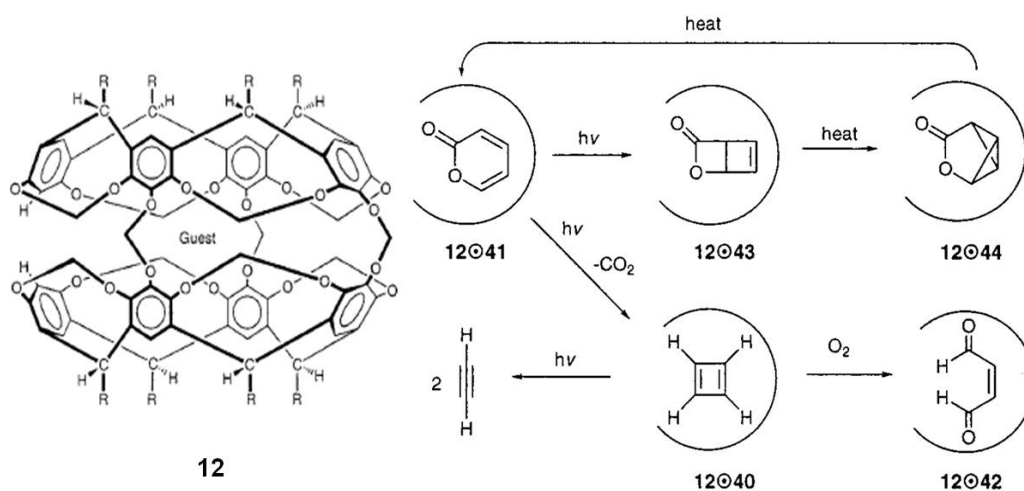
When visible light hits the *cis*-retinal, the *cis*-retinal undergoes an isomerization, or change in molecular arrangement, to all-*trans*-retinal. The new form of *trans*-retinal does not fit as well into the protein, and so a series of geometry changes in the protein begins. As the protein changes its geometry, it initiates a cascade of biochemical reactions that results in changes in charge so that a large potential difference builds up across the plasma membrane. This potential difference is passed along to an adjoining nerve cell as an electrical impulse. The nerve cell carries this impulse to the brain, where the visual information is interpreted.

**1.3.2 Photosynthesis**<sup>32</sup>: In the light reactions, one molecule of the pigment chlorophyll absorbs one photon and loses one electron. This electron is passed to a modified form of chlorophyll called pheophytin which passes the electron to a quinone molecule, allowing the start of a flow of electrons down an electron transport chain that leads to the ultimate reduction of NADP to NADPH. In addition, this creates a proton gradient across the chloroplast membrane; its dissipation is used by ATP synthase for the concomitant synthesis of ATP. The chlorophyll molecule regains the lost electron from a water molecule through a process called photolysis, which releases a dioxygen (O<sub>2</sub>) molecule.



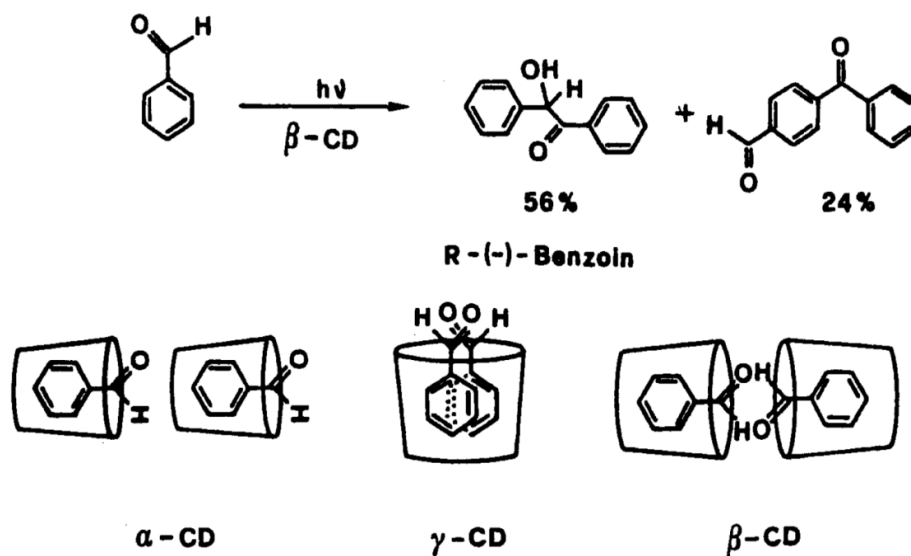
**Figure 1.2** Pictorial depiction of photochemistry and photobiology of *photosynthesis*.

**1.3.3 “Taming” of cyclobutadiene in a carcerand:** Cram et al. first stabilized the highly reactive cyclobutadiene, which is considered to be the “Mona Lisa of organic chemistry”<sup>33</sup>. In the absence of oxygen, 40@12 was stable up to 60 °C. When a solution of 40@12 was oxygenated, inner-phase maleic aldehyde 42 was produced. Prolonged photolysis split incarcerated 40 into two acetylene molecules, which escaped into the bulk phase. A reaction cycle of reactive intermediates was completed inside the inner phase: photolysis at 300 nm converted 41@12 into photopyrone 43@12, which rearranged at 90 °C to 44@12. Upon heating, 44@12 reverted quantitatively to 41@12.



**Figure 1.3** Highly reactive cyclobutadiene stabilized in a carcerand.

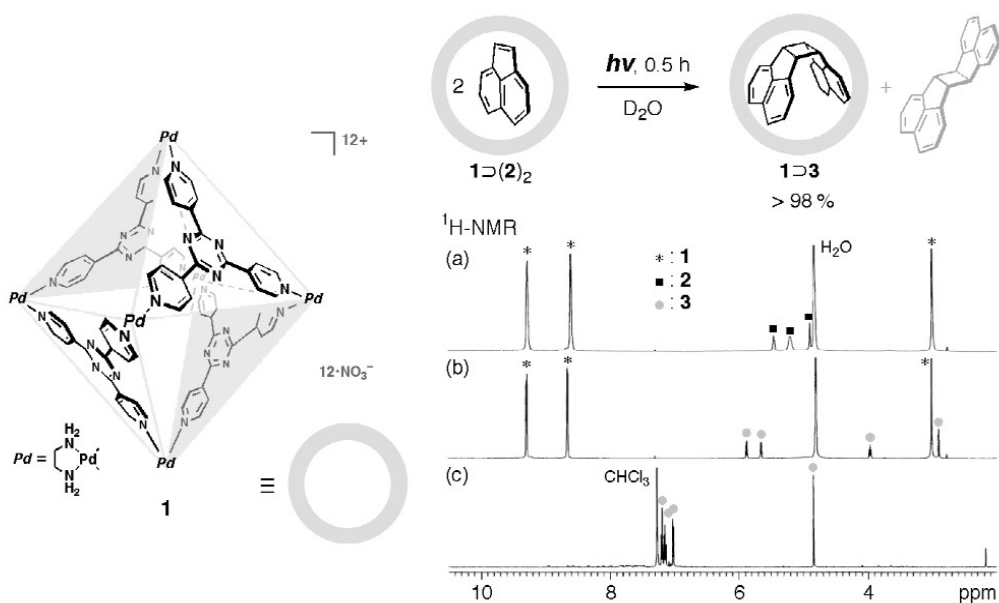
**1.3.4 Achieving high enantio-selectivity inside Cyclodextrins:** Intramolecular H-abstraction leading to enantioselective photoconversions was achieved in the photolysis of benzaldehyde with solid CD complexes.<sup>34</sup> Irradiation of solid  $\beta$ -cyclodextrin complexes of benzaldehyde resulted in an intermolecular reaction to give benzoin and 4-benzoylbenzaldehyde (7:3, 80%). The latter product is not formed in the photolysis of benzaldehyde in organic solvents. Another interesting feature of this solid state irradiation is that the benzoin formed in  $\beta$ -cyclodextrin cavity is optically active and the enantiomeric excess calculated from the optical rotation, is 15 $\pm$ 1 %.



**Figure 1.4** Enantioselective photoconversion of benzaldehyde and dependence of host-guest conformation on the cavity size of CD.

### 1.3.5 Selective photodimerization of acenaphthylene inside Palladium Nanocage:

It was found that [2+2] photodimerization of acenaphthylene (2) proceeds within cage 1 with remarkable rate acceleration and stereo-control to give only the *syn*-isomer 3, as clearly observed by  $^1\text{H}$  NMR.



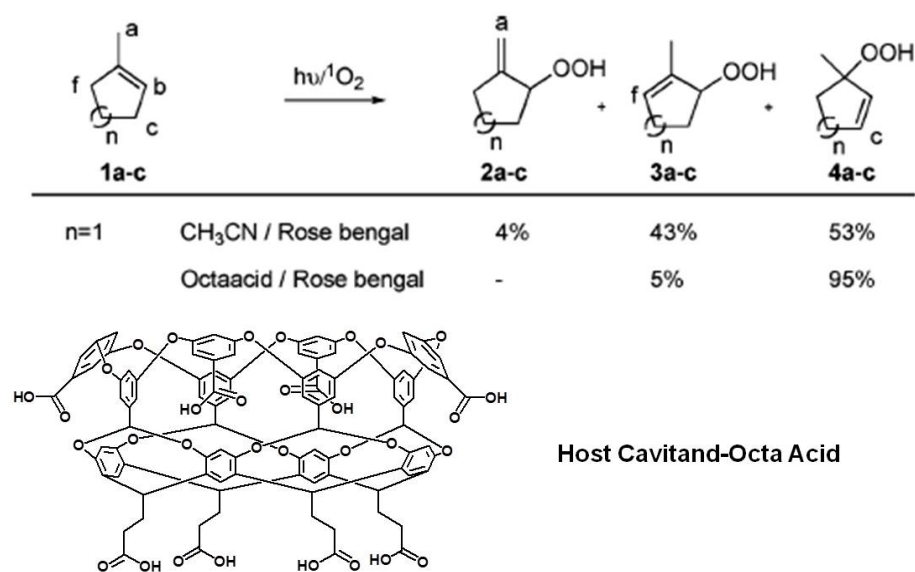
**Figure 1.5** Self-assembled coordination cage 1 (left) and  $^1\text{H}$  NMR spectroscopic analysis ( $\text{D}_2\text{O}$ , r.t.) of the photodimerization of 2 within 1 (a: before irradiation, b: after irradiation for 0.5 h, c: after extraction with  $\text{CDCl}_3$ ) (right).



When the encapsulated complex  $1 \supset (2)$  was irradiated for 0.5 h in  $D_2O$ , the signals of 2 disappeared and one set of new signals emerged. The product was identified as *syn*-dimer 3, and the yield was estimated to be  $>98\%$  based on 2. Within the cage, the formation of *anti*-dimer, which is concomitantly formed in organic media, was not observed. Control experiments revealed that cage 1 dramatically accelerated the reaction and strictly controlled the stereochemistry of the product. It is worth noting that not only stereochemistry but also regio chemistry was highly controlled for the [2+2] photodimerization of 1-methylacetylene. Thus, the photo-irradiation of  $1 \supset (2')$  complex for 3 h gave rise to a head-to-tail *syn*-isomer in a high yield without any other regio- and stereoisomers<sup>35</sup>.

### 1.3.6 High Product selectivity in “ene” reaction when substrate is encapsulated in Octa Acid:

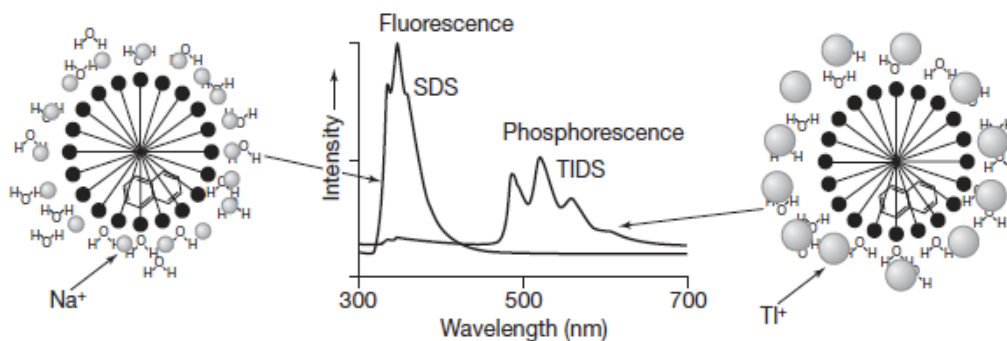
Due to the difficulties in controlling small and highly reactive singlet oxygen, it has not been possible to control the regioselectivity or reactions upon unhindered olefins such as methyl cycloalkenes.



**Figure 1.6** High Product selectivity in “ene” reaction when cycloalkene@OA.

The abstraction of methyl hydrogen by singlet oxygen can be eliminated by encapsulating the methyl cycloalkenes within a water-soluble, deep-cavity cavitand, Octa Acid. It was found that the hydroperoxides formed in the reaction were stable for weeks in aqueous medium as long as they remained within the OA capsule. It can be observed that the tertiary hydroperoxide is formed in high yield when 1 methyl cyclopentadiene (1) is encapsulated inside OA. Whereas, the “ene” reaction of 1 in  $\text{CH}_3\text{CN}$  does not give any product selectivity.<sup>36</sup>

**1.3.7 Phosphorescence of the triplet state is rarely observed in fluid solution:** This is attributed to the reactivity of the triplet state with various impurities in the system. It is expected that micelles may provide sufficient protection for triplet states of probe molecules that phosphorescence may be observed at room temperature and in fluid solution. Such a phenomenon is a rare occurrence in homogeneous solution at room temperature. Although no phosphorescence is observed with naphthalene in aqueous solution, when it is included within a TIDS micelle, a strong phosphorescence ensues.<sup>37</sup>

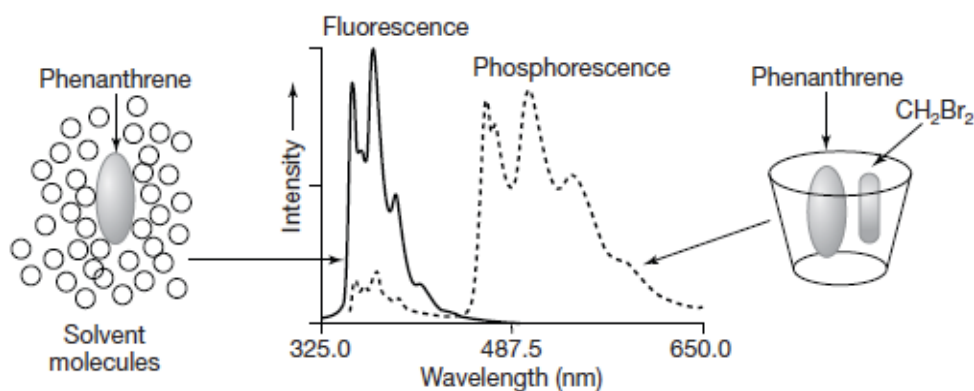


**Figure 1.7** Luminescence of naphthalene@SDS and naphthalene@TIDS.

### 1.3.8 Role of Cyclodextrins in achieving phosphorescence of Aromatic Hydrocarbons (AH):

Cyclodextrins have also proven to be excellent hosts to observe phosphorescence at room temperature when heavy atom containing co-guests are adsorbed together with an AH.

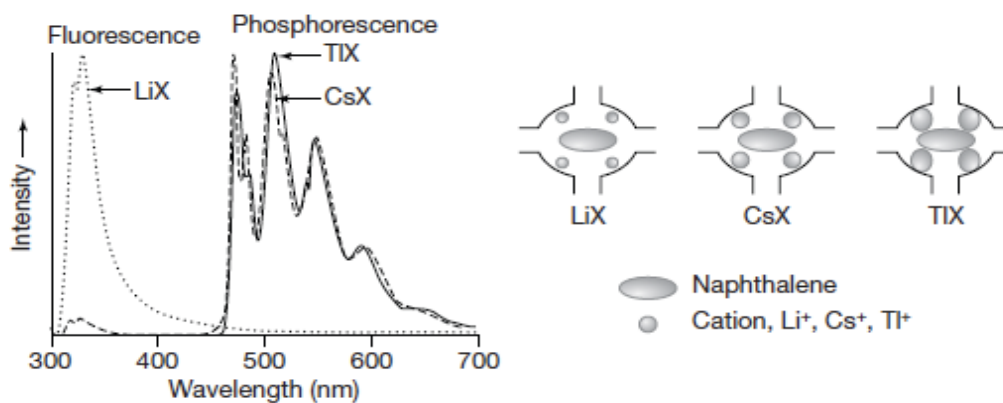
For example, when CDs are used as hosts and brominated co-guests are present, phosphorescence from aromatic molecules such as phenanthrene can be readily observed at room temperature in aqueous solution.<sup>38</sup> the triplet state of phenanthrene is stabilized inside the hydrophobic cavity of cyclodextrins.



**Figure 1.8** Luminescence of phenanthrene@CD in solution in the absence (solid line) and presence of  $\text{CH}_2\text{Br}_2$  (dashed line).

### 1.3.9 Enhancement of phosphorescence of AH in zeolites due to Heavy Atom effect:

The super cages of FAU zeolites contain a large number of exchangeable cations. These cations can be considered as co-guests that can interact with incarcerated guest molecules in the supercages. For example, phosphorescence at room temperature has been observed from a number of AH in a series of heavy atom exchanged AH@zeolites.



**Figure 1.9** Luminescence of naphthalene in FAU zeolites MX as a function of M.

Naphthalene in fluid solution is strongly fluorescent but non-phosphorescent. When naphthalene is incarcerated in the supercages of LiX, intense fluorescence and only weak phosphorescence are observed from naphthalene@LiX. However, naphthalene@CsX and naphthalene@TlX exhibit intense phosphorescence and very little fluorescence<sup>39</sup>.

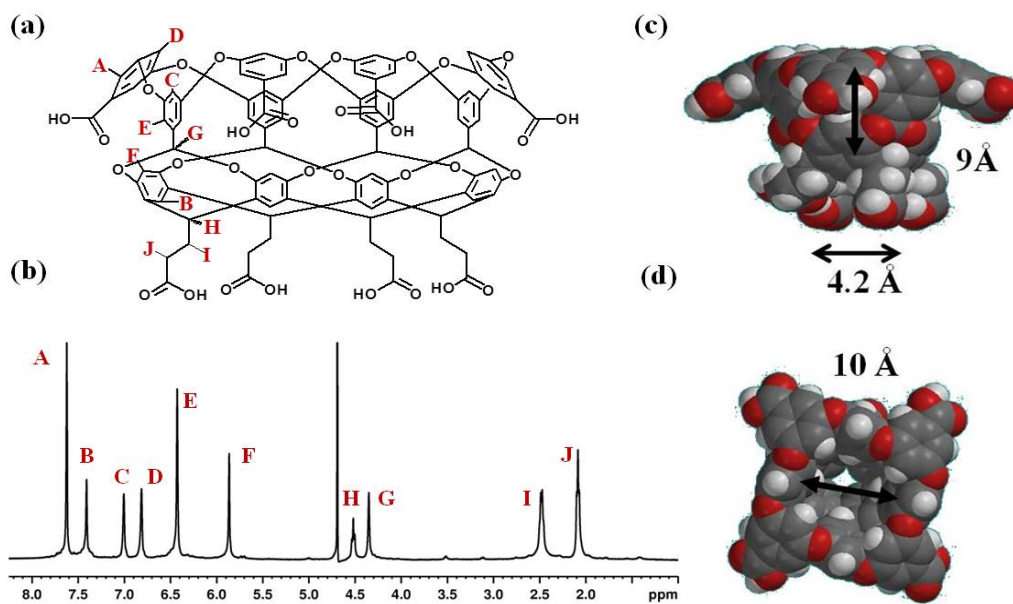
#### **1.4 Brief Description of Supramolecular Hosts used in this Thesis**

This section provides a brief description about all the supramolecular hosts which have been utilized in this research work. A supramolecular organic host possesses a space within which the guests are assembled and react. This space could be visualized in terms of the “reaction cavity” model initially formulated by Cohen and Schmidt<sup>40,41</sup> and expanded by Ramamurthy, Weiss, and Hammond.<sup>42,43</sup> A “reaction cavity” is defined to be a confined space with a well-defined boundary and some amount of “free volume” around the enclosed guest reactant molecule(s). The extent of selectivity within such a reaction cavity depends on the cavity’s size and shape, free volume, flexibility (hard or soft) of the boundary, and the weak interactions that hold the guest molecule(s) within the cavity.<sup>44</sup> Non-covalent interactions between the host and guest, which are usually the driving force for complexation mainly comprise of forces like: hydrophobicity, van der Waals interaction, hydrogen bond, C-H- $\pi$ , charge transfer, and cation- $\pi$  interactions.<sup>45</sup>

A common and most important characteristic from the point of view of “green chemistry”; of all the hosts used in various projects in this research work is that all of them are water soluble. Some being soluble with the aid of sodium borate buffer like Octa Acid, Calixarene [8] and Carboxylic end group dendrimers; others like CB[7], PdNC and Cyclodextrins are soluble in pure water. Phenolic end group dendrimers are

soluble in NaOH basic solution. And CB[8] is partially soluble in water, though upon complexation with the guest it becomes fully soluble.

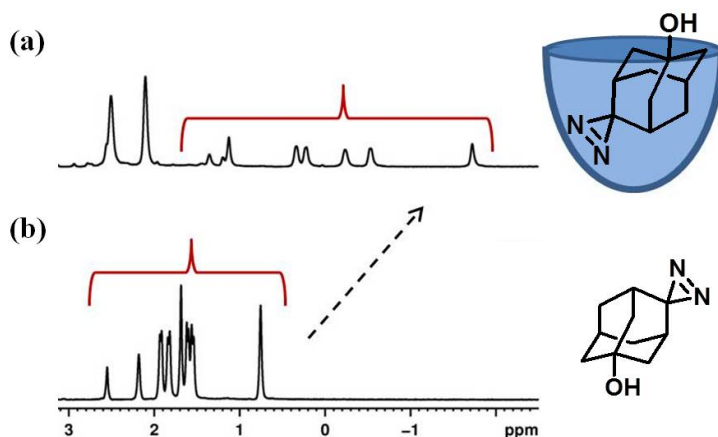
**1.4.1 Octa Acid (OA)** – The most commonly and vividly used host in this thesis is Octa Acid (OA). OA is a resorcinarene-based synthetic cavitand.<sup>46</sup> It possesses an external coat of carboxylic acid groups, due to the presence of the eight -COOH groups, it is soluble in water under slightly alkaline conditions (pH- 9). It has a narrow lower rim and a wider upper rim. The upper rim acts as a portal for the incoming guest while the lower rim is narrow enough not to let the encapsulated molecules pass through (**Figure 1.10 (a)**). More importantly, it possesses an internal hydrophobic pocket approximately 1 nm in width and depth (**Figure 1.10 (c) & (d)**). The major driving force for binding of guests to OA in aqueous solutions is the hydrophobic effect.



**Figure 1.10** (a) Chemical structure of OA with labeled protons A-J, (b) <sup>1</sup>H NMR of 1mM OA in buffered D<sub>2</sub>O, dimensions of the host cavity as calculated by Spartan, (c) Side view, (d) Top view.

The OA host has 4-fold symmetry and is made up of four identical panels containing 10 sets of chemically nonequivalent hydrogens A-J (the total number of

hydrogens is 14) giving a maximum of 10 NMR proton signals in the  $\delta$  region of 2-8 ppm with 6 of these appearing in the  $\delta$  region of 6-8 ppm (shown in **Figure 1.10 (b)**). When a capsule is formed with one symmetrical guest molecule and two molecules of OA, the resultant capsuleplex is symmetrical (the top and bottom halves of the capsule are identical) and displays (despite the presence of eight identical panels, four on top and four on bottom) only six signals in the  $\delta$  region of 6-8 ppm in the  $^1\text{H}$  NMR spectrum. When OA complexes to an unsymmetrical guest, the capsule as a whole is unsymmetrical along the y-z plane. In this case, the top and bottom halves of the capsule are not identical. The inclusion of an asymmetrical guest destroys the symmetry of the capsule and its six proton signals in the  $\delta$  region of 6-8 ppm (equivalent protons in the top and bottom halves) are split, the extent being dependent on the electronic differences between the top and bottom parts of the guest molecule.<sup>46</sup>



**Figure 1.11** Partial  $^1\text{H}$  NMR spectra (500 MHz) of (a) 4-hydroxy aziadamantane@OA in buffered  $\text{D}_2\text{O}$ , (b) 4-hydroxy adamantine in buffered  $\text{D}_2\text{O}$ .

An upfield shift of the guest proton signals in the  $^1\text{H}$  NMR spectra caused by the magnetic shielding provided by the aromatic walls of the host interior serves as an experimental test for inclusion of a guest within the OA cavity (**Figure 1.11**).<sup>47-50</sup>

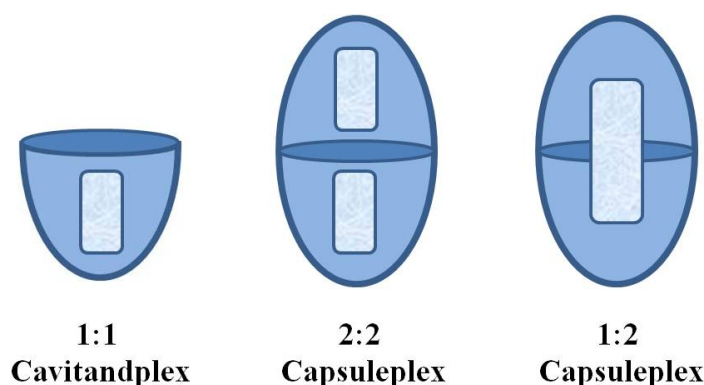
Intelligent exploitation of the cavity of any host requires knowledge of (a) the cavity dimensions, (b) the nature of the cavity's interior (polar or nonpolar), (c) the stoichiometry of the host-guest complex, (d) the types of interactions holding a guest within a host, (e) the strength of the host-guest complexes (binding constants), (f) the dynamics of the host-guest complex, and so on. Some of these features are investigated in detail by our research group and a brief summary have been presented below for a better comprehension of the host OA properties:

(a) Cavity dimensions: The dimensions of host cavity OA, as calculated by Spartan is shown in **Figure 1.10 (c), (d)**.

(b) Nature of cavity's interior: In order to be able to predict the effect of the host cavity on photochemical transformations of a guest it is important to know whether water molecules are present within the OA cavity, especially since the host/guest complexes are prepared in water. The excited-state  $S_1$  lifetime of pyrene included in OA was measured to be 350 ns, indicating that pyrene resides as a single molecule within the OA capsule. The monomer emission with  $I_1/I_3$  ratio of 1.01 is an indication that pyrene is emitting from an environment where there are no water molecules. Comparing  $I_1/I_3$  value obtained in OA with those in various solvents reported in the literature, it was conclude that the polarity of the host/guest capsule is similar to that of benzene. Considering the 24 benzene rings of the OA capsule, this similarity is not surprising.<sup>51</sup>

(c) Stoichiometry of the host-guest complex: Organic molecules with ionic as well as neutral head groups form complexes with OA. Two types of complexes are formed: One of these we term as cavitandplex, an open complex in which a part of the guest is exposed to water; in the second one called capsuleplex, the host completely surrounds the guest

and protects it from the aqueous exterior. Two types of capsuleplexes (1:2 and 2:2), depending on the number of guest molecules (two or one) within a capsule, have been observed (**Figure 1.12**). Molecules with ionic head groups tend to form cavitandplex and all other molecules form a capsuleplex. Molecules longer than 11 Å form 2:1 capsuleplex, and those shorter than 10 Å form both 2:1 and 2: 2 complexes. Smaller molecules having considerable free space within the capsule experience substantial freedom of motion while the larger ones with very little freedom are often forced to adopt folded/coiled conformations.<sup>52</sup>

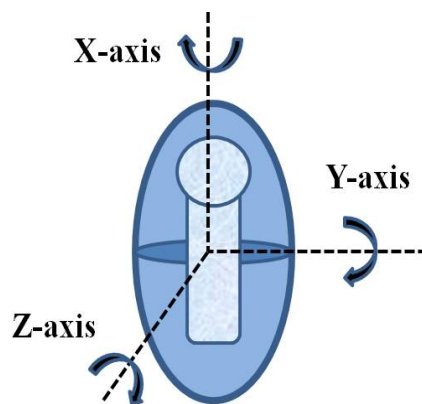


**Figure 1.12** Pictorial representation of possible host-guest stoichiometries for host OA.

(d) Dynamics of the host-guest complex: The guest molecule that is imprisoned within a molecular container is not stationary. But still the rotation of the guests is restricted within the capsule compared to that in water. The extent of freedom is dependent on weak interactions that hold the guest within the container. We have found that all guest molecules undergo fairly rapid rotation (nanosecond range) along the x axis. However, the mobility along the y and z axes varies (**Figure 1.13**). One might note that the symmetry of the capsuleplex would be restored by the free rotation of the guest along the y or z axis. We believe from our recordings of split peaks that such rotation does not occur on the NMR timescale. The two halves of the capsule may experience different



magnetic environments as a result of the absence of rotation along their y or z axis within the OA capsule on the NMR timescale. This observation further confirmed that the C-H-- $\pi$  interaction could restrict the rotational mobility of a guest molecule within an OA capsule, i.e. guest rotation within the OA capsule would be prohibited by the walls of the container. However, molecules could accomplish structural changes equivalent to rotation along y and z axes through coordinated wiggly motions of various parts of the molecule. It has also been postulated that the rotational motion of the guest is dependent on the length of the alkyl chain. Even a small structural change such as the addition of a methyl group makes the guest molecule stationary within the container on the NMR timescale.<sup>53</sup>

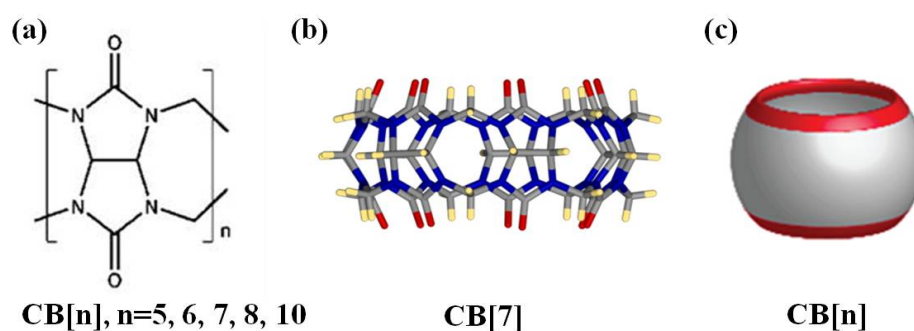


**Figure 1.13** Pictorial representation of the types of rotation possible for a guest@OA<sub>2</sub>.

The possibility of significant alteration of the photophysical and photochemical behavior of organic molecules included within the restrictive space of a capsule comprised of two molecules of Octa Acid (OA) has been extensively investigated in the recent years. It has been shown how high product selectivity can be achieved in a photochemical reactions, like photodimerization of acenaphthylene<sup>54</sup> and methylcinnamates<sup>55</sup>, photo-oxygenation of alkenes<sup>36</sup>, chiral photochemistry<sup>56-58</sup> and photoisomerization<sup>59,60</sup> when the guest is encapsulated inside the host OA. It has been

found that confinement of organic guest molecules inside OA result in a major change in their photophysical properties.<sup>61-63</sup> OA has been found instrumental in taming highly reactive reaction intermediates like carbenes and nitrenes.<sup>47,64</sup> Recently, ultrafast electron transfer and energy transfer processes have been explored when the excited guest was encapsulated inside OA.<sup>65,66</sup> The applications of Octa Acid as a useful host are innumerable, and this research work is a logical extension towards exploring them.

**1.4.2 Cucurbiturils (CB[n])** – CB[n] are macrocyclic containers formed by acid-catalyzed condensation of  $n$  glycoluril units with formaldehyde.<sup>67</sup> Although first made in 1905,<sup>67</sup> the interest towards the CB[n] family has only grown after the full characterization of the parent compound cucurbit[6]uril (CB[6]) in 1981.<sup>68</sup> Subsequently, larger and smaller homologues have been characterized, such that the CB[n] family nowadays comprises CB[5], CB[6], CB[7], CB[8], and CB[10].<sup>69-72</sup> All CB[n] homologues have highly symmetrical structures with a hydrophobic cavity, accessible on both sides through two identical carbonyl-rimmed portals.



**Figure 1.14** (a) Chemical structure of CB[n], (b) Calculated structure, (c) pictorial representation of CB[n]- pumpkin like shape.

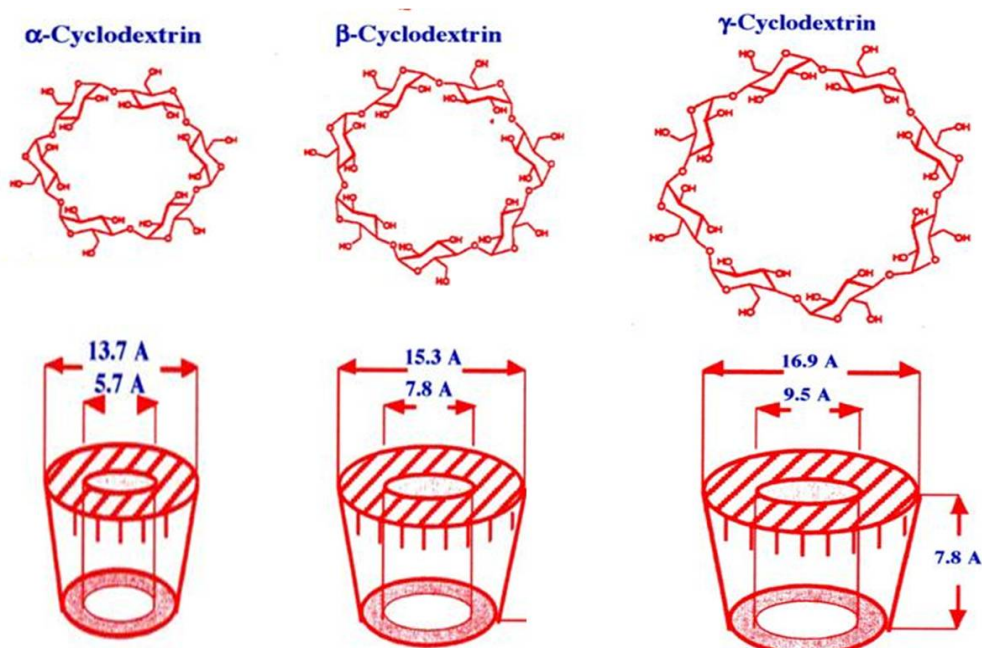
Structurally, CBs constitute highly symmetrical pumpkin-shaped hydrophobic cages of low polarity and polarizability with two identical dipolar portal ends composed

of carbonyl functional groups (**Figure 1.14**). CBs, for example cucurbit[7]uril (CB[7], with seven glycouril units), have been established as versatile and interesting host molecules, which form stable inclusion complexes with small guest molecules organic dyes,<sup>73</sup> metal cations,<sup>73</sup> protonated alkyl and aryl amines<sup>73,74</sup> and cationic dyes such as rhodamines,<sup>75,76</sup> triphenyl methane dyes,<sup>77</sup> via a combination of hydrophobic and ion-dipole interactions.

Several biologically and pharmaceutically relevant applications of cucurbiturils, particularly of CB[7], have been recently reported.<sup>78</sup> With respect to interactions with biomolecules, cucurbiturils have been shown to form host–guest inclusion complexes with selected naturally occurring amino acid residues,<sup>78</sup> which has been used to recognize and self-sort sequences of short peptides.<sup>79-83</sup> Cucurbituril–dye reporter pairs have been successfully employed for assaying the activity of enzymes<sup>84-86</sup> and for amino acid sensing.<sup>87</sup> Cucurbiturils have also shown the potential to bind with either peptide substrates<sup>88</sup> or inhibitors<sup>89</sup> and in this way affect the activity of enzymes. Cucurbiturils have also been employed to immobilize proteins on surfaces by noncovalent interactions.<sup>90</sup> Furthermore, cucurbiturils have shown the capability to refold synthetic oligomers under chemical stimuli response.<sup>91</sup> The fluorescence enhancement and photostabilization of different dye molecules upon cucurbituril encapsulation provides additional potential for biological analysis. This last strategy has been applied to several commonly used dyes such as Rhodamine 6G,<sup>92-94</sup> as well as Brilliant Green and Neutral Red in combination with proteins.<sup>95,96</sup>

**1.4.3 Cyclodextrins (CD)** - A cyclodextrin (CyD) is a cyclic oligomer of R-Dglucose formed by the action of certain enzymes on starch. Naturally occurring  $\alpha$ -,  $\beta$ -, and  $\gamma$ -

cyclodextrins and their higher homologues are truncated cone-shaped molecules with a hollow, tapered cavity of 7.8-Å depth (**Figure 1.15**). The top and bottom diameters of the cavity of most widely used cyclodextrins are 5.7 and 13.7 Å for  $\alpha$ -cyclodextrin, 7.8 and 15.3 Å for  $\beta$ -cyclodextrin, and 9.5 and 16.9 Å for  $\gamma$ -cyclodextrin, respectively.<sup>97</sup>



**Figure 1.15** Chemical structures of  $\alpha$ -,  $\beta$ -,  $\gamma$ -cyclodextrins and their dimensions.

Possessing a hydrophobic central cavity suitable for the inclusion of various organic molecules, cyclodextrin was one of the first receptor molecules whose ability to bind organic molecules was recognized and extensively studied by various experimental techniques.<sup>98-103</sup> The most probable mode of binding involves the insertion of the less polar part of the guest molecule into the cavity, while the more polar and often charged group of the guest is exposed to the bulk solvent just outside the wider opening of the cavity. This picture is derived from both thermodynamic and NMR studies.<sup>98,101,104-112</sup>

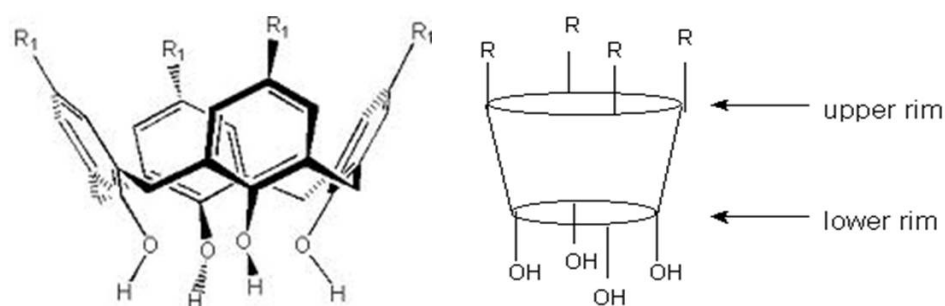
The principal factors involved in binding are believed to be primarily van der Waals and hydrophobic interactions,<sup>99,104,105,107,113-118</sup> although hydrogen bonding and steric effects also have certain roles to play.<sup>105,106</sup> Complexation reactions involving

cyclodextrins are highly important to drug delivery systems technology and also to the separation and food industries.<sup>98,119-123</sup> These reactions also serve as excellent models for understanding general inclusion phenomena, as well as enzyme-substrate interactions.<sup>99</sup> Several classes of compounds which can be included in natural  $\alpha$ -,  $\beta$ -, and  $\gamma$ -cyclodextrins have been subjected to systematic thermodynamic studies. These cover almost every class of compound such as hydrocarbons,<sup>124,125</sup> aliphatic alcohols,<sup>104,107,113,126-128</sup> diols,<sup>127,129</sup> amines and acids,<sup>105</sup> cyclohexane derivatives,<sup>108</sup> amino acids,<sup>129,130</sup> origopeptides,<sup>131</sup> sugars,<sup>132</sup> phenols,<sup>133-135</sup> aromatic amines,<sup>109</sup> azo compounds,<sup>137-140</sup> naphthalene derivatives and other aromatic compounds,<sup>110,141-143</sup> and various drugs.<sup>144-148</sup>

**1.4.4 Calixarenes (CA)** - Calixarenes are synthetic macrocycles formed by the reaction of phenol and formaldehyde<sup>149-151</sup>. Depending on the reaction conditions, it is possible to produce ring structures with differing monomer units (4,6, and 8) which in turn determine the cavity shape and size<sup>152, 153</sup>. It is known that these macrocycles encapsulate small molecules and ions. Calixarenes are flexible macrocycles, since the arene units which form the backbone of the macrocycle are linked by flexible methylene units. Not all calixarenes adopt the basket shape or the “cone” conformation in which all the arene groups point upward.

The binding properties of calixarenes and water soluble calixarenes towards organic cationic substrates have been studied in solid state, gas phase, and in solution by different techniques. Calixarene complexes are significantly stronger than the corresponding inclusion complexes of cyclodextrins and crown ethers with amino acids. In spite of their small cavity, a Calixarene scaffold with appropriate functionalization (sulfonate, phosphate, ammonium etc.) on the upper rim renders this class of receptors as

a template for the design and construction of special receptors for cations, anions and neutral species recognition mimicking biological processes<sup>154,155</sup> Due to their ability to form reversible complexes with both neutral and charged compounds, the calixarenes are also employed in separation chemistry. Exhaustive molecular dynamic studies on liquid–liquid interfaces in assisted ion extraction involving calixarenes pointed out the importance of solvation effects and of small amounts of water on the selectivity.<sup>156</sup>

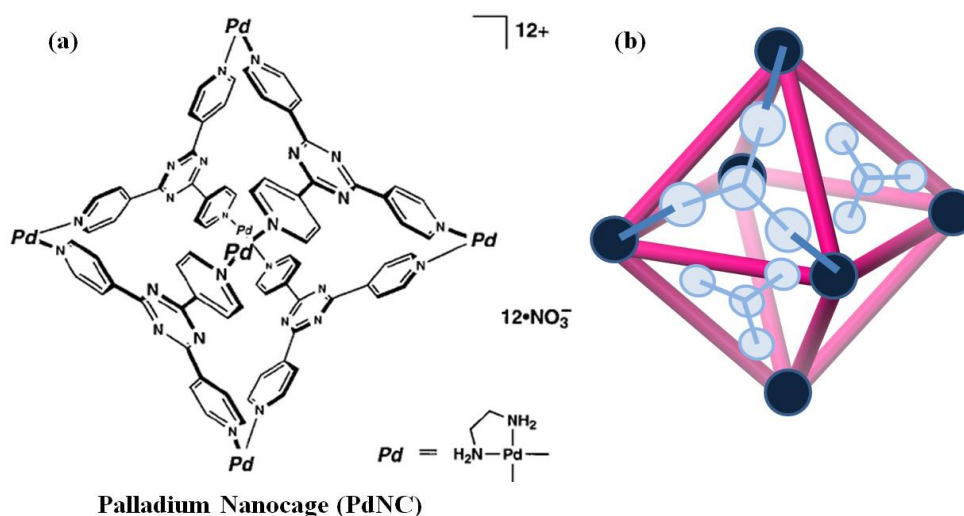


**Figure 1.16** Chemical structure of most basic Calixarene [4].

They present some of the requirements to serve as platforms for the nano-material<sup>157</sup>, analytical<sup>158</sup>, biological<sup>159–161</sup>, and industrial<sup>162</sup> investigations. The poor solubility of most calixarenes precludes their applications in the applications carry out in the aqueous media<sup>163</sup>. Calixarenes present well-defined conformational properties and cavities with molecular dimensions that enable to encapsulate guest drugs.<sup>164</sup>

**1.4.5 Palladium Nanocage (PdNC)** – PdNC, which possess a roughly spherical cavity is spontaneously formed by simply mixing the metal precursors (M) and the organic ligands (L) in a 3:2 ratio.<sup>165</sup> Despite the simple and highly symmetric structure, PdNC possesses several unique characteristics: (1) The diagonal Pd–Pd distance measured by X-ray analysis is quite large (ca. 2 nm). (2) A procedure for large-scale production of up to 100 g scale has been established. (3) The cage is highly water-soluble due to the presence of

six cationic Pd(II). (4) In contrast, the cavity provides a hydrophobic pocket that can bind as many as four neutral organic guests such as adamantane or *o*-carborane through hydrophobic interactions. (5) The molecular recognition in the cage can be easily monitored by NMR. (6) The size and shape of the cage can be modified at will by rational design of new ligands. In fact, we have constructed a variety of cavities from a family of panel-like ligands and transition metals <sup>166</sup>.



**Figure 1.17** (a) Chemical structure of Palladium Nanocage (PdNC) and (b) Cartoon representation of PdNC.

It has been established that the complexation with PdNC is much faster when the guest molecules are smaller. With such small guests as toluene or methoxy-substituted benzenes, the proton signals of complexed and free PdNC are indistinguishable in the NMR time scale. PdNC have been also known to encapsulate larger molecules like four molecules of *o*-carborane, an icosahedral cage molecule with a diameter of 8 Å. Adamantane was also encapsulated by PdNC to form a 1:4 complex. The high upfield shift of <sup>1</sup>H NMR signals of adamantane proved the complexation process. When 1- or 2-adamantanol was employed as a guest, the formation of a stable 1:4 complex was again

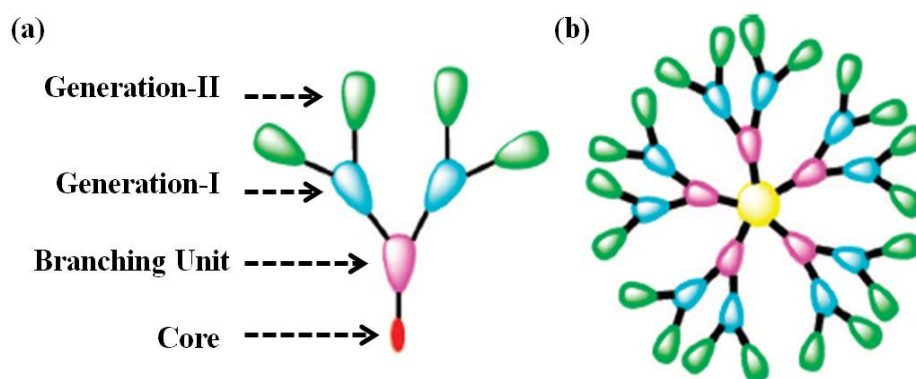
observed. Careful NMR analysis of this complex showed that the signals of the hydrophobic moieties were shifted significantly upfield while those of the hydrophilic moiety were not. This result shows that the interior of host PdNC is highly hydrophobic and the guest molecule is located in the cage such that the hydroxyl group is pointed outward. Significant  $\pi$ -donor-acceptor interactions were observed when 1,3,5-trimethoxybenzene (TMB) was employed as a guest. The very large upfield shift of Ar protons of TMB strongly supports an efficient aromatic stacking between the guest and the interior face of host PdNC. The interior of the nanocage creates not only a hydrophobic but also an electrophilic microspace with properties quite different from those of the bulk phase. It is also noteworthy that the complexation is much faster when the guest molecules are smaller.<sup>167</sup>

Selective recognition and encapsulation of molecules are some of the most attractive features of cage like molecule PdNC<sup>165-168</sup>. Since PdNC can accommodate two or more guest molecules at restricted positions in the cavity, it can act as a molecular flask for intermolecular reactions with high stereo- and regioselectivity. For example, intermolecular [2+2] photodimerization of olefins has been extensively studied in such media as micelles, zeolites, organic hosts (e.g., cyclodextrins), and crystals<sup>169</sup>. It was found that [2+2] photodimerization of acenaphthylene proceeds within PdNC with remarkable rate acceleration and stereocontrol to give only the *syn*-isomer<sup>170</sup>, as clearly observed by <sup>1</sup>H NMR. The labile molecules are most effectively trapped in PdNC if they are prepared in situ from smaller components coming through the small openings of the cage. Polycondensation of trialkoxysilanes (so-called sol-gel condensation) leads to the formation of siloxane networks or ladder polymers inside host PdNC<sup>171</sup>. More recently, it



was revealed that the photoexcitation of self-assembled PdNC accommodating photochemically inert alkane guests led to the regioselective oxidation of the guest within the cage<sup>172</sup>.

**1.4.6 Dendrimers** -The term ‘dendrimer’ refers to macromolecules possessing 100% branched architecture, with molecular weights of several kilo Daltons, which possess near spherical shapes. Developments in the field of dendrimer chemistry began from a few reports that appeared on the synthesis of well-defined dendritic macromolecules in the mid-1980’s.<sup>173</sup> Most of these dendrimers are manmade. However, natural dendritic architectures are also known, for example, glycogen, an energy-storage macromolecule in living organisms has a dendritic structure. A dendritic architecture could be defined by three distinct components, (i) the core, (ii) the interior branches and (iii) the exterior functionalities (Figure 1.18).



**Figure 1.18** Pictorial representation of :(a) various structural units, (b) whole dendrimer.

The assembly of these components creates a dendritic structure, which is radially symmetric and has several tiers. A tier, more often called a generation, refers to a circle enveloped by a set of branch points located symmetrically around the core. The symmetric branching results in (i) exponential growth of the dendritic structure leading to

an exponential increase in the molecular weights with increasing generations, (ii) dense exterior regions and (iii) relatively less-dense interior regions.<sup>174</sup> This unique architectural feature is one of the key aspects, which is exploited in order to realize new functions, among them are in utilizing dendrimers (i) for biological applications<sup>175</sup>, (ii) as organometallic catalysts to mediate carbon-carbon bond formations<sup>176</sup> and (iii) as hosts for encapsulation of metals and aromatic compounds.<sup>177</sup>

The physical and photophysical studies of dendrimers have led to the disclosure of supramolecular properties that are the basis of functional use. In particular, when the generation number increases, the dendrimer becomes globular, the periphery becomes bulkier despite back folding of the terminal groups, and possibilities of encapsulation and dendrimer-substrate interactions (surface, medium, other dendrimer, etc.) also increase. The nature of the peripheral groups governs the solubility and related biological properties such as biocompatibility.<sup>178</sup>

## **1.5 Instruments and techniques used in this research work**

**1.5.1 UV-Visible Spectroscopy:** Molecules containing  $\pi$ -electrons or non-bonding electrons (n-electrons) can absorb the energy in the form of ultraviolet or visible light to excite these electrons to higher anti-bonding molecular orbitals. Hence Absorption spectroscopy gives us valuable information about the ground state of the molecule.

UV-Visible spectroscopy has proved to be a very helpful tool for studying photochemical and photophysical processes in host-guest chemistry in this thesis. For example, the basic information needed to carry out any photochemical reaction inside a host molecule is: the absorbance of the host and the guest. This information is very important, since it can bring into light the mechanism of the photoreaction taking place.

For instance, if the host and the guest absorb the light in the same region and the absorbance for host is more than that of the guest, then upon irradiation the host is going to absorb most of the light energy. This may result in: (a) photo-degradation of host, (b) poor absorption of light by the guest, hence very slow or no reaction, (c) transfer of energy or electron from host to guest. In all the cases, the photoreaction becomes complicated and un-effective. To avoid this various kinds of light filters are used during irradiation.

Similarly, UV-Visible spectroscopy had been extensively used for understanding photophysical processes in host-guest studies. For example, UV-Visible spectroscopy helped in studying the aggregation of dyes in presence of various hosts, since it can give us the information about the ground state environment of a molecule. Also, it has been utilized as a basic tool for understanding FRET process occurring between a donor@host and the acceptor in solution.

**1.5.2 Fluorescence Spectroscopy:** In fluorescence spectroscopy, the organic molecule is first excited, by absorbing a photon from its ground electronic state to one of the various vibrational states in the excited electronic state. The molecule then drops down to one of the various vibrational levels of the ground electronic state again, emitting a photon in the process. Hence, Fluorescence spectroscopy is an invaluable tool for studying the excited state behavior of a molecule.

Fluorescence spectroscopy is a complimentary analytical tool for UV-Visible spectroscopy. The latter elucidates the transition process from ground state to the excited state, while former gives us the information about the transition process from excited state to the ground state. For the same reason, it has been used in Chapter-7 of this thesis.

Fluorescence spectroscopy has proved itself irreplaceable in the study of host-guest chemistry. Since, alteration in the excited state behavior of “probe” guest molecules can impart valuable knowledge about the inner cavities of the hosts. Hence, it has been extensively used in Chapter 8 of this thesis. Also, it was a basic analytical technique used in Chapter 6.

**1.5.3 Time-Resolved Emission Spectroscopy:** Time-resolved Emission spectroscopy is used to monitor molecular interactions and motions that occur in the femtosecond—nanosecond time range, and is especially useful in the analysis of biomolecular structure and dynamics. Time Resolved Emission Spectroscopy (TRES) is frequently used to study the excited state dynamics and kinetics of fluorescent molecules in solutions.

The two major uses of this technique in this thesis work, is studying FRET (Chapter-6) between a donor@host and acceptor molecule and Solvation Dynamics of a fluorescent probe in the vicinity of dendrimers (Chapter 8). Both of the above photophysical processes occur in the time range of femto-nano seconds. Hence, it was essential to use this technique to study these processes. We have gathered very useful information about the host-guest interactions using TRES. For instance, the FRET process studied by TRES supported our proposed model of the donor being encapsulated inside host OA and the acceptor being associated with the exterior of OA through ion-pair interaction. Also, the Solvation Dynamics studies showed that the interior of the dendrimers is very hydrophobic whereas, the external periphery attracts polar guests being polar itself in nature.

**1.5.4 Nuclear Magnetic Resonance Spectroscopy:** NMR spectroscopy is one of the principal techniques used to obtain physical, chemical, electronic and structural

information about molecules due to their chemical shifts. It is a powerful technique that can provide detailed information on the topology, dynamics and three-dimensional structure of molecules in solution and the solid state. The sensitivity of the technique depends on the strength of the magnetic field. In this thesis work, mostly 500 MHz NMR instrument have been utilized. Below are the NMR techniques which have been extensively used in this work:

**(a) One Dimensional  $^1\text{H}$  NMR spectroscopy:**  $^1\text{H}$  NMR is the basic and most important tool which has been vastly used in this thesis work. Specifically, it has been used to ascertain the purity of the various components during host synthesis. Also, it has been utilized as a purity check for different hosts and guests. Since the first and foremost criterion of any chemical undertaking is the purity of the materials used. Secondly, it has been used to study the encapsulation process of a guest inside the host. Since upon encapsulation inside the aromatic cavity of the host, the guest proton signals are much upfield shifted. Another main usage of this technique in this thesis is for conducting titration experiments with the host and the guest, which gives us the valuable information about their binding ratio.

**(b) Two Dimensional Diffusion Spectroscopy (2D DOSY):** The diffusion constant ( $D$ ) can be calculated using the following equation:

$$D = kT/6 \pi\eta R_h$$

Where,  $R_h$  is the hydrodynamic radius of the sphere (the host-guest complex is considered as a sphere),  $k$  is the Boltzmann constant,  $T$  is the temperature in kelvin, and  $\eta$  is the solvent viscosity. From the equation it is clear that diffusion constant of the supramolecular complex depends on its hydrodynamic radius. Hence, the moiety with a

larger volume diffuses slowly on a NMR time scale than a moiety with a smaller hydrodynamic radius. For this reason, this technique is very useful in supramolecular host-guest chemistry. Basically it can tell whether a guest molecule is associated with a host molecule or not, since the diffusion constant of the host-guest complex will be smaller than the free host or guest. Secondly, it can give us information about the dissociation of a complex. And more importantly in the studies in this thesis this technique has been utilized to differentiate between a cavitandplex and a capsuleplex of a guest and host OA. Since a capsuleplex being larger in volume will have a smaller diffusion constant than a cavitandplex which has a smaller volume.

**(c) Two-dimensional correlation spectroscopy (2D COSY):** The first and most popular two-dimension NMR experiment is the homonuclear correlation spectroscopy (COSY) sequence, which is used to identify spins which are coupled to each other. One can thus determine which atoms are connected to one another (within a small number of chemical bonds) by looking for cross-peaks between various signals. This NMR technique is very useful for assigning the proton signals. The correct assignment of proton signals of the host and guests is very important. Since based upon these peak assignments, the *through-space* interactions between a host and guest can be studied. Because of this application, 2D COSY has been a basic NMR tool in this research work. All of the  $^1\text{H}$  NMR signals of the guests and the host OA used in this thesis have been done with the help of 2D COSY NMR.

**(d) Two Dimensional Nuclear Overhauser Effect Spectroscopy (2D NOESY):** In NOESY, the Nuclear Overhauser cross relaxation between nuclear spins during the mixing period is used to establish the correlations. The spectrum obtained is similar to

COSY, with diagonal peaks and cross peaks, however the cross peaks connect resonances from nuclei that are spatially close, i.e. *through-space* coupling rather than those that are *through-bond* coupled to each other. This makes NOESY one of the powerful techniques in understanding the host-guest interaction in the NMR time scale. 2D NOESY in this thesis work has been extensively used to study the specific orientation of the guests inside the host OA. By understanding the guest orientation one can justify the product selectivity of a photoreaction when the guest is encapsulated inside the host OA.

#### **1.5.5 Gas Chromatography /GC-Mass Spectrometry:**

**(a) Gas chromatography (GC):** is a common type of chromatography used in analytical chemistry for separating and analyzing compounds that can be vaporized without decomposition. In gas chromatography, the *mobile phase* (or "moving phase") is a carrier gas, usually an inert gas such as helium or an unreactive gas such as nitrogen. The *stationary phase* is a microscopic layer of liquid or polymer on an inert solid support, inside a piece of glass or metal tubing called a column. The gaseous compounds being analyzed interact with the walls of the column, which is coated with a stationary phase. This causes each compound to elute at a different time, known as the *retention time* of the compound. The comparison of retention times is what gives GC its analytical usefulness.

Typical uses of GC include testing the purity of a particular substance, or separating the different components of a mixture (the relative amounts of such components can also be determined). In some situations, GC may help in identifying a compound. This is one of the most frequently used analytical tools in this research work. GC has been primarily used to check the purity of the synthesized guests in addition with  $^1\text{H}$  NMR. Also, more importantly it has been used to follow a photoreaction and detect

the products obtained after photo-irradiation. GC analysis gives the percentages of the products obtained, which is essential information for understanding the photochemical processes taking place inside a host molecule.

**(b) Gas Chromatogram-Mass Spectrometry (GC-MS):** GC-MS is a method that combines the features of gas-liquid chromatography and mass spectrometry to identify different substances. MS is used for determining the elemental composition of a sample, the masses of particles and of molecules, and for elucidating the chemical structures of molecules, such as peptides and other chemical compounds. Mass spectrometry works by ionizing chemical compounds to generate charged molecules or molecule fragments and measuring their mass-to-charge ratios. In a typical MS procedure, a sample, which may be solid, liquid, or gas, is ionized. The ions are separated according to their mass-to-charge ( $m/z$ ) ratio. The ions are detected by a mechanism capable of detecting charged particles. The signal is processed into the *spectra* (singular spectrum) of the relative abundance of ions as a function of the mass-to-charge ( $m/z$ ) ratio. The atoms or molecules can be identified by correlating known masses by the identified masses or through a characteristic fragmentation pattern.

In this thesis this technique has been used to characterize the small organic molecules which are the product of a photochemical reaction. Although other techniques like NMR can also be utilized for the same purpose but this technique has an advantage over the others. Since the product mixture can be directly injected in GCMS. The GC separates different products and the MS helps to analyze each of them based upon their characteristic fragmentation pattern.



**1.5.6 Electronic Paramagnetic Resonance Spectroscopy (EPR):** Electron paramagnetic resonance (EPR) or electron spin resonance (ESR) spectroscopy is a technique for studying materials with unpaired electrons, hence it is most commonly used for studying radicals. Because most stable molecules have all their electrons paired, the EPR technique is less widely used than NMR. However, this limitation also means that EPR offers great specificity, since ordinary chemical solvents and matrices do not give rise to EPR spectra. The two most informational parameters of an EPR spectrum are:

**(a) Hyperfine coupling constant-** The interaction energy between the electron spin and a magnetic nucleus is characterized by the hyperfine coupling constant “A”. It is known that “ $A_N$ ” for a nitoxide radical is sensitive to the polarity of the solvent in which they are dissolved.

**(b) Rotational Correlation Time ( $\tau_{\text{perp}}$ )** - Rotational correlation time is the time it takes for a molecule to rotate one radian, on average. The  $\tau_{\text{perp}}$  value increases with increasing the mobility of the probe. Hence,  $\tau_{\text{perp}}$  is an important parameter to assign the location of the guest molecule (with unpaired electron) in a supramolecular system. When the guest molecule is within a host molecule, its mobility is restricted and hence  $\tau_{\text{perp}}$  is found to be enhanced compared to the guest in solution.

These two parameters could be used for investigating the interior and vicinity of a host molecule, for this reason, this technique have been utilized to characterize the dendrimers in Chapter-8.

## **1.6 Scope and Aim of this thesis**

The main aim of this thesis was to understand the role of supramolecular hosts in altering the photochemical and photophysical pathways of small organic molecules

encapsulated within them or anchored to their close proximity. It was fascinating to observe that the highly reactive species which are untamable in a free environment are so much under control in a confined environment. Also, this research work aims not to focus entirely on one particular kind of host, but to study many different hosts which are the hot topic for extensive research presently.

**Chapter 2** includes an extensive study of association and photolysis of four substituted carbene precursors within various host systems like, Octa Acid (OA), Cucurbiturils(CB) and Pd Nanocage (PdNC). There are several layers to this study. The first one is the role of different hosts on the photochemistry of the carbene precursors, i.e. how the free space and the “openness” of the hydrophobic cavities of these hosts can govern the photochemical product distribution. Next is how the substitution on the guest can make a crucial difference to its orientation inside the host. And, lastly, the effect of substitution on the photochemical behavior of the guests encapsulated inside the above mentioned hosts.

**Chapter 3** deals with the association of two nitrene precursors, which are positional isomers, into the host OA, CB and PdNC. This study again has two dimensions: one, how the orientation and number of nitrene intermediates encapsulated inside various hosts, can alter the photochemical outcome and secondly and more importantly, we have seen how a highly reactive nitrene intermediate can insert itself into the host OA, to produce a modified host OA.

**Chapter 4** is an extension towards understanding the effect of confinement on the photochemical behavior of highly reactive reaction intermediates, in this case again nitrenes. But this class of nitrenes differs in the sense that they have an in-built

intramolecular triplet sensitizer. Hence, presumably, in this study we dealt with triplet nitrenes. These triplet nitrene precursors have been encapsulated inside the host cavitand OA and it has been observed that the encapsulation have a profound effect on the photochemical product distribution.

**Chapter 5** deals with the studies of another important reactive specie- Singlet Oxygen ( $^1\text{O}_2$ ). Controlling the bimolecular reactivity of singlet oxygen and hence obtaining the desired photoproduct is a major challenge, due to its highly reactive nature. In this chapter, we have tried to control the “ene” reaction between a group of cyclic alkenes and singlet oxygen by encapsulating the alkene guests inside the host OA. Also, this chapter includes the intricate details of the encapsulation and orientation of the guests inside the host cavitand OA, which forms a strong platform for further studies with the host OA.

**Chapter 6** is a subtle transition from the photochemical to photophysical studies. In this chapter we have studied Forster Resonance Energy Transfer (FRET) between a donor which has been encapsulated inside the hydrophobic cavity of host OA and the acceptor which interacts with the anionic exterior of OA. Moreover, we found that FRET occurs at an ultrafast time scale in the above case and the distance between the donor and acceptor comes around 13 Å, which perfectly supports the proposed model. Also, we employed various other hosts like CBs and dendrimers to detach the acceptor from OA, expecting that it may diminish the FRET.

**Chapter 7** is a study of the interaction of cationic dyes and the anionic exterior of the host OA, which finds its application in Chapter 6. The studies in this chapter are unique in the sense that they deal with the direct competition of various hosts among

themselves for the cationic dyes. Different hosts like OA, CBs, Dendrimer, Cyclodextrin and Calixarene offer different kinds of interactions like hydrophobic, Columbic ion-pair and combination of both, to the cationic dye molecules. And, with the help of these experiments we have succeeded in demonstrating that the Columbic ion-pair interactions are more effective than the hydrophobic interactions when the guests are charged specie.

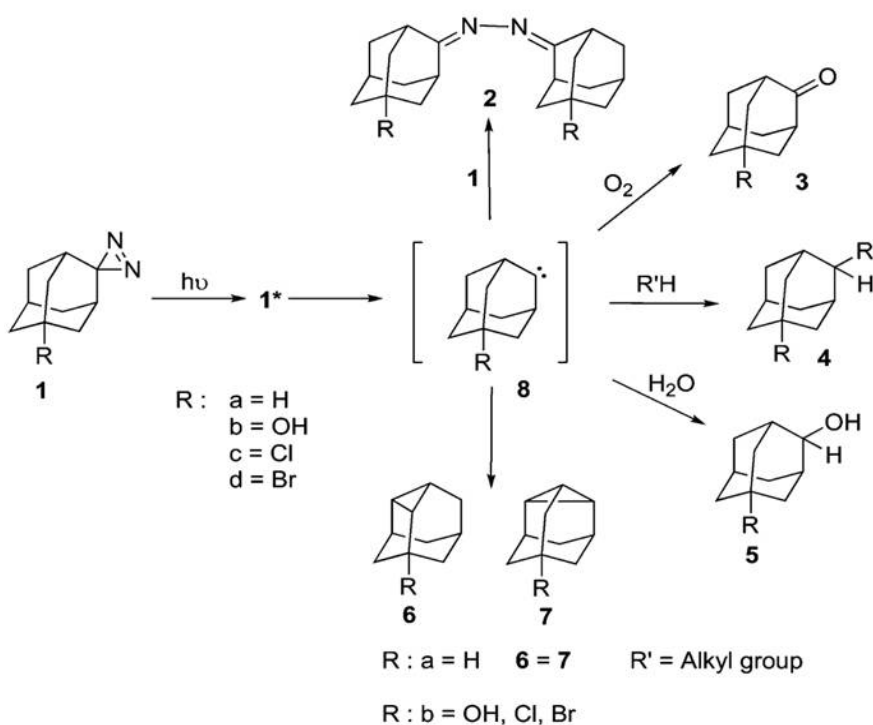
A detailed and all kind of studies pursued with the Dendrimers as water soluble hosts have been summed up in **Chapter 8**. The studies start with probing the interior of the phenolic dendrimers with the probes Pyrene and Coumarins, followed by the solvation dynamics studies. The role of the hydrophobic cavity of these dendrimers in controlling the photolysis reaction of di benzyl ketones and in *cis-trans* isomerization of stilbenes has been explored. Next, the UV-Visible and Fluorescence characterization studies of the carboxylic end groups dendrimers have been performed. The interior of these set of dendrimers have been probed by EPR studies. These dendrimers too have been found to have an effect on the photo-induced electron transfer *cis-trans* isomerization of stilbenes.

## **CHAPTER 2**

### **Photochemical Generation and Reactivity of Carbenes in Various Nanoenvironments**

## 2.1 Overview

Carbenes<sup>179</sup> are species bearing a divalent carbon. In their singlet state, they possess a lone pair and a low-lying unoccupied orbital at the same atom. This special electronic configuration gives them a high reactivity. In fact, methylene has been described as the most indiscriminating reagent in chemistry.<sup>180</sup> For such reactive carbenes, encapsulation in a cavitand permits to reduce the mobility of the intermediate, therefore lessening the number of accessible bonds or lone-pairs that may act as reaction partners and consequently, reducing the amount of side-products. Indeed, the use of a host molecule as a reaction vessel opens up the possibility to synthesize products that would be difficult to obtain in solution<sup>181</sup> or to modify the reaction pathway.<sup>182</sup>



**Scheme 2.1** Photolysis of Carbene Precursors and Possible Products.

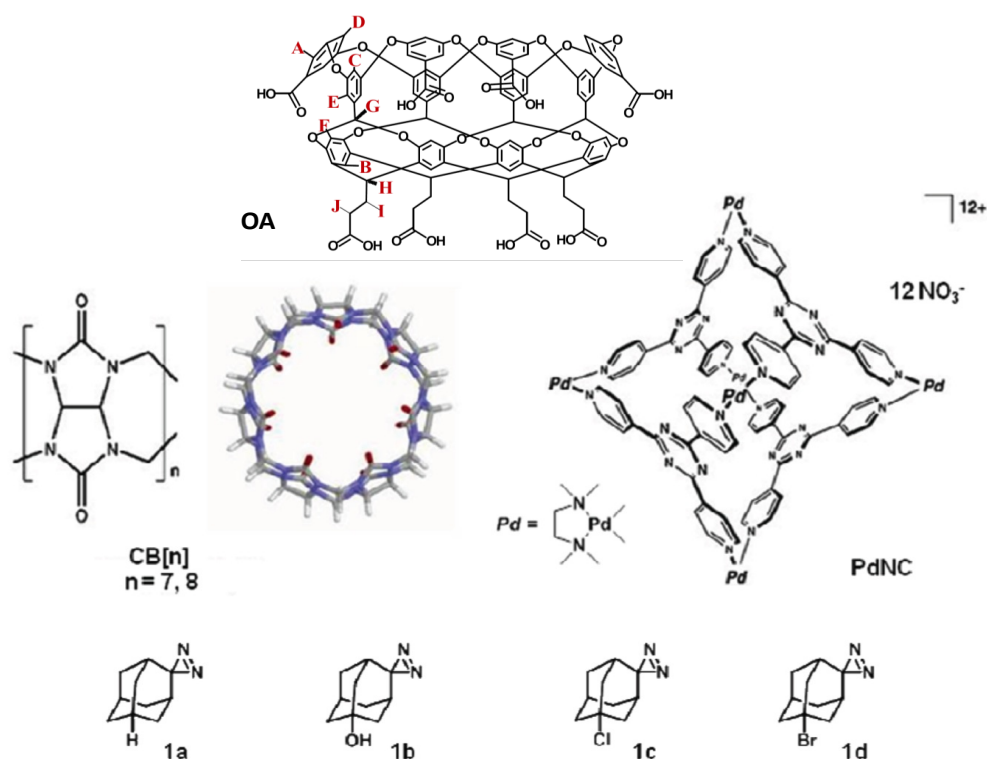
Carbenes can react in various ways during the photolysis of nitrogenous precursors<sup>181</sup> such as diazo compounds. Photolysis of carbene precursors **1a-d** in

hydrocarbon and alcohol solution is reported to give a number of products shown in **Scheme 2.1**<sup>183-188</sup>. Of these, azine **2**, adamantanone **3**, and solvent insertion products **4** and **5** were the major ones. Importantly, intramolecular C-H insertion products **6** and **7** were formed only in trace amounts. In general, the formation of all products listed in **Scheme 2.1** was presumed to involve adamantylidene **8** as the intermediate.

Numerous investigations on controlling the chemical stability and behavior of photochemically generated reactive carbenes intermediates in solution, in the crystalline state, and the solid state as inclusion complexes with zeolites, cyclodextrins, and a resorcinarene- based cavitand have been done recently.<sup>189-192</sup> Solid state photolysis of carbene precursors **1a-d**, majorly gives the products **2 a-d**. In the zeolites, due to close association of the carbenes generated and the water molecule, mostly alcohol **5** and admantanone **3** products are obtained. Whereas, encapsulation of carbene intermediates in cyclodextrins give result to dimeric product **2** and intermolecular insertion product **4**, in major amounts. It has been recently shown that, some percentage of C-H intramolecular insertion products **6 c, d** and **7 c, d** have been obtained when the carbene intermediate **8** was encapsulated in a hemicarcerand.

In this context, we have investigated the photochemical behavior of four adamantanediazirines **1a-d**<sup>193</sup> included in various nanoenvironments, such as cavitand Octa Acid, cucurbit[7]uril (CB[7]),<sup>194-196</sup> cucurbit[8]uril (CB[8]), and Pd nano cage (PdNC)<sup>197, 198</sup> (**Figure 2.1**) in water. The study included examination of the complexation behavior by <sup>1</sup>H NMR, isothermal titration calorimetry (ITC), and computation as well as monitoring of the photochemical product distributions by gas chromatography (GC). Results presented below highlight that carbenes generated within the OA cavitand in

aqueous solution and on a silica surface by photolysis of carbene precursors **1a-d**@OA show a distinctly different chemical behavior from that of free molecules in aqueous solution. The results also suggest that the behavior of photochemically generated adamantanylidene within cucurbiturils and cyclodextrins, comparable containers in terms of size and shape, is distinctly different. In addition, photoreaction within PdNC suggests a possible involvement of triplet adamantanylidene as opposed to singlet adamantanylidene within CBs.



**Figure 2.1** Structures of hosts OA, cucurbiturils CB[7], CB[8], palladium nano cage (PdNC), and guest molecules carbene precursors and its derivatives.

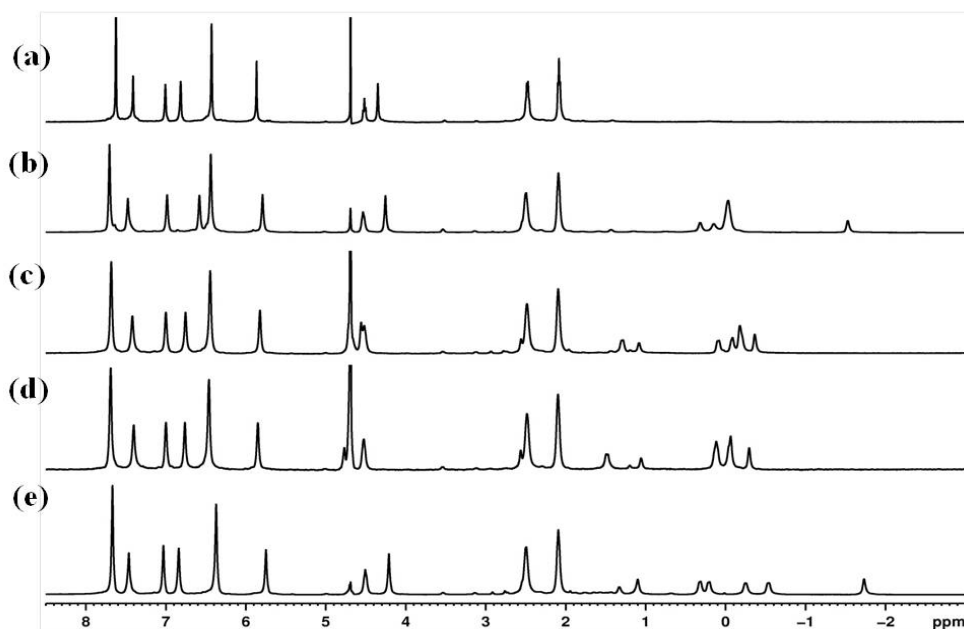
## 2.2 Results and Discussion

### 2.2.1 Encapsulation of carbene precursors **1 a-d** in OA as studied by <sup>1</sup>H NMR

The first host-guest system we investigated was OA and carbene precursors **1a-d**. Host OA is a deep cavity cavitand. Due to its eight carboxylate groups, it can be solubilized in



water using sodium tetra borate buffer. Usually 10 equivalents of the buffer is used for the studies. The pH of the solution is maintained at  $\sim 9.0$ . OA forms variety of host: guest complexes, for example, 2:2 capsuleplex, 2:1 capsuleplex, depending upon the shape and size of the guest molecule.<sup>52</sup>



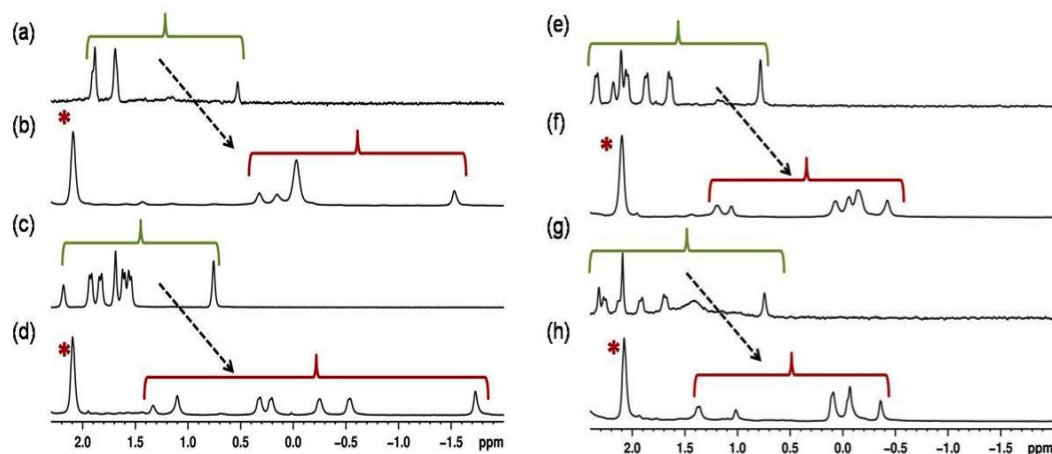
**Figure 2.2**  $^1\text{H}$  NMR spectra of (a) OA in buffered  $\text{D}_2\text{O}$ , (b)  $\mathbf{1a}_2@OA_2$  in buffered  $\text{D}_2\text{O}$ , (c)  $\mathbf{1c}@OA$  in buffered  $\text{D}_2\text{O}$ , (d)  $\mathbf{1d}@OA$  in buffered  $\text{D}_2\text{O}$ , (e)  $\mathbf{1b}@OA$  in buffered  $\text{D}_2\text{O}$ . Buffer: 10 mM sodium tetra borate solution in  $\text{D}_2\text{O}$ .

**Figure 2.2** represents the  $^1\text{H}$  NMR complexation spectra of the guests  $\mathbf{1a-d}$  with host OA. Stirring a 1 mM solution of carbene precursors  $\mathbf{1a-d}$  and OA in water ( $\text{D}_2\text{O}$ ; sodium borate buffer) resulted in a transparent solution whose  $^1\text{H}$  NMR spectra confirmed inclusion of carbene precursors  $\mathbf{1a-d}$  within host OA. On addition of guests  $\mathbf{1a-d}$  in the OA solution, the bound guest proton signals appear in the upfield region usually from 1.0 to -2.0 ppm, which is suggestive of organic guests being included within the host OA. Also, some of the host OA proton signals shift in their position upon complexation with guests, again indicating the association of host and guest. It can be

noticed that the host OA proton signals does not split upon addition of guests, indicating that the complexes formed are symmetric in nature.

Next **Figure 2.3** shows the partial  $^1\text{H}$  NMR spectra of the guests **1a-d** in  $\text{D}_2\text{O}$  and that after complexation with OA. It can be noticed that, guest proton signals are markedly upfield shifted when in association with the host, this upfield shift of the guest protons in comparison to their position in only  $\text{D}_2\text{O}$  solution, confirm its encapsulation inside the OA cavity which is relatively non-polar.

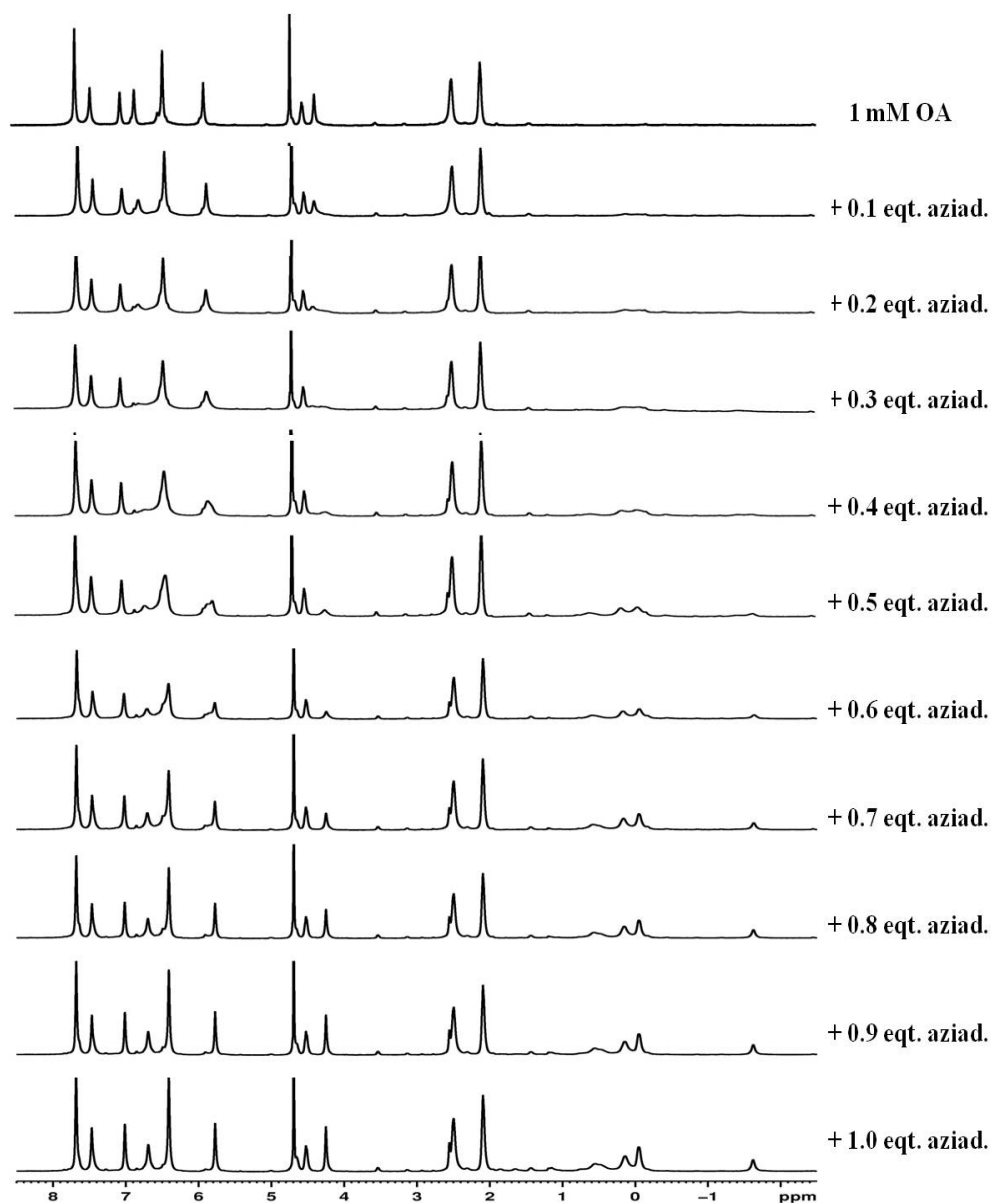
Once it is confirmed that the guest and host form a complex, the next question arises as to what is the nature and the binding ratio of the complex. Non-splitting of the proton signal of the host OA suggest symmetric complex as mentioned before. The binding ratio of the guest: host can be determined by the  $^1\text{H}$  NMR titration of the guest in host solution. As an example, the  $^1\text{H}$  NMR titration spectra of **1a** in OA has been shown in **Figure 2.4**. It can be observed that on subsequent addition of the guest the intensity of the guest proton signals in the upfield region increases. Also, we can observe that the host proton signals first get broadened, and on subsequent addition of the guests, it sharpens. This broadening is possibly due to the presence of complexed as well as uncomplexed host in the solution. As the guest concentration increases, more and more of the complexed host exists, hence the sharpening of the proton signals is observed. Also, on further addition of the guest, uncomplexed guest proton could be observed, indicating the excess or uncomplexed guest. The titration experiment shown in **Figure 2.4**, indicate the host: guest ratio of 1:1.  $^1\text{H}$  NMR titrations performed for all four guests suggested that carbene precursors **1a-d** formed 1:1 (host to guest) stoichiometric complexes with OA in water.



**Figure 2.3** Partial  $^1\text{H}$  NMR spectra of (a) **1a** in buffered  $\text{D}_2\text{O}$ , (b) **1a**<sub>2</sub>@OA<sub>2</sub> in buffered  $\text{D}_2\text{O}$ , (c) **1b** in buffered  $\text{D}_2\text{O}$ , (d) **1b**@OA in buffered  $\text{D}_2\text{O}$ , (e) **1c** in buffered  $\text{D}_2\text{O}$ , (f) **1c**@OA in buffered  $\text{D}_2\text{O}$ , (g) **1d** in buffered  $\text{D}_2\text{O}$ , (h) **1d**@OA in buffered  $\text{D}_2\text{O}$ . Buffer: 10 mM sodium tetra borate solution in  $\text{D}_2\text{O}$ .

The  $^1\text{H}$  NMR titration experiments can only give us the information about the binding ratio of the host and guest. To infer whether the 1:1 complex is a 1:1 cavitandplex or a 2:2 capsuleplex, 2D-DOSY experiments were carried out at room temperature. The diffusion constant of a certain molecular species depends on its effective molecular size, which should change with any intermolecular interactions. It is clear that diffusion constants are intuitively related to aggregation and intermolecular interactions. This means that in diffusion measurements the observable parameters of the bound guest can be predicted<sup>22</sup>. **Table 2.1** shows the diffusion constants of the free host as well as the host: guest complexes. **Figure 2.5**, shows the 2D DOSY NMR spectra of **1a-d**@OA complexes. It can be observed that the proton signals of the host as well as guest moves with the same speed, hence showing their associated nature. The diffusion constant of the free host OA is  $1.88 \times 10^{-5} \text{ cm}^2/\text{sec}$ <sup>52</sup>. On comparison, it could be found that diffusion constant for the bound guest@host complex is less than the diffusion constant for the free host in all the cases. This is probably due to the fact that as the guest

binds to the host, the complex becomes bulky and hence diffuses slowly on the NMR timescale. Also, it can be observed that the diffusion constant for **1a**@OA is  $1.26 \times 10^{-6} \text{ cm}^2/\text{sec}$ , whereas for all the other complexes it is  $\sim 1.56 \times 10^{-6} \text{ cm}^2/\text{sec}$ . This observation indicates that **1a** being relatively smaller in size than its other derivatives forms 2:2 capsuleplex with OA, whereas all the other derivatives, form 1:1 cavitandplex with OA.

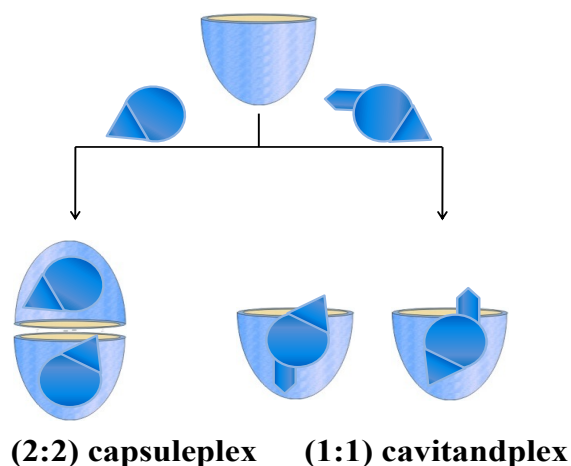


**Figure 2.4**  $^1\text{H}$  NMR Titration of **1a** against 1mM OA in 10 mM buffered  $\text{D}_2\text{O}$ .

**Scheme 2.2** shows the cartoon representation of the mode of complexation of the guest **1a-d** with OA. All the observations are summarized into this cartoon, i.e. guests **1a-d** form complexes with OA, **1a** being symmetric in shape and having lesser volume, forms 2:2 capsuleplex with OA, whereas, all other guests **1b-d** form 1:1 cavitandplex with host OA.

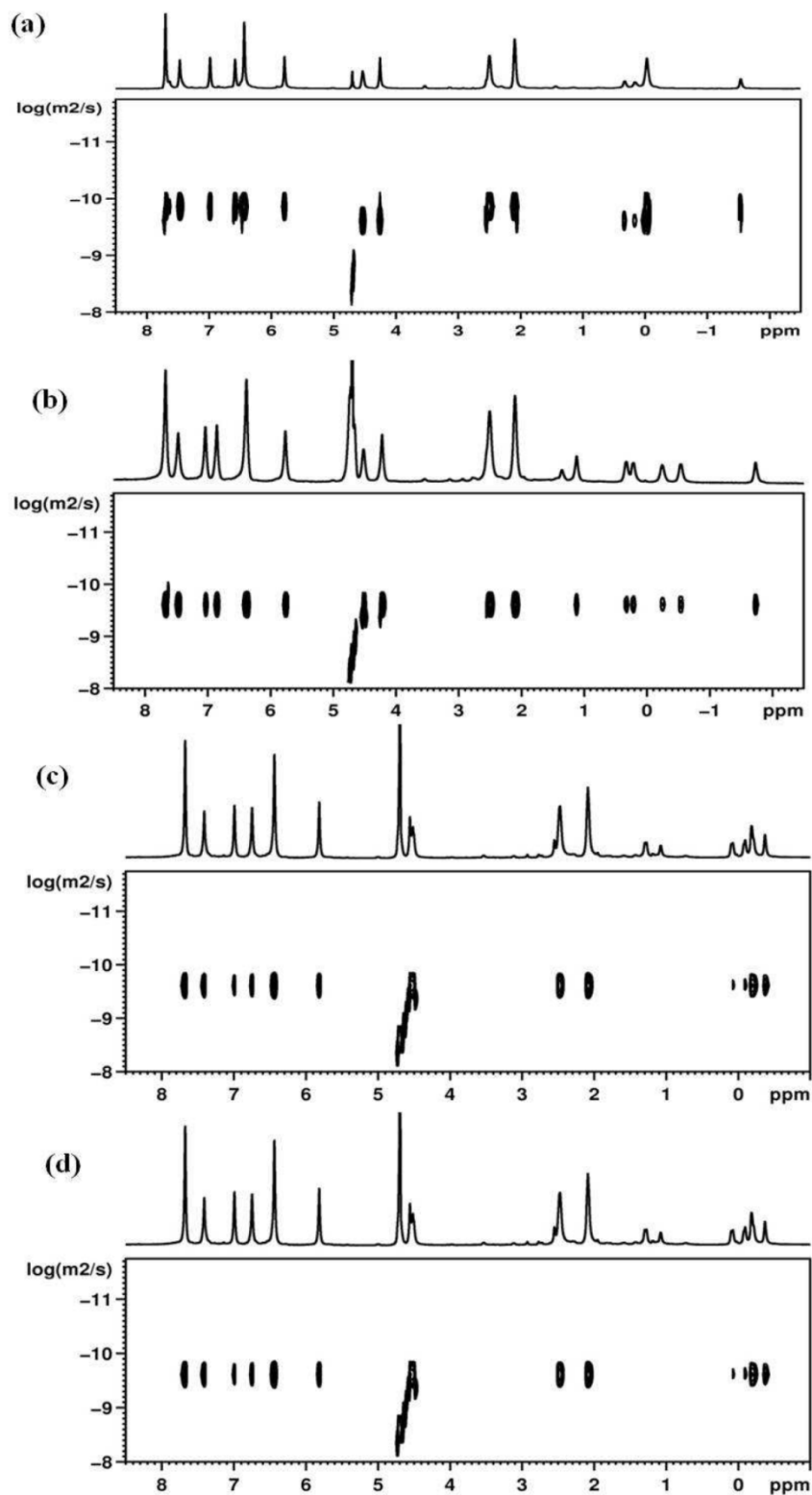
**Table 2.1** The diffusion constants for various guest@host complexes.

Compound	Diffusion Constant ( $\times 10^{-6} \text{ cm}^2/\text{sec}$ )
Free OA	1.88
<b>1a@OA</b>	1.23
<b>1b@OA</b>	1.56
<b>1c@OA</b>	1.56
<b>1d@OA</b>	1.55



**Scheme 2.2** Cartoon representation of the complexation modes of the guest of various size and shape with the host OA

Now, our next step would be to find out the preferred orientation of these guests inside OA, since orientation of the guest plays a strong role in the photochemistry of the guests@OA. For this purpose 2D COSY and 2D NOESY NMR experiments were carried out at room temperature.



**Figure 2.5** 2D DOSY NMR spectra of (a)  $1a_2@OA_2$ , (b)  $1b@OA$ , (c)  $1c@OA$ , (d)  $1d@OA$ .

As, we have mentioned earlier guest **1a** is symmetric in nature, hence its orientation is not of much significance. And guests **1c** and **1d** are similar in nature, hence here we are illustrating only two examples **1b@OA** and **1c@OA**. **Figures 2.6** (a) and (b) represent the partial 2D COSY and NOESY spectra of **1b@OA**, and **Figures 2.7** (a) and (b) represent partial 2D COSY and NOESY spectra of **1c@OA**, respectively. 2D COSY experiments helps us to assign the proton signals of the guests@OA, whereas, the NOESY spectra allow us to assess the orientation of the guest@OA. These experiments suggest that **1b@OA** is oriented in such a way that the OH group faces the opening of the cavity; whereas, in case of **1c@OA** (also **1d@OA**) the halogen group faces the narrower end of the OA cavity. The observed orientation of **1b@OA** can be explained by considering the fact that the hydrophilic OH group likes to orient itself in such a way that it faces the open end of the cavity so that it can freely interact with the aqueous media outside OA, and the diazirine group being relatively non-polar in nature is held tightly at the narrower end of the cavitand. It is quite likely that this tight fit and the hydrogen bonding of the OH group with exterior water molecules lower the mobility of **1b**. In the case of **1c@OA** (also **1d@OA**), the halogen group, prefers the van der Waals interaction with the inner walls of the OA cavity, hence orients itself towards the narrower end of the cavity to get a snug fit. These observations are also supported by ITC and Computational experiments as discussed in **section 2.2.8**

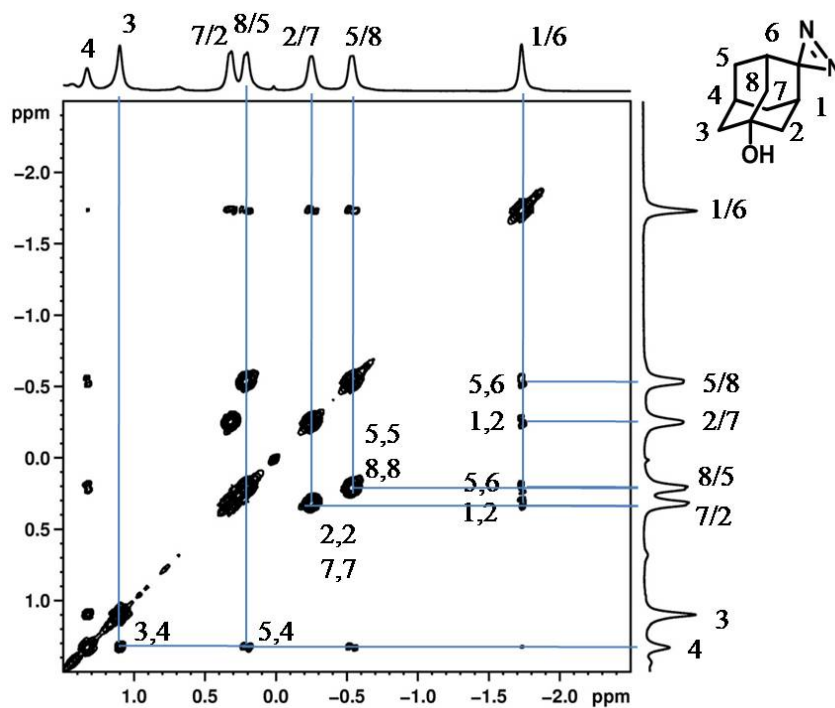


Figure 2.6 (a) 2D COSY NMR spectra of **1b@OA**.

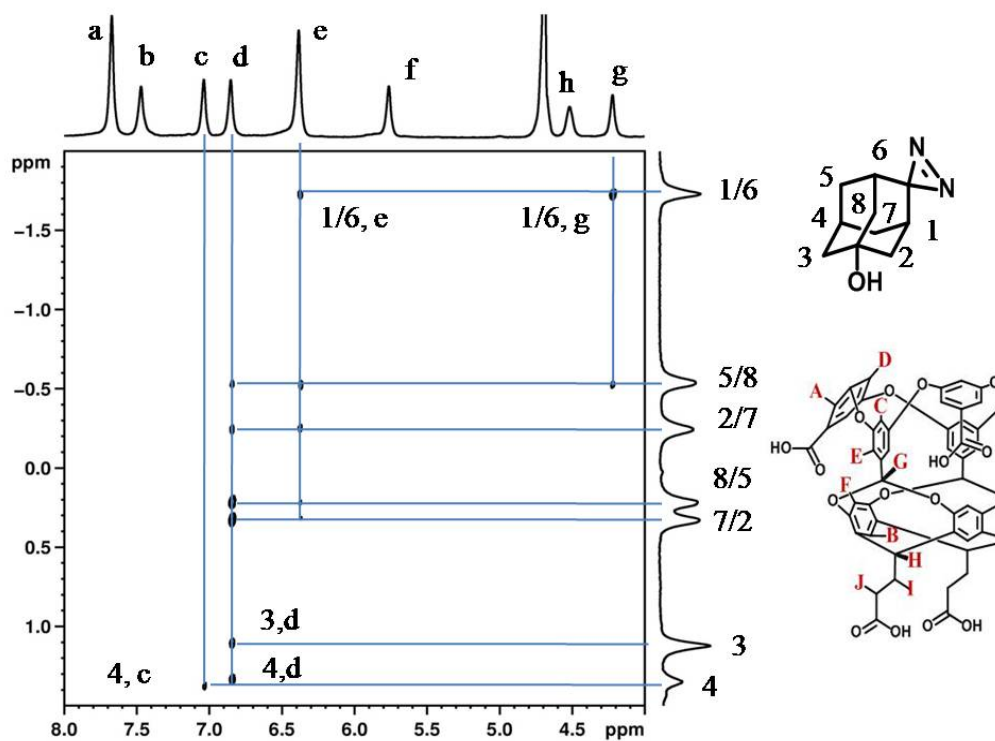


Figure 2.6 (b) 2D NOESY NMR spectra of **1b@OA**.



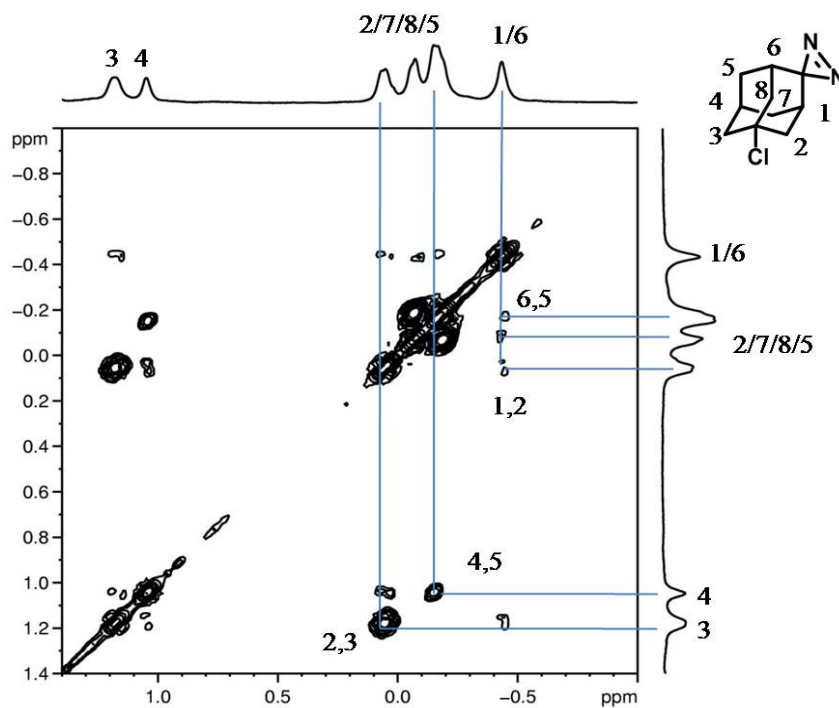


Figure 2.7 (a) 2D COSY NMR spectra of **1c@OA**.

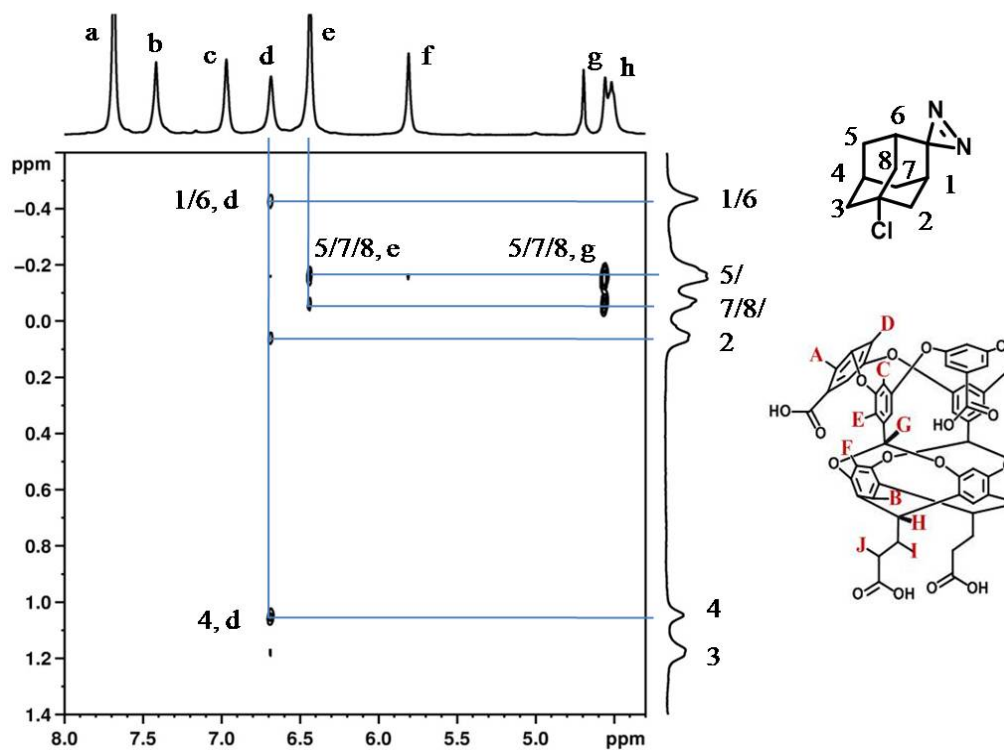


Figure 2.7 (b) 2D NOESY NMR spectra of **1c@OA**.

### 2.2.2 Photolysis of carbene precursors **1a-d@OA** and **1a-d@OA** on silica surface.

Photolysis of carbene precursors **1a-d** in hydrocarbon and alcohol solution is reported to give a number of products shown in **Scheme 2.1**.<sup>183-187</sup> Of these, azine **2**, adamantanone **3**, and solvent insertion products **4** and **5** were the major ones. Importantly, intramolecular C-H insertion products **6** and **7** were formed only in trace amounts. In general, the formation of all products listed in **Scheme 2.1** was presumed to involve adamantylidene **8** as the intermediate. We have carried out photolyses of **1a<sub>2</sub>@OA<sub>2</sub>**, **1b@OA**, **1c@OA**, and **1d@OA** under two different conditions. In one condition, the complex was irradiated in water (sodiumborate buffer), and in the other, the complex was transferred to a silica surface and irradiated as powder. For comparison, irradiations of **1a-d** alone in water were also carried out. The progress of the photolysis was followed by <sup>1</sup>H NMR. As an example we have shown the photolysis experiment of **1a@OA**. **Figure 2.8** (a) shows the <sup>1</sup>H NMR spectra of the host-guest complex before irradiation; **Figure 2.8** (b) shows the <sup>1</sup>H NMR spectra of the host-guest complex after 20 minutes of irradiation, i.e. products@OA. **Figure 2.8** (c) shows the <sup>1</sup>H NMR spectra of the host OA after extraction of products by CDCl<sub>3</sub>. And **figure 2.8** (d) is a control experiment, done for the comparison, in which CDCl<sub>3</sub> was added to only OA solution and then extracted back. It can be noticed that no proton signals from the guest can be observed after extraction. These observations also show that none of the products are attached to the host OA itself. The products were extracted upon completion of the reaction and analyzed by GC. Results are summarized in **Table 2.2**. In water in the absence of OA **1a-d** gave adamantanone **3** and adamantanol **5** as major products (~90%). On the other hand, irradiation of **1a<sub>2</sub>@OA<sub>2</sub>** in aqueous solution gave azine **2a** in 89% yield (**Table 2.2**). Obviously, the formation of azine is an outcome of caging of two

molecules of **1a** within a single capsule. Most likely as soon as the carbene is generated it reacts with the adjacent carbene precursor **1a** molecule, present in the same capsule to yield azine **2a**. This model is consistent with the absence of azines upon photolysis of **1b@OA**, **1c@OA**, and **1d@OA** where only one molecule is present within the OA cavitand. Irradiation of **1b@OA** in water gave 92% of intramolecular insertion products **6b** and **7b**. In this case adamantanone **3** was formed in 8% yield, most likely a result of a reaction between carbene and oxygen. The formation of unprecedented amounts of **6b** and **7b** from **1b@OA** is consistent with its structure wherein the photolytically generated adamantylidene **8b** intermediate would have its reactive end facing the narrower end of the cavitand; such geometry would offer very little option. Based on the proposed structures for **1c@OA** and **1d@OA**, we expect adamantylidenes **8c** and **8d** generated upon photolysis would have the reactive end facing water allowing them to explore options such as reacting with oxygen and water. As seen in **Table 2.2**, **6c** and **7c** are formed in 45% yield from **1c@OA** and **6d** and **7d** in 37% yield from **1d@OA**. Corresponding adamantanones accompanied the above products in larger amounts. Formation of intramolecular insertion products in nearly quantitative yield from **1b@OA** brings out the potential of manipulating the behavior of reactive intermediates such as carbenes by constraining them in a narrow space. Having established that the chemistry of carbenes could be altered within a cavitand in aqueous solution, we were interested in exploring the possibility of transferring the host-guest complexes onto a silica surface and photolyzing them as powders.<sup>199,200</sup> We envisioned that this methodology would also allow us to exclude side reactions such as those with solvents and oxygen. As noted in **Table 2.2**, in all cases the major products were intramolecular insertion products **6** and **7**

(>75%). Even **1a** gave intramolecular insertion products and no azine. As expected, based on the slower diffusion of oxygen on the silica surface, yields of adamantanones **3a-d** were lower than in aqueous solution. For comparison, the guests **1a-d** alone were adsorbed on the silica surface and irradiated under the similar condition. As can be seen from **Table 2.3**, in the case of photolysis of guests **1a-d** on silica surface without the host OA, the products are unevenly distributed, and no selectivity can be observed, emphasizing the role of OA as host.

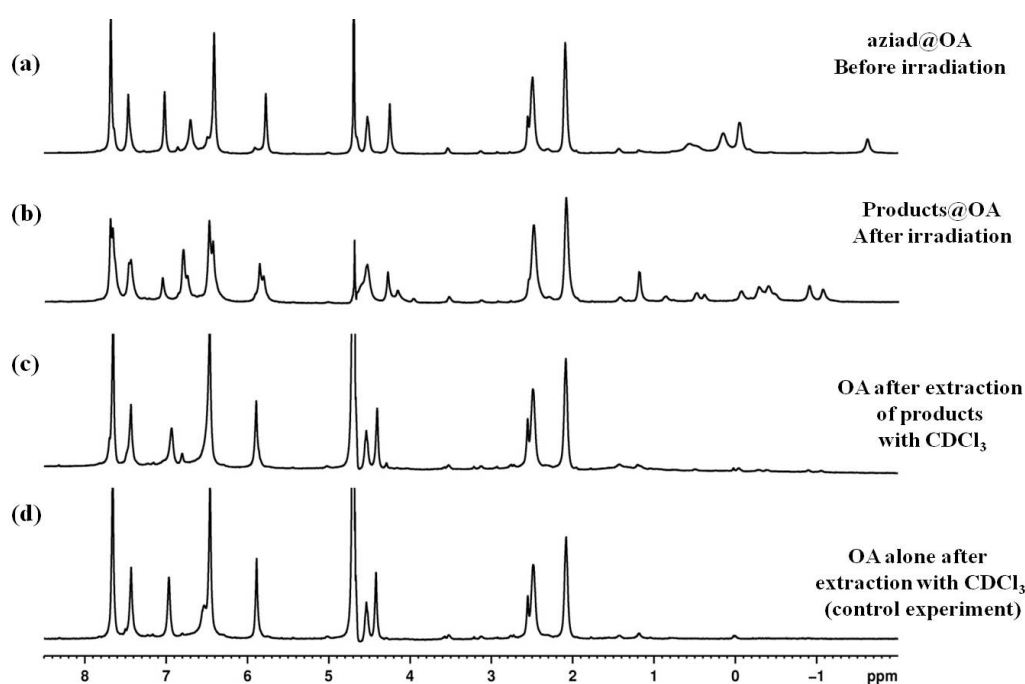
**Table 2.2** Relative percentages of the products upon the photolysis of the guests **1a-d@OA**, **1a-d@OA** on silica surface and in D<sub>2</sub>O.

Guests	Media	2	3	5	6/7
<b>1a</b>	D <sub>2</sub> O	5.5	31.0	62.0	1.5
	1a@OA	89.0	5.0	--	6.0
	1a@OA-SiO <sub>2</sub>	--	16.0	--	84.0
<b>1b</b>	D <sub>2</sub> O	--	3.0	95.0	2.0
	1b@OA	--	8.0	--	92.0
	1b@OA-SiO <sub>2</sub>	--	5.5	--	94.5
<b>1c</b>	D <sub>2</sub> O	8.0	2.5	88.0	1.5
	1c@OA	--	55.0	--	45.0
	1c@OA-SiO <sub>2</sub>	--	24.0	--	76.0
<b>1d</b>	D <sub>2</sub> O	5.0	27.0	62.0	6.0
	1d@OA	--	63.0	--	37.0
	1d@OA-SiO <sub>2</sub>	--	20.2	--	79.8

Irradiation done using medium pressure mercury lamp and 320 nm filter. Reaction was followed by NMR, and following 100% conversion products were analyzed by GC-MS and GC.

**Table 2.3** Relative percentages of the products upon the photolysis of the guests on silica without any host.

Guests	Media	2	3	5	6/7
<b>1a</b>	SiO <sub>2</sub>	52.0	17.0	--	30.0
<b>1b</b>	SiO <sub>2</sub>	40.0	24.0	--	36.0
<b>1c</b>	SiO <sub>2</sub>	34.0	36.5	--	29.5
<b>1d</b>	SiO <sub>2</sub>	19.0	42.0	--	39.0

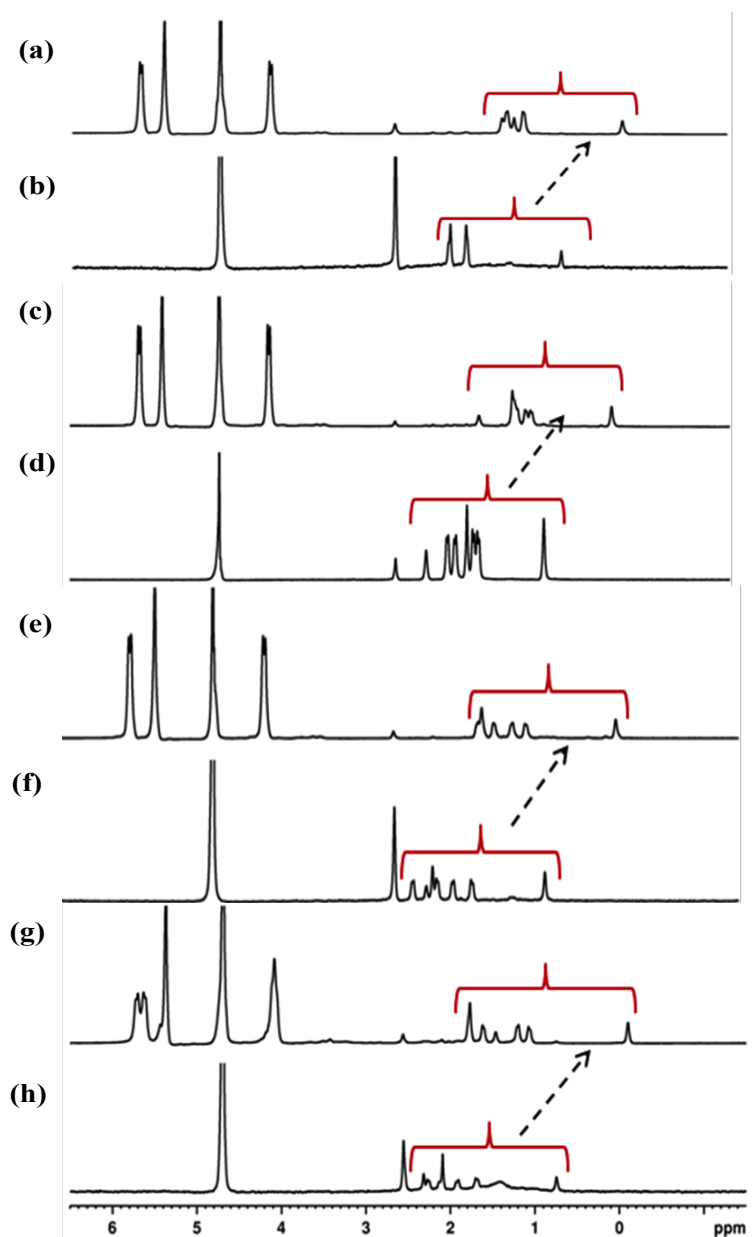


**Figure 2.8** <sup>1</sup>H NMR spectra of (a) **1a**@OA before irradiation, (b) Products@OA after irradiation, (c) OA after extraction of products, (d) control experiment.

### 2.2.3 Encapsulation of carbene precursors **1a-d** in CB[7] and CB[8] as studied by <sup>1</sup>H NMR

Host molecules CB[8] and CB[7], have portal shaped cavity, with carbonyl groups pointing upwards, on the rim. CB[7] is readily soluble in water whereas CB[8] is partially soluble in water, but its solubility increases upon complexation with the guest molecules. CB [7] due to its cavity size usually forms 1:1 complex, whereas CB[8] can

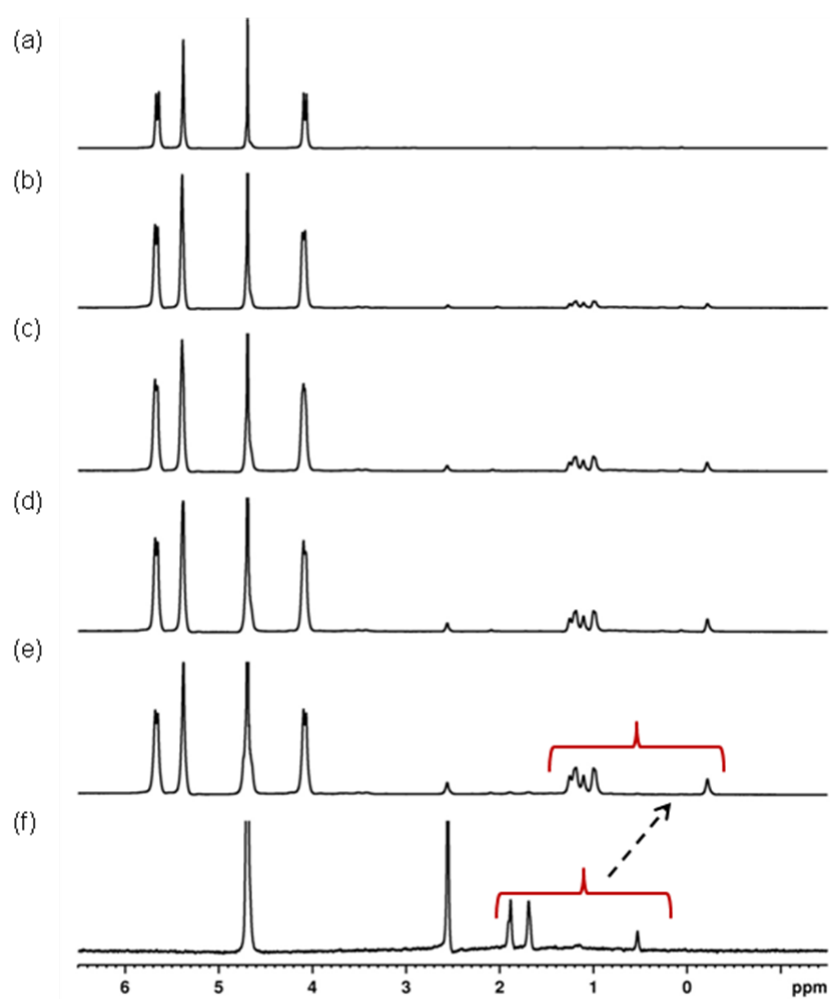
form both 1:1 and 1:2 complexes depending upon the shape and size of the guest molecule.<sup>194-196</sup>



**Figure 2.9** <sup>1</sup>H NMR spectra of (a) **1a** in D<sub>2</sub>O, (b) **1a**@CB[7] in D<sub>2</sub>O, (c) **1b** in D<sub>2</sub>O, (d) **1b**@CB[7] in D<sub>2</sub>O, (e) **1c** in D<sub>2</sub>O, (f) **1c**@CB[7] in D<sub>2</sub>O, (g) **1d** in D<sub>2</sub>O, (h) **1d**@CB[7] in D<sub>2</sub>O

The second host system we tried for the complexation of the guests, **1a-d** were cucurbiturils. We investigated the complexation of host guest by <sup>1</sup>H NMR technique as

mentioned in previous sections. **Figure 2.9** shows the  $^1\text{H}$  NMR spectra of guests **1a-d**@CB[7] and in only  $\text{D}_2\text{O}$  solution. It can be noticed that, the proton signals of the guests **1a-d** shift upfield on the NMR scale, after addition of the host CB[7], which is indicative of the host guest association. Also, on comparison with the proton signals of the guests **1a-d** in  $\text{D}_2\text{O}$ , we can observe that none of these signals appear in the **1a-d**@CB[7]  $^1\text{H}$  NMR spectra. This shows that, no uncomplexed guest molecules exist in the solution.

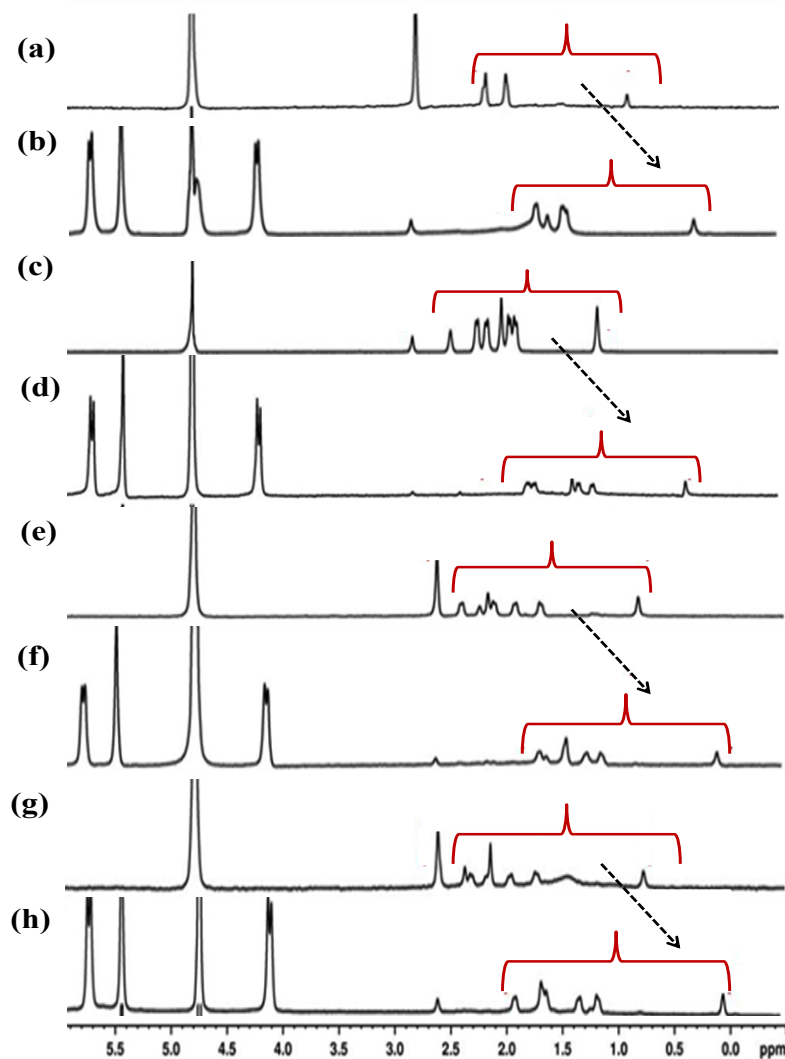


**Figure 2.10**  $^1\text{H}$  NMR spectra of (a) 1 mM of CB[7] in  $\text{D}_2\text{O}$ , (b)-(e) 1 mM CB[7] + 0.2, 0.6, 0.8, 1.0 equivalent of **1a** respectively in  $\text{D}_2\text{O}$ , (f) 1 mM of **1a** in  $\text{D}_2\text{O}$ .

Next, to determine the host guest ratio,  $^1\text{H}$  NMR titrations were carried out.  $\mathbf{1a@CB[7]}$   $^1\text{H}$  NMR titration experiment has been shown in **Figure 2.10** as an example. It can be observed that on subsequent addition of the guest the intensity of the guest proton signals in the upfield region increases. Also, we can observe that the host proton signals first get broadened, and on subsequent addition of the guests, it sharpens. This broadening is possibly due to the presence of complexed as well as uncomplexed host in the solution. As the guest concentration increases, more and more of the complexed host exists, hence the sharpening of the proton signals is observed. Also, on further addition of the guest, uncomplexed guest proton could be observed, indicating the excess of the guest. Such titration experiments were carried out for  $\mathbf{1b-d@CB[7]}$  also, and it was observed that all the four guests  $\mathbf{1a-d}$  form 1:1 complex with host CB[7].

CB[8] also belongs to the family of cucurbiturils with the only difference that it has one extra parent group and hence a bit larger cavity than CB[7]. But this difference in the size of cavity can play an important role in complexation and photoreactivity of the guests. Hence we proceeded to investigate the complexation behavior of guests  $\mathbf{1a-d}$  with host CB[8]. CB[8] is partially soluble in water, so initially a haziness is observed in the solution, but as the guest concentration increases, the solution becomes clearer. **Figure 2.11** show the  $^1\text{H}$  NMR complexation spectra of CB[8] with guests  $\mathbf{1a-d}$ . As can be seen, the guest proton signals are upfield shifted when in association with the host, this upfield shift of the guest protons shows its encapsulation inside the CB[8] cavity which is relatively non-polar. Also, further addition of the guest results in uncomplexed proton signals for the guest molecules as seen by NMR.

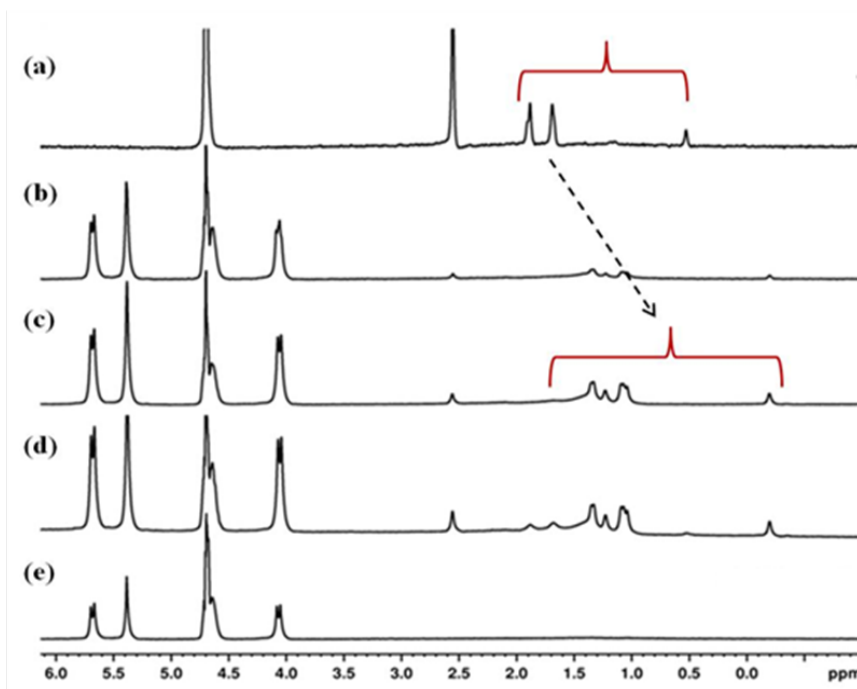




**Figure 2.11**  $^1\text{H}$  NMR spectra of (a) **1a** in  $\text{D}_2\text{O}$ , (b) **1a@CB[8]** in  $\text{D}_2\text{O}$ , (c) **1b** in  $\text{D}_2\text{O}$ , (d) **1b@CB[8]** in  $\text{D}_2\text{O}$ , (e) **1c** in  $\text{D}_2\text{O}$ , (f) **1c@CB[8]** in  $\text{D}_2\text{O}$ , (g) **1d** in  $\text{D}_2\text{O}$ , (h) **1d@CB[8]** in  $\text{D}_2\text{O}$

$^1\text{H}$  NMR titration experiments were carried out for **1a-d@CB[8]** system. **Figure 2.12** is an example showing  $^1\text{H}$  NMR titration of **1a-CB[8]**. Since the host CB[8] is partially soluble in water, hence exact concentration of each addition could not be determined. But when the proton signals of the uncomplexed guest are seen, the addition just before that had been considered to be 1:1 ratio of the host and guest. On the basis of

$^1\text{H}$  NMR titration experiments for all other guests **1b-d**, we concluded that carbene precursors **1a-d** formed 1:1 complexes (guest to host) with CB[8].



**Figure 2.12**  $^1\text{H}$  NMR spectra of (a) 1mM of **1a** in  $\text{D}_2\text{O}$ , (b)-(d)  $\sim 1$  mM CB[8] +  $\sim 0.2$ ,  $0.4$ ,  $1.0$  equivalent of **1a** respectively in  $\text{D}_2\text{O}$ , (e)  $\sim 1$ mM of CB[8] in  $\text{D}_2\text{O}$ .

#### 2.2.4 Photolysis of carbene precursors **1a-d@CB[7]** and **1a-d@CB[8]**.

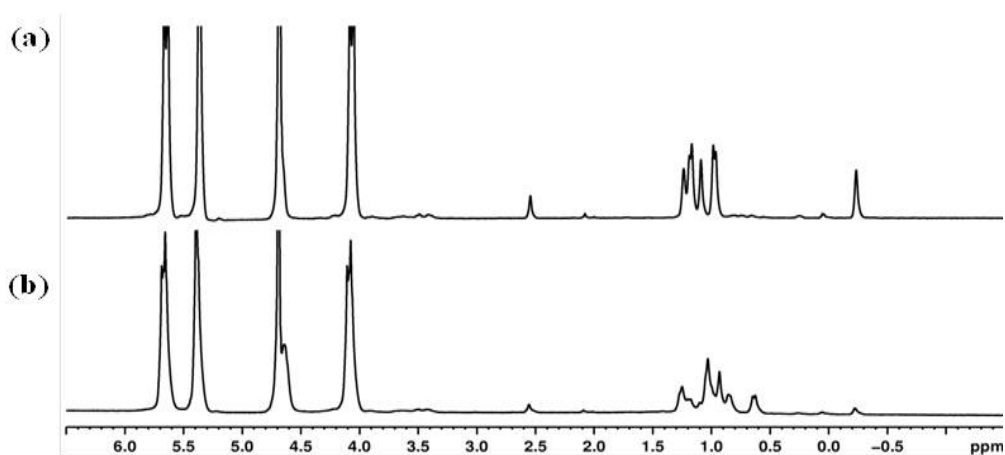
Once the complexation behavior of the guests **1a-d** was determined with the hosts CB[7] and CB[8], photolysis reactions of these systems were carried out. In this study, all irradiations were carried out with a medium pressure mercury lamp fitted with a Corning glass O-52 filter ( $>320$  nm). CB[7] and CB[8] have no absorption above 250 nm and would not sensitize the photoreactions of guests **1a-d**. In all cases, irradiations were conducted to total conversion (1–3 h) as determined by  $^1\text{H}$  NMR. At that stage, products were extracted three times with  $\text{CDCl}_3$ , and the combined concentrated extract was analyzed by GC–MS, GC, and  $^1\text{H}$  NMR.  $^1\text{H}$  NMR and ESI-MS or MALDI-MS spectra

of photolyzed samples did not show any products of reaction between the hosts CB[7], CB[8] and the guest carbene. Product distributions obtained upon photolysis of **1a–d** in water alone and from complexes with CB[7], and CB[8] in water are provided in **Table 2.4** To our surprise and delight, we noted that the intramolecular C–H insertion product **6a** was obtained in >90% yield upon irradiation of **1a** included in CB[7] and CB[8]. To our knowledge for **1a**, no such dominance of formation of intramolecular insertion product in any other medium has been observed. Even in an octa acid capsule with the formation of a 2:2 complex, **6a** was obtained only in 6% yield. It is observed for **1b@CB[7]/CB[8]**, that it gives approximately equal amounts of 1, 3-insertion products and adamantanone **3a–d** as a result of the photolysis. In the case of **1b@OA**, we had observed that azi-group is pointing downwards towards the cavity hence left with no choice but undergo intramolecular insertion reaction. But in the case of CBs the size of the portal on both the ends is equal, unlike OA, where one end of the cavity is much bigger than the other end. So in this case, whichever way the azi-group faces it is equally labile. In the case of **1c@CB[7]/CB[8]** and **1d@CB[7]/CB[8]**, 1, 3-insertion products **6/7c, d** is formed in major quantities followed by the formation of the adamantanones **3c, d**. The completion of the reaction was monitored by  $^1\text{H}$  NMR technique. **Figures 2.13** (a), (b), shows the  $^1\text{H}$  NMR spectra of guest@CB[7] complex before irradiation and products@CB[7] after irradiation respectively. **Figures 2.14** (a), (b), show the  $^1\text{H}$  NMR spectra of the guest@CB[8] before irradiation and products@CB[8] complex after irradiation is completed, respectively. It can be noticed that in spectra (b), most of the starting material is finished and only the products which are still encapsulated inside the host are seen.

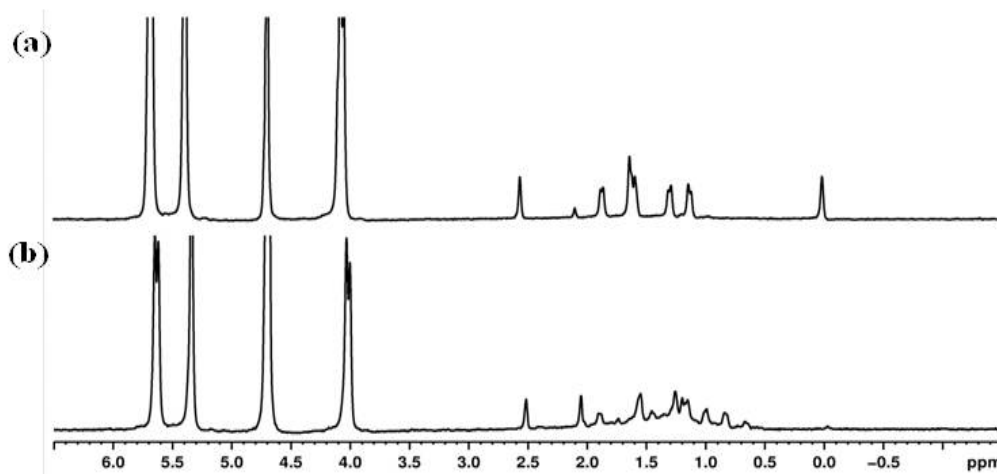
**Table 2.4** Relative percentages of the products upon the photolysis of guests **1a-d**@CB[7], **1a-d**@CB[8] and in D<sub>2</sub>O.

Guests	Media	2	3	5	6/7
<b>1a</b>	D <sub>2</sub> O	5.5	31.0	62.0	1.5
	1a@CB[7]	--	6.0	--	94.0
	1a@CB[8]	--	9.0	--	91.0
<b>1b</b>	D <sub>2</sub> O	--	3.0	95.0	2.0
	1b@CB[7]	--	44.0	--	56.0
	1b@CB[8]	--	51.0	--	49.0
<b>1c</b>	D <sub>2</sub> O	8.0	2.5	88.0	1.5
	1c@CB[7]	--	41.0	--	59.0
	1c@CB[8]	--	21.0	--	79.0
<b>1d</b>	D <sub>2</sub> O	5.0	27.0	62.0	6.0
	1d@CB[7]	--	34.0	--	66.0
	1d@CB[8]	--	40.0	--	60.0

The samples were irradiated using a medium pressure mercury lamp and an O-52 (320 nm) filter. Product yields were determined by GC after total conversion with adamantane as internal standard. Concentration of 1a-d: CB[7], CB[8] = 1 mM/1 mM, concentration of 1a-d in D<sub>2</sub>O = 1 mM. Host/guest complex ratios not included. Compounds 6a and 7a obtained from 1a are identical.



**Figure 2.13** (a) <sup>1</sup>H NMR spectra of **1a**@CB[7] before irradiation, (b) <sup>1</sup>H NMR spectra of Products@CB[7] after irradiation.

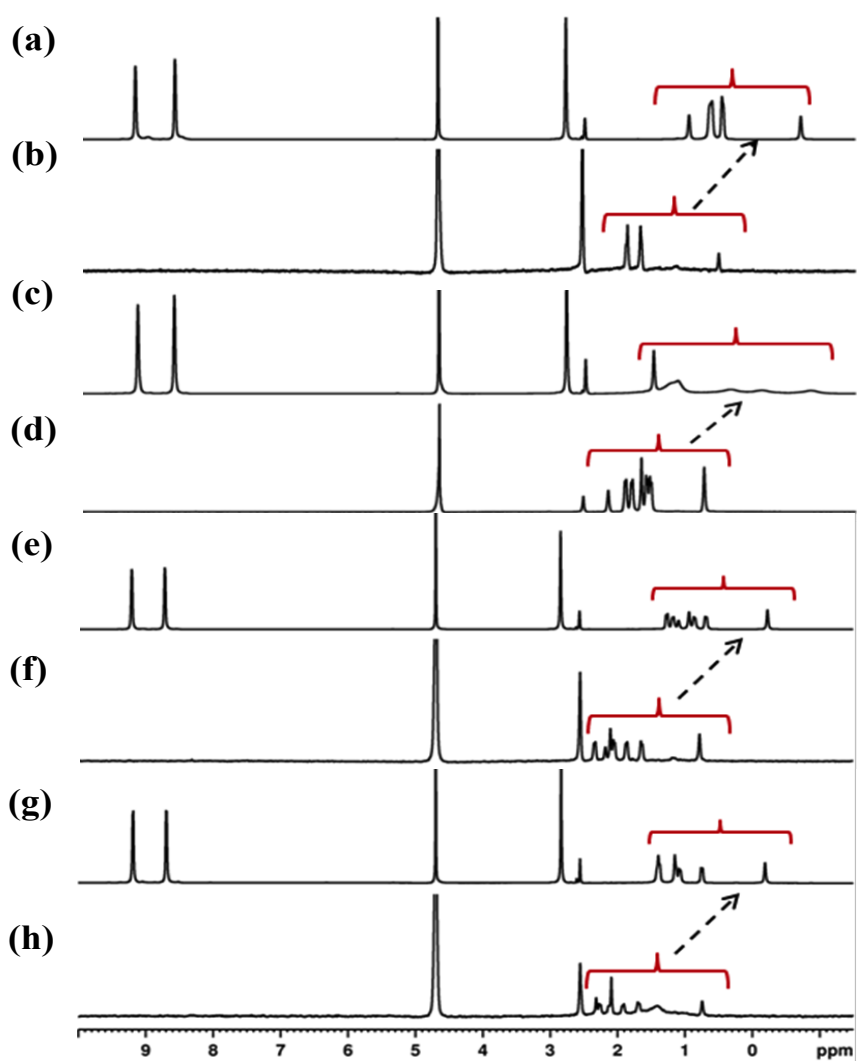


**Figure 2.14** (a)  $^1\text{H}$  NMR spectra of **1a@CB[8]** before irradiation, (b)  $^1\text{H}$  NMR spectra of **Products@CB[8]** after irradiation.

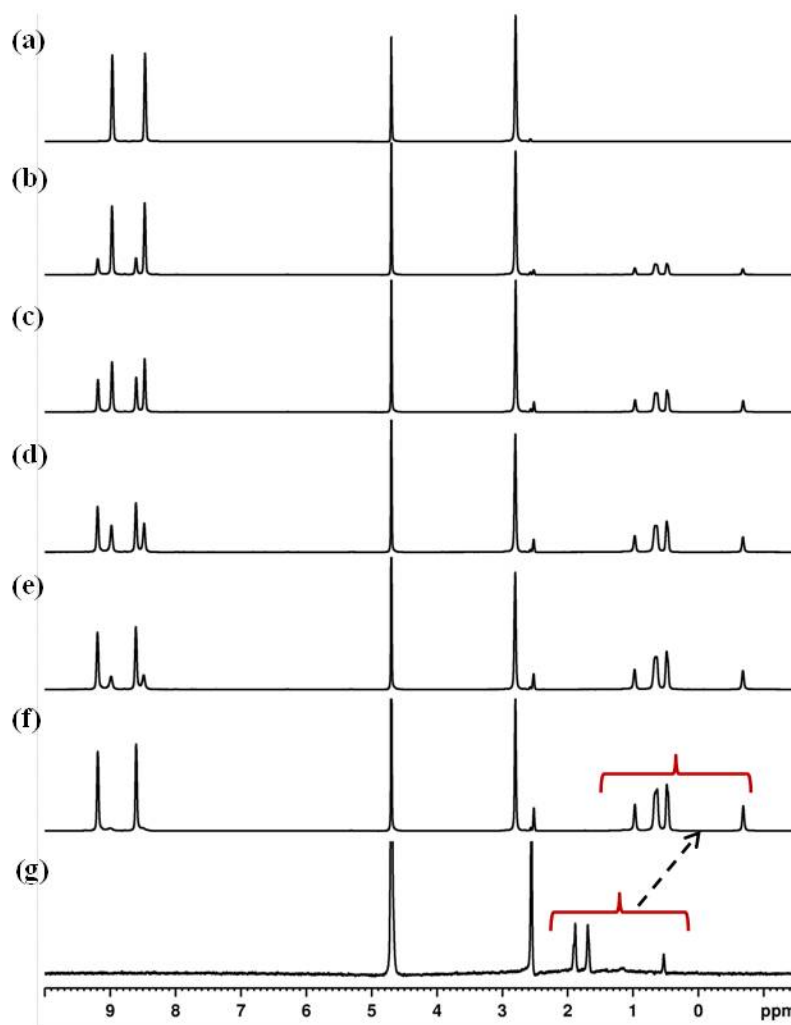
### 2.2.5 Encapsulation of carbene precursors **1a-d** in PdNC as studied by $^1\text{H}$ NMR

The last host we employed in this study was Palladium Nanocage (PdNC). PdNC is a water soluble host and possesses larger cavity<sup>197,198</sup> than the three hosts mentioned earlier OA, CB[7] and CB[8].  $^1\text{H}$  NMR spectra of the guests **1a-d** in  $\text{D}_2\text{O}$  only and in PdNC have been shown in **Figure 2.15**. As in all the above cases, the guest proton signals appear in the upfield region in comparison to its position in the  $\text{D}_2\text{O}$  solution, when associated with the host PdNC. These spectra show that the guests **1a-d** are completely complexed with the host PdNC, no uncomplexed host or guest remains in the solution. Also the sharpness of the proton signals suggests that the host and guests are bound strongly together. Next the  $^1\text{H}$  NMR titration of the guest **1a-d** was carried out with PdNC. As an example the  $^1\text{H}$  NMR spectra of **1a@PdNC** have been shown in **Figure 2.16**, it can be observed that as the guest concentration increases so does the intensity of the guest proton signal in the upfield region. It was very interesting to observe that as the guest concentration is increased, the complexed host proton signals appear along with the uncomplexed host proton signals, and on subsequent addition of

the guest **1a**, complexed host proton signals increase in intensity while a systematic decrease in the uncomplexed host signals can be observed. At the end of the titration experiment only complexed host proton signals remain, indicating the completion of the experiment. It was concluded from this experiment that **1a** formed a 3:1 guest@host complex with PdNC. In all other cases guests **1b-d** also formed 3:1 guest@host complexes with the host PdNC.



**Figure 2.15** <sup>1</sup>H NMR (500 MHz, D<sub>2</sub>O) spectra of (a) **1a**@PdNC, (b) **1a** in D<sub>2</sub>O, (c) **1b**@PdNC, (d) **1b** in D<sub>2</sub>O, (e) **1c**@PdNC, (f) **1c** in D<sub>2</sub>O, (g) **1d**@PdNC, (h) **1d** in D<sub>2</sub>O.



**Figure 2.16**  $^1\text{H}$  NMR spectra of (a) 1 mM of PdNC in  $\text{D}_2\text{O}$ , (b)-(f) 1 mM PdNC + 0.6, 1.2, 1.8, 2.4 and 3.0 equivalents of **1a** respectively in  $\text{D}_2\text{O}$ , (g) 1 mM of **1a** in  $\text{D}_2\text{O}$ .

### 2.2.6 Photolysis of carbene precursors **1a-d**@PdNC

Once it was confirmed that the guests **1a-d** form complexes with the host PdNC, photolysis reactions of **1a-d**@PdNC were carried out. PdNC showing a weak absorption tailing up to 350 nm is likely to absorb a small part of the light that is used to excite the guests, hence sensitization by PdNC cannot be completely ignored<sup>201</sup>. **Table 2.5** shows the product distribution of the irradiation of **1a-d**@PdNC. Irradiation of **1a** included in PdNC resulted in adamantanone **3a** (oxygen addition product) as the major product

(85%) and **6a** in 4% yield. Complete removal of oxygen from water was impossible, and we suspect the presence of some residual dissolved oxygen under our experimental conditions. We speculate the dramatic shift in product distribution in favor of **3a** within PdNC was irradiated at  $\lambda > 320$  nm. Under this condition no adamantanone was detected. Also, when the photoreaction of **1a**@PdNC was followed by  $^1\text{H}$  NMR, no accumulation and disappearance of **2a** was noticed.

**Table 2.5** Relative percentages of the products upon the photolysis of the guests **1a-d**@PdNC and in  $\text{D}_2\text{O}$ .

Guests	Media	2	3	5	6/7
<b>1a</b>	$\text{D}_2\text{O}$	5.5	31.0	62.0	1.5
	<b>1a</b> @PdNC	11.0	85.0	--	4.0
<b>1b</b>	$\text{D}_2\text{O}$	--	3.0	95.0	2.0
	<b>1b</b> @PdNC	6.0	90.0	--	4.0
<b>1c</b>	$\text{D}_2\text{O}$	8.0	2.5	88.0	1.5
	<b>1c</b> @PdNC	13.0	80.0	--	7.0
<b>1d</b>	$\text{D}_2\text{O}$	5.0	27.0	62.0	6.0
	<b>1d</b> @PdNC	4.0	83.0	--	13.0

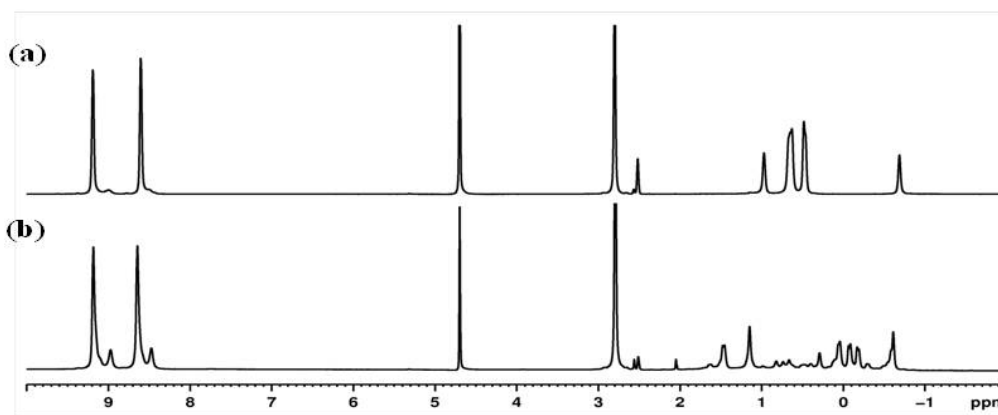
The samples were irradiated using a medium pressure mercury lamp and an O-52 (320 nm) filter. Product yields were determined by GC after total conversion with adamantane as internal standard. Concentration of **1a**–**1d**: PdNC = 3 mM/1 mM, concentration of **1a**–**1d** in  $\text{D}_2\text{O}$  = 1 mM. Host/guest complex ratios not included. Compounds **6a** and **7a** obtained from **1a** are identical.

These observations suggested that formation of adamantanone was not preceded by **2a**. Lack of formation of **2a** in spite of presence of three molecules of **1a** within PdNC could be due to either the triplet adamantanylidene's inertness toward **1a** or improper alignment of adamantanediazirine molecules present within PdNC for a bimolecular reaction. In all other cases, i.e. **1b**, **1c** and **1d**@PdNC, adamantanones **3b**, **3c** and **3d** predominated the product distribution. Azine **2b**, **2c** and **2d** were minor products and 1, 3



intramolecular insertion products were formed in trace amounts. As in the previous sections, the progress and completion of the photoreaction was monitored by  $^1\text{H}$  NMR.

**Figure 2.17** show the  $^1\text{H}$  NMR spectra of **1a**@PdNC before irradiation and products@PdNC after irradiation.



**Figure 2.17** (a)  $^1\text{H}$  NMR spectra of **1a**@PdNC before irradiation, (b)  $^1\text{H}$  NMR spectra of Products@PdNC after irradiation.

### 2.2.7 Comparison of the products obtained in the case of different hosts.

In all the previous sections, we have shown the complexation studies and the photochemistry of the carbene precursors **1a-d** when associated with different hosts like OA, CBs and PdNC. This section summarizes the overall product distribution when these carbene precursors are complexed with different hosts mentioned in this chapter as well as those found in the literature. The aim of this section is to discuss the pros and cons of each host used to encapsulate the above mentioned carbene precursors, how they affect the photochemistry, and hence could be useful in manipulating the product distribution.

Photolysis of **1a-d** in hydrocarbon and alcohol solutions and during thermolysis in the gas phase have been established to generate products shown in **Scheme 2.1** via the corresponding adamantanylidenes **8** as reactive intermediates. In water, the major

products were adamantanones **3** and alcohols **5** resulting from reaction of carbene **8** with oxygen and water, respectively. The most important point to note is that the intramolecular C–H insertion products **6** and **7** were obtained only in trace amounts (<10%) in water, alcohol, and hydrocarbon as solvents. Irradiation of **1a** included in cyclodextrins and **1d** in a resorcinarene-based cavitand in the solid state gave the corresponding insertion products **6** and **7** (note with **1a**, compounds **6a** and **7a** are identical and we denote them by **6a**; **Scheme 2.1**) in about 25% yield. Similar irradiation of **1a** included in the NaX zeolite gave **6a** in ~40% yield. Photolysis of carbene precursors **1a-d**@ $\alpha$ -CD in water afforded two insertion products into the OH groups of the host in addition to parent adamantane, but there was almost no intramolecular C–H insertion product **6a** formed.

**Table 2.6** Relative percentages of the products upon the photolysis of the guests **1a-d**@hosts as mentioned in the literature.

Guests	Media	2	3	4	5	6/7	Adamantane
<b>1a</b>	Hexane	95.0	traces	--	--	5	--
<b>1a</b>	NaY	--	14.0	--	80.0	2.0	3.0
<b>1a</b>	7Cy	33.0	7.0	21.0	2.0	9.0	3.0
<b>1a</b>	8Cy	30.0	10.0	25.0	13.0	9.0	7.0
<b>1c</b>	Solid state	95.0	traces	--	--	traces	--
<b>1d</b>	Solid state	95.0	traces	--	--	traces	--
<b>1d</b>	Carcerand	--	1.0	--	74.0	24.0	--

Unlike most previous studies that were carried out in the solid state, the current ones are performed in aqueous solution. The results<sup>27</sup> noted within the OA host are

distinctly different from what has been recorded within zeolites, cyclodextrins, and a resorcinarene based cavitand.<sup>189-193</sup> Most importantly, complex of **1b** within an octa acid capsule afforded **6b/7b** exclusively. Whereas, complexes of **1c@OA** and **1d@OA** afforded **6c, d / 7c, d** in 37–92% yields, which is a higher percentage than the one obtained in all other hosts reported in the literature. Photolysis of **1a<sub>2</sub>@OA<sub>2</sub>** gave azine **2a** as the major product; this we noticed was due to the encapsulation of two **1a** molecules together in an OA capsule. Thus, here we can see how the complexation and orientation of the carbene precursors within an OA cavitand can manipulate the product distribution.

Moving on to the Cucurbiturils as the hosts, the intramolecular C–H insertion product **6a** was obtained in >90% yield upon irradiation of **1a** included in CB[7] and CB[8]. To our knowledge for **1a**, no such dominance of formation of intramolecular insertion product in any other medium has been observed. Even in an octa acid capsule with the formation of a 2: 2 complex, **6a** was obtained only in 6% yield. Irradiation of CB complexes of **1b**, **1c**, and **1d** in water gave the intramolecular insertion products **6** and **7** in ca. 50–80% yield, which is again much higher than the values reported in recent literature. The results suggest that the behavior of photochemically generated adamantanylidene within cucurbiturils and cyclodextrins, comparable containers in terms of size and shape, is distinctly different. The molecular geometries of these hosts, though closely similar in dimensions and internal shape, are different. In cyclodextrins with several reactive OH groups, intermolecular reactions directly compete with intramolecular C–H insertions of carbenes **8**. In contrast, the inertness of the CB interior helps to promote intramolecular C–H insertions of **8** and prevents bimolecular reactions with the host, which have been shown for cyclodextrins. Compared to cyclodextrins,

cucurbituril complexes have better solubility in water, making CBs better hosts for conducting reactions in water. The last host in our discussion is Palladium Nanocage (PdNC), irradiation of **1a** included in PdNC resulted in adamantanone **3a** (oxygen addition product) as the major product (85%) and **6a** in 4% yield. Complete removal of oxygen from water was impossible, and we suspect the presence of some residual dissolved oxygen under our experimental conditions. We speculate the dramatic shift in product distribution in favor of adamantanone **3a** within PdNC to be due to the heavy atom Pd favoring the spin interconversion of the singlet adamantanylidene to its triplet state.<sup>202-204</sup> To make sure that azine **2a** is not the precursor of adamantanone, **2a** included within PdNC was irradiated at  $\lambda > 320$  nm. Under this condition no adamantanone was detected. Also, when the photoreaction of **1a**@PdNC was followed by <sup>1</sup>H NMR, no accumulation and disappearance of **2a** was noticed. These observations suggested that formation of adamantanone was not preceded by **2a**. In hydrocarbon solution the major product of photolysis is azine **2a**, which according to one possible mechanism is the product of a reaction between adamantanylidenes and adamantanediazirine. However, this was not formed within CB and was only a minor product within PdNC. Its absence in CB is understandable on the basis that each adamantanediazirine and the resulting adamantanylidene species are individually wrapped by the host CB. Lack of formation of **2a** in spite of presence of three molecules of **1a** within PdNC could be due to either the triplet adamantanylidene's inertness toward **1a** or improper alignment of adamantanediazirine molecules present within PdNC for a bimolecular reaction. Consistent with the results on **1a**, PdNC did not favor intramolecular insertion products **6** and **7** with **1b**, **1c**, and **1d** (<13% yield) but favored formation of the corresponding

**Table 2.7** Relative percentages of the products upon the photolysis of the guests **1a-d**@hosts.

<b>Guests</b>	<b>Media</b>	<b>2</b>	<b>3</b>	<b>5</b>	<b>6/7</b>
<b>1a</b>	D <sub>2</sub> O	5.5	31.0	62.0	1.5
	1a@OA	89.0	5.0	--	6.0
	1a@OA-SiO <sub>2</sub>	--	16.0	--	84.0
	1a@CB[7]	--	6.0	--	94.0
	1a@CB[8]	--	9.0	--	91.0
	1a@PdNC	11.0	85.0	--	4.0
	D <sub>2</sub> O	--	3.0	95.0	2.0
<b>1b</b>	1b@OA	--	8.0	--	92.0
	1b@OA-SiO <sub>2</sub>	--	5.5	--	94.5
	1b@CB[7]	--	44.0	--	56.0
	1b@CB[8]	--	51.0	--	49.0
	1b@PdNC	6.0	90.0	--	4.0
	D <sub>2</sub> O	8.0	2.5	88.0	1.5
	1c@OA	--	55.0	--	45.0
<b>1c</b>	1c@OA-SiO <sub>2</sub>	--	24.0	--	76.0
	1c@CB[7]	--	41.0	--	59.0
	1c@CB[8]	--	21.0	--	79.0
	1c@PdNC	13.0	80.0	--	7.0
	D <sub>2</sub> O	5.0	27.0	62.0	6.0
<b>1d</b>	1d@OA	--	63.0	--	37.0
	1d@OA-SiO <sub>2</sub>	--	20.2	--	79.8
	1d@CB[7]	--	34.0	--	66.0
	1d@CB[8]	--	40.0	--	60.0
	1d@PdNC	4.0	83.0	--	13.0

Irradiation done using medium pressure mercury lamp and 320 nm filter. Reaction was followed by NMR, and following 100% conversion products were analyzed by GC-MS and GC.

adamantanones **3** (>80%). could once again be attributed to the role played by Pd as a heavy atom. Thinking along this line, we are tempted to attribute the lower yield of the corresponding insertion products **6** and **7** and the higher yields of the corresponding adamantanones **3** upon irradiation of CB complexes of **1c** and **1d** (as compared to that obtained from the **1a**@CB complex) to a heavy atom effect of the Cl and Br substituents.<sup>202-204</sup> However, we are unable to offer a rationale for the lower yield (significant as it may be) of the corresponding **6b** and **7b** and the higher yield of corresponding adamantanone **3b** resulting upon irradiation of CB complexes of **1b** as compared to that obtained from the **1a**@CB complex. Finally, the contrasting behavior of CB and PdNC highlights the importance of choosing the right container to achieve the desired goal. While the general characteristics of molecular containers could be understood on the basis of concepts such as “confinement” and “weak interactions”, each one is unique and deserves careful scrutiny.<sup>205</sup> In addition, photoreaction within PdNC suggests a possible involvement of triplet adamantanylidene as opposed to singlet adamantanylidene within CBs.

### 2.2.8 Observations supported by ITC and Computational Studies

One way of determining the host: guest ratio is <sup>1</sup>H NMR titration, which we have extensively used in this project. But there is another technique for finding the host:guest ratio, which is Isothermal Calorimetric studies. Along with the host:guest binding ratio, it gives us other useful information, as to what may be the driving force for the complex formation. Similarly, whereas, 2D NMR techniques like 2D DOSY, COSY and NOESY NMR, can be utilized as experimental probes for understanding the mode, nature and orientation of the complex; computational studies come handy in guesstimating the same.

In this section, we show how these techniques have been used along with the ones mentioned in previous sections to study the encapsulation and photochemistry of the carbene precursors **1a-d**. These experiments have been mostly carried out by Dr. Rajib Choudhury.

**Table 2.8** Binding Constants (K) and Relevant Thermodynamic Parameters for Complexation of Adamantanediazirines with OA at 298 K

Guests	$K_a^a$ ( $M^{-1}$ )	$\Delta G^b$ (Kcal/mol)	$\Delta H^c$ (Kcal/mol)	$\Delta S^d$ (cal/mol)	Stoichiometry
<b>1b</b>	$5.5 \pm 0.6 \times 10^4$	$-6.45 \pm 0.06$	$-12.9 \pm 0.5$	$-21.5 \pm 1.5$	$0.80 \pm 0.05$
<b>1c</b>	$9.9 \pm 0.8 \times 10^5$	$-8.20 \pm 0.04$	$-12.0 \pm 0.1$	$-12.8 \pm 0.4$	$0.91 \pm 0.02$
<b>1d</b>	$1.8 \pm 0.1 \times 10^6$	$-8.52 \pm 0.04$	$-11.87 \pm 0.07$	$-11.2 \pm 0.1$	$0.98 \pm 0.04$

<sup>a</sup> Mean values measured from at least three ITC experiments at 25 °C in 1 mM sodium tetra borate, pH ~9.0. Standard deviations are given in parentheses. <sup>b</sup> Gibbs free energy values calculated from  $K_a$  values. <sup>c</sup> Enthalpy values measured by ITC. <sup>d</sup> Entropic contributions to  $\Delta G$  calculated from  $K_a$  and  $\Delta H$  values. A solvent mixture of DMSO and sodium borate buffer in water (2:3) was used for all the titrations.

Thermodynamic parameters for complexation of **1b-d** with OA were estimated by monitoring the heat changes during titration of the guest into a host OA solution. Since guests **1b-d** were not sufficiently soluble in 100% buffer solution, all ITC experiments were carried out in 40% DMSO + 60% sodium borate buffer solution. The association constant (K),  $\Delta G$ ,  $\Delta H$ ,  $\Delta S$ , and stoichiometry of the complex were obtained by fitting the experimental titration curve with the computed one based on an independent binding model (**Table 2.8**). The binding constants in the range of  $10^4$  to  $10^6 M^{-1}$  suggested the complex to be stable in the above solvent mixture. We believe the complexes should be even more stable in 100% water in which photochemical studies were conducted. High enthalpies of binding ( $\sim -12$  kcal/ mol) could be a result of the tight fit of the adamantyl group within the OA cavitand resulting in stronger van der Waals and C-H--- $\pi$  interactions, and in addition a C-X--- $\pi$  interaction (X=Cl and Br) in the case of **1c** and **1d**.

Negative entropies (range -12 to - 21 cal/ mol) are consistent with the loss of freedom of the guest as it binds to the host OA. Based on ITC data, we believe the binding of **1b-d** to host OA is essentially driven by enthalpic rather than entropic considerations.<sup>206,207</sup>

**Table 2.9** Binding Constants (K) and Relevant Thermodynamic Parameters for Complexation of Carbene Precursors with CB[7] at 298 K.

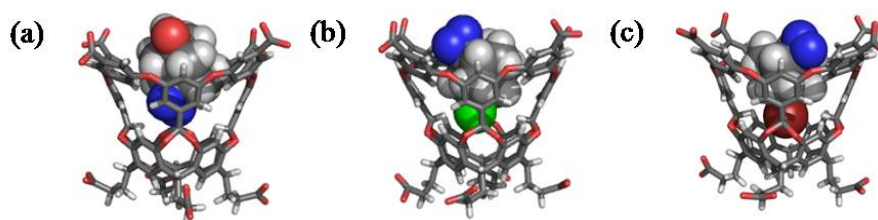
Guests	$K_a^a$ ( $M^{-1}$ )	$\Delta G^b$ (Kcal/mol)	$\Delta H^c$ (Kcal/mol)	$T\Delta S^d$ (cal/mol)	Stoichiometry
<b>1a</b>	$6.5 \pm 0.7 \times 10^5$	$-7.9 \pm 0.06$	$-12.9 \pm 0.1$	$-5.02 \pm 0.2$	$0.9 \pm 0.07$
<b>1b</b>	$1.0 \pm 0.2 \times 10^5$	$-6.8 \pm 0.1$	$-14.4 \pm 0.5$	$-7.59 \pm 0.6$	$0.8 \pm 0.1$
<b>1c</b>	$4.4 \pm 0.4 \times 10^4$	$-6.3 \pm 0.06$	$-15.6 \pm 0.5$	$-9.26 \pm 0.5$	$0.88 \pm 0.03$
<b>1d</b>	$4.6 \pm 0.4 \times 10^4$	$-6.3 \pm 0.05$	$-10.9 \pm 0.1$	$-4.6 \pm 0.1$	$0.92 \pm 0.01$

<sup>a</sup> Mean values measured from at least three ITC experiments at 25 °C in DMSO–water (3:2). Standard deviations are given in parentheses. <sup>b</sup> Gibbs free energy values calculated from  $K_a$  values. <sup>c</sup> Enthalpy values measured by ITC. <sup>d</sup> Entropic contributions to  $\Delta G$  calculated from  $K_a$  and  $\Delta H$  values.

Surprisingly, the entropic loss was much more for the system with the OH substituent **1b** than for the Cl and Br substituted ones (**1c** and **1d**). **Table 2.9** shows the thermodynamic parameters obtained for studying the complexation behavior of **1a-d** with CB[7].<sup>207,208</sup> Thermodynamic parameters for complexation of **1a-d** with CB[7] were determined by monitoring the heat changes during titration of the guest into a host CB solution. Since guests **1a-d** were not sufficiently soluble in aqueous solution, all ITC experiments were carried out in 60% DMSO + 40% water solution. ITC measurements could not be carried out with CB[8] owing to its poor solubility in the above solvent mixture and with PdNC due to lack of programs to deal with 3:1 complexes. The association constant (K),  $\Delta G$ ,  $\Delta H$ ,  $\Delta S$ , and stoichiometry of the complex (guest@CB[7], i.e., guest included in host) were obtained by fitting the experimental titration curve with the computed one based on an independent binding model (**Table 2.9**). The binding constants in the range of  $10^4$ – $10^5 M^{-1}$  suggested all complexes to be stable in the above



solvent mixture. The complexes should be even more stable in 100% water in which the photochemical studies were conducted. Stoichiometry of the host to guest complex (1:1) inferred from ITC data (**Table 2.9**) is consistent with the  $^1\text{H}$  NMR titration studies. Generally, stronger binding to CBs results from Columbic interaction between the negatively polarized carbonyl rim and the positively charged or polarized guest molecules.<sup>16</sup> Such interaction is not expected in the case of **1a–d**. Accordingly, the observed high enthalpies of binding (ca.  $-11$  to  $-16$  kcal/mol) result from van-der-Waals interactions between host and guest. Negative entropies are consistent with the loss of freedom of the guest as it binds to the host. As expected, the gain in enthalpy is compensated by loss in entropy (compare **1c** and **1d** in **Table 2.9**).

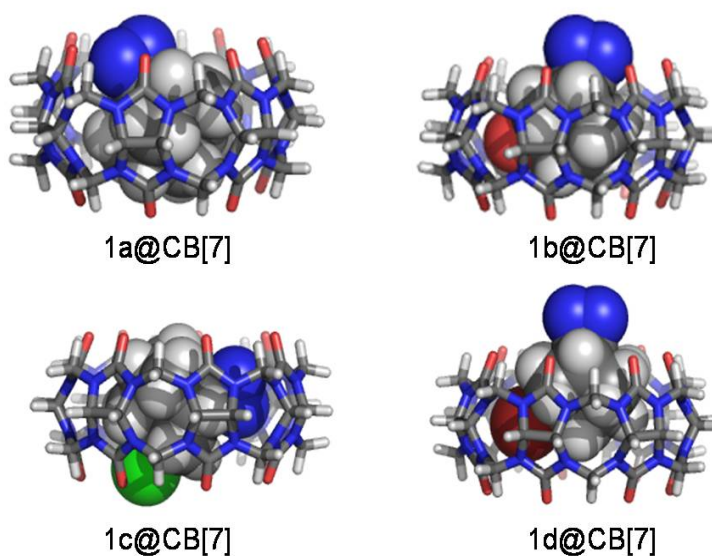


**Figure 2.18** Orientation of the adamantanediazirines in (a) **1b@OA**, (b) **1c@OA**, and (c) **1d@OA** based on molecular dynamics simulations (GROMACS, OPLS-AA force-field). Color code for atoms: C, gray; N, blue; O, red; Cl, green; Br, dark red; H, white.

To gain an insight into the difference in entropic loss between the three molecules, we generated the most likely structure of the three complexes in aqueous solution using the GROMACS program that employs the OPLS-AA force field.<sup>209-212</sup> Most representative structures obtained through the above simulation are provided in **Figure 2.18**. It is readily seen that **1c@OA**, and **1d@OA** have structures different from that of **1b@OA**. As found by 2D NOESY and COSY studies, computational studies also suggest that the hydrophilic group OH points towards the open end of the cavitand OA, interacting with the water molecules outside; whereas, in case of **1c** and **1d@OA**, the

halogen group points towards the narrower end of the cavity hence maximizing the van der Waals interactions.

To gain insight into the structure of the guest@host complexes, we optimized several structures of complexes of **1a–d** with CB[7] at the BLYP/6-31G(d) level of theory using the Gaussian 03 revision D.01 program.<sup>213</sup> The final energies of the optimized structures were improved by performing singlepoint calculations using a 6-311+G(d, p) basis set of the triple- $\zeta$  quality. The dielectric effect of the surrounding water molecules was taken into account using the self-consistent reaction field IEF-PCM method. Of the various structures generated, those with lowest energy in each case presented in **Figure 2.19** clearly show that the bulky adamantyl group is accommodated within the CB cavity and possibly stabilized by van-der-Waals interactions. The structures also suggest that the carbenes that would be generated by photochemical extrusion of nitrogen will be protected to some extent by the cavity in all cases.



**Figure 2.19** BLYP/6-311G (d, p) energy-minimized structures of aziadamantanes within CB[7].

## 2.3 Conclusion

In this report we have shown that carbene precursors **1a-d** form strong host-guest complexes with the organic cavitand octa acid, cucurbiturils and Pd nanocage in water. The nature of the complex (1:1 or 2:2) and orientation of the guest within the host depend on the substituent on the adamantyl framework. Other than **1a**, all other carbene precursors form 1:1 complex with OA, **1a** form a 2:2 capsuleplex. **1a-d** form 1:1 complex with hosts CB[7] and CB[8]. And a 3:1 guest: host complex is formed when **1a-d** are added to PdNC. Although the primary photochemical step is the same in both the presence and absence of octa acid, i.e., formation of a carbene, the resulting final products are distinctly different within a confined space. The formation of large amounts of intramolecular insertion products **6** and **7** within the OA cavitand testifies that there is still room for manipulating reactivity patterns of highly reactive intermediates such as carbenes through supramolecular approaches.

Photolysis of the **1a-d** CB[7]/CB[8] complexes yields products in ratios distinctly different from those in conventional solvents and gas phase. During irradiation, products are believed to arise via carbenes as intermediates. Since carbenes can exist in both singlet and triplet states we tentatively propose that the confined medium may have an effect on the equilibrium between the two states. Thus the spin state control by the confined environment could be used as yet another tool to control product selectivity. CBs favoring intramolecular C-H insertion products may be due to suppression of bimolecular reactions with water and oxygen. Most likely the reactive center is protected by the inert cavity of CB from these reactants. The lifetime of adamantanylidene is reported to be dependent on the water and oxygen content and in dry benzene it is found

to be fairly long (700 ns). In this context, it would be interesting to conduct time-resolved photophysical studies of adamantanediazirines included in various hosts with different internal characteristics. Such studies form a part of our future investigation.

## 2.4 Experimental Section

**Encapsulation of Guest inside Host studied by  $^1\text{H}$  NMR:** For each experiment, a 60 mM stock solution of the guest was prepared in DMSO- $d_6$ , 10  $\mu\text{L}$  of this solution was added to 0.6 mL, 10 mM buffered  $\text{D}_2\text{O}$ , making the concentration of the guest to be  $\sim 1\text{mM}$ , and the  $^1\text{H}$  NMR was recorded at the room temperature. 0.6 mL of 1mM of OA solution was prepared in 10 mM buffered  $\text{D}_2\text{O}$ , and the  $^1\text{H}$  NMR was recorded. To this solution, 10  $\mu\text{L}$  of the 60 mM guest solution was added, the solution was shaken for 5 minutes and the NMR was recorded.

**Stoichiometry of the complexes, determined by  $^1\text{H}$  NMR Titration:** For each experiment, a 60 mM stock solution of the guest was prepared in DMSO- $d_6$ . 1  $\mu\text{L}$  of this solution was added to 0.6 mL of 1mM OA in 10 mM buffered  $\text{D}_2\text{O}$ , making the concentration of the guest to be  $\sim 0.1\text{ mM}$ , the NMR tube was shaken for  $\sim 5$  minutes and the  $^1\text{H}$  NMR was recorded, again another 1  $\mu\text{L}$  of the guest stock solution was added to the above solution, NMR tube was shaken and the  $^1\text{H}$  NMR spectra was recorded. This process was repeated 9 more times.

**Nature of the complexes as determined by DOSY NMR:** Diffusion NMR experiments were performed on Bruker 500 MHz NMR spectrometer. The experiments were performed at 25  $^\circ\text{C}$ , at a host concentration of 1 mM (in 10 mM sodium tetra borate buffered  $\text{D}_2\text{O}$ ). Data was analyzed by using the Bruker Topspin software. Assuming the

complex to be spherical, diffusion constant  $D$  can be calculated according to the following equation:  $R_h = kT/6\pi\eta D$  where  $R_h$  is the hydrodynamic radius of the sphere in meters,  $k$  is the Boltzmann constant,  $T$  is the temperature in Kelvin,  $\eta$  is the solvent viscosity, and  $D$  is the diffusion constant in  $m^2s^{-1}$ . All the calculations and fittings are done with the help of the software.

**Photolysis of the Carbene precursors encapsulated inside the host as studied by  $^1H$  NMR, in solution:**

1:1 ratio of 1mM of the guest@host solution was prepared in 10 mM buffered  $D_2O$ .  $^1H$  NMR of this solution was recorded. Then the solution was evacuated and purged with argon several times. This solution was irradiated inside an irradiation chamber containing medium pressure mercury lamp and 320 nm filter. The  $^1H$  NMR spectra of the solutions were recorded at regular intervals to follow the completion of the reaction. **1a@OA** solution was irradiated for 20 minutes, whereas all other **1b,c,d@OA** were irradiated for 45 minutes.

**Photolysis of the Carbene precursors encapsulated inside the host on silica surface:**

Approximately 1mL of 1mM of the guest@OA solution was prepared in buffered  $D_2O$ . 100 mg of silica was added in the solution and shaken overnight in dark. Later  $D_2O$  was removed and the solid powder was irradiated in a pyrex RB inside an irradiation chamber containing medium pressure mercury lamp. **1a@OA** was irradiated for 1hr, whereas all other **1b,c,d@OA** were irradiated for 2 hrs.

**Photolysis products of the Carbene precursors in water:** Approximately 1mL of 1mM of the guest solution was prepared in  $D_2O$ . Then the solution was evacuated and purged with argon several times. This solution was irradiated inside an irradiation chamber

containing medium pressure mercury lamp and 320 nm filter. The  $^1\text{H}$  NMR spectra of the solutions were recorded at regular intervals to follow the completion of the reaction. All the solutions were irradiated for 3 hours and 15 minutes.

**Photolysis products of the Carbene precursors embedded on silica surface:**

Approximately 1 mL of 1 mM of the guest solution was prepared in  $\text{CHCl}_3$ . 100 mg of silica was added in the solution and shaken overnight in dark. Later  $\text{CHCl}_3$  was removed and the solid powder was irradiated in a pyrex RB inside an irradiation chamber containing medium pressure mercury lamp. All the samples were irradiated for 3 hrs.

**Analysis of the photolysis products and analyzing host OA after irradiation (Inner-molecular Products):**

After the irradiation was over, the products were extracted 3 times using  $\text{CDCl}_3$ , and dried over anhydrous sodium sulfate. The  $\text{CDCl}_3$  solution was concentrated to approximately 0.6 mL and the  $^1\text{H}$  NMR spectra of the products mixture was recorded. Then the solution was further concentrated to approximately 0.1 mL and was injected in the GC. The program used for GC was – starting at 70 °C, held for 5 minutes, applying ramp of 10 °C per minutes, reached to 270 °C and held for 10 minutes. The GC traces gave the percentages of the product obtained. All the reactions were repeated for consistency. The products thus obtained were primarily characterized by  $^1\text{H}$  NMR. The product solution was injected in GCMS. The molecular weight obtained by molecular ion peak and the fragmentation pattern further confirmed their identity. Also, 1, 3-insertion products of aziadamantane and the corresponding azine were synthesized and co-injected with the products obtained. For all other derivatives, it is known from the literature that these aziadamantane derivatives form chiefly 1, 3-insertion products upon thermolysis,

hence they were injected as such in the GC and GCMS, whereupon they would pyrolyze at the injection port, and hence provided the corresponding 1, 3 insertion products. In all the cases, adamantanone and adamantanol and their derivatives were synthesized and co-injected with other products. Corresponding adamantane and its derivatives were commercially available, hence injected as such in GC and GCMS.

**Experimental Procedure for analyzing host after irradiation:** For the control experiment 1mM OA solution in 10 mM buffered D<sub>2</sub>O was taken, to this solution CDCl<sub>3</sub> solution was added and extracted back. The residual OA solution was analyzed by <sup>1</sup>H NMR. For the other cases, for example aziadamantane@OA, the products were extracted by aforementioned technique and the residual OA solution was analyzed by <sup>1</sup>H NMR.

**Encapsulation of Guests in CB[7], CB[8], and PdNC:** For each experiment, a 60 mM stock solution of the guest was prepared in DMSO-d<sub>6</sub>. A 10 μL portion of this solution was added to 0.6 mL of D<sub>2</sub>O, making the concentration of the guest ~1 mM, and a <sup>1</sup>H NMR spectrum was recorded. To a solution of 0.6 mL of 1 mM of CB[7], CB[8], or PdNC D<sub>2</sub>O was added 10 μL of a 60 mM guest solution. The solution was shaken vigorously for 5 min, and the NMR spectra were recorded.

**Stoichiometry of the Complexes As Determined by <sup>1</sup>H NMR Titration:** For each experiment, a 60 mM stock solution of the guest was prepared in DMSO-d<sub>6</sub>. A 1 μL portion of this solution was added to 0.6 mL of 1 mM of CB[7], CB[8], or PdNC in D<sub>2</sub>O, making the concentration of the guest ~0.1 mM. The NMR tube containing the above solution was shaken for ~5 min, and a <sup>1</sup>H NMR spectrum was recorded. This process was repeated by stepwise addition of 1 μL of the guest stock solution. The addition of

guest was stopped when signals due to excess of peaks deriving from unbound guest molecules were detected or broadening of the signals was observed.

**Photolysis of Adamantanediazirines Encapsulated Inside Hosts CB[7], CB[8], and PdNC:**

A D<sub>2</sub>O solution containing a 1:1 ratio of 1 mM of the guest@host for CB[7] and CB[8] and a 3:1 ratio of guest@host for PdNC solution was prepared for irradiation experiments. A <sup>1</sup>H NMR spectrum of the solution prior to irradiation was recorded. The solution was evacuated and purged with argon for 30 min. This solution was irradiated with a medium-pressure mercury lamp (450 W) fitted with a 340 nm cutoff glass filter (Corning O-52). <sup>1</sup>H NMR spectra of the solutions were recorded at regular intervals to follow the completion of the reaction. **1a**@CB[7]:CB[8] and PdNC solutions were irradiated for 45 min, whereas **1b–1d**@CB[7]:CB[8] and PdNC solutions were irradiated for 3 h.

**Characterization of Photoproducts:** After irradiation was complete the products were extracted three times with CDCl<sub>3</sub>. The CDCl<sub>3</sub> solution was dried over anhydrous sodium sulfate and concentrated to approximately 0.6 mL, and a <sup>1</sup>H NMR spectrum was recorded. The solution was further concentrated to approximately 0.1 mL, and was injected into the GC (HP-5). The program used for GC: starting at 70 °C, held for 5 min, applying ramp of 10 °C per min, up to 270 °C, held for 10 min. All reactions were repeated (at least three times) for consistency. The product solution was injected into a GC–MS. The molecular weight obtained from the molecular ion peak and the fragmentation pattern further confirmed the identity of the products. In addition, the 1,3-insertion products from the adamantanylidene **8** and the corresponding azines were



synthesized and co-injected with the products obtained. For all other derivatives, it is known from the literature that these adamantanediazirine derivatives form mostly 1,3-insertion products upon thermolysis. Hence, they were injected as such into the GC and GC–MS, respectively, whereupon they would decompose in the injection port to afford the corresponding 1,3-insertion products. In all cases, adamantanone and adamantanol and their derivatives were synthesized and co-injected with other products. The commercially available corresponding adamantanes and their derivatives were injected as such into GC and GC–MS.

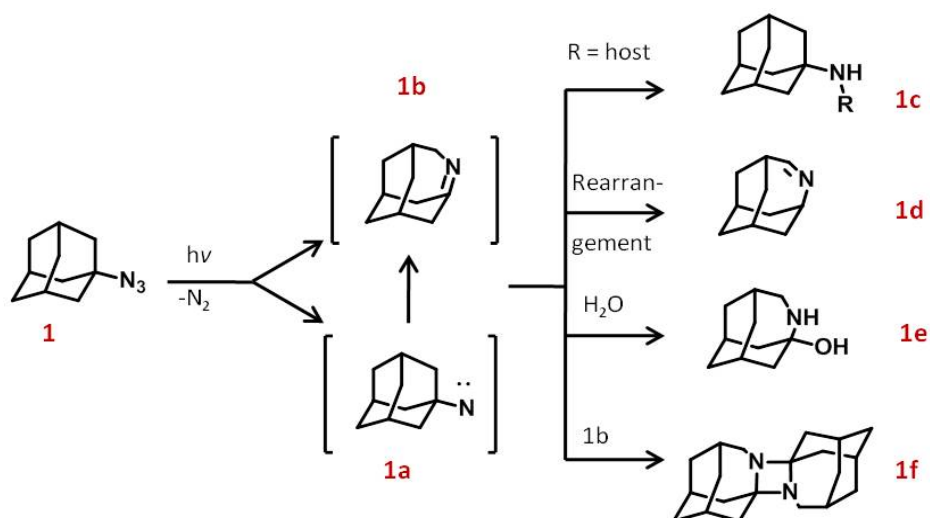
## **CHAPTER 3**

### **Encapsulation and Photoreactions of Nitrene Precursors within Various Host Systems**

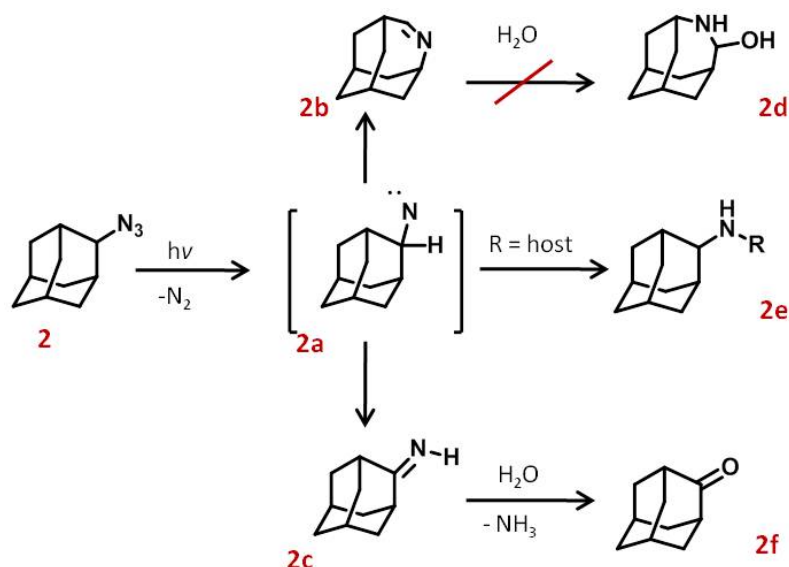
### 3.1 Overview

The chemistry of nitrenes and carbenes is of significant theoretical and practical importance. For example, they can be employed in photoaffinity labeling<sup>214</sup>, and the ring expansion of aryl nitrenes in syntheses of azepines and diazepines.<sup>215</sup> In this chapter our focus is on the reactions of nitrenes encapsulated inside various hosts. The reactions of nitrenes stretch from cycloaddition, to rearrangements, to insertion reactions.<sup>216-217</sup>

Azides<sup>218</sup> have served as nitrene<sup>219</sup> precursors for quite some time. The reactive intermediates are generated after elimination of molecular nitrogen by either thermal or photochemical methods. The mechanism of the photodecomposition of alkyl azides has received considerable attention over the years. There have been proposals that the photolysis of an alkyl azide proceeds via a discrete alkylnitrene intermediate. In the present study we have taken two azides: 1- and 2-azidoadamantanes as the nitrene precursors. The general photoreactions they can undergo are illustrated in **Schemes 3.1** and **3.2**.



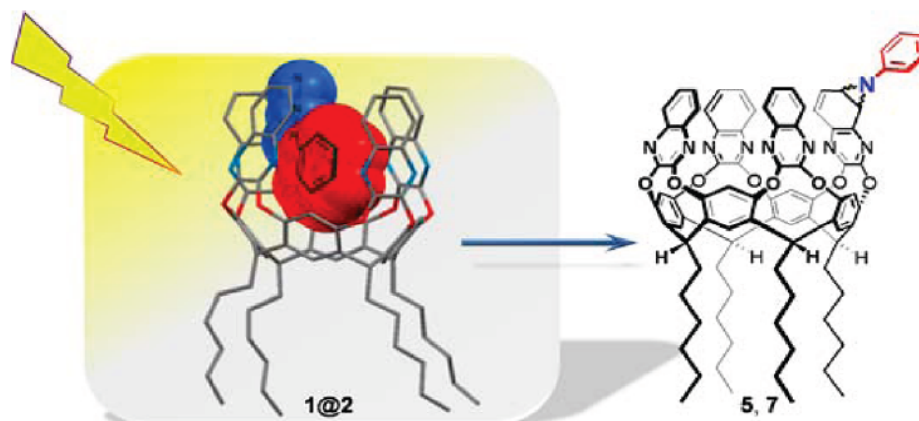
**Scheme 3.1** Photoreaction and possible products from photo-irradiation of 1-azidoadamantane



**Scheme 3.2** Photoreaction and possible products from photo-irradiation of 2-azidoadamantane

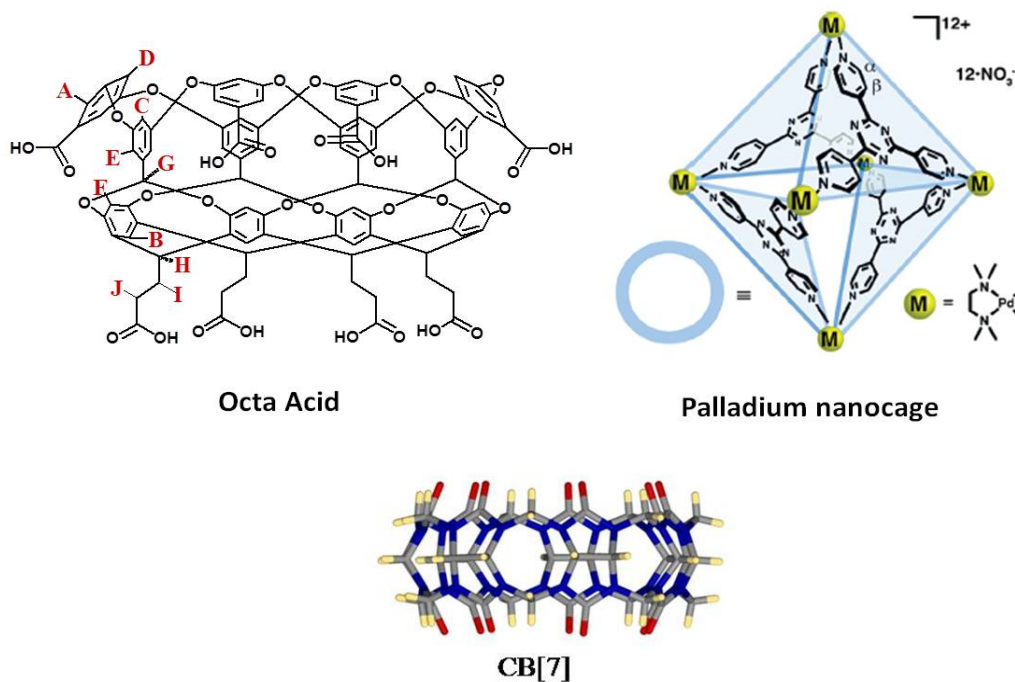
Recent experience shows that nitrenes are powerful tools for photoaffinity labeling. These electron-deficient species can react immediately with surrounding molecules, thus making them useful photoaffinity labels.<sup>220</sup>

Nitrenes have been shown to react with and hence photo-label the host systems in which they were encapsulated. Some recent examples include, nitrene substituted cavitand **5**, **7** shown in **Figure 3.1**. Here phenyl azide has been encapsulated inside this organic cavitand and is then used as a precursor for the generation of nitrene which in turn reacts with the cavitand.<sup>221</sup> In another example, 1- and 2-azidoadamantanes have been encapsulated inside the cyclodextrins and their photolyses is carried out within these hosts.<sup>222</sup> In this article it was probed whether photoaffinity labeling could occur, by intermolecular reaction between the above mentioned guests and host, leading to modified CDs.



**Figure 3.1** Example of a nitrene precursor reacting with the host cavity.

In our quest to understand the reactivity, selectivity and the photoaffinity tendencies of the nitrene precursors 1- and 2-azidoadamantanes, we employed a variety of hosts, like cavitand Octa Acid, Cucurbiturils and Palladium Nanocage, as listed in **Figure 3.2**.



**Figure 3.2** Hosts employed to study the photoreactions of nitrene precursors 1- and 2-azidoadamantanes.

In the present project our paradigm have been to first study the encapsulation behavior of the guests 1- and 2-azidoadamantanes with the hosts mentioned above and then photo-irradiate them to understand their reactivity inside these closed spaces. Both of the above studies have chiefly utilized  $^1\text{H}$  NMR as the basic tool. Though ITC and computational studies have also been utilized, of which the experiments have been carried out by **Dr. Rajib Choudhury**. The photoproducts have been characterized with mass spectrometry, this work have been carried out by **Dr. Jose P. Da Silva**.

On carrying out the photoreactions of nitrenes encapsulated within various hosts, we found that the orientation of the guests, the free space in the host after the guest occupies the inner cavity and the orientation of abstractable hydrogens play an important role in determining the photoproduct and the extent of photolabelling. We hereby present our research work in following sections.

## **3.2 Results and discussion**

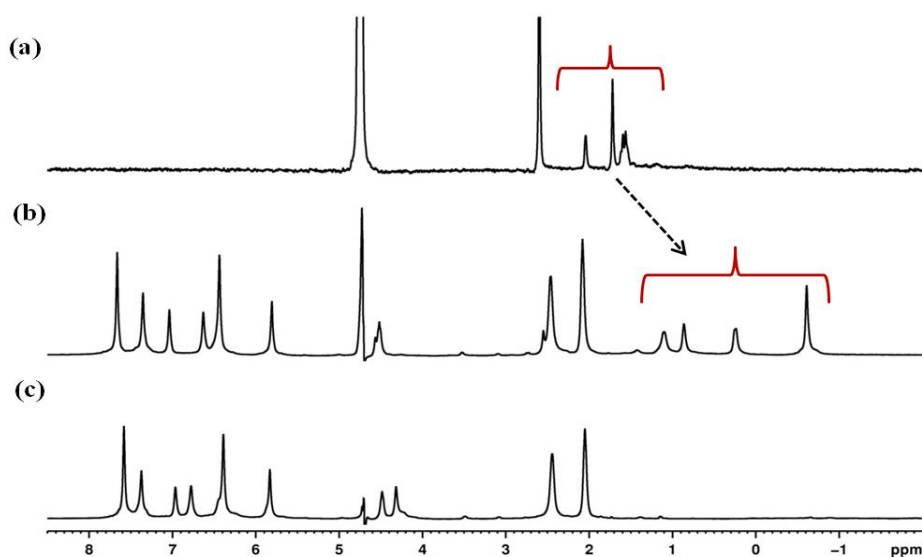
### **3.2.1 Encapsulation and photoreaction of 1-azidoadamantane@OA**

1- azidoadamantane (**1**) being non-polar in nature is sparingly soluble in water formed a stable 1:1 host–guest complex with OA in aqueous borate buffer solution. **Figure 3.3** shows the complexation of 1-azidoadamantane with 1mM OA. It can be noticed that the guest proton signal shifts upfield when the guest is complexed with host OA, in comparison to the guest in sodium borate buffer solution. This characteristic upfield shift signifies the bound nature of the guest to the host OA.

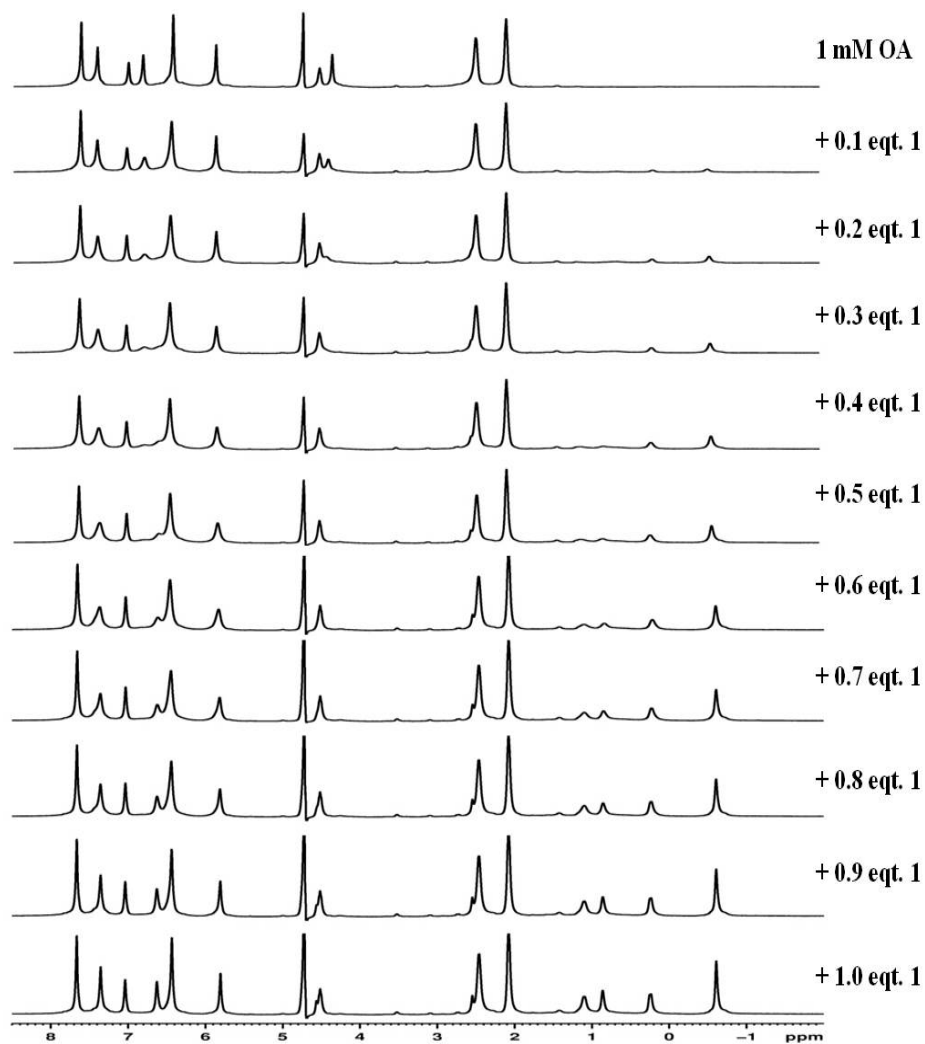
Next came the question as to what could be the guest: host ratio. The host–guest ratio was determined by  $^1\text{H}$  NMR titration experiments. Initially 1 mM OA solution was taken, and to it 0.1 mM guest solution was added step by step and the corresponding

NMR spectrum was recorded. From the  $^1\text{H}$  NMR titration experiment illustrated in **Figure 3.4** it can be noticed that as the guest was added, the bound guest proton signals start appearing in the upfield region. Also, the host proton signals starts broadening, indicating the existence of both complexed and uncomplexed host. As the concentration of guest reaches 1 mM, the host proton signals become sharp. And on the addition of further guest, uncomplexed, i.e. extra guest proton signals could be monitored.

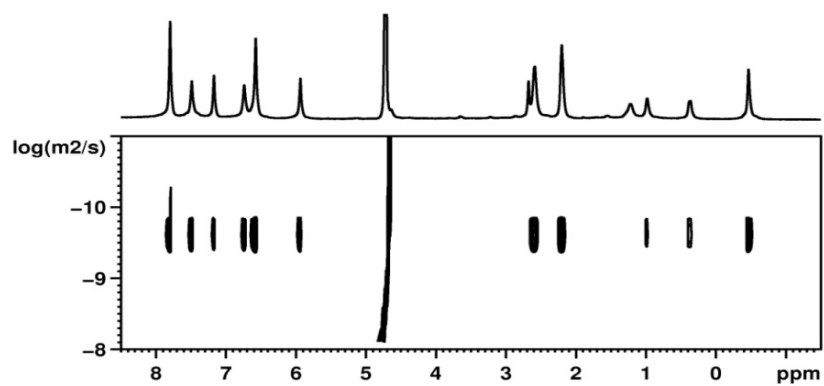
$^1\text{H}$  NMR titration experiments gives us the ratio between the complexed guest and host, but whether the complex is a 1:1 cavitandplex, 1:2 capsuleplex or a 2:2 capsuleplex, could be answered by a 2D DOSY NMR experiment. The diffusion constants obtained by these experiments can actually give a more accurate picture of the complex. The diffusion of free OA is around  $1.8 \times 10^{-6} \text{ cm}^2/\text{sec}$ . whereas; the diffusion constant of **1@OA** comes around  $1.51 \times 10^{-6} \text{ cm}^2/\text{sec}$ . This diffusion constant corresponds to a 1:1 cavitandplex. Hence 1-azidoadamantane forms 1:1 cavitandplex with the host OA. (**Figure 3.5** and **Table 3.1**)



**Figure 3.3**  $^1\text{H}$  NMR spectra of (a) 1-azidoadamantane in buffered  $\text{D}_2\text{O}$ , (b) 1-azidoadamantane@OA, (c) only 1mM OA in buffered  $\text{D}_2\text{O}$ .



**Figure 3.4**  $^1\text{H}$  NMR titration spectra of 1-azidoadamantane with host OA



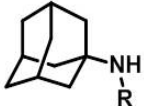
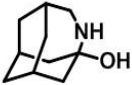
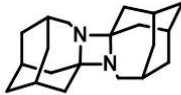
**Figure 3.5** 2D DOSY NMR spectrum of 1-azidoadamantane@OA.



**Table 3.1** Diffusion constant of free OA and **1@OA** as obtained by 2D DOSY NMR

Compound	Diffusion Constant ( $\times 10^{-6} \text{ cm}^2 / \text{sec}$ )
Free OA	1.88
<b>1@OA</b>	1.51

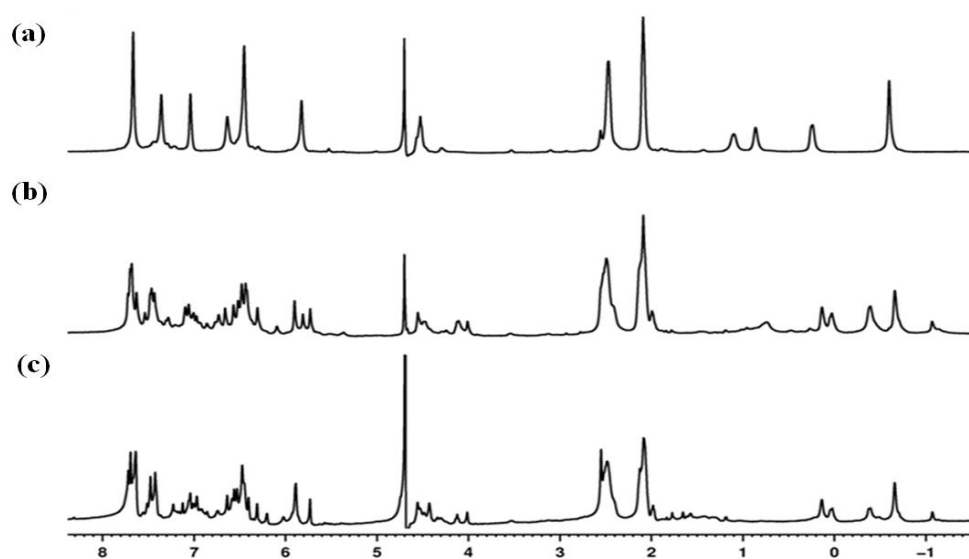
**Table 3.2** Ratio of the photoproducts after the photolysis of **1@OA**.

Media	<b>1c</b>	<b>1e</b>	<b>1f</b>
			
<b>1@OA</b>	86.0	14.0	--

Once it was determined that 1-azidoadamantane formed a stable complex with host OA, the photo-irradiation of the complex was carried out. After purging  $\text{N}_2$  for 30 minutes, the solution of **1@OA** was irradiated using a medium pressure mercury lamp in a pyrex test tube. The progress of the photoreaction was monitored by  $^1\text{H}$  NMR and the completion of the reaction was marked by the disappearance of the bound guest proton signals. The solution thus was treated with  $\text{CDCl}_3$ , to extract the photoproducts. These photoproducts were analyzed with the help of GC and GCMS. **Table 3.2** gives the ratio of the photoproducts after the photolysis of **1@OA**. Please refer **Scheme 3.1** for the labeled compounds.

**Figure 3.6** (b) shows the  $^1\text{H}$  NMR spectrum of the complex after irradiation was complete. It can be observed that the bound guest proton signals disappear whereas some new proton signals, probably corresponding to the photoproduct appear. As mentioned earlier, the solution at this stage was washed with  $\text{CDCl}_3$  to extract any photoproducts

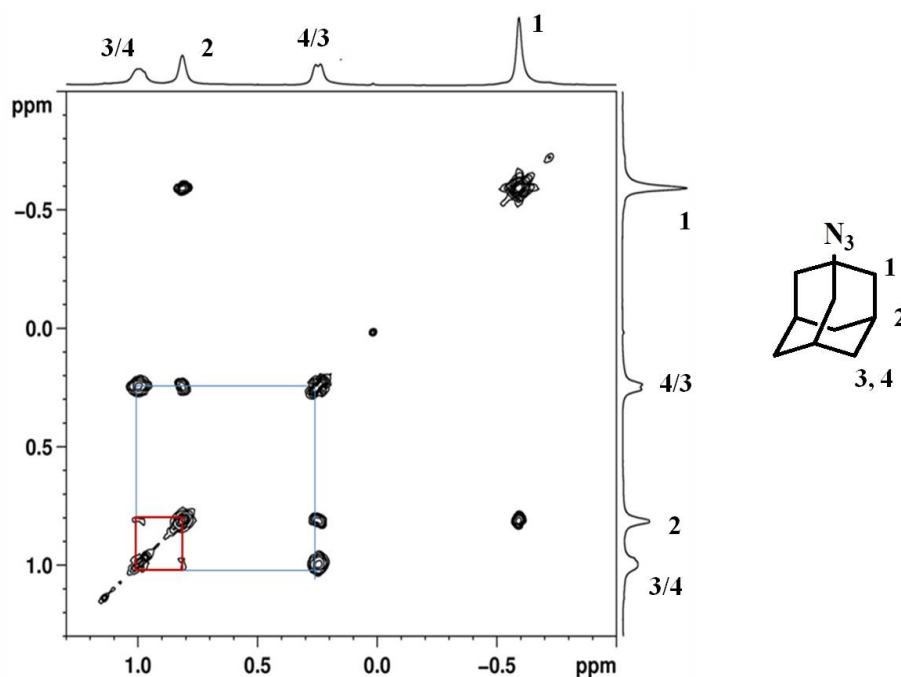
formed. The  $^1\text{H}$  NMR spectrum of the solution after three consecutive  $\text{CDCl}_3$  washes was recorded (**Figure 3.6** (c)). It was observed that some proton signals corresponding to the photoproduct still remained. Also, more importantly, the host proton signals were split and did not come to their original shape, as was expected if all the photoproduct were extracted out and only OA remained in the solution. Hence, this complex was further probed by ESI-MS by Dr. Jose Da Silva, under positive and negative ionization conditions.



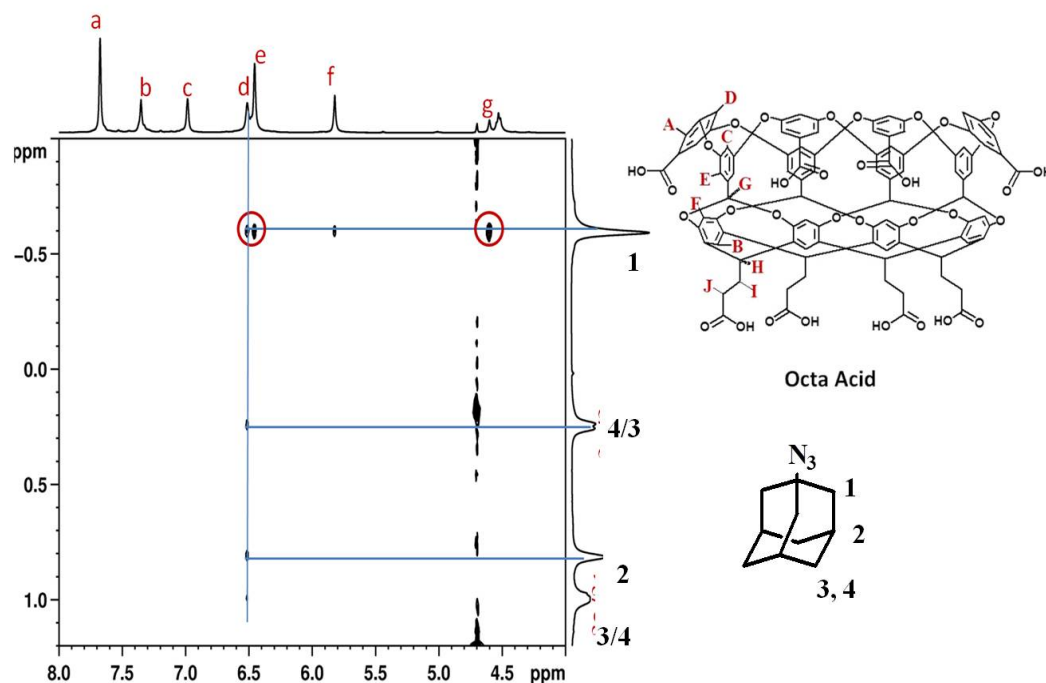
**Figure 3.6**  $^1\text{H}$  NMR spectra of (a)  $\mathbf{1@OA}$  before irradiation, (b) photoproducts of  $\mathbf{1@OA}$  after 40 min of irradiation and (c) photoproducts of  $\mathbf{1@OA}$  after extraction by  $\text{CHCl}_3$ .

**Figure 3.32** in **Section 3.2.8** presents the mass spectrum of the photoproduct monitored under conditions similar to those used for the detection of  $\mathbf{1@OA}$  complex (**Figure 3.30**). A new  $m/z$  value was observed at 938.2 as opposed to 952.6 obtained for  $\mathbf{1@OA}$  complex. However, under hard ionization conditions (desolvation gas flows  $>2$  L/min and capillary exit potentials  $>150$  V), unlike  $\mathbf{1@OA}$  complex (**Figure 3.30**), the ion at  $m/z$  938.2 was stable, suggesting the formation of a covalently linked system.

These two experiments clearly showed the existence of the photoproduct which was the result of a reaction between the generated nitrene and the host OA. In this reaction, the generated nitrene, abstracted the hydrogen “g” of the host which protrudes outward inside the host cavity. 2D COSY and NOESY NMR experiments were done to support these observations. When the guest 1-azidoadamnatane was encapsulated inside host OA, its orientation which could be responsible for the reaction of generated nitrene with the hydrogen “g” of the host was studied with the help of above two experiments as shown in **Figures 3.7** and **3.8**. The 2D COSY NMR experiment was used to assign the guest proton signals and the 2D NOESY NMR experiments based on the intermolecular interactions taking place between the host and the guest gave useful information about the orientation of the guest inside the host OA.



**Figure 3.7** Partial 2D COSY NMR (500 MHz, D<sub>2</sub>O) spectrum of 1@OA. [OA] = 5.0 mM, [1] = 5 mM in 50 mM sodium tetraborate buffer. \* indicates residual water signal.

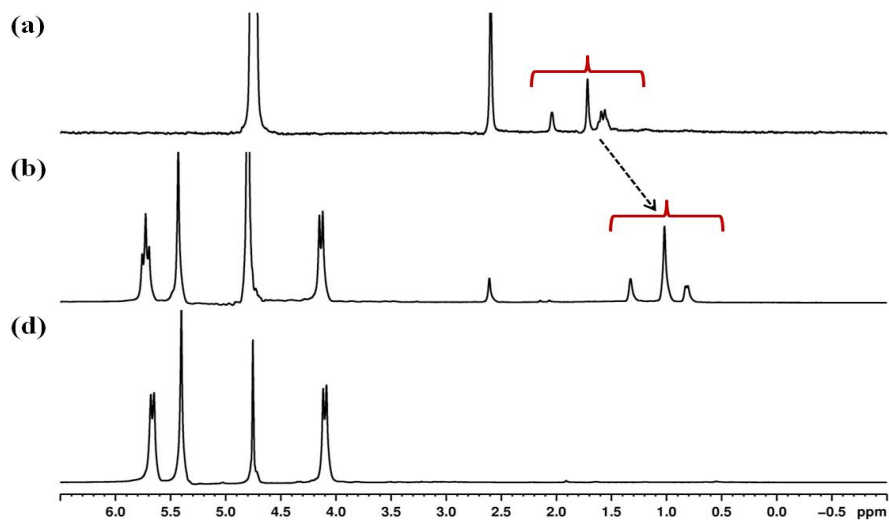


**Figure 3.8** Partial 2D NOESY NMR (500 MHz, D<sub>2</sub>O) spectrum of **1@OA**. [OA] = 5.0 mM, [1] = 5 mM in 50 mM sodium tetraborate buffer.

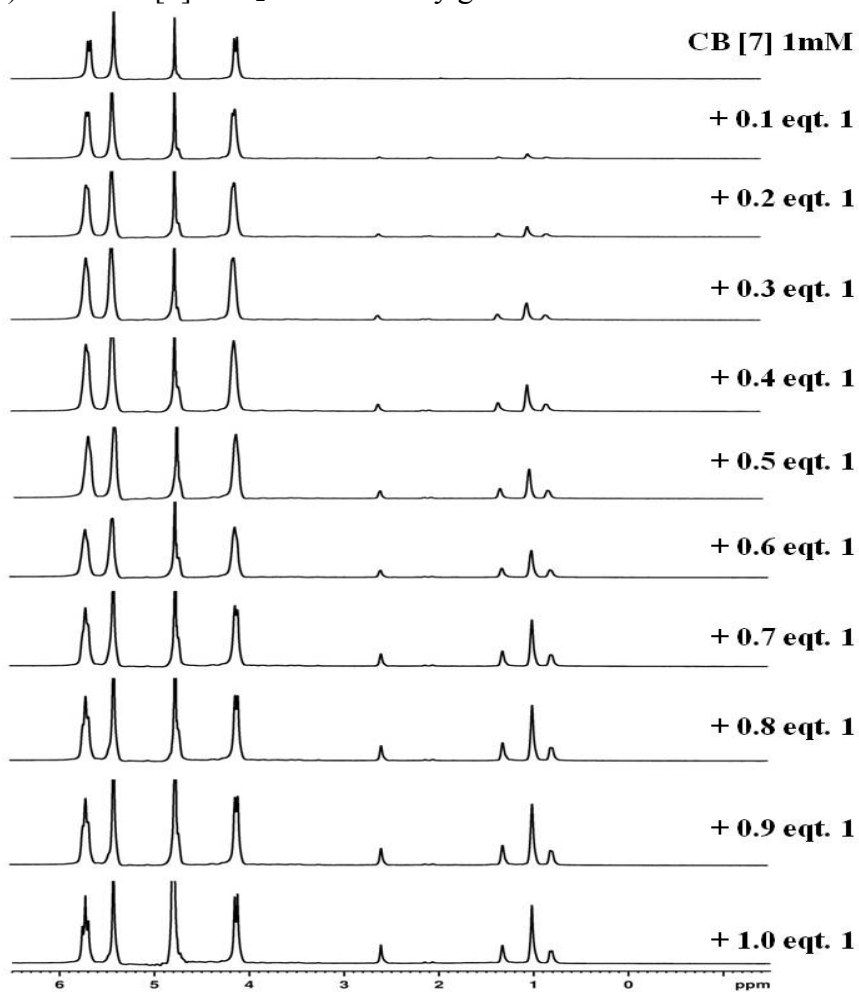
### 3.2.2 Encapsulation and photoreaction of 1-azidoadamantane@CB[7].

After studying the complexation behavior and the photochemistry of 1-azidoadamantane with the host OA, we moved on to another set of hosts-Cucurbiturils. Cucurbiturils have a different shape than host OA. They have a barrel like shape, and are equally opened at both the ends.

**Figures 3.9** shows the complexation of 1-azidoadamantane with CB[7]. It can be noticed, in both the cases, the guest proton signals are upfield shifted in comparison to their position in only buffered D<sub>2</sub>O solution, indicating that the guest is now complexed with the hosts. After this primary experiment, the <sup>1</sup>H NMR titration experiments were done. A <sup>1</sup>H NMR titration of 1-azidoadamantane with 1 mM CB[7] showed that they bind in 1:1 ratio. (**Figure 3.10**)

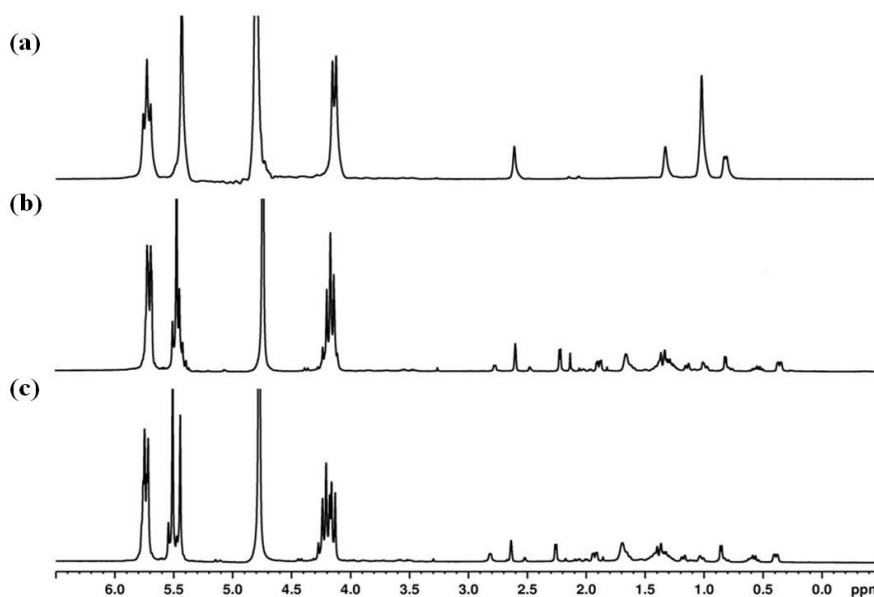


**Figure 3.9**  $^1\text{H}$  NMR spectra of (a) 1-azidoadamantane in buffered  $\text{D}_2\text{O}$ , (b)  $1@CB[7]$  in  $\text{D}_2\text{O}$ , and (c) 1 mM  $CB[7]$  in  $\text{D}_2\text{O}$  without any guest.



**Figure 3.10**  $^1\text{H}$  NMR titration spectra of 1-azidoadamantane with  $CB[7]$ .

Once it was determined that 1-azidoadamantane forms 1:1 complex with host CB[7], the photochemical reaction of the complexes was carried out. After purging N<sub>2</sub> for 30 minutes, the complexes were irradiated using medium pressure mercury lamp in a pyrex test tube. The completion of the reaction was monitored by <sup>1</sup>H NMR. After the irradiation the solution was washed three times with CDCl<sub>3</sub>, to extract the photoproducts.

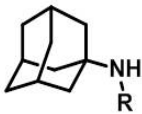
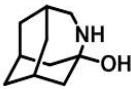
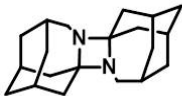


**Figure 3.11** <sup>1</sup>H NMR spectra of (a) **1@CB[7]** in D<sub>2</sub>O before irradiation, (b) photoproducts of **1@CB[7]** after the reaction was complete, and (c) photoproducts of **1@CB[7]** after the solution was washed three times with CDCl<sub>3</sub> to extract the soluble photoproducts

The ratio of the photoproducts thus obtained is listed in **Table 3.3**. In **Figure 3.11** (b) it can be noticed that a set of new proton signals appear in the upfield region of the NMR spectrum signifying the presence of the photoproduct. **Figure 3.11** (c) shows that these proton signals persist even after three washings of the CDCl<sub>3</sub>. One might expect the formation of an inner-molecular insertion compound as was in the case of **1@OA**, hence ESI-MS studies were carried out. In the ESI-MS experiments (covered in detail in **Section 3.2.8**) when photoproducts of **1@CB[7]** complex was treated with methyl

vilogen, the tightly held photoproduct came out of the CB[7] cavity thus confirming that the nitrene generated thereby did not react with the CB[7] cavity. This observation seems logical though. CB[7] cavity has no hydrogen protruding inside of the cavity which might be willing to be abstracted by the *in situ* generated nitrene. The product **1f**, which is probably the result of combination of two nitrenes generated is also not observed, the reason for that could be that no two guest molecules are in close vicinity to react with each other.

**Table 3.3** Ratio of the photoproducts after the photolysis of **1@CB[7]**.

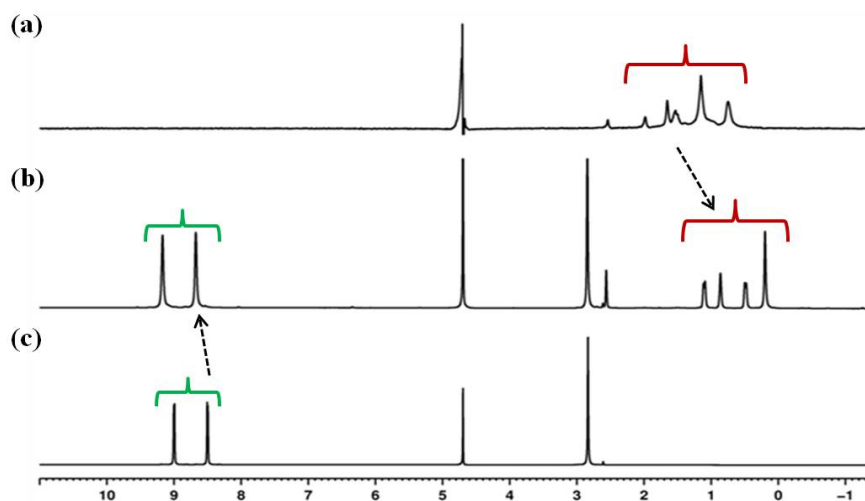
Media	<b>1c</b>	<b>1e</b>	<b>1f</b>
			
<b>1@CB[7]</b>	--	< 95.0	--

### 3.2.3 Encapsulation and photoreaction of 1-azidoadamantane@PdNC

The third host system we have studied with the guest 1-azidoadamantane, is Pd Nanocage (**Figure 3.2**). The reason why we chose this molecule as our next host is that this host molecule is again very different from the ones we used in previous sections, both in terms of shape and size. Pd Nanocage possesses a larger inner cavity, which is octahedron in shape, flagged by Pd on eight corners. Our first step was to check whether 1-azidoadamantane forms a stable complex with the host Pd Nanocage. **Figure 3.12** shows that the guest 1-azidoadamantane proton signals are shifted upfield with respect to their position in only buffered D<sub>2</sub>O, when they are bound to the host PdNC. The host

proton signals too are shifted a bit downfield with respect to their position in unbound state.

**Figure 3.13** shows the  $^1\text{H}$  NMR titration of 1-azidoadamantane with 1 mM of PdNC. Unlike other hosts, the titration experiment shows that PdNC forms a 1:3 host-guest complex with 1-azidoadamantane. It can be observed as the concentration of the guest increases, the intensity of the bound guest proton signal increases too. Also, it is noticeable that the host proton signals gradually broaden and on approaching optimum concentration of the guest, becomes sharp again.

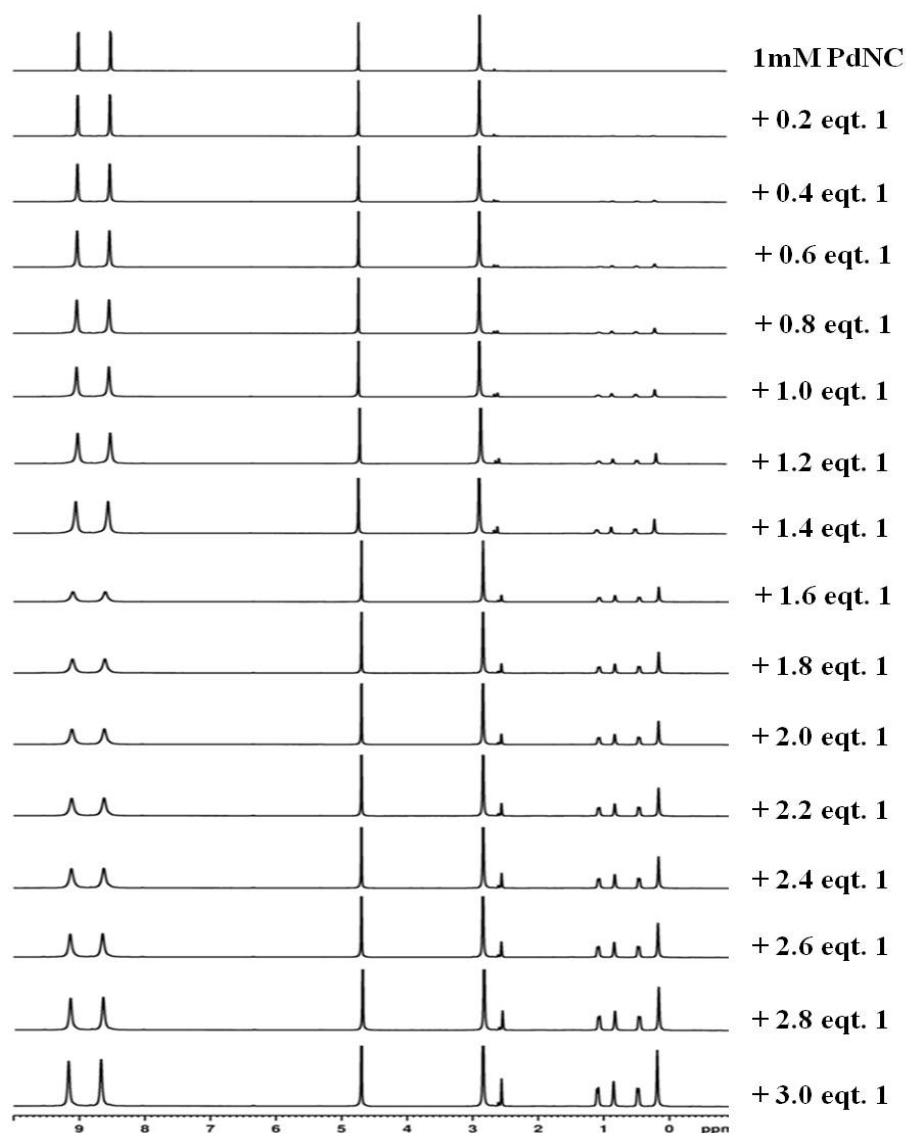


**Figure 3.12**  $^1\text{H}$  NMR spectra of (a) 1-azidoadamantane in buffered  $\text{D}_2\text{O}$ , (b) **1**@PdNC in  $\text{D}_2\text{O}$ , and (c) 1 mM PdNC in  $\text{D}_2\text{O}$ .

After the formation of the complex of 1-azidoadamantane with PdNC, it was irradiated using a medium pressure mercury lamp. The completion of the photoreaction was marked with the  $^1\text{H}$  NMR (**Figure 3.14** (b)). The photoproducts, from the solution were then extracted with  $\text{CDCl}_3$ . The  $^1\text{H}$  NMR spectrum (**Figure 3.14** (c)) of the leftover host PdNC showed that no inner-molecular insertion reaction took place between the generated nitrene and the PdNC. A look at the **Table 3.4** shows that the **1f**, the product formed due to the association of two nitrenes is the major product followed by the


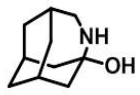
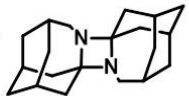


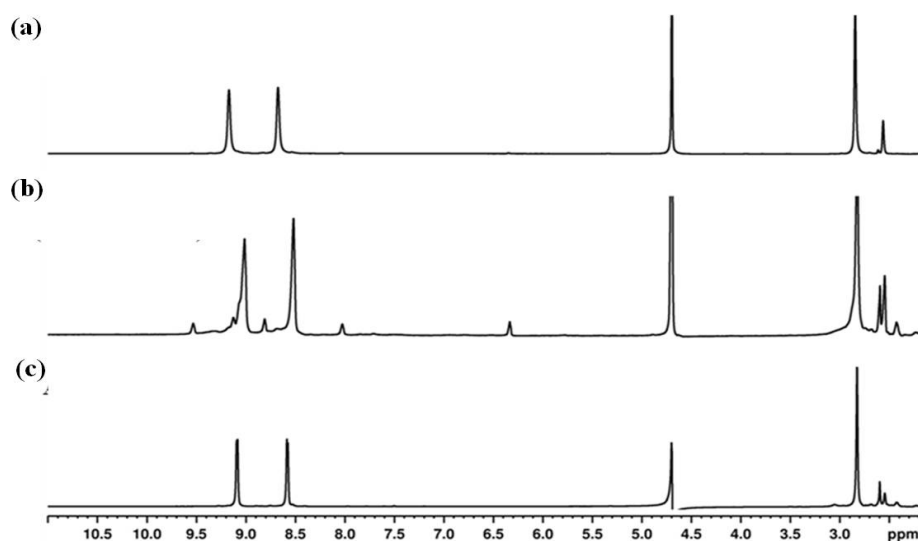
product **1e**. The product obtained here are quite different from the ones obtained in the case of **1@OA** and **1@CB[7]**. The reason for the obtained product set could be the larger cavity size of the host PdNC. PdNC encapsulates three guest molecules, at least two of them are in close proximity of each other to react in an intermolecular fashion to yield product **1f**. And the rest of the guest molecules react with water to form product **1e**, since the cavity is not very hydrophobic in nature and is open to the access of water molecules.



**Figure 3.13**  $^1\text{H}$  NMR titration of 1-azidoadamantane with 1 mM PdNC in  $\text{D}_2\text{O}$ .

**Table 3.4** Ratio of the photoproducts after the photolysis of **1@PdNC**.

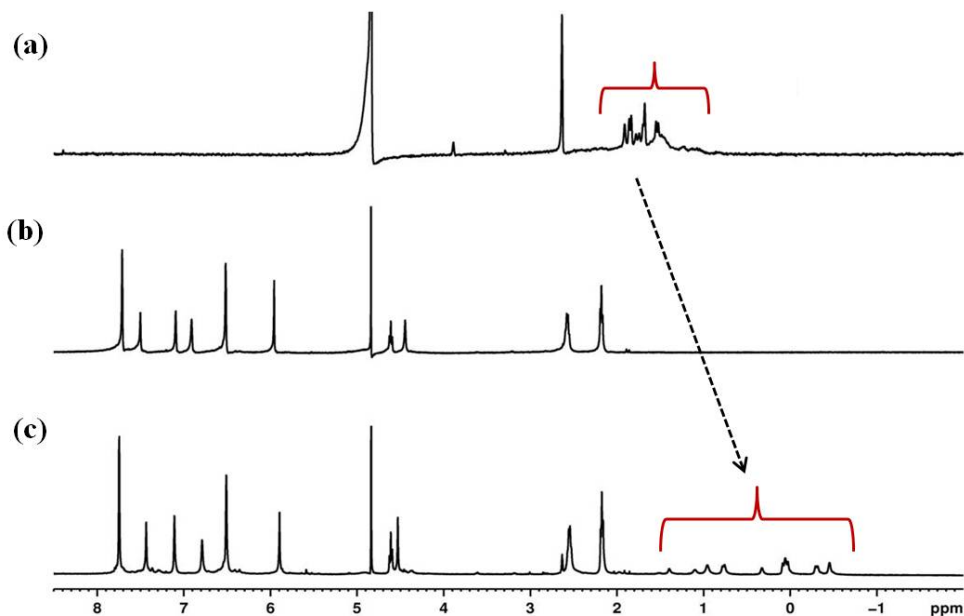
Media	<b>1c</b>	<b>1e</b>	<b>1f</b>
			
<b>1@PdNC</b>	--	41.0	59.0

**Figure 3.14**  $^1\text{H}$  NMR spectra of (a) **1@PdNC** in  $\text{D}_2\text{O}$  before irradiation, (b) photoproducts of **1@PdNC** after the reaction was complete, and (c) PdNC after the solution was washed three times with  $\text{CDCl}_3$  to extract the soluble photoproducts.

### 3.2.4 Encapsulation and photoreaction of 2-azidoadamantane@OA

1- and 2- azidoadamantane, both are nitrene precursors and both have same adamantyl group attached to them, but the major difference between the two, is the position of the azide functional group. Also, the photochemical reactions they undergo are different (**Scheme 3.2**). Unlike 1-azidoadamantane, the endocyclic imine formed is stable and does not readily react with water, on the other hand, the exocyclic imine

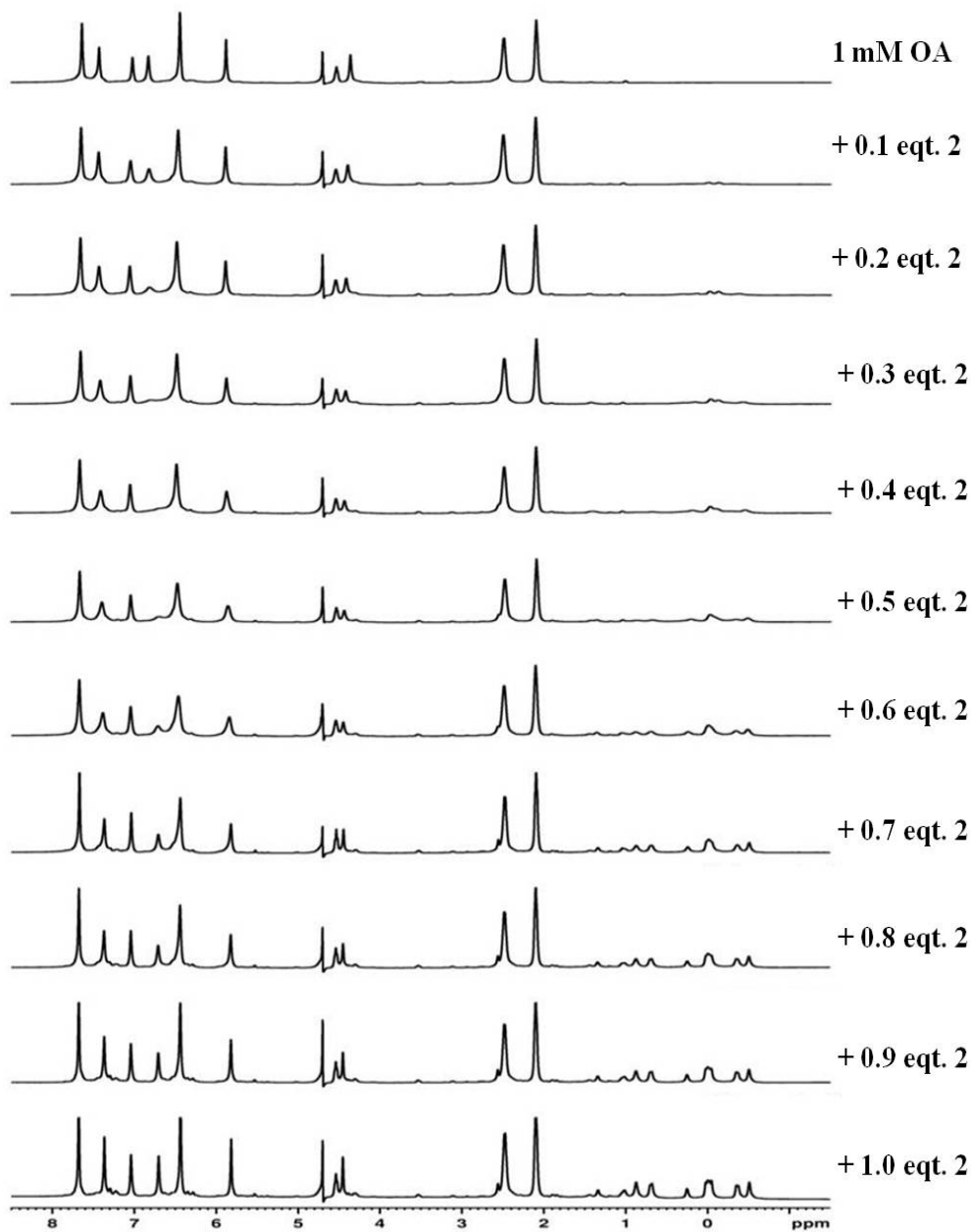
formed reacts with water to give corresponding adamantanone. We expected that the difference in the substituent position of the azide functional group may lead to a different kind of orientation inside the host molecules and hence a difference in the ratio of the photoproducts may be observed.



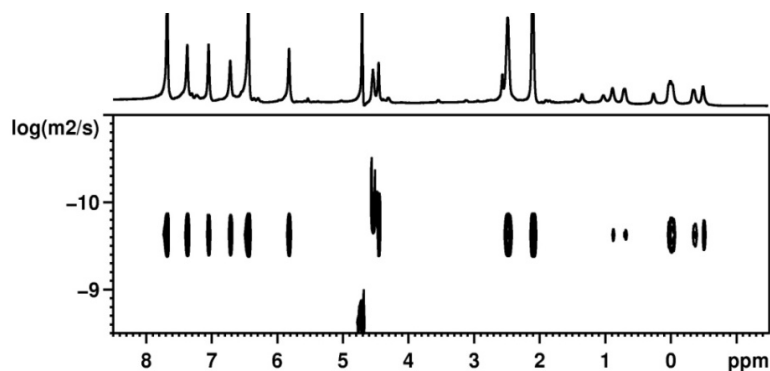
**Figure 3.15**  $^1\text{H}$  NMR spectra (500 MHz) of (a) 2-azidoadamantane in buffered  $\text{D}_2\text{O}$ , (b) only 1mM OA in buffered  $\text{D}_2\text{O}$ , (c) **2@OA**.

In this section we studied the complexation of 2-azidoadamantane with the host cavitand Octa Acid. In the primary experiment we investigated the complexation of the guest with the host. **Figure 3.15** shows that the 2-azidoadamantane proton signals in OA solution are shifted upfield with respect to their position in buffered  $\text{D}_2\text{O}$  solution, indicating the formation of a stable complex between 2-azidoadamantane and host OA. Further  $^1\text{H}$  NMR titration experiments (**Figure 3.16**) were done to obtain the host-guest ratio, which in this case came out to be 1:1. So, we knew that 2-azidoadamantane forms 1:1 complex with the host, but it could be a 1:1 cavitandplex or a 2:2 capsuleplex. To ascertain which one, we carried out 2D DOSY NMR experiments. The diffusion

constants obtained from these experiments (**Figure 3.17** and **Table 3.5**) clearly showed that 2-azidoadamantane forms a 1:1 cavitandplex with the host OA. The ITC experiments done by Rajib Choudhury also confirmed the formation of 1:1 complex.



**Figure 3.16**  $^1\text{H}$  NMR titration spectra of 2-azidoadamantane with 1mM OA.




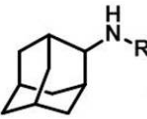
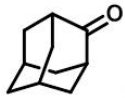
**Figure 3.17** 2D DOSY NMR (500 MHz, room temperature) spectrum of **2@OA**.

**Table 3.5** Diffusion Constants for free OA and **2@OA**, as obtained by 2D DOSY experiments.

Compound	Diffusion Constant ( $\times 10^{-6} \text{ cm}^2/\text{sec}$ )
Free OA	1.88
<b>2@OA</b>	1.56

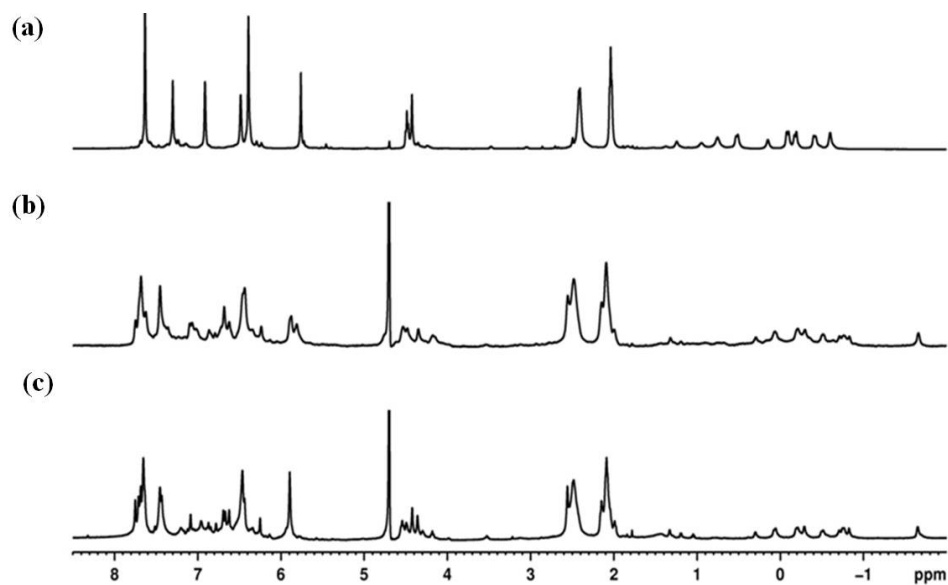
After the complexation experiments, irradiation of **2@OA** was carried out under medium pressure mercury lamp. The completion of the reaction was marked with the  $^1\text{H}$  NMR experiment. It was found that similar to the case of **1@OA**, all the photoproducts do not come out in the extraction of the photo irradiated **2@OA** solution, as can be seen from **Figure 3.18** (c).

**Table 3.6** Ratio of the photoproducts after the photolysis of **2@OA**.

Media	<b>2b</b>	<b>2e</b>	<b>2f</b>
			
<b>2@OA</b>	19.0	71.0	10.0

Hence, the solution was further probed by ESI-MS (**Section 3.2.8**). And it was found that 2 azidoadamantane too, after generating a *in situ* nitrene, forms an inner-molecular insertion with the host OA. The product ratios are listed in **Table 3.6**. Inner-

molecular insertion product being the major product, is followed by the stable imine and adamantanone respectively.

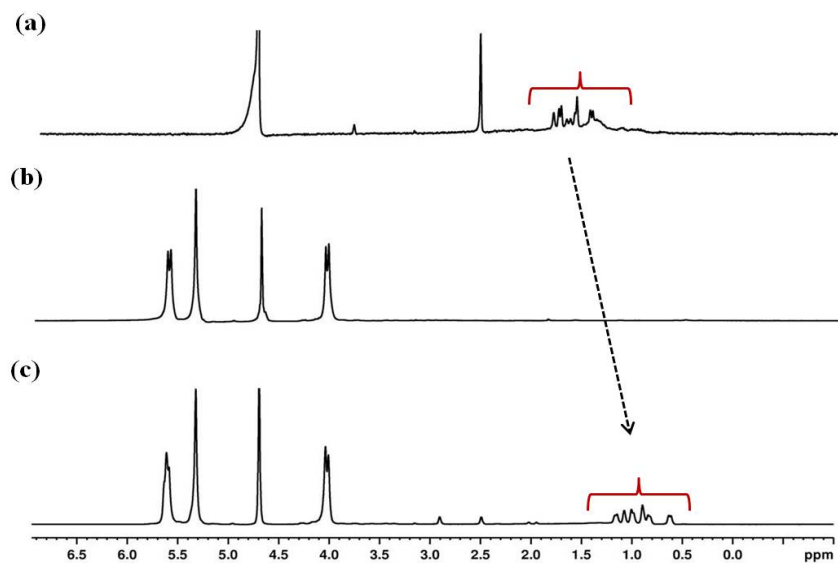


**Figure 3.18**  $^1\text{H}$  NMR spectra of (a)  $2@OA$  before irradiation, (b) photoproducts of  $2@OA$  after 40 min of irradiation and (c) photoproducts of  $2@OA$  after extraction by  $\text{CDCl}_3$ .

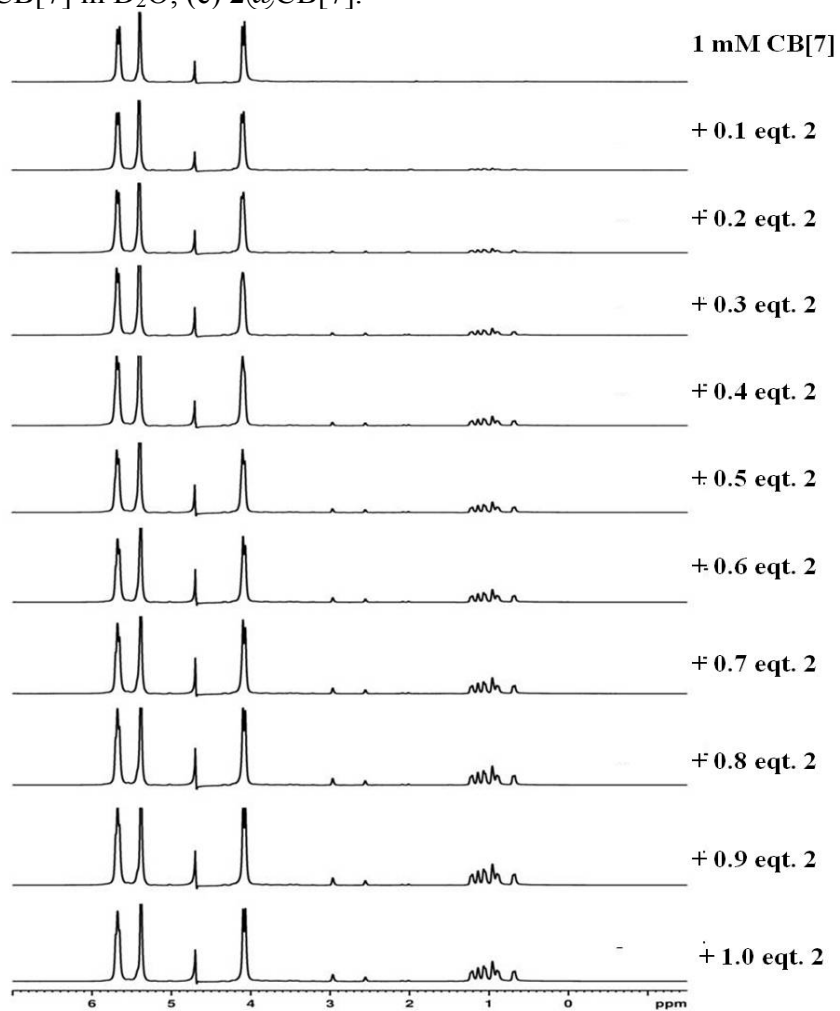
### 3.2.5 Encapsulation and photoreaction of 2-azidoadamantane@CB[7]

Complexation of 2-azidoadamantane with CB[7] was also studied. **Figures 3.19** shows that 2-azidoadamantane binds successfully with CB[7] host molecule. This experiment was followed by the  $^1\text{H}$  NMR titration experiments which showed that both the above host form 1:1 complex with the guest 2-azidoadamantane, as can be seen from **Figures 3.20**.

Once the complexation behavior of 2-azidoadamantane with the host molecule CB[7] was examined, the complexes were irradiated, and the reaction progress was followed by  $^1\text{H}$  NMR. **Table 3.7** gives the ratio of the photoproducts obtained.


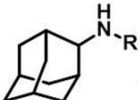
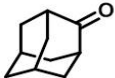


**Figure 3.19**  $^1\text{H}$  NMR spectra (500 MHz) of (a) 2-azidoadamantane in buffered  $\text{D}_2\text{O}$ , (b) only 1 mM CB[7] in  $\text{D}_2\text{O}$ , (c)  $2@CB[7]$ .



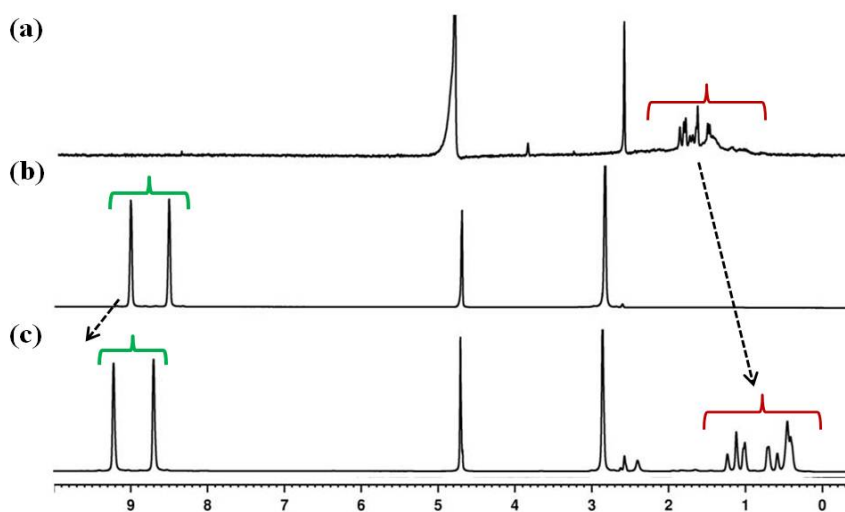
**Figure 3.20**  $^1\text{H}$  NMR titration spectra of 2-azidoadamantane with 1 mM CB[7] in  $\text{D}_2\text{O}$ .

**Table 3.7** Ratio of the photoproducts obtained after the irradiation of **2**@CB[7].

Media	<b>2b</b>	<b>2e</b>	<b>2f</b>
			
<b>2</b> @CB[7]	> 95.0	--	--

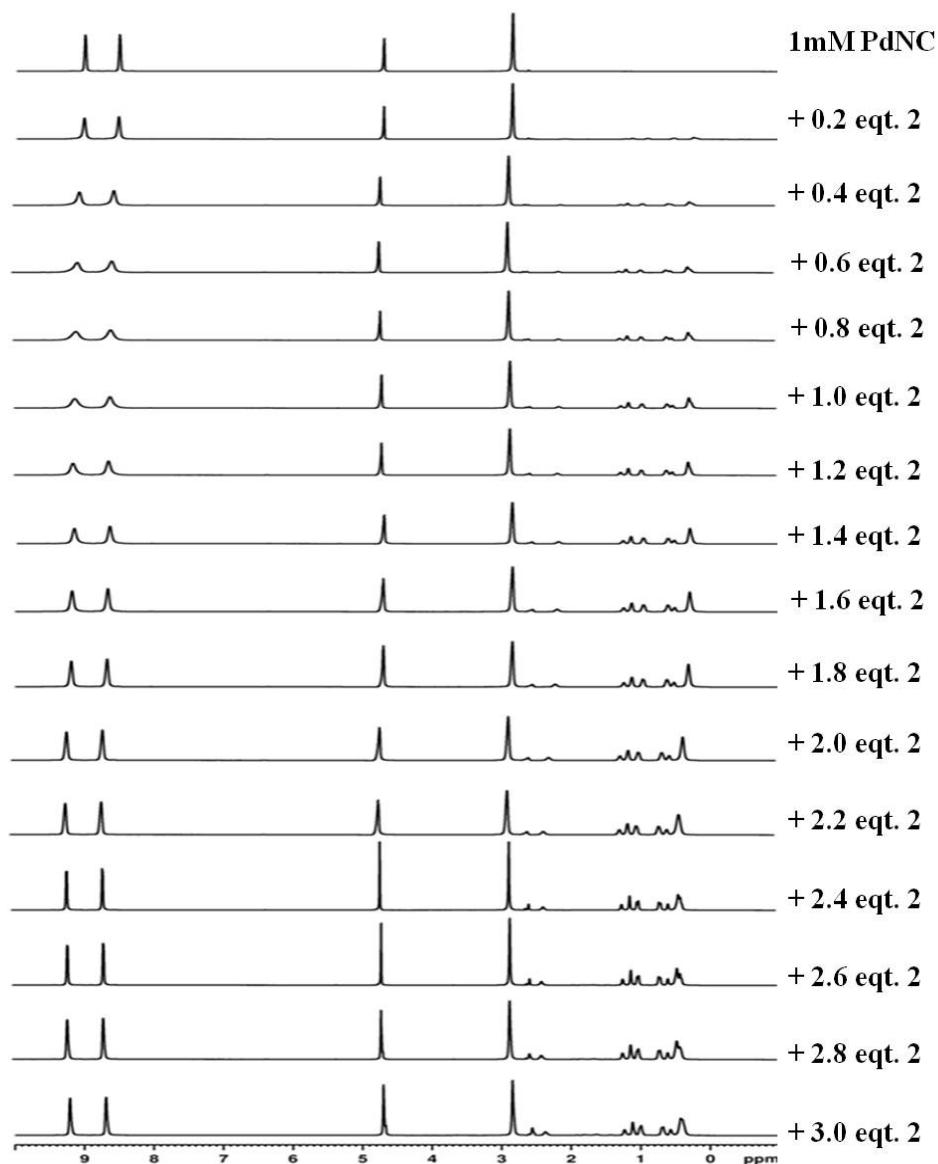
### 3.2.6 Encapsulation and photoreaction of 2-azidoadamantane@PdNC

We investigated the complexation of 2-azidoadamantane with the host Pd Nanocage, and observed that it forms a stable complex with the host PdNC (**Figure 3.21**). A concentrated solution of 2-azidoadamantane was gradually stepwise added to 1mM solution of PdNC in D<sub>2</sub>O, in a <sup>1</sup>H NMR titration (**Figure 3.22**). It was observed that first the host proton signals broadened and then sharpened after reaching the optimum guest concentration, as was observed in the case of 1-azidoadamantane@PdNC. The titration experiment showed that a 1:3 host-guest complex is formed between 2-azidoadamantane and PdNC.



**Figure 3.21** <sup>1</sup>H NMR spectra (500 MHz) of (a) 2-azidoadamantane in buffered D<sub>2</sub>O, (b) 1mM PdNC in D<sub>2</sub>O and (c) **2**@PdNC in D<sub>2</sub>O.




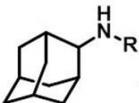
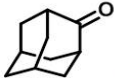


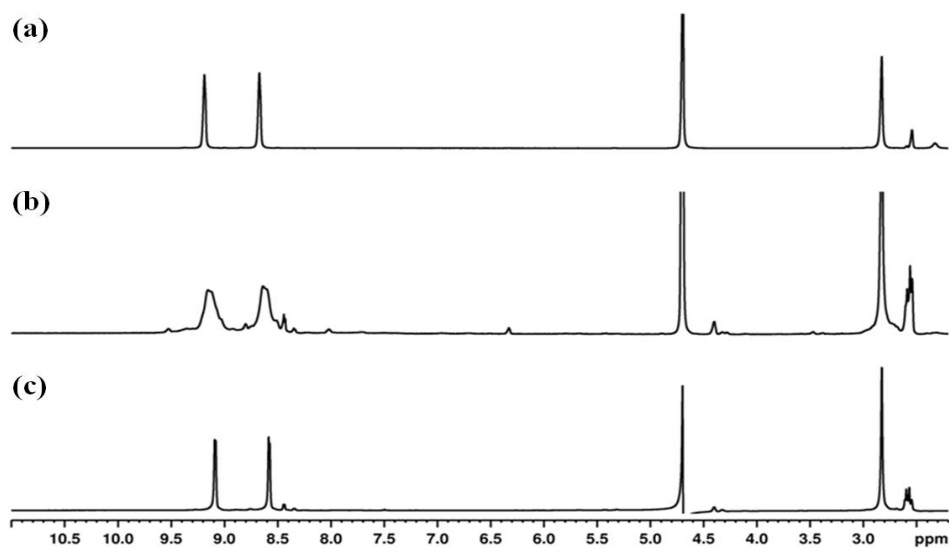
**Figure 3.22**  $^1\text{H}$  NMR titration spectra of 2-azidoadamantane with 1 mM of PdNC.

After the formation of the complex, it was irradiated using a medium pressure mercury lamp for about 40 minutes, in a pyrex test tube. **Table 3.8** shows the ratio of the photoproducts thus obtained. It can be noticed that adamantanone is the major product followed by the endocyclic imine. The reason for the large amount of adamantanone formation could be the open nature of the PdNC cavity.  $\text{H}_2\text{O}$  molecules are easily accessible to the exocyclic unstable imine formed to yield adamantanone. Also, **Figure**

**3.23** shows that the host proton signals are resume to their former shape after the photoproducts are extracted from the irradiated solution, indicating that no inner-molecular insertion reaction has taken place between the generated nitrene and the host cavity, like as observed in the case of **2@OA**.

**Table 3.8** Ratio of the photoproducts obtained after the irradiation of **2@PdNC**.

Media	<b>2b</b>	<b>2e</b>	<b>2f</b>
			
<b>2@PdNC</b>	28.0	--	72.0



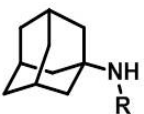

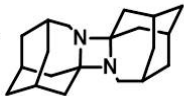
**Figure 3.23** Partial  $^1\text{H}$  NMR spectra of (a) host PdNC before irradiation, (b) host PdNC after 40 min of irradiation and (c) host PdNC after extraction of photoproducts by  $\text{CDCl}_3$ .

### 3.2.7 Comparative studies of 1- and 2-azidoadamantanes included in various hosts.

Being the popular nitrene precursors, photolysis of 1- and 2-azidoadamantanes have been studied extensively. The photoreactions have been carried out in different

media including solid state, alkane solutions and more recently when the above mentioned guests were included in cyclodextrins. In this section we have compiled together the ratio of the photoproducts obtained in various media, including the ones studied by us in this project. By doing so, we hope to compare and increase our comprehension of the role of various media in manipulating the irradiation outcome.

**Table 3.9** Ratio of the photoproducts of 1-azidoadamantane irradiated in various media.

Substrate/Media	<b>1c</b>	<b>1e</b>	<b>1f</b>
			
1-Solid state	--	--	84
1-Alkane	--	--	88
1@ $\alpha$ -CD	--	94.0	--
1@ $\beta$ -CD	--	91.0	--
1@OA	86.0	14.0	--
1@CB[7]	--	> 95.0	--
1@PdNC	--	41.0	59.0

**Table 3.9** gives us the ratio of the photoproducts, when 1-azidoadamantane was irradiated in various media. **1** in solid state chiefly forms **1f**, which is outcome of the nitrene generated attacking the other nitrene. The same result is observed in the case when **1** is irradiated in an alkane solution. The formation of **1f** is justified by the close proximity and approachable distance between the two generated nitrenes in the solid state and the alkane solution. For the next set of irradiation experiment, **1** was encapsulated in  $\alpha$  and  $\beta$  cyclodextrins. In both the case, **1e** was the major product, owing to the open nature of the CD cavity, water molecule have easy accessibility to the nitrenes generated


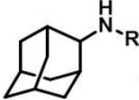
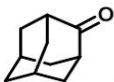
*in situ*. In all the above cases, nitrene generated was not able to undergo inner-molecular insertion reaction with the host. In case, when **1** was encapsulated inside the host OA, we observed that the major product was **1c**. But this was again not the case for **1@CB[7]**, though both the cavities offer a snug fit and a closed environment to the nitrene precursor.

The reason for this, on investigation was found to be the correct orientation of the nitrene precursor inside the cavity, along with the ease in availability of the abstractable hydrogen. In the case of OA, Hydrogen “g” protruding inside the cavity was readily available for the insertion reaction, hence the product **1c**, but in the case of CB[7], no such hydrogen existed. However, when **1** was encapsulated inside the host PdNC, the major products were **1f** followed by **1e**. Here too the close proximity of two nitrene precursors and the open nature of the cavity played an important role in giving **1f** and **1e** as the major product.

Moving on to 2-azidoadamantane (**2**), when **2** is irradiated in solid state, the major product is found to be the endocyclic imine **2b**, followed by some adamantanone **2f**. Though formation of product **2b** is quite straightforward, but the formation of **2f** could be a result of some moisture entrapped in the solid mixture. Irradiation of **2** in alkane solution gave pretty much same kind of product distribution, with the nominal decrease in the product **2f**. When **2** was encapsulated in  $\alpha$  and  $\beta$  cyclodextrins the major products was still **2b** followed by **2f**. Here we have noticed that no inner-molecular insertion product could be formed. But when we irradiated **2** encapsulated inside the host cavitand OA, we found that we get product **2c**, i.e. the inner-molecular insertion product in a quantitative yield. Imine **2b** is the major product in the case of **2@CB[7]**. CB[7] probably provides

nitrene precursor **2** with a shielded cavity hence **2b** is the major product. When **2@PdNC** was irradiated the major product came out to be **2f** followed by **2b**, this observation again could be attributed to the open cavity of the host PdNC.

**Table 3.10** Ratio of the photoproducts of 2-azidoadamantane irradiated in various media.

Substrate/Media	<b>2b</b>	<b>2e</b>	<b>2f</b>
			
2-Solid state	84.0	--	15.0
2-Alkane solution	87.0	--	5.0
2@ $\alpha$ -CD	81.0	--	10.0
2@ $\beta$ -CD	77.0	--	23.0
2@OA	19.0	71.0	10.0
2@CB[7]	> 95.0	--	--
2@PdNC	28.0	--	72.0

### 3.2.8 Mass spectrometry, ITC and Computational experiments done to support the above studies

Though the basic experiments of this projects were based on  $^1\text{H}$  NMR and irradiation of the complexes, but ITC, computational studies, and more importantly ESI-MS studies proved to be very useful in reaching to solid conclusion. The ITC studies done by Rajib Choudhury, were mainly useful for supporting the complexation ratio of the host and the guest as elucidated by the  $^1\text{H}$  NMR titrations.<sup>224</sup> Thermodynamic parameters for complexation of **1** and **2** with OA were determined by monitoring the heat changes during titration of the guest into a host solution. Since **1** and **2** were not sufficiently soluble in aqueous solution, all ITC experiments were carried out in 50%

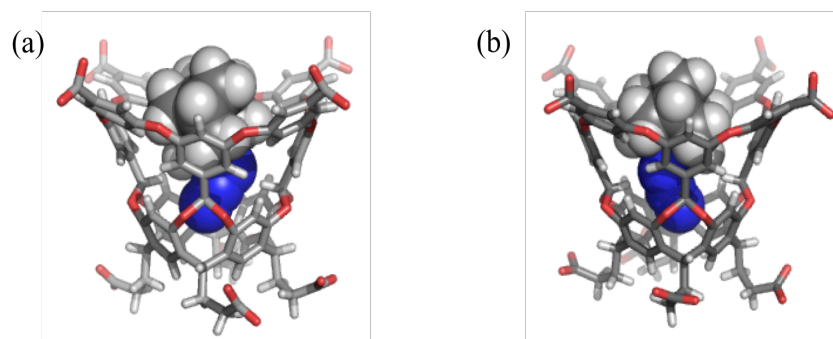
DMSO + 50% water mixture. The association constant ( $K$ ),  $\Delta G$ ,  $\Delta H$ ,  $\Delta S$ , and stoichiometry of the complex were obtained by fitting the experimental titration curve with the computed one based on an independent binding model (**Table 3.11**). The binding constants in the range of  $10^5$ – $10^6$   $M^{-1}$  suggested all complexes to be stable in the above solvent mixture. Since the guest inclusion within host OA is driven by a hydrophobic effect, the complexes should be more stable in 100% water in which the photochemical studies were conducted. We believe that the observed high enthalpies of binding ( $\sim$ ca. 8 kcal/mol) result from van der Waals interactions between host and guest. Stoichiometry of the host to guest complex (1:1) inferred from ITC data (**Table 3.11**) is consistent with the above  $^1H$  NMR titration and 2D-DOSY results.

To visualize the structure of the two host–guest complexes the most likely structures were generated using the molecular docking program AutoDock Vina.<sup>225</sup> Iterated local search global optimizer with Broyden–Fletcher–Goldfarb–Shanno (BFGS) method was used for the local optimization.<sup>226</sup> A rectangular region,  $10 \text{ \AA} \times 9 \text{ \AA} \times 9 \text{ \AA}$  with a grid spacing of  $1 \text{ \AA}$ , was selected to define the binding site of OA. The atomic partial charges were calculated by the Kollman method, and other docking parameters were set as default. The program determined the total interaction energies between random pairs of ligands and various selected portions of OA to determine docking poses. For each guest molecule a total of 10 different poses were obtained, and the structures with lowest energy for **1@OA** and **2@OA** are provided in **Figure 3.24**. It is readily seen from these cartoon representations that the  $N_3$  group in these structures is pointed toward the narrower part of OA.

**Table 3.11** Binding constants (K) and relevant thermodynamic parameters for complexation of 1- and 2-azidoadamantanes with OA at 25 °C.

Media	$K_a^a$ ( $M^{-1}$ )	$\Delta G^b$ (kcal/mol)	$\Delta H^c$ (kcal/mol)	$\Delta S^d$ (kcal/mol)	Stoichiometry
1@OA	$1.95(\pm 0.5) \times 10^6$	$-8.6 \pm 0.1$	$-8.25 \pm 0.3$	$0.36 \pm 0.2$	$0.98 \pm 0.07$
2@OA	$7.04(\pm 0.2) \times 10^5$	$-8.0 \pm 0.02$	$-7.68 \pm 0.1$	$0.34 \pm 0.1$	$0.99 \pm 0.03$
1@CB[7]	$1.20(\pm 0.2) \times 10^6$	$-8.3 \pm 0.1$	$-17.3 \pm 0.3$	$-9.0 \pm 0.3$	$0.90 \pm 0.04$
2@CB[7]	$1.40(\pm 0.2) \times 10^6$	$-8.4 \pm 0.1$	$-14.0 \pm 0.2$	$-5.6 \pm 0.5$	$0.90 \pm 0.004$

<sup>a</sup> Mean values measured from at least three ITC experiments at 25 °C in DMSO-water (1:1). Standard deviations are given in parentheses. <sup>b</sup> Gibbs free energy values calculated from  $K_a$  values. <sup>c</sup> Enthalpy values measured by ITC. <sup>d</sup> Entropic contributions to  $\Delta G$  calculated from  $K_a$  and  $\Delta H$  values. A solvent mixture of DMSO and sodium borate buffer in water (1:1) was used for all the titrations.

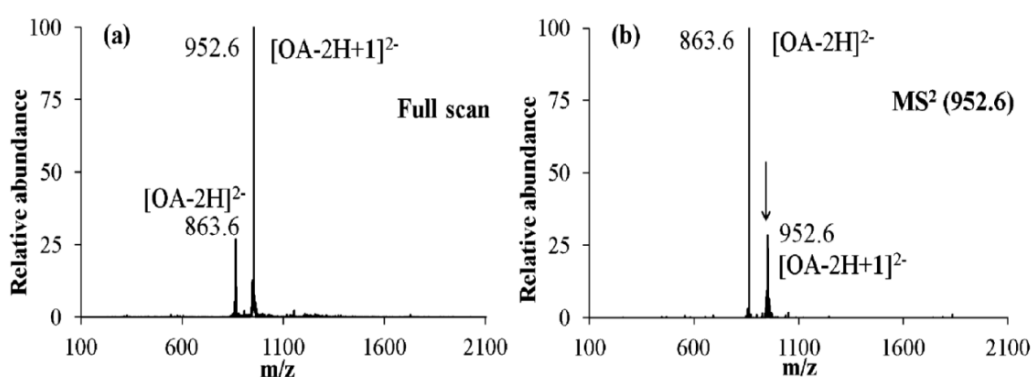


**Figure 3.24** Orientations of the azidoadamantanes in (a) 1@OA and (b) 2@OA based on molecular docking experiment (AutoDock Vina). Color code for atoms: C, gray; N, blue; O, red; H, white.

Further confirmation for formation of 1:1 complex came from electrospray ionization mass spectrometry (ESI-MS) data. This part of the research work has been done by **Dr. Jose P. Da Silva**. The ESI-MS technique provides valuable information regarding the stoichiometry, reactivity, and binding constants of host-guest complexes as well as of higher order supramolecular assemblies in gas phase.<sup>227-229</sup> Employing ESI-MS studies, we recently reported one of the few examples of gas-phase-stable capsuleplexes (2:2 and 2:1) with Octa Amine as host.<sup>230</sup> However, to our knowledge, there are no known examples of stable gas phase complexes of OA. Free OA was readily seen in the gas phase under ESI-MS in both negative and positive polarities. The spray of an aqueous solution of OA containing  $NH_3$  (1  $\mu L/mL$ ) gave rise to peaks at  $m/z$  863.6 ( $[OA - 2H]^{2-}$ ) and 1747.4 ( $[OA + NH_3 + H]^+$ ) in the negative and positive modes, respectively. The

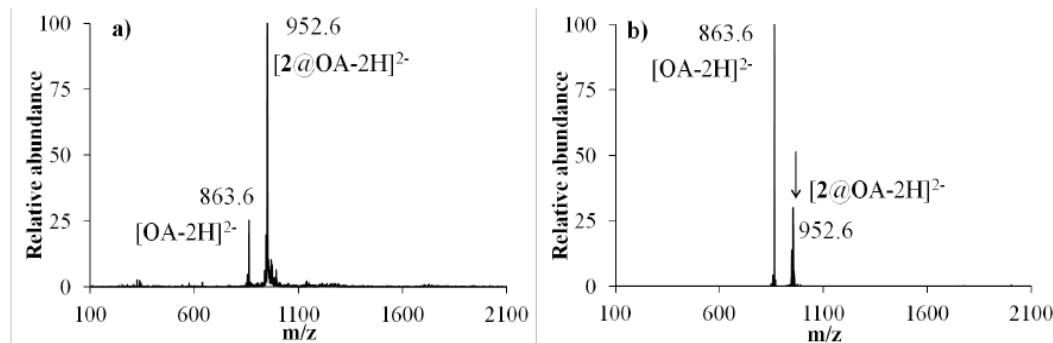
addition of **1** to OA gave rise to a new doubly charged ion peaking at  $m/z$  952.6 (**Figure 3.25 (a)**) under negative ESI-MS. Its fragmentation led to release of the guest and observation of free OA (**Figure 3.25(b)**). We therefore assign the peak at  $m/z$  952.6 to **1@OA** complex.

A similar behavior was observed for **2@OA** (**Figure 3.26**). The azidoadamantane–OA complexes were observed under gentle ionization conditions, namely low desolvation gas flows (<2 L/min) and low capillary exit potentials (<150 V). Under harder ionization conditions (desolvation gas flows >2 L/min and capillary exit potentials >150 V) only free OA was observed, indicating that guest is being released. To our knowledge, this is the first example of a stable gas-phase 1:1 complex of OA host with any guest. As there are no solvent molecules in the gas phase pure hydrophobic effect is absent. The observation of gas-phase stable 1:1 cavitandplexes suggests van der Waals interaction to be likely responsible for the binding and is in agreement with the observed high enthalpies of binding. From the above  $^1\text{H}$  NMR, ITC, and ESI-MS studies it is clear that 1-azidoadamantane and 2-azidoadamantane form stable 1:1 cavitandplexes with OA.



**Figure 3.25** ESI-MS of an aqueous solution of **1@OA** complexes in the presence of  $\text{NH}_3$  (1  $\mu\text{L}/\text{mL}$ ): (a) full scan spectrum; (b) fragmentation ( $\text{MS}^2$ ) of  $m/z$  952.6 (**1@OA**). The arrow indicates the fragmented peak. Assignments:  $m/z$  863.6  $[\text{OA} - 2\text{H}]^{2-}$ ; 952.6  $[\text{OA} - 2\text{H} + 1]^{2-}$ .

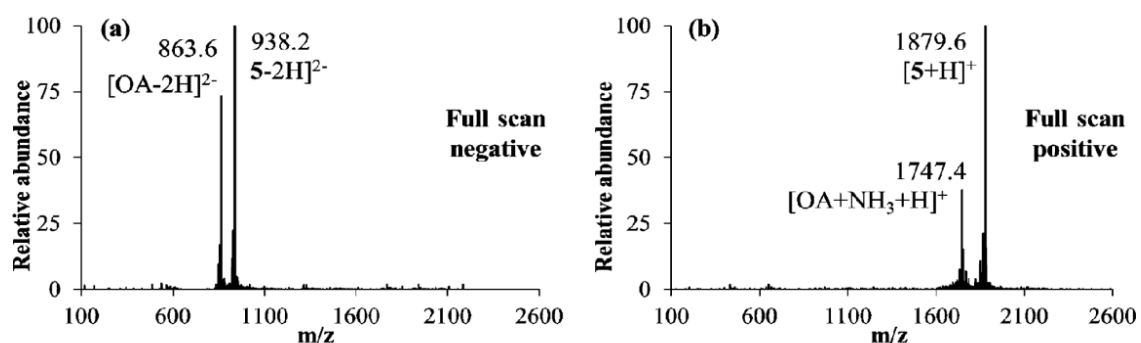




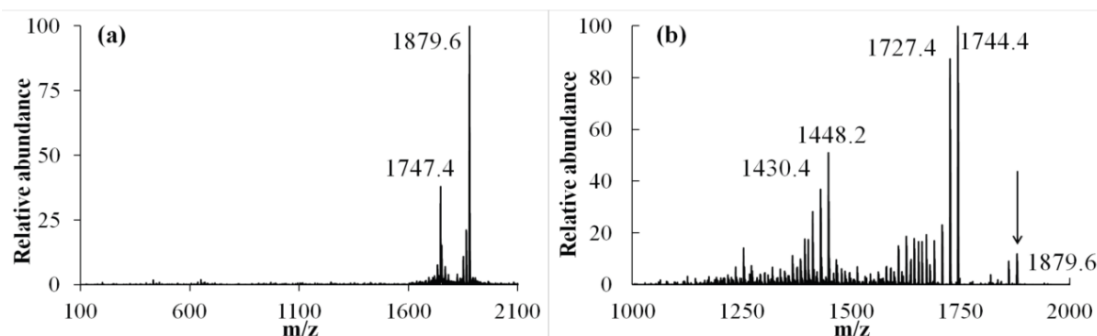
**Figure 3.26** ESI-MS spectra of an aqueous solution of **2@OA** complexes in the presence of  $\text{NH}_3$  (1  $\mu\text{L}/1$  mL). (a) Full scan spectrum and (b) fragmentation ( $\text{MS}^2$ ) of  $m/z$  952.6 (**2@OA**). The arrow indicates the fragmented peak. Assignments:  $m/z$  863.6  $[\text{OA}-2\text{H}]^{2-}$ ; 952.6  $[\text{2@OA}-2\text{H}]^{2-}$ .

The photoproduct **1c** was further probed by ESI-MS under positive and negative ionization conditions to obtain further support for the conclusion that it is the result of reaction between 1-adamantylnitrene and OA. **Figure 3.27 (a)** presents the mass spectrum of the photoproduct **1c** monitored under conditions similar to those used for the detection of **1@OA** complex (**Figure 3.25 a**). A new  $m/z$  value was observed at 938.2 as opposed to 952.6 obtained for **1@OA** complex. However, under hard ionization conditions (desolvation gas flows  $>2$  L/min and capillary exit potentials  $>150$  V), unlike **1@OA** complex (**Figure 3.25 (a)**), the ion at  $m/z$  938.2 was stable, suggesting the formation of a covalently linked system. The fragmentation of  $m/z$  938.2 ( $\text{MS}^2$ ) gave rise to neutral losses of 18 and 44, corresponding to  $\text{H}_2\text{O}$  and  $\text{CO}_2$ , respectively a pattern different from that of **1@OA** complex, in which the release of the guest and free OA formation was observed (**Figure 3.25 (b)**). The fragmentation ( $\text{MS}^2$ ) of the doubly charged negative ion of free OA showed the same neutral losses. These observations are consistent with the photoproduct being a result of a chemical reaction between 1-adamantanylnitrene and OA. ESI-MS under positive polarity gave further insight into the structure of the photoproduct. The spray of an aqueous solution of the photoproduct in

the presence of  $\text{NH}_3$  (1  $\mu\text{L}/\text{mL}$ ) in the positive mode gave rise to a base peak at  $m/z$  1879.6 and to the already observed signal for free OA ( $m/z$  1747.4) (**Figure 3.27 (b)**). The isotope distributions obtained using time of flight (TOF) analyzer and the correspondent theoretical patterns near  $m/z$  1879 are consistent with a product of reaction between the host OA and 1-adamantanylnitrene or a strong noncovalent complex between 1-adamantanylnitrene-derived product and OA. With highly reactive molecules having precedence<sup>231</sup> in being trapped in capsules we fancied that the above mass peak might correspond to a strong noncovalent host–guest complex of the highly reactive **1b** with OA. Unlike the negative ions the fragmentation of the single positively charged OA and photoproduct are different and reflect the presence of the adamantyl moiety in the photoproduct. While the fragmentation of OA indicates the loss of  $\text{NH}_3$  and  $\text{H}_2\text{O}$ , the major losses in the case of the photoproduct are 135 and 150 Da, corresponding to the adamantyl and amino adamantyl moieties, respectively. Based on the above analysis of mass spectral data, we believe that the 1-adamantanylnitrene generated from 1-azidoadamantane has inserted itself at the C–H<sub>g</sub> site of OA.



**Figure 3.27** ESI-MS spectra (full scans) of (a) photolyzed **1@OA** in the negative polarity, (b) photolyzed **1@OA** in the positive polarity. Assignments:  $m/z$  863.6  $[\text{OA} - 2\text{H}]^{2-}$ ; 938.2  $[5 - 2\text{H}]^{2-}$ ; 1747.4  $[\text{OA} + \text{NH}_3 + \text{H}]^+$ ; 1879.6  $[5 + \text{H}]^+$ .

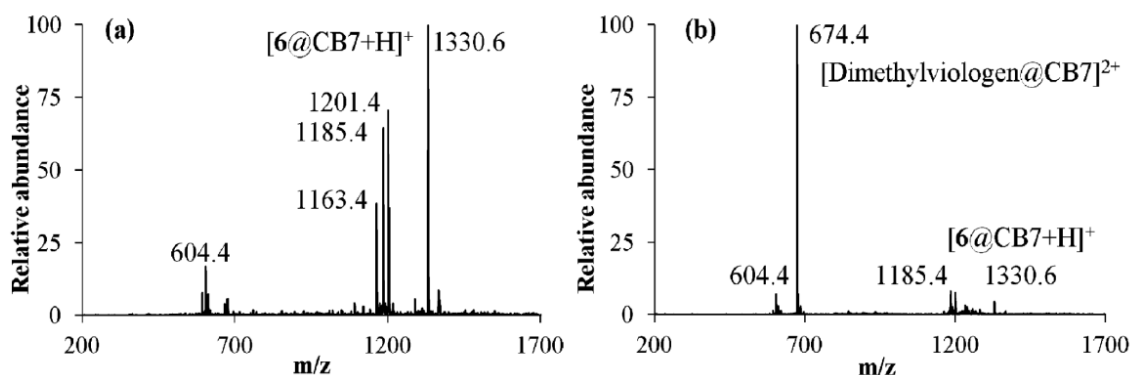


**Figure 3.28** ESI-MS spectra of (a) photoproduct **2e** ( $m/z$  1879.6) in the positive polarity (full scan) and (b) fragmentation ( $MS^2$ ) of  $m/z$  1879.6. The arrow indicates the fragmented peak.

Irradiation of **2@OA** in aqueous borate buffer solution ( $\lambda > 280$  nm) resulted in a nitrene insertion product **2e** similar to **1c** with the  $^1H$  NMR spectrum also bearing close similarity to it. To probe this further, the ESI-MS of the photoproduct was recorded under positive and negative modes. Under the positive mode, the  $m/z$  value (1878.46), the fragmentation behavior, and the experimental and simulated isotope distributions (**Figures 3.28**) support the conclusion that the photoproduct is **2e**.

Mass spectra recorded by ESI-MS technique gave the mass ion corresponding to 1:1 complex for **1@CB[7]** and **2@CB[7]**. The ESI-MS spectrum of the extract of **1@CB7** showed a major peak at  $m/z$  1330.6 (**Figure 3.29** (a)), a value corresponding to a system containing both **1e** and CB[7]. To get further insight into the nature of this ion we performed MS/MS studies. The fragmentation of  $m/z$  1330.6 gave rise to a major peak at 1312.6, which corresponds to the loss of  $H_2O$ , together with free CB[7] at  $m/z$  1163.4 and further fragmentation of former leading to the breaking of the remaining guest and release of CB[7]. The release of guest fragments upon fragmentation of CB host–guest complexes has been reported when the binding is strong.<sup>232, 233</sup> These results could mean either CB[7] was functionalized with 1-adamantyl nitrene or **1e** was tightly held within CB[7]. Interestingly when the ESI-MS of the extract was recorded after the addition of

dimethyl viologen<sup>2+</sup> the signal at 1330.6 gave rise to a new signal at 674.4 corresponding to dimethyl viologen<sup>2+</sup>@CB7 complex (**Figure 3.29** (b)), a result we interpreted as displacement of the photoproduct that was tightly held within CB[7].



**Figure 3.29** ESI-MS spectra (full scans) of (a) photoproduct of **1**@CB7 and (b) photoproduct of **1**@CB7 in the presence of dimethylviologen<sup>2+</sup>. Assignments:  $m/z$  604.4 [CB[7] + 2Na]<sup>2+</sup>; 674.4 [Dimethylviologen@CB[7]]<sup>2+</sup>; 1163.4 [CB[7] + H]<sup>+</sup>; 1185.4 [CB[7] + Na]<sup>+</sup>; 1201.4 [CB[7] + K]<sup>+</sup>; 1330.6 [CB[7] + 6 + H]<sup>+</sup>.

For photoproducts of **2**@CB[7], based on ESI-MS data of the irradiated sample in the absence and presence of dimethyl viologen<sup>2+</sup> and on the fragmentation of the ion at  $m/z$  1312.6 we concluded that the photoproduct **2b** is tightly held within CB[7].

### 3.3 Conclusion

In order to carry out molecular reactions in a nano reaction vessel, with focus on product selectivity, it is important to understand the properties of these vessels. Some important questions in this aspect would be: what is the preferred orientation of the guest inside these, whether these vessels themselves are capable of reacting with the reactive intermediate or not? In order to answer these questions keeping in mind the host systems we extensively use, like Octa Acid, Cucurbiturils and Pd Nanoage, the above study was carried out. In the above studies we studied the complexation behavior of two nitrene

precursors 1- and 2-azidoadamantane followed by their photolyses when encapsulated within these hosts.

The interior of octa acid contains four hydrogens that could be susceptible for abstraction by an excited carbonyl compound, a radical, or a carbene. Thus far, none of them are reported to react with the host OA. We have shown in this presentation that nitrenes generated by photolysis of azidoadamantanes undergo intermolecular C–H insertion and thereby get attached to OA. As far as we are aware this is the first report demonstrating that OA is not as inert as it is believed to be. This observation suggests that one needs to be watchful when using OA as the host. Along with OA, we have been employing cucurbiturils as reaction cavities in our research. In this case, the abstractable hydrogens are at the exterior. As expected, there was no functionalization of CB when photolysis of azidoadamantanes included in CB was carried out. However, we were surprised to note that the product was non-covalently bound to the host and could not be extracted by conventional means. The product had to be displaced with the help of a stronger binding guest. Also, Pd Nanocage though a very useful for carrying out selective photo-dimerization reactions<sup>234</sup>, was unable to show such selectivity of the products in the photolyses of nitrene precursors.

In summary, it would be worthwhile for organic chemists to study new nitrenes, new methods to generate nitrenes, and the reactions of nitrenes within various nanocontainers, which might act as a template to the more prominent or interesting building blocks found in biochemistry (and in medicinal chemistry).

### 3.4 Experimental Section

**Materials:** Hosts octa acid, cucurbit[7]uril and azidoadamantanes, and 3-hydroxy-4-azatricyclo[4.3.1.1]undecane (**1e**) were prepared as reported in literature.<sup>46,235,236</sup> All other chemicals of the highest available purity were purchased from commercial suppliers.

#### **Nature of the Complexes Probed by 1D <sup>1</sup>H NMR and 2D DOSY NMR experiments:**

To 0.6 mL of a D<sub>2</sub>O solution of host OA (1 mM OA in 10 mM Na<sub>2</sub>B<sub>4</sub>O<sub>7</sub>) in an NMR tube were added increments of 0.25 equivalents of guests (2.5 μL of a 60 mM solution in DMSO-d<sub>6</sub>) followed by a 5 min sonication after each addition, and <sup>1</sup>H NMR recorded. Formation of the complex was monitored by the gradual increase in intensity of bound guest signals. After addition of 1.25 equiv of guest, signals due to free, unbound guest were observed. To a solution of 0.6 mL of 1 mM of CB[7] in D<sub>2</sub>O was added 10 μL of a 60 mM guest solution, the solution was shaken vigorously for 5 min, and the <sup>1</sup>H NMR spectra were recorded. For the titration experiment 1mM of CB[7] solution in D<sub>2</sub>O was prepared to this 1.0 μL of 60 mM guest solution was added in steps of 0.1 equivalent. For the titration experiment of 1- and 2- azidoadamantane with the host PdNC, 1mM of PdNC solution was taken in D<sub>2</sub>O, to this 1.0 μL of 60 mM guest in DMSO-d<sub>6</sub>, was added in steps of 1 equivalent until the concentration of the guest reached 3 mM. The diffusion constants (D) of the complexes were determined by diffusion ordered spectroscopy (2D DOSY NMR), a technique useful in separation based on <sup>1</sup>H NMR signals and, in particular, as a supramolecular entity is expected to diffuse slower than the smaller individual components. All diffusion experiments were performed on a 500 MHz NMR instrument at 25 °C. The concentration of both host and guest was 1 mM in 10 mM sodium tetraborate buffer. Formation of the complexes was monitored by adding guests

(10.0  $\mu\text{L}$  of a 60 mM solution in  $\text{DMSO-d}_6$ ) to a host solution (1 mM in 10 mM sodium tetraborate buffer) followed by sonication for 5 min.

### **Experimental Procedure for Photolysis and Characterization of Products:**

Photolysis was performed by irradiation with a medium pressure mercury lamp (450 W) of guest@host complex in sodium tetraborate buffer solution contained in a Pyrex tube ( $\lambda > 280 \text{ nm}$ ), after purging with nitrogen for 30 min. The conversion was confirmed by comparison of the  $^1\text{H}$  NMR spectrum of the solution prior to irradiation and 1D  $^1\text{H}$  NMR spectroscopy post irradiation. Complete conversion of reactants to products was observed for **1@OA** and **2@OA** complexes after irradiation for 40 min ( $\lambda > 280 \text{ nm}$ ), while **1/2@CB[7]** solutions were irradiated for 1 h. After the irradiation, the products were extracted five times using  $\text{CDCl}_3$  and dried over anhydrous sodium sulfate. The  $\text{CDCl}_3$  solution was concentrated to approximately 0.1 mL and was injected into the GC. The GC program used for OA samples: starting at 70  $^\circ\text{C}$ , held (for 1 min for OA and 2 min for CB[7]), applying ramp of 10  $^\circ\text{C}$  per min, up to 270  $^\circ\text{C}$ , held for 10 min. All reactions were repeated (at least three times) for consistency. The product solution was injected into a GC–MS. The molecular weight obtained from the molecular ion peak and the fragmentation pattern confirmed the identity of the products. Comparison with authentic sample further confirmed the identity of the products. On the other hand, the aqueous extract was concentrated to 0.6 mL and further 1D and 2D NMR (COSY, NOESY) experiments were performed.

### **Mass Spectrometry:**

**Sample Preparation.** The ESI-MS studies of OA and OA photoproducts were performed using 100  $\mu\text{M}$  aqueous solutions prepared with Milli-Q water containing 1  $\mu\text{L/mL}$  of

ammonia. The host–guest complexes were prepared in a 1:1 ratio at 100  $\mu\text{M}$  concentration and using a 50 mM stock solution of each guest in DMSO and Milli-Q water with 1  $\mu\text{L}/\text{mL}$  of ammonia. The solutions were sonicated for 10 min and allowed to equilibrate for 30 min before analysis. The complexes were also prepared by addition of a single crystal of the solid guest to a 100  $\mu\text{M}$  solution of the host, followed by sonication for 30 min and equilibration overnight. Similar spectral distributions were obtained for both methods but the signal intensities are lower when DMSO is used. The CB[7] complexes were prepared by addition of a single crystal of the solid guest to a 100  $\mu\text{M}$  solution of the host, followed by sonication for 30 min and equilibration overnight.

#### **ESI-MS System:**

ESI-MS spectra were obtained using mass spectrometers equipped with time-of-flight (TOF) and ion trap analyzers. The ions were continuously generated by infusing the aqueous sample solution into the source at 4  $\mu\text{L}/\text{min}$ . The solutions were studied in the negative and positive polarities. For the observation of host–guest complexes of OA soft desolvation conditions are required. Typical experimental conditions for the observation of these host–guest complexes in negative polarity were: capillary voltage (CE): 3.0 kV; capillary exit voltage:  $-80$  V; skimmer voltage:  $-15$  V; drying gas temperature:  $300$   $^{\circ}\text{C}$ ; drying gas flow: 1 L/ min; nebulizer gas pressure: 40 psi. Host–guest complexes with CB7 can be observed under positive polarity in the following conditions: capillary voltage (CE):  $-4.0$  kV; capillary exit voltage: 105 V; skimmer voltage: 35 V; drying gas temperature:  $300$   $^{\circ}\text{C}$ ; drying gas flow: 6 L/ min; nebulizer gas pressure: 30 psi. The photoproducts with OA as well as the host–guest complexes of the photoproducts with CB7 can be seen in a wide range of spray and ion optics conditions. Typically the main



parameters in the positive polarity were: capillary voltage (CE): -4.0 kV; capillary exit voltage: 300 V; skimmer voltage: 100 V; drying gas: 300 °C at 6 L/min; nebulizer gas pressure: 40 psi.

#### **Preparation of Compounds 1c and 2e:**

**Compound 1c-** Compound **1c** was obtained after photolysis of **1@OA** complexes by irradiation with a medium-pressure mercury lamp (450 W) in sodium tetraborate buffer contained in a Pyrex tube ( $\lambda > 280$  nm), after purging with nitrogen for 30 min. After irradiation, the products were extracted five times using  $\text{CDCl}_3$ . The organic layer was discarded and the aqueous extract was concentrated to 0.6 mL and further 1D and 2D NMR (COSY, NOESY) experiments were performed.  $^1\text{H}$  NMR (500 MHz,  $\text{D}_2\text{O}$ )  $\delta\text{H}$ : -0.94 (1H), -0.65 (6H), -0.4 (3H), 0.05 (3H), 0.18 (3H), 2.1 (8H), 2.5 (8H), 4.4 (2H), 5.7–5.9 (6H), 7.6–7.8 (9H). HRMS (ESI): calculated for the first peak of the isotope series of  $\text{C}_{106}\text{H}_{80}\text{O}_{32}\text{N}$   $[\text{M} + \text{H}]^+$  1878.4658, found 1878.4543.

**Compound 2e-** Compound **2e** was prepared following the procedure described for compound **1c** but using **2@OA** complexes.  $^1\text{H}$  NMR (500 MHz,  $\text{D}_2\text{O}$ )  $\delta\text{H}$ : -1.7 (2H), -0.9 (1H), -0.85 (2H), -0.75 (1H), -0.55 (2H), -0.35 (2H), -0.2 (2H), 0.4 (1H), 1.35 (1H), 2.1 (8H), 2.5 (8H), 5.9 (4H). HRMS (ESI): calculated for the first peak of the isotope series of  $\text{C}_{106}\text{H}_{80}\text{O}_{32}\text{N}$   $[\text{M} + \text{H}]^+$  1878.4658, found 1878.4454.

## **CHAPTER 4**

**Photolysis Studies of Triplet Nitrene Precursors**

**Encapsulated Inside Octa Acid Cavitand**

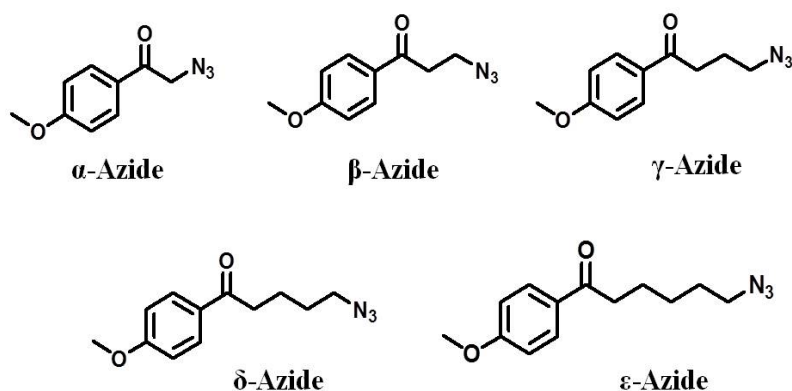
## 4.1 Overview

Singlet nitrene intermediates are useful in applications such as photoaffinity labeling, crosslinking polymers, and modification of surfaces.<sup>237-245</sup> The use of singlet nitrenes in these applications is due to their ability to insert efficiently into surrounding chemical bonds.<sup>246</sup> The most suitable nitrenes are those that insert more efficiently than they rearrange or intersystem-cross to their triplet state. In the last Chapter (**Chapter 3**), we investigated the photolysis of alkyl azides converting into most probably singlet nitrenes, which underwent H-abstraction reaction with the host Octa Acid, to afford a modified host OA.<sup>64</sup>

In this Chapter, we investigated the photolysis of nitrene precursors, encapsulated within the host cavitand Octa Acid, which were designed to produce corresponding triplet nitrenes. It has been theorized that triplet nitrenes have potential applications as organic magnets due to their high spin properties.<sup>247-249</sup> However, high-spin nitrene units can only be assembled from triplet nitrenes that are highly unreactive. Furthermore, singlet alkylnitrene cannot intersystem cross to their triplets, because the energy gap is too large. Therefore, we have to depend on sensitization. And hence, their use in photoaffinity labeling and surface modifications can also be complicated by H-atom abstraction reactions. Thus, to use triplet nitrenes in useful applications, it is essential to be able to predict whether the triplet nitrenes decay by H-atom abstraction processes. Also, azido aryl ketones are valuable in organic synthesis and can be transformed to yield a wide variety of organic molecules such as heterocyclic compounds.<sup>250, 251</sup>

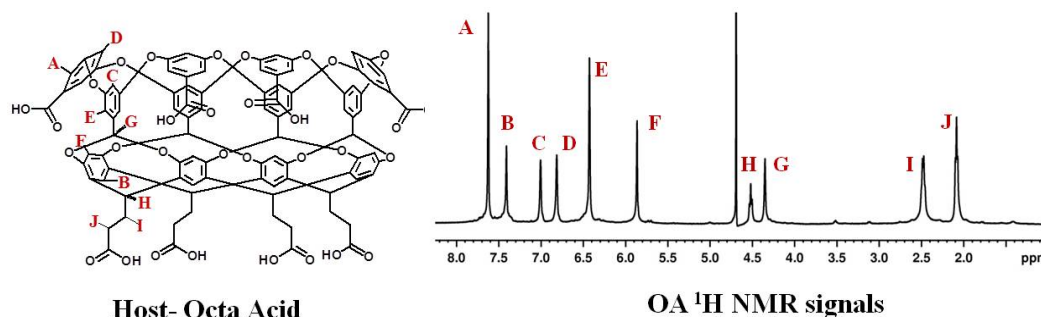
It has been known that the excited state of various ketones and aromatics can be quenched by alkyl azides.<sup>252</sup> Hence, the azido aryl ketones were designed in a way that

they possess both the parts- aromatic ketone and alkyl azide. The aromatic ketone serves as intramolecular triplet sensitizer for generating triplet nitrenes from the alkyl azide.



**Scheme 4.1** Chemical structures of the azido aryl ketones, used as guests in this study.

The chemical structures of the guests used in this study are shown in **Scheme 4.1**. These azido aryl ketones have been provided by **Dr. Anna Gudmundsdottir**, from University of Cincinnati. It has been shown that the photolysis of these azido aryl ketones, leads to products that come from trapping triplet alkyl nitrene intermediates.<sup>253</sup> For this study we have a series of azido aryl ketones, starting from alpha to epsilon azide. Each azide undergoes photolysis and yield different set of products, and each one follows a particular reaction mechanism. We wanted to investigate whether there would be any change in the excited state behavior of these aryl keto azides upon encapsulation inside the host OA (**Scheme 4.2**). In past, we have seen how the free space in the OA cavity governs the product distribution in the photolysis reaction of *para*-alkyl dibenzyl ketone.<sup>254</sup> Another important question was like the azidoadamantanes, which generated presumably singlet nitrenes, whether the triplet nitrenes generated here attack, the cavitand or not. We expected Octa Acid to play a specific role in determining the major products from the photolysis of these guest molecules.



**Scheme 4.2** Chemical structure and <sup>1</sup>H NMR peak assignment of host Octa Acid.

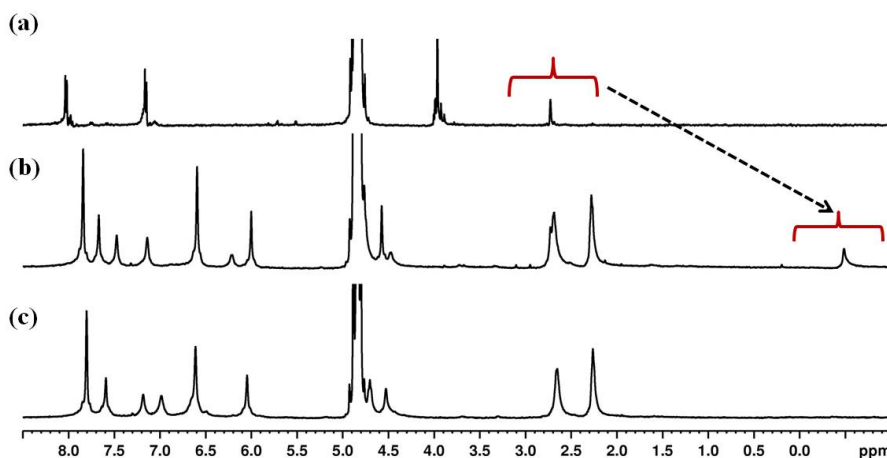
## 4.2 Results and Discussion

In this study, we have found that though the guests listed in **Scheme 4.1** are not very much soluble in water themselves but they form a stable complex with the host Octa Acid, in water. The guest:host ratio depends upon the size of the guest molecules. Upon encapsulation within OA, these azido ayl ketones, show different products upon photolysis. The studies have been categorized based upon each guest's encapsulation and photolysis studies within host OA.

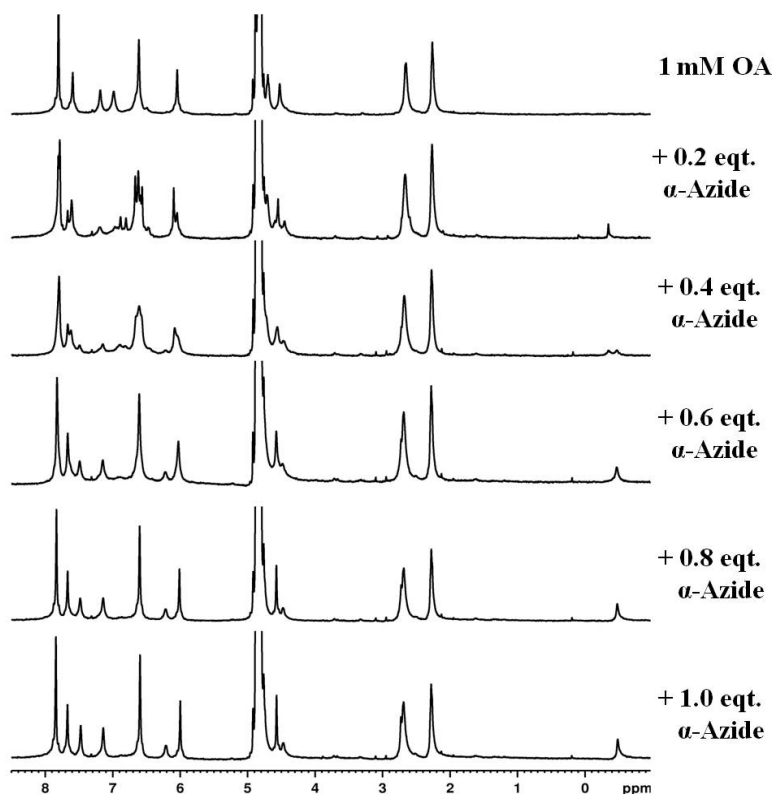
### 4.2.1 Encapsulation and photochemistry of $\alpha$ -Azide@OA

The first compound in the series of guest azides is  $\alpha$ -Azide. Our initial question was whether or not  $\alpha$ -Azide forms a complex with the host OA. **Figure 4.1** shows the <sup>1</sup>H NMR spectra of free and complexed  $\alpha$ -Azide. The proton signals of the bound  $\alpha$ -Azide are much upfield shifted in comparison to free  $\alpha$ -Azide in buffered D<sub>2</sub>O. This indicates that  $\alpha$ -Azide indeed forms a stable complex with OA. Next <sup>1</sup>H NMR titration of  $\alpha$ -Azide with host OA was carried out (**Figure 4.2**). When 0.1 eqts. of  $\alpha$ -Azide was added to 1 mM OA solution, a major change in host proton signals was observed with appearance of a tiny guest peak in far upfield region. On addition of further guest, the host protons broadened and the intensity of the upfield shifted guest peak increased. At 0.5 eqts. of the guest, the host peaks of OA were still broad, on addition of further guest, the OA proton

signals gradually sharpened, and at 1.0 eqt. of guest, the host OA proton signals were very sharp. Further guest addition made the solution turbid, indicating the presence of insoluble free guest. These observations led us to the conclusion that  $\alpha$ -Azide forms a 1:1 guest:host complex with OA.



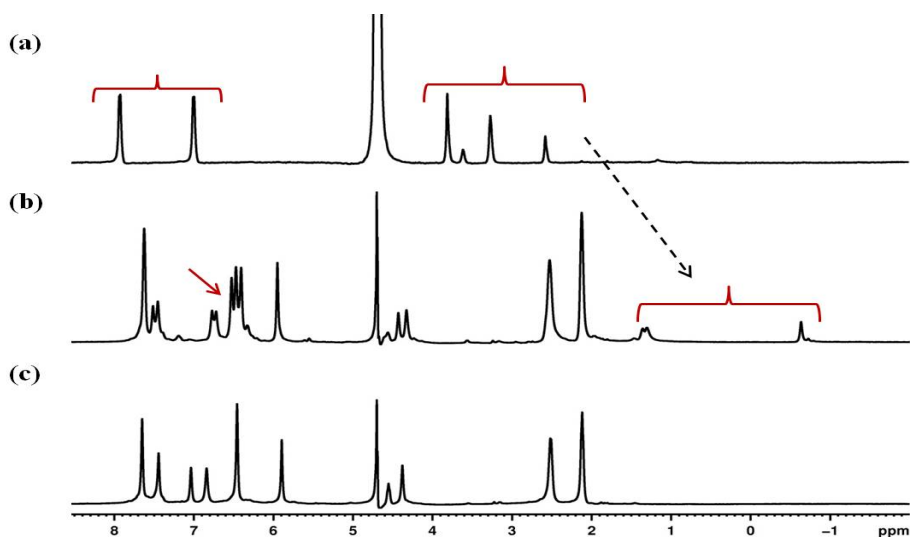
**Figure 4.1**  $^1\text{H}$  NMR spectra (500 MHz,  $\text{D}_2\text{O}$ ) of (a)  $\alpha$ -azide in buffered  $\text{D}_2\text{O}$ , (b)  $\alpha$ -azide@OA, (c) 1mM OA alone.



**Figure 4.2**  $^1\text{H}$  NMR Titration of  $\alpha$ -azide against 1mM OA in 10 mM buffered  $\text{D}_2\text{O}$ .

#### 4.2.2 Encapsulation and photochemistry of $\beta$ -Azide@OA

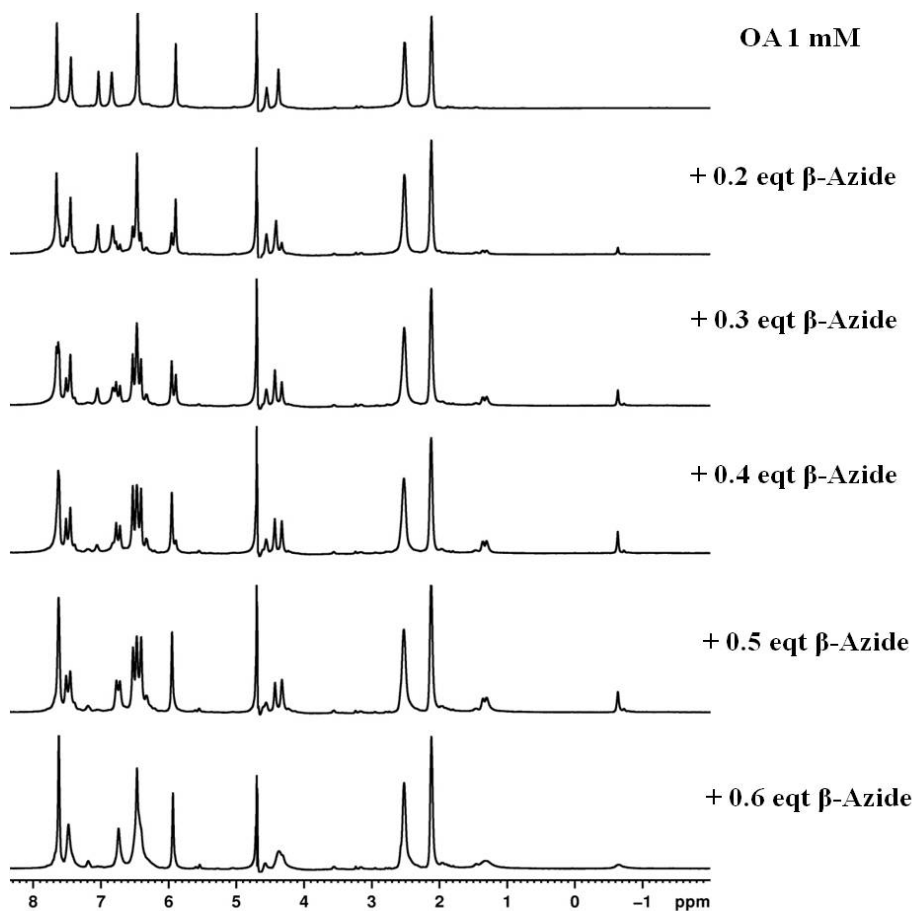
As a primary experiment, the complexation of  $\beta$ -azide was investigated with the host OA. **Figure 4.3**, shows the  $^1\text{H}$  NMR complexation spectra of  $\beta$ -azide with the host OA. From the spectra it can be observed that the guest proton signals are upfield shifted when associated with the host, in comparison to their position in buffered  $\text{D}_2\text{O}$ . Also, we could observe a change in the shape of the host proton signals, when the guest is present in the solution. From the chemical structure of the guest, we can decipher that probably it does not form a symmetrical complex with the two host cavitands; hence we can observe the splitting in the host proton signals. **Figure 4.4** shows the  $^1\text{H}$  NMR titration spectra of the guest  $\beta$ -azide with the host OA.



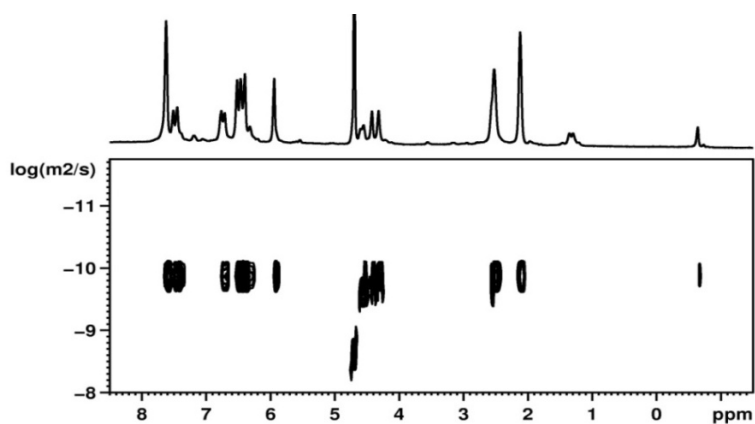
**Figure 4.3**  $^1\text{H}$  NMR spectra (500 MHz,  $\text{D}_2\text{O}$ ) of (a)  $\beta$ -azide in buffered  $\text{D}_2\text{O}$ , (b)  $\beta$ -azide@OA, (c) 1mM OA alone.

The titration is started with 1 mM of host OA. As the concentration of the guest is increased the changes are noticed in the intensity of the guest proton signals as well as the shape of the host proton signals. When the ratio between the guest and the host reaches 0.5:1, we can observe the maximum change. But when the guest ratio is further increased to 0.6:1, we can observe that the host proton signals start broadening. This broadening of

the host proton signals could be due to formation of a loose or an unstable complex with the guest. Hence, we took 0.5:1 as the final guest: host ratio. This implied that the guest forms a 1: 2 capsular complex with the host OA.



**Figure 4.4**  $^1\text{H}$  NMR Titration of  $\beta$ -azide against 1mM OA in 10 mM buffered  $\text{D}_2\text{O}$ .



**Figure 4.5** 2D DOSY NMR spectra of  $\beta$ -azide@OA<sub>2</sub>.

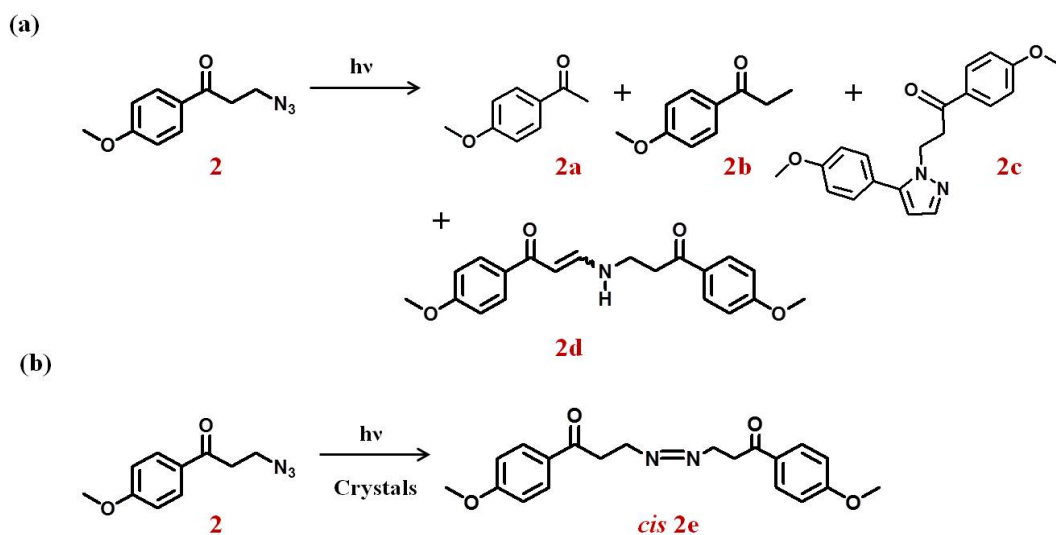


Next a 2D DOSY NMR experiment was conducted to ascertain the observations made above. The diffusion constant for the above complex came out to be  $1.28 \times 10^{-6}$  cm<sup>2</sup>/sec, which indeed corresponds to the 1:2 capsular complex.

**Scheme 4.3** illustrates the photolysis reactions that  $\beta$ -azide could undergo in solution as well as in solid state. The initial step upon irradiation of  $\beta$ -azide is the expulsion of N<sub>2</sub>, followed by the formation of nitrene intermediate.  $\beta$ -azide with a built-in intramolecular sensitizer is designed in such a way, that it is not able to undergo  $\alpha$ -cleavage.<sup>255</sup> In the case of  $\beta$ -azide, due to the methoxy group substitution at the *para* position in aromatic ring, the  $\pi, \pi^*$  configuration is the lowest triplet excited state of the ketone moiety, hence the nitrene formed from  $\beta$ -azide is not photoreactive, since it has been observed that triplet ketones with  $\pi, \pi^*$  configuration do not undergo intramolecular H-atom abstraction efficiently.<sup>256</sup> Hence,  $\beta$ -azide yields only one major compound in the solution, **2c**, which comes from the formation of the azo dimer. Two nitrene intermediates combine to form an azo dimer, which has a co-existing tautomer, this tautomer after losing one water molecule cyclizes to form the product **2c**. No formation of *p*-methoxy propiophenone from photolysis of  $\beta$ -azide was observed<sup>257</sup>, because in the azo dimer formed, the methoxy-acetophenone chromophore absorbs much more strongly above 300 nm than the azo chromophore. Since the azo chromophore cannot absorb the light directly, hence it cannot form propiophenone radical expelling a nitrogen molecule.

Hence it was proposed that the photolysis of  $\beta$ -azide in solution, results in the formation of alkyl nitrene, which are long-lived intermediates because they decay by dimerization, rather than reacting with the solvent or its precursor.<sup>257</sup> **Scheme 4.3** (b) shows the result of solid-state photolysis of  $\beta$ -azide. In this case *cis*-**2e** is formed

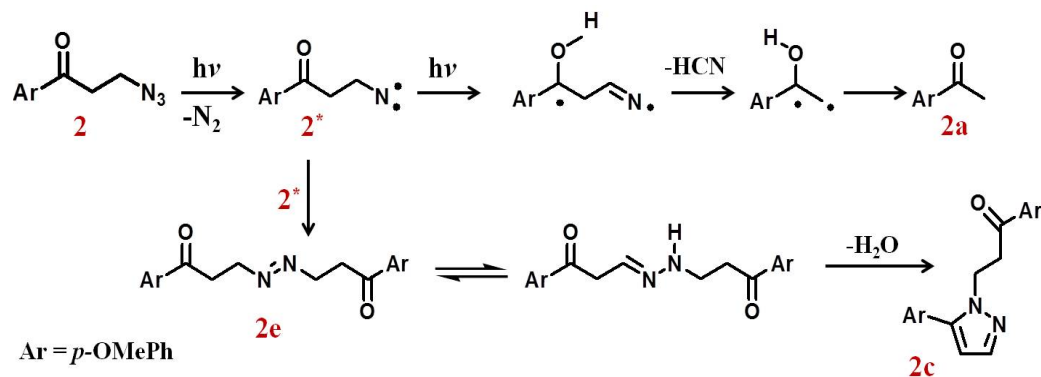
selectively, via dimerization between two nitrene molecules. Crystal packing of  $\beta$ -azide indicates that dimerization does not take place between nearest neighboring N-atoms on nitrenes, but rather between N-atoms that are further apart and have better molecular orbital alignment. It can be theorized that alkyl nitrenes are long-lived in crystals as well, and that the restriction of the crystal lattice forces them to form *cis*-**2e**, stereoselectively.<sup>258</sup>



**Scheme 4.3** Photolysis reactions  $\beta$ -azide undergoes in (a) solution and (b) crystals.

Having some understanding about the photolysis reactions of  $\beta$ -azide in solution and solid state, we proceeded with the photolysis of  $\beta$ -azide@OA<sub>2</sub>. The  $\beta$ -azide@OA<sub>2</sub> complex was irradiated using Rayonet reactor. About 30 % conversion of the starting material was achieved. The solution was not further irradiated, so as to avoid any secondary photolysis products. As could be seen in **Table 4.1**, the major product formed is the corresponding acetophenone **2a**. The formation of acetophenone inside OA could be explained on the basis of the reaction mechanism illustrated in **Scheme 4.4**. Since, OA encapsulates only one  $\beta$ -azide molecule, and also two OA cavitands come together to

form a capsular complex, hence the nitrene intermediate generated inside OA, cannot react with the other nitrene intermediate which would be residing in another OA capsular complex. Since no two nitrene intermediates could approach each other, the corresponding azo dimer could not be formed, as was the case when  $\beta$ -azide was irradiated in solution. The azo-dimer was responsible for the formation of product **2e** in solution, by losing one water molecule. Hence, the only option left for the nitrene intermediate generated inside OA, is to form an imine biradical which produces corresponding acetophenone by losing one HCN molecule. This mechanism is known to take place in argon matrix.<sup>257</sup> So, here we witnessed how encapsulation of a reactive intermediate could alter the course of reaction to give entirely different product with appreciable selectivity.



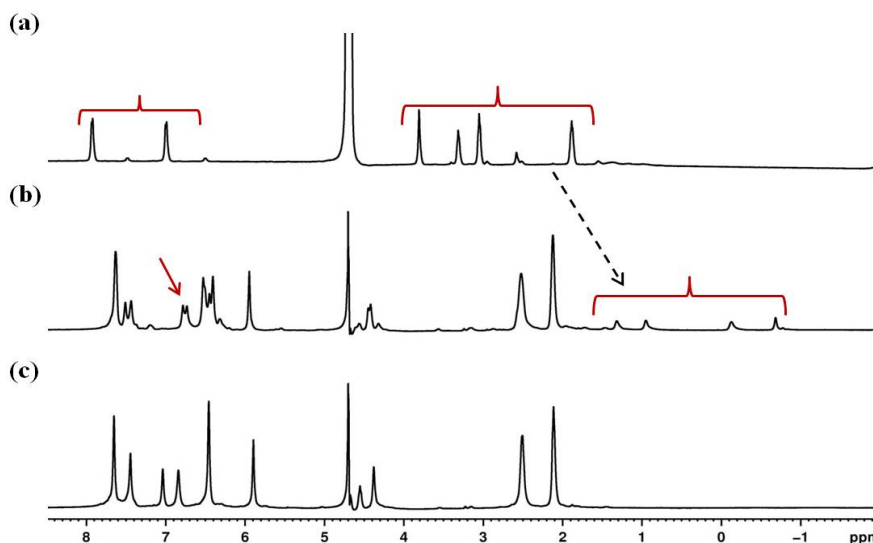
**Scheme 4.4** Proposed Reaction mechanism for the photolysis of  $\beta$ -azide.

**Table 4.1** Relative Percentages of the products obtained upon irradiation of  $\beta$ -azide in solution and in OA.

Guest	Media	2a	2b	2c	2d
2	Toluene	0.0	0.0	100.0	0.0
2	OA	99.0	0.0	0.0	0.0

### 4.2.3 Encapsulation and photochemistry of $\gamma$ -Azide@OA

$\gamma$ -azide is different from  $\beta$ -azide in the way that it has one extra methylene group, but this increase in its chain length can have crucial effect on its photochemistry when it is encapsulated inside the host OA, as we will see in the following discussion. We carried out the same preliminary complexation experiment with the next guest in the series- $\gamma$ -azide. **Figure 4.6**, shows the  $^1\text{H}$  NMR spectra of the guest  $\gamma$ -azide in buffered  $\text{D}_2\text{O}$  and when it is complexed with the host OA. We observe the upfield shifted guest proton signals, when  $\gamma$ -azide is complexed with the host OA, which is characteristic of the formation of a stable guest@host complex. We also observe the splitting in the host OA proton signals. This indicates that the two OA host cavitands face different kind of chemical environment, which could be due to the unsymmetrical nature of the guest  $\gamma$ -azide which occupies the OA cavity.



**Figure 4.6**  $^1\text{H}$  NMR spectra (500 MHz,  $\text{D}_2\text{O}$ ) of (a)  $\gamma$ -azide in buffered  $\text{D}_2\text{O}$ , (b)  $\gamma$ -azide@OA, (c) 1mM OA alone.

The ratio of the guest:host was determined by  $^1\text{H}$  NMR titration experiments (**Figure 4.7**). It was observed that  $\gamma$ -azide formed 1:2 guest: host complex. This

observation was also supported by the 2D DOSY NMR studies. 2D DOSY NMR spectra (Figure 4.8) of  $\gamma$ -azide@OA<sub>2</sub> showed that the complex was stable and the diffusion constant for the complex came out to be  $1.26 \times 10^{-6} \text{ cm}^2/\text{sec}$ , which corresponds to a 1:2 OA capsular assembly.

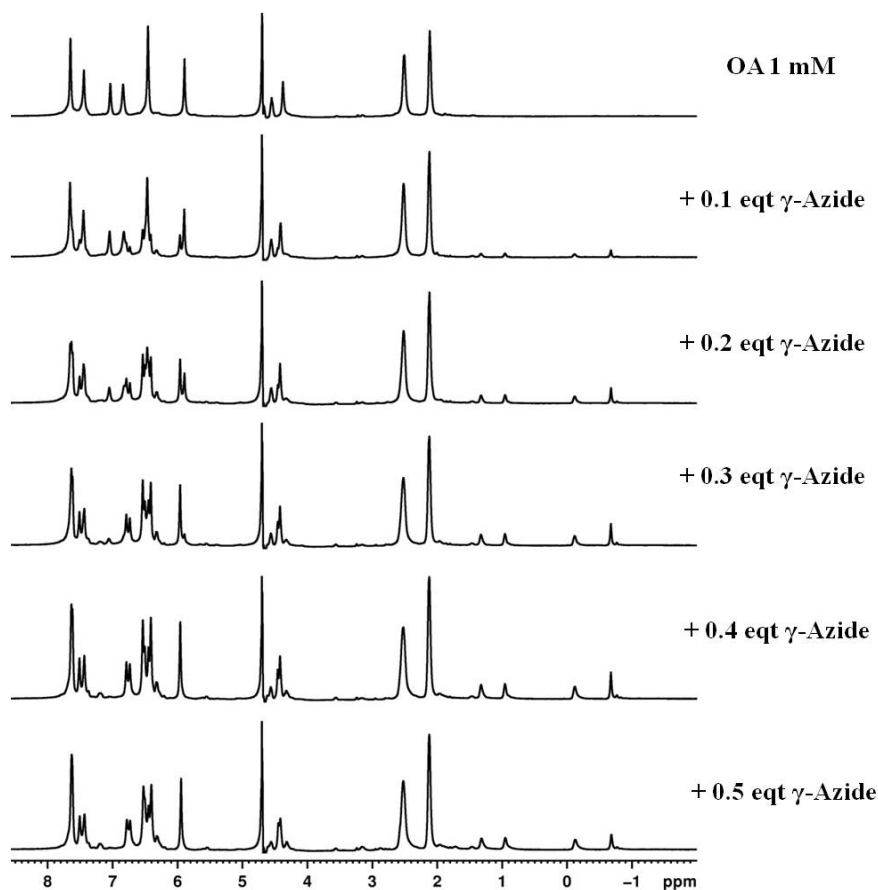


Figure 4.7 <sup>1</sup>H NMR Titration of  $\gamma$ -azide against 1 mM OA in 10 mM buffered D<sub>2</sub>O.

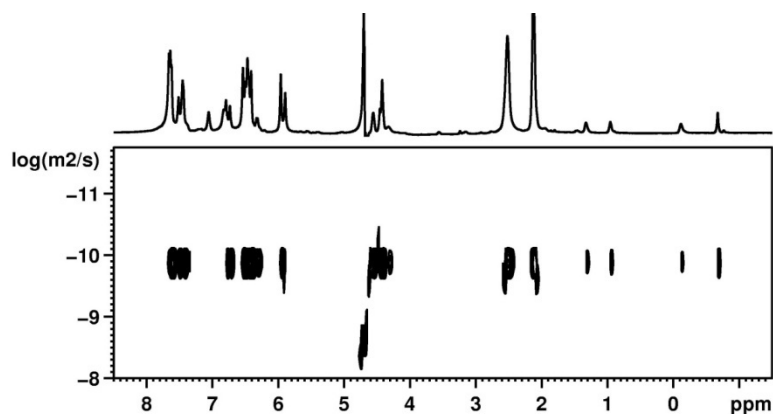
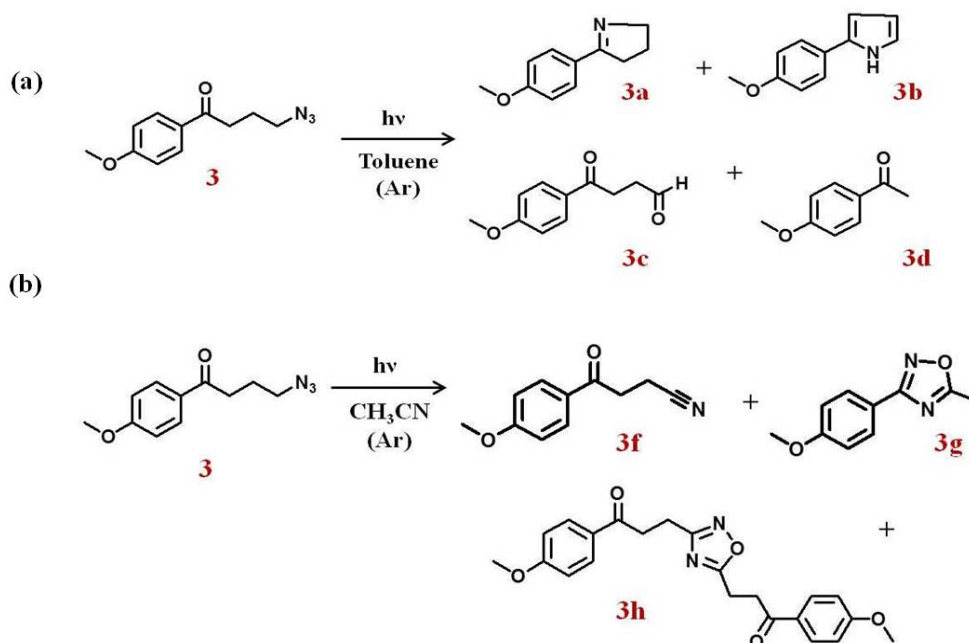


Figure 4.8 2-D DOSY NMR spectra of  $\gamma$ -azide@OA<sub>2</sub>.

Next a 2D DOSY NMR experiment was conducted to ascertain the observations made above. The diffusion constant for the above complex came out to be  $1.28 \times 10^{-6}$   $\text{cm}^2/\text{sec}$ , which indeed corresponds to the 1:2 capsular complex.

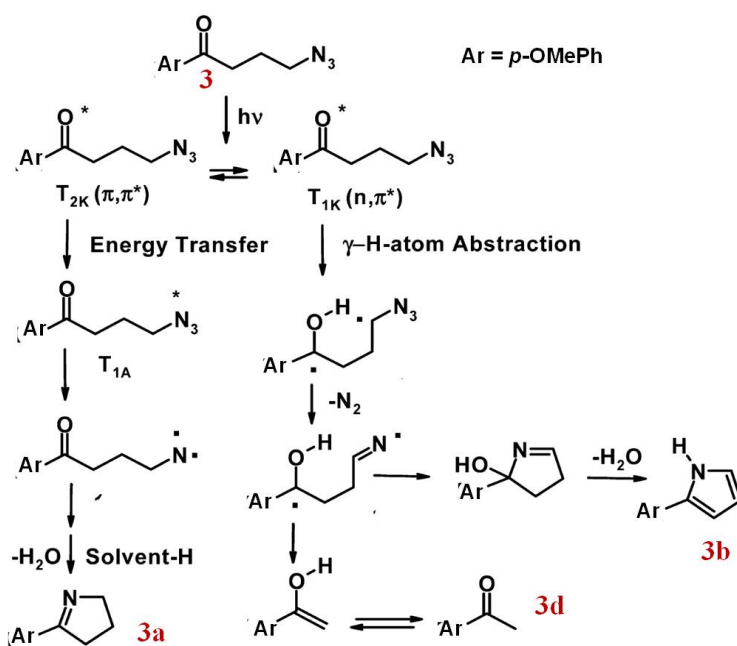
Photolysis of  $\gamma$ -azide can give a myriad of products under various experimental conditions. Photolysis of  $\gamma$ -azide in different solution yields different sets of products with different ratios. **Scheme 4.5** shows the products formed when  $\gamma$ -azide was dissolved in Toluene, Acetonitrile and Chloroform. In **Table 4.2**, we have only included the percentages of the products when  $\gamma$ -azide was dissolved in Toluene in presence of Ar and  $\text{O}_2$ , respectively. Cyclic product **3b** is the major product when  $\gamma$ -azide is irradiated in Ar, whereas, when  $\gamma$ -azide is irradiated in presence of  $\text{O}_2$ , an aldehyde **3c** is the major product.



**Scheme 4.5** Products obtained from the photolysis of  $\gamma$ -azide under various experimental conditions.

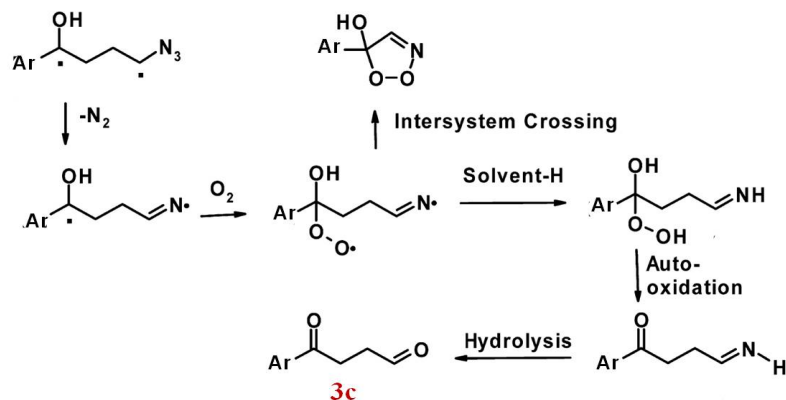
It has been proposed that the lowest excited triplet ketone ( $T_{1K}$ ) of  $\gamma$ -azide (**Scheme 4.6**), that presumably has a  $(n,\pi^*)$  configuration, abstracts a  $\gamma$ -H-atom to form

biradical. Expulsion of a nitrogen molecule from this biradical results in iminyl radical, which cyclizes and dehydrates to give **3b**. However, a small fraction of the biradical must cleave to form 1-phenylethenol, which tautomerizes to corresponding acetophenone. Based on the comparison with valerophenone derivatives, where the first two triplet states are close in energy,<sup>258</sup> it has been theorized that the second excited state of the triplet ketone ( $T_{2K}(\pi,\pi^*)$ ) of  $\gamma$ -azide undergoes energy transfer to form the triplet excited state of the azido chromophore ( $T_{1A}$ ) of  $\gamma$ -azide, which falls apart to yield triplet alkyl nitrene and eventually results in formation of **3a**<sup>260</sup> (Scheme 4.6).



**Scheme 4.6** Proposed Reaction mechanism for the photolysis of  $\gamma$ -azide in Toluene (Ar).

It has also been suggested that in oxygen-saturated toluene, biradical must be intercepted with oxygen to form imine biradical (Scheme 4.7). Imine biradical presumably decays by abstracting H-atoms from the solvent, followed by autoxidation to form the corresponding imine, which is hydrolyzed to **3c**.<sup>260</sup>



**Scheme 4.7** Proposed Reaction mechanism for the photolysis of  $\gamma$ -azide in Toluene ( $O_2$ ).

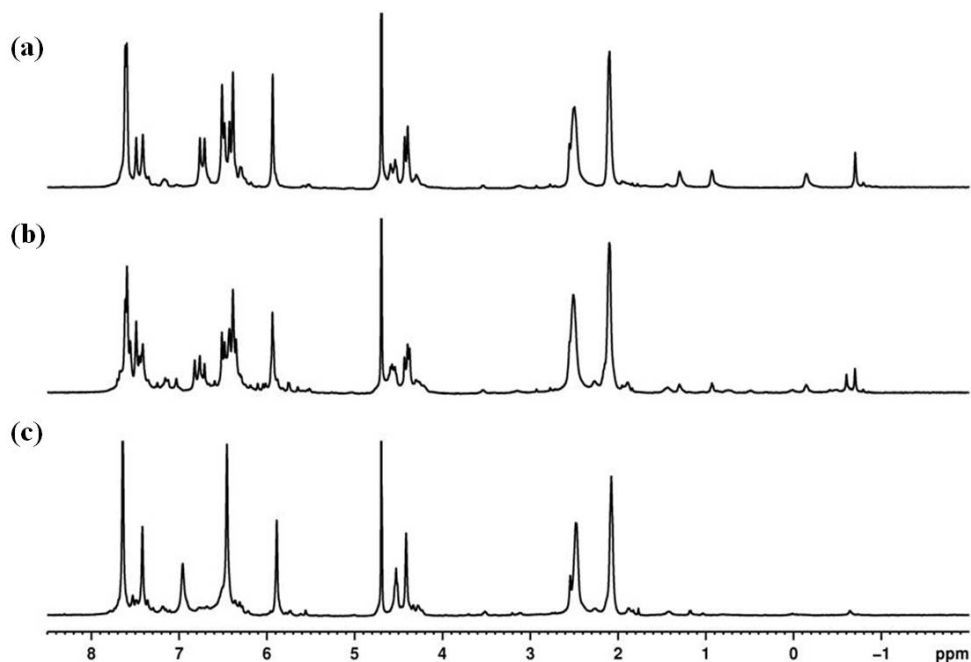
However, when  $\gamma$ -azide@OA<sub>2</sub> solution was irradiated, the major product formed was the cyclized product **3b**. This product is presumably formed upon intramolecular  $\gamma$ -H abstraction. Products **3a** and **3c** are observed in traces. The reason for this could be, that the reaction intermediates formed being encapsulated inside the hydrophobic OA cavity are well protected from the protic solvent (which is essential for the formation of **3a**) and  $O_2$  (which is essential for the formation of **3c**), which is dissolved in the solvent. This special product distribution again stresses the role of encapsulation of a reaction intermediate. Encapsulation plays a big role in determining the accessibility of the reactants to the reaction intermediates in the bimolecular reactions. Moreover, the free space and the orientation of the abstractable Hs also are key factors in deciding the resultant product ratio in the reactions involving very reactive intermediates.

**Table 4.2** Relative Percentages of the products obtained upon irradiation of  $\gamma$ -azide in solution and in OA.

Guest	Media	3a	3b	3c	3d
3	CH <sub>3</sub> CN (Ar)	100.0	0.0	0.0	0.0
3	CH <sub>3</sub> CN ( $O_2$ )	0.0	34.0	55.0	3.0
3	OA	5.0	90.0	5.0	0.0



After the irradiation of the above complex, the products were extracted using  $\text{CDCl}_3$ . The remaining host OA was analyzed by the  $^1\text{H}$  NMR after that (**Figure 4.9**). The resultant OA was almost same as the original OA solution and no adduct formation between the reactive intermediate and host OA was detected in this case.



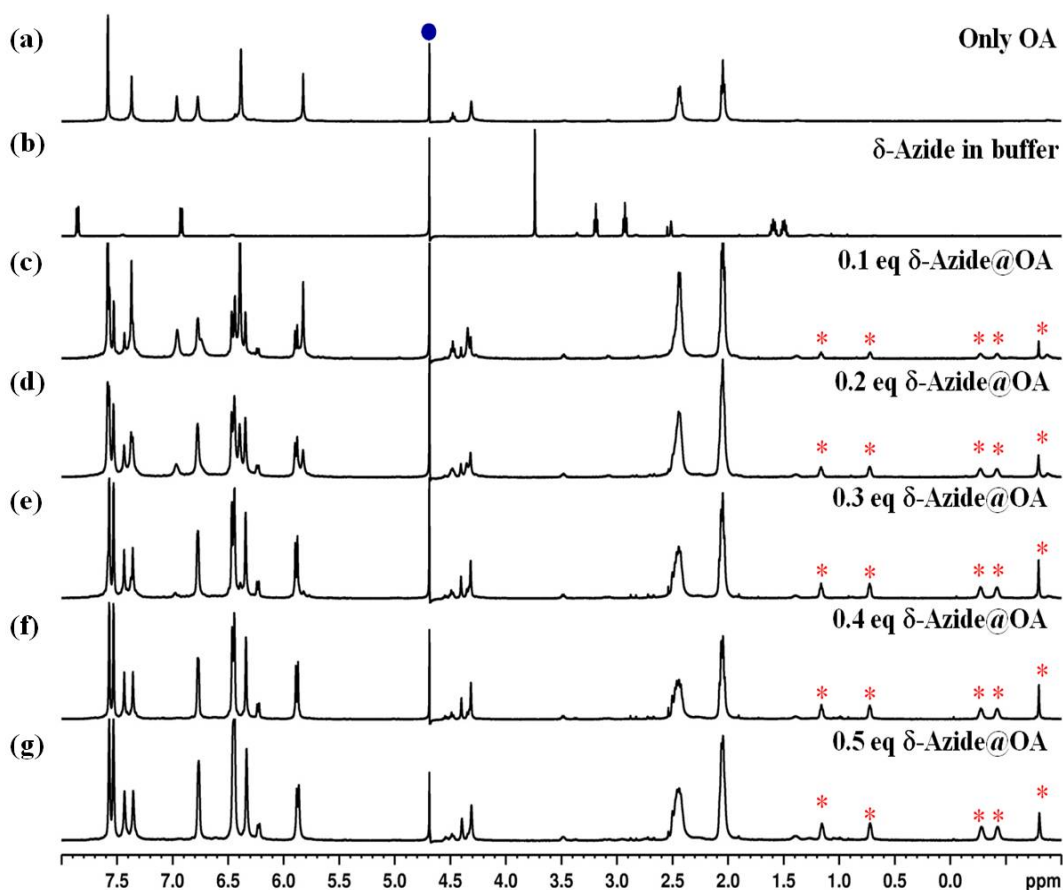
**Figure 4.9**  $^1\text{H}$  NMR spectra of (a)  $\gamma$ -azide@OA<sub>2</sub> before irradiation, (b) Products@OA after irradiation, (c) OA after extraction of products.

#### 4.2.4 Encapsulation and photochemistry of $\delta$ -Azide@OA

Next in the series of guest azides is  $\delta$ -Azide. This guest has been studied by **Pradeep Jagadesan**. It has been included here to maintain the synchrony in the guest series. Like all the previous guest azides,  $\delta$ -Azide too formed a stable complex with the host OA as can be seen from **Figure 4.10**.  $^1\text{H}$  NMR titration experiments showed that it formed 1:2 complex with the host OA.

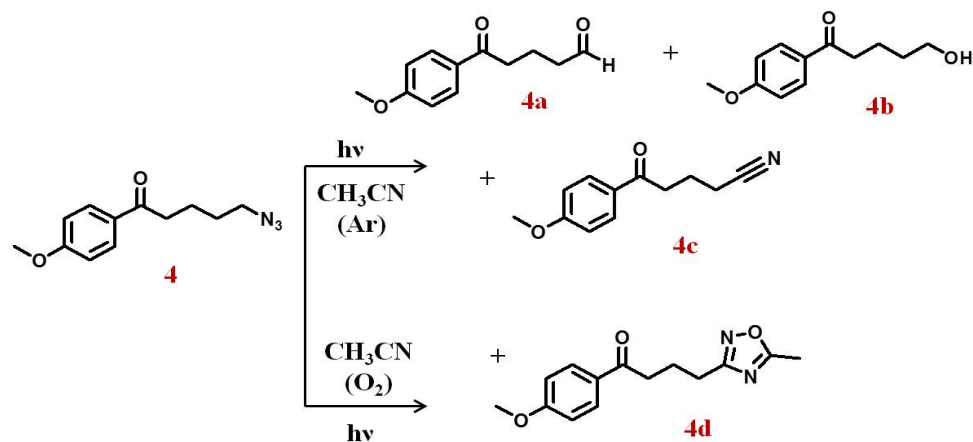
**Scheme 4.8** shows the products which are obtained upon the photolysis of  $\delta$ -Azide under various experimental conditions. **Table 4.3** gives the relative percentages of these

products. It can be observed that in Argon saturated Acetonitrile solution, the major product is corresponding aldehyde **4a** followed by the corresponding nitrile **4c**, with some amount of alcohol **4b**. But in the case when  $\delta$ -Azide is dissolved in O<sub>2</sub> saturated Acetonitrile solution, the major product is the cyclized **4d** followed by **4c**.



**Figure 4.10** <sup>1</sup>H NMR spectra (500 MHz, D<sub>2</sub>O) of: (a) only OA 1mM, (b) 1mM  $\delta$ -Azide in buffered D<sub>2</sub>O, (c) 1mM OA +0.1 eqt.  $\delta$ -Azide, (d) 1mM OA +0.2 eqt.  $\delta$ -Azide, (e) 1mM OA +0.3 eqt.  $\delta$ -Azide, (f) 1mM OA +0.4 eqt.  $\delta$ -Azide, (g) 1mM OA +0.5 eqt.  $\delta$ -Azide.

When  $\delta$ -azide@OA<sub>2</sub> solution is irradiated, the two products **4a** and **4b** are formed in major quantity. Product **4d** is completely absent. The reason attributed to this observation could be the unavailability of the free space inside OA for the formation of relatively bigger **4d** also, less access to the O<sub>2</sub> dissolved in the solvent.



**Scheme 4.8** Products obtained upon photolysis of  $\delta$ -Azide under various experimental conditions.

**Table 4.3** Relative Percentages of the products obtained upon irradiation of  $\delta$ -azide in solution and in OA.

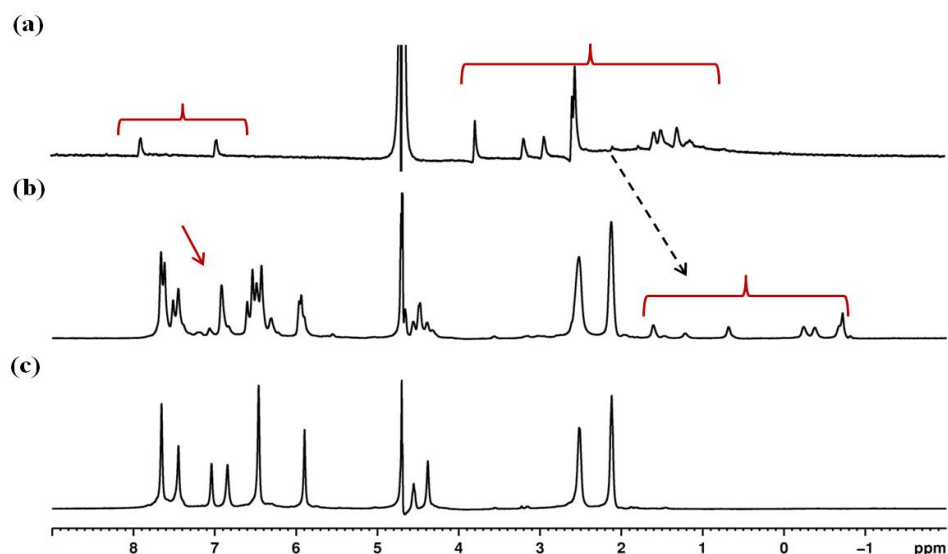
Guest	Media	4a	4b	4c	4d
4	CH <sub>3</sub> CN (Ar)	56.0	20.0	24.0	0.0
4	CH <sub>3</sub> CN (O <sub>2</sub> )	0.0	0.0	34.0	66.0
4	OA	56.0	44.0	0.0	0.0

#### 4.2.5 Encapsulation and photochemistry of $\varepsilon$ -Azide@OA

The last guest azide in this series is  $\varepsilon$ -Azide. **Figure 4.11** shows the <sup>1</sup>H NMR complexation spectra of  $\varepsilon$ -Azide with OA. The upfield shifted proton signals of  $\varepsilon$ -Azide, in presence of the host OA, shows that the two are complexed with each other. Also, the sharpness of the guest as well as host proton signals are the indication towards the formation of a stable complex.

Another observation which we had previously encountered is that the OA host proton signals are well split. This is usually the case when the two OA cavitands experience different chemical environment. In other words, the host proton signals are split when the guest is unsymmetrical in nature and more importantly its motion (probably rotational motion about x-axis) is slower in regard to the NMR time scale. If

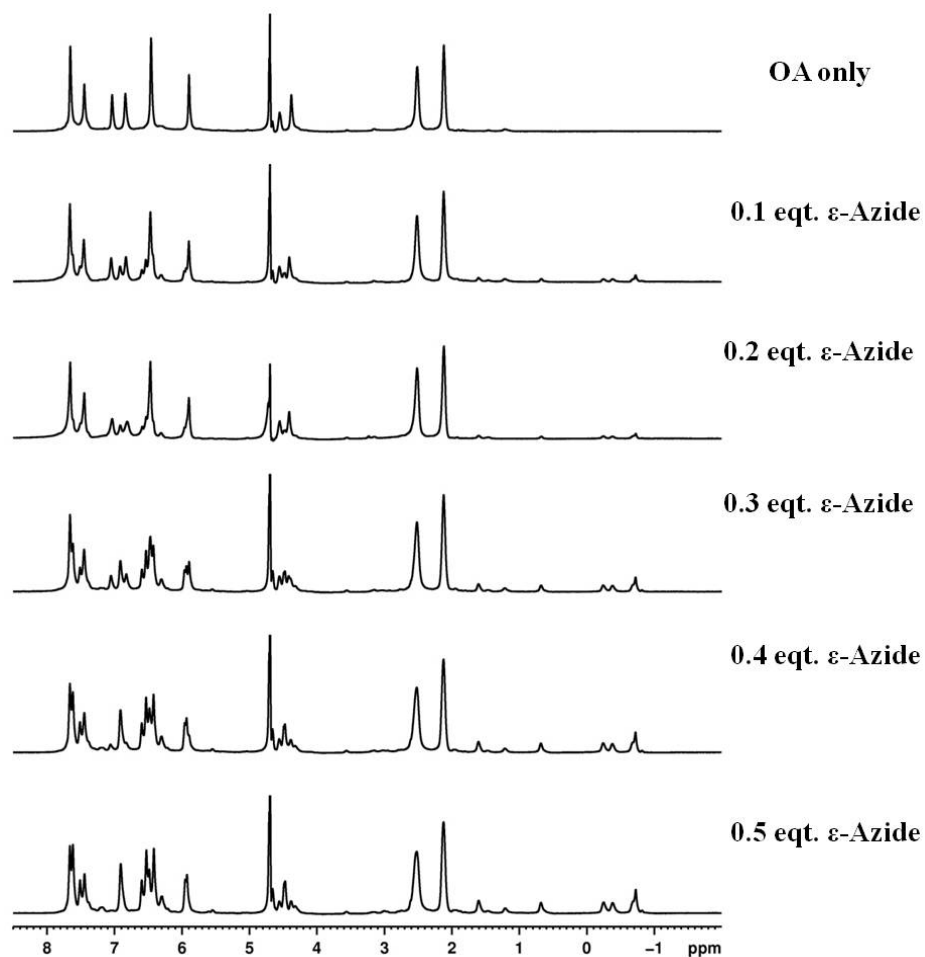
this rotational motion is too fast in comparison to the NMR time scale, then the NMR spectra would show us the time averaged resonance signals, and would not be able to differentiate between the two chemically different atmospheres offered to two host cavitations OA, by the unsymmetrical guest molecule.



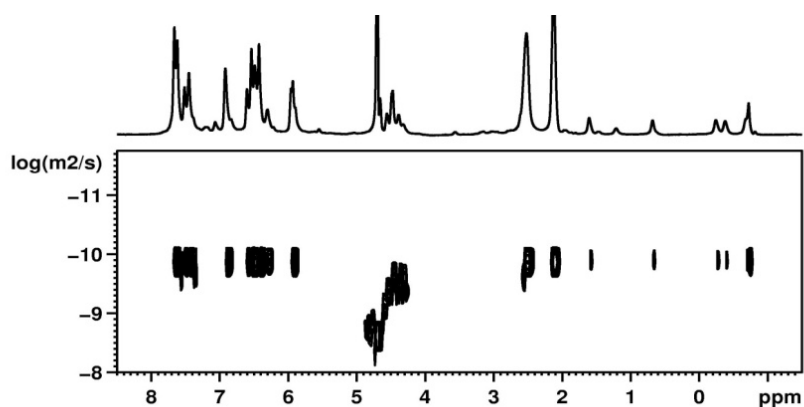
**Figure 4.11** <sup>1</sup>H NMR spectra (500 MHz, D<sub>2</sub>O) of (a) ε-azide in buffered D<sub>2</sub>O, (b) ε-azide@OA, (c) 1mM OA alone.

<sup>1</sup>H NMR titration studies (**Figure 4.12**) of ε-azide with 1mM OA solution showed that it forms a 1:2 guest@host complex with the host OA. 2D DOSY NMR studies (**Figure 4.12**) supports the above observation. The 2D DOSY spectra show that ε-azide@OA<sub>2</sub> complex is a stable one. Also the diffusion constant for the ε-azide@OA<sub>2</sub> is  $1.23 \times 10^{-6} \text{ cm}^2/\text{sec}$ , which corresponds to a 1:2 capsular complex with OA. If we compare the diffusion constants of β-azide@OA<sub>2</sub>, γ-azide@OA<sub>2</sub> and ε-azide@OA<sub>2</sub>, which are  $1.28$ ,  $1.26$  and  $1.23 \times 10^{-6} \text{ cm}^2/\text{sec}$ , respectively, we could observe that there is a continuous decrease in the diffusion constant. This decrease in the diffusion constant value is attributed to the increase in the chain length of the guest azides. As the size of the

guest azide increases, the capsular complex becomes heavier; hence it diffuses more slowly on the NMR time scale, giving us lower diffusion constant.

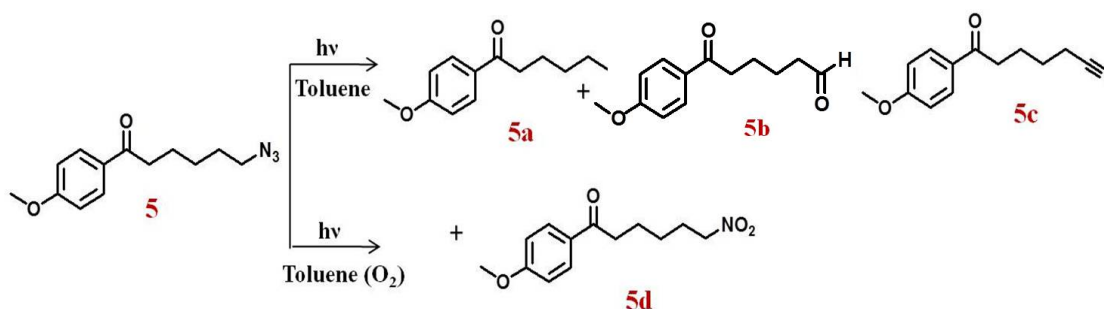


**Figure 4.11**  $^1\text{H}$  NMR Titration of  $\epsilon$ -azide against 1mM OA in 10 mM buffered  $\text{D}_2\text{O}$ .

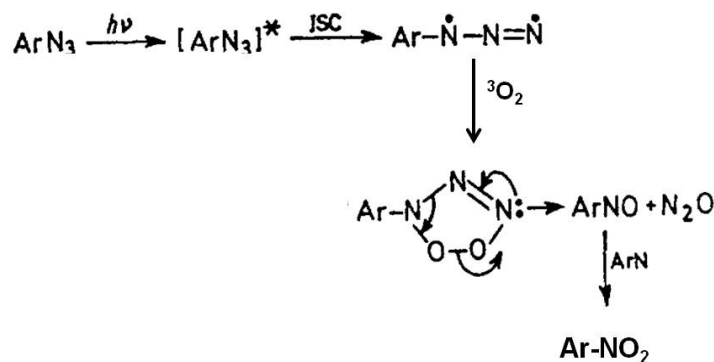


**Figure 4.12** 2D DOSY NMR spectra of  $\epsilon$ -azide@OA<sub>2</sub>.

When  $\epsilon$ -azide is irradiated in the presence and absence of toluene, again a lot of products are obtained without much selectivity as can be observed from **Table 4.4**. **Scheme 4.9** shows the products thus obtained. When  $\epsilon$ -azide is dissolved in argon saturated toluene and irradiated the major product is seven-membered cyclic imine **5b**, followed by the corresponding nitrile **5c** and ketone **5a**, respectively. Whereas, when the photolysis of  $\epsilon$ -azide is dissolved in  $O_2$  saturated toluene is carried out, the major product is nitrile **5c** followed by the cyclic imine **5b** and an additional nitro product **5d**.



**Scheme 4.9** Products obtained upon photolysis of  $\epsilon$ -Azide under various experimental conditions.



**Scheme 4.10** Probable mechanism for the formation of nitro products from the photolysis of  $\epsilon$ -azide in presence of molecular  $O_2$ .

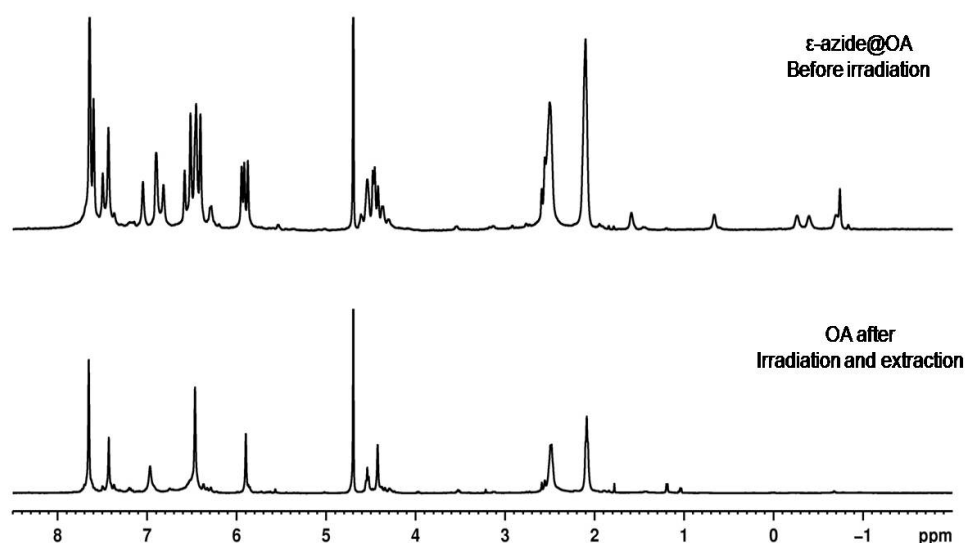
**Scheme 4.10** shows the probable mechanism of the formation of nitro product **5d** from the photolysis of  $\epsilon$ -Azide in presence of molecular oxygen. It has been established that nitro-aromatic compounds are formed by trapping triplet aryl nitrenes with triplet  $O_2$ ,

and that the addition of oxygen to photo-excited triplet azido-groups gives nitro products.<sup>261</sup>

**Table 4.4** Relative Percentages of the products obtained upon irradiation of  $\epsilon$ -azide in solution and in OA.

Guest	Media	5a	5b	5c	5d
5	Toluene (Ar)	16.0	55.0	29.0	0.0
5	Toluene (O <sub>2</sub> )	0.0	23.0	60.0	17.0
5	OA	3.0	3.0	94.0	0.0

However, when  $\epsilon$ -azide@OA<sub>2</sub> complex was irradiated in a Rayonet reactor, so that approximately 30-40% photo-conversion is achieved, the major product formed was the corresponding nitrile compound **5c**, followed by the traces of compounds **5a** and **5b**. The absence of compound **5d** in this case, highlighted the fact that the reactive triplet nitrene produced inside the OA capsule, was not able to react with the molecular O<sub>2</sub> dissolved in the solvent which surrounded the exterior of the capsule.



**Figure 4.13** <sup>1</sup>H NMR spectra of  $\epsilon$ -azide@OA<sub>2</sub> before irradiation and OA after extraction of products.

This observation once again draws our attention to the fact that the confinement of the guest inside a hydrophobic host plays a very important role in governing their photochemical outcome. Also, we checked the residual OA after the extraction of products with  $\text{CDCl}_3$  from the irradiated  $\varepsilon$ -azide@OA<sub>2</sub> complex. **Figure 4.13** shows the resultant NMR spectra of OA which resembles the original OA compound. It can be observed that no adduct formation is detected between the host OA and the reactive triplet nitrene intermediate.

### 4.3 Conclusion

The formation of aryl and alkyl nitrenes from corresponding azides has been studied extensively for the last several decades.<sup>262</sup> Since nitrenes undergo bimolecular reactions they have been used for photoaffinity labeling bio-organic molecules and in several industrial processes such as microlithography.

Here, we have extended our effort to understand the role of encapsulation of the otherwise very reactive intermediates. Usually, being so reactive, these intermediate undergo fast reactions which results in unselective product distribution. Or some times, one particular kind of product is obtained with very high selectivity, leaving no scope for getting another possible product. It was for these reasons that we were interested in exploiting host-guest chemistry for taming the reactive intermediates like carbenes and nitrenes.

In the previous chapter, we studied guests which yielded singlet nitrenes which formed an adduct with the host cavitand OA, by abstracting viable Hs from the cavitand. In this chapter, we studied the guests which yielded presumably triplet nitrene. Another important fact about this series of guests was that it had an in-built triplet sensitizer, i.e.



an aromatic ketone. From the above studies, we could conclude that, encapsulation of the guest inside the OA capsule played an important role in regard to the outcome of the photoreaction, for instance in this case: (1) a triplet nitrene is formed in high yield in a hydrophobic environment, since only one particular mechanism of nitrene formation and further reaction is prevalent inside the OA capsule, (2) the molecular walls of the OA capsule prohibits nitrene to diffusion out of the binding site or other species to venture in, rendering only very few options to the generated nitrene to react. These conclusions are supported by the product selectivity we achieve in the case of  $\beta$ -,  $\gamma$ - and  $\epsilon$ -azides. For example, for  $\beta$ -azide, the cyclic dimer product which is a major product in solution is just not possible inside the OA capsule, owing to its big molecular volume, so the only photoproduct we obtain is *p*-methoxy acetophenone. Similarly, for  $\epsilon$ -azide, the major product is the corresponding nitrile in high yield, whereas in the solution there are other products present and the product selectivity is low.

The studies done above and in the previous chapters, concerning the encapsulation of nitrene and carbene intermediates opens up a wide range of scientific opportunities for further investigations. For example, it would be interesting to perform an azide “click” reaction inside the OA capsule. Also, to try to generate a long lived triplet nitrene or carbene with the help of the stabilizing effect of the interior of the host molecules.

#### 4.4 Experimental Section

**Encapsulation of Guest inside Host studied by  $^1\text{H}$  NMR:** For each experiment, a 60 mM stock solution of the guest was prepared in DMSO- $d_6$ . 10  $\mu\text{L}$  of this solution was added to 0.6 mL, 10 mM buffered  $\text{D}_2\text{O}$ , making the concentration of the guest to be  $\sim$  1mM, and the  $^1\text{H}$  NMR was recorded at the room temperature. 0.6 mL of 1mM of OA

solution was prepared in 10 mM buffered D<sub>2</sub>O, and the <sup>1</sup>H NMR was recorded. To this solution, 10 μL of the 60 mM guest solution was added, the solution was shaken for 5 minutes and the NMR was recorded.

**Stoichiometry of the complexes, determined by <sup>1</sup>H NMR Titration:** For each experiment, a 60 mM stock solution of the guest was prepared in DMSO-d<sub>6</sub>. 1 μL of this solution was added to 0.6 mL of 1mM OA in 10 mM buffered D<sub>2</sub>O, making the concentration of the guest to be ~0.1 mM, the NMR tube was shaken for ~5 minutes and the <sup>1</sup>H NMR was recorded, again another 1 μL of the guest stock solution was added to the above solution, NMR tube was shaken and the <sup>1</sup>H NMR spectra was recorded. This process was repeated 9 more times.

**Nature of the complexes as determined by DOSY NMR:** Diffusion NMR experiments were performed on Bruker 500 MHz NMR spectrometer. The experiments were performed at 25°C, at a host concentration of 1 mM (in 10 mM sodium tetraborate buffered D<sub>2</sub>O). Data was analyzed by using the Bruker Topspin software. Assuming the complex to be spherical, diffusion constant  $D$  can be calculated according to the following equation:

$$R_h = kT / 6\pi\eta D$$

where  $R_h$  is the hydrodynamic radius of the sphere in meters,  $k$  is the Boltzmann constant,  $T$  is the temperature in Kelvin,  $\eta$  is the solvent viscosity, and  $D$  is the diffusion constant in m<sup>2</sup>s<sup>-1</sup>. All the calculations and fittings are done with the help of the software.

**Photolysis of the Azido aryl ketone guests encapsulated inside the host as studied by <sup>1</sup>H NMR, in solution.**

**Experimental Procedure:** 1:1 ratio of 1mM of the guest@host solution was prepared in 10 mM buffered D<sub>2</sub>O. <sup>1</sup>H NMR of this solution was recorded. Then the solution was

evacuated and purged with argon several times. This solution was irradiated inside Rayonet reactor for 1, 2, 5, 7 minutes. The  $^1\text{H}$  NMR spectra of the solutions were recorded at these intervals to follow the reaction. Usually the reaction was stopped at 30-40% conversion of the starting material, to avoid any secondary photoreactions.

### **Analysis of the photolysis products and analyzing host OA after irradiation (Intramolecular Products)**

**Experimental Procedure for product analysis and characterization:** After the irradiation was over, the products were extracted 3 times using  $\text{CDCl}_3$ , and dried over anhydrous sodium sulfate. The  $\text{CDCl}_3$  solution was concentrated to approximately 0.6 mL and the  $^1\text{H}$  NMR spectra of the products mixture was recorded. Then the solution was further concentrated to approximately 0.1 mL and was injected in the GC. The program used for GC was – starting at  $65^\circ\text{C}$ , held for 5 minutes, applying ramp of  $10^\circ\text{C}$  per minutes, reached to  $270^\circ\text{C}$  and held for 10 minutes. The GC traces gave the percentages of the product obtained. All the reactions were repeated for consistency. The products thus obtained were primarily characterized by  $^1\text{H}$  NMR. The product solution was injected in GCMS. The molecular weight obtained by molecular ion peak and the fragmentation pattern further confirmed their identity.

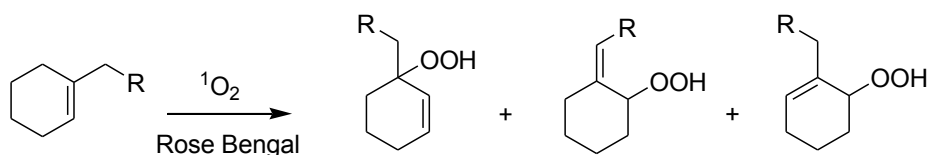
**Experimental Procedure for analyzing host after irradiation:** For the control experiment 1mM OA solution in 10 mM buffered  $\text{D}_2\text{O}$  was taken, to this solution  $\text{CDCl}_3$  solution was added and extracted back. The residual OA solution was analyzed by  $^1\text{H}$  NMR.

## **CHAPTER 5**

### **Photo-oxygenation of Alkyl-cyclohexenes by Singlet Oxygen in Solution and inside Confined Media**

## 5.1 Overview

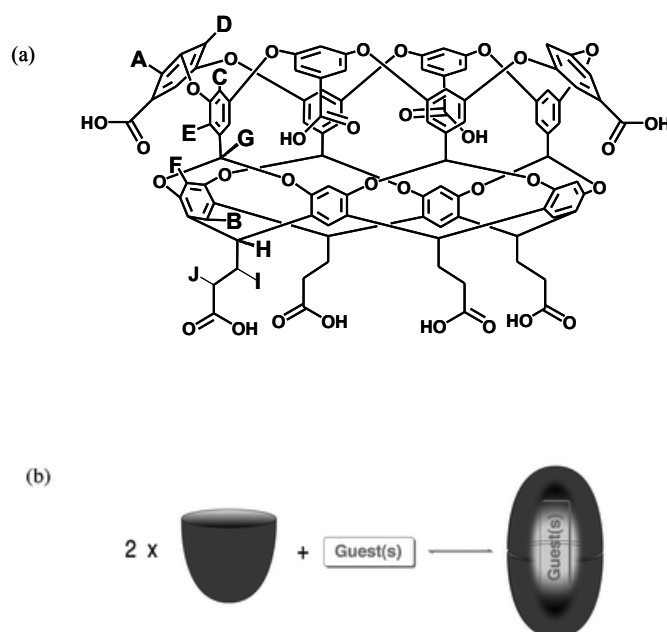
The study of chemical/photochemical reactions of substrates encapsulated in a supramolecular host system is driven by the ultimate goal of enzyme mimetics. It is the enforced proximity and local environment offered by the “active site” of the enzyme that catalyzes unique reactions. A large array of supramolecular host systems has been used ever since to enhance, control and catalyze the reactivity of a substrate in various chemical and photochemical reactions.<sup>263-275, 169a</sup>



**Scheme 5.1** The products of the “ene” reaction, when alkylcycloalkenes are used as substrates.

One relevant photoreaction calling for the controlled reactivity is “ene” reaction. Addition reactions of singlet oxygen to olefins, also known as “ene” reaction, have been the subject of inquiry since the discovery of singlet oxygen by Kautsky over a century ago.<sup>276-278</sup> Singlet molecular oxygen is produced by energy transfer from triplet sensitizers to ground state triplet oxygen. The specie thus produced is chemically and kinetically very reactive. It is a very useful synthetic “reagent”.<sup>279</sup> Many processes which involve singlet oxygen provide informative model systems through which a range of chemical and physical phenomenon can be investigated. One such well known chemical model reactions of singlet oxygen is the hydroperoxidation of alkenes containing allylic hydrogens, often called “ene” reactions.<sup>280,281</sup> Reaction with substrates containing more than one allylic hydrogens produce several products in solution<sup>282</sup> (**Scheme 5.1**).

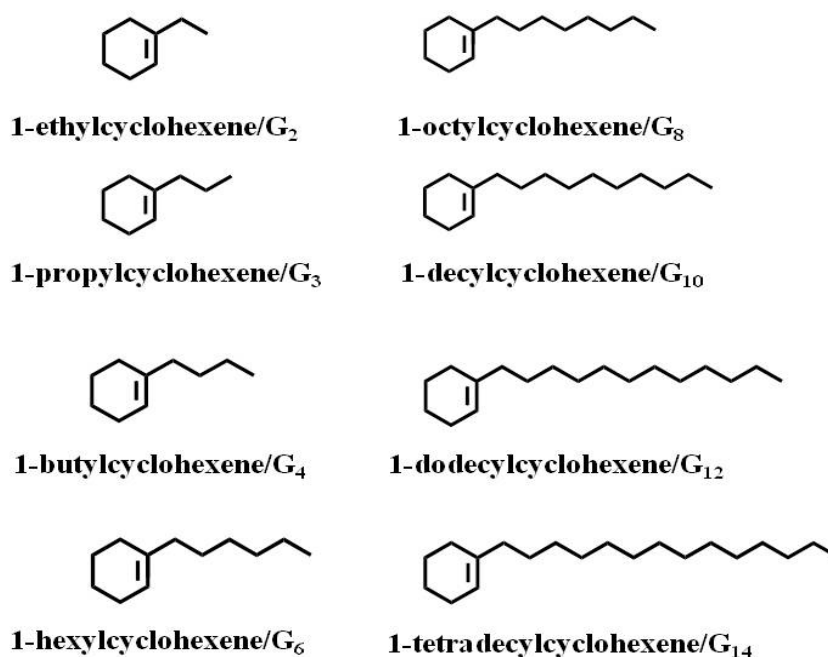
Due to the difficulties in controlling highly reactive singlet oxygen, it has not been possible to control the regioselectivity of reactions upon unhindered olefins, for eg. alkyl-cycloalkenes.<sup>283</sup> In the recent past, preferential abstraction of hydrogen from the methyl group of methyl cycloalkenes could be achieved by pre-organization of the olefins through cation- $\pi$  interactions within zeolites.<sup>284</sup> In yet another report by our group OA has been used as a reaction vessel to control the “ene” reaction product selectivity.<sup>36</sup> In this report we have further explored the strategy to control the product distribution in photochemical “ene” reaction by using a water soluble deep cavity cavitand called octa acid<sup>46</sup> as host.



**Figure 5.1** (a) The chemical structure of the host cavitand Octa Acid and the  $^1\text{H}$  NMR assignment A-J. (b) The formation of capsule.

Host OA is a water-soluble synthetic with eight carboxylic acid groups, in the form of a traditional “lampshade” arranged with four acid groups each at the top and the bottom. In presence of a guest, two molecules of the host come together and form a capsular assembly (Figure 5.1b). These capsular assemblies, in which the templating

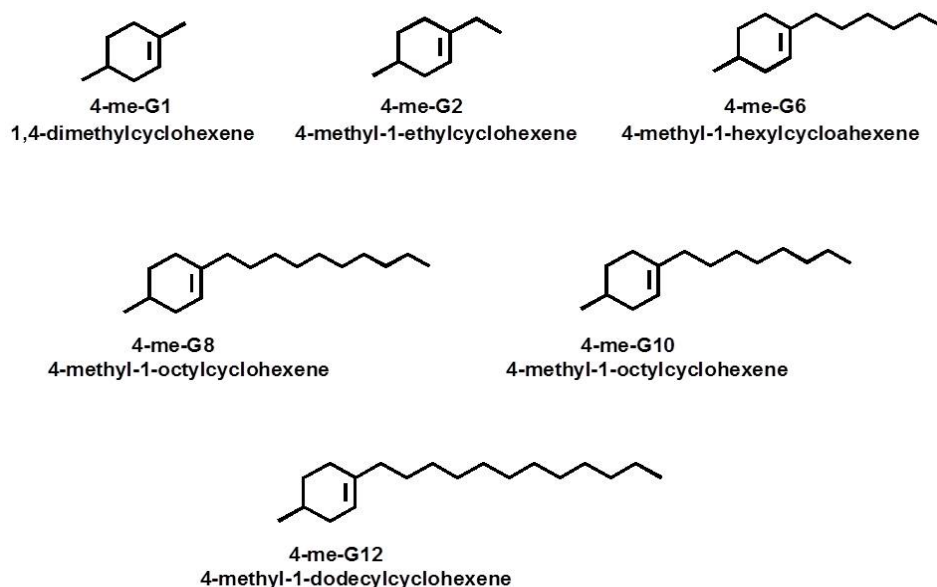
guest or guests reside within an essentially dry and non polar interior<sup>46</sup>, are held together by weak interactions such as van der Waals and CH- $\pi$  interactions and hydrophobic effect. The capsular assembly can template distinct conformations of the guest residing within the nanospace.<sup>285</sup> It can induce supramolecular stereochemistry by directing the position or orientation of guests.<sup>56</sup> It can also accelerate or re-direct a reaction.



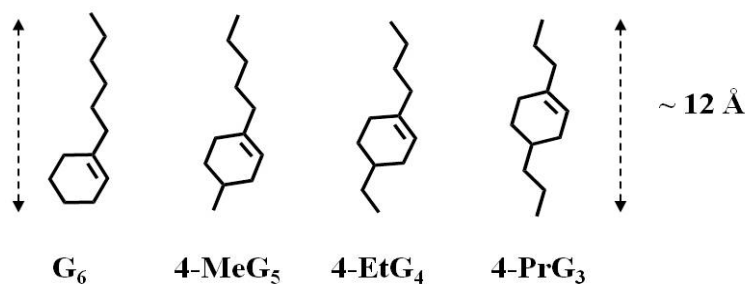
**Scheme 5.2** Two sets of guests 1-alkylcyclohexene studied for the “ene” reactions.

The result and discussion section of this chapter has been broadly divided into four parts. The first part consists of the detailed study on the encapsulation and “ene” reaction of the 1-alkyl alkylcyclohexene in OA (**Scheme 5.2**). The second part shows the study of encapsulation and photochemistry of 1-alkyl-4-methylcyclohexene in OA (**Scheme 5.3**). By introducing a methyl group at 4-position in the cycloalkene ring, we anticipated a change in the encapsulation properties of these guests in OA, as well as a change in the product distribution of the “ene” reaction. In the third part, encapsulation

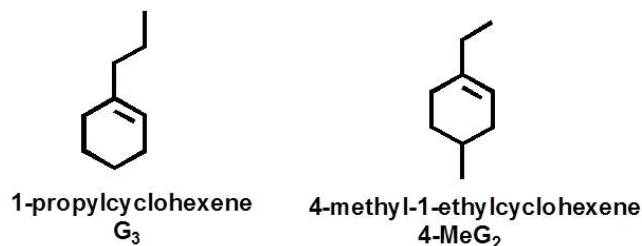
and photochemistry of four cyclohexene guests, of approximately same molecular length but different substitutions, inside OA (as shown in **Scheme 5.4**) were carried out. Finally, the anomalous encapsulation pattern of two cyclohexenes guest molecules  $G_3$  and 4-Me $G_2$  have been discussed briefly (**Scheme 5.5**).



**Scheme 5.3** Two sets of guests 1-alkyl-4-methylcyclohexene studied for the “ene” reactions.



**Scheme 5.4** Chemical structure of guests cycloalkenes with almost similar molecular length.



**Scheme 5.5** Chemical structure of guests cycloalkenes with intermediate molecular size.

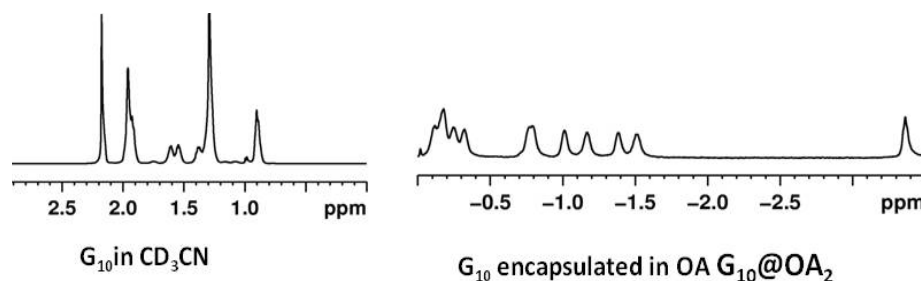


First three of the four subsections are principally divided into two parts: (1) the encapsulation of the aforementioned guest inside the host. (2) The photochemical “ene” reaction in solution and in the confinement of the host OA. The former study, i.e. encapsulation of the guests inside the host molecule has extensively utilized 1D  $^1\text{H}$  NMR spectroscopy, for illustrating the step by step process of capsule formation. 2D COSY NMR experiments have been carried out to assign the peaks of the guest molecules in the capsular complex. And 2D NOESY NMR experiments have been performed to bring into light the orientation of the guest inside the capsular complex. Diffusion NMR spectroscopy have also been used to draw conclusions regarding the capsular assembly.<sup>286</sup> The latter part of the study, i.e., the photochemical “ene” reaction, has been carried out in solution as well as in OA and monitored by GC and the identity of the products being confirmed with GCMS and NMR spectroscopy.

## 5.2 Results and Discussions

### 5.2.1 Encapsulation and “ene” reaction of 1-alkylcycloalkenes inside Host OA

**(a) Stoichiometry of the complexes:** The alkyl and cyclohexyl proton signals appear as an indistinguishable cluster in  $\text{CD}_3\text{CN}$  whereas, are upfield shifted and can be distinctly located when encapsulated inside OA, suggesting that the interior of the OA provides a non-polar environment and can distinguish between various protons of the bound guest. **Figure 5.2** illustrate this, with the help of an example of  $\text{G}_{10}$  and  $\text{G}_{10}@\text{OA}$ . Once it is ascertained that the guest forms a complex with the host OA,  $^1\text{H}$  NMR titration experiments are carried out. These experiments along with the 2D DOSY NMR experiments can give detailed information on the complexation ratio of the guest and host.

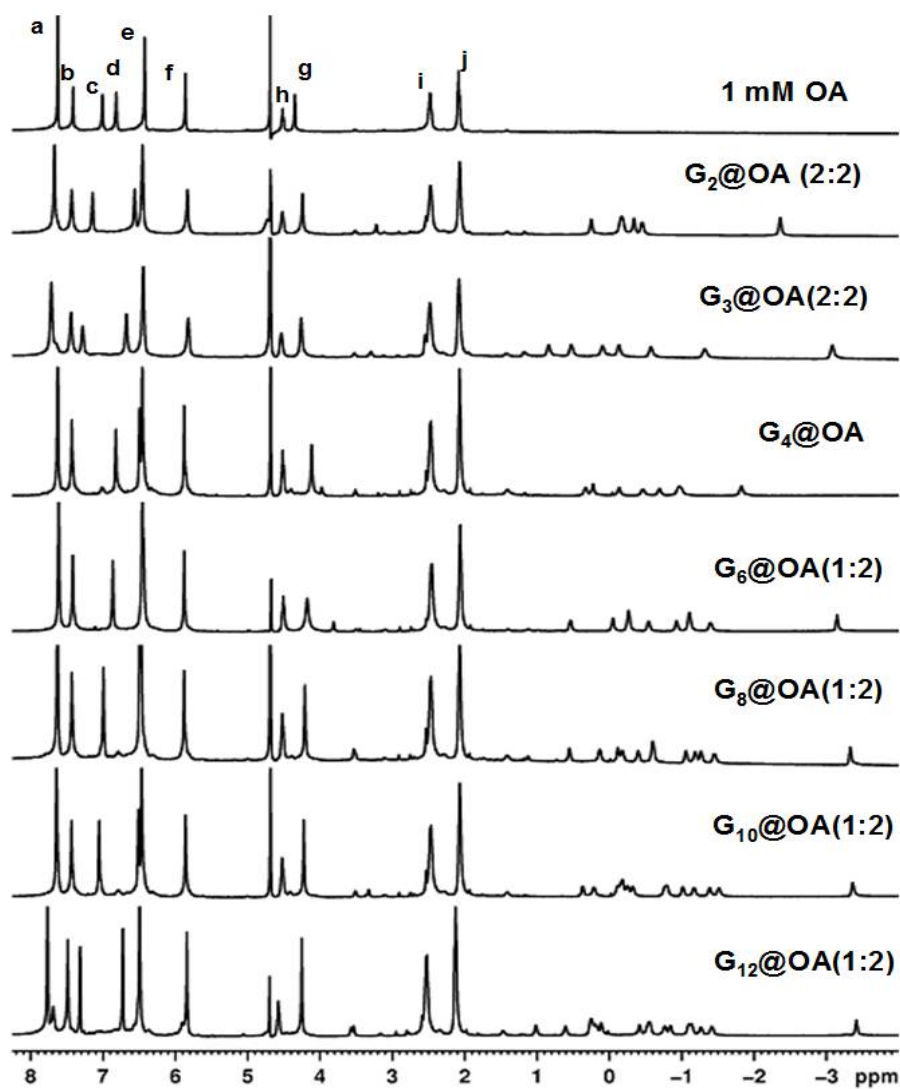


**Figure 5.2** Partial  $^1\text{H}$  NMR spectra of  $\text{G}_{10}$  in  $\text{CD}_3\text{CN}$  and in OA.

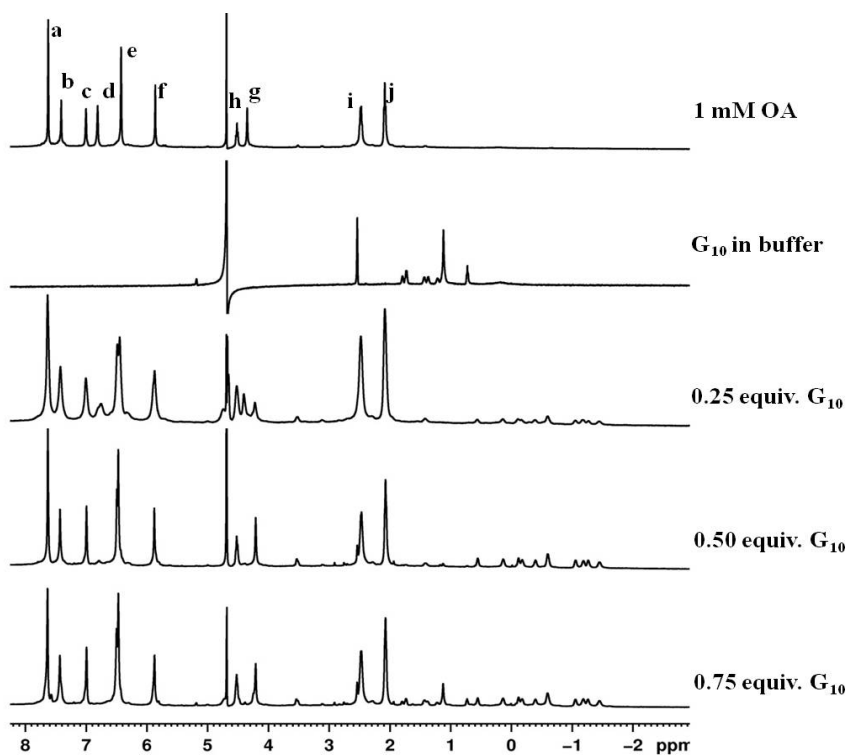
**Figure 5.3** shows various host-guest complexes and gives the ratio of the guest@host. It is observed that for smaller chain length cyclohexenes like ethyl and propyl, (2:2) capsuleplex is formed. The hexyl to dodecyl cyclohexenes bear long chain, hence essentially form (2:1) complexes. The above stoichiometry is based upon the  $^1\text{H}$  NMR titration study. Two examples of  $^1\text{H}$  NMR titrations experiments are illustrated in **Figures 5.4** and **5.5**. In **Figure 5.4**,  $^1\text{H}$  NMR titration of  $\text{G}_{10}$  is shown. Guest  $\text{G}_{10}$  is added in 0.25 equivalent slots to the 1mM host solution. It can be observed that on addition of first 0.25 equivalents  $\text{G}_{10}$ , the guest proton signals appear in the upfield region, showing that the guest is complexing with the host OA. But, the host proton signals remain broad, indicating that some uncomplexed host is still remaining in the solution. On addition of another 0.25 equivalent  $\text{G}_{10}$  (total 0.50 equivalents), all the host as well as guest proton signals get sharpened indicating that none of the host or guest is uncomplexed in the solution. When another 0.25 equivalent of  $\text{G}_{10}$  is added, it can be observed that the guest proton signals corresponding to the uncomplexed guest appear in the spectrum. Hence, this series of observation lead to the fact that  $\text{G}_{10}$  forms a 1:2 complex with the host OA. As another example  $^1\text{H}$  NMR titration of  $\text{G}_2$  with host OA is shown in **Figure 5.5**. 0.1 equivalents of  $\text{G}_2$  is added to 1mM of OA solution, and the  $^1\text{H}$  NMR spectrum recorded.

This process is repeated for next nine times. On addition of each 0.1 equivalents  $\text{G}_2$ , the intensity of the guest proton signals which appear in the upfield region increases. But

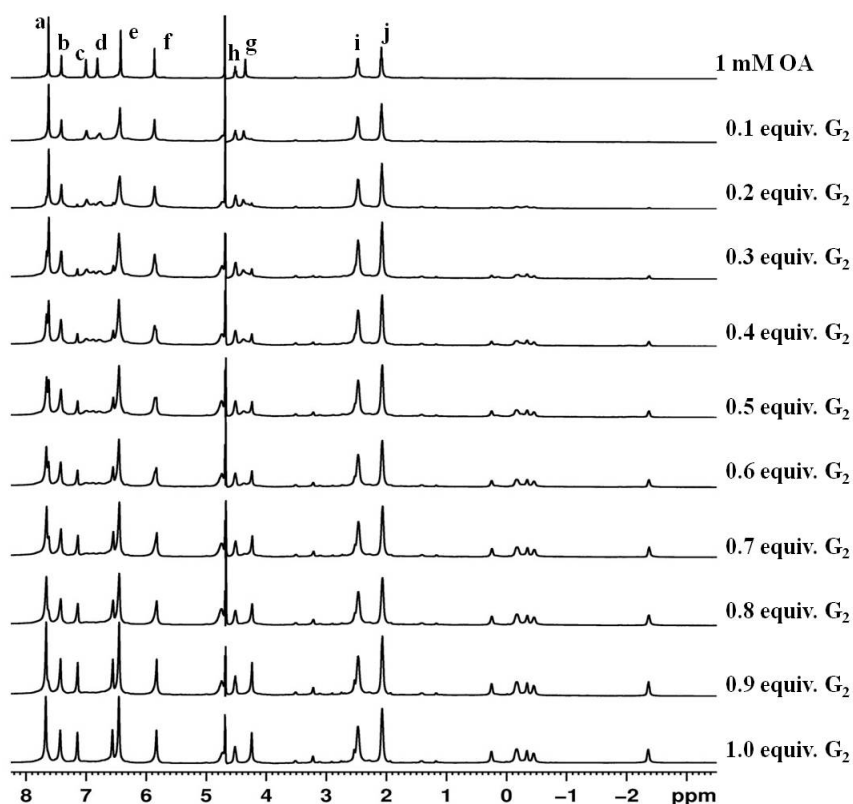
whether the complexation is complete or not is determined by observing the host OA peaks. On Addition of around 0.5 equivalents of  $G_2$ , the host OA proton signals are still broad so the guest ration is increased gradually. On addition of 1.0 equivalents of  $G_2$ , the host as well as guest proton signals get sharpened, indicating the formation of a strong complex with the guest host ratio as 1:1. On forming a capsuleplex neither free host, nor free guest  $^1\text{H}$  signals can be seen. Integration of the guests also confirms the stoichiometry.



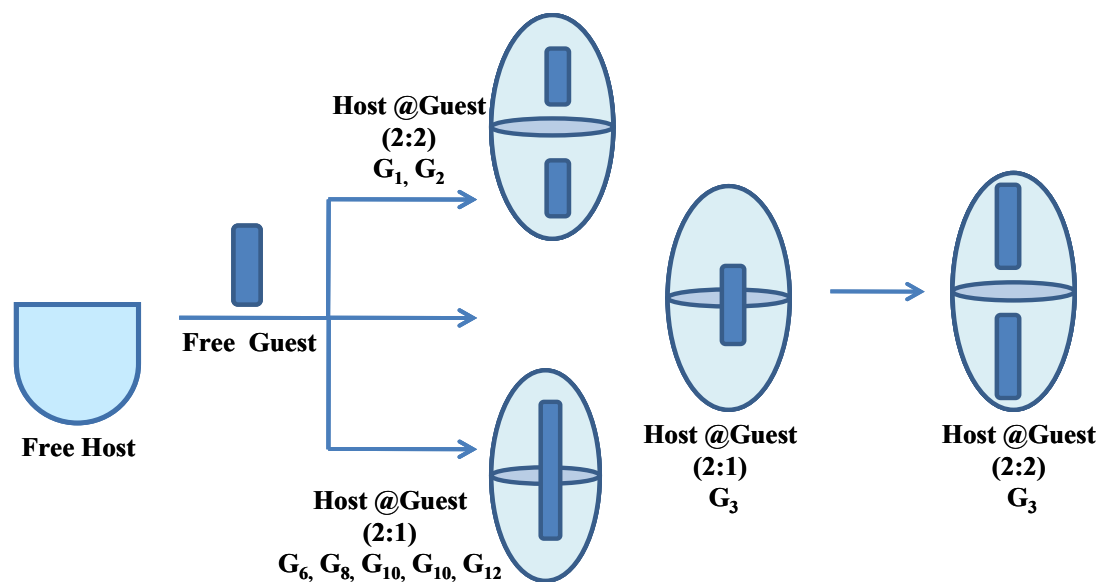
**Figure 5.3** Various guest@host complexes in  $\text{D}_2\text{O}$  and the stoichiometric ratio of complexes; 500 MHz,  $25^\circ\text{C}$ .



**Figure 5.4**  $^1\text{H}$  NMR titration spectra of G<sub>10</sub>@OA. [G<sub>10</sub>] = 0.25 -0.75 mM, [OA] = 1mM. Spectra recorded in 500 MHz NMR and at room temperature.



**Figure 5.5**  $^1\text{H}$  NMR titration spectra of G<sub>2</sub>@OA. [G<sub>10</sub>] = 0.10 -1.0 mM, [OA] = 1mM. Spectra recorded in 500 MHz NMR and at room temperature.

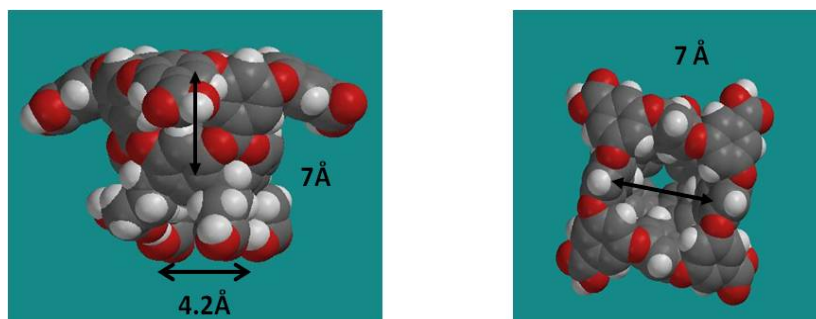


**Figure 5.6** The formation of (2:1), (2:2) and both the complexes simultaneously in presence of various guests.

**(b) Calculations of length and volume of the guest molecules using Spartan:** The length of the inner cavity of the host is 7 Å and hence of a capsule is 14 Å, and the total volume of the host cavity is 740 Å<sup>3</sup>. The volume of the guests calculated also supports the aforementioned stoichiometry of the host guest complex for eg. the host volume is 740 Å<sup>3</sup> and the G<sub>6</sub> volume is 217.51 Å<sup>3</sup>, so two such guest molecules may not fit in the host, suggesting a 2:1 complex. At first, the lengths do not seem to be compatible with the stoichiometry, but it has been suggested by Gibb<sup>287</sup>, that the alkyl chain adopt folded conformations<sup>288, 289</sup> to fit within the confines of the capsule. We observe that the above statement is true, but there is a limit of encapsulation. In this case, dodecylcyclohexene is the limit. We have tried to encapsulate tetradecylcyclohexene, but even after long hours of heating and sonication, no guest can be encapsulated inside OA. The calculated length and volume of tetradecylcyclohexene also suggest the same. Extensive study on the stoichiometric aspect of complexation has been done by our group.<sup>52</sup>

**Table 5.1** The length and volume for each guest molecule. Spartan has been utilized and the energy is minimized for each structure. The guest molecule is taken in linear conformation.

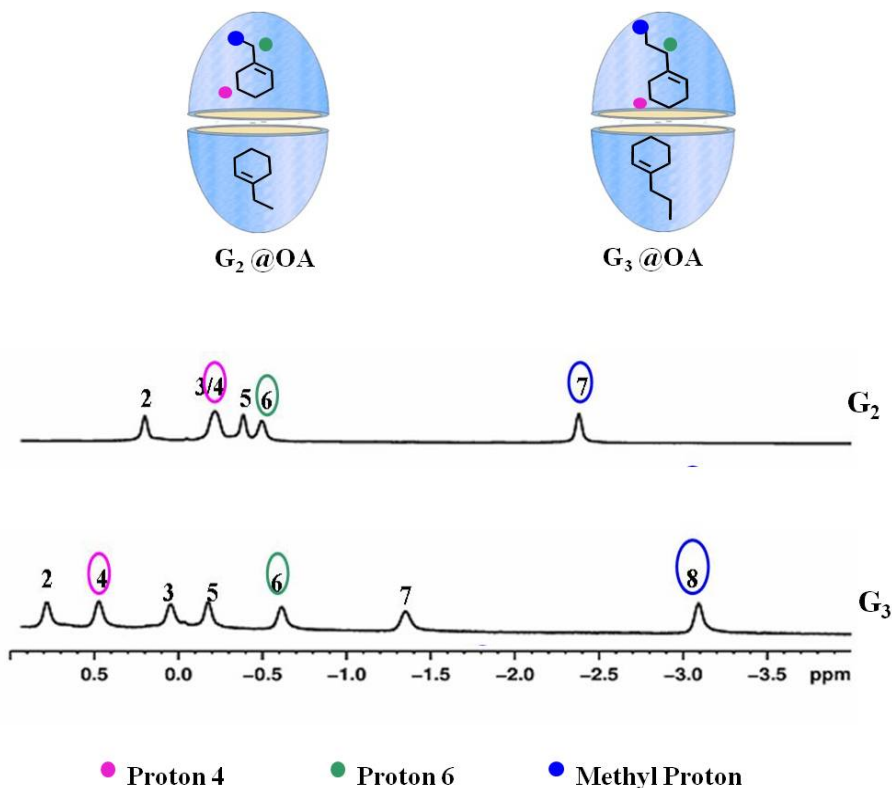
Guest Compounds	Length (Å)	Volume (Å <sup>3</sup> )
1- methylcyclohexene	5.9	125.9
1-ethylcyclohexene	7.2	144.2
1-propylcyclohexene	8.5	162.4
1-butylcyclohexene	9.6	180.8
1-pentylcyclohexene	10.9	199.1
1-hexylcyclohexene	12.0	217.5
1-octylcyclohexene	14.8	254.0
1-decylcyclohexene	17.1	290.8
1-dodecylcyclohexene	19.6	327.4
<b>1-tetradecylcyclohexene</b>	<b>22.3</b>	<b>363.9</b>



**Figure 5.7** The dimensions of the host cavity, as calculated by Spartan.

(c) **<sup>1</sup>H NMR structural characterization of 1-alkylcyclohexene@host complexes:** This section is subdivided into two parts (i) signals for the alkyl chain and cyclohexyl ring of the guest and (ii) the host aromatic region. The guest and host peaks are assigned on the basis of 2D COSY NMR spectroscopy.

(i) **Signals for the alkyl chain and cyclohexyl ring of the guest.** The significant upfield shift of guest signals revealed that all the guests were held within the essentially dry and non polar interior of the capsule.<sup>52</sup> For all the guests it is the methyl group (represented by a blue dot and circle in the following figures) which is most upfield shifted, indicating that it is situated deep into the cavity.

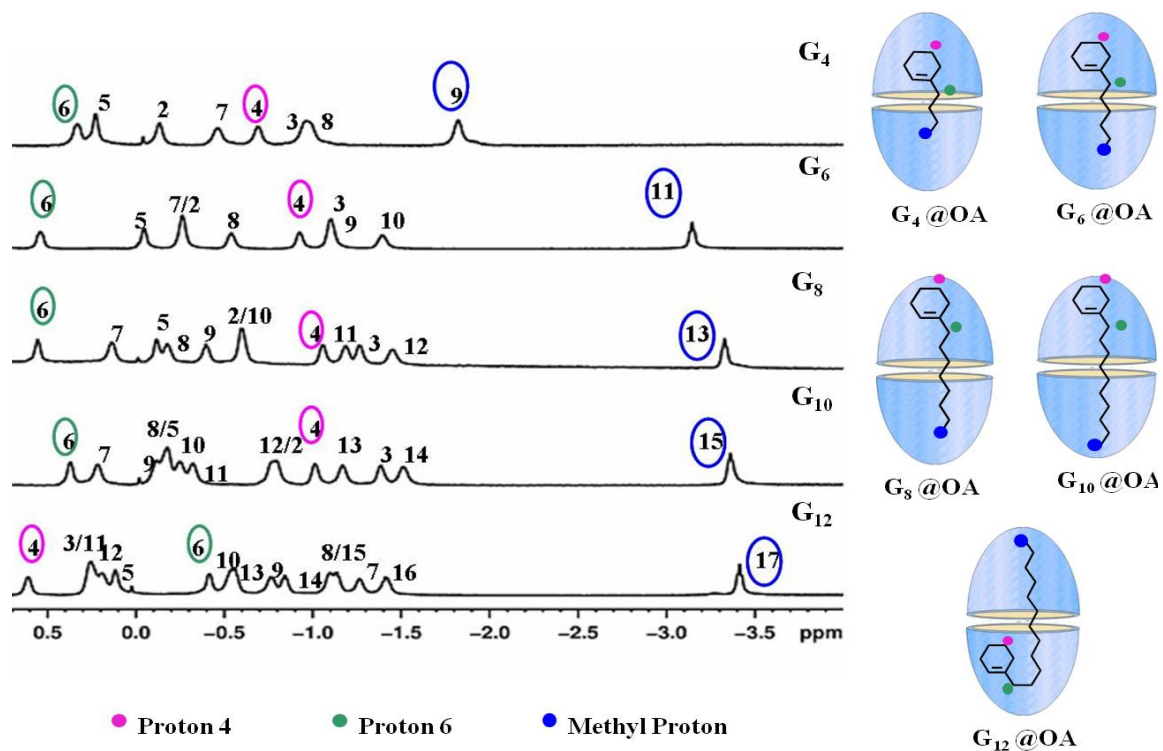


**Figure 5.8** The expanded  $^1\text{H}$  NMR upfield region (depicting the guest protons) for  $\text{G}_2@OA$  and  $\text{G}_3@OA$ . The guest protons have been assigned on the basis of 2D COSY NMR experiments for the above complexes.

**Figure 5.8** shows the  $^1\text{H}$  NMR upfield guest region of  $\text{G}_2@OA$  and  $\text{G}_3@OA$ . These two guests  $\text{G}_2$  and  $\text{G}_3$  have been grouped into one figure because both of them form 2:2 complexes with host OA. It is observed that the methyl group of  $\text{G}_3$  is more upfield shifted in comparison with  $\text{G}_2$ , suggesting that since  $\text{G}_3$  is larger in length, so it is deeper in the cavity. If we continue to look on from **Figure 5.8** to **Figure 5.9**, we would observe

that the methyl group of  $G_4$  is downfield shifted in comparison to  $G_3$ , this could be since  $G_3$  forms (2:2) complex, so the methyl proton is deeper in the cavity, whereas  $G_4$  forms (2:1) complex so methyl proton is located in the mid-space of the cavity, hence downfield. It is also noteworthy that cyclohexyl ring protons show up at the relatively downfield region for  $G_2$  and  $G_3$ , indicating that the ring is located at the centre of the cavity. **Figure 5.9** shows the  $^1\text{H}$  NMR upfield guest region of  $G_4@OA$ ,  $G_6@OA$ ,  $G_8@OA$ ,  $G_{10}@OA$ , and  $G_{12}@OA$ . The methyl proton keeps shifting upfield from  $G_4$  to  $G_8@OA$  complexes, indicating that as the alkyl chain length of the guest cyclohexene increases, it occupies more cavity space, methyl group heading towards the narrower end of the cavity. From  $G_8$  through  $G_{12}$  we see marginal upfield shift in methyl proton position indicating that  $G_8$  methyl group acquires optimal depth inside the cavity. It can be observed that the cyclohexyl ring protons, particularly proton 4 (proton 4 represented by pink dot and circle) for  $G_4$  through  $G_{10}$  is upfield shifted, suggesting that the cyclohexyl ring try to burry itself in the other end of the cavity as the alkyl chain length increases. In case of  $G_{12}$ , we observe that proton 4 is shifted downfield, suggesting that it is located near the mid of the cavity. On comparing the position of proton 6, which is the first proton on the alkyl chain adjoining the cyclohexene ring (proton 6 represented by green dot and circle) it can be observed that proton 6 is located in downfield region in case of  $G_4@OA$  to  $G_{10}@OA$ , whereas, in case of  $G_{12}@OA$ , it is much upfield shifted. The shift in proton 6 position is complementary to the shift in position of proton 4. These observations suggest the possible conformations of the guests@OA as shown in **Figure 5.9**.



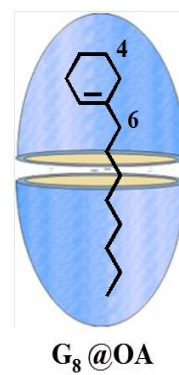
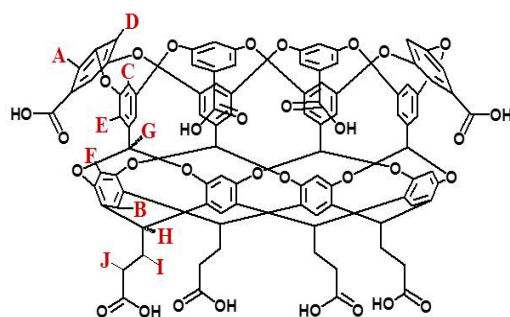
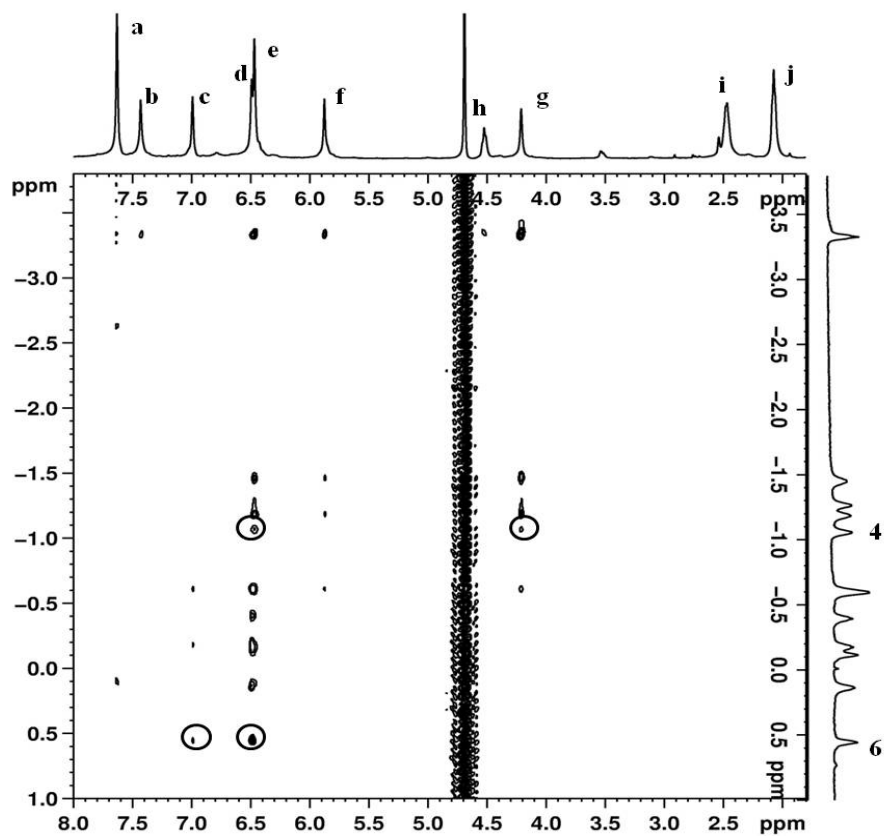


**Figure 5.9** The expanded  $^1\text{H}$  NMR upfield region (depicting the guest protons) for G<sub>4</sub>@OA, G<sub>6</sub>@OA, G<sub>8</sub>@OA, G<sub>10</sub>@OA and G<sub>12</sub>@OA. The guest protons have been assigned on the basis of 2D COSY NMR experiments for the above complexes.

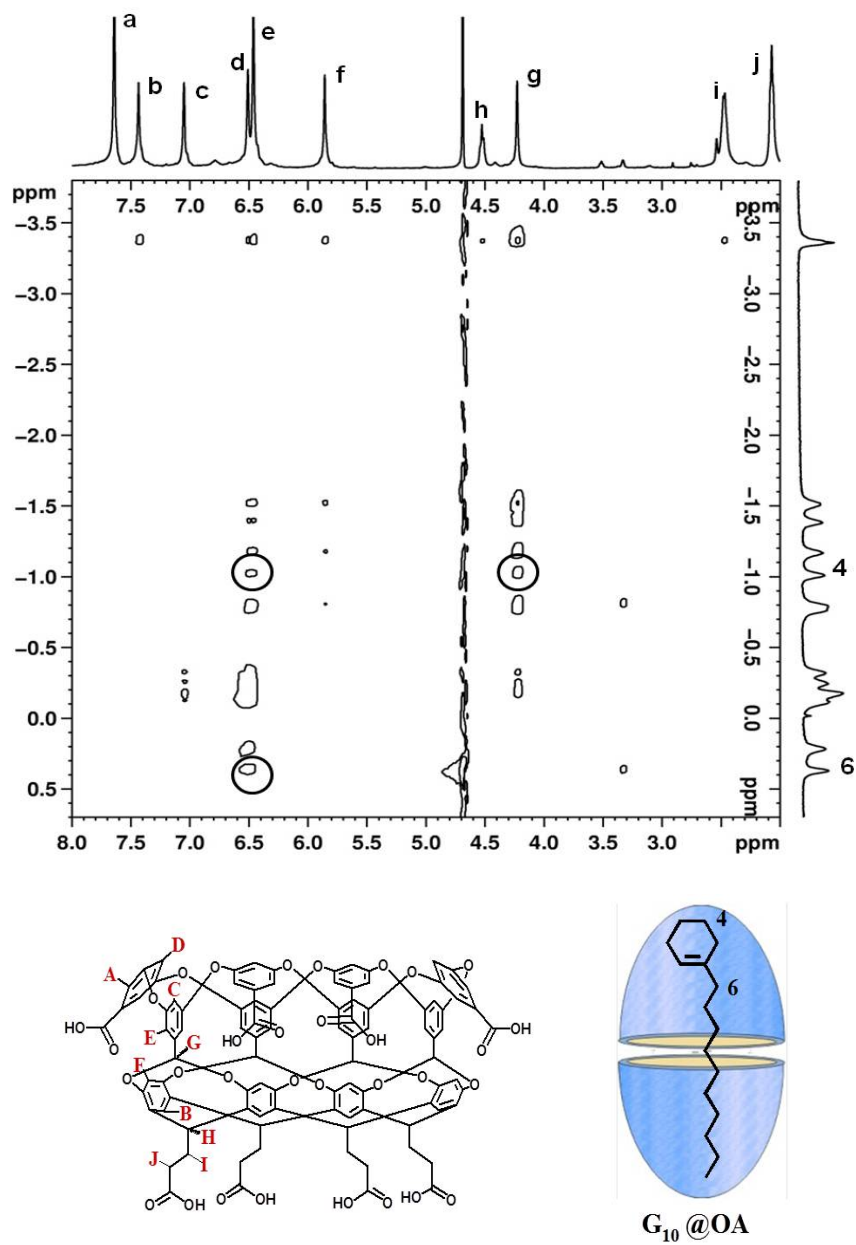
Apart from 1D  $^1\text{H}$  NMR studies of these complexes, 2D COSY and NOESY NMR have been extensively utilized to support the above observations. **Figures 5.10, 5.11 and 5.12** show the 2D NOESY NMR spectra of complexes G<sub>8</sub>@OA, G<sub>10</sub>@OA and G<sub>12</sub>@OA, respectively. A 2D NOESY NMR spectrum gives us the information about the interaction of the guest with the host, since in this spectrum we can observe the intermolecular correlation between the guest and host proton signals. Focusing on **Figures 5.10 and 5.11**, we can observe that the proton 4, which is a proton in the cyclohexene ring in G<sub>8</sub>@OA and G<sub>10</sub>@OA complexes shows a correlation with protons “g” and “e” of host OA. Protons “g” and “e” in host OA are located towards the narrower end and mid space of the cavity, respectively. Hence the correlation between proton 4 of guests G<sub>8</sub> and G<sub>10</sub>

with the protons “g” and “e” of host OA, indicates that the cyclohexene ring of these guests may be located at the narrower end of the cavity. Whereas, proton 6 which is the first proton in the alkyl chain adjoining the cyclohexene ring, shows a correlation with protons “d” and “c” of the host OA. Protons “d” and “c” in host OA are located towards the broader end of the cavity or the open space in the capsular complex. The correlation between proton 6 and protons “c” and “d” of the host OA, may indicate that the alkyl chain tends to be at the middle of the capsular assembly.

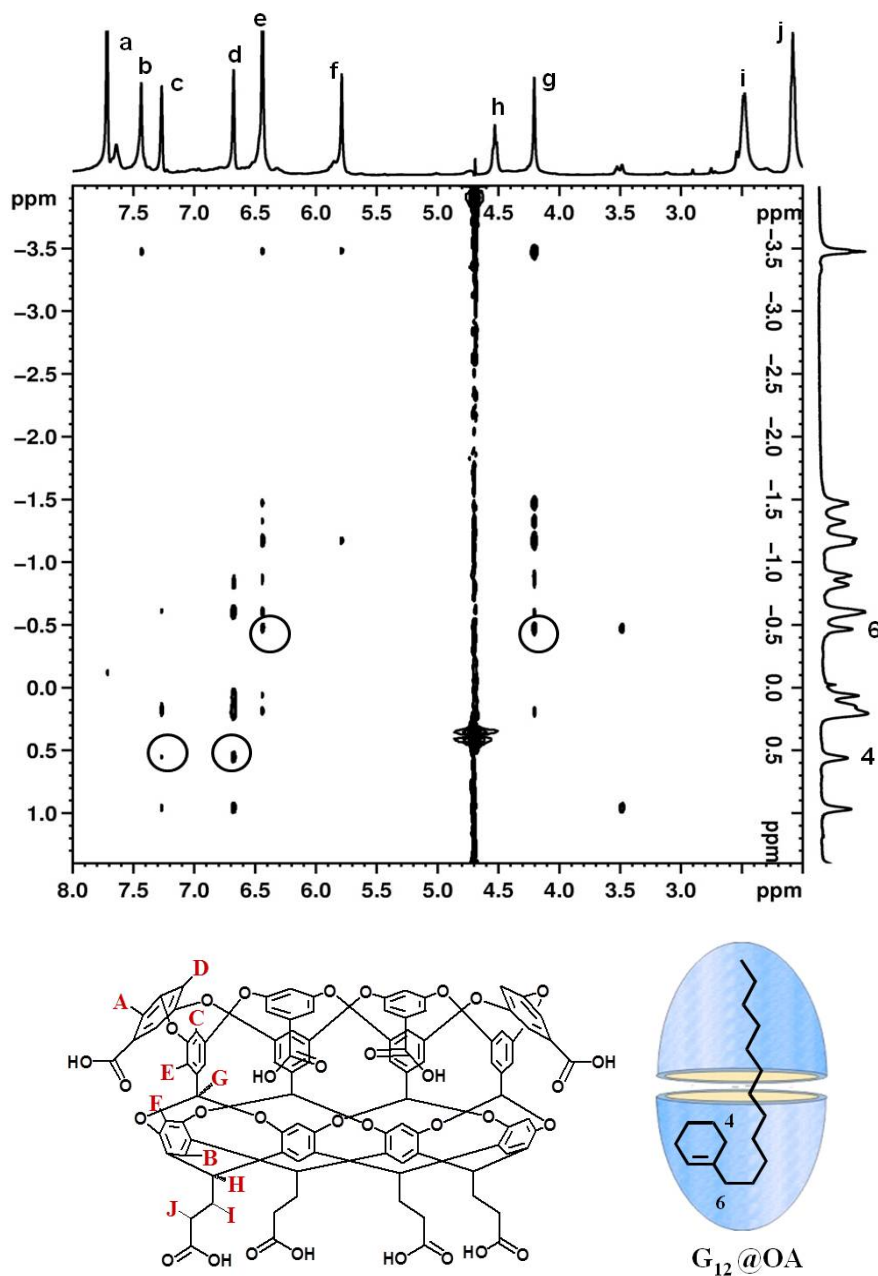
Now moving on to  $G_{12}@OA$  complex, **Figure 5.12** shows the 2D NOESY NMR spectrum of  $G_{12}@OA$ . It can be observed that here the positions of guest proton signals 4 and 6 are switched in comparison to the complexes  $G_8@OA$  and  $G_{10}@OA$ . Proton 6 of  $G_{12}$  shows a correlation with protons “g” and “e” of host OA, whereas, proton 4 of guest  $G_{12}$  shows a correlation with protons “c” and “d” of host OA. These correlations support the bent conformation for the guest  $G_{12}$ , inside the host cavity OA. We speculate that, as the alkyl chain length increases from  $G_4$  to  $G_{10}$ , the cyclohexene ring keeps on moving towards the deeper end of the cavity (proton 4 shows up in the upfield region and correlates with protons “g” and “e” of the host OA) and occupy the optimal position. But when the alkyl chain length is further increased to  $G_{12}$ , since there is no more space in the capsule, hence, the cyclohexene ring bents and finds itself more comfortable in the mid region of the capsule (proton 4 in the downfield region and correlating with protons “c” and “d” of host OA and proton 6 correlating with protons “e” and “g” of the cavity).



**Figure 5.10** 2D NOESY NMR spectrum of  $G_8@OA$ . Spectrum recorded in 500 MHz NMR and at room temperature.



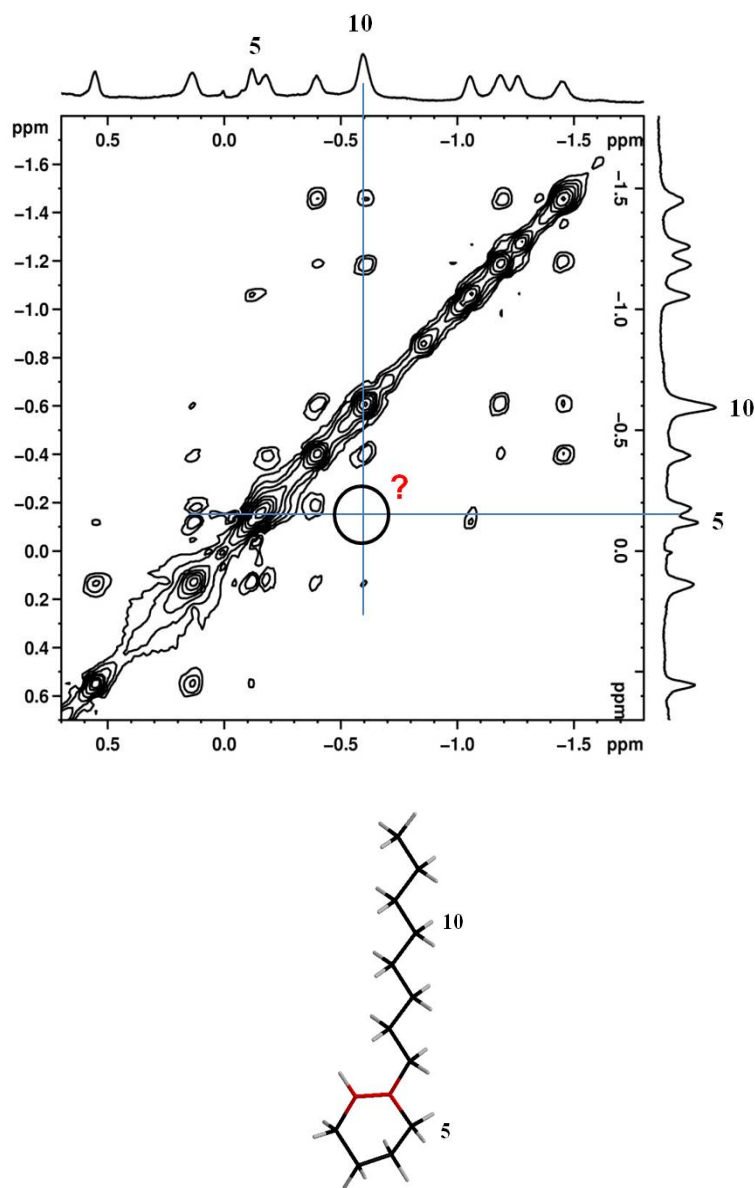
**Figure 5.11** 2D NOESY NMR spectrum of  $G_{10}@OA$ . Spectra recorded in 500 MHz NMR and at room temperature.



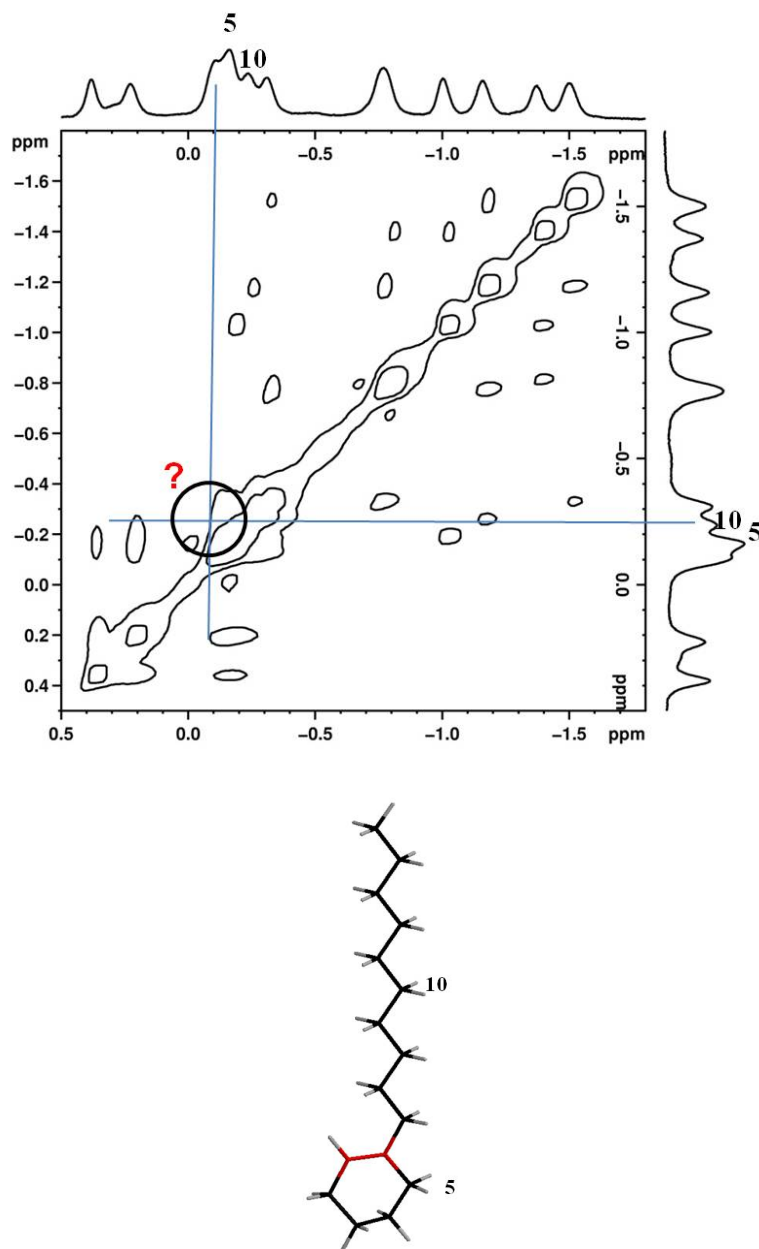
**Figure 5.12** 2D NOESY NMR spectrum of  $G_{12}@OA$ . Spectra recorded in 500 MHz NMR and at room temperature.

Below we present another set of observations which further supports the bent conformation of  $G_{12}$  molecule inside host OA. **Figures 5.13, 5.14 and 5.15**, show the expanded upfield region of 2D NOESY spectra of  $G_8@OA$ ,  $G_{10}@OA$  and  $G_{12}@OA$ , showing the intermolecular (through space) guest-guest proton signal interactions. By

observing **Figures 5.13** and **5.14**, we can notice that there exist no correlation between protons 5 and 10 of the guests  $G_8$  and  $G_{10}$ .

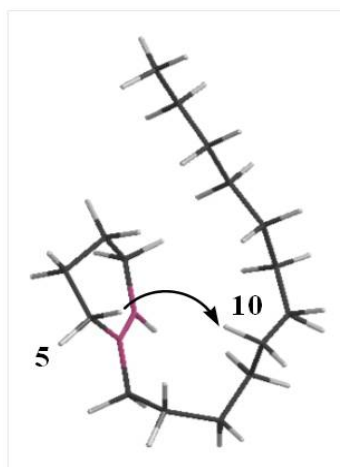
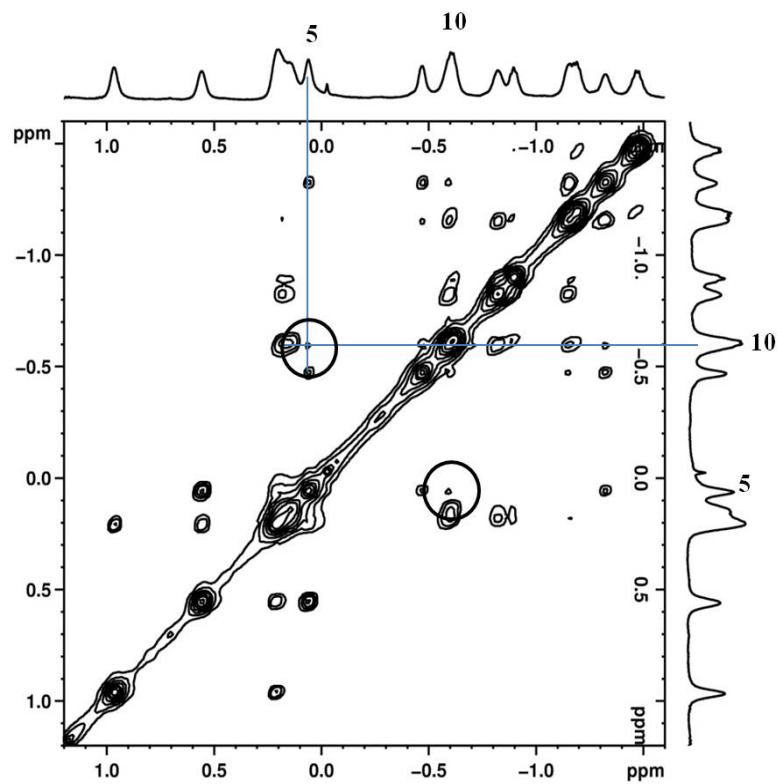


**Figure 5.13** Expanded upfield region of 2D NOESY NMR, (depicting intermolecular guest-guest proton correlations) spectrum of  $G_8@OA$ . Spectra recorded in 500 MHz NMR and at room temperature.



**Figure 5.14** Expanded upfield region of 2D NOESY NMR, (depicting intermolecular guest-guest proton correlations) spectrum of  $G_{10}@OA$ . Spectra recorded in 500 MHz NMR and at room temperature.

But **Figure 5.15** clearly shows a correlation signal between the protons 5 and 10 of the guest  $G_{12}$  when encapsulated inside OA. This correlation could only occur when the protons 5 and 10 of the guest  $G_{12}$  are positioned nearby, which in turn is only possible when the cyclohexene ring is bent, so that the protons 5 and 10 confront each other.

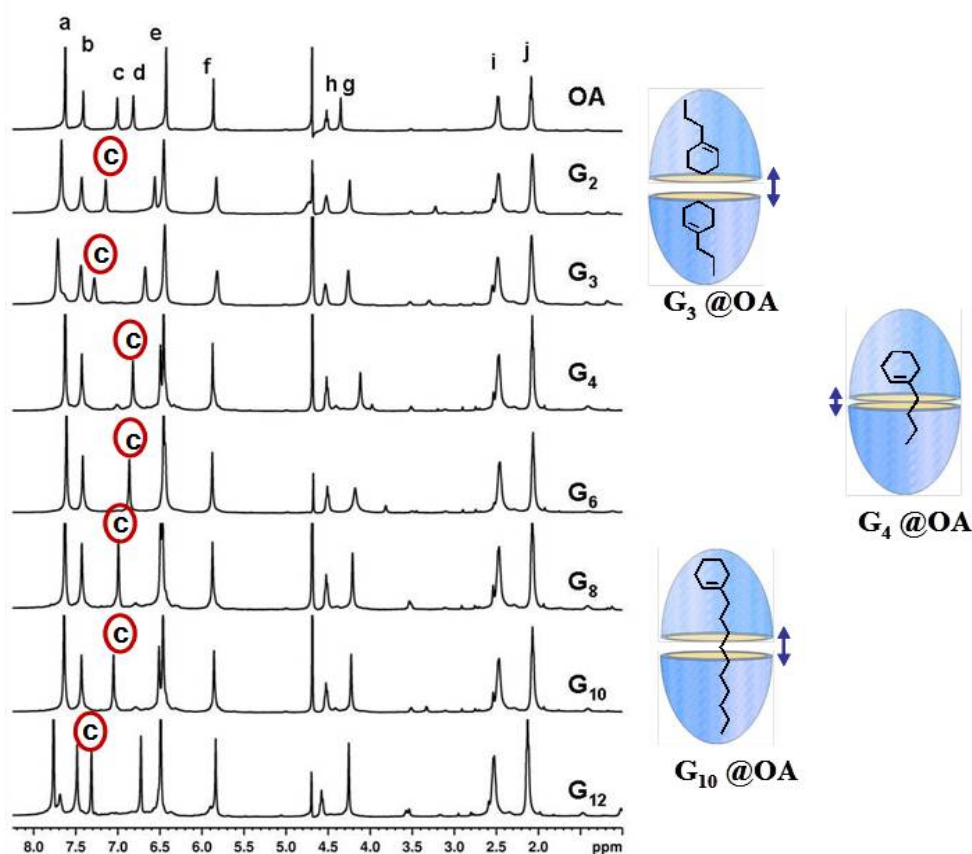


**Figure 5.15** Expanded upfield region of 2D NOESY NMR, (depicting intermolecular guest-guest proton correlations) spectrum of  $G_{12}@OA$ . Spectra recorded in 500 MHz NMR and at room temperature.

In the next subsection, we focus on the overall compactness of the guest@OA capsular assembly.



(ii) **The host aromatic region.** The “c”  $^1\text{H}$  signal for the OA represents the proton at the periphery of the capsule (**Figure 5.1 a**). This proton may shift upfield when another part of the capsule comes on top of it, due to the shielding effect of the aromatic proton from that part. So peak “c” tells how compactly the two parts of the capsule are held together.

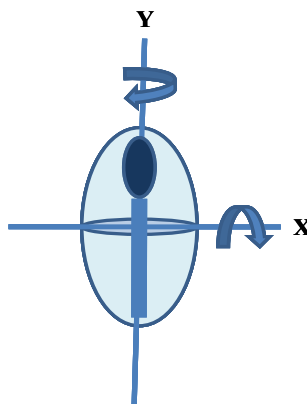


**Figure 5.16** The aromatic host region, shows  $^1\text{H}$  signal “c” shift of the host, upon forming various complexes.

Above, we can notice that from ethyl to propyl the “c” peak shifts more downfield as with the increase in the size of the guest the two parts of OA, come a bit apart. The same observation is consistent for the (2:1) complexes of  $G_4$ - $G_{12}$ @OA. Also, it can be noted that, the host peaks does not split, indicating that there is no kind of asymmetry present inside the capsule. There could be two reasons behind this observation; first, since both the ends of the guest contain alkyl protons, except one alkene proton, hence

host cannot distinguish much between the two parts. But a more plausible reason could be that the guest is tumbling too fast on the NMR scale, so as to account for the symmetry present. If the guest rotates around Y axis inside the capsule, one side of the guest would be most of the time residing in one particular part of OA, and hence no splitting of host peaks be observed.<sup>51</sup> Whereas, if the guest molecule rotates around the x axis, then there will be asymmetry, and splitting of the host peak should be observed. But if this rotation around x axis is fast on the NMR timescale then we may not observe any splitting of the host peaks.

**(d) Diffusion Constant:** The diffusion constant of a certain molecular species depends on its effective molecular size, which should change with any intermolecular interactions. It is clear that diffusion constants are intuitively related to aggregation and intermolecular interactions. This means that in diffusion measurements the observable parameters of the bound guest can be predicted.<sup>286</sup> In above case the diffusion constant of the free host<sup>291</sup> is  $1.88 \times 10^{-5} \text{ cm}^2/\text{sec}$ . On comparison, we find that diffusion constant for the bound guest@host complex is less than the diffusion constant for the free host in all the cases. This is probably due to the fact that as the guest binds to the host, the complex becomes bulky and hence diffuses slowly on the NMR timescale.



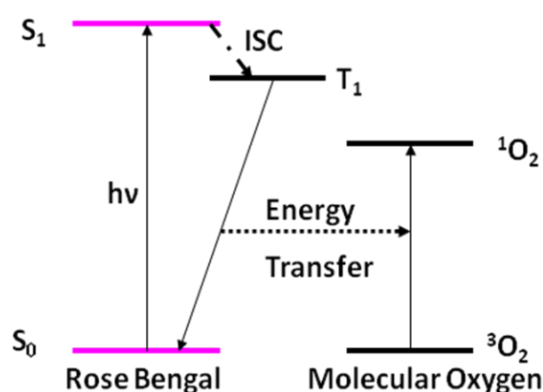
**Figure 5.17** Possible axes of rotation for the guest inside host.

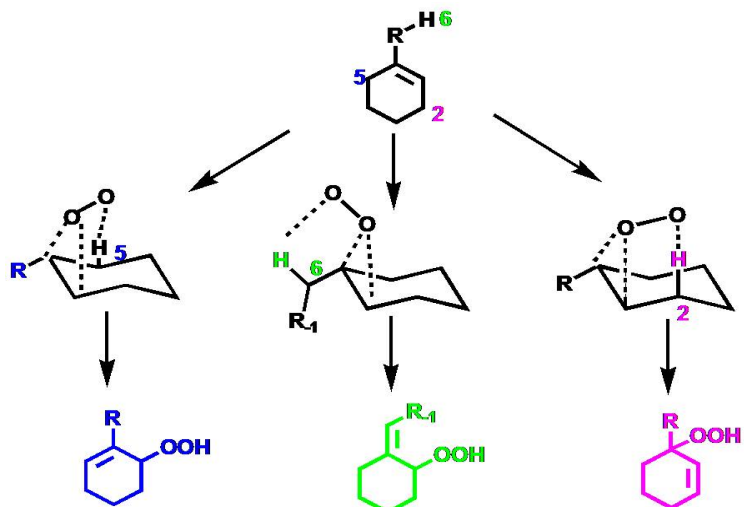
**Table 5.2** The diffusion constants for various guest@host complexes.

Guest Compounds	Diffusion Constant
1-ethylcyclohexene	$1.19 \times 10^{-6} \text{ cm}^2/\text{sec}$
1-propylcyclohexene	$1.10 \times 10^{-6} \text{ cm}^2/\text{sec}$
1-butylcyclohexene	$1.24 \times 10^{-6} \text{ cm}^2/\text{sec}$
1-hexylcyclohexene	$1.22 \times 10^{-6} \text{ cm}^2/\text{sec}$
1-decylcyclohexene	$1.21 \times 10^{-6} \text{ cm}^2/\text{sec}$
1-dodecylcyclohexene	$1.19 \times 10^{-6} \text{ cm}^2/\text{sec}$

2 mM OA in 20 mM sodium tetraborate buffer solution, 500 MHz, 25°C.

**(e) Photochemical “ene” reaction in solution and inside OA:** First, singlet oxygen is generated by triplet sensitizer Rose Bengal. Rose Bengal on irradiation goes from singlet ground state to singlet excited state. From there by inter system crossing (ISC) goes to the excited triplet state and while relaxing back to the original ground state, it transfers its energy to the triplet ground state molecular oxygen to generate singlet excited state of molecular oxygen called singlet oxygen. The singlet oxygen thus produced can undergo “ene” reactions with the cycloalkenes yielding various products in solution.

**Figure 5.18** Sensitization of singlet oxygen by Rose Bengal.



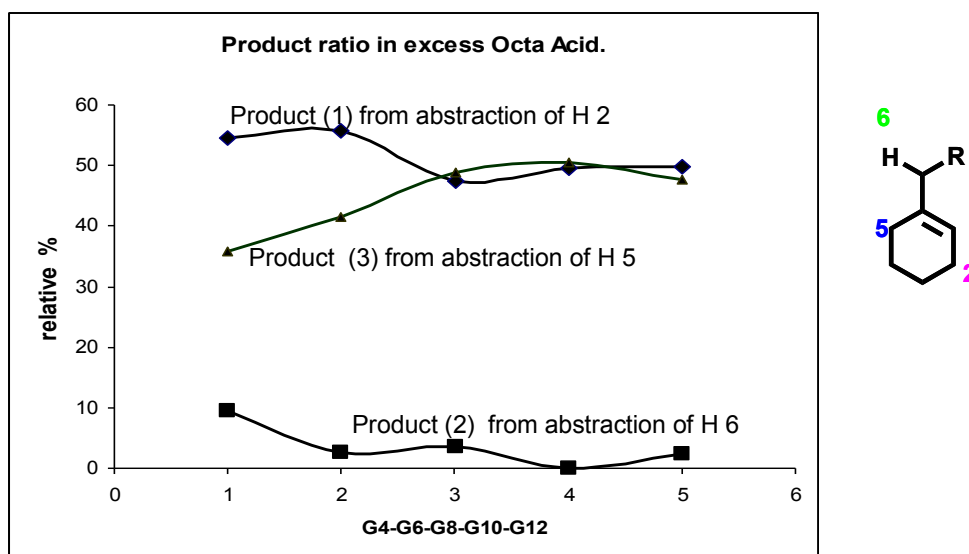
**Scheme 5.6** Possible products of “ene” reaction in solution.

**Table 5.3** Product ratio for “ene” reaction in solution and inside OA.

Relative Percentages (based on GC analysis)				
1-methylcyclohexene <sup>#</sup> (G <sub>1</sub> )	Solution	36	44	20
	<b>Octa Acid</b>	<b>90</b>	<b>10</b>	-
1-ethylcyclohexene (G <sub>2</sub> )	Solution	42	43	15
	<b>Octa Acid</b>	<b>52</b>	<b>40</b>	<b>8</b>
1-propylcyclohexene (G <sub>3</sub> )	Solution	37	35	28
	<b>Octa Acid</b>	<b>58</b>	<b>9</b>	<b>33</b>
1-butylcyclohexene (G <sub>4</sub> )	Solution	39	34	26
	<b>Octa Acid</b>	<b>55</b>	<b>10</b>	<b>36</b>
1-hexylcyclohexene (G <sub>6</sub> )	Solution	41	21	40
	<b>Octa Acid</b>	<b>56</b>	<b>3</b>	<b>42</b>
1-octylcyclohexene (G <sub>8</sub> )	Solution	41	20	39
	<b>Octa Acid</b>	<b>48</b>	<b>4</b>	<b>49</b>
1-decylcyclohexene (G <sub>10</sub> )	Solution	39	21	40
	<b>Octa Acid</b>	<b>50</b>	<b>0.0</b>	<b>50</b>
1-dodecylcyclohexene (G <sub>11</sub> )	Solution	40	22	38
	<b>Octa Acid</b>	<b>50</b>	<b>2</b>	<b>48</b>

Started with 100 % pure starting material, used 420 nm filter and irradiated for 10 min.

When the cycloalkenes are captured inside the OA, then we see product selectivity. The cycloalkene containing capsuplex probably opens up to allow singlet oxygen to diffuse in, where it reacts with guest molecules. Because the cycloalkene containing host, holds its guests in a particular orientation within the cavity, so some parts of the cycloalkene are more accessible for chemical reaction than others. The singlet oxygen therefore predominantly attacks the cycloalkene at the most accessible position yielding majorly one product and limiting the formation of other product.



**Figure 5.19** Graph showing the relative percentages of the product of “ene” reaction inside OA.

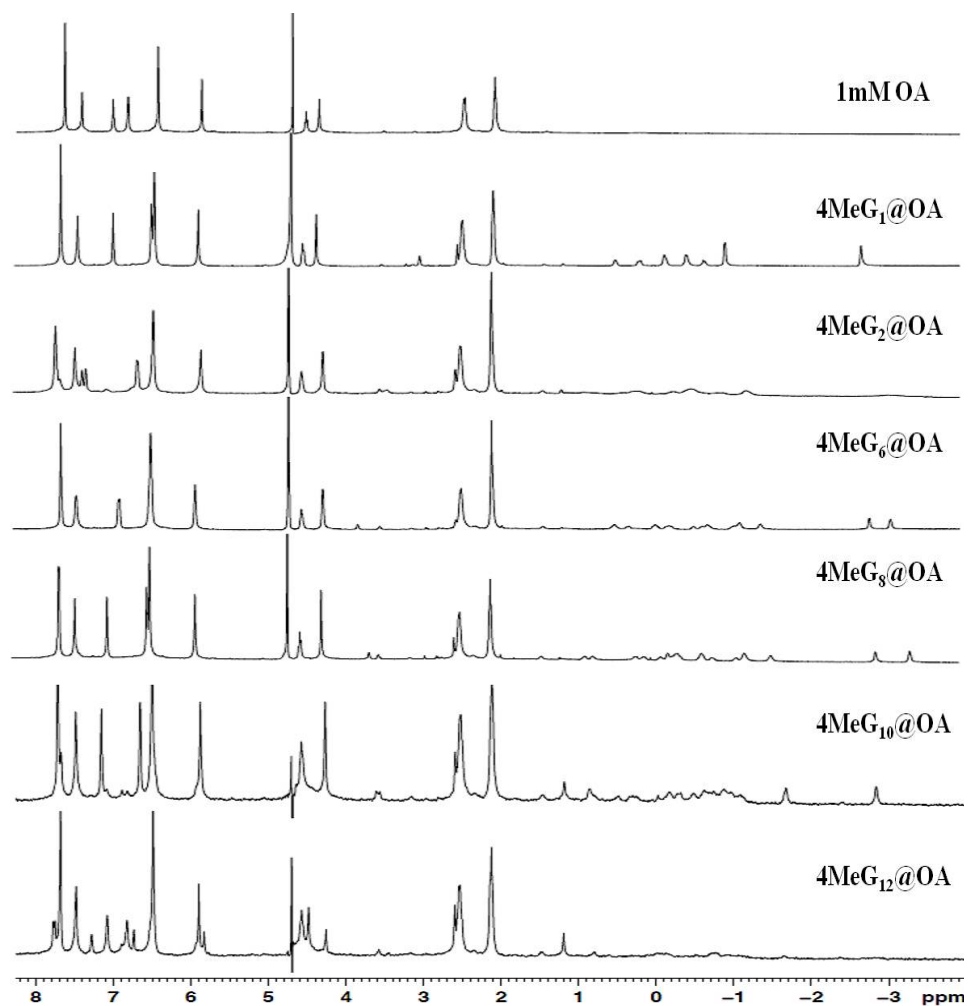
In a recent report by our group the above strategy has been very clearly illustrated. The table above shows the product distribution of “ene” reaction with a series of guest in  $\text{CD}_3\text{CN}$  solution, in absence of host. Correspondingly, it also shows the product selectivity when guest is encapsulated inside the host. It can be observed that when the guest is encapsulated inside the host, chiefly tertiary-peroxide product is formed and the formation of exocyclic peroxide is subsided. The product ratio alters in a

symmetrical fashion based upon the increase in alkyl chain length. In **Figure 5.19**, we see that product from abstraction of hydrogen 2 decreases as the chain length increases, this could be, because with the increase of the chain length hydrogen 2 shifts deeper inside the cavity and hence is least accessible for the chemical reaction with singlet oxygen.

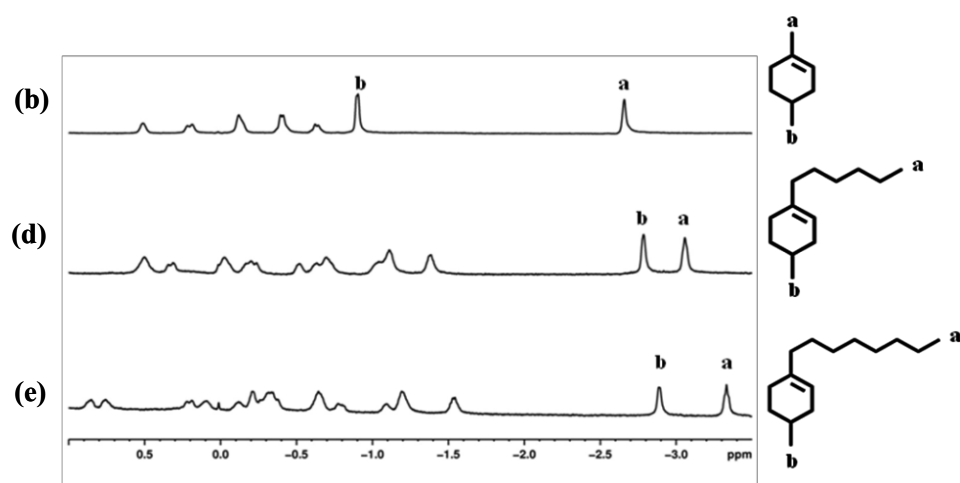
The above graph summarizes the result for all (1:2) guest@host complexes. We also observe that for  $G_4$  and  $G_6$ , product from abstraction of proton 2 is more and eventually for  $G_8$ ,  $G_{10}$  and  $G_{12}$ , the ratio of the products from abstraction of proton 2 as well as proton 5 is almost equal, with very less product present from abstraction of H 6.

### 5.2.2 Encapsulation and “ene” reaction of 1-alkyl-4-methylcycloalkenes inside OA

**(a) Stoichiometric aspects:** The **Figure 5.20** below shows the complex of 4-methyl-1-alkylcyclohexene@OA. Here 4-Me- $G_1$  forms a (2:2) guest@host complex. 4-Me- $G_2$  forms first (2:1) followed by (2:2) complex, and 4-Me- $G_6$ , 4-Me- $G_8$  and 4-Me- $G_{10}$  forms (2:1) complex. 4-Me- $G_{12}$  does not form a complex with the host OA. In the next figure, is given the expansion of the guest region. Here the peaks have been assigned based on the fact that “a” being singlet in case of 4-Me- $G_1$  and triplet in case of 4-Me- $G_6$  and 4-Me- $G_8$  is the alkyl chain methyl group, whereas, “b” being doublet is the 4-substituted methyl group. The proton signal assignments are also supported by the 2D COSY NMR experiments done for the above complexes.

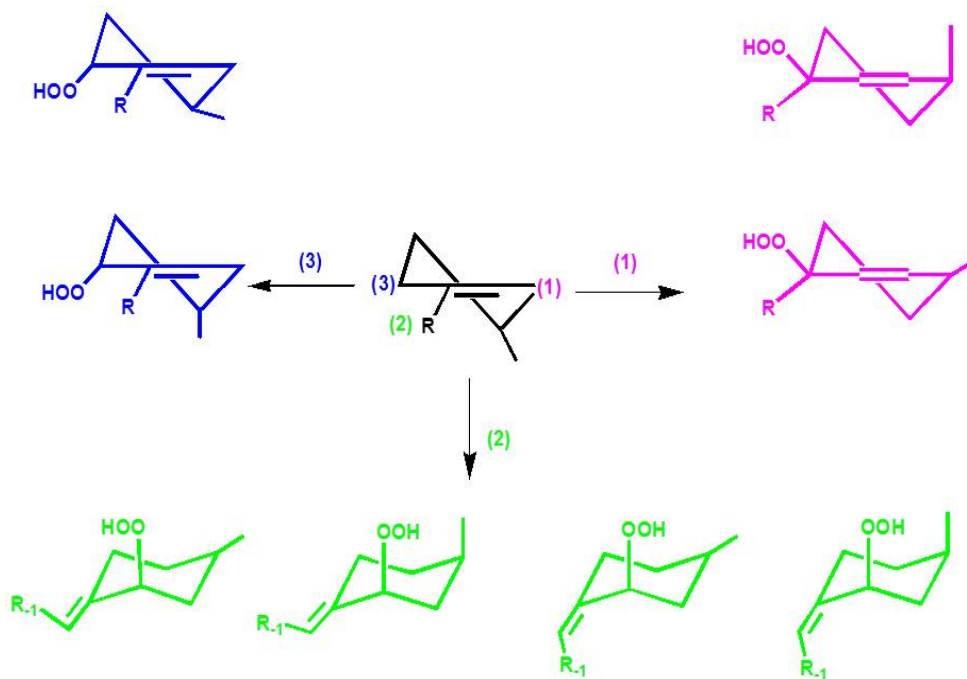


**Figure 5.20** The  $^1\text{H}$  NMR spectra showing the complexation of 4-MeGs@OA, in  $\text{D}_2\text{O}$ , at  $25^\circ\text{C}$ , 500 MHz



**Figure 5.21** The expanded guest region, assignment of two methyl peaks on the basis of multiplicity.

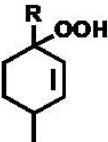
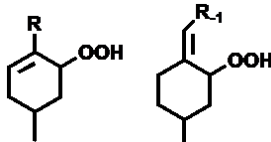
**(b) Photochemical “ene” reaction for 4-Me-1-alkylcyclohexene:** These guest molecules also follow the same trend as for 1-alkylcyclohexene, but the only difference here is that each product formed now can exist in two conformations, axial and equatorial. Hence we observe following possible products (**Scheme 5.6**). We have analyzed these products with the help of GC and GCMS, and we observed that only the first product, i.e. tertiary peroxide is isolated from the rest of the products on the GC, the rest of the product peaks are in some case indistinguishable from each other, hence here we report the product ratio as follows. It is observed that for this set of guests, the percentage of the tertiary-peroxide product further enhances, in comparison to the products obtained in solution probably indicating one favorable orientation of the guest molecule inside the host.



**Scheme 5.7** Possible “ene” reaction products in case of 4-Me-1-alkylcyclohexene guests.



**Table 5.4** Product ratio for “ene” reaction in solution and inside OA\*.

Relative Percentages (based on GC analysis)**			
4-Me-G <sub>1</sub>	Solution	30	70
	<b>Octa Acid</b>	<b>77</b>	<b>23</b>
4-Me-G <sub>6</sub>	Solution	42	58
	<b>Octa Acid</b>	<b>70</b>	<b>30</b>
4-Me-G <sub>8</sub>	Solution	32	68
	<b>Octa Acid</b>	<b>68</b>	<b>32</b>
4-Me-G <sub>10</sub>	Solution	51	49
	<b>Octa Acid</b>	<b>73</b>	<b>27</b>

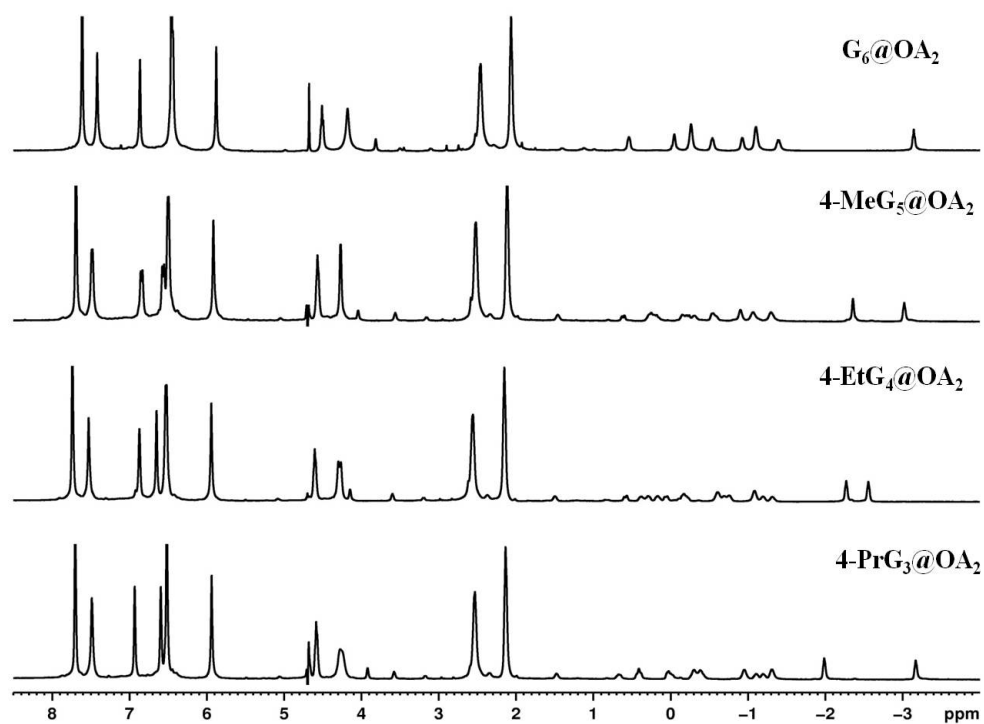
\*Started with 100 % pure starting material, used 420 nm filter and irradiated for 10 min.

\*\* Identity of the structure of the chief product confirmed by the fragmentation pattern obtained by GCMS.

### 5.2.3 Encapsulation and “ene” reaction of four cycloalkene guests of similar molecular length inside Host OA

In an earlier report, we have shown how pre-orientation of methyl cyclohexene within zeolites, through cation- $\pi$  interactions resulted exclusively in product from abstraction of methyl hydrogen. In yet another report, we discussed how the product from abstraction of same methyl hydrogen can be altogether eliminated by anchoring it in the deep cavity of host OA. We believe that space filling and weak CH- $\pi$  interactions are the two main driving forces responsible for specific orientation of a guest inside OA. In order to establish this notion further, we synthesized 4 di-substituted cyclohexenes – 1-hexylcyclohexene (G<sub>6</sub>), 4-methyl-1-pentylcyclohexene (4-Me-G<sub>5</sub>), 4-ethyl-1-butylcyclohexene (4-Et-G<sub>4</sub>) and 1,4-dipropylcyclohexene (4-Pr-G<sub>3</sub>) (**Scheme 5.4**). Though the guest molecules are of approximately same molecular length and are

constitutional isomers of each other, yet with the help of 1D and 2D NOESY/COSY NMR we observed distinct packing for each of them inside the host OA. This clearly indicates that host OA is capable of inducing “orientational isomerism” in its guest molecules. This orientational distinction amongst the guest molecules within OA plays a critical role in photooxygenation reaction of these cyclohexenes and explains the reason behind exquisite product selectivity in one case while none in the other. Herein, we present the results of these observations.

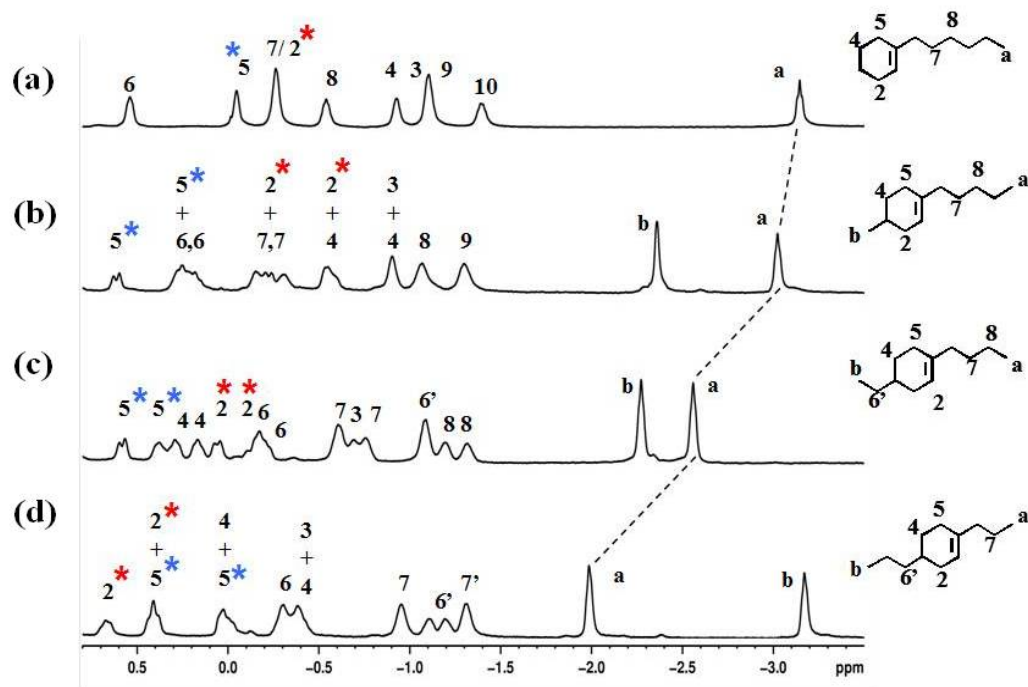


**Figure 5.22**  $^1\text{H}$  NMR spectra showing the complexation of  $\text{G}_6@OA$ ,  $4\text{-MeG}_5@OA$ ,  $4\text{-EtG}_4@OA$  and  $4\text{-PrG}_3@OA$ , respectively, in  $\text{D}_2\text{O}$ , at  $25^\circ\text{C}$ , 500 MHz

First 1 mM of aqueous OA solution in borate buffer, 60 mM of  $\text{G}_6/4\text{-Me-G}_5/4\text{-Et-G}_4/4\text{-Pr-G}_3$  dissolved in  $\text{DMSO-d}_6$  was added in steps of 0.25 equivalents. At 0.5 equivalents it was observed that neither free host nor free guest proton signals existed, suggesting that 2:1 host guest complex was formed in each case. The encapsulation of the

guest was indicated by the significant upfield shift of the guest proton signal (relative to  $\text{CD}_3\text{CN}$ ). In order to compare the packing of the guest molecules, we assigned all the proton signals of each guest@OA<sub>2</sub> with the help of 2-D COSY NMR. **Figure 5.22** shows the <sup>1</sup>H NMR spectra of G<sub>6</sub>@OA, 4-MeG<sub>5</sub>@OA, 4-EtG<sub>4</sub>@OA and 4-PrG<sub>3</sub>@OA.

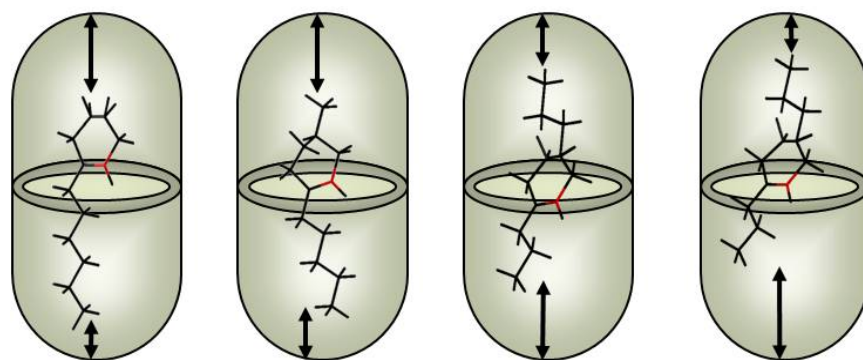
**Figure 5.23** shows the assigned 1D NMR spectra of all four guests@OA<sub>2</sub>. The guest proton signals have been assigned with the help of corresponding 2D COSY NMR spectra of the complexes. As evident, the movement of methyl “a” proton signal downfield from G<sub>6</sub> to 4-Pr-G<sub>3</sub> shows that the guest molecule is probably moving upwards in the cavity (**Figure 5.23**). Whereas, the eventual shifting of methyl “b” proton signal upfield suggests that it is moving deeper into the cavity. This observation can be explained on the basis of two driving forces we mentioned earlier, namely- space filling and more CH- $\pi$  interactions. In the case of G<sub>6</sub>, the proton signals of the chain are more upfield shifted than the proton signals for cyclohexene ring, it suggests that while the hexyl chain is anchored deeper in one end of the capsule, the cyclohexene ring prefer to be located in the middle of the capsule. Next, in 4-Me-G<sub>5</sub> 4-substituted methyl too has a propensity to anchor deeper into the capsule. But more CH- $\pi$  interactions of the pentyl chain with host OA win over and as a result though the molecule moves a bit upward in the capsule, but does not drastically shifts to the other end.



**Figure 5.23** Partial  $^1\text{H}$  NMR of (a)  $\text{G}_6@OA_2$  (b)  $4\text{-Me-G}_5@OA_2$  (c)  $4\text{-Et-G}_4@OA_2$  (d)  $4\text{-Pr-G}_3@OA_2$

This observation is duly supported by the position of the proton signals of  $4\text{-Me-G}_5@OA_2$ . Now, in the case of  $4\text{-Et-G}_4$ , we observe that methyl “a” proton signal has shifted downfield, but methyl “b” proton signal has remained at its position. Though former observation is consistent with the idea of guest molecule moving upward, the anomaly in the latter observation can be explained by the fact that the ethyl is substituted axially at position 4 in the ring. Axial conformations of the 4-substituted alkyl chain are supported by the fact that in COSY NMR, the vicinal coupling between protons 2 and 3 is very weak, overlapped or missing in most cases. This would happen only when proton 3 is in equatorial position. Since equatorial-equatorial and equatorial-axial vicinal coupling is very weak. Secondly, interactions between protons 6'-3 and 6'-4 exist, as elucidated by 2D intramolecular NOESY NMR, which are possible only when the 4-substituted alkyl chain is in axial position.

Moving on to the case of 4-Pr-G<sub>3</sub>, since we have equal chain length on each side of the molecule, so we should expect this guest molecule to be perfectly balanced in the middle of the cavity. But this is not so, here again space filling and CH- $\pi$  interactions win over. In **Figure 5.23** (d) we can see methyl “b” proton signal has shifted much upfield suggesting that the 4-substituted chain anchors deeper to the other end of the capsule, folds and acquires as much space, hence pulling the other end of the guest molecule in the mid of the capsule, as evident by the slight downfield shift of methyl “a” proton signal. This is probably because this side of the guest molecule being more non-planer and devoid of  $\pi$  bond offers maximum CH- $\pi$  interactions with host OA. The idea of the guest molecules redistributing and hence balancing themselves in the free space available, in order to maximize their CH- $\pi$  interactions is further confirmed by the shifting of cyclohexene ring protons (**2, 3, 4, 5**) downfield from G<sub>6</sub> to 4-Pr-G<sub>3</sub>, indicating the movement of cyclohexene ring towards the middle of the capsule. The cartoon representation of the structures predicted from the above observations, for G<sub>6</sub>@OA, 4-MeG<sub>5</sub>@OA, 4-Et-G<sub>4</sub>@OA and 4-PrG<sub>3</sub>@OA have been shown in **Figure 5.24**.



**Figure 5.24** Probable position of guest@OA<sub>2</sub>.

To confirm the above observations, photo-oxidation of G<sub>6</sub>/4-Me-G<sub>5</sub>/4-Et-G<sub>4</sub>/4-Pr-G<sub>3</sub> within OA and in CD<sub>3</sub>CN was performed. To 1 mM of D<sub>2</sub>O solution of G<sub>6</sub>/4-Me-G<sub>5</sub>/4-Et-G<sub>4</sub>/4-Pr-G<sub>3</sub>@OA<sub>2</sub> triplet sensitizer Rose bengal was added. The solution was irradiated at > 400 nm for 10 min under continuous oxygen atmosphere. The hydro peroxides thus produced remain inside the OA. These hydro peroxides were extracted with CDCl<sub>3</sub>. Tri-phenylphosphine was added to this solution to reduce hydro peroxides to alcohols. The product ratio was monitored by GC. The peak assignments were done by co-injecting the individual pure products synthesized by solution chemistry. The results of the photo-oxidation reactions in OA and in CD<sub>3</sub>CN are given in **Scheme 5.6**. In all the cases, compared to the solution, we observed that tertiary peroxide product which comes from the abstraction of hydrogen **2** enhances when the guest is encapsulated within OA. This could be because of two reasons; first, hydrogen **2** is located towards the middle of the capsule and second the tertiary peroxide formed as a result fits better inside the capsule in comparison to the secondary peroxides which would increase the width of the guest molecule, hence inviting more steric repulsion and less stability inside the host OA. Now when we compare the reactivity of G<sub>6</sub>/4-Me-G<sub>5</sub>/4-Et-G<sub>4</sub>/4-Pr-G<sub>3</sub> within OA, we find that the product ratio for G<sub>6</sub> and 4-Me-G<sub>5</sub> is almost similar. If we observe, the position of proton **2** has not changed much, but proton **5** in case of 4-Me-G<sub>5</sub> has shifted downfield, but the axial orientation of 4-substituted methyl could be preventing abstraction of hydrogen 5, hence approximately same product ratio is obtained.

Moving on to the case of 4-Et-G<sub>4</sub>, we see the product selectivity further decreases. Here we can see that both the methyl groups have moved downfield, also the cyclohexene ring proton have moved downfield, indicating that the cyclohexene ring is

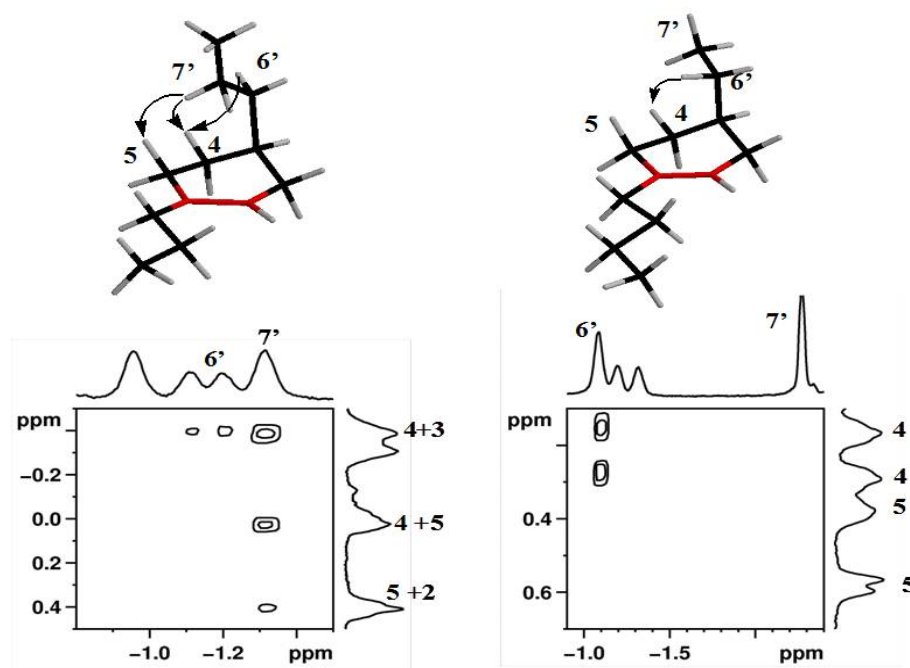
probably situated in the center of the capsule and hence equally exposing all its allylic hydrogens for abstraction by singlet oxygen, which results in poor selectivity. But in the case of 4-Pr-G<sub>3</sub>, we see that majorly tertiary peroxide product is formed. There are subtle reasons behind this enormous product selectivity. First as we can see in **Figure 5.23** protons **2** and **5** have interchanged their positions suggesting that in this case only, proton **2** is most exposed. Secondly, when we compare the intramolecular NOESY interactions (**Figure 5.25**) of 4-Et-G<sub>4</sub>/4-Pr-G<sub>3</sub> within OA, we find that though both the 4 substituted alkyl chain are axial, but in case of **1c** proton **7'** is not interacting with proton **4** or **5**. Whereas, in case of 4-Pr-G<sub>3</sub> we can see that proton **7'** is interacting

**Table 5.5** Product ratio for “ene” reaction in solution and inside OA\*.

$R_1 = C_5H_{11}$ $R_2 = H$	$CD_3CN$ Octaacid	40 % 56 %	60 % 44 %
$R_1 = C_4H_9$ $R_2 = CH_3$	$CD_3CN$ Octaacid	49 % 60%	51 % 40 %
$R_1 = C_3H_7$ $R_2 = C_2H_5$	$CD_3CN$ Octaacid	41 % 48 %	59 % 52%
$R_1 = C_2H_5$ $R_2 = C_3H_7$	$CD_3CN$ Octaacid	37 % 92 %	63 % 8 %

\*Started with 100 % pure starting material, used 420 nm filter and irradiated for 10 min.

\*\* Identity of the structure of the chief product confirmed by the fragmentation pattern obtained by GCMS.



**Figure 5.25** Partial 2D NOESY NMR (depicting guest-guest through space interactions) spectra of 4-EtG<sub>4</sub>@OA and 4-PrG<sub>3</sub>@OA.

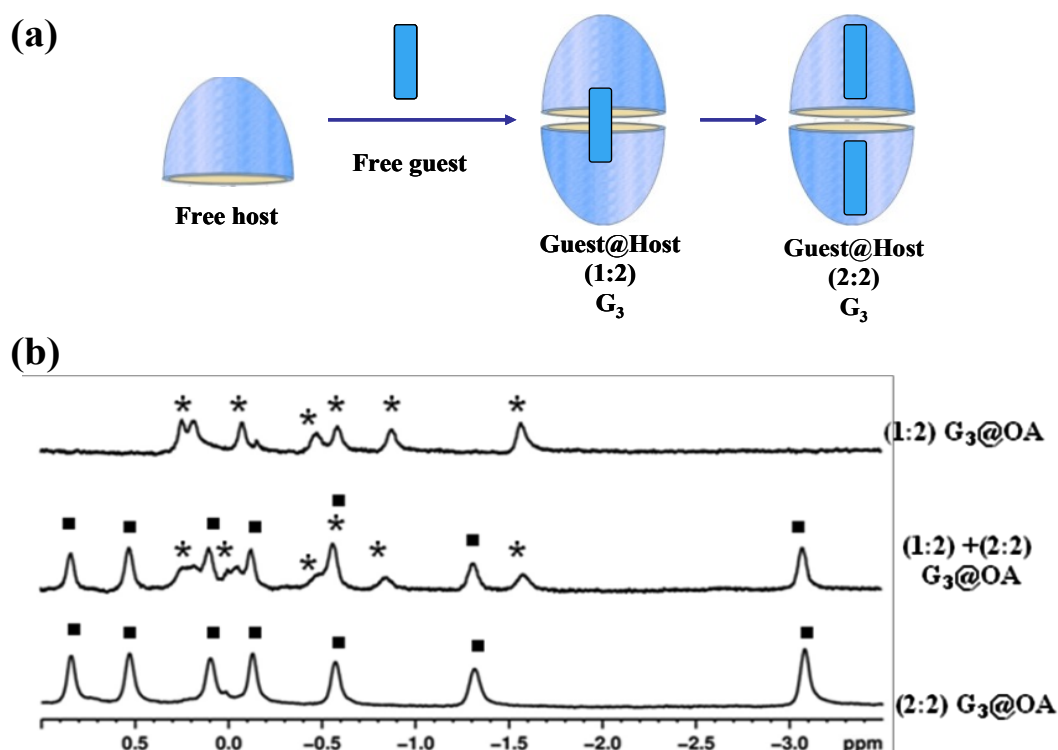
with cyclohexene ring protons especially protons **4** and **5** and hence posing steric hindrance for the approach followed by abstraction of hydrogen **5** by singlet oxygen. Hence, exclusive exposure of hydrogen **2** and strong steric hindrance for abstraction of hydrogen **5** explains the exquisite product selectivity in case of 4-Pr-G<sub>3</sub>.

#### 5.2.4 Encapsulation studies of guest molecules (G<sub>3</sub>, 4-Me-G<sub>2</sub> and 4-EtG<sub>1</sub>) of intermediate size

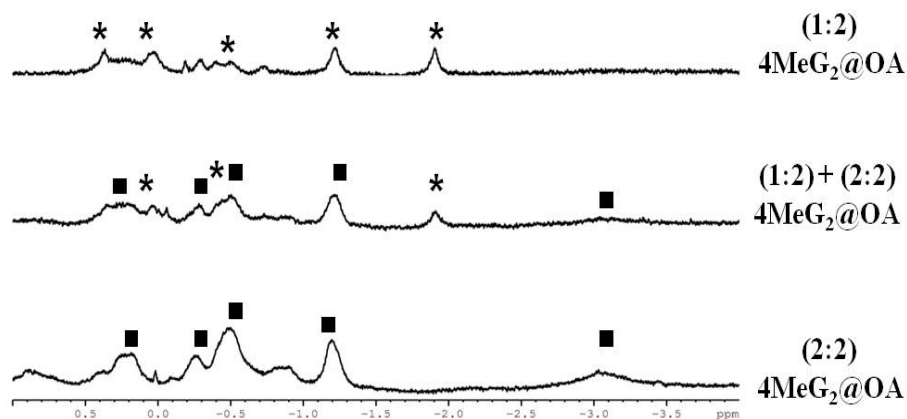
In course of studies carried out in previous sections, we came across a group of guest molecules which possess an intermediate size with respect to the size of the host OA cavity. These guest molecules are a bit too big to form a simple 2:2 or 1:1 complex with OA like G<sub>2</sub> and 4-MeG<sub>1</sub>, and a bit smaller to form a straightforward 1:2 complex with OA, like G<sub>6</sub> or 4-MeG<sub>8</sub>, either. Hence these molecules show anomalous complexation behavior with OA. In this section we present two such guest molecules G<sub>3</sub> and 4-MeG<sub>2</sub> (Scheme 5.5).



Above is shown (**Figure 5.26**) the partial  $^1\text{H}$  NMR titration spectra of 1-propylcyclohexene ( $G_3$ ) with host OA. Here we can see that on adding the guest to the host, first one set of peaks appear, indicating one type of complex, then on increasing the concentration of the guest, gradually second set of peaks appear, and finally first set of peaks vanish and only second set of peaks remain. Also for second set of peaks, the methyl group peak is shifted more upfield indicating that probably it is (2:2) guest@host complex. This explains that in this case first, (2:1) complex is formed, at one stage both the complexes exist and finally a (2:2) complex is formed.



**Figure 5.26** (a) Pictorial representation, (b) expansion of the guest region of the  $^1\text{H}$  NMR spectra of  $G_3@OA$  showing first the formation of (1:2) complex, followed by both complexes and eventually only (2:2)  $G_3@OA$  complex. \* Represents the peaks from (2:2) complex and ■ represents peaks from (2:1) complex.



**Figure 5.27** Expansion of the guest region of the  $^1\text{H}$  NMR spectra of  $4\text{-MeG}_2\text{@OA}$  showing first the formation of (1:2) complex, followed by both complexes and eventually only (2:2)  $\text{G}_3\text{@OA}$  complex. \* Represents the peaks from (2:2) complex and ■ represents peaks from (2:1) complex.

Similarly, for the guest 4-MeG<sub>2</sub>, we can observe that on addition of guest to the host solution first one set of proton signals are sighted, in which the guest protons are comparatively downfield shifted, signifying formation of 1:2 guest-host complex. And on addition of further guest solution, first set of signals gradually vanish giving way to the next set of proton signals, indicating the formation of 2:2 complex.

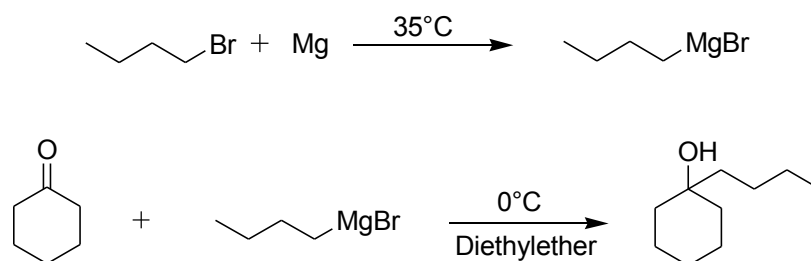
### 5.3 Conclusion

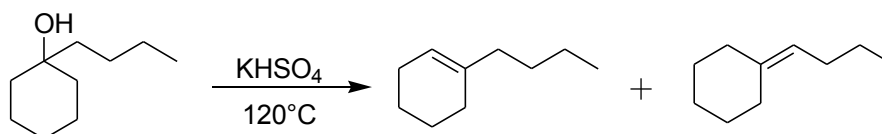
In nutshell, space filling and weak CH- $\pi$  interactions play a critical role in allowing host OA to offer “orientational isomerism” to its occupant guest molecules. Seemingly similar guest molecules acquire different packing patterns inside the host OA and result in exquisite product selectivity in photo- oxygenation reaction. Since the guest molecules in the present case contain no functional group other than one double bond, the systems gives us an opportunity to understand and study the above mentioned two driving forces at a molecular level. In the present study, we have prepared a variety of 1-alkyl and 4-me-

1-alkylcycloalkenes. Their encapsulation behavior inside the host has been studied. Also their photooxygenation by singlet oxygen in solution and inside the host OA have been studied. In the solution, no product selectivity is observed. Hence, we have tried to manipulate and control the product selectivity by encapsulating the guest inside host molecule. We have succeeded in doing so. Out of three possible products, the ratio for one product enhances and the other product decreases to  $\sim 8$ -2%. These results along with the elaborate NMR studies show that the guest molecule while inside the host prefers particular orientation and this orientation pre-determines their reactivity. In this line of action we have also explored the preferential orientation and hence the resultant product selectivity of the 4 cyclohexene molecules with approximately similar molecular length. This study shows how the substitution and the orientation of the substituted alkyl group of the cyclohexenes guest molecule, encapsulated inside the host OA, can manipulate the product distribution.

## 5.4 Experimental Section

**Materials:** Host OA was synthesized according to the literature.<sup>285a</sup> The different alkylcyclohexenes were synthesized by the general procedure outlined below (**Scheme 5.8**). Cyclohexanone, 4-methylcyclohexanone and the alkylbromides were obtained from Aldrich and used as such.





**Scheme 5.8** Synthetic reactions for the formation of 1-substituted cyclohexene.

**Step 1:** 1.46 g (0.0609 mol) Mg turnings were taken in a three necked 100 mL R.B. and to it 25 mL dry Et<sub>2</sub>O was added. In another 100 mL R.B. (0.0508 mol) of bromoalkane was taken and dissolved in 10 mL of dry Et<sub>2</sub>O. The setup was heated upto 35°C, to initiate Grignard reagent formation. Bromoalkane mixture was slowly added to the reaction mixture since the reaction is exothermic, and the heat was also switched off once the reaction started, the reaction mixture was stirred for 10 min.

**Step 2:** To another R.B. 2.0 g (0.0203 mol) of cyclohexanone was mixed with 10 mL of Et<sub>2</sub>O and this was slowly added to the above reaction mixture maintaining the temperature at 0° C. the reaction was left stirring overnight. Then the reaction mixture was poured over ice and 10 % HCl was slowly added to it while stirring. The tertiary alcohol formed was extracted using petroleum ether, and was purified by column chromatography with 1-10 % Ethylacetate and Hexanes.

**Step 3:** The above tertiary alcohol (2.0 g), thus obtained, was treated with powdered potassium bisulfate and refluxed at 120° C for at least 3-9 h. Endo and exocyclic cycloalkenes were obtained in the ratio 88:12. The 100 % pure endocyclic cycloalkene was obtained by following method.

**Purification using silver impregnated silica:** First 15 % silver nitrate solution in methanol was prepared (20 g of silver nitrate + 153 mL of methanol, 70 mL of water was added to dissolve silver nitrate ) to it was added 66 g of silica (230 x 400 mesh). The

solution was gradually stirred so that all the solvent evaporates, once the silica became free flowing, the beaker was covered by aluminum foil and placed inside the oven for overnight drying. It was then cooled in a dessicator and used. The column- 36 cm in height and 1.5 cm in diameter was packed with the silver impregnated silica and eluted with 500 mL of Pentane/ Hexane. The purity of the product was confirmed by  $^1\text{H}$  NMR and GC.

**Protocols for NMR binding studies:** NMR experiments were performed on an 500 MHz spectrometer. All binding studies involved titration of cyclohexenes to the host solution to confirm the stoichiometry of the complexes. The general protocol was as follows: 0.6 mL of 1 mM host and 10 mM sodium borate in  $\text{D}_2\text{O}$  were titrated with aliquots of 1  $\mu\text{L}$  of a 60 mM solution of guest in  $\text{DMSO-d}_6$ . To perform COSY experiments, 5 mM solutions of the complexes were prepared: 5 mM host, 300 mM guest and 50 mM sodium tetra borate in  $\text{D}_2\text{O}$ .

**Protocols for NMR Diffusion Measurements:** Diffusion NMR experiments were performed on 500 MHz. The experiments were performed at  $25^\circ\text{C}$ , at a host concentration of 2 mM (in 20 mM sodium tetraborate).

**Protocol for Photochemistry experiments:** Irradiation was carried out using a medium-pressure Hg lamp, and 420 nm filter. All samples were bubbled with  $\text{O}_2$  during photochemical “ene” reaction. Solutions of the guest was prepared by adding 4  $\mu\text{L}$  of neat cycloalkene in 0.6 mL  $\text{CD}_3\text{CN}$  followed by 12  $\mu\text{L}$  of 0.2 mM Rose Bengal and irradiated in an NMR tube for 10 min. Reaction conversion of 30-50% was achieved during this period.

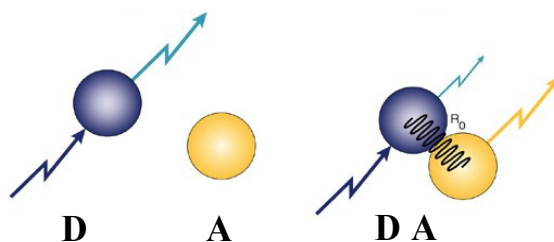
A 1 mM stock solution of host was prepared in sodium tetra borate buffer 10mM in D<sub>2</sub>O. 60 mM of stock solution of guest was prepared in DMSO-d<sub>6</sub>. To 0.6 mL of host solution, guest was added in the ratio (4:1). The formation of the complex was confirmed by NMR. To this was added same amount of Rose Bengal and the solution was irradiated for 10 min using 420 nm filter. The products were extracted using CDCl<sub>3</sub> and to it PPh<sub>3</sub> was added to reduce the peroxides to the corresponding alcohol. The products were analyzed by GC and GCMS. The Structure of the products were determined based upon the fragmentation pattern of the mass spectrum, by NMR alaysis and by anology of the previous work reported in the literature.<sup>292</sup>

## **CHAPTER 6**

**Ultrafast FRET Between the Donor  
Encapsulated inside and Acceptor Non-covalently  
Attached to the Walls of Nano Cavitand OA**

## 6.1 Overview

Fluorescence resonance energy transfer (FRET) has been widely used in all applications of fluorescence, including medical diagnostics, DNA analysis, and optical imaging. FRET occurs between a donor (D) molecule in the excited state and an acceptor (A) molecule in the ground state. Energy transfer occurs without the appearance of a photon and is the result of long range dipole–dipole interactions between the donor and acceptor<sup>293</sup> (**Figure 6.1**). The rate of energy transfer depends upon the extent of spectral overlap of the emission spectrum of the donor with the absorption spectrum of the acceptor, the quantum yield of the donor, the relative orientation of the donor and acceptor transition dipoles, and the distance between the donor and acceptor molecules, according to **equation 6.1**.<sup>294</sup>



**Figure 6.1** Pictorial Representation of FRET occurring through dipole-dipole interaction.

$$k_{\text{FRET}} = \frac{1}{\tau_{\text{rise}}^{\text{A}}} = \frac{1}{\tau_{\text{D}}^0} \left( \frac{R_0}{R_{\text{DA}}} \right)^6 \quad \text{Eqn. 6.1}$$

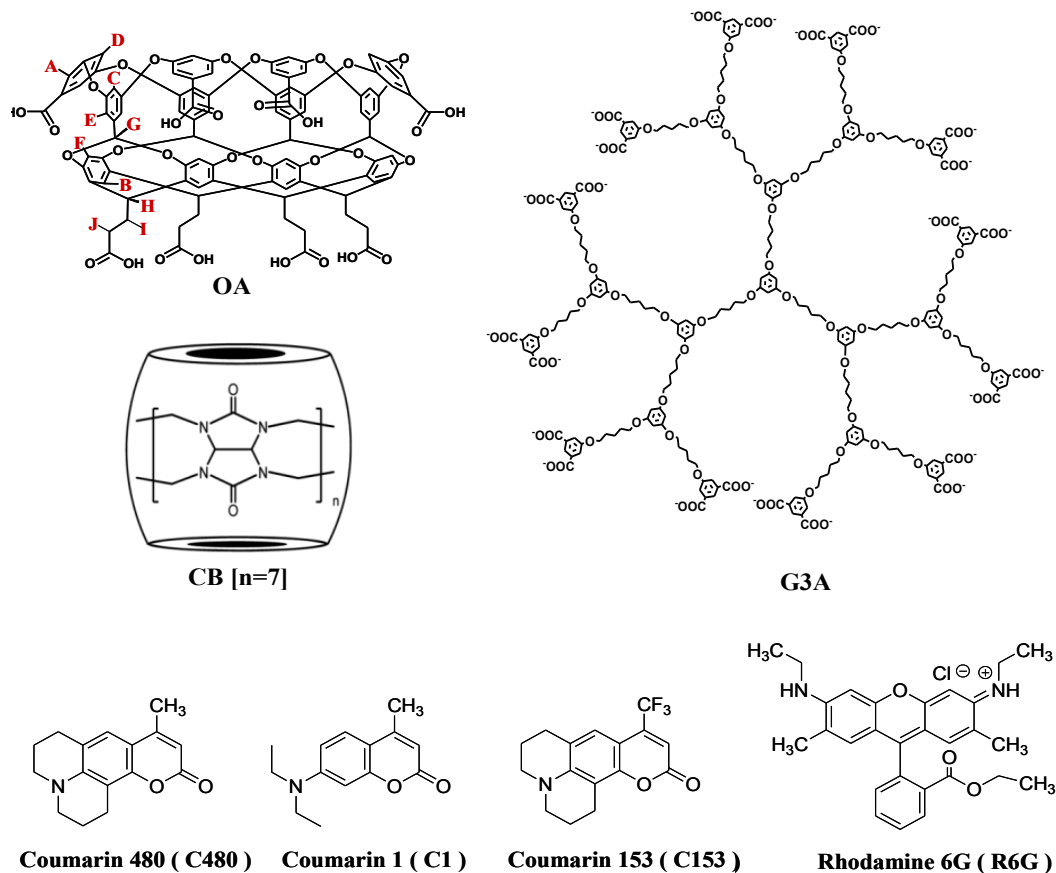
Where,  $\tau_{\text{D}}^0$  is the lifetime of the donor in the absence of acceptor and  $\tau_{\text{rise}}^{\text{A}}$ , is the rise time of acceptor emission in presence of donor. At a donor-acceptor distance  $R_{\text{DA}}=R_0$ , the efficiency of energy transfer is 50% and  $k_{\text{FRET}} = (1/\tau_{\text{D}}^0)$ .

In the course of our research, we came across an interesting question - whether the excited state behavior of a guest molecule enclosed in the Octa Acid (OA) capsule could be influenced by a molecule present outside.<sup>295-299,42</sup> Hence, in recent years, our



group started investigating the molecular communication between the two molecules, one encapsulated inside OA and other outside it. In this regard, we established the interaction of two nitroxide molecules separated by the wall of the OA capsule.<sup>300,301</sup> This was believed to be facilitated by orbital overlap between the two nitroxides through the walls of OA (super exchange process). Next, we wanted to investigate whether singlet-singlet energy transfer between an encapsulated donor and a free acceptor could occur, similar to spin-spin exchange, across the capsular wall. For this, we employed the concept of FRET. The importance of such a choice lies in the microenvironment complexity of the system. For such systems, few key features are highly desirable: first, is sensitivity, since in FRET we can monitor both, the decrease in donor emission and increase in acceptor emission, the sensitivity in this method is two-fold in comparison to the methods bearing only one reporter dye.<sup>302</sup> Secondly, there is a need of a FRET system which can resolve ultrafast events, i.e. events that are faster than those in the range of nanoseconds, and finally, to design a system with precise spatial arrangements of the fluorophores.

In this project, we use the cavitand OA to encapsulate the donor dyes Coumarin1 (C1), Coumarin480 (C480) and Coumarin153 (C153), (**Scheme 6.1**). The main feature of this cavitand is that it has hydrophobic inner pockets and in the presence of a suitable guest, it forms a ternary complex<sup>52</sup>, which we refer to as a “closed nanocontainer”. The second important feature of OA is the eight carboxylic groups located on the top and bottom rim; under slightly basic condition (pH ~ 9.0) these form carboxylate groups and help solubilizing OA in aqueous medium. We have exploited this feature of OA by introducing a cationic acceptor dye R6G, which fairly binds with the carboxylate groups through columbic attraction.



**Scheme 6.1** Chemical Structures of hosts – OA with Proton Signals Assigned from A-J, CB[7], G3A and Structures of Donors C480, C1, and C153 and Acceptor R6G.

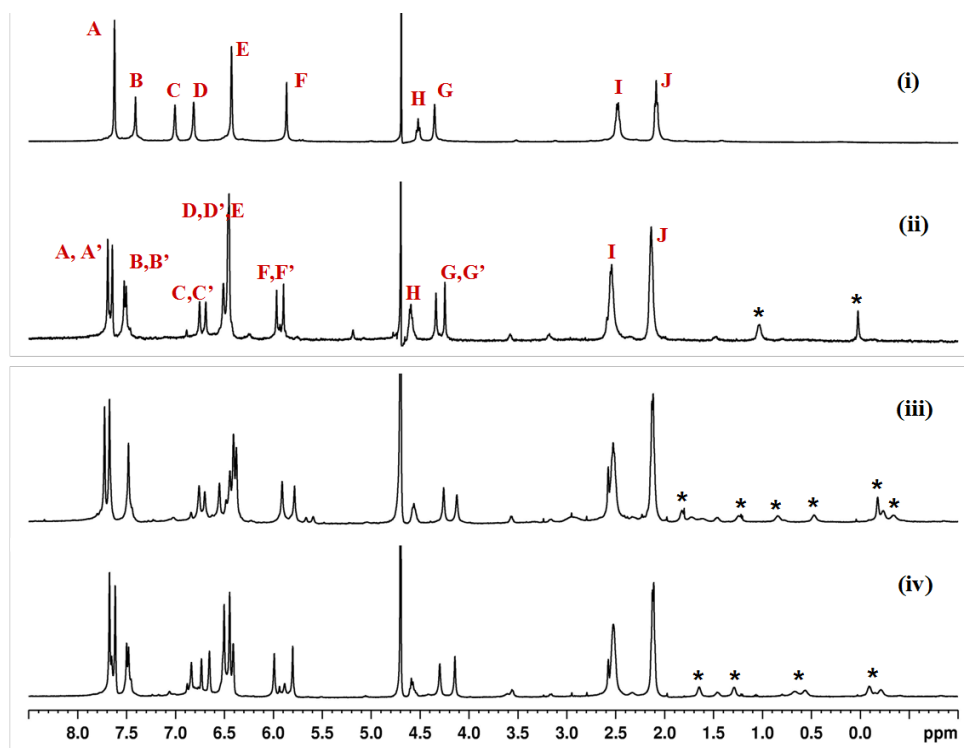
When we have a donor molecule encapsulated inside the hydrophobic pocket of OA and an acceptor molecule hanging outside OA; we observe a quenching in donor emission whereas an enhancement in acceptor emission indicating FRET could be taking place. To further prove the occurrence of FRET, we measured the donor lifetime in presence of acceptor. On a nanosecond level we could not detect any change, but the decay of the donor lifetime at femtosecond level and rise-time of the acceptor in presence of the donor, both studied by picosecond and femtosecond emission spectroscopy supported the ultrafast FRET taking place between the donor@OA and the acceptor. To further prove this observation, we employed two host molecules: third generation acid

dendrimer (G3A) and cucurbituril, CB[7] to detach the acceptor molecule, former through ion-pair interaction and latter through hydrophobic interaction, from the rim of OA; hoping that the observed FRET might diminish. With the help of ultrafast fluorescence spectroscopy we observed that the D-A distance increased when these hosts were added into the system. In the next section, we elaborate our investigation.

## 6.2 Results and Discussion

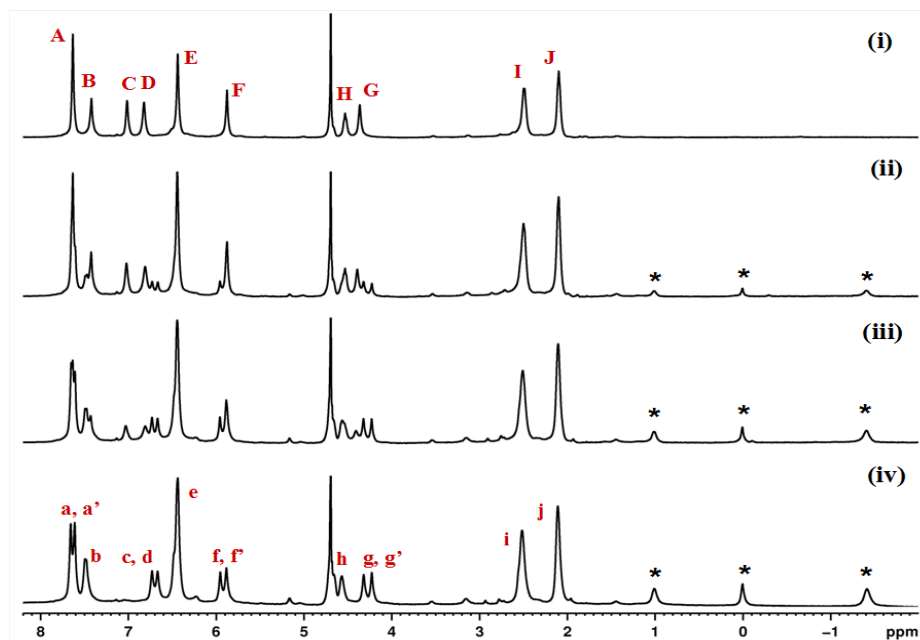
### 6.2.1 Encapsulation of Donor within OA

In presence of a hydrophobic neutral guest molecule/s, two OA molecules assemble together to form either a 1:1, 1:2 or 2:2 complex. Formation of this complex can be determined by using  $^1\text{H}$  1D NMR. The ratio of the guest:host can be determined by doing step by step  $^1\text{H}$  NMR titration. In **Figure 6.2**,  $^1\text{H}$  NMR titration of C1@OA<sub>2</sub> has been shown as an example. For such experiment, to 1 mM of aqueous OA solution in 10 mM borate buffer, 60 mM of the donor molecule C1 dissolved in DMSO-d<sub>6</sub>, was added in steps of 0.25 equivalents. At 0.5 equivalents it was observed that neither uncomplexed host nor uncomplexed guest proton signals existed, suggesting the formation of 1:2 guest:host complex. In **Figure 6.3**,  $^1\text{H}$  NMR spectra of three donor@host complexes-C1@OA<sub>2</sub>, C153@OA<sub>2</sub>, C480@OA<sub>2</sub> have been shown. The encapsulation of the guest is indicated by the significant upfield shift of the guest proton signal. Also, defined splitting of the host proton signal can be observed, on encapsulation of guest. The splitting of host proton signals can be attributed to the asymmetric structure or the restricted motion (in the NMR time scale) of the guest molecule inside OA.

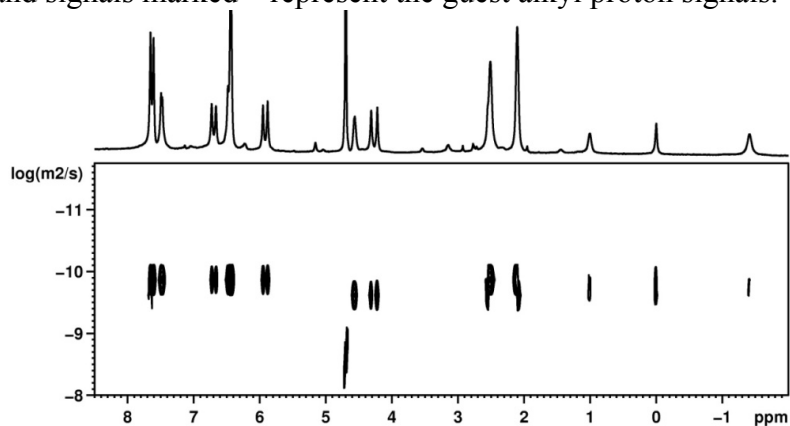


**Figure 6.2**  $^1\text{H}$  NMR (500 MHz,  $\text{D}_2\text{O}$ ) spectra of (i) OA (1mM, in buffered  $\text{D}_2\text{O}$ ), (ii)  $\text{C1@OA}_2$  (0.5mM: 1mM in buffered  $\text{D}_2\text{O}$ ), (iii)  $\text{C480@OA}_2$  (0.5mM: 1mM in buffered  $\text{D}_2\text{O}$ ), (iv)  $\text{C153@OA}_2$  (0.5mM: 1mM in buffered  $\text{D}_2\text{O}$ ). Signals marked A-J in represent uncomplexed OA protons; signals marked a, a' - j, j' represent complexed OA protons; and signals marked \* represent the guest alkyl proton signals.

Another way of determining the formation of a 1:2 complex, is by carrying out DOSY NMR experiments, since the diffusion constant for the free host, 1:1, 1:2 and 2:2 complexes are different. Alternatively, as the complex becomes heavier; it diffuses slowly in the bulk solvent, which can be observed by the DOSY NMR experiments. In this case, the diffusion constant for free OA is measured to be  $1.88 \times 10^{-6} \text{ cm}^2/\text{s}$ . Whereas, the diffusion constant measured for the  $\text{C1@OA}_2$  complex is  $1.27 \times 10^{-6} \text{ cm}^2/\text{s}$ , consistent with the formation of 1:2 complexes.<sup>51</sup> DOSY NMR spectrum of  $\text{C1@OA}_2$  has been shown in **Figure 6.4**. The diffusion constants for  $\text{C480@OA}_2$  and  $\text{C153@OA}_2$ ,  $1.27 \times 10^{-6} \text{ cm}^2/\text{s}$  and  $1.24 \times 10^{-6} \text{ cm}^2/\text{s}$  respectively, were also observed to be in the same range. Thus, we visualize that the donor coumarin dye molecules are held tightly within the OA capsule.



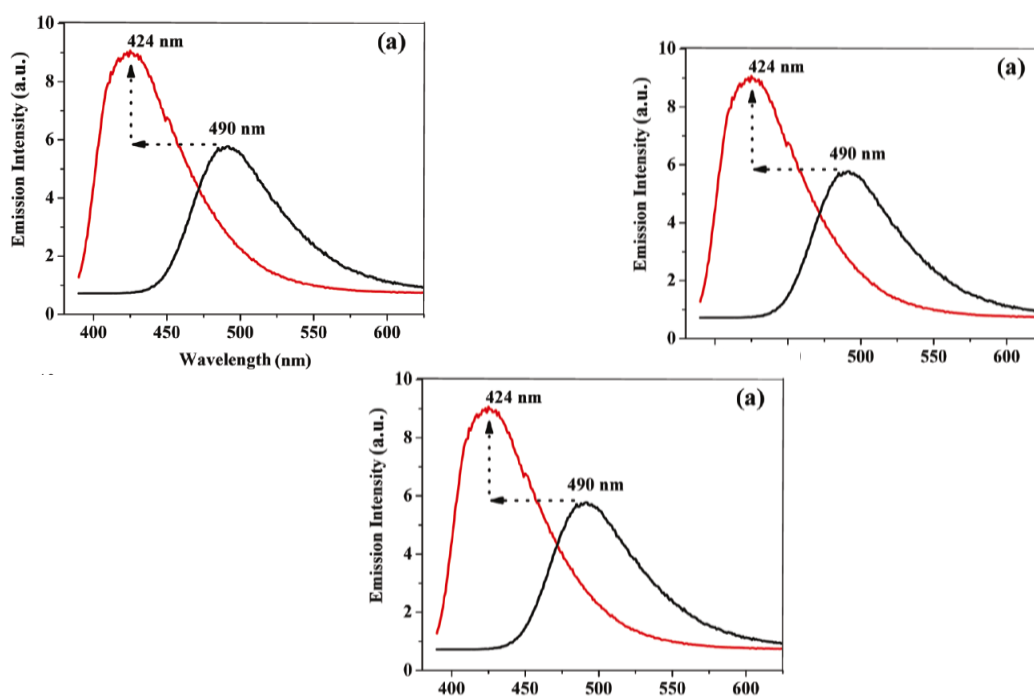
**Figure 6.3**  $^1\text{H}$  NMR (500 MHz,  $\text{D}_2\text{O}$ ), spectra of (i) OA (1mM) alone in sodium borate buffered  $\text{D}_2\text{O}$ , (ii) C1@OA (1:8), (iii) C1@OA (1:4), (iv) C1@OA (1:2). Signals marked A-J in represent uncomplexed OA protons; signals marked a,a'-j,j' represent complexed OA protons; and signals marked \* represent the guest alkyl proton signals.



**Figure 6.4** DOSY NMR(500 MHz,  $\text{D}_2\text{O}$ ) spectra of C1@OA<sub>2</sub> (1:2) complex. [OA] = 1 mM in 10 mM buffered  $\text{D}_2\text{O}$  and [C1] = 0.5 mM.

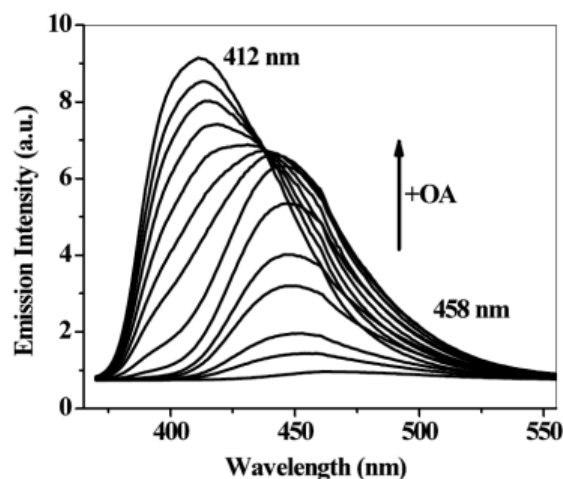
The above observations are also supported by the steady-state fluorescence data provided below. Coumarins C1, C153, and C480 belong to a family of laser dyes whose fluorescence maximum, quantum yield, and lifetime depend on the solvent polarity.<sup>303,304</sup> The emission spectra of these in water, in the presence and absence of OA are shown in

**Figure 6.5.** Upon excitation at 370 nm, C480 (10  $\mu\text{M}$ ) in water showed a fluorescence maximum at 490 nm. On gradual addition of OA, the  $\lambda_{\text{em}}$  max shifted gradually to 424 nm with an increase in intensity by a factor of 2. Similarly, upon exciting C1 at 360 nm, a blue shift of 46 nm from 458 nm in bulk water to 412 nm in aqueous-OA solution with a 3-fold increase in fluorescence intensity was noted. A similar trend was observed for C153 as well ( $\lambda_{\text{em}}$  max = 547 nm in bulk water; 480 nm in aqueous-OA solution; and a 4-fold increase in fluorescence intensity). These marked blue shifts of the emission maxima and increase in emission intensity indicated that the donor molecules reside in a relatively nonpolar (dry) hydrophobic environment.



**Figure 6.5** Fluorescence spectra of (a) C480 (10  $\mu\text{M}$ ) in water (black line) and in the presence of OA (80  $\mu\text{M}$  in 0.8 mM borate buffer) (red line),  $\lambda_{\text{ex}}$  = 370 nm; (b) C1 (20  $\mu\text{M}$ ) in water (black line) and in the presence of OA (120  $\mu\text{M}$  in 1.2 mM borate buffer) (red line),  $\lambda_{\text{ex}}$  = 360 nm; (c) C153 (16  $\mu\text{M}$ ) in water (black line) and in the presence of OA (80  $\mu\text{M}$  in 0.8 mM borate buffer) (red line),  $\lambda_{\text{ex}}$  = 400 nm (a.u. = arbitrary units).

Having previously established the hydrophobic nature of the OA capsule,<sup>51</sup> we believe the above results support a model where the three donor molecules discussed in this presentation reside within the capsule protected from water. In all three guest systems, the shift reached a saturation point when the OA amount reached about 5-8 equiv. of the guest amount. Further addition of OA did not result in a significant shift, suggesting that under such conditions no guest molecules remain free in solution. As an example, fluorescence titration of C1@OA<sub>2</sub> has been shown in **Figure 6.6**. Note that since the concentrations used for NMR and emission studies are different, different amounts of the host are needed to shift the equilibrium toward complete complexation. For energy transfer studies, an excess of OA was used to make sure that all donor molecules remain complexed.

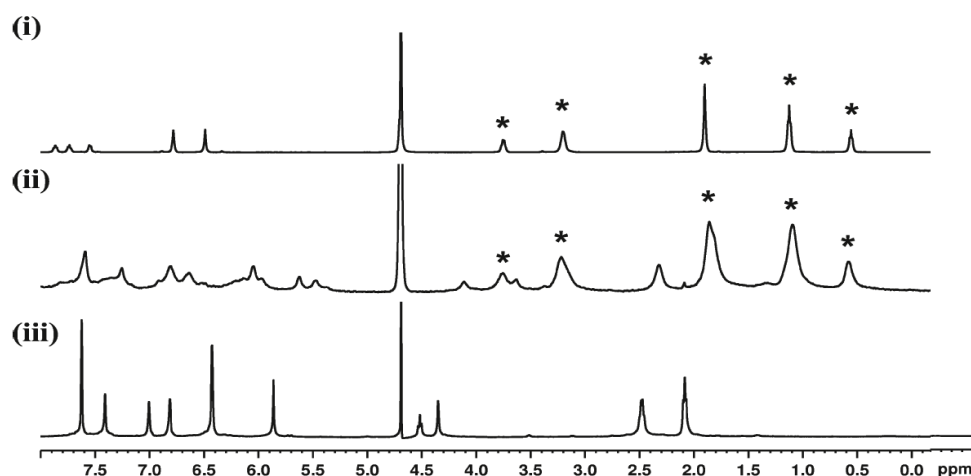


**Figure 6.6** Emission spectra of C1 (20  $\mu\text{M}$ ) in water and on gradual increase of OA (0-120  $\mu\text{M}$ ). Increasing OA concentration stepwise. Concentration of stock solution of OA = 10 mM in 100 mM buffered H<sub>2</sub>O.  $\lambda_{\text{ex}} = 360$  nm (a. u. = arbitrary units)

### 6.2.2 Association of Acceptor Rhodamine 6G to the Capsule's Exterior

<sup>1</sup>H NMR studies of free OA, free R6G and OA with R6G showed marked difference, as can be observed in **Figure 6.7**. Unlike donor@OA, in this case we do not

observe any upfield shift of acceptor R6G protons, when OA is present in the solution, which indicates the acceptor molecule not being encapsulated inside the OA cavity. Instead we observe a broadening of the acceptor proton signals, probably showing the slowing of its motion at NMR time scale and hence its attachment to the outer rim of OA. The diffusion constants for OA and R6G by themselves as measured by DOSY experiments were found to be  $1.88 \times 10^{-6} \text{ cm}^2/\text{s}$  and  $2.6 \times 10^{-6} \text{ cm}^2/\text{s}$  showed a decrease to  $1.41 \times 10^{-6} \text{ cm}^2/\text{s}$  and  $0.9 \times 10^{-6} \text{ cm}^2/\text{s}$ , respectively, when present together. This reduction in diffusion constants for both OA and R6G also suggests the associated nature of these molecules when present together in solution.

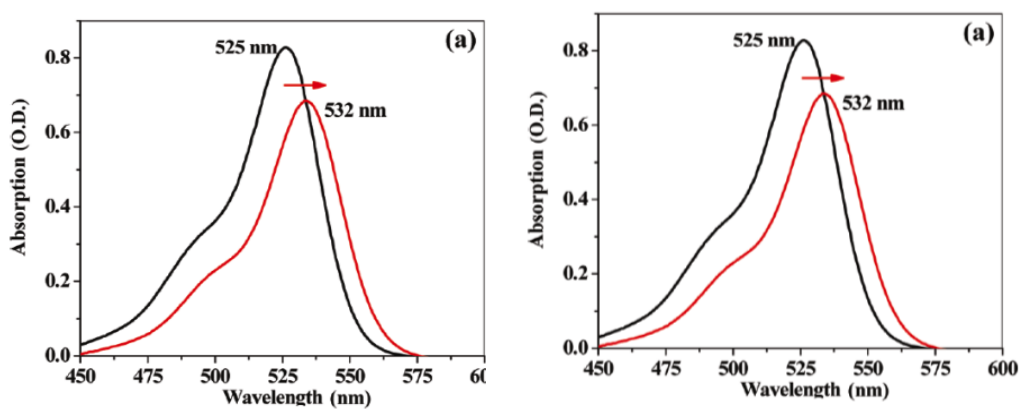


**Figure 6.7**  $^1\text{H}$  NMR (500 MHz,  $\text{D}_2\text{O}$ ) spectra of (i) 0.5mM R6G alone in  $\text{D}_2\text{O}$ , (ii) 0.5mM OA and 0.5mM R6G in 5mM sodium borate buffered  $\text{D}_2\text{O}$ , and (iii) 0.5mM OA alone in 5 mM sodium borate buffered  $\text{D}_2\text{O}$ . Signals due to R6G protons are marked with a symbol \*.

Further support for association of R6G to OA comes from the red shift in the absorption and emission spectra of R6G in the presence of OA (**Figure 6.8**). As shown in **Figure 6.8**, unlike the blue shift observed in the case of donors@OA<sub>2</sub> (**Figure 6.5**), a red shift in R6G absorption and emission maxima is noted. Such shifts are known to result from electrostatic interaction between R6G and perturbing molecules.<sup>305,306</sup> On the basis



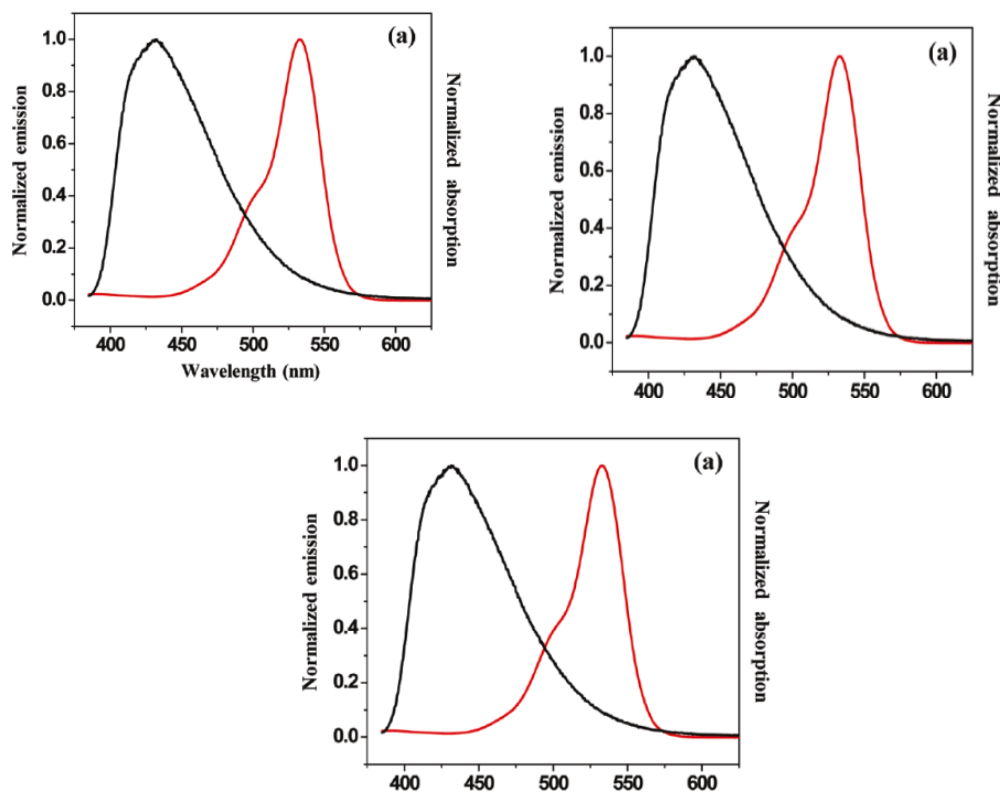
of DOSY data,  $^1\text{H}$  NMR, absorption, and emission spectra, we believe that the acceptor R6G electrostatically interacts with the exterior of the OA cavitand. This type of interaction is consistent with R6G being positively charged and the OA exterior being negatively charged with eight carboxylate anion groups.



**Figure 6.8** (a) Absorption and (b) emission spectra of 50  $\mu\text{M}$  of R6G in the absence (black line) and in the presence (red line) of 150  $\mu\text{M}$  of OA in 1.5 mM sodium borate buffered water,  $\lambda_{\text{ex}} = 525$  nm. (The abbreviations O.D. = optical density and a.u. = arbitrary unit.)

### 6.2.3 Confirmation of spectral overlap between the donor emission and acceptor absorption

Before initiating the energy transfer studies, we wanted to confirm the existence of overlap between the donor emission and acceptor absorption, a requirement for FRET. The spectra for the three pairs are shown in **Figure 6.9**. In the figure, black line indicates emission spectra of donor@OA and red line indicates R6G in presence of OA. It is interesting to observe that after the marked blue shift in the donor emission and red shift in the acceptor absorption in presence of OA, there still exists some spectral overlap, sufficient to move forward with FRET studies. Also, it is obvious that the extent of overlap varies between the pairs, and it is the least for the C1-R6G pair.

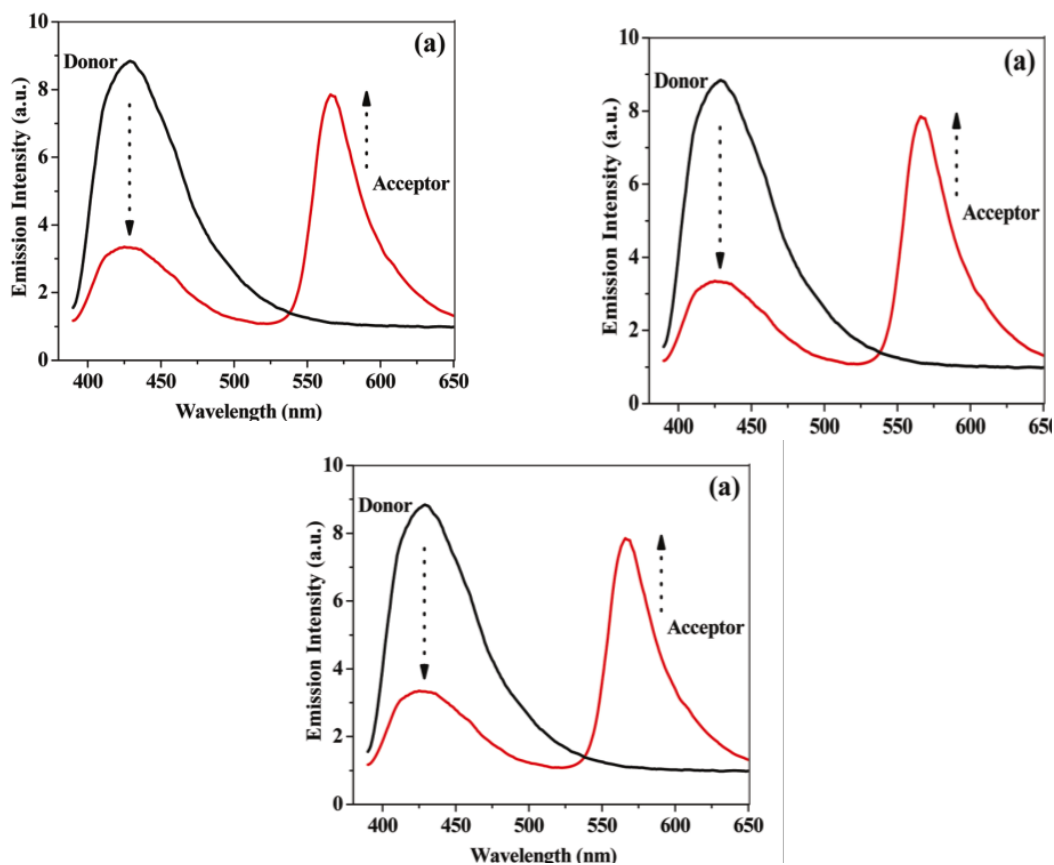


**Figure 6.9** Representations of spectral overlap between (a) the emission of C480@OA (black line) and the absorption of R6G in the presence of OA (red line); (b) the emission of C1@OA (black line) and the absorption of R6G in the presence of OA (red line); and (c) the emission of C153@OA (black line) and the absorption of R6G in the presence of OA (red line). Excitation wavelength ( $\lambda_{ex}$ ) in all cases is 375 nm.

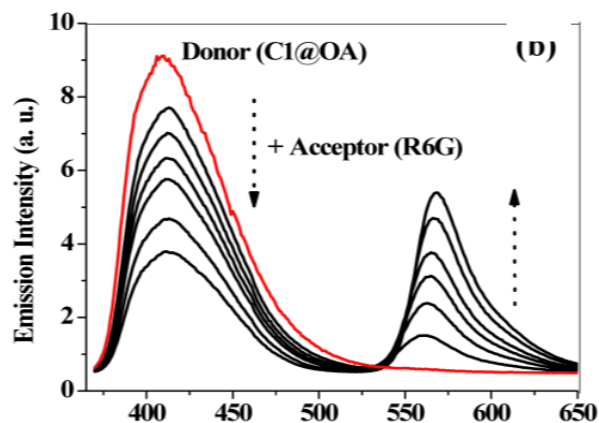
#### 6.2.4 Steady-state emission studies

For clarity reasons, only two traces for each dye are provided in **Figure 6.10**, one dye@OA<sub>2</sub> in the absence and the other dye@OA<sub>2</sub> in the presence of 50  $\mu$ M R6G. Excitation of coumarin dye clearly results in the emission of R6G indicative of singlet-singlet energy transfer. In the absence of the donor coumarins, at the excitation wavelength used in this study, R6G absorbed light and emission resulted. However, the extent of absorption by R6G is expected to be negligible when the donor coumarins are present in solution. As can be seen from **Figure 6.11**, with a gradual increase in R6G

concentration, the emission intensity of the donor C1 steadily decreased, and that of the acceptor increased. From the steady-state spectra, the character of the quenching (static or dynamic) could not be deciphered due to the lack of changes in the lifetime of the OA included donor dyes. To probe this further, femtosecond time-resolved experiments were carried out.



**Figure 6.10** Steady-state fluorescence spectra demonstrating FRET between donor coumarins and acceptor R6G. (a) C480@OA and R6G; (b) C1@OA and R6G; and (c) C153@OA and R6G. The black line represents emission by the donor alone in the absence of the acceptor R6G, and the red line represents the emission in the presence of the acceptor. In this case, both donor and acceptor emissions are seen. Conditions for the spectra: (a) C480 at 10  $\mu\text{M}$ , OA at 80  $\mu\text{M}$ , R6G at 30  $\mu\text{M}$  in 0.8mM buffered water;  $\lambda_{\text{ex}}=370$  nm; (b) C1 at 20  $\mu\text{M}$ , OA at 120  $\mu\text{M}$ , R6G at 50  $\mu\text{M}$  in 1.2mM buffered water;  $\lambda_{\text{ex}}=360$  nm; and (c) C153 at 16  $\mu\text{M}$ , OA at 80  $\mu\text{M}$ , R6G at 48  $\mu\text{M}$  in 0.8mM buffered water;  $\lambda_{\text{ex}}=400$  nm.

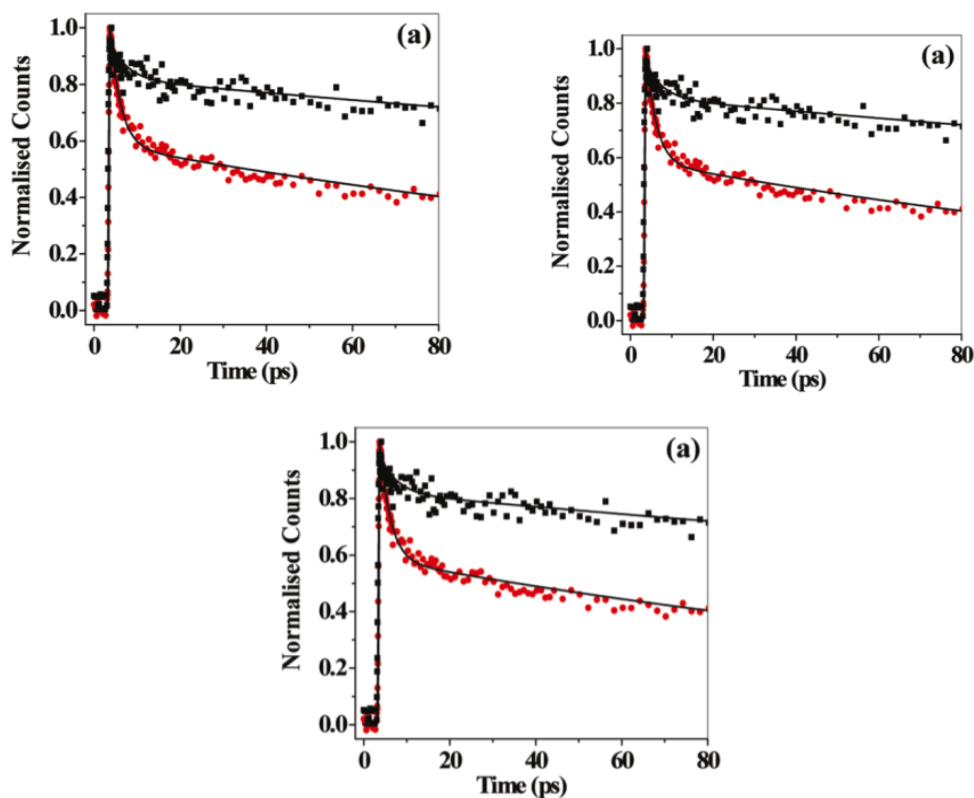


**Figure 6.11** Steady state fluorescence spectra demonstrating FRET between C1 (20  $\mu\text{M}$ )@OA (120  $\mu\text{M}$  in 1.2 mM buffered water) only (red line) and on addition of R6G (0-50  $\mu\text{M}$ ) (black lines),  $\lambda_{\text{ex}} = 360 \text{ nm}$ . In this case donor@OA concentration is kept constant and acceptor R6G is increased stepwise. (a. u. = arbitrary units)

### 6.2.5 Time-Resolved Emission Studies

This work had been carried in association with Dr. Bhattacharya's research group at IACS-Kolkata. This group has been exploring ultrafast FRET between donors and acceptors in micelles and reverse micelles recently.<sup>307-309</sup> In the picosecond studies, the excited singlet lifetime of the three donors included in OA (C480, C1, and C153) was found to be unaffected by the addition of acceptor R6G. This suggested that non-FRET donor molecules (i.e., donor alone in a cavity not being quenched by the acceptor) dominated the steady state fluorescence. Under such conditions, occurrence of FRET could be detected by monitoring the rise time of the emission for the acceptor. In general, the donors that undergo FRET have a shorter decay. The acceptor molecules participating in FRET would exhibit a rise in their emission. This prompted us to probe the occurrence of ultrafast FRET between the donor and the acceptor through the walls of OA by the rise of the acceptor emission. **Figure 6.12** shows the femtosecond (fs) decay of the donors trapped within the OA capsule in the presence and absence of the acceptor R6G. Due to

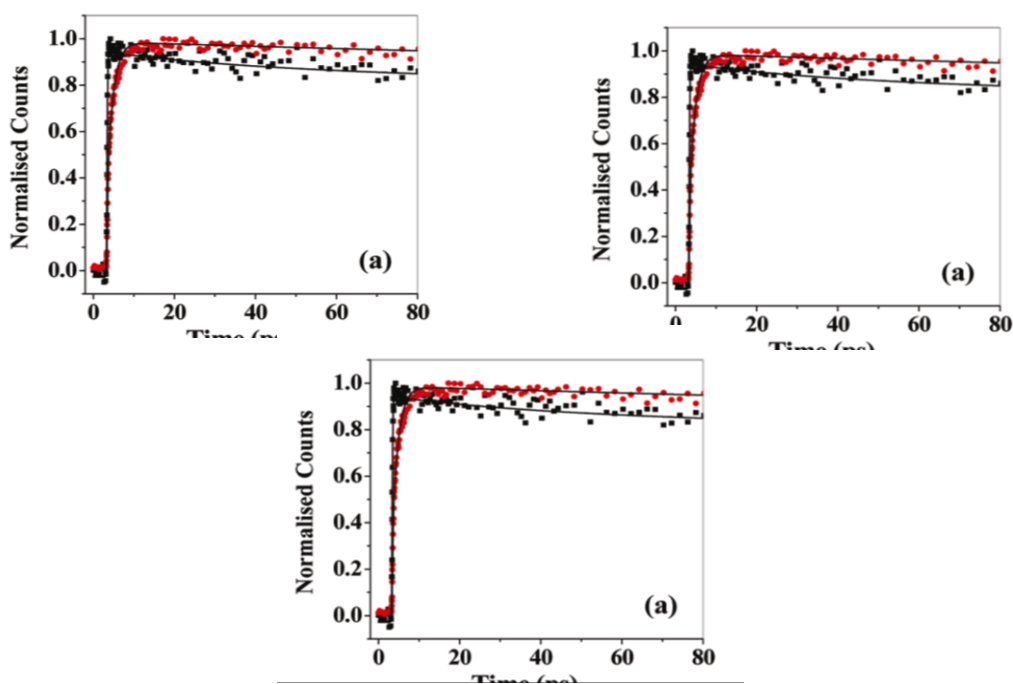
poor water solubility and low quantum yield of fluorescence emission, the lifetimes of C1 and C153 could not be measured in water in the absence of OA



**Figure 6.12** Femtosecond transient decays of donor coumarins: (a) C480 (10  $\mu\text{M}$ )@OA (80  $\mu\text{M}$  in 0.8 mM buffered water) alone (black dots), and on addition of R6G (30  $\mu\text{M}$ ) (red dots),  $\lambda_{\text{ex}} = 375$  nm,  $\lambda_{\text{em}} = 440$  nm; (b) C1 (20  $\mu\text{M}$ )@OA (120  $\mu\text{M}$  in 1.2 mM buffered water) alone (black dots) and on addition of R6G (50  $\mu\text{M}$ ) (red dots),  $\lambda_{\text{ex}} = 375$  nm,  $\lambda_{\text{em}} = 420$  nm; (c) C153 (16  $\mu\text{M}$ )@OA (80  $\mu\text{M}$  in 0.8 mM buffered water) alone (black dots) and on addition of R6G (48  $\mu\text{M}$ ) (red dots),  $\lambda_{\text{ex}} = 375$  nm,  $\lambda_{\text{em}} = 470$  nm. Transient decays were recorded by monitoring the donor emission. The black line indicates the fit line to the recorded femtosecond transients.

The lifetime of C480 in water is reported to be 5.9 ns.<sup>303</sup> In the presence of the acceptor, the donor displays a short initial decay component ( $\sim 10$ -30 ps). We believe that the short decay of donors (close to the origin) in **Figure 6.12** results from ultrafast FRET between the capsule included donors (C480, C1, C153) and the acceptor R6G at short distances.

Conclusive evidence in favor of ultrafast FRET in the OA cavity is provided by the rise of the acceptor emission captured in a fs upconversion experiment. **Figure 6.13** provides the rise of the acceptor R6G emission in the presence of the OA trapped donors, C480, C1, and C153, respectively.



**Figure 6.13** Femtosecond transient decays of: (a) R6G (30  $\mu\text{M}$ ) alone (black dots) and on addition of C480 (10  $\mu\text{M}$ )@OA (80  $\mu\text{M}$  in 0.8 mM buffered water) (red dots) and  $\lambda_{\text{ex}} = 375$  nm,  $\lambda_{\text{em}} = 560$  nm; (b) R6G (50  $\mu\text{M}$ ) alone (black dots) and on addition of C1 (20  $\mu\text{M}$ )@OA (120  $\mu\text{M}$  in 1.2 mM buffered water) (red dots) and  $\lambda_{\text{ex}} = 375$  nm,  $\lambda_{\text{em}} = 570$  nm; (c) R6G (48  $\mu\text{M}$ ) alone (black dots) and on addition of C153 (16  $\mu\text{M}$ )@OA (80  $\mu\text{M}$  in 0.8mM buffered water) (red dots) and  $\lambda_{\text{ex}} = 375$  nm,  $\lambda_{\text{em}} = 570$  nm. The black line indicates the fit line to the recorded femtosecond transients.

### 6.2.6 Comparison of parameters involved in calculation of $R_{\text{DA}}$

The emission of the acceptor exhibits a rise time of 1.5, 3.5, and 1.0 ps (**Table 6.1**) for OA trapped donors, C480, C1, and C153, respectively. Using these rise times, the donor-acceptor distance,  $R_{\text{DA}}$ , was calculated using **equations 6.1 and 6.2**.

**Table 6.1** Femtosecond Decay Parameters of the Acceptor in the Presence and Absence of the Donors.

System	$\lambda_{\text{ex}}(\text{nm})$	$\lambda_{\text{em}}(\text{nm})$	$\tau_1^{\text{a}} (a_1^{\text{b}})$ (ps)	$\tau_2^{\text{a}} (a_2^{\text{b}})$ (ps)	$\tau_3^{\text{a}} (a_3^{\text{b}})$ (ps)
R6G+OA	375	570	40 (0.09)	1100 (0.17)	5000 (0.83)
R6G+C153@OA	375	570	1.0 (-.24, 100%)	1800 (0.16)	6000 (0.84)
R6G+OA	375	560	40 (0.09)	1100 (0.17)	5000 (0.83)
R6G+C480@OA	375	560	1.5 (-1.4, 100%)	1600 (0.17)	5100 (0.83)
R6G+OA	375	570	40 (0.09)	1100 (0.17)	5000 (0.83)
R6G+C1@OA	375	570	3.5 (-1.56, 100%)	1600 (0.13)	5500 (0.87)

$$R_0 = 0.211 [\kappa^2 n^{-4} Q_D J(\lambda)]^{1/6} \quad \text{Eqn. 6.2}$$

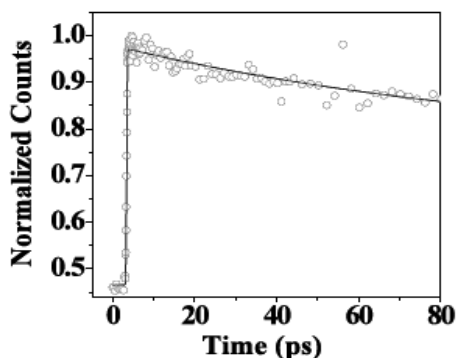
Here,  $n$  is the refractive index of the medium ( $\sim 1.4$  for macromolecules in water),  $Q_D$  is the quantum yield of the donor in the absence of acceptor,  $\kappa^2$  is the orientation factor and  $J(\lambda)$  is the spectral overlap between the donor emission and the acceptor absorption. **Table 6.2** lists the values of experimentally obtained  $R_0$ ,  $\tau_D^0$ ,  $\tau_{\text{rise}}^A$ , and calculated  $R_{\text{DA}}$  for the three donor-acceptor pairs: C480@OA<sub>2</sub> and R6G; C1@OA<sub>2</sub> and R6G; and C153@OA<sub>2</sub> and R6G. It is interesting that similar values were obtained despite the varying parameters for calculating  $R_{\text{DA}}$  in these systems. This observation leads to the conclusion that varying fundamental conditions for FRET like spectral overlap, donor lifetime (in the absence of acceptor), or acceptor rise time (in the presence of donor) among various donor-acceptor pairs could still result in efficient ultrafast FRET provided the pair is in close proximity (13 Å in this case). One might wonder why the most pronounced difference in the decays occurs for the D-A pair exhibiting the worst spectral overlap. We believe that due to low magnitude of overlap between the D-A pair (C1-R6G) the rate of FRET becomes slower, and hence the rise is more distinct compared to

the transient in the absence of donor. The difference is only captured in our up-conversion setup (IRF, resolution~350 fs). One might argue that the absence of change in lifetime of the donor in the presence of an acceptor (in the picosecond time scale) could be due to trivial energy transfer. In our study, the trivial energy transfer (donor emission being reabsorbed by the acceptor) is ruled out due to the delay noted for the emission of the acceptor R6G upon excitation of the donors.

**Table 6.2** Comparison of Parameters for Calculating  $R_{DA}$

System	$\tau_{\text{rise}}^A$	$\tau_D^0$	$R_0$	$R_{DA}$
C480@OA+R6G	1.5 ps	4900 ps	48.8 Å	13±1 Å
C153@OA+R6G	1.0 ps	7400 ps	55.7 Å	13±1 Å
C1@OA+R6G	3.5 ps	4300 ps	42.5 Å	13±1 Å

An additional point to note is the lack of any rise at the red end of the emission spectra of the coumarin dyes indicating the absence of solvation dynamics inside the OA cavity **Figure 6.14**, consistent with our earlier conclusion of a nonpolar, water excluded interior of the capsule.<sup>51</sup> This also supports that FRET is not due to donor molecules present in water. Demonstration of energy transfer in an environment lacking water molecules suggests the capsule to have remained closed.



**Figure 6.14** Femtosecond decay of C480 (10  $\mu\text{M}$ ) in presence of OA (80  $\mu\text{M}$  in 0.8 mM buffered water),  $\lambda_{\text{ex}}=375\text{ nm}$   $\lambda_{\text{em}}=530\text{ nm}$  (red end of C480 emission spectrum)



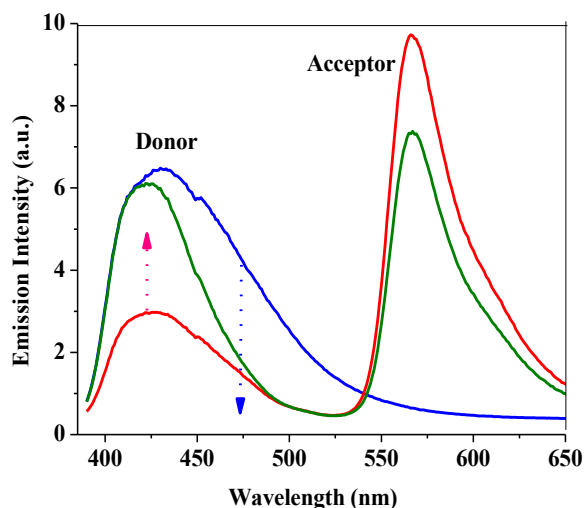
### 6.3 Diminishing FRET between donor@OA and acceptor-OA by introducing another host

After establishing the occurrence of FRET between the donor dyes encapsulated within the hydrophobic cavity of the nanocavitand OA and the acceptor dye being attached to the outer walls of OA through ion-pair interaction, we moved on to a more complex system. We introduced a new host into the system, which could attract the acceptor dye R6G. The hosts we used for our studies were third generation acid dendrimer (G3A), which could attract R6G through ion-pair interaction and Cucubituril [7] (CB[7]), which could attract R6G by hydrophobic interactions (**Scheme 6.1**). The idea was to detach the acceptor R6G from the walls of OA and see if the FRET taking place would diminish. Below we summarize our observations.

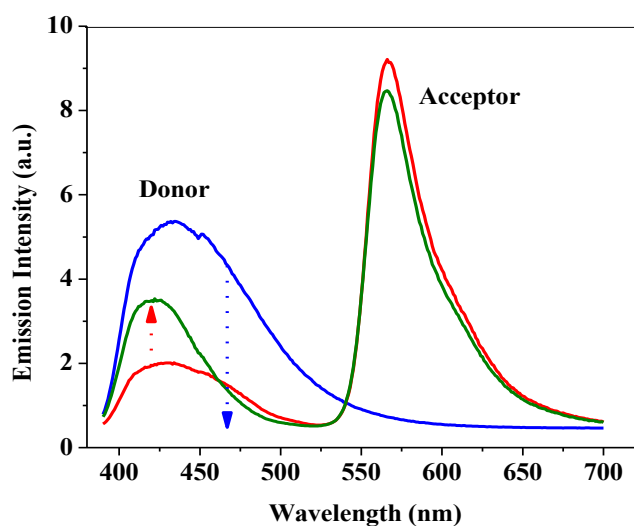
#### 6.3.1 Steady-state emission studies

In these experiments, we first recorded the emission spectrum of donor@OA and to this solution, we added the acceptor R6G. As stated in earlier sections, we could observe that the emission intensity of the donor@OA decreased and emission intensity of the acceptor R6G increased, indicating the occurrence of FRET. Now to this solution we added the second host gradually and recorded the emission spectra. In **Figure 6.15**, blue line denotes the emission spectrum of donor C1@OA<sub>2</sub> alone. Red line denotes the emission spectrum of the system when the acceptor R6G is added to the above solution; we can observe the decrease in the emission intensity of the donor and increase in the emission intensity of the acceptor R6G. Next, green line in the figure denotes the emission spectrum of the system when 40  $\mu\text{M}$  of G3A was added to the above solution. Here, we could observe, that the emission intensity of the donor is almost regained, whereas, the emission intensity of the acceptor has partially decreased. This observation

points towards the reversal or diminishing of FRET taking place between the donor and the acceptor.



**Figure 6.15** Steady state fluorescence spectra of C1 (20  $\mu\text{M}$ )@OA (120  $\mu\text{M}$  in 1.2 mM buffered water) only (blue line); on addition of R6G (50  $\mu\text{M}$ ) (red line), and on addition of G3A (40  $\mu\text{M}$ ) (green line)  $\lambda_{\text{ex}}=360$  nm. The blue arrow indicates the decrease in emission intensity of donor on addition of the acceptor and red arrow indicates the regain in the emission intensity of the donor on addition of another host G3A into the above solution. (a. u. = arbitrary units).



**Figure 6.16** Steady state fluorescence spectra of C1 (20  $\mu\text{M}$ )@OA (120  $\mu\text{M}$  in 1.2 mM buffered water) only (blue line); on addition of R6G (50  $\mu\text{M}$ ) (red line), and on addition of CB[7] (30  $\mu\text{M}$ ) (green line)  $\lambda_{\text{ex}}=360$  nm. The blue arrow indicates the decrease in emission intensity of donor on addition of the acceptor and red arrow indicates the regain in the emission intensity of the donor on addition of another host CB[7] into the above solution. (a. u. = arbitrary units).

Similarly, **Figure 6.16**, shows how the intensity of FRET taking place between the donor C1@OA<sub>2</sub> and the acceptor partially decreased on addition of the host CB[7] to the system. As, in earlier cases, we carried on time resolved studies to obtain a better picture of the events taking place in this system.

### 6.3.2 Time Resolved Emission Studies

As observed in the previous **Section 6.2.5**, in the picoseconds studies the excited singlet lifetime of the three donors included in OA (C480, C1, and C153) was found to be unaffected by the addition of acceptor R6G; so was the case when we introduced the second host into the system as can be seen from **Table 6.3**. For exploring the system further, femtosecond experiments were carried out. We monitored the rise time (**Table 6.4**) of the acceptor R6G in the presence of the donor@OA as well as on addition of the second host G3A/CB[7] into the system. As can be seen that the rise time of the acceptor R6G in presence of C480@OA was 1.5 ps, whereas on addition of the hosts CB[7] and G3A it increased to 5.0 ps and 4.0 ps respectively. As stated in **Section 6.2.6**, the increase in the rise time of the acceptor could be due to the decreased rate of FRET between the D-A pair. And the decrease in the rate of FRET is possible when the D-A distance is increased.

**Table 6.3** Picosecond Decay Parameters of C480-R6G-OA systems + G3A/ CB[7]

system	$\tau_1^a (a_1^b) \text{ (ps)}^*$	$\tau_2^a (a_2^b) \text{ (ps)}^*$
C480+R6G+OA	1600 (0.17)	5100 (0.83)
C480+R6G+OA+CB[7]	2000 (0.10)	5500 (0.90)
C480+R6G+OA+G3A	1100 (0.22)	5300 (0.78)

\*( $\lambda_{\text{ex}} = 375 \text{ nm}$ ,  $\lambda_{\text{em}} = 560 \text{ nm}$ )

**Table 6.4** Femtosecond Decay Parameters of C480-R6G-OA systems + G3A/ CB[7]

System	$\tau_1^a$ ( $a_1^b$ ) (ps)*	$\tau_2^a$ ( $a_2^b$ ) (ps)*	$\tau_3^a$ ( $a_3^b$ ) (ps)*
C480+R6G+OA	1.5 (-1.40, 100%)	1600 (0.40, 17%)	5100 (2.00, 83%)
C480+R6G+OA+CB[7]	5.0 (-0.53, 100%)	2000 (0.15, 10%)	5500 (1.38, 90%)
C480+R6G+OA+G3A	4.0 (-0.31, 100%)	1100 (0.29, 22%)	5300 (1.02, 78%)

\*( $\lambda_{\text{ex}} = 375$  nm,  $\lambda_{\text{em}} = 560$  nm )

**Table 6.5**, shows the  $R_{\text{DA}}$  calculated from the values of the rise time given in **Table 6.4**. It can be observed that the distance ( $R_{\text{DA}}$ ) between the donor and the acceptor increased slightly on addition of the second host (G3A/CB[7]) into the system, suggesting that these hosts could be attracting the acceptor R6G towards themselves, hence detaching them from OA.

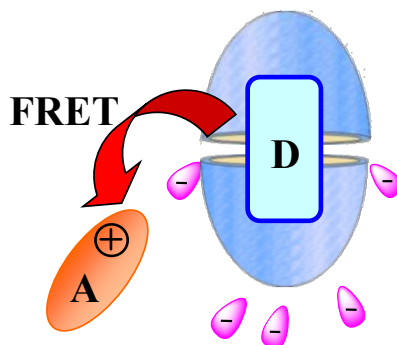
**Table 6.5** Calculated Donor-Acceptor distances

System	$\tau_{\text{rise}}$ (ps)	$R_{\text{D-A}}$ (Å)
C480+R6G+OA	1.5	12.7
C480+R6G+OA +CB[7]	5.0	15.5
C480+R6G+OA +G3A	4.0	14.9

## 6.4 Conclusion

This work demonstrates the occurrence of ultrafast FRET between a donor (coumarin dyes) enclosed in an OA capsule and a cationic acceptor attached to the capsule's anionic exterior. Though steady-state experiments gave us a glimpse of singlet-singlet energy transfer, time-resolved femtosecond studies gave us a clear and concise picture of the events occurring at the ultrafast time scale. These studies also unambiguously proved our proposed supramolecular model for the donor@OA and

acceptor assembly, **Figure 6.17** is a pictorial representation of this model. As a next step, we by introducing other host molecules into the system, we showed that by detaching the acceptor from the rim of OA, rate of ultrafast FRET could diminish as a result of increased D-A distance. We wish to ultimately incorporate this system in higher-order supramolecular assemblies as a building block.



**Figure 6.17** Pictorial representation of ultrafast FRET taking between the donor@OA and acceptor-OA.

## 6.4 Experimental Section

**Materials:** Laser grade dyes coumarin 1, coumarin 153, and coumarin 480 (and rhodamine 6G) were obtained from Exciton and used as received. The octa-acid was synthesized and purified according to the published procedure.<sup>46</sup>

**Steady-State Fluorescence Experiments:** Fluorescence emission and excitation spectra were recorded on an Edinburgh FS920CDT steady-state fluorimeter, and nanosecond lifetime measurements were carried out on an Edinburgh FL900CDT fluorescence lifetime spectrometer. Stock solutions of 10 mM of OA in 100 mM of sodium tetraborate buffer and known concentration of coumarins in water were made and used for steady-state and time-resolved fluorescence studies. For experiments with C1 in the presence of

OA, 20  $\mu\text{M}$  of C1 was taken in a cuvette, and 6 equiv, i.e., 120  $\mu\text{M}$  of OA, was added. Then the solution was made up to a volume of 3 mL, by addition of water. Similarly, for 16  $\mu\text{M}$  of C153, 5 equiv (80  $\mu\text{M}$ ) of OA, and for 10  $\mu\text{M}$  of C480, 8 equiv (80  $\mu\text{M}$ ) of OA were used to prepare 3 mL of donor@OA solutions. For FRET experiments, 5 mM Rhodamine 6G aqueous stock solution was added stepwise to the donor@OA solution, until no further change in the spectra was observed. For the experiments, involving hosts G3A and CB[7], these hosts were gradually added to the solution containing donor@OA and R6G to the final concentration of 40 and 30  $\mu\text{M}$  respectively.

**Picosecond and Femtosecond Fluorescence Experiments:** Femtosecond up-conversion setup (FOG 100, CDP) (IRF  $\sim$  350 fs) used in this study has been described previously.<sup>308</sup> To fit the fs transient, we first determined the long ps components (400-7000 ps) using a TCSPC setup (IRF $\sim$ 90 ps) described earlier.<sup>308</sup> The long ps components were kept fixed to fit the fs data. The ultrafast components (1-3 ps) were determined from the fs up-conversion setup. The rate of FRET ( $k_{\text{FRET}}$ ) was calculated following Förster Theory<sup>293</sup>

$$k_{\text{FRET}} = \frac{1}{\tau_{\text{rise}}^{\text{A}}} = \frac{1}{\tau_{\text{D}}^0} \left( \frac{R_0}{R_{\text{DA}}} \right)^6$$

Where,  $\tau_{\text{D}}^0$  is the lifetime of the donor in the absence of acceptor and  $\tau_{\text{rise}}^{\text{A}}$ , is the rise time of acceptor emission in presence of donor. At a donor-acceptor distance  $R_{\text{DA}}=R_0$ , the efficiency of energy transfer is 50% and  $k_{\text{FRET}} = (1/\tau_{\text{D}}^0)$ .

The procedure to evaluate  $R_0$  is described in one of our groups' previous publications.<sup>307-</sup>

**General Protocol for Guest Binding Studies Probed by  $^1\text{H}$  NMR:** A  $\text{D}_2\text{O}$  stock solution (600  $\mu\text{L}$ ) of host OA (1 mM) and sodium borate buffer (10 mM) taken in a NMR tube was titrated with the guest by sequential addition of 0.125 equiv of guest (1.25  $\mu\text{L}$  of a 60 mM solution in  $\text{DMSO-d}_6$ ). The complexation was achieved by shaking the NMR tube for about five minutes.  $^1\text{H}$  NMR spectra were recorded at room temperature under aerated conditions on a Bruker 500 MHz NMR. Addition of guest beyond 0.5 equiv led to a turbid solution at which stage the NMR spectrum demonstrated the presence of free guest in addition to the capsular complex.

**Protocols for Measurements by  $^1\text{H}$  NMR DOSY Studies:** Diffusion NMR experiments were recorded on a Bruker 500MHz NMR spectrometer. The experiments were performed at  $25^\circ\text{C}$ , at a host concentration of 1 mM (in 10 mM sodium tetraborate). Assuming the complex to be spherical  $R_h$  can be calculated using the measured  $D$  according to the following equation

$$R_h = kT/6\pi\eta D$$

where  $R_h$  is the hydrodynamic radius of the sphere in meters;  $k$  is the Boltzmann constant;  $T$  is the temperature in Kelvin;  $\eta$  is the solvent viscosity; and  $D$  is the diffusion constant in  $\text{m}^2 \text{s}^{-1}$ .<sup>310</sup> Since the molecular size of 1:1 and 1:2 complexes is different, the value of  $R_h$  is an indirect reflection of the nature of the complex.

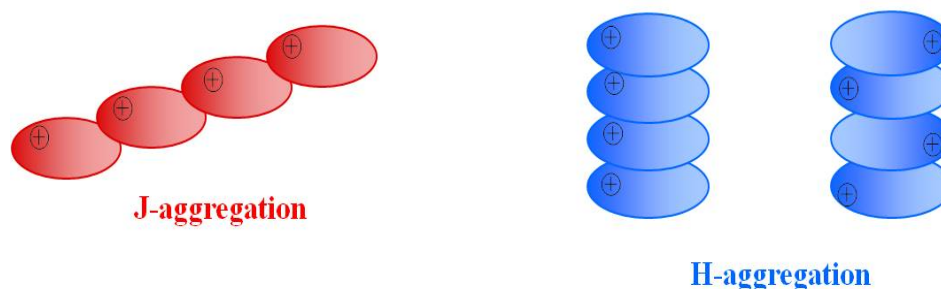
## **CHAPTER 7**

### **Study of the Hydrophobic and Columbic Association of Dyes with Various Organic Supramolecular Hosts**



## 7.1 Overview

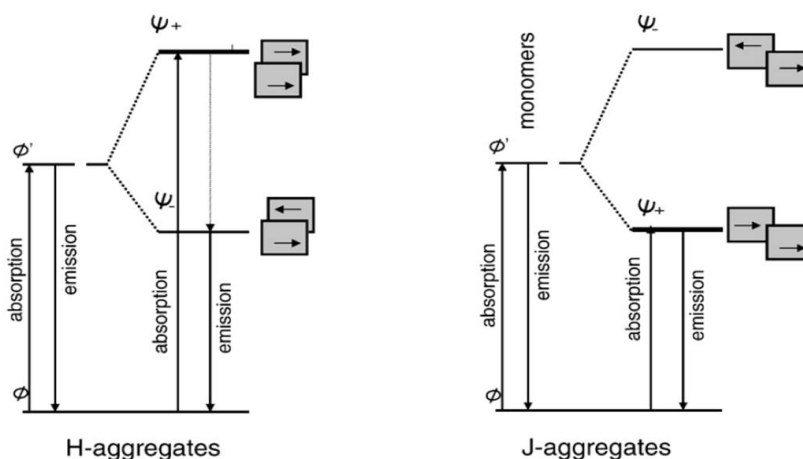
Organic dyes may change colour and other optical and chemical properties in relation to their chemical environment. Therefore, dyes have often been used as probes or sensors in various scientific fields.<sup>311</sup> Dyes play an important role as sensitizers in photographic processes, laser components, photographic filter layers, and chemotherapy.<sup>312,313</sup> Recently, dyes have also been studied extensively as sensitizers in photo-electrochemical solar energy conversion systems.<sup>314-316</sup> Broadly classifying, dyes find applications in two important areas: coloration of materials such as fibers and in photochemical processes such as photography and dye lasers. In both of these areas, knowledge of aggregation equilibria is important.



**Figure 7.1** Pictorial representation of J- and H-aggregates.

The molecular aggregation could be a result of hydrophobic interactions, which is a general tendency of non-polar molecules to associate physically in aqueous solutions. The presence of non-polar molecules in water disrupts the hydrogen bond network of water molecules, resulting in a loss of translational and rotational degrees of freedom of the solvent within the hydrophobic hydration shell. Such a mechanism is generally referred to as a loss of entropy of the system. In dyes, the aggregation principally forms dimers except at high concentrations in solvents with a high dielectric constant.

There are two main types of dye molecular aggregates, formally and originally assigned according to their optical properties, but closely related to their structure and the type of intermolecular association. H-aggregates are based on a sandwich-type intermolecular association. Less frequent J-aggregates are formed by head-to-tail intermolecular interactions **Figure 7.1** illustrates a pictorial representation of H- and J-aggregates.

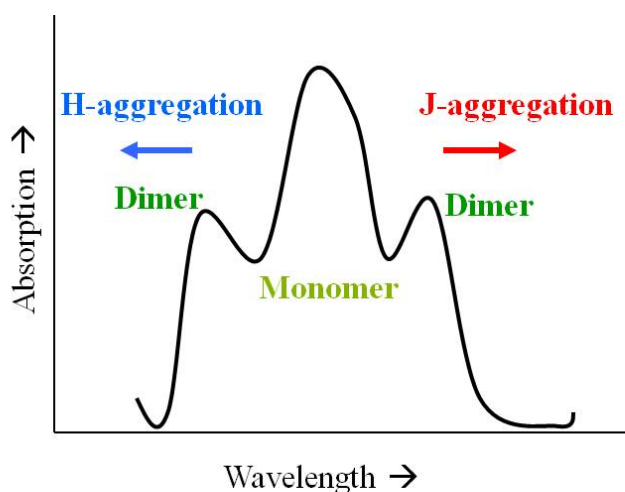


**Figure 7.2** Energy graphs for the dye dimers of H- and J-type types according to a molecular exciton theory.  $\Psi^+$ —directions of the transition moments are parallel, and the transition is non-zero.  $\Psi^-$ —directions of the transition moments are anti-parallel, and the transition is zero.

In the H-aggregates, coupled transition moments could be oriented in either the parallel or anti-parallel fashion. The anti-parallel orientation ( $\Psi^-$ ) of an H-dimer has a lower energy state, due to the electrostatic attraction between the transition moments. In the J-aggregates, anti-parallel moments ( $\Psi^-$ ) result in a higher energy due to electric repulsion. Resulting dipole for the anti-parallel arrangements of the transition moments is always zero; and therefore, the transitions to such states are symmetry forbidden. Only the transitions to the states with parallel orientations ( $\Psi^+$ ) are allowed, which is to the

lower energy state for the J-aggregates and to the higher energy state for the H-aggregates, as we can see in **Figure 7.2**.<sup>311</sup>

Hence, interpreting this energy level diagram in terms of UV-visible absorption spectra, we can expect to observe a band arising in the lower wavelength region due to a H-aggregate of the corresponding monomer of a given dye molecule. Or a band that is sharp and appears in the high wavelength region with respect to the band corresponding to the monomer, could be assigned due to the existence of J-aggregates in the solution. For a clearer visualization of the facts, **Figure 7.3** gives a pictorial representation of the location of expected band due to J- and H- aggregates.



**Figure 7.3** Pictorial representation of the location of H- and J-aggregates on UV-visible absorption spectra.

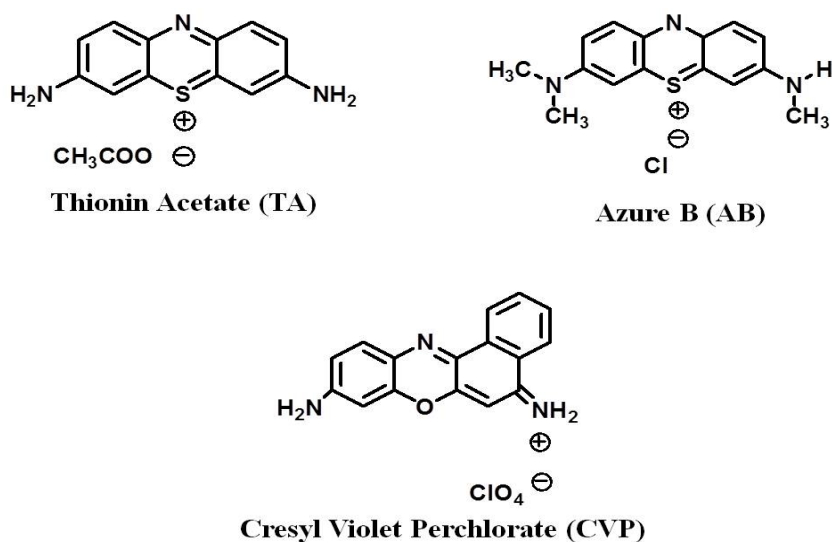
The perfect H- and J-aggregates are just two ideal states of all possible forms and variations of molecular assemblies. Many dyes may form such assemblies, which include the structural features of both the H- and J-aggregates. In such cases, the molecular aggregates absorb light with energies corresponding to both the higher and lower energy states. The assignments of the bands absorbing at the low- and high-energy transitions indicate the structural features of the dye supramolecular assemblies.

Aggregation and de-aggregation of the dyes can be well managed by introducing macromolecules in the system. Hence, photochemical activation of organic dyes in controlled molecular environments has become an important area of research for application in photo-devices and renewable energy sources.<sup>317,318</sup> Different micro-heterogeneous environments such as micelles, thin films, and silicate materials<sup>319-322</sup> are employed as models for photochemical processes occurring in photosynthesis and in solar energy conversion devices.<sup>323-325</sup> The aggregation of the dye molecules on a semiconductor surface has been generally viewed as detrimental to the performance of light energy conversion devices.<sup>326,327</sup> Thus controlling the ratio of different aggregates and monomer form of the dyes are some issues which need to be scientifically addressed.

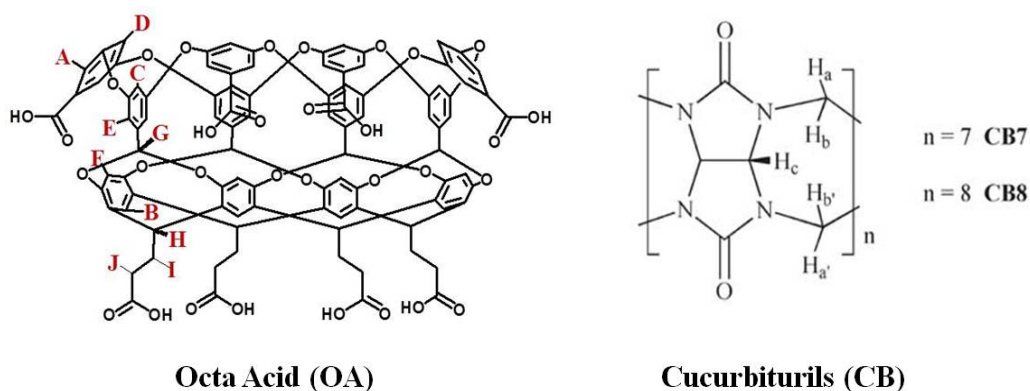
Recently, to modulate the aggregation of dyes through encapsulating dye in the cages of supramolecular assemblies has caused much interest.<sup>328-330</sup> A classical example is cucurbit[n]uril (CBs) which can strongly influence the photophysical properties of dyes by forming host/guest inclusion complexes with organic dyes.<sup>75</sup> Depending on the size and preferred orientation of guests, CBs can accommodate one or two dye molecule(s) either fully or partially to form 1:1 or 1:2 complex through the ion-dipole and hydrophobic interaction. Werner M. Nau *et al*, and J. C. Scaiano *et al* have done much works in this field.<sup>331-334</sup>

In this project, we have investigated the interaction between some cationic dyes (as shown in **Scheme 7.1**) and host cavitand Octa Acid (OA) (**Scheme 7.2**) by monitoring the change in the absorption and emission spectra of these dyes. Due to the hydrophobic characteristic of OA cavity, it can form two types of cavity complexes depending on the type of guests: one is termed as cavitandplex, an open complex in which a part of the

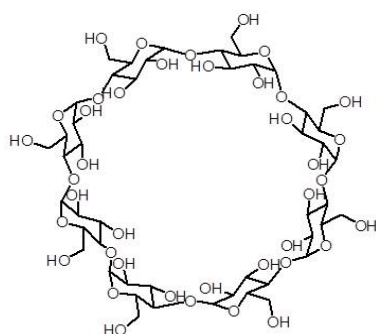
guest is exposed to water; the other one is capsuleplex, in which the host completely surrounds the guest and protects it from the aqueous exterior.<sup>52</sup> For a long time, the four acid groups each at the top and the bottom (as shown in **Scheme 7.2**) have been considered as hydrophilic groups, just to improve the solubility of OA in aqueous solution, only few attention has been paid on their ability to bind to a positively charged groups. It's very obvious to assume that a Coulombic attraction would exist between the carboxylate groups of OA with negative charge and any other groups with positive charge in aqueous solution.



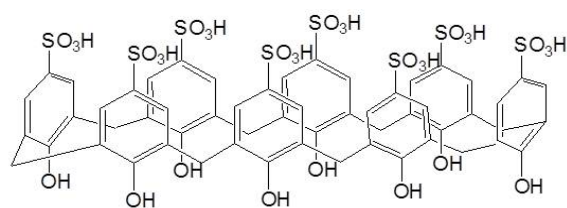
**Scheme 7.1** Chemical structures of the cationic dyes used for these studies.



**Scheme 7.2** Chemical structures of the hosts Octa Acid and Cucurbiturils.

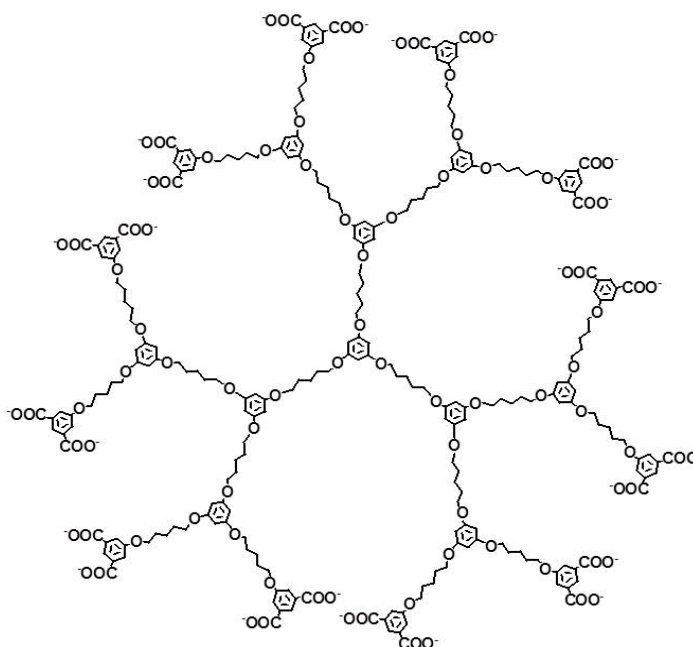


**$\gamma$ -Cyclodextrin  
( $\gamma$  CD)**



**Calixarene [8] (Cal 8)**

**III-Generation Acid  
Dendrimer (G<sub>3</sub>A)**



**Scheme 7.3** Chemical structures of the other hosts involved in this study.

We have also compared the interaction of the above dyes with the hosts, CB[7] and CB[8], to clearly differentiate the hydrophobicity offered by these hosts in comparison to the Columbic interaction association with the host cavitand OA. Dr. **Yao Pang Zhao** did the preliminary research work on this project which has been included in **Section 7.2.4**. After a getting a clear and profound understanding of the interactions of cationic dyes with the exterior of Octa Acid, we moved on to some other host systems like Cyclodextrins, Calixarene and dendrimers (**Scheme 7.3**) for further understanding the interplay of hydrophobic and Columbic interactions offered by these host systems.

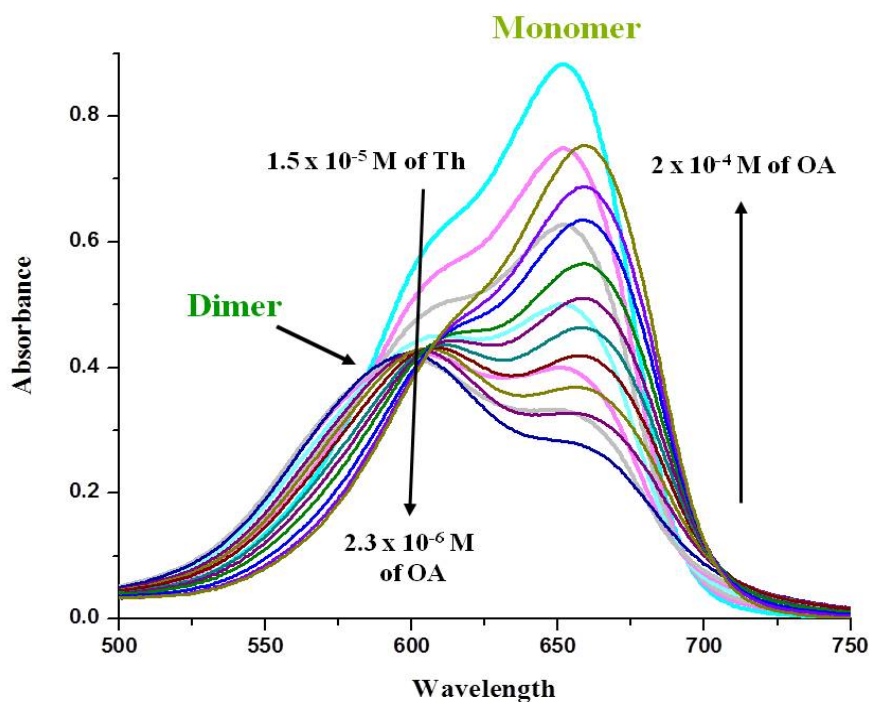
## 7.2 Results and discussion

### 7.2.1 Interaction of Azure B and Thionin Acetate with OA

We initiated our studies with two dyes, Azure B (AB) and Thionin Acetate (Th), these are laser grade dyes and were used as such, without any further purification. Both the dyes exist in their cationic states in the aqueous sodium borate buffer. In aq. sodium borate buffer medium, all eight carboxylic acid groups of OA gets converted to corresponding carboxylates.. A 10 mM stock solution of the host OA was prepared in 100 mM borate buffer. And it was added to 3 mL of the stated concentration of the dyes in very small increments stepwise. The resultant absorption and fluorescence spectra of titration of Th against OA have been showed in **Figure 7.4** and **7.5** respectively. In **Figure 7.4**, the bright blue color spectrum is for  $1.5 \times 10^{-5}$  M Thionin in aq. solution. A well defined monomer peak at  $\lambda_{\max}$  652 nm along with a faint shoulder at a lower wavelength assigned as the dimer peak could be observed for the free Thionin. The primary observation we made from the absorption and emission spectra was that for almost all the dyes we have used in these studies, chiefly a monomer exist in the aq. solution with a slight amount of dimer. This dimer is attributed to the presence of a blue shifted weak shoulder band in the absorption spectra of the aq. solution of dyes. Hence we inferred that this dimer is a part of the H-aggregates of the dye.

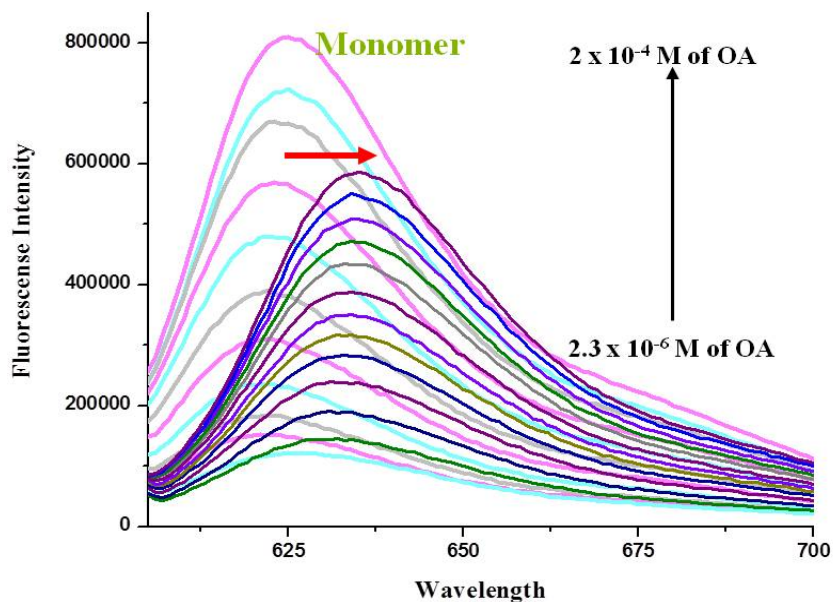
Host OA was gradually added to the above solution. As the OA concentration increased the monomer band kept on decreasing and the relative intensity of the dimer band increased. At  $2.3 \times 10^{-6}$  M concentration of OA, we observed that the solution equilibrium shifted more towards the dimer, i.e. at this stage more of the dimer existed in the solution. When the concentration of OA was further increased, the band for monomer

started reappearing while dimer band disappearing slowly. At  $2.0 \times 10^{-4}$  M of OA, the solution equilibrium favored the formation of monomer. On further increasing the concentration of OA, no further change in the spectrum was observed. One important observation is that the new monomer peak is 4-5 nm red shifted in comparison to the initial monomer peak. **Figure 7.5** shows the corresponding fluorescence spectra. Here again, we initially observe a peak due to the monomer, but when host OA is added to the solution, the intensity of this peak decreases. Unlike absorption spectra, here we do not observe any peak corresponding to the dimer, since dimers are mostly non-emissive. After  $2.3 \times 10^{-6}$  M concentration of OA, the monomer peak starts reviving back, and at  $2.0 \times 10^{-4}$  M of OA, the monomer peak intensity reaches to its maxima. In this case too we observe a 10-11 nm red shift in the final emission spectra.

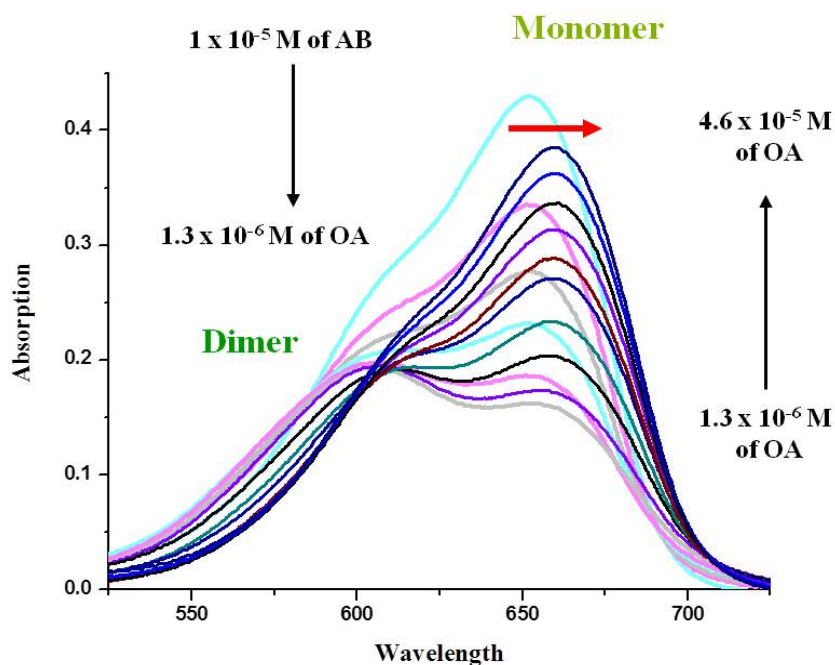


**Figure 7.4** UV-visible spectra of Thionin Acetate (Th) titrated with OA at room temperature. Lighter color lines represent the increase of [OA] to  $2.3 \times 10^{-6}$  M and the darker shade lines represent the increase in [OA] from  $2.3 \times 10^{-6}$  M to  $2.0 \times 10^{-4}$  M. Wavelength measured in nanometers.



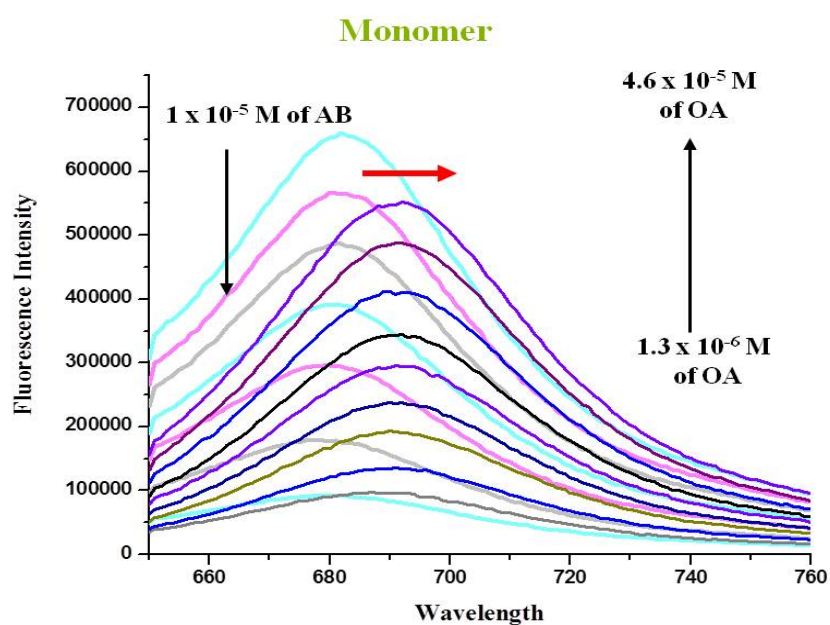


**Figure 7.5** Fluorescence spectra of Thionin Acetate (Th) titrated with OA at room temperature. Lighter color lines represent the increase of [OA] to  $2.3 \times 10^{-6}$  M and the darker shade lines represent the increase in [OA] from  $2.3 \times 10^{-6}$  M to  $2.0 \times 10^{-4}$  M. Wavelength in nanometer.



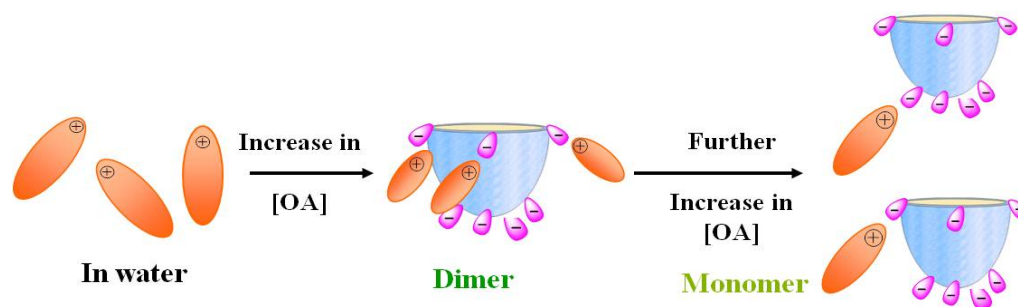
**Figure 7.6** UV-visible spectra of Azure B (AB) titrated with OA at room temperature. Lighter color lines represent the increase of [OA] to  $1.3 \times 10^{-6}$  M and the darker shade lines represent the increase in [OA] from  $1.3 \times 10^{-6}$  M to  $4.6 \times 10^{-5}$  M. Wavelength measured in nanometers.

The second dye we utilized for the same study was Azure B. We started the UV-Visible and fluorescence titration with  $1 \times 10^{-5}$  M of aq. solution of Azure B. We initially observed a monomer peak at 650 nm with a faint shoulder peak at around 610 nm corresponding to the dimer (**Figure 7.6**). To this solution we gradually added host OA. As was observed in the case of Thionin, the intensity of the monomer peak gradually decreased, and at  $1.3 \times 10^{-6}$  M of OA, most of the dimer existed.



**Figure 7.7** Fluorescence spectra of Azure B (AB) titrated with OA at room temperature. Lighter color lines represent the increase of [OA] to  $1.3 \times 10^{-6}$  M and the darker shade lines represent the increase in [OA] from  $1.3 \times 10^{-6}$  M to  $4.6 \times 10^{-5}$  M. Wavelength measured in nanometers.

When the concentration of OA was further increased the monomer peak increased in intensity with a 3-4 nm red shift. And at  $4.6 \times 10^{-5}$  of OA, there was no further change in the spectra. In the case of fluorescence spectra, initially the monomer peak was observed for Azure B, but with the increase of OA concentration this peak diminished, and on further increase in OA concentration a red shifted monomer peak reappeared (**Figure 7.7**).



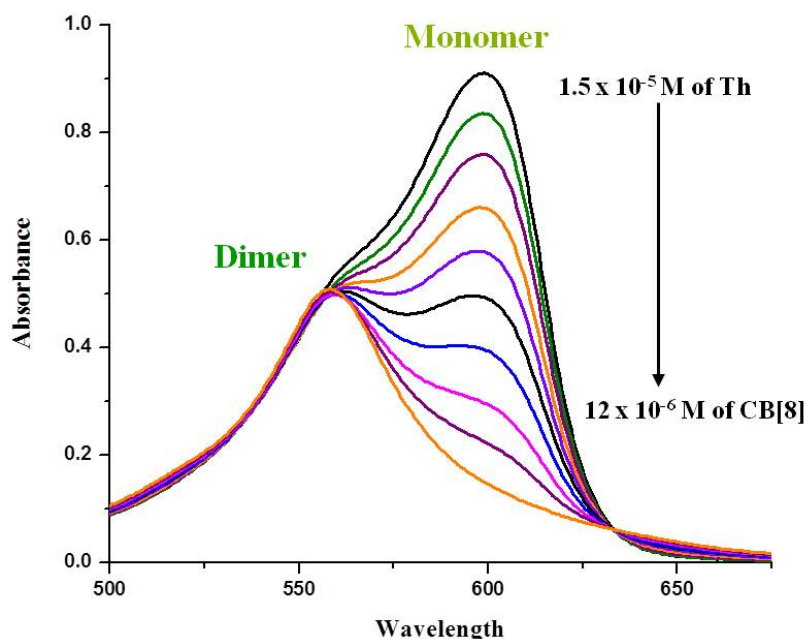
**Figure 7.8** Cartoon representations of the probable mechanism of formation of dimer followed by monomer of the cationic dyes due to the interaction with the anionic exterior of the host OA.

**Figure 7.8** can be used to illustrate the observed phenomenon in the above two cases. Initially the dyes existed in a monomer/dimer equilibrium in the aq. solution, where monomer specie predominated. When OA was added to the aqueous solution of these dyes, at the beginning the concentration of OA was very less when compared to the concentration of dyes; hence every OA molecule could be surrounded by many dye molecules due to the Columbic attraction between cationic dye and anionic exterior of host OA. This attraction resulted in the increase in local concentration of the dyes, which facilitated the aggregation of the dye molecules. This was reflected by the sharp decrease in absorption and fluorescence intensity of the dye monomer in **Figures 7.4** and **7.6**. However, along with addition of more and more OA, the aggregated dye molecules dispersed to the surrounding of more OA, and the aggregation effect of OA began to disappear. This was also reflected by the absorption and fluorescence spectra of the dye monomer which started increasing, when the concentration of OA was further increased.<sup>335</sup>

### 7.2.2 Interaction of Thionin Acetate with CB[7] and CB[8]

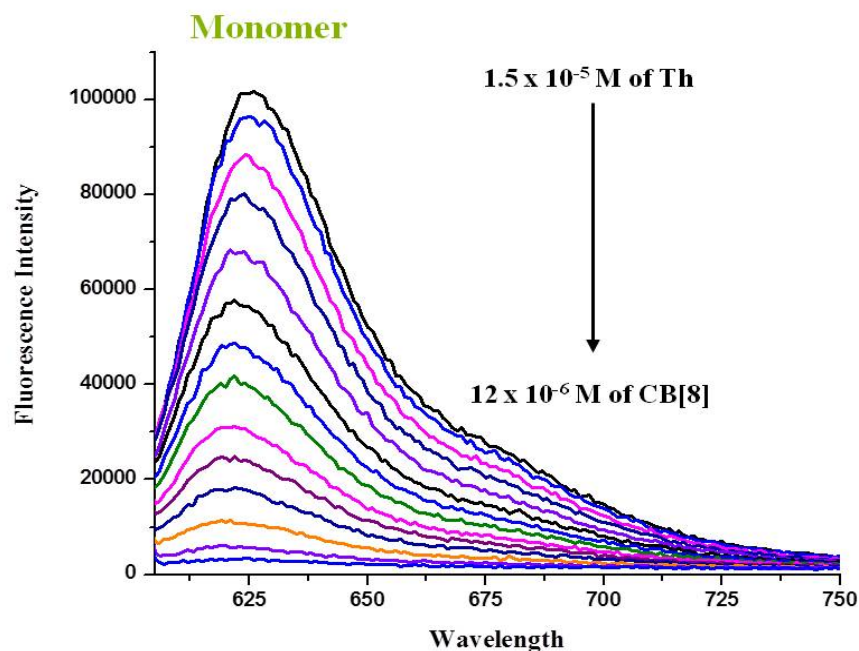
Cucurbiturils are known to bind the positively charged dyes effectively due to hydrophobic interactions.<sup>336</sup> Kaifer and co-workers have recently reported that the extent

of J- and H-aggregation of two cyanine dyes can be controlled by complexation with CB[6] and CB[7].<sup>337</sup> We carried out the absorption and fluorescence titration experiments with the positively charged dye Thionin Acetate and the hosts CB[7] and CB[8], to confirm the observations made by other research group. Also, we were interested to find if there are any differences in the interaction of the dye with CB[7] and CB[8], since they have different portal sizes.



**Figure 7.9** UV-Visible spectra of Thionin Acetate (Th) titrated with CB[8] at room temperature. [Th] =  $1.5 \times 10^{-5}$  M and CB[8] = 0 to  $12 \times 10^{-6}$  M. Wavelength is measured in nanometers.

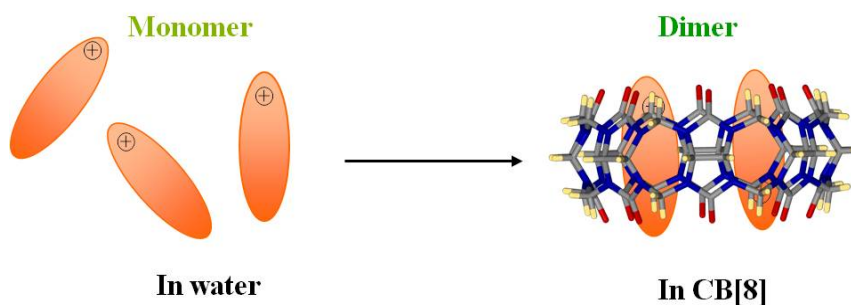
In this set of experiments we started with the aq. solution of dye Thionin acetate and then gradually added the hosts CB[7] and CB[8] in different experiments. Absorption and fluorescence spectra were recorded for each step. The experiments were stopped when no change in the spectra was observed after adding more host solution. The primary observation here too was same, that Thionin Acetate existed mostly as a monomer in aq. solution with a slight amount of H-aggregate dimer.



**Figure 7.10** Fluorescence spectra of Thionin Acetate (Th) titrated with CB[8] at room temperature.  $[\text{Th}] = 1.5 \times 10^{-5} \text{ M}$  and  $\text{CB}[8] = 0$  to  $12 \times 10^{-6} \text{ M}$ . Wavelength is measured in nanometers.

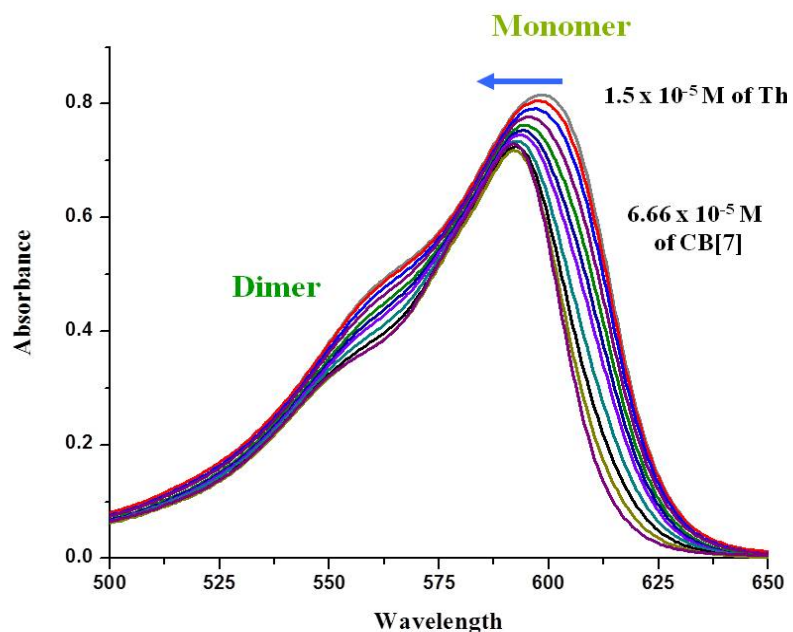
We started with  $1.0 \times 10^{-5} \text{ M}$  aq. solution of Thionin Acetate, and recorded the absorption as well as emission spectra (**Figures 7.9** and **7.10**). To this solution, a concentrated solution of the host CB[8] was gradually added, and the corresponding spectra were recorded. As we can observe, as the concentration of CB[8] increased the monomer peak diminished both in absorption as well as fluorescence spectra. The absorption spectra indicated that at  $12 \times 10^{-6} \text{ M}$  of CB[8], mostly dimer existed in the solution. This dimer peak was blue shifted in comparison to the weak shoulder band for the dimer which initially existed, indicating that the dye aggregates were present in a more hydrophobic environment. Corresponding fluorescence spectra also confirmed this observation, as after a gradual increase in the concentration of CB[8], the monomer emission band decreased with a continuous blue shift, and at the end diminished altogether.

**Figure 7.11** illustrates the above observed phenomenon. Initially, Thionin Acetate exist as a mixture of monomer and dimer in the aq. solution and at an optimum concentration of the host CB[8], two dye molecules occupy the portal cavity in preferably head to tail fashion. The dimerization is thought to be driven by the strong hydrophobic environment offered by the CB[8] host molecules to the organic dye molecules.

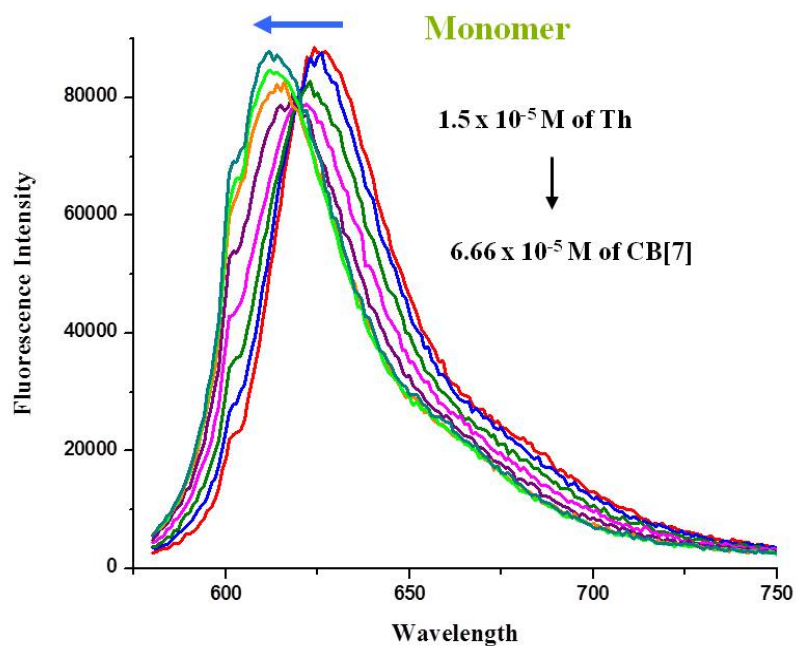


**Figure 7.11** Cartoon representations of the probable mechanism of the formation of the dimer in presence of host CB[8].

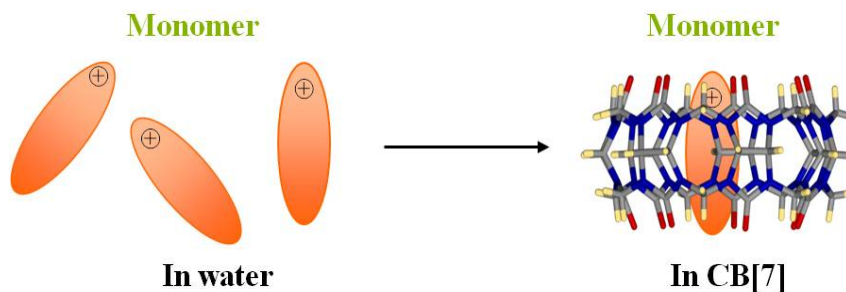
Similar experiments were carried out for the host CB[7]. Initially a  $1.5 \times 10^{-5}$  M of aq. solution of Thionin Acetate was taken. To this concentrated aq. solution of CB[7] was added in gradual steps. We went upto  $6.6 \times 10^{-5}$  M concentration of CB[7], but the observed spectral change was very less. There was a slight decrease in the absorption band intensity with a marked blue shift of 7-8 nm (**Figure 7.12**). A similar pattern was noticed in the corresponding fluorescence spectra (**Figure 7.13**). First there was a slight decrease in the monomer emission band, and then the monomer band intensity increased with a blue shift. Here we noticed a new monomer band approximately 8-10 nm shifted from the original monomer band.



**Figure 7.12** UV-Visible spectra of Thionin Acetate (Th) titrated with CB[7] at room temperature.  $[\text{Th}] = 1.5 \times 10^{-5} \text{ M}$  and  $[\text{CB}[7]] = 0$  to  $6.6 \times 10^{-5} \text{ M}$ . Wavelength is measured in nanometers.



**Figure 7.13** Fluorescence spectra of Thionin Acetate (Th) titrated with CB[7] at room temperature.  $[\text{Th}] = 1.5 \times 10^{-5} \text{ M}$  and  $[\text{CB}[7]] = 0$  to  $6.6 \times 10^{-5} \text{ M}$ . Wavelength is measured in nanometers.



**Figure 7.14** Cartoon representations of the probable mechanism of the formation of the dimer followed in presence of host CB[8].

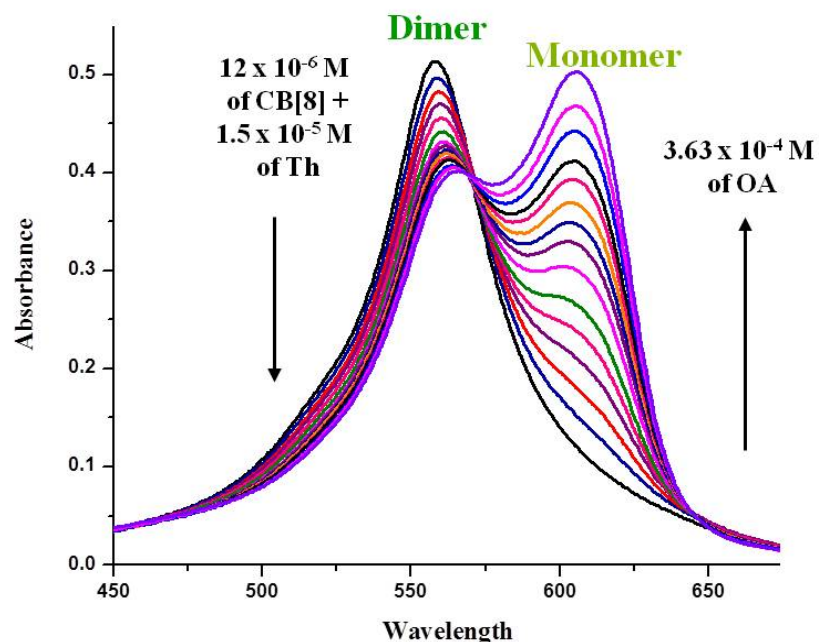
**Figure 7.14** explains the phenomenon which we think is taking place in the above mentioned experiments. As usual, the initial aq. solution of the dye Thionin Acetate consists of a mixture of monomer and dimers at  $1.5 \times 10^{-5}$  M concentration. When the host CB[7] is added gradually, these dye molecules face a hydrophobic environment, hence a blue shift is observed in both absorption as well as emission spectra. But since the portal size of CB[7] is less than that for CB[8], CB[7] is able to accommodate only a single dye molecule inside its cavity unlike CB[8], which accommodated two dye molecules. As a result, we observe a monomer peak but which is blue shifted since now this monomer is encapsulated inside the host CB[7] and enjoys a relatively more hydrophobic environment.

### 7.2.3 Comparative studies of OA vs. CB[8] and OA vs. CB[7] for Thionin Acetate

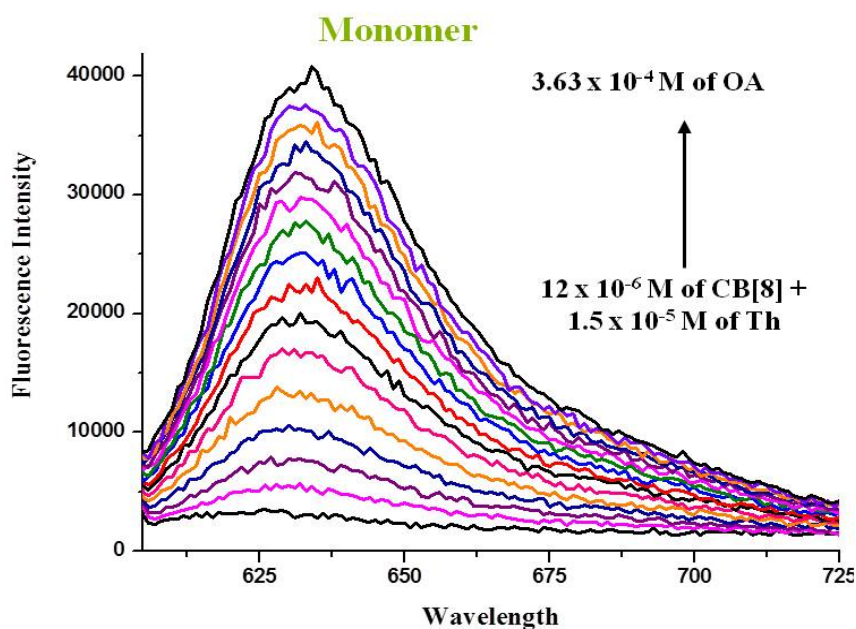
After studying the effects of OA and CBs on the cationic dyes, we sought the comparative studies of binding of these dyes in the presence of two hosts simultaneously in the solution. The main idea behind the above studies was actually to clearly distinguish between the two kinds of interactions, i.e. hydrophobic and Columbic ion-pair interactions, which a positively charged dye can face in presence of two different kinds of hosts, and also which interaction could dominate over the other.



In the first experiment, initially  $1.5 \times 10^{-5}$  M aq. solution of Thionin Acetate was taken. To this concentrated aq. solution CB[8] was added in steps. For the resultant absorption and fluorescence spectra please refer **Figures 7.9** and **7.10**. In both the cases, increase in concentration of CB[8] resulted in the formation of dimer of the dye which was attributed to the hydrophobic interaction offered by CB[8] inner cavity. The final concentration of CB[8] after which no further change in the spectra was noticed, was  $12 \times 10^{-6}$  M. After this a concentrated solution of OA was added to the above solution containing the dye dimers inside CB[8] (**Figure 7.15**). With the increase in the concentration of OA, it was noticed that the absorption peak due to the dimer gradually decreased, giving way to the red shifted monomer peak. After  $3.63 \times 10^{-4}$  M of OA, no further change in the absorption spectra was observed. At this point we observed the presence of chiefly red shifted monomer which indicated that the dye molecules segregated and interacted with OA molecules by an ion- pair interaction; along with a blue shifted dimer peak, which showed that probably some dye molecules preferred to be in dimer form in the presence of CB[8] in the solution. The corresponding emission spectra (**Figure 7.16**), initially due to the formation of dimer showed practically no emission bands, but with the gradual increase in the concentration of OA, the red shifted monomer emission band re-appeared, though the intensity of the band was not very high. The re-appearing of this band, supported the prior observation in the absorption spectra, that these spectral changes could be due to the preferential monomer formation of the positively charged dye molecules in the presence of anionic OA host.

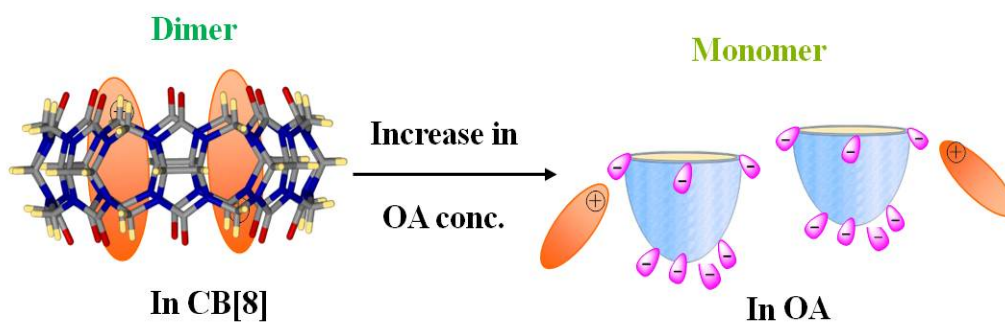


**Figure 7.15** UV-Visible spectra of Thionin Acetate (Th) first titrated with CB[8] (0-  $12 \times 10^{-6}$  M) followed by OA (0-  $3.63 \times 10^{-4}$  M) at room temperature. Initial concentration of Th =  $1.5 \times 10^{-5}$  M. Wavelength is measured in nanometers.



**Figure 7.16** Fluorescence spectra of Thionin Acetate (Th) first titrated with CB[8] (0-  $12 \times 10^{-6}$  M) followed by OA (0-  $3.63 \times 10^{-4}$  M) at room temperature. Initial concentration of Th =  $1.5 \times 10^{-5}$  M. Wavelength is measured in nanometers.

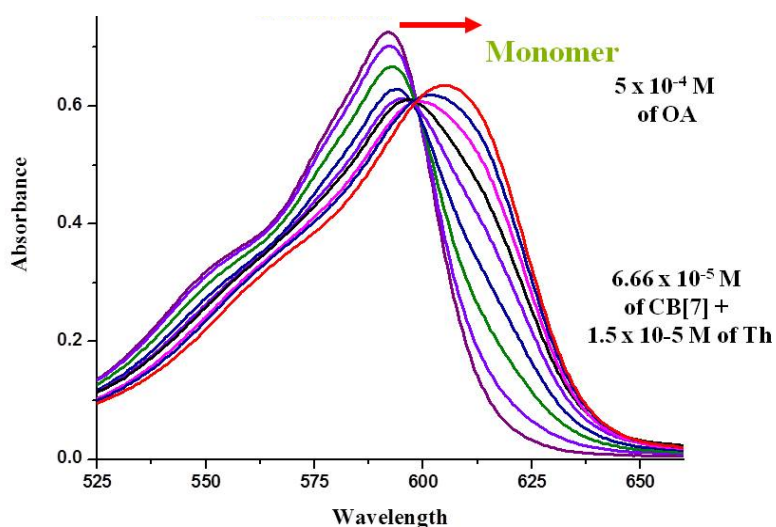
**Figure 7.17** tries to explain the phenomenon which could be likely taking place, when the two host molecules offering two different kind of interaction were mixed with a positively charged dye solution. This experiment clearly shows that though organic dye molecules prefer hydrophobic interactions for maximum stability, yet they cannot overcome the strong ion-pair interaction offered by the anionic exterior of the host OA.



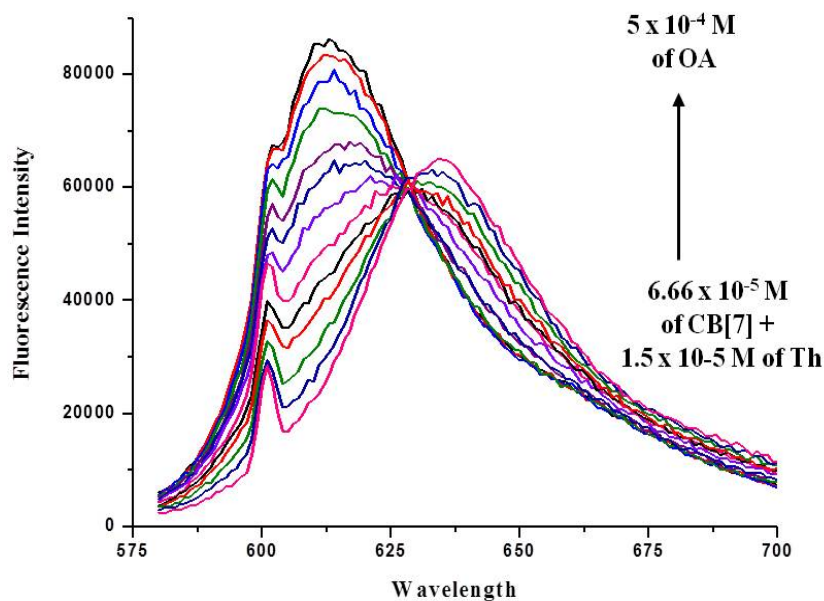
**Figure 7.17** Cartoon representations of the probable mechanism of the formation of the dimer in CB[8] followed by formation of monomer in presence of host OA.

In the next set of experiments, we compared the interaction of Thionin Acetate with the hosts CB[7] and OA. The main difference between this and the previous experiment is that, in the case of CB[8] vs. OA, the competition was between a hydrophobic dimer and the ion-pair monomer. But in the case of CB[7] vs. OA, the competition is between a hydrophobic monomer and the ion-pair monomer. In this experiment initially  $1.5 \times 10^{-5}$  M Thionin acetate was taken in an aq. solution, to this a concentrated aq. solution of CB[7] was added stepwise, the resultant absorption and emission spectra is shown in **Figures 7.12** and **7.13**. Both the spectra showed that on addition of CB[7], a new blue shifted monomer peak appeared indicating the existence of a dye monomer which was encapsulated inside a CB[7] host molecule. At  $6.66 \times 10^{-5}$  M of CB[7], no further change in the spectra were noticed, hence concentrated aq. solution

of OA was gradually added at this point. We noticed a gradual red shift in the monomer absorption and emission band of the dye, with a slight decrease in intensity, as the concentration of OA was increased (Figures 7.18 and 7.19). After reaching  $5 \times 10^{-4}$  M of OA, no further change in the spectra was observed.

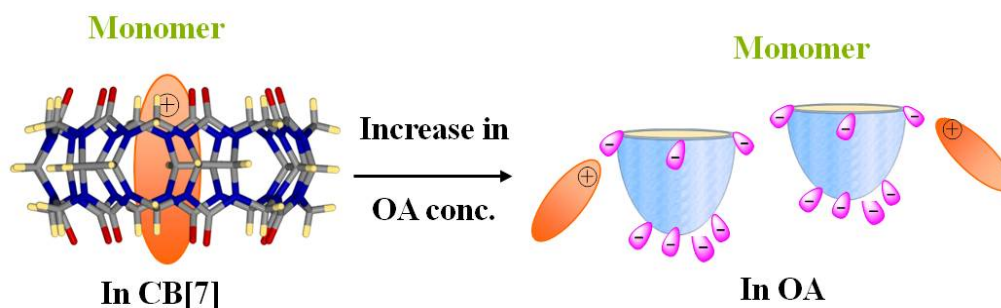


**Figure 7.18** UV-Visible spectra of Thionin Acetate (Th) first titrated with CB[7] ( $0-6.66 \times 10^{-5}$  M) followed by OA ( $0-5.0 \times 10^{-4}$  M) at room temperature. Initial concentration of Th =  $1.5 \times 10^{-5}$  M. Wavelength is measured in nanometers.



**Figure 7.19** Fluorescence spectra of Thionin Acetate (Th) first titrated with CB[7] ( $0-6.66 \times 10^{-5}$  M) followed by OA ( $0-5.0 \times 10^{-4}$  M) at room temperature. Initial concentration of Th =  $1.5 \times 10^{-5}$  M. Wavelength is measured in nanometers.

**Figure 7.20** illustrates the likely phenomenon taking place. In this experiment too it is observed that the cationic dye molecules prefer Columbic ion-pair interaction with anionic exterior of OA, over the hydrophobic interaction offered by the host CB[7].

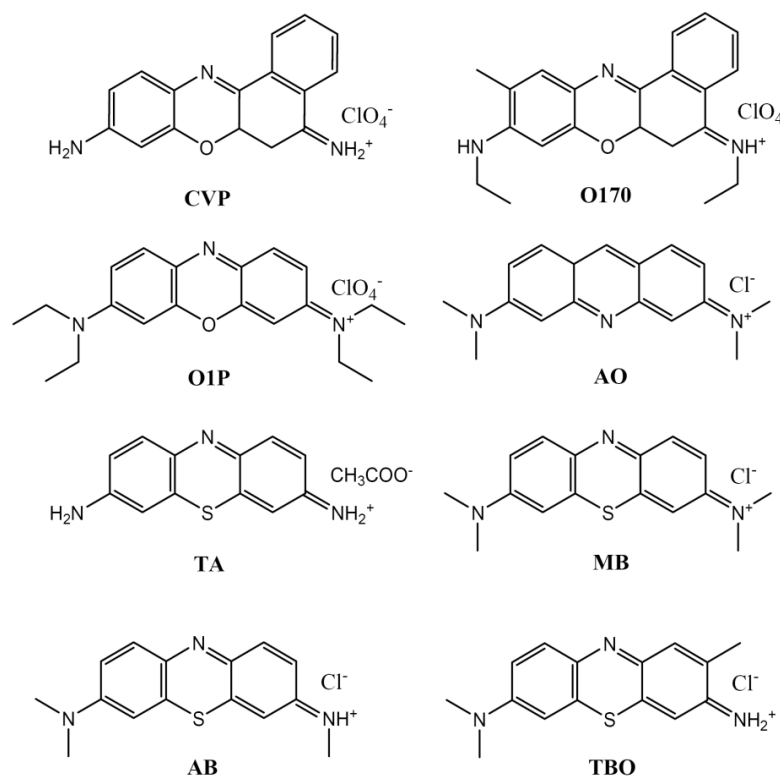


**Figure 7.20** Cartoon representations of the probable mechanism of the formation of the dimer in CB[8] followed by formation of monomer in presence of host OA.

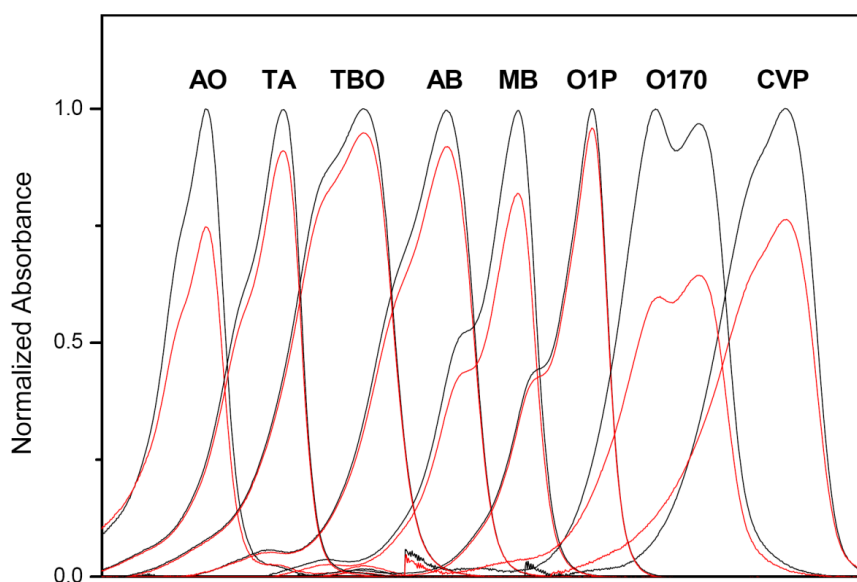
#### 7.2.4 Basic experiments done with various cationic dyes to support above observations and inferences

Prior to the above experiments, some basic experiments were performed in order to form a platform for the above studies, along with the experiments to generalize the above observations. These experiments have been done in collaboration with **Dr. Yao Pang Zhao**. To generalize the above observed concepts, the same set of experiments was carried out with other six cationic dyes listed in **Scheme 7.4**.

Because the OA was dissolved in a borate buffer solution, hence in order to differentiate the effect of borate buffer from that of OA, the normalized absorption spectra of these dyes in neutral aqueous solution and buffer solution were recorded respectively, as shown in **Figure 7.21**.



**Scheme 7.4** Chemical structures of cationic dyes used for the studies- Cresyl Violet Perchlorate (CVP), Oxazine 170 (O170), Oxazine 1 Perchlorate (O1P), Acridine Orange (AO), Thionin Acetate (TA), Methylene Blue (MB), Azure B (AB), and Toluidine Blue (TBO).



**Figure 7.21** The absorption spectra of dyes in neutral aqueous (black lines) and borate buffer (red lines) ( $\geq 6$  mM) solution at room temperature.

We have observed that, in comparison to the neutral solution, the absorption intensity of the dyes has decreased in the presence of borate buffer solution. This change could be attributed to the difference in pH and ionic strength of the neutral aqueous solution and the borate buffer solution (6 mM) (pH = 9 when 10 mM). Also, another major observation is that except the dye O170, all the other dyes exhibited a stronger monomer absorption band with a slight blue shifted shoulder which was attributed mainly to the H-aggregate dimer.

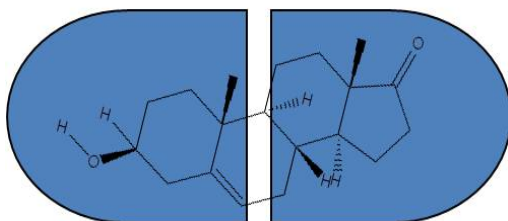
**Table 7.1** Red shift observed for the  $\lambda_{\max}$  of the cationic dyes in presence of host OA.

<b>Dyes</b>	<b>Absorption (<math>\lambda_{\max}/\text{nm}</math>)</b>		<b>Fluorescence</b>	
	<b>No OA</b>	<b>OA</b>	<b>No OA</b>	<b>OA</b>
<b>CVP</b>	588	604	630	640
<b>O170</b>	618	615	653	648
<b>O1P</b>	654	662	677	684
<b>AO</b>	491	498	531	531
<b>TA</b>	552	560	625	635
<b>TBO</b>	629	638	675	680
<b>AB</b>	652	660	682	692
<b>MB</b>	664	670	692	702

In another set of experiments, the absorption and emission spectra of all the above eight dyes were recorded in the absence and presence of the host OA. All the experiments were titration experiments in which the concentrated aq. solution of host OA was added gradually to the dilute aq. solution of the cationic dye. The shift in the  $\lambda_{\max}$  values is shown in **Table 7.1**. As can be observed from this table, in absorption and fluorescence spectra, the  $\lambda_{\max}$  of almost all the dyes have an obvious red-shift upon addition of OA as

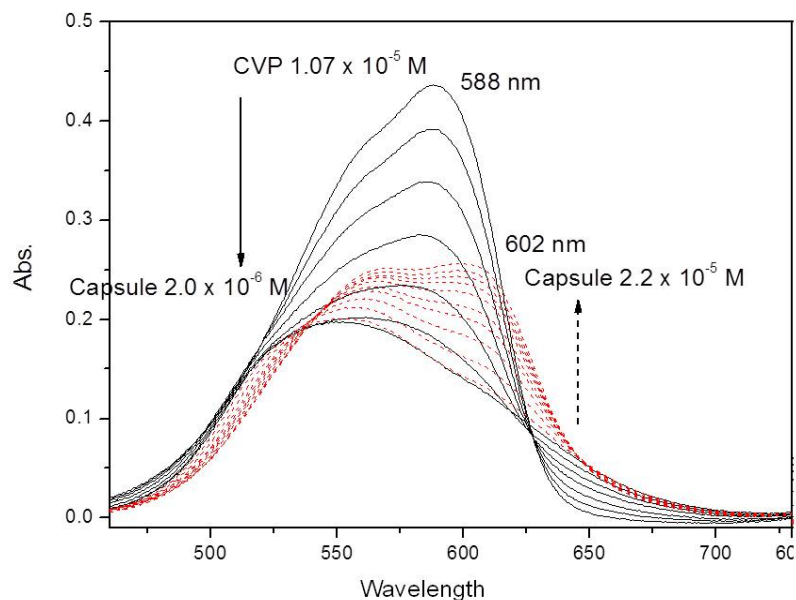
compared to with the spectra without OA. This phenomenon is attributed to the formation of ion-pair involving the dye's cations and OA carboxylate anions in aqueous solution.<sup>335</sup>

Apart from the eight carboxyl groups with negative charge, another important characteristic of OA is the hydrophobic wall of the cavity. It's reasonable to think a hydrophobic interaction between the cationic organic dyes and OA can also play an associative role to a certain extent. However, does this hydrophobic interaction takes place with the cationic dyes in question? It has been already reported that the OA molecule is very often used to form various capsular complexes with small hydrophobic guests.<sup>51</sup> In order to clarify this, the following experiment has been done. Compound **DHAS** can strongly complex with OA to form a very stable capsular complex with two molecules of OA<sup>46</sup>, as seen in **Scheme 7.5**. **Figure 7.22** shows the change in absorption spectra of cationic dye Cresyl Violet Perchlorate (CVP) when titrated with **DHAS@OA2** capsular complex. As can be observed in **Figure 7.22**, when the concentration of **DHAS@OA2** capsular complex is low, the absorption of CVP monomer was decreased; along with the further addition of **DHAS@OA2** capsular complex, the absorption of CVP monomer were recovered. This is exactly the observation in absence of any guest occupying the inner cavity of the host OA. This indicates that the inner cavity of OA plays a less important role in the interaction between the cationic dyes and OA.



**Scheme 7.5** Capsular complex of **DHAS@OA<sub>2</sub>**.





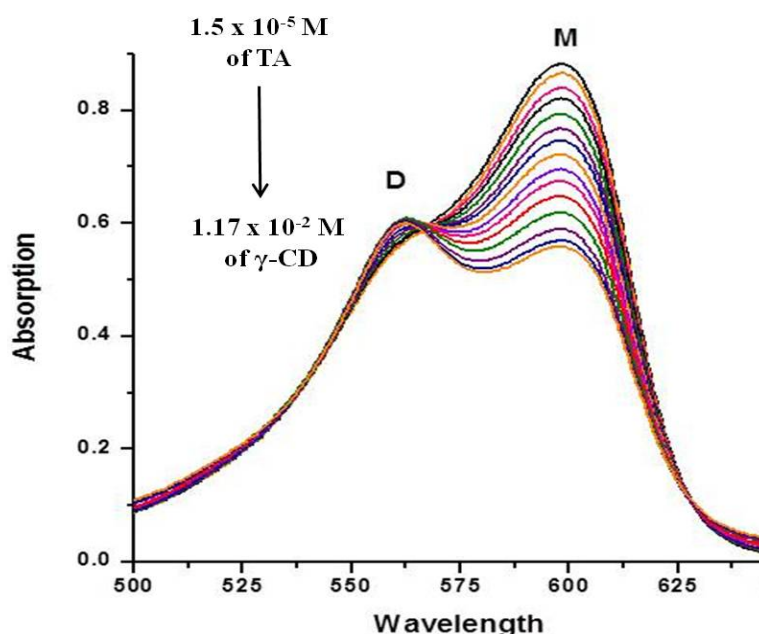
**Figure 7.22** Absorption spectra of CVP ( $1.07 \times 10^{-5}$  M) titrated with aq. solution of DHAS@OA<sub>2</sub> capsular ( $0-2.2 \times 10^{-5}$  M).

### 7.2.5 Comparative binding studies for the dyes Thionin Acetate and Cresyl Violet Perchlorate between the hosts-Cyclodextrin, Dendrimers, Calixarene vs. Octa Acid

In this section, we present the comparative binding studies between the cationic dyes and various host systems. We carried out these studies with two cationic dyes- Thionin Acetate and Cresyl violet Perchlorate. Here we have chosen Thionin Acetate as the representative cationic dye to be shown in this chapter. And we have already studied the interaction of these dyes with the hosts Octa Acid and Cucurbiturils CB[7] and CB[8] in detail, as mentioned in previous sections. In the comparative studies done with Thionin Acetate for OA vs. CB[7] and OA vs. CB[8], we have observed that the Columbic ion-pair effect offered by anionic exterior of OA plays a stronger role than the hydrophobic effect offered by the inner cavities of cucurbiturils in stabilizing the cationic dyes in an aq. solution. In this section we incorporated various other hosts for the comparative studies. These hosts include  $\gamma$ -Cyclodextrin ( $\gamma$ -CD), Third generation carboxylic acid

dendrimer ( $G_3A$ ) and Calixarene [6], as shown in **Scheme 7.3**. All these hosts are compared against a common host OA.

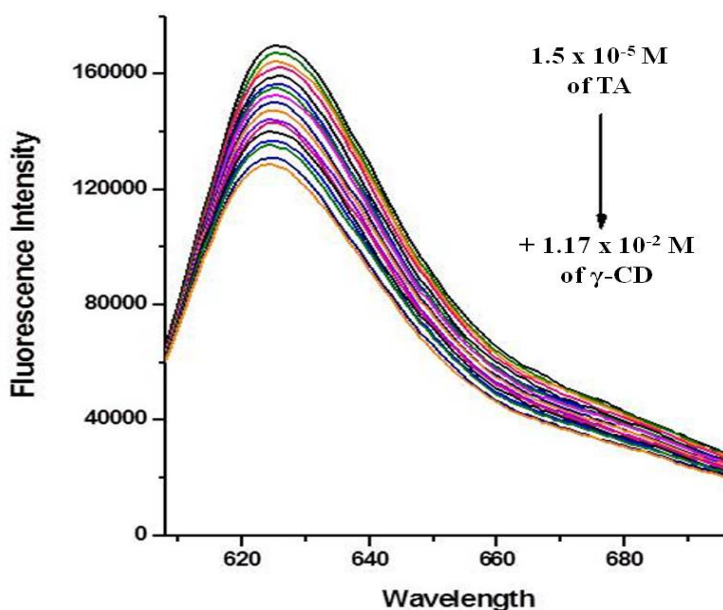
**7.2.5 (a)  $\gamma$ -CD vs. OA- Binding studies for Thionin Acetate:** In this set of experiments, initially  $1.5 \times 10^{-5}$  M aq. solution of Thionin Acetate was taken. To this an aq. solution of  $\gamma$ -CD was added stepwise.



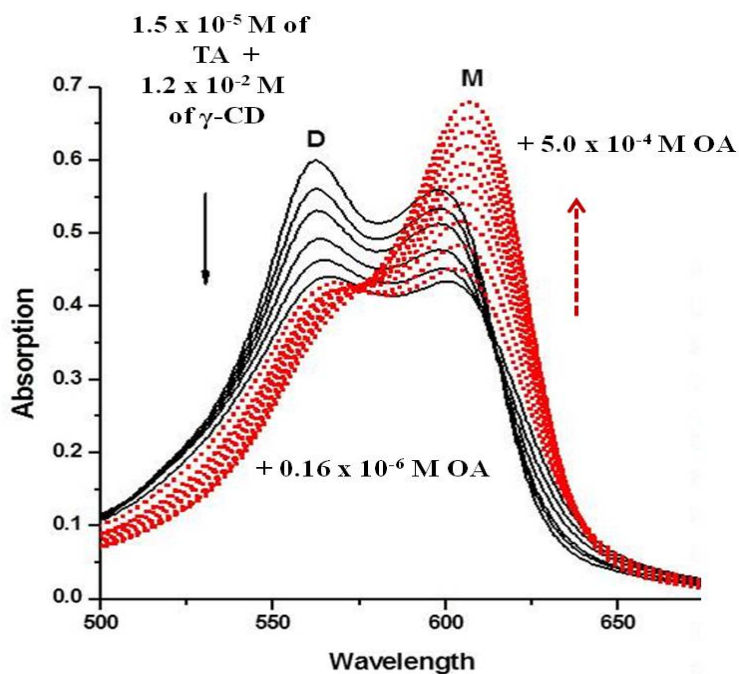
**Figure 7.23** UV-Visible spectra of Thionin Acetate (TA) titrated with  $\gamma$ -CD (0-  $1.17 \times 10^{-2}$  M) Initial concentration of TA =  $1.5 \times 10^{-5}$  M. Wavelength is measured in nanometers.

**Figure 7.23** shows the changes in the absorption spectra. It can be observed that as the concentration of  $\gamma$ -CD increased the monomer band absorption decreased with a simultaneous increase in dimer band intensity. At  $1.17 \times 10^{-2}$  M of  $\gamma$ -CD, no further change in the spectra was observed. The same trend was noticed in the emission spectra as shown in **Figure 7.24**. As the dimer is non-emissive, the fluorescence intensity of the monomer peak decreased with the increase in  $\gamma$ -CD concentration.  $\gamma$ -CD is known to encapsulate small organic molecules through hydrophobic interactions.<sup>338,339</sup> The above observations indicate that at an optimum concentration of  $\gamma$ -CD, preferentially two dye

molecules gets encapsulated inside the  $\gamma$ -CD host molecule and hence a stronger dimer peak is observed in the absorption spectra.

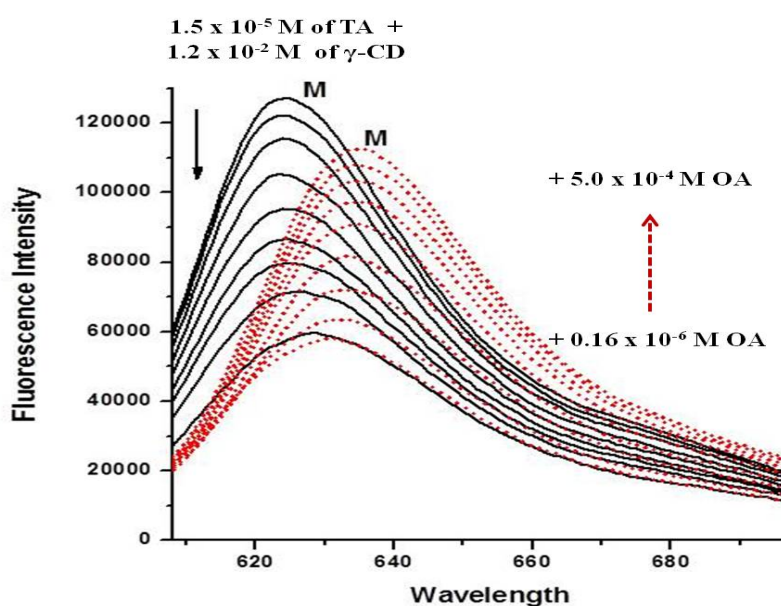


**Figure 7.24** Fluorescence spectra of Thionin Acetate (TA) titrated with  $\gamma$ -CD (0-  $1.17 \times 10^{-2}$  M) Initial concentration of TA =  $1.5 \times 10^{-5}$  M. Wavelength is measured in nanometers.



**Figure 7.25** UV-Visible spectra of Thionin Acetate (TA) first titrated with  $\gamma$ -CD (0-  $1.17 \times 10^{-2}$  M), followed by OA (0-  $1.6 \times 10^{-6}$  M solid black lines) ( $1.6 \times 10^{-6}$  M- $5.0 \times 10^{-4}$  M dotted red lines). Initial concentration of TA =  $1.5 \times 10^{-5}$  M. Wavelength is measured in nanometers.

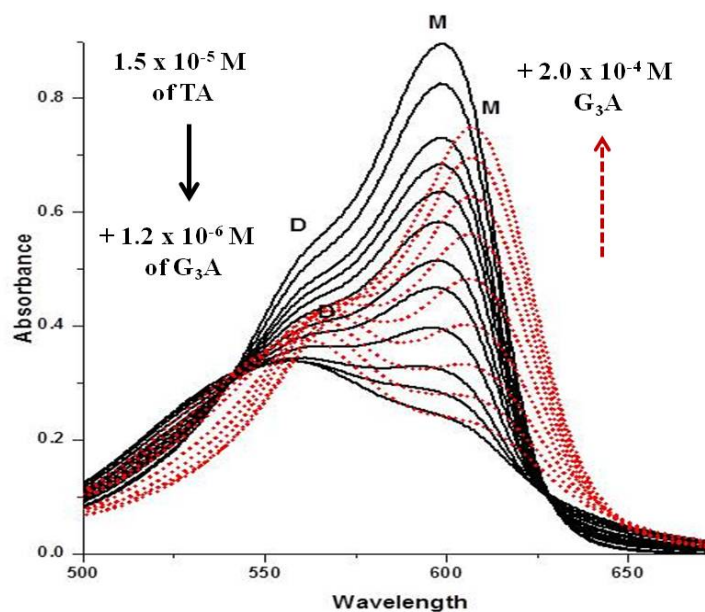
To the above solution, a concentrated aq. solution of OA is added. **Figures 7.25** and **7.26** show the resultant absorption and emission spectra. **Figure 7.25** shows that as the concentration of OA is increased first there is a simultaneous decrease in the peak intensity of both dimer and monomer. But at  $0.16 \times 10^{-6}$  M of OA, this change ceases. On further addition of OA, a red shifted monomer peak starts developing. At  $5.0 \times 10^{-4}$  M of OA, there is no further change in the spectra is observed.



**Figure 7.26** Fluorescence spectra of Thionin Acetate (TA) first titrated with  $\gamma$ -CD ( $0-1.17 \times 10^{-2}$  M), followed by OA ( $0-0.16 \times 10^{-6}$  M solid black lines) ( $0.16 \times 10^{-6}$  M - $5.0 \times 10^{-4}$  M dotted red lines). Initial concentration of TA =  $1.5 \times 10^{-5}$  M. Wavelength is measured in nanometers.

Similarly, in the emission spectra (**Figure 7.26**), first the intensity of the monomer peak decreases on addition of OA, then on further increase in OA concentration a red shifted monomer peak evolves. Similar to the case of CBs, these observations too indicate that the cationic dye prefers the Columbic ion-pair interaction offered by anionic exterior of OA more than the hydrophobic interior offered by the  $\gamma$ -CD cavity. A red shifted monomer band is a clear indication of the ion-pair monomer of the dye.

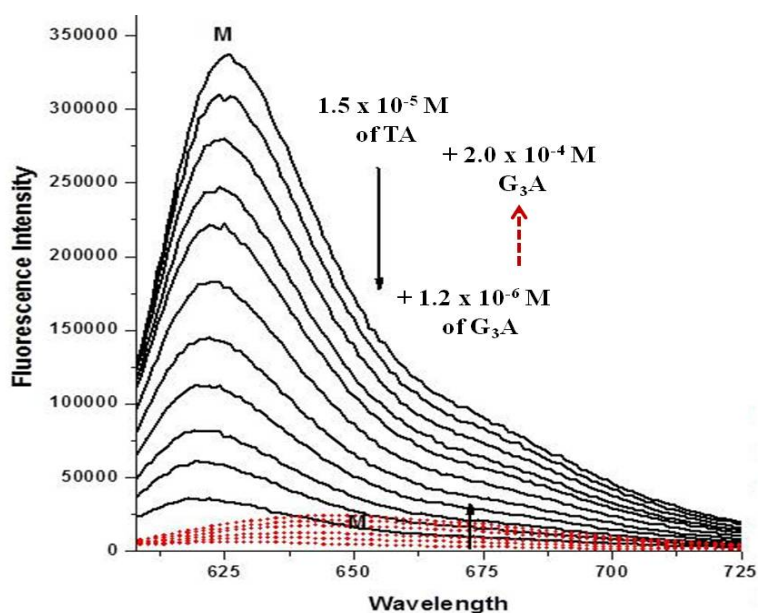
**7.2.5 (b) G<sub>3</sub>A vs. OA- Binding studies for Thionin Acetate:** The second host system we investigated consisted of Third generation dendrimer with twenty four carboxylic acid groups at its periphery.  $1.5 \times 10^{-5}$  M aq. solution of Thionin Acetate was taken. To this, the concentrated aq. solution was added gradually stepwise. In the absorption spectra (**Figure 7.27**), first the absorption of the monomer band decreased and a blue shifted broad dimer peak appeared.



**Figure 7.27** UV-Visible spectra of Thionin Acetate (TA) titrated with G<sub>3</sub>A (0-  $1.2 \times 10^{-6}$  M, solid black lines) and ( $1.2 \times 10^{-6}$  M –  $2.0 \times 10^{-4}$  M, red dotted lines) Initial concentration of TA =  $1.5 \times 10^{-5}$  M. Wavelength is measured in nanometers.

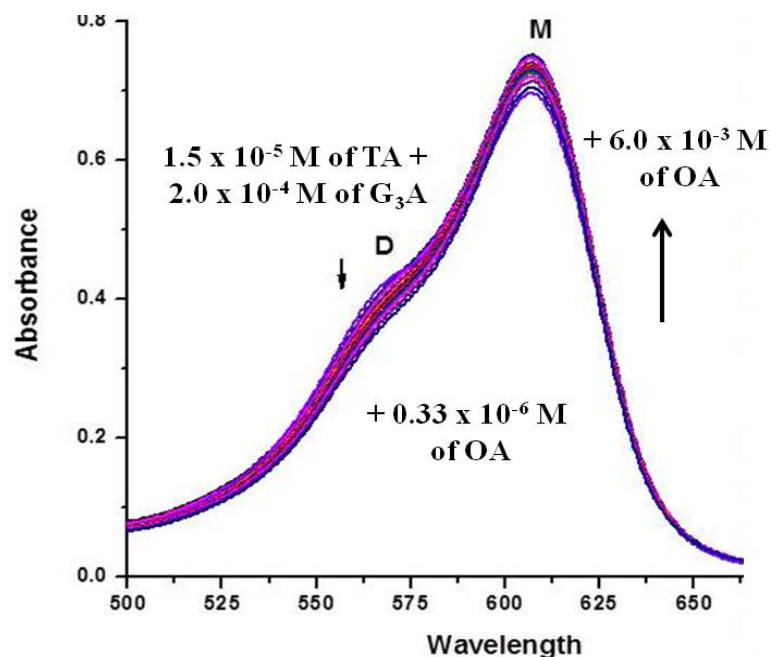
A broad dimer peak indicated that at this particular concentration ( $1.2 \times 10^{-6}$  M) of the dendrimer, the dye molecules are all clustered around the periphery of the dendrimer. As the concentration of the dendrimer was increased, the change in the absorption spectra reversed. The broad dimer peak started giving way to a red shifted monomer peak. And at  $2.0 \times 10^{-4}$  M of dendrimer a red shifted stronger monomer peak appears with a weak dimer shoulder.

This observation is quite similar to the case of OA, in which first the dye molecule form aggregates in presence of OA, but as the OA concentration increases, these aggregates break up and form dye monomers. The same happens in the case of dendrimers, at lower concentration of dendrimers, first the dye aggregates are formed and later on increasing the concentration of the dendrimers these aggregates disperse to form individual monomers around the now abundant dendrimer periphery.



**Figure 7.28** Fluorescence spectra of Thionin Acetate (TA) titrated with  $G_3A$  ( $0$ -  $1.2 \times 10^{-6}$  M, solid black lines) and ( $1.2 \times 10^{-6}$  M –  $2.0 \times 10^{-4}$  M, red dotted lines) Initial concentration of TA =  $1.5 \times 10^{-5}$  M. Wavelength is measured in nanometers.

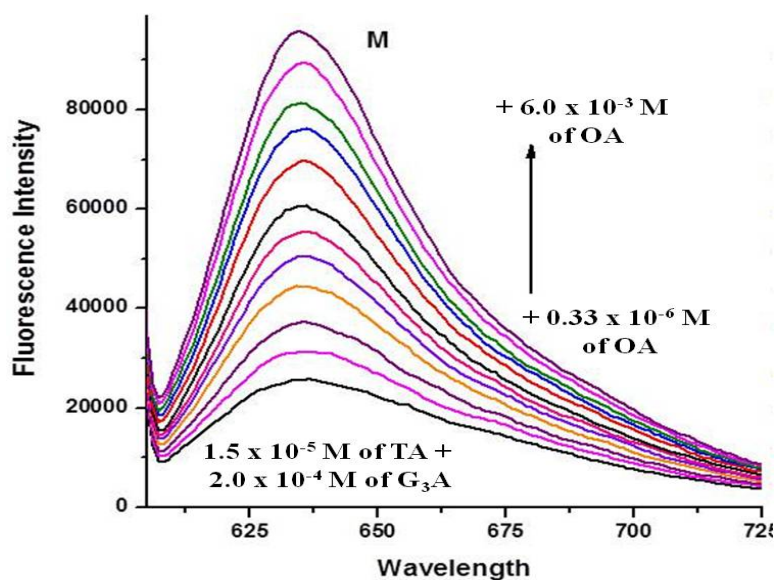
One more fact to notice here is that, though the monomer absorption band revived, but it is still not that intense as the original monomer absorption band. In the emission spectra (**Figure 7.28**), we encountered the same observations. First on subsequent addition of dendrimer, the monomer emission band gradually diminished and then on further addition of dendrimer it re-appeared but the resultant intensity was not too much.



**Figure 7.29** UV-Visible spectra of Thionin Acetate (TA) first titrated with G<sub>3</sub>A (0-  $2.4 \times 10^{-4}$  M), followed by OA (0-  $6.0 \times 10^{-3}$  M). Initial concentration of TA =  $1.5 \times 10^{-5}$  M. Wavelength is measured in nanometers.

To the above solution, OA was added gradually. **Figures 7.29** and **7.30** give the corresponding absorption and emission spectra respectively. In the absorption spectra it can be observed that the change was not too much even after adding  $6.0 \times 10^{-3}$  M of OA. But in emission spectra we observed that the red shifted monomer band intensity increased on increasing the OA concentration. These observations can be explained by considering the structures of the two hosts- third generation carboxylic acid dendrimer and OA. Both of them contain carboxylate groups on their external periphery, though the dendrimer contains three times as much carboxylate group as OA. Hence, the initial behavior of the dye in presence of dendrimer is quite similar to, as in the presence of OA. And also, when OA is added to the solution containing both the dye and the dendrimer, not much change is observed, since both the hosts are similar in nature and moreover the

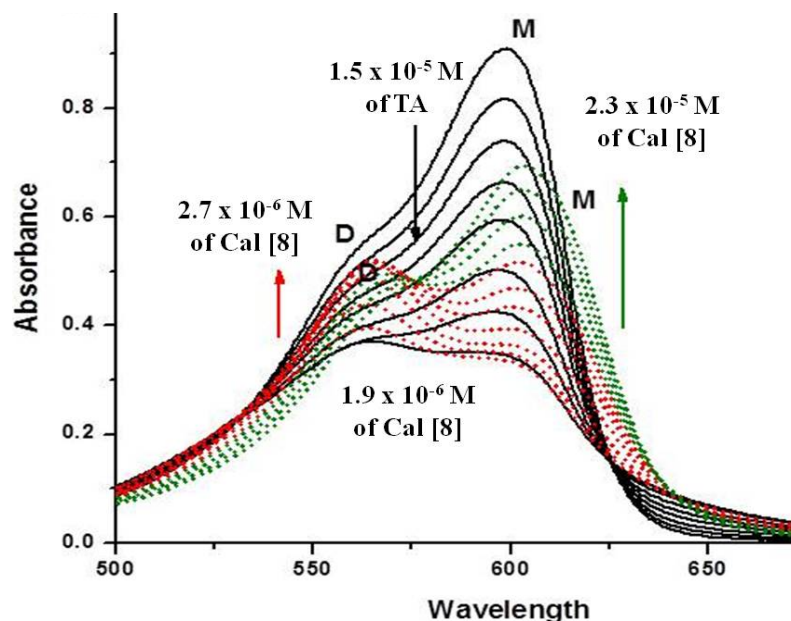
binding mode of the two hosts to the cationic dye is similar, which is Columbic ion-pair interaction.



**Figure 7.30** Fluorescence spectra of Thionin Acetate (TA) first titrated with G<sub>3</sub>A (0-  $2.0 \times 10^{-4}$  M), followed by OA (0-  $6.0 \times 10^{-3}$  M). Initial concentration of TA =  $1.5 \times 10^{-5}$  M. Wavelength is measured in nanometers.

**7.2.5 (c) Cal [8] vs. OA- Binding studies for Thionin Acetate:** The third host in this series is Calixarene [8]. The first two hosts were different in the sense that Cyclodextrins are known mostly to interact with smaller organic molecules through hydrophobic interactions. Dendrimers on the other hand have dual nature; they are capable of encapsulating neutral small organic molecules and their negatively charged periphery can interact with other positively charged molecules through Columbic ion-pair attraction. Calixarenes, combine the properties of above two hosts. It can offer hydrophobic environment to its organic guests by encapsulating them inside its cavity, whereas it can also stabilize them by its negatively charged rim.<sup>340-342</sup> In this set of experiments, we started with  $1.5 \times 10^{-5}$  M of aq. solution of Thionin Acetate. To this a concentrated aq. solution of Cal [8] was added stepwise.

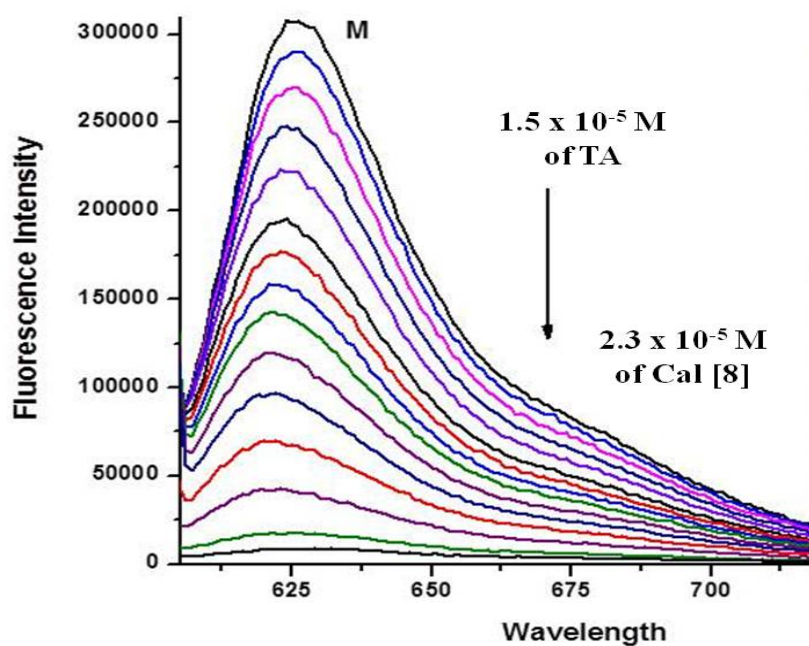




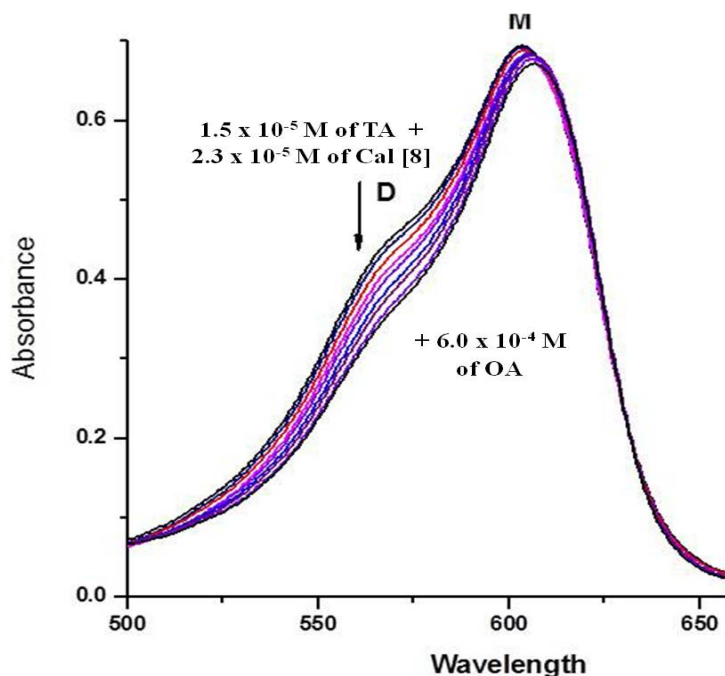
**Figure 7.31** UV-Visible spectra of Thionin Acetate (TA) titrated with Cal [8] ( $0-1.9 \times 10^{-6}$  M, solid black lines); ( $1.9 \times 10^{-6}$  M –  $2.7 \times 10^{-6}$  M, red dotted lines) and ( $2.7 \times 10^{-6}$  M –  $2.3 \times 10^{-5}$  M, dotted green lines). Initial concentration of TA =  $1.5 \times 10^{-5}$  M. Wavelength is measured in nanometers.

In the absorption spectra we observed that initially the dye monomer absorption decreased. At  $1.9 \times 10^{-6}$  M of Cal [8], we observed a broad dimer peak along with a weaker monomer absorption peak. As the concentration of Cal [8] was increased, the absorption both the dimer as well as monomer band increased simultaneously. On further increasing the Cal [8] concentration (green dotted lines in the **Figure 7.31**), we observed that the dimer peak gradually diminished and a stronger red shifted monomer peak appeared. Though in the corresponding emission spectra (**Figure 7.32**) the only change we could monitor was lowering of the intensity of the original dye monomer peak, on increasing the concentration of Cal [8]. We added concentrated aq. OA solution to the above Thionin Acetate and Cal [8] mixture in steps. The resultant absorption and emission spectra are shown in **Figures 7.33** and **7.34** respectively. As we had observed in the case of OA vs. dendrimer, here too we observed a minute change in the absorption

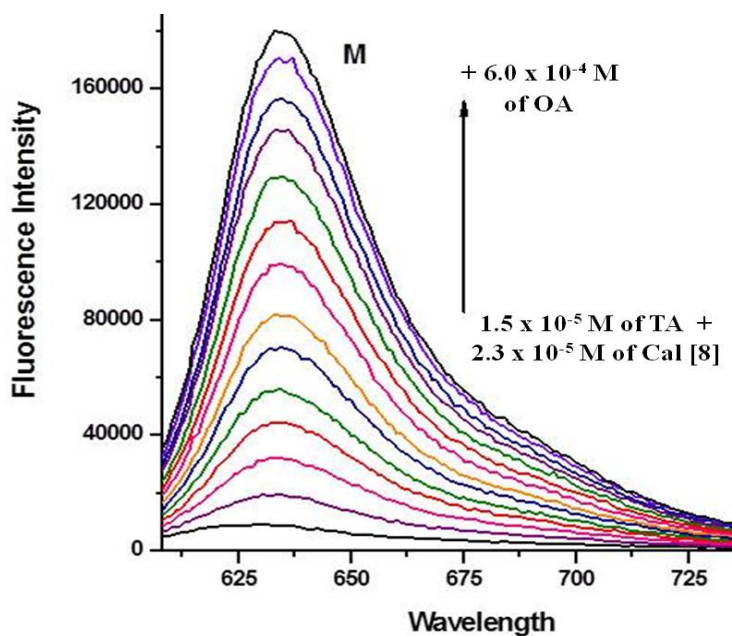
spectra, with an increase in the intensity of the monomer peak in the emission spectra. This observation indicates that the just like OA Calixarene [8] too have eight negatively charged groups on its rim which could interact with the cationic dye molecules through Columbic io-pair interactions. But it is apparent from both the cases- OA vs. dendrimer and OA vs. Cal [8], that OA has some additional interaction which eventually helps the dye to remain in its monomer form.



**Figure 7.32** Fluorescence spectra of Thionin Acetate (TA) titrated with Cal [8] (0-  $2.3 \times 10^{-5}$  M). Initial concentration of TA =  $1.5 \times 10^{-5}$  M. Wavelength is measured in nanometers.



**Figure 7.33** UV-Visible spectra of Thionin Acetate (TA) first titrated with Cal [8] (0-  $2.3 \times 10^{-5}$  M), followed by OA (0-  $6.0 \times 10^{-4}$  M). Initial concentration of TA =  $1.5 \times 10^{-5}$  M. Wavelength is measured in nanometers.



**Figure 7.34** Fluorescence spectra of Thionin Acetate (TA) first titrated with Cal [8] (0-  $2.3 \times 10^{-5}$  M), followed by OA (0-  $6.0 \times 10^{-4}$  M). Initial concentration of TA =  $1.5 \times 10^{-5}$  M. Wavelength is measured in nanometers.

### 7.3 Conclusion

A central goal in supramolecular chemistry has been the development of host–guest systems with binding affinities as high as those reached in biological systems, which often permit selective binding at concentrations in the nanomolar or picomolar regimes. In this project we have qualitatively investigated various hosts for their binding affinities towards positively charged dyes. A simple and straightforward contribution of these studies is to achieve the goal of enhancing dye solubilization, de-aggregation, fluorescence enhancement, increase in brightness, prolongation of fluorescence lifetimes, and photo-stabilization of the dyes.

In this chapter we have investigated the effect of various hosts on the aggregation properties of the positively charged dyes. We had carried out our experiments with eight dyes in total to generalize the observations made, but have chosen Thionin Acetate, as the representative dye. The primary observation we made was that the dyes at an optimum concentration were present as a monomer along with a slight amount of the dimer. These dimers were conferred to be H- aggregates, since the absorption band responsible for them was weak and blue shifted relative to the monomer band.

The positively charged dyes preferred to exist as monomers within CB[7] whereas dimers in CB[8]. The most probable reason behind this distinction was the difference in the portal size of the two hosts. CB[8] possess a bigger inner cavity than CB[7]. Also, blue shift in the absorption band of the monomer and the dimer indicated that the dye molecules were present in a relatively hydrophobic environment. So we can conclude that CBs bind with the positively charged dye molecules by offering them a hydrophobic environment.

Cavitand Octa Acid, which has till date been much exploited for its versatile inner cavity, was shown to have a useful exterior as well in this project. The exterior part of OA has eight carboxylic acid groups which turn to the corresponding carboxylate groups in the borate buffer solution. These carboxylate groups were found to strongly attract the positively charged dyes. This observation proved to be very useful in designing further projects using OA. This newly explored capability of OA was used to hold an acceptor cationic dye close to the cavitand for studying ultrafast FRET from the donor encapsulated inside the cavity.<sup>66</sup> Also, the same property of OA to be able to attach cationic molecules to its anionic exterior has been used for many studies.<sup>343, 344, 65</sup>

As a step further, we compared the binding affinity of OA to the cationic dyes, in the presence of other organic hosts. Like CBs,  $\gamma$ -Cyclodextrin too offered hydrophobic environment to the cationic dyes and they mostly existed as dimers inside a  $\gamma$ -CD. OA, in comparison helped these dimers to come out and interact with its anionic exterior in the form of monomers, through Columbic ion-pair interaction. Dendrimers, on the other hand offered the same situation to the cationic dye molecules as OA, since they too possessed twenty four carboxylate groups on their periphery. Cyclodextrins acted as versatile hosts since, they offered both hydrophobic as well as Columbic ion-pair interactions to their dye guest molecules. In this case too it was found that the cationic dyes preferred to associate more with the negatively charged rim of Calixarene rather than being encapsulated inside them through hydrophobic interactions. But both in the case of dendrimers as well as Calixarene, when compared with OA, it was observed that the dye molecules still preferred to associate with OA in their monomeric form through Columbic

ion-pair interaction. Though the reason for this preference is unclear, but it may be attributed to the unique shape of the cavitand.

## 7.4 Experimental Section

The dyes were used as received from Kodak (Cresyl Violet perchlorate, Oxazine 170 perchlorate, Oxazine 1 perchlorate), Fluka (Acridine Orange chlorate), Aldrich (Thionine acetate), Fisher (Methylene Blue, Azure B, Toluidine Blue O). The optimized synthetic procedure has been used to prepared CBs and OA.<sup>345, 46</sup>

Absorption and emission spectra were recorded in a standard ~3 mL quartz cell. Absorption spectra were recorded using a UV-Vis spectrophotometer. Fluorescence emission spectra were recorded on an Edinburgh FS920CDT steady-state fluorimeter. A stock solution of known concentration was made for the dyes. The dyes were weighed on a wax paper, and quickly transferred to a 25 mL volumetric flask, and Millipore water was added to make up to the full volume. The volumetric flask was covered with aluminum foil to avoid the interaction of dyes with the light and the solution was generally stored in a dark place. These stock solutions of dyes were diluted with Millipore water to reach the desired concentration for the experiments.

A stock solution of the hosts was prepared in a glass vial. The usual concentration of the stock was maintained at 10 mM. CBs were dissolved in only Millipore water. Notably, CB[8] is sparingly soluble in water, so prior to its use, it was always sonicated and heated for at least 1 hour to form a uniform suspension. It was observed that, it completely dissolved in presence of the dyes in the cuvette. 10 mM of OA was dissolved using 100 mM sodium borate buffer solution, in Millipore water.

Cyclodextrin was dissolved in simple Millipore water. And Calixarene was also dissolved using sodium borate buffer.

The titration experiments were usually conducted in one go not being dragged to another day and the time between the addition of host at every step was strictly maintained for the consistency of the experiment. The stock solution of the host was added using a microlitre syringe and the cuvette was closed using a vinyl white cap and the solution was shaken gently few times before recording the spectra. Care was taken not to spill any solution during shaking and addition of the host. Also, the micro liter syringe was handled carefully, to avoid the contamination of the needle by the solution in the cuvette.

All the experiments were repeated at least twice for consistency. The absorption spectra were recorded usually from 300-800 nm. And the emission spectra were recorded based on the calculation done for the limits based upon the excitation wavelength. The excitation wavelength for each dye was different. As a rule of thumb, the wavelength where the absorbance was recorded as 0.2 was taken as the excitation wavelength.

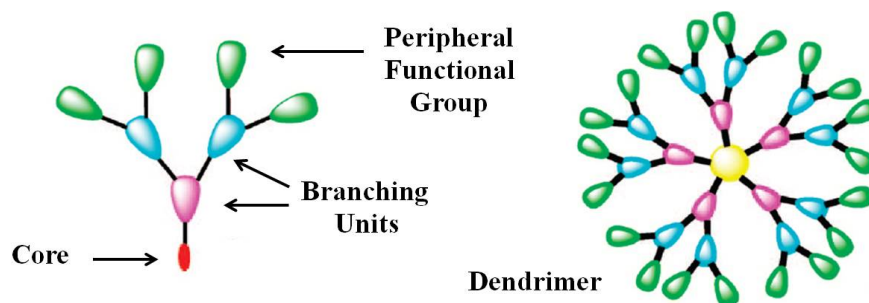
## **CHAPTER 8**

### **Characterization and Use of Dendrimers as Micro- and Nano- Molecular Reactors**



## 8.1 Overview

Dendrimers represent a novel type of polymeric material that has generated much interest in diverse areas due to their unique structure and properties. To increase our fundamental understanding of highly branched architecture, as well as its promising potential for material and life science applications, motivates intensive research efforts in the expanding field of “dendrimer” chemistry.<sup>346,347</sup> “Dendrimers” are highly branched macromolecules with precisely controlled size, shape and end-group functionality.<sup>348,349</sup> The term “dendrimer”, first proposed by Tomalia in 1985, comes from the Greek word ‘dendron,’ meaning tree, and was chosen due to their structural shape. Dendrimers are different from traditional polymers in that they have a multi-branched, three dimensional architecture, with very low poly-dispersity and high functionality. A typical dendrimer is comprised of three different topological parts: (a) a focal core, (b) building blocks with several interior layers composed of repeating units, and (c) multiple peripheral functional groups (**Scheme 8.1**). The first part, the focal core, can encapsulate various chemical species that exhibit unparalleled properties due to the special nano environment surrounded by extensive dendritic branching. Next, the several interior layers composed of repeating units can provide a flexible space created within the voids of dendritic building blocks, which can possibly encapsulate various small guest molecules. Finally, the third part of a dendrimer is the multivalent surface, which can accommodate a large number of functionalities that can interact with the external environment, thereby defining the dendrimer’s macroscopic properties.<sup>350</sup> Dendrimers can be synthesized starting from the central core and working out toward the periphery (divergent synthesis) or in a top-down approach starting from the outermost residues (convergent synthesis).



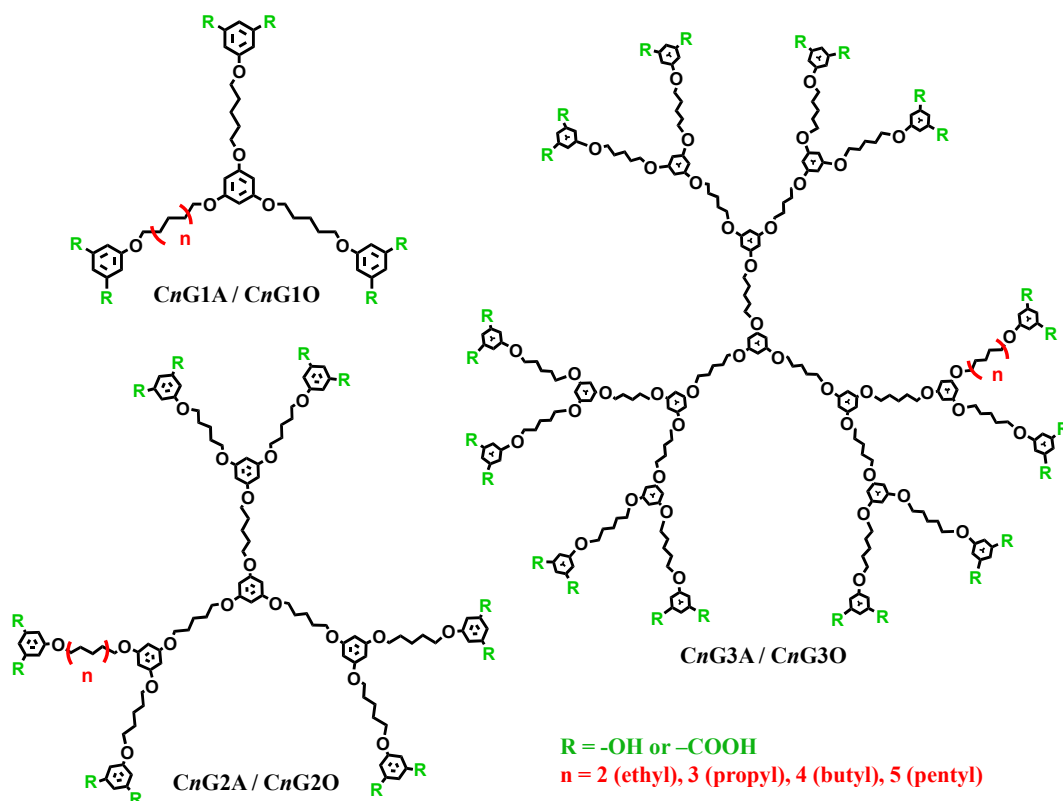
**Scheme 8.1** Cartoon representation of the topological parts of a dendrimer.

The well-defined structure renders dendritic macromolecules unique properties for versatile applications, especially in the biomedical field. For example, phosphorus-containing dendrimers have shown anti-prion activity and can potentially be used as mediators for gene therapy<sup>351</sup>; Boronated starburst PAMAM (i.e. polyamidoamine) dendrimer-monoclonal antibody immune conjugates have been used as potentially efficient anti-cancer reagents involving boron capture of neutron. Commercially available dendrimers such as PAMAM and PPI (polypropyleneimine) dendrimer have also been employed as magnetic resonance imaging contrast agents potentially to improve the quality of the clinical diagnostics.<sup>352</sup> They can be synthetically designed to mimic various biological functions of metalloproteins and enzymes such as supramolecular self-assembly; molecular recognition and complexation, etc.<sup>353</sup> Based on their dimensional length scaling, narrow size distribution, and other biomimetic properties, dendrimers are often referred to as artificial proteins.<sup>354-358</sup>

Dendrimers have been extensively used as micro and nano-reactors. The initial example of dendrimers as microreactor for photoreactions was reported by Fréchet's group.<sup>359</sup> They designed and synthesized a series of amphiphilic dendrimers with a benzophenonyl core as oxygen sensitizer, apolar interior and polar exterior, and

applied them to the photoinduced oxidation of cyclopentadiene in O<sub>2</sub>-saturated methanol. The experiment results manifest the higher generation dendrimers lead to faster reaction and higher conversion rate. The same dendrimers were also used for the photosensitized oxygenation of sulfides by Shiraishi's group, giving a similar conclusion.<sup>360</sup> Recently, carboxylic acid terminated poly (aryl ether) dendrimers have been used as microreactors to conduct photo-oxidation of olefins in aqueous media. The experiments demonstrated that the photo-oxidation pathways can be successfully controlled by encapsulating the substrate and sensitizer molecules in same or different sets of dendrimers.<sup>361</sup> Our research group<sup>362,363</sup> synthesized several poly (alkyl aryl ether) dendrimers with hydroxyl or carboxyl groups at the peripheries and applied them as microreactors to conduct photoreactions. It has been demonstrated that these dendrimers can act as "unimolecular micelles" and offer much better constraint than traditional micelles, although their hydrophobic pockets are not totally "leak-proof" for encapsulated guests.

In this chapter we have outlined our efforts to characterize poly (alkyl aryl ether) dendrimers with hydroxyl and carboxyl groups (**Scheme 8.2**) at the peripheries by different techniques like UV-visible, fluorescence, EPR spectroscopies and solvation dynamics; and use them as micro and nano-reactors for carrying out different photoreactions. **Scheme 8.2** shows the chemical structure of the two classes of dendrimers we have extensively used for our work.



**Scheme 8.2** Chemical structures of poly (aryl alkyl ether) dendrimers with phenolic (*CnGO*) and carboxylic acid (*CnGA*) peripheral group.

The poly (alkyl aryl ether) dendrimers with carboxylic acid end group have been synthesized in our lab by the given procedure<sup>364</sup> and the poly (alkyl aryl ether) dendrimers ending with phenolic group have been generously provided by Dr. Jayaraman, I.I.Sc. Bangalore and have been meticulously prepared by Dr. Bhaskar Natarajan. In these dendrimers, the phloroglucinol moiety acts as the core as well as the branch junctures and these branch junctures are linked with the aid of ethyl-pentamethylene linkers (spacers) in the case of phenolic end group dendrimers and only pentamethylene linker in the case of acidic end group dendrimers. The peripheral groups are phenol or carboxylic acid accordingly. In an effort to modify the peripheries of these

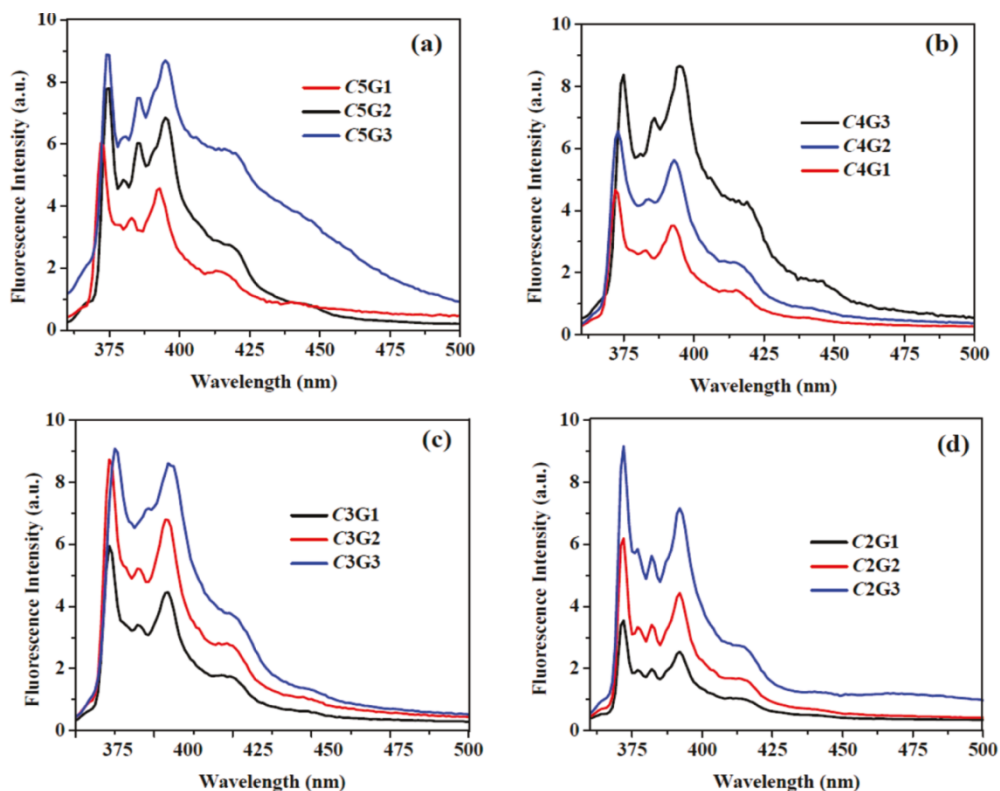
phloroglucinol-based dendrimers with functional groups that would allow water solubility, carboxylic acid terminated dendrimers were synthesized.

## 8.2 Results and Discussion

### 8.2.1 Probing the microenvironment of phenolic end group dendrimers ( $C_nGO$ ) with fluorescence probes

**(a) Assessing Dynamic Inner Cavity with Pyrene as Probe:** As, illustrated in **Scheme 8.1**, the core of the dendrimers is the focal point of the symmetrical structure. The branch points and the linkers together make nano or micro size spaces which are referred to as dendritic dynamic inner cavities. These dynamic inner cavities are capable of encapsulating small molecules. Microenvironments resulting from dynamic inner cavities of dendrimers were assessed with pyrene and coumarins as probes. In order to assess polarities of microenvironments generated at the dendritic interior cavities, fluorescence spectra of pyrene in aqueous basic solutions of dendrimer were recorded (**Figure 8.1**). The ratio of vibrational band intensities  $I_3/I_1$  of pyrene fluorescence is known to depend on the microenvironment polarity.<sup>365,366</sup> Pyrene solubilized aqueous basic dendrimer solutions (200  $\mu$ M) were prepared, and the  $I_3/I_1$  values arising from pyrene fluorescence were measured (**Table 8.1**). A higher  $I_3/I_1$  value indicates a hydrophobic environment and vice versa. It was found that across the dendrimer generations (G1O-G3O) with uniform spacer lengths,  $I_3/I_1$  increased with increasing generations. On the other hand, within a dendrimer generation with various spacer units  $C_2$ - $C_5$ ,  $I_3/I_1$  was found to increase progressively from ethyl to n-pentyl spacer. The third generation  $C_5$ ,  $C_4$ , and  $C_3$  spaced dendrimers exhibited higher hydrophobic interior ( $I_3/I_1 = 0.84, 0.75, 0.79$ , respectively), whereas third generation  $C_2$  spaced dendrimers showed lower microenvironment polarity ( $I_3/I_1 = 0.61$ ). Among second generation dendrimers,  $I_3/I_1$  for  $C_5$  spaced

dendrimers was 0.78, which was  $\sim 1.2$ -  $1.5$  times higher than propyl ( $C_3$ ) and ethyl ( $C_2$ ) spaced dendrimers. In the case of first generation dendrimers, there was no increment in the  $I_3/I_1$  values, which reflected the absence of a hydrophobic interior arising from this series of dendrimers, except for the  $C_5G1O$  dendrimer ( $I_3/I_1 = 0.67$ ).



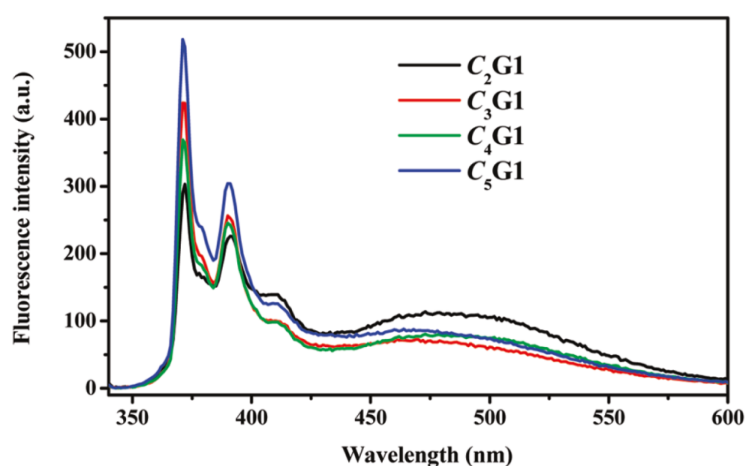
**Figure 8.1** Emission spectra of pyrene in the presence of dendrimers. [pyrene] = 0.01 mM and [dendrimer] = 0.2 mM in aq. NaOH (0.1 M), excitation wavelength = 335 nm.

A broad excimer emission of pyrene was detected for the first generation dendrimers (**Figure 8.2**), which weakened further for the second generation dendrimers. Third generation dendrimers did not exhibit detectable excimer emission. Excimer emission results from the association of an excited state pyrene molecule with ground state molecule. This also could result from ground state aggregation of pyrene molecules. Aggregation is more likely in a hydrophilic environment and the appearance of an excimer in G1O but not in G3O dendrimer is in agreement with the micropolarity

reported by pyrene molecules. The higher the polarity (G1O dendrimer; lower  $I_3/I_1$ ), the higher are the chances of aggregation and excimer emission is more probable.

**Table 8.1** Relative  $I_3/I_1$  Fluorescence Band Intensity of Pyrene in Aqueous Basic Solutions of Dendrimers.

Aqueous solution of dendrimer (200 $\mu$ M)		$I_3/I_1$
G1O	$C_2$	0.52
	$C_3$	0.56
	$C_4$	0.56
	$C_5$	0.67
G2O	$C_2$	0.53
	$C_3$	0.63
	$C_4$	0.64
	$C_5$	0.78
G3O	$C_2$	0.61
	$C_3$	0.79
	$C_4$	0.75
	$C_5$	0.84

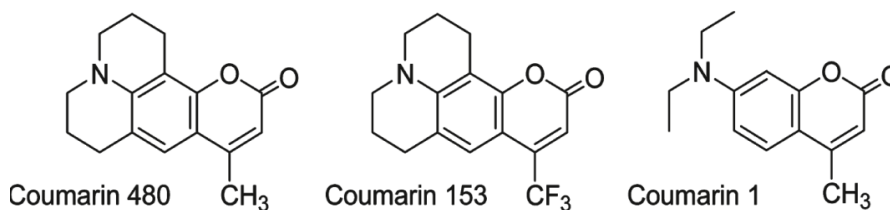


**Figure 8.2** Emission spectra of pyrene in the presence of first generation dendrimers  $C_2G1O$ - $C_5G1O$  in aq alkaline medium (0.2mM),  $\lambda_{ex}=335$  nm.

The local concentration of pyrene is likely to be more in G1O than in the G3O dendrimer, which could also be the cause for excimer emission in the G1O dendrimer.

Further, C<sub>5</sub>G2O showed higher microenvironmental polarity than C<sub>2</sub>G3O and to an extent C<sub>3</sub>G3O, thereby indicating that the role of the alkyl chain constituting the interfacial region is as important as a higher generation of the dendrimer.

**(b) Assessing Dynamic Inner Cavity with Coumarins as Probes:** The next set of probes which we utilized to study the microenvironments of the dendrimers belongs to coumarin dyes, comprising Coumarin 480 (C480), Coumarin 1 (C1), Coumarin 153 (C153) (**Figure 8.3**). Coumarins belong to a family of laser dyes whose fluorescence quantum yield and lifetime increase with the decrease in solvent polarity.<sup>367</sup> These probes are used extensively in various supramolecular assemblies.<sup>51, 307</sup>



**Figure 8.3** Molecular structures of coumarins used as fluorescent probes.

Fluorescence spectra of C1, C480 (20  $\mu$ M), and C153 (40  $\mu$ M) in water and in aqueous basic solutions containing dendrimers (300-800  $\mu$ M) (pH  $\sim$ 10) were recorded. In a titration experiment, aqueous basic dendrimer solution was added to aqueous coumarin solutions, until no further spectral change was observed. **Tables 8.2, 8.3, 8.4** show the emission  $\lambda_{\text{max}}$  of C480, C1, and C153 after the addition of C<sub>n</sub>G1O-C<sub>n</sub>G3O dendrimers; the next column shows the blue shift (in nm) from the emission  $\lambda_{\text{max}}$  of coumarins in water. A blue shift in  $\lambda_{\text{em}}$  was observed in general, upon addition of a dendrimer to coumarin, which indicated a decrease in the polarity of the microenvironment possessing the probe.<sup>368, 369</sup> It is observed that across the dendritic generations (G1O-G3O) with uniform spacer lengths, blue shift increased with increasing dendrimer generations. As in



case of C480, the blue shift for C<sub>5</sub>G3O dendrimer was observed to be 15 nm, for C<sub>5</sub>G2O -8 nm, and for C<sub>5</sub>G1O no shift was observed. Similarly, for C153, the blue shift for C<sub>5</sub>G3O dendrimer was observed to be 36 nm, for C<sub>5</sub>G2O dendrimer-26 nm and for C<sub>5</sub>G1O again no shift was observed. For the case of C1, addition of C<sub>5</sub>G3O dendrimer afforded a blue shift of 18 nm, C<sub>5</sub>G2O afforded a blue shift of 14 nm and no shift was observed in case of C<sub>5</sub>G1O dendrimers. Negligible blue shift in the emission spectra of probes on addition of G1O dendrimers is in accordance with the results obtained for pyrene solubilization where no change in I<sub>1</sub>/I<sub>3</sub> ratio is observed on addition of first generation dendrimers, indicating the absence of hydrophobic interior.

**Table 8.2** Blue shift in emission  $\lambda_{\max}$  and  $E_T$  30 value of Coumarin 480 in various dendrimer solutions.\*

Aq. solution of dendrimers (200 $\mu$ M)	Emission $\lambda_{\max}$ (nm)	Blue Shift (nm)	$E_T$ 30 value (Kcal/mole)
C <sub>2</sub> G1	487	0	63.1
C <sub>3</sub> G1	487	0	63.1
C <sub>4</sub> G1	487	0	63.1
C <sub>5</sub> G1	487	0	63.1
C <sub>2</sub> G2	487	0	63.1
C <sub>3</sub> G2	483	4	60.3
C <sub>4</sub> G2	479	8	58.5
C <sub>5</sub> G2	479	8	58.5
C <sub>2</sub> G3	477	10	57.7
C <sub>3</sub> G3	475	12	57.0
C <sub>4</sub> G3	472	15	55.4
C <sub>5</sub> G3	472	15	55.4

\* [C480] =  $2.0 \times 10^{-5}$  M; emission  $\lambda_{\max}$  for C480 in water = 487 nm. [C<sub>n</sub>G1O] =  $4.0 \times 10^{-4}$  M in  $1.0 \times 10^{-1}$  M aq. NaOH; [C<sub>n</sub>G2O] and [C<sub>n</sub>G3O] =  $3.0 \times 10^{-4}$  M in  $1.0 \times 10^{-1}$  M aq. NaOH.

On the other hand, within a dendrimer generation with various spacer units, blue shift was found to be higher for C<sub>5</sub>, C<sub>4</sub> spacer, when compared to other spacer dendrimers. For example, for C480, within the third generation dendrimers, blue shift was 15 nm (from 487 nm to 472 nm) for C<sub>5</sub>G3O, whereas 10 nm (from 487 nm to 477 nm) for C<sub>2</sub>G3O dendrimer. Similarly, for C153, blue shift for C<sub>5</sub>G3O was 36 nm whereas for C<sub>2</sub>G3O was 22 nm. The same trend has been observed in case of C1. As predicted by pyrene probe, the above results also indicate that across the generations, third generation dendrimers possess more hydrophobic pockets, whereas, within a generation there is a continuous decrease in hydrophobicity of the pockets with systematic decrease in spacer length.

**Table 8.3** Blue shift in emission  $\lambda_{\max}$  and E<sub>T</sub> 30 value of Coumarin 1 in various dendrimer solutions.\*

Aq. solution of dendrimers (200 $\mu$ M)	Emission $\lambda_{\max}$ (nm)	Blue Shift (nm)	E <sub>T</sub> 30 value (Kcal/mole)
C <sub>2</sub> G1	470	0	63.1
C <sub>3</sub> G1	470	0	63.1
C <sub>4</sub> G1	470	0	63.1
C <sub>5</sub> G1	470	0	63.1
C <sub>2</sub> G2	466	4	53.0
C <sub>3</sub> G2	462	8	51.8
C <sub>4</sub> G2	459	11	50.8
C <sub>5</sub> G2	456	14	49.9
C <sub>2</sub> G3	456	14	49.9
C <sub>3</sub> G3	456	14	49.9
C <sub>4</sub> G3	454	16	49.2
C <sub>5</sub> G3	452	18	48.5

\* [C1] = 2.0 x 10<sup>-5</sup> M; emission  $\lambda_{\max}$  for C1 in water = 470 nm. [C<sub>n</sub>G1O] = 4.0 x 10<sup>-4</sup> M in 1.0 x 10<sup>-1</sup> M aq. NaOH; [C<sub>n</sub>G2O] and [C<sub>n</sub>G3O] = 3.0 x 10<sup>-4</sup> M in 1.0 x 10<sup>-1</sup> M aq. NaOH.

Another careful observation from the study of three different coumarins revealed, that more blue shift is observed in case of C153 in comparison to C1, C480 (18, 15 nm respectively). It is well known that the fluorescence properties of the coumarin dyes depend critically on the pattern of substitution.<sup>303</sup> Hence, C153 being comparatively more non-polar due to  $-CF_3$  group tends to occupy hydrophobic sites of the dendrimer more readily, hence showing greater blue shift.

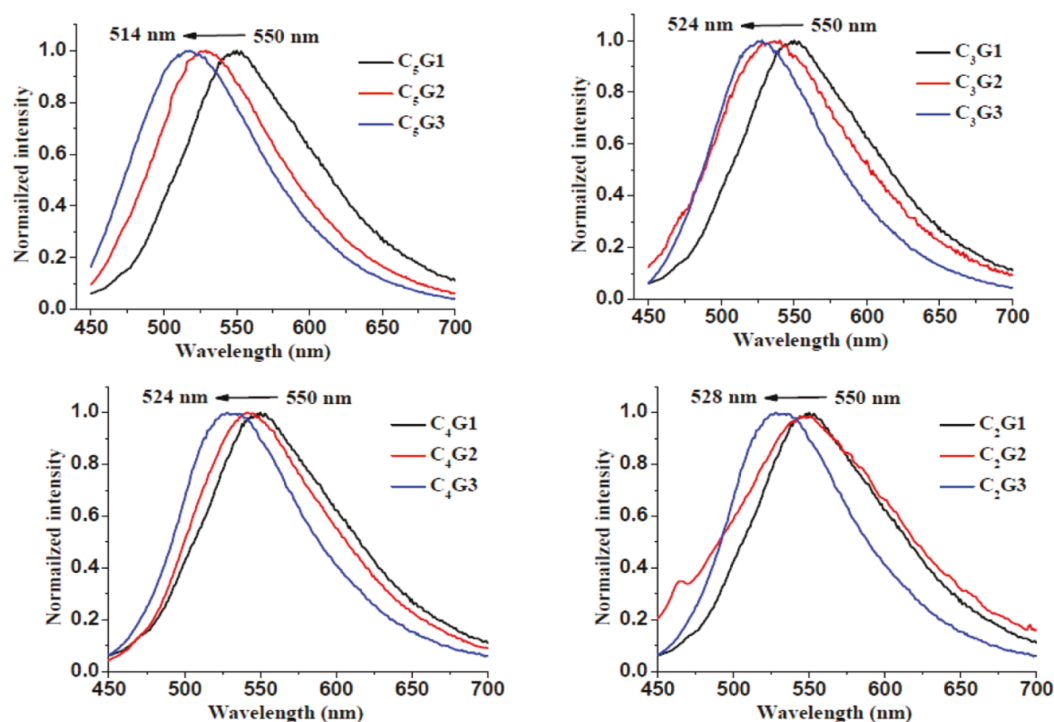
**Table 8.4** Blue shift in emission  $\lambda_{\max}$  and  $E_T$  30 value of Coumarin 153 in various dendrimer solutions.

Aq. solution of dendrimers (200 $\mu$ M)	Emission $\lambda_{\max}$ (nm)	Blue Shift (nm)	$E_T$ 30 value (Kcal/mole)
C <sub>2</sub> G1	550	0	63.1
C <sub>3</sub> G1	550	0	63.1
C <sub>4</sub> G1	550	0	63.1
C <sub>5</sub> G1	550	0	63.1
C <sub>2</sub> G2	548	2	51.7
C <sub>3</sub> G2	534	16	48.1
C <sub>4</sub> G2	530	20	47.1
C <sub>5</sub> G2	524	26	45.5
C <sub>2</sub> G3	528	22	46.6
C <sub>3</sub> G3	524	26	45.5
C <sub>4</sub> G3	524	26	45.5
C <sub>5</sub> G3	514	36	43.0

\* [C153] =  $4.0 \times 10^{-5}$  M; emission  $\lambda_{\max}$  for C153 in water = 550 nm. [C<sub>n</sub>G1O] =  $8.0 \times 10^{-4}$  M in  $1.0 \times 10^{-1}$  M aq. NaOH; [C<sub>n</sub>G2O] and [C<sub>n</sub>G3O] =  $6.0 \times 10^{-4}$  M in  $1.0 \times 10^{-1}$  M aq. NaOH.

Apart from the magnitude of the blue shifts, the polarity of the microenvironments located inside the dendrimers has also been reported on an  $E_T$  30 scale, for all the three coumarins. Usually the more hydrophobic the environment, lesser is the  $E_T$  30 value.<sup>370</sup> The  $E_T$  30 values obtained in all the cases correspond to the observed magnitude of the blue shifts. As for example, across the generations, for C480,

$E_T$  30 value for  $C_5G3O$  is 55.4 kcal/mole, whereas for  $C_5G1O$  is 63.1 kcal/mole. Similarly, within a generation, but across the spacers,  $E_T$  30 value for  $C_5G3O$  is 55.4 kcal/mole whereas for  $C_2G3O$  is 57.7 kcal/mole. The above assessment of microenvironments at dendritic interiors reiterates previous observations that alkyl chain length connecting the branch junctures of dendritic structure is an important criterion, in addition to dendrimer generations.



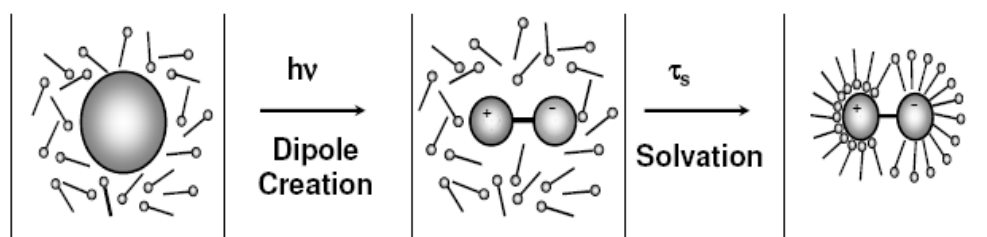
**Figure 8.4** Emission spectra of C153 in the presence of various generation dendrimers ( $C_nG1O$  -  $C_nG3O$ ,  $n = 2, 3, 4, 5$ ) [ $C_nG1O$ ] = 0.8mMin 0.1M aq NaOH; [ $C_nG2O$ ] and [ $C_nG3O$ ] = 0.6 mM in 0.1 M aq NaOH; [C153] = 0.04 mM;  $\lambda_{ex}$  = 400 nm and  $\lambda_{em}$  for C153 in water = 550 nm.

### 8.2.2 Probing the microenvironment of phenolic end group dendrimers ( $C_nGO$ ) by Solvation Dynamics

Most chemical reactions and biological functions take place in solution.

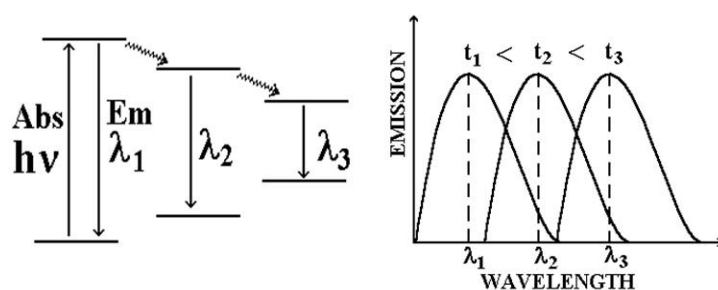
This simple fact has spurred a tremendous research effort aimed at elucidating the effects

of the solvent on the chemical or biochemical reactivity. The study of the dynamics of water in nano-confined systems has attracted great attention during the last years.<sup>371</sup> Most recently, there have been attempts to understand the dynamics in different regions of an organized assembly. Hence dynamics of a solvent in a confined environment is a subject of very active recent research.<sup>372</sup> The research field which focuses on the study of dynamics of the solvents around a solute is referred to as “solvation dynamics”. Solvation dynamics is the study of how a solvent interacts with molecules as a function of time. A single solute molecule, depending on its size, can be surrounded by tens to thousands of liquid molecules, each one tumbling and interacting with other solvent molecules and the solute.<sup>374</sup> When a probe molecule is excited with a photon, its electrons rearrange, changing its physical and chemical nature. The solvent, which was accustomed to seeing a ground state molecule, are now confronted with a transient excited state species. They start to move and rearrange to accommodate this change. **Figure 8.5** demonstrate this phenomenon. Now, looking back at the molecule - if the excited state molecule is sensitive to its environment, it will sense the motion of the solvent. This will affect the light it emits. The molecule serves both as the *trigger* which starts the solvent change, and the *camera* which can view the dynamics.



**Figure 8.5** Rearrangement of solvent molecules around the excited probe molecule.

After excitation, the solvent molecules 'relax' around the excited state species. This relaxation often results in an increased electric field across the molecule. As the electric field increases, the gap between the first singlet excited state and the ground state decreases in energy, causing the photons that are emitted are redder and redder in color as time goes on. Superimposing emission spectra at various times after emission show a spectrum whose center of mass keeps shifting to the red until a new equilibrium is reached. (**Figure 8.6**)



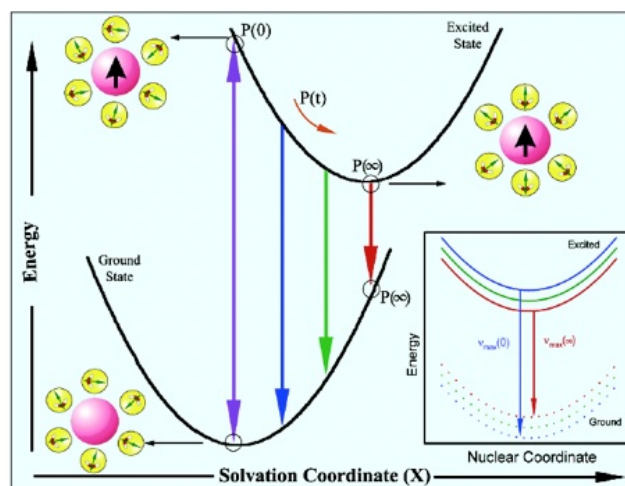
**Figure 8.6** Processes of Solvation Dynamics

The whole process of solvation dynamics is summarized in **Figure 8.7**. For disordered media, the solvation process is usually expressed via the solvation time correlation function:

$$C(t) = \frac{\langle E(t) \rangle - \langle E(\infty) \rangle}{\langle E(0) \rangle - \langle E(\infty) \rangle}$$

Where  $E(0)$  and  $E(\infty)$  are the energy of the system at the beginning and at the end of the dynamics (i.e. corresponding to initial polarization  $P(0)$  and final polarization  $P(\infty)$  in **Figure 8.7**), while  $E(t)$  is the energy at some intermediate time during the dynamics. The correlation function typically exhibits a multi exponential decay with time scales of <200 fs, some 100s of fsec and a few psec to several tens of psec, depending on the solvent, or its surroundings. Hence, solvation dynamics can be measured experimentally by looking

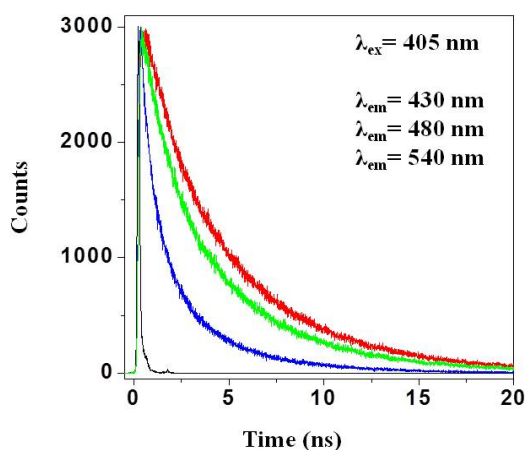
for solvent interactions with spectroscopic probes, like time-resolved fluorescence. The advantage of fluorescence is the ability to introduce an instantaneous change to the solute, which then perturbs the solvent in a time dependent manner. According to computer simulations, about 85% of the solvation dynamics arises from the first solvation layer around the solvation probe.<sup>373</sup> As a result, solvation dynamics may be utilized to probe regions of sizes around 1 nm in a heterogeneous assembly. By using solvatochromism, the fluorescent probes in different regions of such an assembly may be selectively excited through variation of the excitation wavelength. Excitation at a short wavelength (blue end) selects the solvatochromic (e.g. coumarin 480, C480) probe in a relatively nonpolar (hydrophobic) environment and gives rise to a blue-shifted emission spectrum. On the other hand, excitation at a longer wavelength (red end) selects the probe in a relatively polar (hydrophilic) environment and gives rise to a red-shifted emission spectrum. Solvation dynamics in bulk water (and other polar solvents) is ultrafast and occurs in a time scale  $< 1$  ps.<sup>374</sup>



**Figure 8.7** Schematic illustration of the potential energy surfaces involved in the solvation dynamics of water. (Reproduced from Pal et al, *J. Phys. Chem. B*, **2002**, 106, 12376-12395)

However, many organized assemblies exhibit a slow component on a 100-1000 ps time scale.<sup>375-387</sup> This includes cyclodextrin,<sup>376</sup> protein,<sup>377</sup> micelle,<sup>378</sup> reverse micelle,<sup>379</sup> DNA,<sup>380</sup> nanoporous solgel glass,<sup>381</sup> lipid,<sup>382</sup> and polymer and polymer surfactant aggregates.<sup>383</sup>

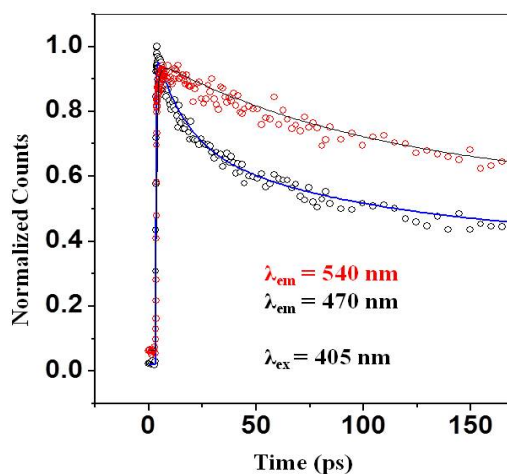
We have tried to explore the structure of the poly alkyl (aryl) dendrimers ending with phenolic group (C<sub>5</sub>G3O) (**Scheme 8.2**), with the help of solvation dynamics. This work has been done in association with Dr. Kankan Bhattacharya (IACS) Kolkata, and the dendrimers are provided by Dr. N. Jayaraman, (IISc) bangalore. We have utilized two well known fluorescent probes for this work, Coumarin 480 (C480) and coumarin 153 (C153) (**Figure 8.3**). Time resolved picoseconds experiments have been carried out for the dendrimer C<sub>5</sub>G3O with the probe C480. A mixture of the aqueous solution of the probe C480 and the dendrimer C<sub>5</sub>G3O was excited at 405 nm and the lifetime was monitored at different wavelengths (430, 480, 530 nm). It was observed that the long component ( $\sim 5$  ns) of the lifetime of the probe increased with increasing the emission wavelength (**Figure 8.8**).



**Figure 8.8** Picosecond time-resolved experiments for the probe C480 and C<sub>5</sub>G3O dendrimer.



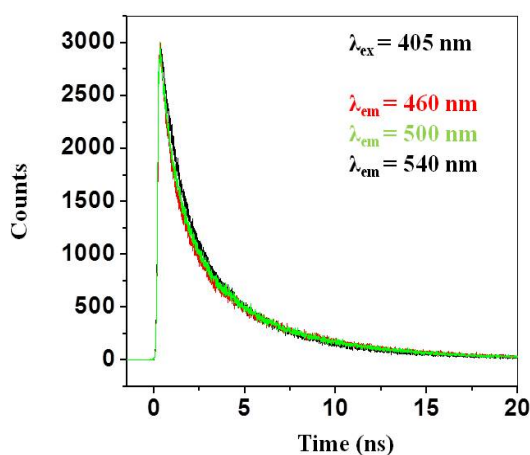
This indicated that the solvation dynamics might be taking place in the dendrimer vicinity. To confirm this, femtosecond lifetime experiments were carried out. The probe was again excited at 405 nm and the lifetime was monitored at two emission wavelengths 470 and 540 nm. In both the cases, no rise component was detected (**Figure 8.9**). This indicated that though the solvation dynamics for the probe C480 was taking place in the vicinity of the dendrimer C<sub>5</sub>G3O, but it was as fast as bulk water. To measure such fast component more sophisticated instruments are called for. The inference drawn from these experiments were that C480 being comparatively a polar probe is stabilized by the polar part that is the polar phenolic end groups of the dendrimer, and hence it likes to reside outside in the bulk solution, exhibiting the solvation dynamics of the bulk solution.



**Figure 8.9** Femtosecond time-resolved experiments for the probe C480 and C<sub>5</sub>G3O dendrimer.

Likewise, the picoseconds time resolved experiments for C153 as probe were carried out. The aqueous mixture C153 and dendrimer C<sub>5</sub>G3O was excited at 405 nm. And the lifetime was monitored at emission wavelengths 460, 500 and 540 nm. No change in the lifetime of the probe was monitored (**Figure 8.10**). This indicated absence

of solvation dynamics. Absence of solvation dynamics for the probe C153, could mean that C153 being a relatively non-polar probe is more stabilized in the hydrophobic cavities of the dendrimers, where no solvent molecules are present, hence no solvation dynamics is observed in this case. In other words, as in the previous case, the absence of solvation dynamics indicated that the probe was present in the hydrophobic pocket of the dendrimers. Hence these experiments illustrate the structure of the dendrimers in question, by showing that these dendrimers possess polar periphery whereas, non-polar inner cavities.



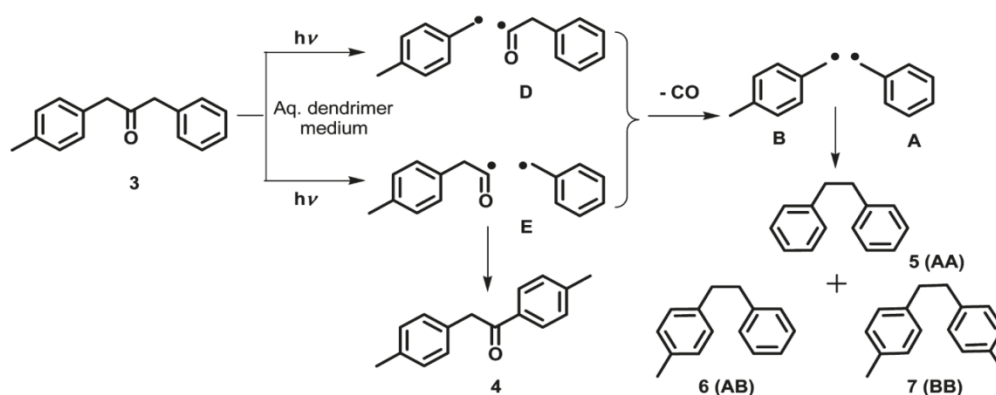
**Figure 8.10** Picosecond time-resolved experiments for the probe C153 and C<sub>5</sub>G3O dendrimer.

### 8.2.3 Phenolic end group dendrimers (C<sub>n</sub>GO) as reaction media for Photolysis of 1-Phenyl-3-p-tolyl-propane-2-one

The studies with polarity probes pyrene and coumarin indicate the presence of hydrophobic pockets inside the third generation dendrimers. The solvation dynamics studies too show the existence of the hydrophobic inner cavities in the dendrimers. In this instance, abilities of poly(alkyl aryl ether) dendrimers to mediate various photochemical reactions were assessed previously.<sup>362, 363</sup> In continuation, it was deemed necessary to probe the mobility of guest molecules in the hydrophobic environments of dendrimers

with varying interfacial regions resulting from different spacer groups within a dendrimer generation. The series within third generation dendrimers, constituted with C<sub>2</sub>-C<sub>5</sub> alkyl chain length, was chosen, in order to conduct photolysis of dibenzyl ketone (**Scheme 8.3**).<sup>388</sup>

Irradiation of 1-phenyl-3-p-tolyl-propane-2-one **3** in hexane solution resulted in an R-cleavage, yielding the primary radical pairs D and E, followed by decarbonylation, to afford a secondary radical pair A and B. In hexane solution, no product from the radical pairs D and E was detected. Three diaryl ethanes **5** (AA), **6** (AB) and **7** (BB), resulting from the radical pairs A and B, were formed in the ratio 1:2:1. In restricted environments, the rearrangement product **4** is formed from the radical pair E.<sup>389</sup> When the radical pairs A and B were held within a cage with little translational mobility, the only product expected was **6** (AB).<sup>390-392,273</sup>



**Scheme 8.3** Photolysis of Dibenzylketone inside Aqueous Basic Solutions of Dendrimers.

The cage effect  $(AB - AA - BB)/(AA + AB + BB)$  and the yield of rearrangement product **4** provide information concerning the “leakiness” of the reaction cavity with respect to radical pairs D, E, A, and B. The results of photolysis of 1-phenyl-3-p-tolyl-propane-2-one **3** in hexane and in aqueous basic third generation dendrimers with various

spacer groups are summarized in **Table 8.5**. It was observed that in case of C<sub>5</sub>G3O dendrimer the cage effect was 1.0 with the formation of rearrangement product 4 in 31% yield. As the spacer length decreased to C<sub>4</sub>G3O, the cage effect also decreased to 0.62. The cage effect for C<sub>3</sub>G3O was observed to be 0.54, whereas negligible cage effect was observed in the case of C<sub>2</sub>G3O dendrimer. These results indicated that the third generation dendrimers with the pentamethylene linker possessed higher hydrophobicity, as concluded from the above solubilization and photophysical studies. As the spacer length decreased, the hydrophobicity also decreased.

**Table 8.5** Photolysis of 1-Phenyl-3-p-tolyl-propan-2-one in Aqueous Basic Dendrimer Solutions<sup>a,b</sup>

Medium	AA	AB	BB	2	Cage effect
Hexane	21	51	29	-	0.05
<b>C<sub>2</sub>G3</b>	30	46	24	-	-
<b>C<sub>3</sub>G3</b>	10	77	13	-	0.54
<b>C<sub>4</sub>G3</b>	9	81	10	-	0.62
<b>C<sub>5</sub>G3</b>	-	69	-	31	1.0

a. [C<sub>n</sub>G3] = 1.0 x 10<sup>-3</sup> M in 1.0 x 10<sup>-2</sup> M aq. NaOH. b. Cage effect = (AB-BB-AA)/(AA+AB+BB)

#### 8.2.4 Photochemical Isomerizations of Stilbenes inside Phenolic end group dendrimers (C<sub>n</sub>GO)

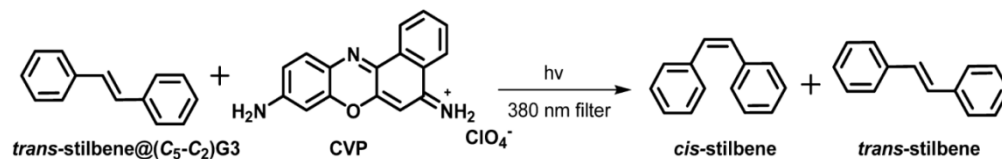
Continuing the efforts to utilize dynamic inner cavities of dendrimers as reaction cavities in an aqueous medium, we undertook studies of photochemical isomerization of stilbenes, well-investigated system in solution. Photochemical isomerization of stilbene proceeds via rotation of the C=C bond. The experiments were performed in aqueous

dendrimers solutions (pH ~10, aq NaOH) upon encapsulation of stilbene. After purging with N<sub>2</sub>(g) for 30 min, the solutions in Pyrex test tubes were irradiated using a medium-pressure Hg lamp for 6 h and extracted with diethyl ether, and the products were analyzed by gas chromatography. As a comparison, irradiations were also conducted in ethanol solution in the absence of the dendrimer. As shown in **Table 8.6**, in aqueous solutions containing dendrimers, conversion of *trans*-isomer to *cis*-isomer was complete. In addition to *cis*-isomer, a considerable amount of phenanthrene was formed with C<sub>5</sub>G3 and C<sub>4</sub>G3 dendrimers as well as in EtOH solution. Although stilbene dimerization in aqueous solutions, probably due to aggregation, to afford cyclobutane was known previously,<sup>393</sup> in none of the irradiations did tetraphenylcyclobutane, resulting from [2 + 2] cycloaddition, formed. The absence of dimers suggested that stilbene molecules were confined to the hydrophobic interior of dendrimers. Exclusive formation of only the *cis*-isomer within C<sub>3</sub>G3O and C<sub>2</sub>G3O dendrimers suggested that the *cis*-isomer was not favored to isomerize to the *trans*-form or cyclize to phenanthrene. This may also be an indication of the *cis*-isomer being more easily accommodated than the *trans*-isomer within the dendritic hydrophobic cavities. Formation of phenanthrene in solutions containing C<sub>5</sub>G3O and C<sub>4</sub>G3O dendrimers suggested that cyclization was becoming facile as the linker lengths constituting the dendrimers increased. Thus, among *cis*- and *trans*-isomers and phenanthrene, *cis*-isomer appeared to be the preferred resting state inside dendrimer cavities, followed by phenanthrene. The dominant role of cavity sizes in photoisomerization could thus be observed within a dendrimer generation by varying linkers connecting the branch points.

**Table 8.6** Isomerization of *trans*-Stilbene in Aqueous Dendrimer Solutions and in EtOH.

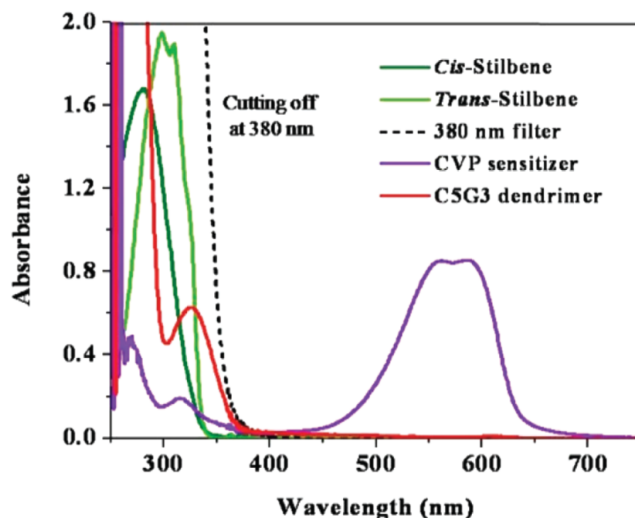
	<i>trans</i> -Stilbene (%)	<i>cis</i> -Stilbene (%)	Phenanthrene (%)
<b>EtOH</b>	15	56	29
<b>C<sub>5</sub>G3</b>	-	72	28
<b>C<sub>4</sub>G3</b>	-	91	9
<b>C<sub>3</sub>G3</b>	-	99	trace
<b>C<sub>2</sub>G3</b>	-	99	trace

Having established that the dendrimer interior favors the *cis*-isomer formation, we were curious whether such would be the case when the isomerization was prompted by a photoinduced electron-transfer process. It is well-known that photoinduced electron transfer of stilbene in organic solvents favors the *trans*-isomer.<sup>394-396</sup> We chose cresyl violet perchlorate (CVP) as the electron-transfer sensitizer (**Scheme 8.4**) for the following reasons: (a) CVP, a positively charged dye (**Scheme 8.4**), being polar in nature<sup>397</sup> would prefer to be in the bulk aqueous solution and posed no competition to the encapsulation of *trans*-stilbene inside the dendrimers. Also, being positively charged, it was likely to interact with the negatively charged periphery of dendrimers. (b) The absorption spectra of *trans*-stilbene, *cis*-stilbene, CVP, and the CS-380 cutoff filter are shown in **Figure 8.11**. From the absorption spectra it is clear that CVP could be selectively excited in the presence of stilbenes. (c) Based on the known values of the oxidation and reduction potentials of the donor and the acceptor and the excitation energy of CVP, the photoinduced electron transfer is expected to be exothermic by  $-0.29$  eV ( $E_{\text{ox}}[\textit{trans}\text{-stilbene}] = 1.43$  V vs SCE;  $E_{\text{red}}[\text{CVP}] = -0.46$  V vs SCE; ES1 (Cresyl violet) = 2.118 eV (corresponding to 586 nm)).



**Scheme 8.4** Photoisomerization of *trans*-Stilbene@(C<sub>5</sub>–C<sub>2</sub>)G3O Dendrimers in the Presence of CVP as Electron-Transfer Sensitizer.

First, we established that CVP-sensitized isomerization of *trans*-stilbene in ethanol favors the *trans*-isomer. As indicated in **Table 8.7**, consistent with literature reports, CVP sensitization gave very little *cis*-isomer in ethanol without the presence of a dendrimer.



**Figure 8.11** Absorption spectra of *cis*-, *trans*-stilbenes, C<sub>5</sub>G3O, CVP, and 380 nm filter.

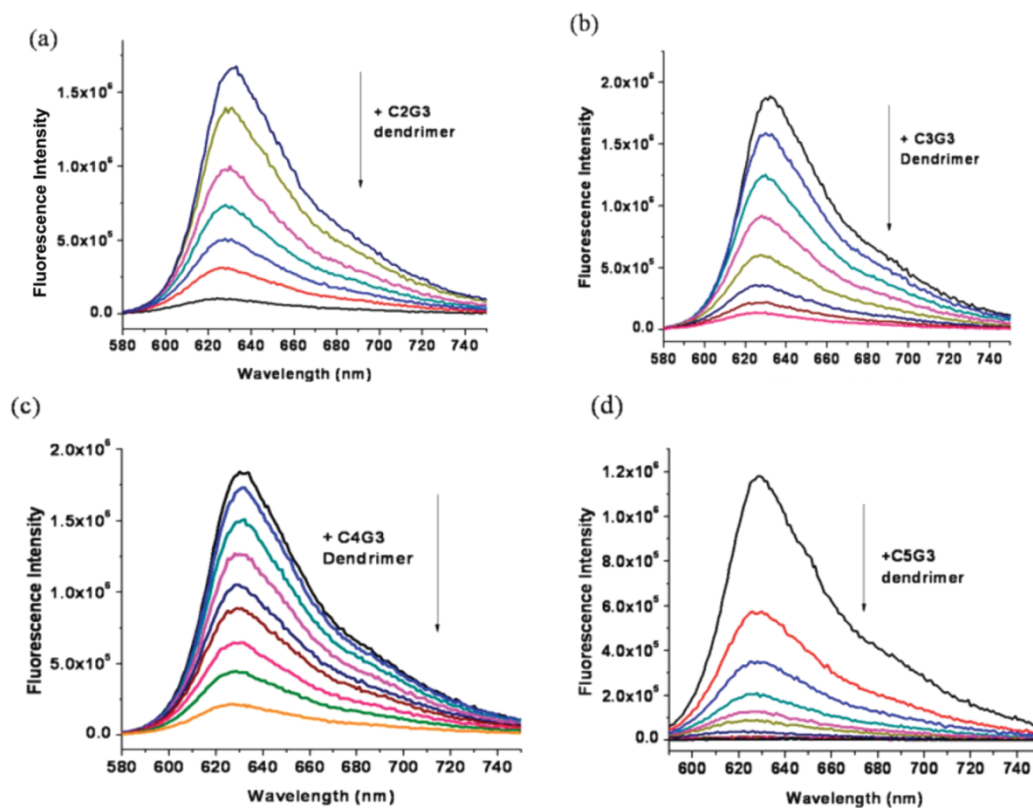
For photoinduced dendrimers was achieved similar to that during direct irradiation experiments. Selective excitation of the sensitizer in the presence of *trans*-stilbene<sup>398</sup> was conducted for 2 h using a Corning 380 nm filter. Similar to direct irradiation, CVP sensitization of *trans*-stilbene also led to *cis*-stilbene as the main product. **Table 8.7** lists the relative percentages of *cis*- and *trans*-stilbenes encapsulated within C<sub>5</sub>G3O–C<sub>2</sub>G3O dendrimers, obtained after the photosensitized irradiation, in the presence of CVP. We observed that in going from C<sub>5</sub> to C<sub>2</sub> linker in the third-generation

dendrimers, the percentage of *cis*-isomer increased. This supports the inference drawn from results of direct irradiation that a decrease in the size of inner cavities stabilizes *cis*-stilbene inside the dendrimers. Given the closeness of the oxidation potential of the linker trialkoxybenzene units ( $E_{\text{ox}}$  [TMB = G3(OH)24] = 1.5 V vs SCE) with that of *trans*-stilbene, the linker units mediating the electron-transfer unit cannot be ruled out. To probe this possibility, the fluorescence of CVP was monitored with increased addition of dendrimers. As shown in **Figure 8.12**, addition of C<sub>2</sub>G3O–C<sub>5</sub>G3O dendrimers resulted in a decrease in CVP fluorescence intensity. Given that the excited singlet energy of the linker unit is higher than that of CVP, we believe that the quenching is likely to be due to electron transfer from linker units to excited CVP. The Stern–Volmer plot due to the above fluorescence quenching showed a nonlinear upward curve, indicating the quenching process to be under both dynamic and static mechanisms.

**Table 8.7** Photo-isomerization of *trans*-Stilbene Encapsulated within C<sub>2</sub>G3O–C<sub>5</sub>G3O Dendrimers, in the Presence of CVP as Electron-Transfer Sensitizer Dye, Using a 380 nm Filter and Irradiation for 2 h.

<b>Dendrimer</b>	<i>trans</i> -stilbene	<i>cis</i> -stilbene
Ethanol	98%	2%
C <sub>5</sub> G3	16%	84%
C <sub>4</sub> G3	5%	95%
C <sub>3</sub> G3	1%	99%
C <sub>2</sub> G3	2%	98%



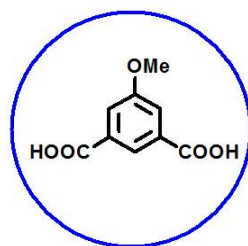


**Figure 8.12** Fluorescence studies of CVP in presence of various (a–d) ( $C_2G_3O$ – $C_5G_3O$ ) dendrimers respectively.  $[CVP] = 3 \times 10^{-5}$  M in water.  $[C_nG_3] = 0.33 \times 10^{-6}$  M to  $1.7 \times 10^{-4}$  M.  $\lambda_{ex} = 580$  nm.

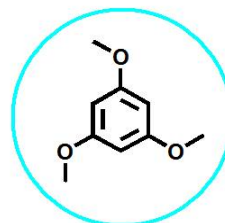
### 8.2.5 Characterization of poly alkyl aryl dendrimers ending with carboxylic acid group ( $C_5G_1A$ – $C_5G_3A$ ) with UV-visible and Fluorescence Spectroscopies

In this study, UV-visible and fluorescence spectroscopies have been used to characterize the structure of  $C_5G_1A$ – $C_5G_3A$  dendrimers possessing carboxylic acid as external peripheral groups. These carboxylic acid groups are converted to carboxylate groups under basic buffer conditions (sodium borate buffer, pH 9) and render anionic surface to the dendrimers. In contrast to the precise compositional and constitutional aspects of these dendrimers, their shapes and morphologies needed to be defined by direct spectroscopic methods. But methods such as X-ray analysis could not be used due to their gummy nature. Hence we have utilized UV-visible and fluorescence spectroscopy

to probe these dendrimers. In previous reports, the fluorescence spectroscopy was used to investigate a series of n.5-generation dendrimers possessing anionic surfaces of sodium carboxylate groups.<sup>399-401</sup>



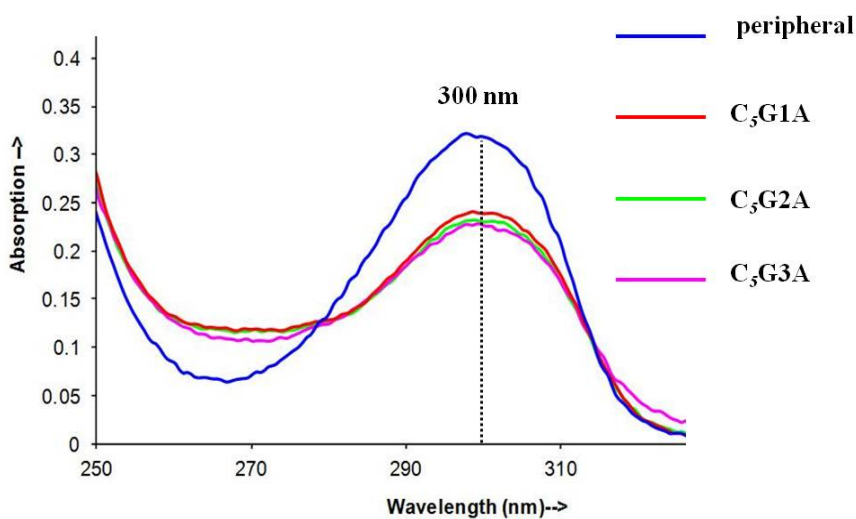
**1-methoxyisophthalic acid**  
**Peripheral Molecule**



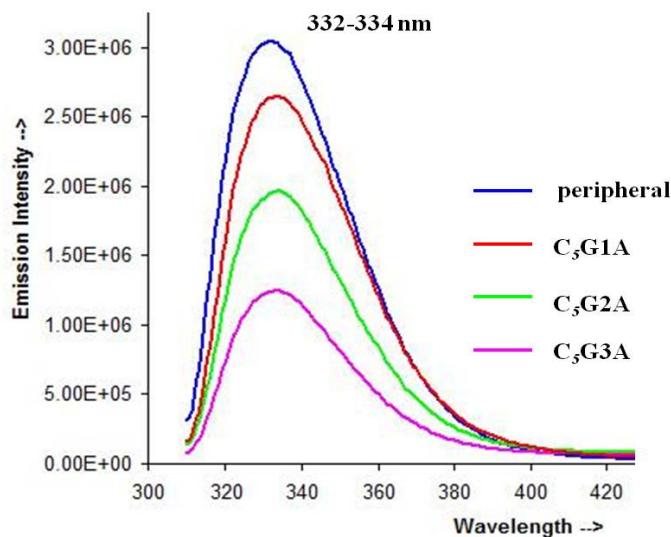
**1,3,5-Trimethoxybenzene**  
**TMB**

**Scheme 8.5** Chemical structures of Peripheral Molecule and TMB.

Along with the C<sub>5</sub>G1A-C<sub>5</sub>G3A dendrimers three additional molecules are introduced in this study, out of which two were synthesized as shown in **Scheme 8.5**. We named the first molecule as the “peripheral molecule” since it represents the periphery of the dendrimers in question. The next one is the third generation dendrimer with the corresponding carboxylic ester as the end group at its periphery (C<sub>5</sub>G3(COOMe)) and the last one is trimethoxybenzene, which represents the core of these dendrimers.

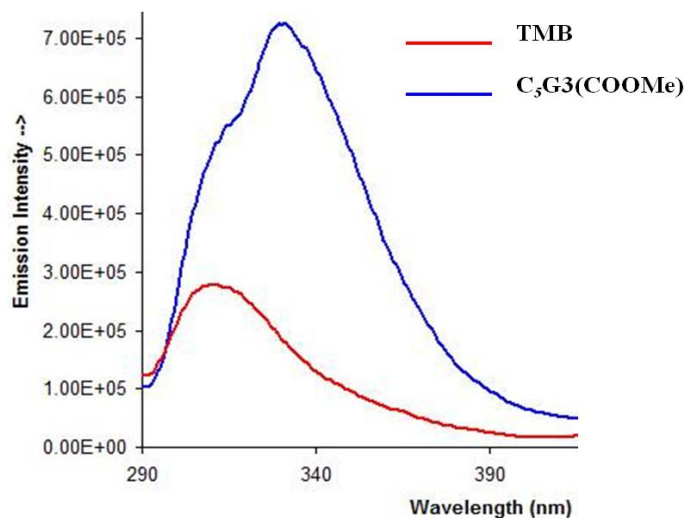


**Figure 8.13** UV-visible spectra of first, second and third generation dendrimers along with the peripheral molecule.



**Figure 8.14** Fluorescence spectra of first, second and third generation dendrimers along with the peripheral molecule.

Initially we carried out the UV-visible studies of the three dendrimers C<sub>5</sub>G1A to C<sub>5</sub>G3A and the peripheral molecule (**Figure 8.13**), followed by the fluorescence studies (**Figure 8.14**). The concentration of all the samples was maintained constant as 0.1 mM. It can be observed that the UV maxima for all the four molecules lie at nearly 300 nm, whereas, the fluorescence maximum wavelength lies between 332-334 nm for these molecules. Though the number of peripheral groups increases with the increase in the generation of the dendrimer, the UV-visible and fluorescence maximum wavelength remains almost same for all of them. Also, this  $\lambda_{\text{max}}$  corresponds to the “peripheral molecule”. These observations suggest that the UV-visible and fluorescence properties exhibited by these dendrimers arise due to the peripheral group represented by the “peripheral molecule”.



**Figure 8.15** UV-visible spectra of third generation dendrimer ending with ester group along with the trimethoxybenzene (representing the core of the dendrimer).

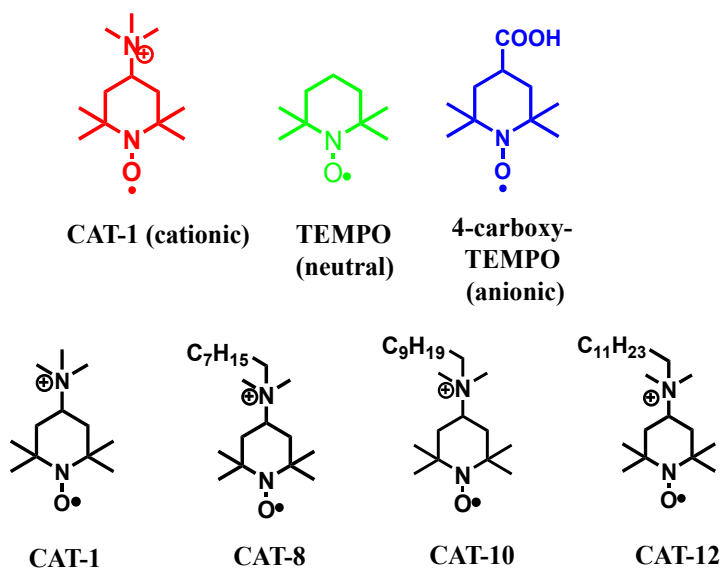
In another experiment fluorescence spectra of the third generation dendrimer ending with the carboxylic ester groups and trimethoxybenzene (representing the core of the dendrimer) were recorded. **Figure 8.15** shows that the fluorescence spectra of  $C_5G_3(COOMe)$  possesses a slight shoulder corresponding to the emission maxima of trimethoxybenzene (TMB). Hence, this observation suggests that the core consisting of trimethoxybenzene moiety have very slight contribution in the photophysical properties of these dendrimers.

To extensively probe the structure of these dendrimers, including its external nature and the internal hydrophobic cavities various kinds of experiments were carried out as presented in following sections.

### **8.2.6 Characterization of poly alkyl aryl dendrimers ending with carboxylic acid group ( $C_5G_1A-C_5G_3A$ ) with EPR Spectroscopy**

Host-guest systems made from dendrimers have enormous possibilities in the areas of membrane transport and drug delivery.<sup>402-404</sup> The interest in dendrimeric macromolecules for such applications stems from their distinctive dual-natured properties, an external periphery bearing multiple functional groups for solubility in

aqueous media combined with an internal hydrophobic core for large molecule transport. Hence, a more complete characterization of the dendrimer surface would require information on its binding capability, the extent of ionization in different experimental conditions, the ability to interact with molecules or ions, and the ability of molecules and ions to penetrate the internal core of the dendrimers. EPR studies have proved to be very informative in determining the binding and structural properties of host molecules and surfaces in the case of various spin labels and spin probes as guest molecules. Nitroxide radicals with an attached carbon chain of different lengths were shown to be valuable probes for identifying hydrophilic and hydrophobic interacting and binding sites at the surface of the dendrimers.<sup>405</sup> Recently, the electron paramagnetic resonance (EPR) technique has been employed to monitor the interactions occurring between dimyristoylphosphatidylcholine (DMPC) vesicles and polyamidoamine starburst dendrimers (SBDs).<sup>405,406</sup>



**Scheme 8.6** Nitroxide radical probes used for the characterization of dendrimers using EPR.

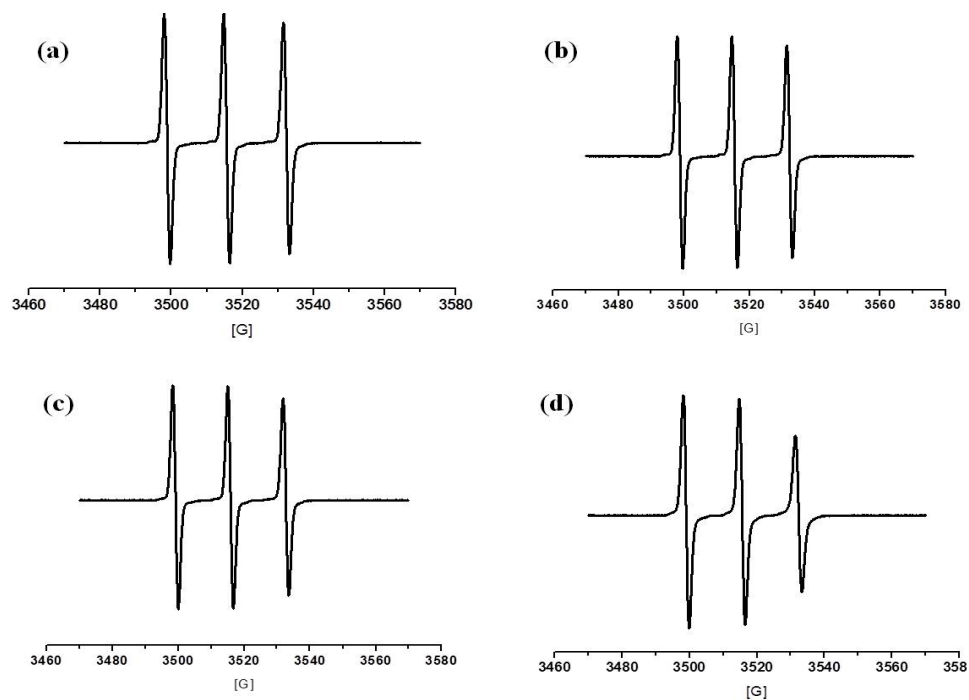
EPR analysis can be carried out by the evaluating two important factors: First, rotational correlation time of the radical probe and the hyperfine coupling constant. These two factors can be evaluated experimentally as well as by computational means by following the well-established procedure developed by Schneider and Freed.<sup>407</sup> The correlation time,  $\tau_c$ , is the time characteristic for the rotational diffusion and is related to the rotational diffusion coefficient,  $D$ , by the relationship  $\tau_c = 1/6D$ . The correlation time ( $\tau$ ) for the rotational diffusion motion of the spin probe provides information about the guest rotation within the host molecule. A decrease in the  $\tau_c$  would mean the encapsulation of the guest probe into the host cavity. The evaluation of hyperfine coupling constant  $\langle A_N \rangle$  can be performed by measuring peak to peak distances in the experimental spectra.  $\langle A_N \rangle$  is a good parameter to measure the environmental polarity,<sup>408</sup> since the electron spin density at the nitrogen nucleus increases if the NO moiety is surrounded by more polar molecules. An increase in the environmental polarity enhances the  $\langle A_N \rangle$  tensor components owing to the increased electron spin density on the nitrogen nucleus of the NO group of the nitroxide probe.<sup>408,409</sup> Monitoring the  $\langle A_N \rangle$  tensor can help us to ascertain the location of guests in the presence of the host.

In this preliminary study, nitroxide radicals were used to investigate the structural properties of poly alkyl (aryl) dendrimers with carboxylic end groups (C<sub>5</sub>G1A-C<sub>5</sub>G3A) and their interactions with the radical molecules. We have carried out two kinds of studies. In the first study, we used one anionic, cationic and neutral radical probe to investigate the characteristic of the external periphery of the dendrimers, whereas, in the other set of experiments we used long chain cationic radical probes to investigate the interior hydrophobic pockets of the dendrimers. The EPR computational studies could be

carried out to support the experimental results obtained, as presented below. The radical probes used in this study are shown in **Scheme 8.6**.

Firstly, 1:10 ratio of the CAT-1: C<sub>5</sub>G1A-C<sub>5</sub>G3A solution was prepared in sodium borate buffer of 10 mM concentration. This solution was analyzed by the EPR. Similarly, the aqueous buffer solutions of 1:10 -TEMPO: C<sub>5</sub>G1A-C<sub>5</sub>G3A and 4-carboxy TEMPO: C<sub>5</sub>G1A-C<sub>5</sub>G3A were also prepared and the EPR spectra were recorded. For the comparison, the EPR spectra of the buffer solution of all three probes, CAT-1, TEMPO, and 4-carboxy TEMPO alone without any host were also recorded. All the studies were carried out at room temperature. The EPR spectra thus obtained were analyzed and the hyperfine coupling constants were measured using ORIGIN software and the rotational correlation times were calculated according to the procedure given in the literature. **Figures 8.16**, show the EPR spectra of CAT-1, a cationic probe in different media, like buffer solution and C<sub>5</sub>G1A- C<sub>5</sub>G3A solution. **Table 8.8**, shows the obtained hyperfine coupling constants and the rotational correlation time in each case. From the EPR spectra (three hyperfine lines:  $2I_N+1=3$ ) it can be noticed that the high field hyperfine line gets broader and broader as the generation of the dendrimer increases from 1 to 3. Also, **table 8.8**, shows that the hyperfine coupling constant  $\langle A_N \rangle$  decreases slightly on association with the dendrimers in comparison to the buffer solution, probably indicating that the probe faces some change in its environment. Rotational correlation time  $\tau_c$  changes from 27 to 112 ps, from buffer to C<sub>5</sub>G3A solution. This significant increase in  $\tau_c$  shows that the cationic probe CAT-1 prefers to attach itself to the periphery of the dendrimer. The question arises: why periphery and not the interior of the dendrimer? Probably, because CAT-1 is comparatively polar in nature and positively charged, and prefers the columbic

interaction with the carboxylate (negatively charged) end group containing periphery of the dendrimer. This hypothesis is supported by the minimal change in the hyperfine coupling constants, which is a parameter effected by the polarity of the environment of the probe, in the case of buffer- $C_5G1-3A$  dendrimers. In support of this hypothesis, a positively charged nitroxide have been shown to bind electrostatically with the negatively charged n.5-SBD surface.<sup>405</sup>



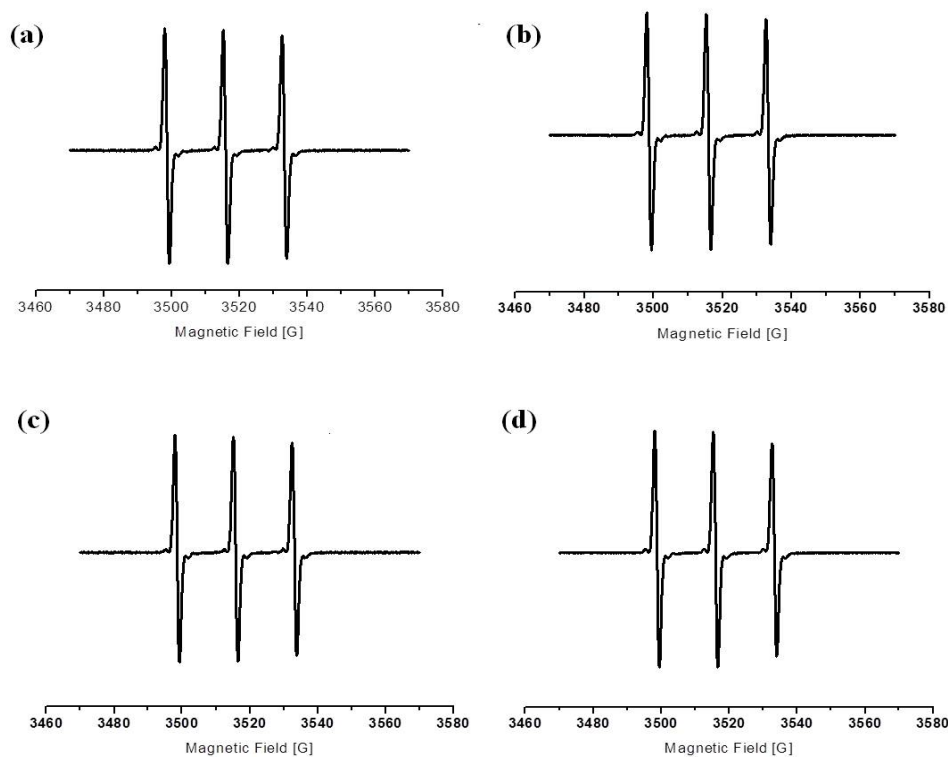
**Figure 8.16** EPR spectra of CAT-1 in (a) buffer solution, (b)  $C_5G1A$ , (c)  $C_5G2A$ , (d)  $C_5G3A$ .  $[CAT-1] = 0.1$  mM,  $[C_5G1-3A] = 1$  mM,  $[buffer] = 10$  mM. Spectra recorded at room temperature.

**Table 8.8** Hyperfine coupling constant and rotational correlation time for CAT-1 in different media.

CAT-1	$A_N$ [G]	$\tau_c$ [ns]
Buffer	16.8	0.027 ns
G1A	16.7	0.041 ns
G2A	16.7	0.059 ns
G3A	16.6	0.112 ns



To probe the dendrimers further, and collect evidence in support of our hypothesis as mentioned above, we employed TEMPO as the next EPR probe. TEMPO is a neutral molecule. As can be observed from the EPR spectra in Figure X, the broadening in the high field hyperfine line is not as prominent as was in the case of CAT-1 as a probe. Also, **Table 8.9**, suggest that there is not much change in the hyperfine coupling constants  $\langle A_N \rangle$  traversing from the buffer solution to the dendrimer solutions, probably indicating that the EPR probe does not prefer to occupy the internal hydrophobic cavities of the dendrimers. The rotational correlation time,  $\tau_c$  differs from 9 ps to 42 ps, in the case of buffer solution to C<sub>5</sub>G3A solution. The increase in this case is not as prominent as was in the case of cationic probe CAT-1. This observation supports our idea that CAT-1 being cationic prefers to interact with the negatively charged periphery of the dendrimers.

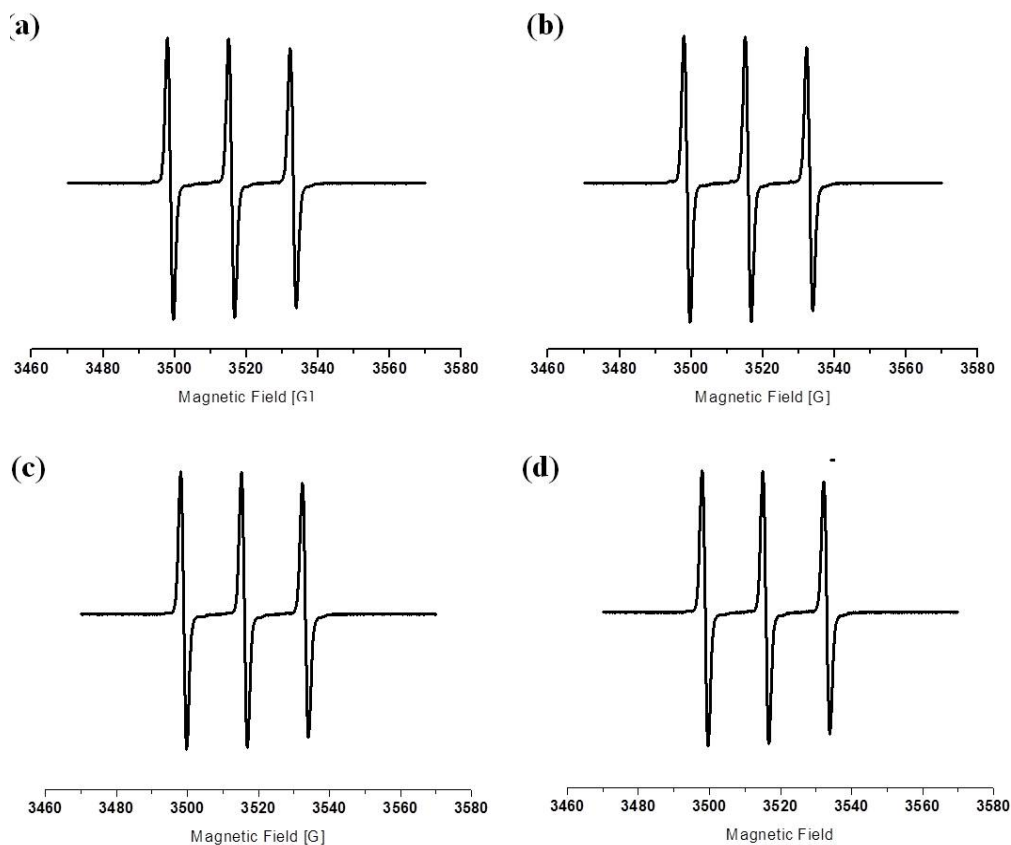


**Figure 8.17** EPR spectra of TEMPO in (a) buffer solution, (b) C<sub>5</sub>G1A, (c) C<sub>5</sub>G2A, (d) C<sub>5</sub>G3A. [TEMPO] = 0.1 mM, [C<sub>5</sub>G1-3A] = 1 mM, [buffer] = 10 mM. Spectra recorded at room temperature.

**Table 8.9** Hyperfine coupling constant and rotational correlation time for TEMPO in different media.

TEMPO	$A_N$ [G]	$\tau_c$ [ns]
Buffer	17.19	0.009 ns
G1A	17.20	0.014 ns
G2A	17.29	0.019 ns
G3A	17.20	0.042 ns

Lastly in this series, we utilized 4-carboxy TEMPO, an anionic molecule under the experimental conditions as the next EPR probe. **Figure 8.18** again shows minimum changes in the high field hyperfine line, advancing from buffer to C<sub>5</sub>G3A solution. **Table 8.10**, shows almost no or minimum change in the hyperfine coupling constants  $\langle A_N \rangle$  in all the cases. And the rotational correlation time  $\tau_c$  changes from 33 ps to 39 ps. This increase in the  $\tau_c$  seems almost negligible in comparison to the increase in the case of cationic probe CAT-1 and is much lower from the increase in the case of neutral probe TEMPO. Summing up these observations, we can conclude that the EPR probes CAT-1, TEMPO and 4-carboxy TEMPO, all prefer to reside outside the dendrimers. Also, CAT-1 being cationic in nature attaches itself to the negatively charged periphery of the dendrimers, as exhibited by the increase in the  $\tau_c$ . Neutral probe TEMPO does not mind to be in the vicinity of the dendrimers, and 4-carboxy TEMPO, being anionic in nature suffers from columbic repulsion from the periphery of the dendrimers, as indicated by the minimal change in EPR parameters.



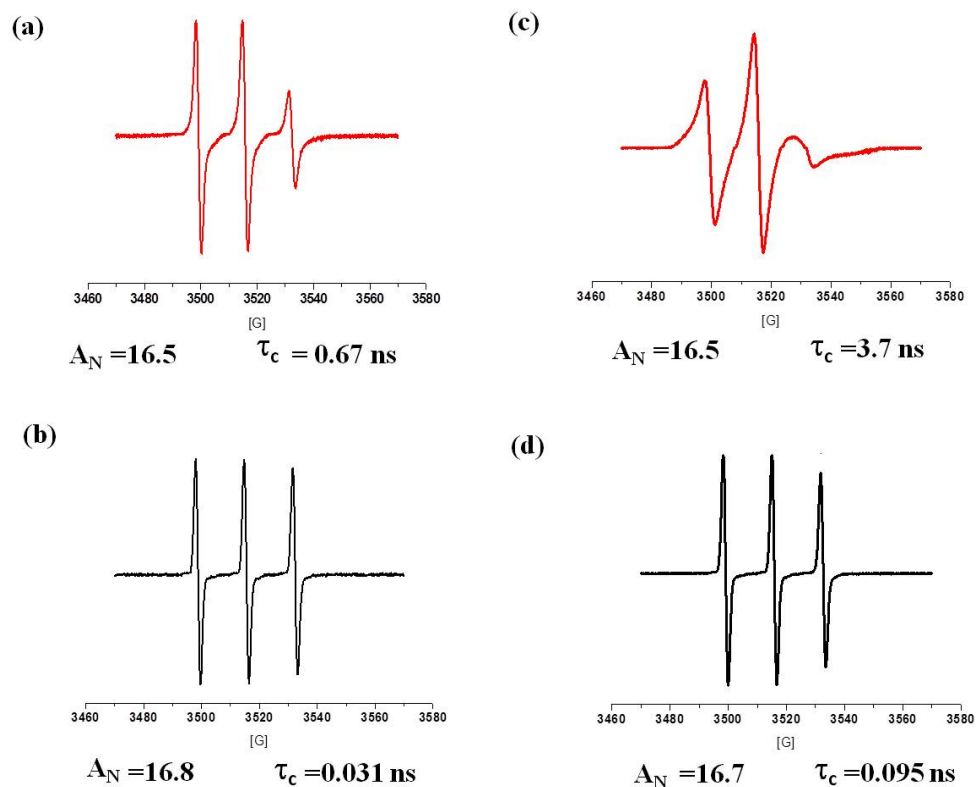
**Figure 8.18** EPR spectra of 4-carboxy-TEMPO in (a) buffer solution, (b) C<sub>5</sub>G1A, (c) C<sub>5</sub>G2A, (d) C<sub>5</sub>G3A. [4-carboxy-TEMPO] = 0.1 mM, [C<sub>5</sub>G1-3A] = 1 mM, [buffer] = 10 mM. Spectra recorded at room temperature.

**Table 8.10** Hyperfine coupling constant and rotational correlation time for 4-carboxy TEMPO in different media.

4-Carboxy TEMPO	$A_N$ [G]	$\tau_c$ [ns]
Buffer	17.10	0.033
G1A	17.10	0.036
G2A	17.10	0.037
G3A	17.05	0.039

Long chain nitroxide radicals have been shown to be very profitable EPR probes in studying the micellization process and the properties of micellar solutions, since the

hydrophobic chain of these nitroxides may be inserted in the hydrophobic core of the micelles.<sup>410-416</sup>



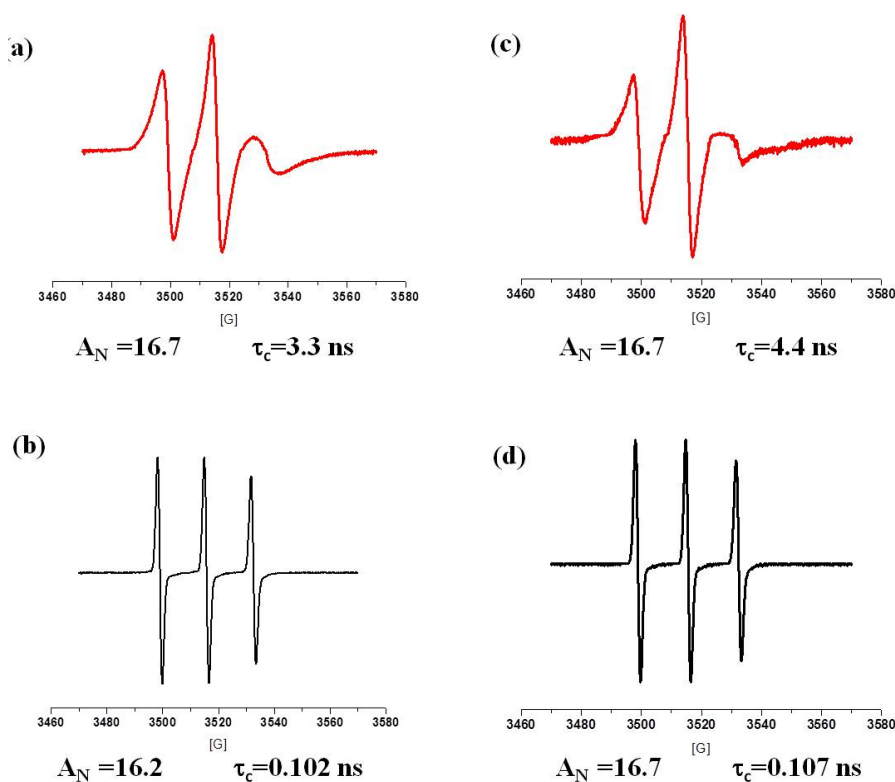
**Figure 8.19** EPR spectra, hyperfine coupling constants and rotational correlation time of (a) CAT-1 in C<sub>5</sub>G3A, (b) CAT-1 in buffer, (c) CAT-8 in C<sub>5</sub>G3A, (d) CAT-8 in buffer. [CAT-1] = 0.01 mM, [CAT-8] = 0.01 mM, [C<sub>5</sub>G1-3A] = 1 mM, [buffer] = 10 mM. EPR spectra recorded at room temperature.

In a previous investigation<sup>405</sup> the CAT-*n* probes were shown to interact with the SBD (Star Burst Dendrimers) surface both at the hydrophilic head groups of the surfactant and with more hydrophobic sites close to the SBD surface. Based on these reports, we anticipated that increasing the length of the alkyl chain of the EPR probe CAT could influence the rotational mobility of the probe. Hence, in this study, four EPR-active cationic nitroxide probes CAT-1, CAT-8, CAT-10 and CAT-12 (**Scheme 8.6**) have been utilized. CAT-10 and CAT-12 probes were investigated to generalize the hypothesis. We chose long chain “cationic” EPR probes because in the previous

experiments we have observed that the cationic probe CAT-1 interacts best with the periphery of the dendrimers. Since the best probe-dendrimer interactions were observed in the case of third generation dendrimer hence we carried out our further studies with C<sub>5</sub>G3A dendrimer.

For comparing of the mobility parameters, the concentrations of both the radicals (0.01 mM) and the C<sub>5</sub>G3A dendrimer were the same for all samples. And to minimize the perturbation effect of the probe, the ratio of concentration was fixed at [CAT-n]/[C<sub>5</sub>G3A] = 1:100. The concentration of the radicals was maintained as low as possible to avoid self-aggregation of the surfactant probes. **Figures 8.19** and **8.20** show the EPR spectra, along with the corresponding hyperfine coupling constants and the rotation correlation time of the probes CAT-n in the absence and presence of the C<sub>5</sub>G3A dendrimers. For comparison, the EPR spectra of the probes CAT-n in buffer solution, in the absence of the dendrimer were also recorded. It can be observed that the high field hyperfine line is significantly broadened when the dendrimer solution is added to the probes CAT-n. Also, in the absence of C<sub>5</sub>G3A, the increase in chain length causes a small decrease (0.031- 0.107 ns) of mobility which is expected since the rotation of the nitroxide group is increasingly hindered as the attached chain grows in length. This effect is strongly enhanced (0.67- 4.4 ns) when C<sub>5</sub>G3A is present. The mobility of CAT-n decreases with increasing n, up to n = 12. Since the positively charged group is always the same and common to all of the probes, the quenching in mobility can only be ascribed to the presence of the hydrophobic chain. The hydrophobic chains may interact with hydrophobic sites in the internal cavities of C<sub>5</sub>G3A dendrimer, and this immediately explains the increase in  $\tau_c$  with the increase in chain length. The hyperfine coupling

constant is observed to be almost same in all the cases, suggesting that the positively charged group of the CAT-n probe prefers to bind to the external periphery of the dendrimer. Hence these experimental results support the conclusion that the probes anchor their chain at internal sites into the C<sub>5</sub>G3A dendrimer. Furthermore, similar results have been observed for cationic surfactants interacting with star burst dendrimers (SBD) and polyanions.<sup>405, 417</sup>



**Figure 8.20** EPR spectra, hyperfine coupling constants and rotational correlation time of (a) CAT-10 in C<sub>5</sub>G3A, (b) CAT-10 in buffer, (c) CAT-12 in C<sub>5</sub>G3A, (d) CAT-12 in buffer. [CAT-1] = 0.01 mM, [CAT-8] = 0.01 mM, [C<sub>5</sub>G1-3A] = 1 mM, [buffer] = 10 mM. EPR spectra recorded at room temperature.

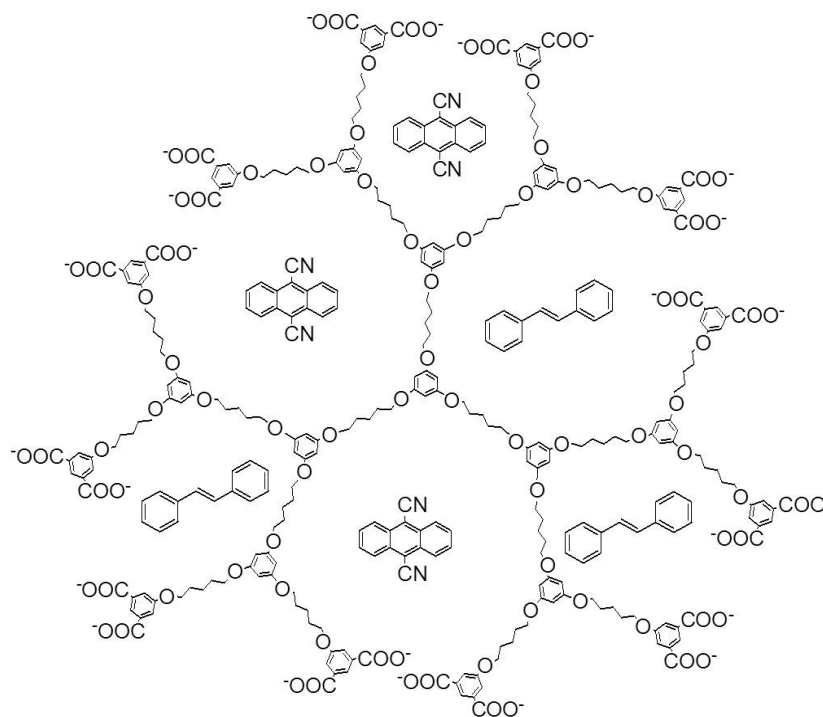
On commencing the studies with C<sub>5</sub>G1A to C<sub>5</sub>G3A dendrimers, we tried to explore C<sub>5</sub>G10-G30 dendrimers (ending with phenolic group). We carried out several experiments, but in all the experiments we observed very broad hyperfine lines. Though considerable concentration of the probe was maintained but the EPR spectra did not seem to be very informative. This observation suggested some kind of quenching of the probe

could be taking place. On exploring the literature we found out that TEMPO can reversibly abstract a hydrogen atom from phenolic-OH groups to form the corresponding hydroxylamine TEMPOH.<sup>418,419</sup> Also, phenols have been widely used as scavengers for free radicals involved in oxidative stress in living organisms. Their chain breaking antioxidant action is based on the trapping of radicals involved in the oxidative chain by efficient hydrogen transfer.<sup>420-422</sup> Hence, this brief study suggested that the phenolic dendrimers seemed to be very strong quenchers of the nitroxide radical probes.

### **8.2.7 Photochemical Isomerizations of Stilbenes Inside Carboxylic acid end group dendrimers (C<sub>n</sub>GA)**

As described in **Section 8.2.4**, in this study too we employed C<sub>5</sub>G3A dendrimers to study the photoinduced electron transfer process taking inside these dendrimers. *Trans*-stilbene was taken as the guest molecule. It was solubilized in sodium borate buffer of the C<sub>5</sub>G3A dendrimers. In this study we chose two well known photoinduced electron transfer (PET) sensitizers- N-methyl Acridinium salt (NMA) and Dicyanoanthracene (DCA).<sup>423</sup> This led us to investigate the system in two scenarios. First, when the PET sensitizer is encapsulated inside the internal hydrophobic cavities of the dendrimers, and secondly, where the PET sensitizer could attach itself to the polar periphery of the dendrimers. The experiments were performed in aqueous dendrimers solutions (pH ~10, aq NaOH) upon encapsulation of stilbene. After purging with N<sub>2</sub>(g) for 30 min, the solutions in Pyrex test tubes were irradiated using a medium-pressure Hg lamp for 3 h and extracted with chloroform, and the products were analyzed by gas chromatography. As a comparison, irradiations were also conducted in acetonitrile solution in the absence of the dendrimer.

Stilbenes dimerize in aqueous solutions, probably due to aggregation, to afford cyclobutane.<sup>393</sup> But in none of the irradiations did tetraphenylcyclobutane, resulting from [2 + 2] cycloaddition, formed, suggesting that stilbene molecules were confined to the hydrophobic interior of dendrimers. Also, it is well-known that photoinduced electron transfer of stilbene in organic solvents favors the *trans*-isomer.<sup>394-396</sup>



**Figure 8.21** Interaction of carboxylic acid functionalized third generation dendrimer with Dicyanoanthracene and *trans*-stilbene.

**Table 8.11** Isomerization of *trans*-Stilbene in Aqueous Dendrimer Solutions and in CH<sub>3</sub>CN.

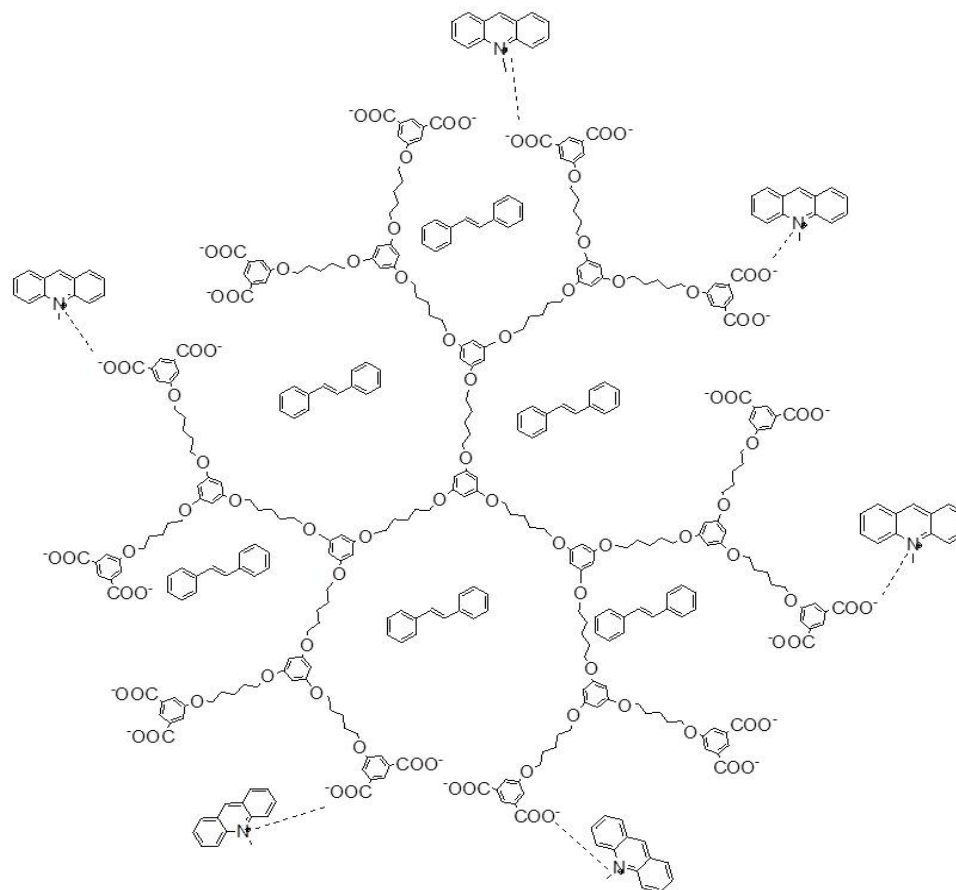
Media	Sensitizer	<i>trans</i> -Stilbene (%)	<i>cis</i> -Stilbene (%)
C <sub>5</sub> G3A	DCA	90	10
CH <sub>3</sub> CN	DCA	98	2
C <sub>5</sub> G3A	NMA	95	5
CH <sub>3</sub> CN	NMA	99	1



First, we analyzed the case where we took DCA as the PET sensitizer. DCA unlike water soluble PET sensitizers like CVP and NMA, being non-polar in nature likes to reside in hydrophobic region of the dendrimers. A cartoon representation of the *trans*-stilbene and DCA in dendrimer is shown in **Figure 8.21**. First we carried out the DCA-sensitized isomerization of *trans*-stilbene in acetonitrile and showed that it favors the *trans*-isomer. As indicated in **Table 8.11**, consistent with literature reports, DCA sensitization gave only 1% of *cis*-isomer in acetonitrile without the presence of a dendrimer. Selective excitation of the sensitizer in the presence of *trans*-stilbene<sup>398</sup> was conducted for 3 h using a Corning 400 nm filter. DCA sensitized irradiation of *trans*-stilbene led to 10% of *cis*-stilbene. **Table 8.11** lists the relative percentages of *cis*- and *trans*-stilbenes encapsulated within C<sub>5</sub>G3A dendrimer, obtained after the photosensitized irradiation, in the presence of DCA. One major drawback of this system was that DCA competes with *trans*-stilbene for encapsulation inside the dendrimer. This leads to poor solubilization of the *trans*-stilbene. To overcome this issue, we carried on our experiments with NMA as PET sensitizer.

NMA is positively charged under the given experimental condition, and we propose that it could be attaching itself to the negatively charged periphery of the dendrimer by columbic interactions. Hence, preferring to be in the bulk aqueous solution and posing no competition to the encapsulation of *trans*-stilbene inside the dendrimers. A cartoon representation of this system is shown in **Figure 8.22**. In this case too *trans*-stilbene was the major product when the NMA sensitized irradiation was carried out in acetonitrile in absence of dendrimers (supporting the literature). In the presence of

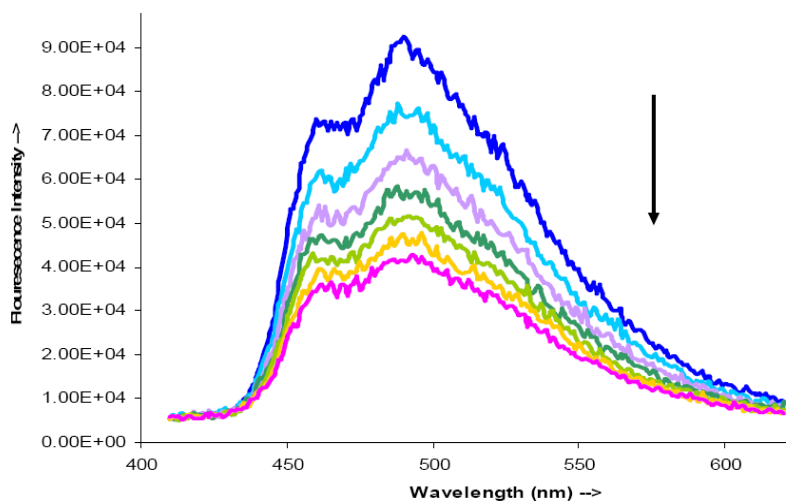
C<sub>5</sub>G3A dendrimers, upon NMA sensitized irradiation, still *trans*-stilbene was in abundance.



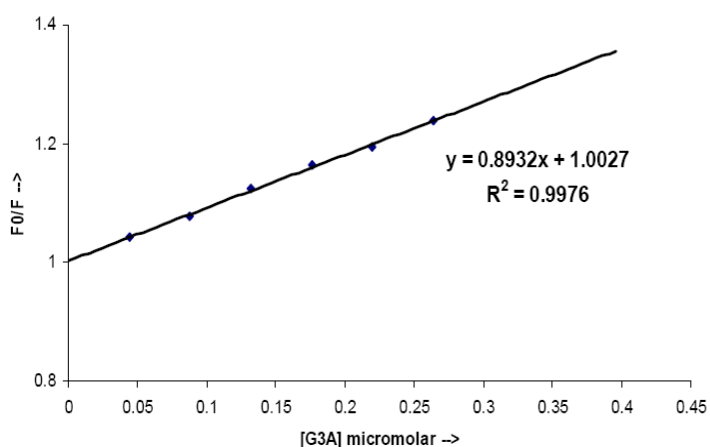
**Figure 8.22** Interaction of carboxylic acid functionalized third generation dendrimer with N-methyl acridinium Iodide (NMA) and *trans*-stilbene.

Though dendrimers having phenolic end groups showed the prominent presence of *cis*-stilbene in almost similar scenario, the carboxylic acid end group dendrimers show the prominence of *trans*-stilbene. This could be due to the fact that the phenolic dendrimers are more hydrophobic than the carboxylic acid dendrimers. In fact the cage effect results suggest that the G-3 phenolic dendrimer is more confining (less open) than the G-3 acid dendrimer. Hence, the snug fit provided by the C<sub>5</sub>G3O dendrimer for the formation of *cis*-stilbene is clearly lacking in the case of C<sub>5</sub>G3A dendrimers.<sup>363</sup> Also, as

was observed in the case of PET occurring in C<sub>5</sub>G3O dendrimers, the oxidation potential of the linker trialkoxybenzene units ( $E_{\text{ox}}$  [TMB = G3(COOH)<sub>24</sub>] = 1.5 V vs SCE), (a similar unit in C<sub>5</sub>G3A dendrimers), is quite close to that of *trans*-stilbene, hence in this case too, the linker units could be mediating the electron-transfer process. In support of this hypothesis, the fluorescence of NMA was monitored with increased addition of dendrimers.



**Figure 8.23** Quenching of Fluorescence of NMA upon addition of dendrimer.



**Figure 8.24** Graph of fluorescence intensity vs. dendrimer concentration to calculate the quenching.

As shown in **Figure 8.23**, addition of C<sub>5</sub>G3A dendrimer resulted in a decrease in NMA fluorescence intensity. Given that the excited singlet energy of the linker unit is

higher than that of NMA, we believe that the quenching is likely to be due to electron transfer from linker units to excited CVP. The Stern–Volmer plot (**Figure 8.24**) due to the above fluorescence quenching showed a linear nature, with a quenching constant of  $3.6 \times 10^{13} \text{ M}^{-1}\text{sec}^{-1}$ .

### 8.3 Conclusion

In this chapter, we have extensively worked towards characterizing the poly alkyl aryl ether dendrimers ending with phenolic and carboxylic groups. Initially, we carried out the studies on poly alkyl aryl ether dendrimers ending with phenolic group, and having various linkers with varying alkyl chain length i.e. from ethyl to pentyl group. We used well known fluorescence probes like pyrene and coumarins to study the inner cavities of the dendrimers and found that higher generation dendrimer with pentyl linker possess most hydrophobic pockets. We utilized solvation dynamics studies to probe the structures of the dendrimers. The picoseconds and femtosecond time resolved experiments with probes C480 and C153 showed that, probe C480 being relatively polar, faces the solvation dynamics of the bulk solvent, suggesting that it prefers to interact with the periphery of the dendrimers whereas C153 being a non polar probe exhibits no solvation dynamics, probably suggesting that it resides in the hydrophobic inner cavities of the dendrimers where no solvent molecules are present.

On the basis of these studies, we were prompted to utilize these dendrimers as micro and nano-reactors. In this line of actions, we carried out two well known photo-reactions in presence of these dendrimers. First being the photolysis of di-benzyl ketones. These reactions showed that the higher generation pentyl linked dendrimers had maximum cage effect and hence could act as efficient hydrophobic micro or nano-

reactors. The second class of reactions we carried out were isomerization of stilbenes by direct irradiation as well as by photoinduced electron transfer pathways. In both the cases it was observed that, the hydrophobic closed packed inner cavities of the dendrimers play an important role in these reactions. Since, as opposed to the solvent photochemistry, formation of phenanthrene and *cis*-stilbene were preferred inside the dendrimers.

In order to make the poly alkyl aryl dendrimers ending with phenolic group more water soluble under normal experimental conditions these dendrimers were synthetically modified to the dendrimers ending with the carboxylic end groups. We initially characterized these dendrimers with the help of UV-visible and fluorescence spectroscopies. It was observed that the  $\lambda_{\max}$  in both the cases coincided with the  $\lambda_{\max}$  of the peripheral molecule (1-methoxyisophthalic acid). Also, EPR spectroscopy was also utilized to elucidate the structures of these dendrimers. The EPR experiments showed that cationic probe CAT-1 binds well with the negatively charged periphery of these dendrimers, whereas, neutral probe TEMPO remained indifferent to the proximity of the dendrimers and anionic probe 4-carboxy TEMPO showed columbic repulsion from the periphery of the dendrimers. Also, the study including long chain cationic radical probes CAT-n with the dendrimers showed that these dendrimers possessed hydrophobic inner cavities, which can preferably accommodate the long alkyl chain of these probe molecules. We expect, theoretical EPR calculations would prove to be supportive to these experiments. As in the earlier case, after characterization of the dendrimers, we proceeded to employ them as molecular vessels to carry out photoreactions. In this case, we probed photoinduced electron transfer isomerization of *trans*-stilbene in presence of two different PET sensitizers- dicynoanthracene (DCA) and N-methyl acridinium iodide

(NMA). In both the cases, the results were not as remarkable as were in the case of dendrimers ending with phenolic groups. This study supporting the previous studies,<sup>363</sup> supported the fact that the dendrimers ending with carboxylic end groups are more “open” in nature and hence could not give as much product selectivity as was in the case of dendrimers ending with the phenolic group.

We expect that the studies on dendrimers hold a very promising future, since the high level of control over the architecture of dendrimers, their size, shape, branching length and density, and their surface functionality, makes these compounds ideal carriers in biomedical applications such as drug delivery, gene transfection and imaging. The bioactive agents may either be encapsulated into the interior of the dendrimers or they may be chemically attached or physically adsorbed onto the dendrimer surface, with the option to tailor the properties of the carrier to the specific needs of the active material and its therapeutic applications. Furthermore, the high density of surface groups allows attachment of targeting groups as well as groups that modify the solution behavior or toxicity of dendrimers.

## 8.4 Experimental Section

**Encapsulation of Pyrene in Dendritic Interior:** A solution of dendrimer (2  $\mu\text{mol}$ ) and pyrene (5 mg) in THF (1 mL) was prepared, and the solvent was removed in *vacuo*. The resulting residue was added with aq. NaOH (1.1 molar equiv per hydroxyl group) solution (10 mL) (pH  $\sim$ 10), the mixture was stirred for 12 h in the dark, filtered (0.45  $\mu$ ), and extracted with PhMe (4 - 5 mL), and the organic portion was evaporated in *vacuo*. The resulting residue was dissolved in EtOH (3mL), and the amount of pyrene was determined by UV-vis spectroscopy ( $\epsilon_{335} 50,734 \text{ mol}^{-1} \text{ cm}^{-1}$ ).

**Fluorescence Measurements:** Fluorescence spectra were recorded at room temperature on an steady-state fluorimeter. The concentrations of the probes were [C1] and [C480] = 0.02 mM, and [C153] = 0.04mM in water. The excitation wavelength for C480 and C1 was 375 nm, and for C153 it was 400 nm. A stock solution of the dendrimer (10mM) was prepared in aq. NaOH (100mM). These dendrimer solutions were added step-by-step to an aq. solution of coumarins. Each consecutive step was 1 mol equiv to the probe concentration. The dendrimer solution was added until no further change in the spectra could be observed. The concentration of pyrene was 0.01 mM, and the excitation wavelength was 335 nm. The required amount of pyrene was taken in a test tube, 3 mL of 0.2 mM dendrimer solution was added to it, and the mixture was stirred for 24 h. The solutions were filtered, nitrogen was purged for 30 min, and the fluorescence spectra were recorded at room temperature.

**Solvation dynamics experiments:** These experiments have been carried out in IACS Kolkata, in collaboration with dr. Kankan Bhattacharya. A 10 mM aq. NaOH solution of C5G3O dendrimer was prepared. Laser grade coumarin 480 and C153 were used as received. In femtosecond upconversion setup (FOG 100, CDP) the sample was excited at 375, 405, and 435 nm, respectively, using the second harmonic of a mode-locked Ti:sapphire laser (Tsunami, Spectra Physics), pumped by a 5 W Millennia (Spectra Physics). In order to generate the second harmonic, we used a nonlinear crystal (1 mm BBO,  $\theta = 25^\circ$ ,  $\theta = 90^\circ$ ). The fluorescence emitted from the sample was upconverted in a nonlinear crystal (0.5 mm BBO,  $\theta = 38^\circ$ ,  $\theta = 90^\circ$ ) using the fundamental beam as a gate pulse. The upconverted light is dispersed in a monochromator and detected using photon counting electronics. A cross-correlation function obtained using the Raman scattering

from ethanol displayed a full width at half maximum (fwhm) of 350 fs. The femtosecond transients were fitted using a Gaussian shape for the exciting pulse. The femtosecond transients are fitted keeping the long picoseconds components fixed. To determine the picosecond components, the samples were excited at 375, 405, and 435 nm using picoseconds diode lasers (IBH nanoleds) in an IBH Fluorocube apparatus. The emission was collected at a magic-angle polarization using a Hamamatsu MCP photomultiplier (5000U-09). The time-correlated single photon counting (TCSPC) setup consists of an Ortec 9327 CFD and a Tennelec TC 863 TAC. The data were collected with a PCA3 card (Oxford) as a multichannel analyzer. The typical form of the system response using a liquid scatterer is about 90 ps. The picosecond fluorescence decays were deconvoluted using IBH DAS6 software. All experiments were done at room temperature (293 K). The time-resolved emission spectra (TRES) were constructed using the parameters of best fit to the fluorescence decays and the steady state emission spectrum following the procedure described by Maroncelli and Fleming. The solvation dynamics is described by the decay of the solvent correlation function  $C(t)$ , defined as:  $C(t) = [\nu(t) - \nu(\infty)] / [\nu(0) - \nu(\infty)]$ , where  $\nu(0)$ ,  $\nu(t)$ , and  $\nu(\infty)$  are the emission maxima (frequencies) at time 0,  $t$ , and  $\infty$ , respectively.

**Photolysis of Substrate-Dendrimer Complex:** 1-Phenyl-3-*p*-tolyl- propane-2-one (3) was synthesized as described in the literature. A solution of substrate 3 in  $\text{CHCl}_3$  (4\_10\_4 M) was taken in a test tube, solvents were removed carefully, the residue was added to an aqueous basic solution of dendrimer ( $1 - 10^{-3}$  M) (2-5 mL), and the mixture was stirred in dark for 12 h, while continuously purging with  $\text{N}_2$ . The mixture was filtered through an Acrodisc filter, and the filtrate in a Pyrex tube was irradiated with a 450 W medium-



pressure Hg lamp, while purging with N<sub>2</sub>. Irradiation for 12 h resulted in 30% conversion for substrate 3. Absorption by the dendrimer might have been responsible for the low conversion.

**Extraction of Photoproducts and Reactants from Dendrimer:** After photolysis, the solution was acidified with aq. HCl (10%), extracted with EtOAc/acetonitrile (7:3) solvent mixture, dried (Na<sub>2</sub>SO<sub>4</sub>), concentrated, and analyzed on a gas chromatograph, fitted with an HP-5 column.

**Characterization of Photoproducts:** Peaks in the GC traces were identified by co-injecting with authentic samples that were prepared by solution irradiation. Photoproducts 5 (AA) and 7 (BB) were commercially available. Photoproduct 6 (AB) was identified on the basis of the GC-MS fragmentation pattern. Mass spectral data m/z (relative intensity): 196 (M<sub>b</sub>, 17%), 105 (100%), 91 (12%), 77 (11%). Photoproduct 4 isolated from irradiation was characterized by <sup>1</sup>H NMR spectroscopy and GC mass spectrometry.

**Solubilizations of Stilbene in Aqueous Dendrimer Solutions:** A solution of stilbene (5–7 mg) and CnG3 dendrimer (100 μM) in THF (2 mL) was evaporated. The resulting residue was admixed aq. NaOH solution (5 mL, pH >10), stirred for 12 h in dark at ambient temperature, and filtered (0.45 μm), and the concentration of solubilized guest molecule was analyzed by UV–vis spectroscopy (ε<sub>295</sub> 29000 M<sup>-1</sup> cm<sup>-1</sup> for stilbene; ε<sub>321</sub> 19950 M<sup>-1</sup> cm<sup>-1</sup> for azobenzene).

**Isomerization of Stilbene in Aqueous Dendrimer Solutions:** A solution of stilbene (10 mg) and CnG3 dendrimer (1 mM) in THF (5 mL) was evaporated. The resulting residue

was admixed aq. NaOH solution (10 mL, pH >10), stirred for 12 h in the dark at ambient temperature, and filtered (0.45  $\mu\text{m}$ ). The filtrate was purged with  $\text{N}_2$  (g) for 30 min and subjected to irradiation in a Pyrex tube under a high-pressure Hg lamp (400 W) for 6 h. The solution was extracted in  $\text{Et}_2\text{O}$  ( $3 \times 10$  mL), dried ( $\text{Na}_2\text{SO}_4$ ), concentrated, and analyzed by gas chromatography, using a fused silica column. Peaks were identified by co-injecting with authentic samples.

**Isomerization of Stilbene in Aqueous Dendrimer Solutions in the Presence of CVP:**

*trans*-Stilbene was dissolved in  $\text{CHCl}_3$ , and a known amount was added to a test tube (to make up a final concentration of  $4 \times 10^{-4}$  M).  $\text{CHCl}_3$  was carefully removed, and to this 2–5 mL of a solution of CnG3 dendrimer ( $1 \times 10^{-3}$  M) was added. This solution was stirred in dark for 12 h, while continuously purging  $\text{N}_2$ , and then it was filtered through an Acrodisc filter to remove any floating particles. One milliliter of 1 mM CVP solution in water was added to the above solution. The solution was irradiated while purging  $\text{N}_2$  in a Pyrex tube with a 450 W medium-pressure Hg lamp for 2 h. The solution was extracted in  $\text{Et}_2\text{O}$  ( $3 \times 10$  mL), dried ( $\text{Na}_2\text{SO}_4$ ), concentrated, and analyzed by gas chromatography on a gas chromatograph fitted with an HP-5 column. Peaks in the GC trace were identified by co-injection with authentic samples, which are commercially available.

**UV-visible and Fluorescence Measurements for C<sub>3</sub>GA dendrimers:** UV spectra were recorded on UV-visible spectrophotometer and fluorescence spectra were recorded at room temperature on a steady-state fluorimeter. The concentrations of all the dendrimers from first to third generation and the peripheral molecule was maintained at 0.1 mM. The excitation wavelength for fluorescent experiments was 300 nm. The dendrimers were dissolved in 100 mM of sodium tetraborate buffer solution.

**Isomerization of Stilbene in Aqueous Dendrimer (C<sub>5</sub>G3A) Solutions in the Presence of DCA and NMA:** *trans*-Stilbene was dissolved in CHCl<sub>3</sub>, and a known amount was added to a test tube (to make up a final concentration of  $4 \times 10^{-4}$  M). CHCl<sub>3</sub> was carefully removed, and to this 2–5 mL of a solution of CnG3A dendrimer ( $1 \times 10^{-3}$  M) was added. This solution was stirred in dark for 12 h, while continuously purging N<sub>2</sub>, and then it was filtered through an Acrodisc filter to remove any floating particles. One milliliter of 1 mM NMA solution in water was added to the above solution. The solution was irradiated while purging N<sub>2</sub> in a Pyrex tube with a 450 W medium-pressure Hg lamp for 2 h. The solution was extracted in Et<sub>2</sub>O ( $3 \times 10$  mL), dried (Na<sub>2</sub>SO<sub>4</sub>), concentrated, and analyzed by gas chromatography on a gas chromatograph fitted with an HP-5 column. Peaks in the GC trace were identified by co-injection with authentic samples, which are commercially available. For DCA experiments, DCA was dissolved in CHCl<sub>3</sub>, and a known amount was added to a test tube (to make up a final concentration of  $4 \times 10^{-4}$  M). CHCl<sub>3</sub> was carefully removed, and to this 2–5 mL of a solution of CnG3A dendrimer ( $1 \times 10^{-3}$  M) was added. This solution was stirred in dark for 12 h, while continuously purging N<sub>2</sub>, and then it was filtered through an Acrodisc filter to remove any floating particles. Equal amounts of the dendrimer solutions containing DCA and *trans*-stilbene were admixed and the irradiation was carried out using 400 nm corning filter for 3 hrs. The products were extracted and analyzed as mentioned above.

## References

1. Ramamurthy, V., Turro N. J., *Chemical Reviews*, **93**, 2 (1993).
2. Pape M., BASF AG, *Hauptlaboratorium*, (1975).
3. Chan B. P., *Tissue Engineering: Part B* **16**, 5, 509-522, (2010)
4. Clausen M., *Chemie in unserer Zeit*, **7**, 141, (1973).
5. Janistyn H., *Handbuch der Kosmetika und Riechstoffe*, **III**, 708, (1973).
6. Data provided by Quarzlampen Gesellschaft, Hanau (1974).
7. Ohloff F., Klein E., Schenck G. O., *Angew. Chem.*, **73**, 578, (1961).
8. Warashina T., Kai T., *Japan Plastics Age*, **19** (1972).
9. Moss T., Dimitrov S. I., Houde D., *Methods* **11**, 225, (1997).
10. Ifkovits J. L., Burdick J. A., *Tissue Eng.* **13**, 2369, (2007).
11. Nguyen K. T., West J. L., *Biomaterials*, **23**, 4307, (2002).
12. (a) Lehn, J. M., Atwood, J. L., Davies, J. E. D., MacNicol, D. D., Vogtle, F., *Series Ed. Comprehensive Supramolecular Chemistry* ; Pergamon: New York, (1996). (b) Lehn, J.-M. *Supramolecular Chemistry* ; VCH: Weinheim, (1995).
13. (a) Lehn, J. M. *Science*, **260**, 1762-1763 (1993). (b) Lehn, J. M. *Angew. Chem., Int. Ed. Engl.*, **29**, 1304 – 1319 (1990). (c) Lehn, J.-M. *Angew. Chem., Int. Ed. Engl.*, **27**, 89 – 112 (1988). (d) Lehn, J.-M. *Science*, **227**, 849 – 856 (1985). (e) Lehn, J.-M. *Pure Appl. Chem.*, **50**, 871 – 892 (1978).
14. For general reviews on supramolecular chemistry, see: (a) Fyfe, M. C. T.; Soddart, J. F. *Acc. Chem. Res.*, **30**, 393 – 401 (1997). (b) Chapman, R. G.; Sherman, J. C. *Tetrahedron*, **53**, 15911 – 15945 (1997). (c) Whitesides, G. M.; Simanek, E. E.; Mathias, J. P.; Seto, C. T.; Chin, D. N.; Mammen, M.; Gordon, D. M. *Acc. Chem. Res.*, **28**, 37 – 44 (1995) (d) Mascial, M. *Contemp. Org. Synth.*, **1**, 31 – 46, (1994).
15. Desiraju, G. R. *Angew. Chem., Int. Ed. Engl.*, **34**, 2311 – 2327 (1995). Mammen, M.; Gordon, D. M. *Acc. Chem. Res.*, **28**, 37 – 44 (1995). (d) Mascial, M. *Contemp. Org. Synth.*, **1**, 31 - 46 (1994).
16. Hamasaki, K. Uneo, A. Toda, F. *J. Chem. Soc. Chem. Commun.*, 331-333 (1993).
17. Bates, P.S. Katakya, R., Parker, D.J. *Chem. Soc. Perkin Trans. 2*, 669-675, (1994).

18. Breslow, R. Graff, A. *J. Am. Chem. Soc.*, **115**, 10988-10989, (1993).
19. Andersson, T., Nillson, K., Sundhal, M., Westman, G, Wennerstrom, O. *J. Chem. Soc. Chem. Commun.*, 604-606, (1992).
20. Litzinger, D. C. Huang, L. *Biochem. Biophys. Acta*, **1113**, 201-207, (1992).
21. Atik, s.s., Thomas, J. K. *J. Am. Chem. Soc.*, **103**, 3543-3550, (1981).
22. Chapman, R. G.; Sherman, J. C. *Tetrahedron*, **53** , 15911 – 15945, (1997).
23. Conn, M. M.; Rebek, J., Jr. *Chem. Rev.*, **97**, 1647 – 1668, (1997).
24. (a) Maverick, E.; Cram, D. J. *In Comprehensive Supramolecular Chemistry*; Lehn, J.-M., Atwood, J. L., Davies, J. E. D., MacNicol, D. D., Vogtle, F., Series Ed.; Pergamon: New York; Vol.2, 367-418, (1996). (b) Cram, D. J.; Cram, J. M. *Container Molecules and Their Guests*; Royal Society of Chemistry: Cambridge, (1994); Vol. 4. (c) Sherman, J. C. *In Large Ring Molecules*; Semlyen, J.A., Ed.; J. Wiley & Sons: West Sussex, England, (1996); 507-524. (d) Sherman, J. C. *Tetrahedron*, **51**, 3395-3422, (1995).
25. (a) Rudkevich, D. M.; Hilmersson, G.; Rebek, J., Jr. *J. Am. Chem. Soc.*, **119**, 9911-9912, (1997). (b) Boerrigter, H.; Verboom, W.; Reinhoudt, D. N. *J. Org. Chem.*, **62**, 7148-7155, (1997). (c) Timmerman, P.; Verboom, W.; Reinhoudt, D. N. *Tetrahedron*, **52**, 2663-2704, (1996). (d) von dem Bussche-Hunnefeld, C.; Helgeson, R. C.; Buhlig, D.; Knobler, C. B.; Cram, D. J. *Croat. Chem. Acta*, **69**, 447-458, (1996). (e) Schierbaum, K. D.; Weiss, T.; Thoden van Velzen, E. U.; Engbersen, J. F. J.; Reinhoudt, D. N.; Gopel, W. *Science*, **265**, 1413-1415, (1994).
26. (a) Cram, D. J. *Science*, **219**, 1177-1183, (1983). (b) Cram, D. J. *Nature*, **356**, 29-36, (1992).
27. (a) Bonar-Law, R. P.; Sanders, J. K. M. *J. Am. Chem. Soc.*, **117**, 259-271, (1995). (b) Bonar-Law, R. P.; Sanders, J. K. M. *Tetrahedron Lett.*, **34**, 1677-1680, (1993).
28. (a) Whang, D.; Heo, J.; Park, J. H.; Kim, K. *Angew. Chem., Int. Ed.* **37**, 78-80, (1998). (b) Jeon, Y.-M.; Kim, J.; Whang, D.; Kim, K. *J. Am. Chem. Soc.*, **118**, 9790-9791, (1996).
29. (a) Breslow, R. *Acc. Chem. Res.*, **28**, 146-153, (1995). (b) Easton, C. J.; Lincoln, S. F. *Chem. Soc. Rev.*, **25**, 163-170, (1996). (c) Szejtli, J. *Cyclodextrins and Their Inclusion Complexes*; Akademiai Kiado: Budapest, (1982). (d) Bender, M. L.; Komiyama, M. *Cyclodextrin Chemistry*; Springer-Verlag: New York, (1978).

30. For lead references and an overview, see: (a) Ikeda, A.; Shinkai, S. *Chem. Rev.*, **97**, 1713-1734, (1997). (b) Bohmer, V. *Angew. Chem., Int. Ed. Engl.* **34**, 713-745, (1995). (c) Gutsche, C. D. *Adi Chim. Acta*, **28**, 3-9, (1995).
31. Rebek, J., Jr. *Chem. Soc. Rev.*, **25**, 255-264, (1996).
32. Deisenhofer, D. ; Huber, R. ; Michel, H. *Nobel Prize in Chemistry*, (1988).
33. Cram, D. J.; Tanner, M. E.; Thomas, R. *Angew. Chem., Int. Ed. Engl.*, **30**, 1024-1027, (1991).
34. Rao, V. P.; Turro, N. J.; *Tetrahedron Lett.*, **30**, 4641, (1989).
35. Yoshizawa M., Takeyama Y., Kusukawa T., Fujita M.. *Angew. Chem., Int. Ed.* **41**, 1347 (2002).
36. Natarajan, A., Kaanumalle, L. S., Jockusch, S., Gibb, C. L. D., Gibb, B. C., Turro, N. J., Ramamurthy, V., *J. Am. Chem. Soc.*, **129**, 4132-4133, (2007).
37. Kalayansundaram, K., Grieser, F., Thomas, J. K., *Chem. Phys. Lett.*, **51**, 501-505, (1997).
38. Scypinski S., Love C. L. J., *Anal. Chem.* **56**, 322, (1984).
39. Ramamurthy, V., Caspar J. V., Eaton D.F., Kuo E. W., Corbin D. R., *J. Am. Chem. Soc.* **114**, 3882, (1992).
40. D. Ginsberg, G. M. J. Schmidt, *Solid State Photochemistry*, Verlag Chemie, New York, (1976).
41. Cohen M. D., *Angew. Chem.*, **87**, 439-447, (1975); *Angew. Chem. Int. Ed. Engl.*, **14**, 386-393, (1975).
42. Turro N. J., Ramamurthy V., Scaiano J. C., *Modern Molecular Photochemistry of Organic Molecules*, University Science Books, Sausalito, CA, (2010).
43. (a) Ramamurthy V., Weiss R. G., Hammond G. S. in *Advances in Photochemistry* (Eds.: Volman D. H., Hammond G. S., Neckers D. C.), Wiley-Interscience, New Jersey, 67-234, (1993); (b) Weiss R. G., Ramamurthy V., Hammond G. S., *Acc. Chem. Res.*, **26**, 530-536, (1993).
44. Ramamurthy V., Parthasarathy, A. *Isr. J. Chem.*, **51**, 817-829, (2011).
45. (a) Meyer E. A., Castellano R. K., Diederich F., *Angew. Chem.*, **115**, 1244-1287, (2003); *Angew. Chem. Int. Ed.*, **42**, 1210-1250, (2003).

46. C. L. D. Gibb, B. C. Gibb, *J. Am. Chem. Soc.*, **126**, 11408–11409, (2004).
47. Gupta, S., Choudhury, R., Krois, D., Wagner, G., Brinker, U. H. Ramamurthy, V. *Org. Lett.*, **13**, , 6074-6077, (2011).
48. Sundaresan, A. K.; Ramamurthy, V. *Photochem. Photobiol. Sci.*, **7**, 155–1564, (2008).
49. Natarajan, A.; Kaanumalle, L. S.; Jockusch, S.; Gibb, C. L. D.; Gibb, B. C.; Turro, N. J.; Ramamurthy, V. *J. Am. Chem. Soc.*, **129**, 4132–4133, (2007).
50. Sundaresan, A. K.; Ramamurthy, V. *Org. Lett.*, **9**, 3575–3578, (2007)
51. Porel, M., Jayaraj, N., Kaanumalle, L. S., Maddipatla, M. V. S. N., Parthasarathy, A., Ramamurthy V. *Langmuir*, **25**, 3473-3481, (2009).
52. Jayaraj, N., Zhao, Y., Parthasarathy, A., Porel, M., Liu, R. S. H., Ramamurthy, V., *Langmuir*, **25**, 10575–10586, (2009).
53. Kulasekharan, R., Jayaraj, N., Porel, M., Choudhury, R., Sundaresan, A. K., Parthasarathy, A., Ottaviani, M. F., Jockusch, S., Turro, N. J., Ramamurthy, V. *Langmuir*, **26**, 6943–6953, (2010).
54. Kaanumalle, L.S., Ramamurthy, V. *Chem. Commun.*, 1062–1064, (2007).
55. Parthasarathy, A., Samanta, S. R., Ramamurthy, V. *Res Chem Intermed* **39**, 73–87, (2013).
56. Sundaresan, A.K., Gibb, C. L. D., Gibb, B. C., Ramamurthy, V., *Tetrahedron* **65**, 7277–7288, (2009).
57. Sundaresan, A. K., Kaanumalle, L.S., Gibb, C. L. D., Gibb, B. C., Ramamurthy, V., *Dalton Trans.*, 4003–4011, (2009).
58. Kulasekharan, R., Maddipatla, V. S. N., Parthasarathy, A., Ramamurthy, V. *J. Org. Chem.*, **78**, 942–949, (2013).
59. Parthasarathy, A., Kaanumalle, L.S., Ramamurthy, V., *Org. Lett.*, **9**, 5059-5062, (2007).
60. Samanta S. R., Parthasarathy A., Ramamurthy V. *Photochem. Photobiol. Sci.*, **11**, 1652–1660, (2012).
61. Baldrige, A.; Samanta, S. R.; Jayaraj, N.; Ramamurthy, V.; Tolbert, L. M. *J. Am. Chem. Soc.*, **132**, 1498, (2010).



62. Baldrige, A.; Samanta, S. R.; Jayaraj, N.; Ramamurthy, V.; Tolbert, L. M. *J. Am. Chem. Soc.*, **133**, 712, (2011).
63. Jayaraj, N.; Maddipatla, M. V. S. N.; Prabhakar, R.; Jockusch, S.; Turro, N. J.; Ramamurthy, V. *J. Phys. Chem. B*, **114**, 14320, (2010).
64. Choudhury, R., Gupta, S., Da Silva, J. P., Ramamurthy, V. *J. Org. Chem.*, **78**, 1824–1832, (2013).
65. Porel, M., Chuang, C., Burda, C., Ramamurthy, V. *J. Am. Chem. Soc.*, **134**, 14718–14721, (2012).
66. Gupta, S., Adhikari, A., Mandal, A. K., Bhattacharyya, K., Ramamurthy, V. *J. Phys. Chem. C*, **115**, 9593–9600, (2011).
67. R. Behrend, E. Meyer and F. Rusche, *Justus Liebigs Ann. Chem.*, **339**, 1–37, (1905).
68. Freeman W. A., Mock W. L., Shih N. Y., *J. Am. Chem. Soc.*, **103**, 7367–7368, (1981).
69. Kim J., Jung I. S., Kim S. Y., Lee E., Kang J. K., Sakamoto S., Yamaguchi K., Kim K., *J. Am. Chem. Soc.*, **122**, 540–541, (2000).
70. Day A., Arnold A. P., Blanch R. J., Snushall B., *J. Org. Chem.*, **66**, 8094–8100, (2001).
71. Day A. I., Blanch R. J., Arnold A. Lorenzo P., S., Lewis G. R., Dance I., *Angew. Chem., Int. Ed.*, **41**, 275–277, (2002).
72. J. Lagona, P. Mukhopadhyay, S. Chakrabarti and L. Isaacs, *Angew. Chem., Int. Ed.*, **44**, 4844–4870, (2005).
73. (a) Lee J. W., Samal S., Selvapalam N., Kim H.-J., Kim K., *Acc. Chem. Res.*, **36**, 621–630, (2003); (b) Lagona J., Mukhopadhyay P., Chakrabarti S., Isaacs L., *Angew. Chem., Int. Ed.*, **44**, 4844–4870, (2005).
74. Marquez C., Hudgins R. R., Nau W. M., *J. Am. Chem. Soc.*, **126**, 5806–5816, (2004).
75. Mohanty J., Nau W. M., *Angew. Chem., Int. Ed.*, **44**, 3750–3754, (2005).
76. Nau W. M., Mohanty J., *Int. J. Photoenergy*, **7**, 133–141, (2005).
77. Bhasikuttan A. C., Mohanty J., Nau W. M., Pal H., *Angew. Chem., Int. Ed.*, **46**, 4120–4122, (2007).

78. Buschmann H. J., Jansen K. Schollmeyer E., *Thermochim. Acta*, , **317**, 95–98, (1998).
79. Buschmann H. Schollmeyer J., E., Mutihac L., *Thermochim. Acta*, **399**, 203–208, (2003).
80. Bush M. E., Bouley N. D. Urbach A. R., *J. Am. Chem. Soc.*, **127**, 14511–14517, (2005).
81. Heitmann L. M., Taylor A. B. Hart, P. J., Urbach A. R., *J. Am. Chem. Soc.*, , **128**, 12574–12581, (2006).
82. Rekharsky M. V., Yamamura H., Ko Y.H., Selvapalam N., Kim K., Inoue Y., *Chem. Commun.*, 2236–2238, (2008).
83. Reczek J. J., Kennedy A. A., Halbert B. T., Urbach, A. R. *J. Am. Chem. Soc.*, **131**, 2408–2415, (2009).
84. Hennig A., Bakirci H., Nau W. M., *Nat.Methods*, **4**, 629–632, (2007).
85. Nau W. M., Ghale G., Hennig A., Bakirci H., Bailey D. M., *J. Am. Chem. Soc.*, **131**, 11558–11570, (2009).
86. Florea M., Nau W. M., *Org. Biomol. Chem.*, (2010).
87. Bailey D. M., Hennig A., Uzunova V. D. Nau W.M., *Chem.–Eur. J.*, **14**, 6069–6077, (2008).
88. Hennig A., Ghale G., Nau W. M., *Chem. Commun.*, 1614– 1616, (2007).
89. Wyman I., Macartney D., *J. Org. Chem.*, **74**, 8031–8038, (2009).
90. Hwang I., Baek K., Jung M., Kim Y., Park K. M., Lee D. W., Selvapalam N., Kim K., *J. Am. Chem. Soc.*, **129**, 4170–4171, (2007).
91. S. Liu, P. Y. Zavalij, Y. F. Lam and L. Isaacs, *J. Am. Chem. Soc.*, **129**, 11232–11241, (2007).
92. Nau W. M., J. Mohanty, *Int. J. Photoenergy*, **7**, 133–141, (2005).
93. Mohanty J., Nau W. M., *Angew. Chem., Int. Ed.*, **44**, 3750– 3754, (2005).
94. Koner A. L., Nau W. M., *Supramol. Chem.*, **19**, 55–66, (2007).

95. Bhasikuttan A. C., Mohanty J., Nau W. M., Pal H., *Angew. Chem., Int. Ed.*, , **46**, 4120–4122, (2007).
96. Shaikh M., Mohanty J., Bhasikuttan A. C., Uzunova V. D., Nau W.M., Pal H., *Chem. Commun.*, 3681–3683, (2008).
97. Li, S.; Purdy, W. C. *Chem. Rev.*, **92**, 1457-1490, (1992).
98. Szejtli, L. *Cyclodextrin Technology*; Kluwer Academic: Dordrecht, The Netherlands, (1988).
99. Bender, M. L.; Komiyama, M. *Cyclodextrin Chemistry*; Springer-Verlag: Berlin, (1978).
100. Lehn, J. M. *Supramolecular Chemistry*; VCH: Weinheim, Germany, (1995).
101. Bergeron, R. J. In *Inclusion Compounds*; Atwood, J. L., Davies, J. E. D., MacNicol, D. D., Eds.; Academic: London; Vol. 3, 391-443, (1984).
102. Cramer, F. *Einschlussverbindungen*; Springer: Berlin, (1954).
103. Saenger, W. In *Inclusion Compounds*; Atwood, J. L., Davies, J. E. D., MacNicol, D. D., Eds.; Academic Press: London; Vol. 2, 231-259, (1984).
104. Halle'n, D.; Scho'n, A.; Shehatta, I.; Wadso", I. *J. Chem. Soc., Faraday Trans.*, **88**, 2859-2863, (1992).
105. Rekharsky, M. V.; Mayhew, M. P.; Goldberg, R. N.; Ross, P. D.; Yamashoji, Y.; Inoue, Y.; *A J. Phys. Chem.*, **101**, 87-100, (1997).
106. Ross, P. D.; Rekharsky, M. V. *Biophys. J.*, **71**, 2144-2154, (1996).
107. Matsui, Y.; Mochida, K. *Bull. Chem. Soc. Jpn.*, **52**, 2808- 2814, (1979).
108. Rekharsky, M. V.; Schwarz, F. P.; Tewari, Y. B.; Goldberg, R. N.; Tanaka, M.; Yamashoji, Y. *J. Phys. Chem.*, **98**, 4098- 4103, (1994).
109. Rekharsky, M. V.; Goldberg, R. N.; Schwarz, F. P.; Tewari, Y. B.; Ross, P. D.; Yamashoji, Y.; Inoue, Y. *J. Am. Chem. Soc.*, **117**, 8830-8840, (1995).
110. Inoue, Y.; Hakushi, T.; Liu, Y.; Tong, L.-H.; Shen, B.-J.; Jin, D.- S. *J. Am. Chem. Soc.*, **115**, 475-481, (1993).
111. Wood, D. J.; Hruska, F. E.; Saenger, W. *J. Am. Chem. Soc.*, **99**, 1735-1740, (1977).

112. Hamilton, J. A.; Sabesan, M. N.; Steirauf, L. K.; Geddes, A. *Biochem. Biophys. Res. Commun.* **73**, 659-664, (1976).
113. Barone, G.; Castronuovo, G.; Del Vecchio, P.; Elia, V.; Muscetta, M. *J. Chem. Soc., Faraday Trans. 1*, **82**, 2089-2101, (1986).
114. Fujiwara, H.; Arakawa, H.; Murata, S.; Sasaki, Y.; *Bull. Chem. Soc. Jpn.*, **60**, 3891-3894, (1987).
115. Saenger, W. *Angew. Chem., Int. Ed. Engl.*, **19**, 344-362, (1980).
116. Sanemasa I.; Osajima, T.; Deguchi, T. *Bull. Chem. Soc. Jpn.*, **63**, 2814-2818, (1990).
117. Harrison, J. C.; Eftink, M. R. *Biopolymers*, **21**, 1153-1166, (1982).
118. Tabushi, I.; Kiyosuke, Y.; Sugimoto, T.; Yamamura, K. *J. Am. Chem. Soc.*, **100**, 916-919, (1978).
119. Szejtli, J. In *Inclusion Compounds. Volume 3: Physical Properties and Applications*; Adwood, J. L., Davies, J. E. D., MacNicol, D. D., Eds.; Academic: New York, 331-390, (1984).
120. Schurig, V.; Jung, M., Recent Advances in Chiral Separations, *Proceedings of the Chromatography Society International Symposium Chiral Separation, 2nd Meeting*; Stevenson, D.; Wilson, I. D., Eds.; Plenum: New York; 117-133, (1991).
121. Amato, M. E.; Djedaini-Pilard, F.; Perly, B.; Scarlata, G. *J. Chem. Soc., Perkin Trans. 2*, 2065-2069, (1992).
122. Berthod, A.; Li, W.; Armstrong D. W. *Anal. Chem.* **64**, 873- 879, (1992).
123. Yamashoji, Y.; Ariga, T.; Asano, S.; Tanaka, M. *Anal. Chim. Acta*, **268**, 39-47, (1992).
124. Wishnia, A.; Lappi, S. J. *J. Mol. Biol.*, **82**, 77-89, (1974).
125. Tucker, E. E.; Christian, S. D. *J. Am. Chem. Soc.*, **106**, 1942-1945, (1984).
126. Sasaki, K. J.; Christian, S. D.; Tucker, E. E. *Fluid Phase Equilib.*, **49**, 281-289, (1989).
127. Andini, S.; Castronuovo, G.; Elia, V.; Gallotta, E. *Carbohydr. Res.*, **217**, 87-97, (1991).
128. Rekharsky, M. V.; Schwarz, F. P.; Tewari, Y. B.; Goldberg, R. N. *J. Phys. Chem.*, **98**, 10282-10288, (1994).

129. Bastos, M.; Briggner, L.-E.; Shehatta, I.; Wadso, I. *J. Chem. Thermodyn.*, **22**, 1181-1190, (1990).
130. Kinoshita, T.; Iinuma, F.; Tsuji, A. *Chem. Pharm. Bull.*, **22**, 2413-2420, (1974).
131. Castronuovo, G.; Elia, V.; Fessas, D.; Giordano, A.; Velleca, F. *Carbohydr. Res.*, **272**, 31-39, (1995).
132. Mwakibete, H.; Bloor, D. M.; Wyn-Jones, E. *J. Inclusion Phenom. Mol. Recognit. Chem.*, **10**, 497-505, (1991).
133. Danil de Namor, A. F.; Blackett, P. M.; Cabaleiro, M. C.; Al Rawl, J. M. A. *J. Chem. Soc., Faraday Trans.*, **90**, 845-847, (1994).
134. Lin, S.-F.; Connors, K. A. *J. Pharm. Sci.*, **72**, 1333-1338, (1983).
135. Bertrand, G. L.; Faulkner, J. R.; Han, S. M.; Armstrong, D. W. *J. Phys. Chem.*, **93**, 6863-6867, (1989).
136. Hilbers, H. W.; Jansen, A. C. A.; Janssen, L. H. M. In *Proceedings of 5th Minutes International Symposium on Cyclodextrins*; Puchene, J., Ed.; Sante: Paris, 213-216, (1990).
137. Yoshida, N.; Seiyama, A.; Fujimoto, M. *J. Phys. Chem.*, **94**, 4246-4253, (1990).
138. Cramer, F.; Saenger, W.; Spatz, H.-C. *J. Am. Chem. Soc.*, **89**, 14-20, (1967).
139. Danil de Namor, A. F.; Traboulssi, R.; Lewis, D. F. V. *J. Am. Chem. Soc.*, **112**, 8442-8447, (1990).
140. Yoshida, N.; Seiyama, A.; Fujimoto, M. *Chem. Lett.*, 703-706, (1984).
141. Connors, K. A.; Lin, S.-F.; Wong, A. B. *J. Pharm. Sci.*, **71**, 217-222, (1982).
142. Wong, A. B.; Lin, S.-F.; Connors, K. A. *J. Pharm. Sci.*, **72**, 388-390, (1983).
143. Connors, K. A.; Paulson, A.; Toledo-Velasquez, D. *J. Org. Chem.*, **53**, 2023-2026, (1988).
144. Orienti, I.; Fini, A.; Bertasi, V.; Zecchi, V. *Eur. J. Pharm. Biopharm.*, **37**, 110-112, (1991).
145. Menard, F. A.; Dedhiya, M. G.; Rhodes, C. T. *Drug Dev. Ind. Pharm.*, **16**, 91-113, (1990).

146. Miyaji, T.; Kurono, Y.; Uekama, K.; Ikeda, K. *Chem. Pharm. Bull.*, **24**, 1155-1159, (1976).
147. Min, S. H. *J. Pharm. Soc. Korea*, **15**, 8-15, (1971).
148. Hardee, G. E.; Otagiri, M.; Perrin, J. H. *Acta Pharm. Suec.*, **15**, 188-199, (1978).
149. Baeyer, A.: Ueber die verbindungen der aldehyde mit denphenolen. *Chem. Ber.* **5**, 280–282 (1872).
150. Zinke, A., Ziegler, E.: Zur kenntnis des härtungsprozesses von phenol-formaldehyd-harzen. X. mitteilung. *Chem. Ber.* **77**, 264–272 (1944).
151. Gutsche, C.D., Muthukrishnan, R. *J. Org. Chem.* **43**, 4905–4936 (1978).
152. Zhang Li, H., Wang, Y., Xiong X., Bai D., , Y., *Mater. Lett.*, **61**, 1474–1477 (2007).
153. Mokhtari, B., Pourabdollah, K., *Asian J. Chem.*, **23**, 4717–4734 (2011).
154. Nimse S. B., J. Kim, V. Ta, H. Kim, K. Song, C. Jung, V. Nguyen and T. Kim, *Tetrahedron Lett.*, **50**, 7346–7350, (2009).
155. Nimse S. B., Nguyen V., Kim J., Kim H., Song K., Eoum W., Jung C., Ta V., Seelam S. R. and Kim T., *Tetrahedron Lett.*, **51**, 2840–2845, (2010).
156. Sieffert N., Chaumont A. and Wipff G., *J. Phys. Chem. A*, **113**, 10610–10622, (2009).
157. Vicens, J., Harrowfield, J., Baklouti, L.: *Calixarenes in the nanoworld*. Springer, Dordrecht (2007)
158. Mokhtari, B., Pourabdollah, K., Dalali, N., *J. Incl. Phenom. Macrocycl. Chem.* **69**, 1–55 (2011).
159. Mokhtari, B., Pourabdollah, K., Dalali, N., *J. Coord. Chem.* **64**, 743–794 (2011).
160. Mokhtari, B., Pourabdollah, K., *J. Coord. Chem.* **64**, 3189–3204, (2011).
161. Mutihac, L., Lee, J.H., Kim, J.S., Vicens, J., *Chem. Soc. Rev.* **40**, 2777–2796 (2011).
162. Mokhtari, B., Pourabdollah, K., Dallali, N., *J. Radioanal. Nucl. Chem.* **287**, 921–934 (2011).

163. Ding, C., Qu, K., Li, Y., Hu, K., Liu, H., Ye, B., Wu, Y., Zhang, S., *J. Chromatogr. A* **1170**, 73–81 (2007).
164. Rodik, R.V., Boyko, V.I., Kalchenko, V.I., *Curr. Med. Chem.* **16**, 1630–1655, (2009).
165. M. Fujita, D. Oguro, M. Miyazawa, H. Oka, K. Yamaguchi, K. Ogura. *Nature* **378**, 469 (1995). Coordination cage **1** is now commercially available from Wako Chemical Co. Ltd. (Pd- Nanocage).
166. For a review: M. Fujita, K. Umemoto, M. Yoshizawa, N. Fujita, T. Kusukawa, K. Biradha. *Chem. Commun.* 509 (2001).
167. Kusukawa, T., Fujita, M., *Angew. Chem. Int. Ed.*, **37**, 3142-3144, (1998).
168. Yoshizawa M., Tamura M., Fujita M.. *J. Am. Chem. Soc.* **126**, 6846 (2004).
169. (a) Ramamurthy V. *Tetrahedron* **42**, 5753 (1986); (b) Ramamurthy V. Venkatesan, K..*Chem. Res.* **87**, 433 (1987); (c) Bouas-Laurent H., Castellan, A. J.-Desvergne P., Lapouyade R.. *Chem.Soc. Rev.* **29**, 43 (2000).
170. Yoshizawa M., Takeyama Y., Kusukawa T., Fujita M.. *Angew. Chem., Int. Ed.* **41**, 1347 (2002).
171. (a) Baney R. H., Itoh M., Sakakibara A., Suzuki T.. *Chem. Rev.* **95**, 1409 (1995); (b) Loy D. A., Shea K. J., *Chem. Rev.* **95**, 1431 (1995); (c) Murugavel R., Voigt A., Walawalkar M. G., Roesky H.W.. *Chem. Rev.* **96**, 2205 (1996).
172. Yoshizawa M., Miyagi S., Kawano M., Ishiguro K., Fujita M.. *J. Am. Chem. Soc.* **126**, 9172 (2004).
173. (a) Tomalia, D. A., Baker, H., Dewald J., Hall M., Kallos G., Martin S., Roeck J., Ryder J., Smith P., *Polym.*, **17**, 117–132, (1985). (b) Hawker C. J., Fréchet J. M. J., *J. Am. Chem. Soc.*, **112**, 7638–7647, (1990). (c) Fréchet J. M. J., *Science*, **263**, 1710–1715, (1994).
174. Jayaraman, N. *Resonance*, 60, (2007).
175. Lee C. C., MacKay J. A., Fréchet J. M. J., Szoka F. C., *Nature Biotech.*, **23**, 1517–1526, (2005).
176. Astruc, D., Lu F., Aranzas, J. R. *Angew. Chem. Int. Ed.*, **44**, 7852–7872, (2005).
177. Morgan M. T., Carnahan M. A., Immoos C. E., Ribeiro A. A., Finkelstein S., Lee S. J., Grinstaff M. W., *J. Am. Chem. Soc.*, **125**, 15485–15489, (2003).

178. Astruc, D., Boisselier, E., Ornelas, C. *Chem. Rev.*, **110**, 1857–1959, (2010).
179. Brinker, U. H., *Advances in Carbene Chemistry*, Volume **3**, Elsevier, (2001).
180. M. Jones Jr., *Sci. Am.*, **234**, 101–113, (1976).
181. (a) Takahashi K., *Chem. Rev.*, **98**, 2013–2034, (1998); (b) Breslow R., Dong S. D., *Chem. Rev.*, **98**, 1997–2012, (1998); (c) Vriezema D. M., Comellas-Aragones M., Elemans J. A. A. W., Cornelissen L. M., Rowan A. E., Nolte R. J. M., *Chem. Rev.*, **105**, 1445–1490, (2005).
182. (a) Brinker U. H., Rosenberg M. G., in: *Advances in Carbene Chemistry*, vol. 2 (Ed.: U. H. Brinker), JAI Press, Stamford, CT, 29–41, (1998); (b) Rosenberg M. G., Brinker U. H., in: *Adv. Phys. Org. Chem.*, vol. 40 (Ed.: J. P. Richard), Academic Press, New York, 1–47, (2005); (c) Rosenberg M. G., Brinker U. H., *Eur. J. Org. Chem.*, 5423–5440, (2006).
183. Moss, R. A.; Chang, M. J. *Tetrahedron Lett.*, **22**, 3749, (1981).
184. Isaev, S. D.; Sherstyuk, O. F.; Kozlov, O. F.; Skripkin, V. V.; Yanku, I. *Teoreticheskaya i Eksperimental' naya Khimiya*, **27**, 211, (1991).
185. Morgan, S.; Jackson, J. E.; Platz, M. S. *J. Am. Chem. Soc.*, **113**, 2782, (1991).
186. Bayley, H.; Knowles, J. R. *Biochem. J.*, **17**, 2420, (1978).
187. Modarelli, D. A.; Morgan, S.; Platz, M. S. *J. Am. Chem. Soc.*, **114**, 7034, (1992).
188. Bobek, M. M.; Brinker, U. H. *J. Am. Chem. Soc.*, **122**, 7430, (2000).
189. Krois, D.; Brecker, L.; Werner, A.; Brinker, U. H. *Adv. Synth. Catal.*, **346**, 1367, (2004).
190. Brinker, U. H.; Buchkremer, R.; Kolodziejczyk, M.; Kupfer, R.; Rosenberg, M. G.; Poliks, M. D.; Orlando, M.; Gross, M. L. *Angew. Chem., Int. Ed. Engl.*, **32**, 1344, (1993).
191. Kupfer, R.; Poliks, M. D.; Brinker, U. H. *J. Am. Chem. Soc.*, **116**, 7393, (1994).
192. Wagner, G.; Knoll, W.; Bobek, M. M.; Brecker, L.; van Herwijnen, H. W. G.; Brinker, U. H. *Org. Lett.*, **12**, 332, (2010).
193. Knoll, W.; Kaneno, D.; Bobek, M. M.; Brecker, L.; Rosenberg, M. G.; Tomoda, S.; Brinker, U. H. *J. Org. Chem.*, **77**, 1340, (2012).



194. Masson, E.; Ling, X.; Joseph, R.; Mensah, L.-K.; Lu, X. *RSC Adv.*, **2**, 1213, (2012).
195. Lagona, J.; Mukhopadhyay, P.; Chakrabarti, S.; Isaacs, L. *Angew. Chem., Int. Ed.*, **44**, 4844, (2005).
196. Lee, J. W.; Samal, S.; Selvapalam, N.; Kim, H.-J.; Kim, K. *Acc. Chem. Res.*, **36**, 621, (2003).
197. Inokuma, Y.; Kawano, M.; Fujita, M. *Nature Chem.*, **3**, 349, (2011).
198. Murase, T.; Fujita, M. *Chem. Rec.*, **10**, 342, (2010).
199. De Mayo, P. *Pure Appl. Chem.*, **54**, 1623, (1982).
200. Turro, N. J. *Tetrahedron*, **43**, 1589, (1987).
201. Yoshizawa, M.; Miyagi, S.; Kawano, M.; Ishiguro, K.; Fujita, M. *J. Am. Chem. Soc.*, **126**, 9172, (2004).
202. Turro, N. J.; Ramamurthy, V.; Scaiano, J. C. *Modern Molecular Photochemistry of Organic Molecules*; University Science Books: Sausalito, CA, (2010).
203. Skell, P. S.; Valenty, S. J.; Humer, P. W. *J. Am. Chem. Soc.*, **95**, 5041, (1973).
204. Havals, Z.; Michl, J. *Collect. Czech. Chem. Commun.*, **63**, 1485, (1998).
205. Ramamurthy, V., *Photochemistry in Organized & Constrained Media*; Ed.; VCH: New York, (1991).
206. Meyer, E. A.; Castellano, R. K.; Diederich, F. *Angew. Chem., Int. Ed.*, **42**, 1210, (2003).
207. Rekharsky, M. V.; Inoue, Y. *Chem. Rev.*, **98**, 1875, (1998).
208. Williams, D. H.; Stephens, E.; O'Brien, D. P.; Zhou, M. *Angew. Chem., Int. Ed.*, **43**, 6596, (2004).
209. Jorgensen, W. L.; Tirado-Rives, J. *J. Am. Chem. Soc.*, **110**, 1657, (1988).
210. Kaminski, G. A.; Friesner, R. A.; Tirado-Rives, J.; Jorgensen, W. L. *J. Phys. Chem. B*, **105**, 6474, (2001).
211. Spoel, D. v. d.; Lindahl, E.; Hess, B.; Groenhof, G.; Mark, A. E.; Berendsen, H. J. C. *J. Comput. Chem.*, **26**, 1701, (2005).

212. Lindahl, E.; Hess, B.; Spoel, D. v. d. *J. Mol. Model.*, **7**, 306, (2001).
213. Frisch, M. J. et al., In Gaussian 03, Rev. D.01; Gaussian, Inc.: Wallingford, CT, (2004).
214. (a) H. Bayley, J. R. Knowles, *Methods Enzymol.*, **46**, 69, (1977). (b) S. A. Fleming, *Tetrahedron*, **51**, 12479, (1995). (c) M. Hashimoto, Y. Hatanaka, *Eur. J. Org. Chem.*, 2513, (2008).
215. (a) N. P. Gritsan, M. S. Platz, *Chem. Rev.*, **106**, 3844, (2006). b) A. Reisinger, R. Koch, P. V. Bernhardt, C. Wentrup, *Org. Biomol. Chem.*, **2**, 1227, (2004). (c) C. Addicott, C. Wentrup, *Aust. J. Chem.*, **61**, 592, (2008).
216. Quast, H.; Eckert, P. Liebigs *Ann. Chem.*, 1727, (1974).
217. Dunkin, I. R.; Shields, C. J.; Quast, H.; Seiferling, B. *Tetrahedron Lett.*, **24**, 3887, (1983).
218. Radziszewski, J. G.; Downing, J. W.; Jawdosiuk, M.; Kovacic, P.; Michl, J. *J. Am. Chem. Soc.*, **107**, 594, (1985).
219. (a) *Organic Azides: Syntheses and Applications* (Eds.: Bräse S., Banert K.), John Wiley & Sons, New York, (2010); (b) Bräse S., Gil C., Knepper K., V. Zimmermann, *Angew. Chem. Int. Ed.*, **44**, 5188, (2005); (c) Hassner A., in: *Azides and Nitrenes: Reactivity and Utility* (Ed.: E. F. V. Scriven), Academic, New York, 35–76, (1984).
220. (a) Platz M. S., in: *Reactive Intermediate Chemistry* (Eds.: Moss R. A., Platz M. S., Jones M. Jr), John Wiley & Sons, Hoboken, NJ, 501–559, (2004); (b) Scriven E. F. V., *Azides and Nitrenes: Reactivity and Utility*, Academic, New York, (1984); (c) Wentrup C., *Reactive Intermediates*, John Wiley & Sons, New York, (1984); (d) Lwowski W., *Nitrenes*, John Wiley & Sons, New York, (1970).
221. (a) Lwowski W., *Ann. N. Y. Acad. Sci.*, **346**, 491, (1980); (b) Vodovozova E. L., *Biochem. (Moscow)*, **72**, 1, (2007); (b) Wagner G., Arion V. Brecker B., L., Krantz C., Mieusset J.-L., Brinker U. H., *Org. Lett.*, **11**, 3056, (2009).
222. Wagner G., Arion, V. B., Brecker, L., Krantz, C., Mieusset, J. C., Brinker, U. H., *Org. Lett.*, **11**, 3056–3058, (2009).
223. Brinker, U. H., Walla, P., Krois, D., Arion, V. B., *Eur. J. Org. Chem.*, 1249–1255, (2011).
224. Rekharsky, M. V.; Inoue, Y. *Chem. Rev.*, **98**, 1875, (1998).

225. Trott, O.; Olson, A. J. *J. Comput. Chem.*, **31**, 455, (2010).
226. Nocedal, J.; Wright, S. J. *Numerical Optimization*, 2nd ed.; Springer Verlag: Berlin, (1999).
227. Zadnarm, R.; Kraft, A.; Schrader, T.; Linne, U. *Chem.Eur. J.*, **10**, 4233, (2004).
228. Kogej, K.; Schalley, C. A. *Analytical Methods in Supramolecular Chemistry*; John Wiley & Sons: Chichester, (2007).
229. Rozhenko, A. B.; Schoeller, W. W.; Letzel, M. C.; Decker, B.; Agena, C.; Mattay, J. *Chem.Eur. J.*, **12**, 8995, (2006).
230. Da Silva, J. P.; Kulasekharan, R.; Cordeiro, C.; Jockusch, S.; Turro, N. J.; Ramamurthy, V. *Org. Lett.*, **14**, 560, (2012).
231. Warmuth, R. *Eur. J. Org. Chem.*, 423, (2012).
232. Da Silva, J. P.; Jayaraj, N.; Jockusch, S.; Turro, N. J.; Ramamurthy, V. *Org. Lett.*, **13**, 2410, (2011).
233. Jayaraj, N.; Porel, M.; Ottaviani, M. F.; Maddipatla, M. V. S. N.; Modelli, A.; Da Silva, J. P.; Bhogala, B. R.; Captain, B.; Jockusch, S.; Turro, N. J.; Ramamurthy, V. *Langmuir*, **25**, 13820, (2009).
234. Karthikeyan S., Ramamurthy, 2006. *J. Org. Chem.*, **71** , 6409 – 6413, (2006).
235. Day, A.; Arnold, A. P.; Blanch, R. J.; Snushall, B. *J. Org. Chem.*, **66**, 8094, (2001).
236. Sasaki, T.; Eguchi, S.; Katada, T.; Hiroaki, O. *J. Org. Chem.*, **42**, 3741, (1977).
237. Saman E., Claeysens M., Kersters-Hilderson H., De Bruyne C. K., *Carb. Res.*, **30**, 207, (1973).
238. Lwowski W., *Ann. N.Y. Acad. Sci.*, **346**, 491, (1980).
239. Schnapp K. A., Poe R., Leyva E., Soundararajan N., Platz M. S., *Bioconjug. Chem.*, **4**, 172, (1993).
240. Platz M. S., *Photochem. Photobiol.*, **65**, 193, (1997).
241. Polshakov D., Rai S., Wilson R. M., Mack E. T., Vogel M., Krause J. A., Burdzinski G., Platz M. S., *Biochemistry*, **44**, 11241, (2005).
242. Cline M. R., Mandel S. M., Platz M. S., *Biochemistry*, **46**, 1981, (2007).

243. Jadhav A. V., Gulgas C. G., Gudmundsdottir A. D., *Euro. Poly. J.*, **43**, 2594, (2007).
244. Voskresenska V., Wilson R. M., Panov M., Tarnovsky A. N., Krause J. A., Vyas S., Winter A. H., Hadad C. M., *J. Am. Chem. Soc.*, **131**, 11535, (2009).
245. Mecomber J. S., Murthy R. S., Rajam S., Singh P. N. D., Gudmundsdottir A. D., Limbach P. A., *Langmuir*, **24**, 3645, (2008).
246. Platz M. S., in *Reactive Intermediate Chemistry*, (Eds: R. A. Moss, M. S. Platz Jr.), John Wiley, Hoboken, 501, (2004).
247. Subhan W., Rempala P., Sheridan R. S., *J. Am. Chem. Soc.*, **120**, 11528, (1998).
248. Tomioka H., in *Reactive Intermediate Chemistry* (Eds: R. A. Moss, M. S. Platz Jr), John Wiley, Hoboken, 375, (2004).
249. Lahti P. M., in *Magnetic Properties of Organic Materials* (Ed.: P. M. Lahti), Marcel Dekker, NY, 661, (1999).
250. (a) Milligan, G. L.; Mossman, C. J.; Aube, J. *J. Am. Chem. Soc.*, **117**, 10449, (1995); (b) Kim, S.; Joe, G. H.; Do, J. Y. *J. Am. Chem. Soc.*, **116**, 5521, (1994); (c) Aube, J.; Milligan, G. L. *J. Am. Chem. Soc.*, **113**, 8965, (1991).
251. (a) Scriven, E. F. V.; Trunbull, K. *Chem. Rev.*, **88**, 298 (1989); (b) Takeuchi, H.; Yanagida, S.; Ozaki, T.; Hagiwara, S.; Eguchi, S. *J. Org. Chem.*, **54**, 431, (1989).
252. (a) Lewis F.D., Saunders W.H. Jr., *J. Am. Chem. Soc.* **90**, 7033, (1968); (b) Lewis F.D., Saunders W.H. Jr., *J. Am. Chem. Soc.* **90**, 7031, (1968); (c) Lewis F.D., Saunders W.H. Jr., *J. Am. Chem. Soc.* **89**, 645, (1967).
253. (a) Mandel S.M., Krause Bauer J.A., Gudmundsdóttir A.D., *Org. Lett.* **3** 523, (2001); (b) Singh P.N.D., Mandel S.M., Robinson R.M., Zhu Z., Franz R., Ault B.S., Gudmundsdottir A.D., *J. Org. Chem.*, in press.
254. Sundaresan, A. K., Ramamurthy, V., *Photochem. Photobiol. Sci.*, **7**, 1555–1564, (2008).
255. Klima, R. F.; Jadhav, A. V.; Singh, P. N. D.; Chang, M.; Vanos, C.; Sankaranarayanan, J.; Vu, M.; Ibrahim, N.; Ross, E.; McCloskey, S.; Murthy, R. S.; Krause, J. A.; Ault, B. S.; Gudmundsdottir, A. D. *J. Org. Chem.*, **72**, 6372, (2007).
256. (a) Wagner, P. J. In *Rearrangements in Ground and Excited States*; De Mayo, P., Ed.; Academic Press: New York; Vol. 42-3, 381, (1980). (b) Wagner, P. J. *Top. Curr. Chem.*, **66**, 1, (1976).

257. Singh P. N. D., Mandel, S. M., Sankaranarayanan, J., Muthukrishnan, S. Chang, M., Robinson, R. M., Lahti, P. M., Ault, B. S., Gudmundsdottir, A. D., *J. Am. Chem. Soc.*, **129**, 16263-16272, (2007).
258. Sankaranarayanan, J., Bort, L.N., Mandel, S. M., Chen, P., Krause, Elwood, J. A., Brooks, E., Tsang, P. Gudmundsdottir, A. D. *Org. Lett.*, **10**, (2008).
259. Wagner, P. J.; Kemppainen, A. E.; Schott, H. N. *J. Am. Chem. Soc.*, **95**, 5604, (1973).
260. Muthukrishnan, S., Sankaranarayanan, J., Klima, R. F., Pace, T. C. S., Bohne, C., Gudmundsdottir, A. D., *Org. Lett.*, **11**, 2345-2348, (2009).
261. Abramovitch R. A., S. R. Challand, *J.C.S. Chem. Comm.*, 964, (1972).
262. (a) Schuster G.B., Platz M.S., *Adv. Photochem.* **17**, 70, (1992); (b) Borden W.T., Gritsan N.P., Hadad C.M., Karney W.L., Kemnitz C.R., Platz M.S., *Acc. Chem. Res.* **33**, 765 (2000); (c) Platz M.S., *Adv. Carbene Chem.* **2**, 133, (1998).
263. D'Souza, V. T.; Bender, M., L. *Acc. Chem. Res.*, **20**, 146–152, (1987).
264. Breslow, R. *Chem. Br.*, **19**, 126; 128; 130-131, (1983).
265. Breslow, R. *Pure Appl. Chem.*, **66**, 1573–1582, (1994).
266. Breslow, R.; Dong, S. D. *Chem. Rev.*, **98**, 1997–2011, (1998).
267. Paulini, R.; Muller, K.; Diederich, F. *Angew. Chem., Int. Ed.*, **44**, 1788–1805, (2005).
268. Meyer, E. A.; Castellano, R. K.; Diederich, F. *Angew. Chem., Int. Ed.*, **42**, 1210–1250, (2003).
269. Weiss, R. G. *Tetrahedron*, **44**, 3413–3475, (1988).
270. Whitten, D. G. *Acc. Chem. Res.*, **26**, 502–509, (1993).
271. Whitten, D. G.; Russell, J. C.; Schmehl, R. H. *Tetrahedron*, **38**, 2455–2487, (1982).
272. Tung, C.-H.; Wu, L.-Z.; Zhang, L.-P.; Chen, B. *Acc. Chem. Res.*, **36**, 39–47, (2003).
273. Turro, N. J. *Acc. Chem. Res.*, **33**, 637–646, (2000).

274. Turro, N. J.; Graetzel, M.; Braun, A. M. *Angew. Chem., Int. Ed. Engl.*, **19**, 675–696, (1980).
275. Scaiano, J. C.; Garcia, H. *Acc. Chem. Res.*, **32**, 783–793, (1999).
276. Kautsky, H.; de Bruijn, H.; Neuwirth, R.; Baumeister, W. *Ber. Dtsch. Chem. Ges.*, **66B**, 1588-1600, (1933).
277. Rebek, J., Jr. *Tetrahedron*, **35**, 723-731, (1979).
278. Greer, A. *Acc. Chem. Res.*, **39**, 797-804, (2006).
279. Clennan, E. L.; Pace, A. *Tetrahedron*, **61**, 6665-6691, (2005).
280. (a) Griesbeck, A. G. *CRC Handbook of Organic Photochemistry and Photobiology*, 301-310, (1995). (b) Wasserman, H. H.; Murray, R. W. Eds.; *Singlet Oxygen: New York*, (1979).
281. Foote, C. S. *Pure Appl. Chem.*, **27**, 635-45, (1971).
282. Jefford, C. W.; Rimbault, C. G. *Tetrahedron Lett.*, **22**, 91-94, (1981).
283. Prien, M.; Adam, W. *Angew Chem., Int. Ed. Engl.*, **35**, 477, (1996).
284. Shailaja, J.; Sivaguru, J.; Robbins, R. J., Ramamurthy, V.; Sunoj, R. B.; Chandrashekar, J.; *Tetrahedron*, **56**, 6927-6943, (2000).
285. (a) Gibb, C. L.; Gibb, B. C. *J. Am. Chem. Soc.*, 1635-1637, (2007). (b) Gibb, C. L.; Gibb, B. C. *J. Am. Chem. Soc.*, **128**, 16498-16499, (2006).
286. Cohen, Y.; Avram, L.; Frish, L. *Angew. Chem. Int. Ed.*, **44**, 520-554, (2005).
287. Gibb, C. L. D.; Gibb, B. C. *Chem. Commun.*, 1635-1637, (2007).
288. Sacro A., Tremleau. L., Rebek, J. Jr. *J. Am. Chem. Soc.*, **126**, 13512-13518, (2004).
289. J. Rebek, Jr., *Angew. Chem., Int. Ed.*, **44**, 2068-2078, (2005).
290. Scarso, A.; Onagi, H.; Rebek, J. Jr. *J. Am. Chem. Soc.*, **126**, 12728-12729, (2004)
291. Gibb, C. L. D.; Sundaresan, A. K.; Ramamurthy, V.; Gibb, B. C. *J. Am. Chem. Soc.*, **130**, 4069-4080, (2008).
292. Griesbeck, A. G.; Cho, M. *Org. Lett.*, **9**, 611-613, (2007).

293. Lakowicz J. R., *Principles of Fluorescence Spectroscopy*, Plenum, New York, (1983).
294. Valeur B., *Molecular Fluorescence Principles and Applications*, Wiley-VCH, (2001).
295. Farran, A.; Deshayes, K.; Matthews, C.; Balanescu, I. *J. Am. Chem. Soc.*, **117**, 9614, (1995).
296. Farran, A.; Deshayes, K. *J. Phys. Chem.*, **100**, 3305, (1996).
297. Parola, A. J.; Pina, F.; Ferreira, E.; Maestri, M.; Balzani, V. *J. Am. Chem. Soc.*, **118**, 11610, (1996).
298. Pina, F.; Parola, A. J.; Ferreira, E.; Maestri, M.; Armaroli, N.; Ballardini, R.; Balzani, V. *J. Phys. Chem.*, **99**, 12701, (1995).
299. Place, I.; Farran, A.; Deshayes, K.; Piotrowiak, P. *J. Am. Chem. Soc.*, **120**, 12626, (1998).
300. Jockusch, S.; Zieka, O.; Jayaraj, N.; Ramamurthy, V.; Turro, N. J. *J. Phys. Chem. Lett.*, **1**, 2628, (2010).
301. Chen, J. Y. C.; Jayaraj, N.; Jockusch, S.; Ottaviani, M. F.; Ramamurthy, V.; Turro, N. J. *J. Am. Chem. Soc.*, **130**, 7206, (2008).
302. Kainmuller E. K., Bannwarth W., *Helvetica Chimica Acta*, **89**, 3056, (2006).
303. Jones, G. I.; Jackson, W. R.; Choi, C. Y.; Bergmark, W. R. *J. Phys. Chem.*, **89**, 294, (1985).
304. Nag, A.; Chakrabarty, T.; Bhattacharyya, K. *J. Phys. Chem.*, **94**, 4203, (1990).
305. Micheau, J. C.; Zakharova, G. V.; Chibisov, A. K. *Phys. Chem. Chem. Phys.*, **6**, 2420, (2004).
306. Kohn, F.; Hofkens, J.; Schryver, F. D. *Chem. Phys. Lett.*, **321**, 372, (2000).
307. Das, D. K.; Das, A. K.; Mondal, T.; Mandal, A. K.; Bhattacharyya, K. *J. Phys. Chem. B*, **114**, 13159, (2010).
308. Adhikari, A.; Das, D. K.; Sasmal, D. K.; Bhattacharyya, K. *J. Phys. Chem. A*, **113**, 3737, (2009).
309. Ghosh, S.; Dey, S.; Adhikari, A.; Mandal, U.; Bhattacharyya, K. *J. Phys. Chem. B*, **111**, 7085, (2007).

310. Gunther, H. *NMR Spectroscopy*; John Wiley: Chichester, 1992.
311. Bujdák, B., *Applied Clay Science* **34**, 58–73, (2006).
312. Hamer F. M., *The Cyanine Dyes and Related Compounds*, Wiley, New York, (1964).
313. Schafer F. P., ed. *Dye Lasers*, Springer-Verlag, Berlin, (1973).
314. (a) Arden W., Fromherz P., *Ber. Bunsenges. Phys. Chem.*, **82**, 868, (1978); (b) Arden W., Fromherz P., *J. Electrochem. Soc.*, **127**, 372, (1980); (c) Inacker, H. Kuhn, D. Mobius, and G. Debuch, *Z. Phys. Chem. (Frankfurt am Main)*, **101**, 337, (1976).
315. (a) Hoffman M., Lichtin N. N., *Solar Energy Chemical Conversion and Storage*, eds. R. R. Hautala, R. B. King, and C. Kotal, The Human Press Inc., New Jersey, 153-187; (b) Clark W. D. K., J. A. Eckert, *Sol. Energy.*, **17**, 147, (1975).
316. (a) Albery W. J., Foulds A. W., *J. Photochem.*, **10**, 41, (1979); (b) Albery W. J., Archer M. D., *Nature (London)*, **270**, 399, (1977); *J. Electroanal. Chem.*, **86**, 19, (1978).
317. Kamat, P. V. *J. Phys. Chem. C*, **111**, 2834–2860, (2007).
318. Tvrđy, K.; Kamat, P. V. *J. Phys. Chem. A*, **113**, 3765–3772, (2009).
319. Gil, M.; Wang, S.; Organero, J. A.; Teruel, L.; Garcia, H. Douhal. *J. Phys. Chem. C*, **113**, 11614–11622, (2009).
320. Bruhwiler, D.; Gfeller, N.; Calzaferri, G. *J. Phys. Chem. B*, **102**, 2923–2929, (1998).
321. Bussemer, B.; Munsel, D.; Wunscher, H.; Mohr, G. J.; Grummt, U. *J. Phys. Chem. B*, **111**, 8–15, (2007).
322. Fujii, K.; Iyi, N.; Hashizume, H. *Chem. Mater.*, **21**, 1179–1181, (2009).
323. Harris, C.; Kamat, P. V. *ACS Nano*, **3**, 682–690, (2009).
324. Yui, T.; Tsuchino, T.; Itoh, T.; Ogawa, M.; Fukushima, Y.; Takagi, K. *Langmuir*, **21**, 2644–2646, (2005).
325. Fujii, K.; Iyi, N.; Sasai, R.; Hayashi, S. *Chem. Mater.*, **20**, 2994–3002, (2008).
326. Eswaramoorthi, S.; Natarajan, P. *J. Porous Mater.*, **15**, 343–349, (2008).



327. Kongkanand, A.; Kamat, P. V. *ACS Nano*, **1**, 13–21, (2007).
328. Koner, A. L., Nau, W. M., *Supramolecular Chemistry*, **19**, 55–66, (2007).
329. Biedermann, F., Elmalem, E., Ghosh, I., Nau, W. M., Scherman, O. A., *Angew. Chem. Int. Ed.*, **51**, 7739–7743, (2012).
330. Batchelor, E. K., Gadde, S., Kaifer, A. E., *Supramolecular Chemistry*, **22**, 40–45, (2010).
331. Praetorius, A., Bailey, D. M., Schwarzlose, T., Nau, W. M., *Org. Lett.*, **10**, , 4089-4092, (2008).
332. Navajas, P. M., Gonz'alez-B'ejar, M., Scaiano, J. C., Garc'ia, H., *Photochem. Photobiol. Sci.*, **8**, 1743–1747, (2009).
333. Alarcon, E. I., Gonz'alez-B'ejar, M., Navajas, P. M., Garcia, H., Lissicand, E.A., Scaiano, J.C., *Photochem. Photobiol. Sci.*, **11**, 269–273, (2012).
334. Gonzalez-Bejar, M., Navajas, P.M., Garc'ia, H., Scaiano, J. C. *Langmuir*, **25**, 10490–10494, (2009)
335. Oliveira C.S. et al. *Spectrochimica Acta Part A* **58** 2971-2982, (2002).
336. Ghale, G., Ramalingam, V., Urbach, A. R., Nau, W. M., *J. Am. Chem. Soc.*, **133**, 7528–7535, (2011).
337. Gadde, S., Batchelor, E. K., Weiss, J. P., Ling, Y., Kaifer, A. E., *J. Am. Chem. Soc.*, **130**, 17114–17119, (2008).
338. Bortulus, P.; Monti, S. *Adv. Photochem.*, **21**, 1–133, (1996).
339. Zhang, X.; Gramlich, G.; Wang, X.; Nau, W. M. *J. Am. Chem. Soc.*, **124**, 254–263, (2002).
340. Ikeda, A.; Shinkai, S. *Chem. Rev.*, **97**, 1713–1734, (1997).
341. Abraham, W. J. *Incl. Phenom. Macrocycl. Chem.*, **43**, 159–174, (2002).
342. Diamond, D.; McKervey, M. A. *Chem. Soc. Rev.*, **25**, 15–24, (1996).
343. Porel M., Jockusch S., Parthasarathy A., Rao V. J., Turro N. J., Ramamurthy V. *Chem. Commun.*, **48**, 2710-2712, (2012).
344. Porel M., Klimczak A., Freitag M., Galoppini E., Ramamurthy V., *Langmuir*, **28**, 3355-3359, (2012).

345. Lee, J. W., Samal S., Selvapalam N., Kim, H., Kim, K., *Accounts of Chemical Research*, **36**, 621-630, (2003).
346. Chai, M. *Proc. R. Soc. A*, **466**, 1441–143, (2010).
347. (a) Bosman, A. W., Schenning, A. P. H. J., Janssen, R. A. J. & Meijer, E. W. *Chem. Ber.* **130**, 725–728, (1997); (b) Boas, U. & Heegaard, P. M. H., *Chem. Soc. Rev.* **33**, 43–63, (2004); (c) Lee, C. C., MacKay, J. A., Fréchet, J. M. & Szoka, F. C. *Nat. Biotechnol.* **23**, 1517–1526, (2005); (d) Agarwal, A., Asthana, A., Gupta, U. & Jain, N. K. *J. Pharm. Pharmacol.* **60**, 671–688, (2008); (e) Hwang, S.-H., Moorefield, C. N. & Newkome, G. R. *Chem. Soc. Rev.* **37**, 2543–2557, (2008).
348. Janga, W., Selimb K.M. K., Leea, C., *Inn-Kyu Kangb*, **34**, 1–23, (2009).
349. Tomalia D.A., Baker H., Dewald J., Hall M., Kallos G., Martin S., et al. *Polym J*, **17**, 117–32, (1985).
350. Bosman A.W., Janssen H.M., Meijer E.W., *Chem Rev*; **99**, 1665–88, (1999).
351. Solassol, J. et al. *J. Gen. Virol.* **85**, 1791–1799, (2004).
352. Kobayashi, H., Kawamoto, S., Jo, S.-K., Bryant Jr, H. L., Brechbiel, M. W. & Star, R. A. *Bioconjugate Chem.* **14**, 388–394, (2003).
353. Thayumanavan, S., Bharathi, P., Sivanandan, K. & Vutukuri, D. R., *C. R. Chim.* **6**, 767–778, (2003).
354. S. Hecht, J.M.J. Fre'chet, *Angew. Chem., Int. Ed. Engl.*, **40**, 74–91, (2001).
355. Jiang D.L., Aida T., *Chem. Commun.*, 1523–1524, (1996).
356. Dandliker P.J., Diederich F., Zingg A., Gisselbrecht J.P., Gross M., Louati Sanford A., E., *Helv. Chim. Acta* , **80**, 1773– 1801, (1997).
357. Weyermann P., Gisselbrecht J.P., Boudon C., Diederich F., Gross M., *Angew. Chem., Int. Ed. Engl.*, **38**, 3214– 3219, (1999).
358. Arima H., Kihara F., Hirayama F., Uekama K., *Bioconjug. Chem.*, **12**, 476–484, (2001).
359. Hecht S., Frechet J. M. J., *J. Am. Chem. Soc.*, **123**, 6959-6960, (2001).
360. Shiraishi Y., Koizumi H., Hirai T., *J. Phys. Chem. B*, **109**, 8580-8586, (2005).
361. Yuan Z., Zheng S. J., Zeng Y., Chen J. P., Han Y. B., Li Y. Y., Y. Li, *New J. Chem.*, **34**, 718-722, (2010).

362. Kaanumalle L. S., Nithyanandhan J., Pattabiraman M., Jayaraman N., Ramamurthy V., *J. Am. Chem. Soc.*, **126**, 8999-9006, (2004).
363. Kaanumalle L. S., Ramesh R., Maddipatla V. S. N. M., Nithyanandhan J., Jayaraman N., Ramamurthy V., *J. Org. Chem.*, **70**, 5062-5069, (2005).
364. Kaanumalle L. S., Nithyanandhan J., Pattabiraman M., Jayaraman N., Ramamurthy V., *J. Am. Chem. Soc.*, **126**, 8999-9006, (2004).
365. Kalyanasundaram, K.; Thomas, J. K. *J. Am. Chem. Soc.*, **99**, 2039, (1977).
366. Dong, D. C.; Winnik, M. A. *Can. J. Chem.*, **62**, 2560–2565, (1984).
367. Nag, A.; Chakrabarty, T.; Bhattacharyya, K. *J. Phys. Chem.*, **94**, 4203, (1990).
368. Wagner, B. D. *Molecules*, **14**, 210–237, (2009).
369. Grant, C. D.; DeRitter, M. R.; Steege, K. E.; Fadeeva, T. A.; Castner, E. W., Jr. *Langmuir*, **21**, 1745–1752, (2005).
370. Reichardt, C. *Solvents and Solvent Effects in Organic Chemistry*; Wiley-VCH: Weinheim, (2003).
371. (a) Bhattacharyya K., *Chem. Commun.*, 2848–2857, (2008); (b) Bagchi B., *Chem. Rev.*, **105**, 3197–3219, (2005); (c) Pal S. K., Zewail A. H., *Chem. Rev.*, **104**, 2099–2124, (2004); (d) Nandi N., Bhattacharyya K., Bagchi B., *Chem. Rev.*, **100**, 2013–2046, (2000); (e) Bhattacharyya K., *Acc. Chem. Res.*, **36**, 95–101, (2003).
372. Sen, P., Roy, D., Mondal, S. K., Sahu, K., Ghosh, S., Bhattacharyya, K., *J. Phys. Chem. A*, **109**, 9716-9722, (2005).
373. Maroncelli M., Fleming G. R., *J. Chem. Phys.*, **89**, 5044–5069, (1988).
374. (a) Fecko, C. J.; Eaves, J. D.; Loparo, J. J.; Tokmakoff, A.; Geissler, P. L. *Science*, **301**, 1698, (2003). (b) Jimenez, R.; Fleming, G. R.; Kumar, P. V.; Maroncelli, M. *Nature*, **369**, 471, (1994). (c) Jarzeba, W.; Walker, G. C.; Johnson, A. E.; Kahlow, M. A.; Barbara, P. F. *J. Phys. Chem.*, **92**, 7039, (1988). (d) Nandi, N.; Roy, S.; Bagchi, B. *J. Chem. Phys.*, **102**, 1390, (1995).
375. (a) Nandi, N.; Bhattacharyya, K.; Bagchi, B. *Chem. Rev.*, **100**, 2013, (2000). (b) Pal, S. K.; Zewail, A. H. *Chem. Rev.*, **104**, 2099, (2004). (c) Bhattacharyya, K. *Acc. Chem. Res.*, **36**, 95, (2003). (d) Bhattacharyya, K.; Bagchi, B. *J. Phys. Chem. A*, **104**, 10603, (2000).

376. (a) Vajda, S.; Jimenez, R.; Rosenthal, S. J.; Fidler, V.; Fleming, G. R.; Castner, E. W., Jr. *J. Chem. Soc., Faraday Trans.*, **91**, 867, (1995). (b) Nandi, N.; Bagchi, B. *J. Phys. Chem.*, **100**, 13914, (1996). (c) Sen, S.; Sukul, D.; Dutta, P.; Bhattacharyya, K. *J. Phys. Chem. A*, **105**, 10635, (2001).
377. (a) Jordanides, X. J.; Lang, M. J.; Song, X.; Fleming, G. R. *J. Phys. Chem. B*, **103**, 7995, (1999). (b) Nandi, N.; Bagchi, B. *J. Phys. Chem. B*, **101**, 10954, (1997). (c) Pal, S. K.; Peon, J.; Zewail, A. H. *Proc. Natl. Acad. Sci. U.S.A.*, **99**, 1763, (2002). (d) Pal, S. K.; Mandal, D.; Sukul, D.; Sen, S.; Bhattacharyya, K. *J. Phys. Chem. B*, **105**, 1438, (2001). (e) Sen, P.; Mukherjee, S.; Dutta, P.; Halder, A.; Mandal, D.; Banerjee, R.; Roy, S.; Bhattacharyya, K. *J. Phys. Chem. B*, **107**, 14563, (2003).
378. (a) Hara, K.; Kuwabara, H.; Kajimoto, O. *J. Phys. Chem. A*, **105**, 7174, (2001). (b) Mandal, D.; Sen, S.; Tahara, T.; Bhattacharyya, K. *Chem. Phys. Lett.*, **359**, 77, (2002). (c) Shirota, H.; Tamoto, Y.; Segawa, H. *J. Phys. Chem. A*, **108**, 3244, (2004). (d) Hazra, P.; Chakrabarty, D.; Chakraborty, A.; Sarkar, N. *Biochem. Biophys. Res. Commun.*, **314**, 543, (2004).
379. (a) Dutta, P.; Sen, P.; Mukherjee, S.; Halder, A.; Bhattacharyya, K. *J. Phys. Chem. B*, **107**, 10815, (2003). (b) Satoh, T.; Okuno, H.; Tominaga, K.; Bhattacharyya, K. *Chem. Lett.*, **33**, 1090, (2004). (c) Willard, D. M.; Riter, R. E.; Levinger, N. E. *J. Am. Chem. Soc.*, **120**, 4151, (1998). (d) Corbeil, E. M.; Riter, R. E.; Levinger, N. E. *J. Phys. Chem. B*, **108**, 10777, (2004). (e) Pant, D.; Levinger, N. E. *J. Phys. Chem. B*, **103**, 7846, (1999).
380. (a) Gearheart, L. A.; Somoza, M. M.; Rivers, W. E.; Murphy, C. J.; Coleman, R. S.; Berg, M. A. *J. Am. Chem. Soc.*, **125**, 11812, (2003). (b) Brauns, E. B.; Madaras, M. L.; Coleman, R. S.; Murphy, C. J.; Berg, M. A. *Phys. Rev. Lett.*, **88**, 158101-1, (2002).
381. (a) Scodinu, A.; Reilly, T.; Fourkas, J. T. *J. Phys. Chem. B*, **106**, 1041, (2002). (b) Farrer, R. A.; Fourkas, J. T. *Acc. Chem. Res.*, **36**, 605, (2003). (c) Sen, P.; Mukherjee, S.; Patra, A.; Bhattacharyya, K. *J. Phys. Chem. B*, **109**, 3319, (2005). (d) Baumann, R.; Ferrante, C.; Kneuper, E.; Deeg, F.- W.; Brauchle, C. *J. Phys. Chem. A*, **107**, 2422, (2003).
382. (a) Pal, S. K.; Sukul, D.; Mandal, D.; Bhattacharyya, K. *J. Phys. Chem. B*, **104**, 4529, (2000). (b) Sykora, J.; Kapusta, P.; Fidler, V.; Hof, M. *Langmuir*, **18**, 571, (2002). (c) Chattopadhyay, A.; Mukherjee, S. *Langmuir*, **15**, 2142, (1999).
383. (a) Frauchiger, L.; Shirota, H.; Uhrich, K. E.; Castner, E. W., Jr. *J. Phys. Chem. B*, **106**, 7463, (2002). (b) Sen, S.; Sukul, D.; Dutta, P.; Bhattacharyya, K. *J. Phys. Chem. B*, **106**, 3763, (2002). (c) Halder, A.; Sen, P.; Das Burman, A.; Bhattacharyya, K. *Langmuir*, **20**, 653, (2004).

384. (a) Bandyopadhyay, S.; Chakraborty, S.; Balasubramanian, S.; Bagchi, B. *J. Am. Chem. Soc.*, **127**, 4071, (2005). (b) Marchi, M.; Sterpone, F.; Ceccarelli, M. *J. Am. Chem. Soc.*, **124**, 6787, (2002).
385. (a) Pal, S.; Balasubramanian, S.; Bagchi, B. *J. Phys. Chem. B*, **107**, 5194, (2003). (b) Bruce, C. D.; Senapati, S.; Berkowitz, M. L.; Perera, L.; Forbes, M. D. E. *J. Phys. Chem. B*, **106**, 10902, (2002).
386. (a) Faeder, J.; Albert, M. V.; Ladanyi, B. M. *Langmuir* 2003, **19**, 2514. (b) Senapathy, S.; Chandra, S. *J. Phys. Chem. B*, **105**, 5106, (2001). (c) Senapati, S.; Berkowitz, M. L. *J. Chem. Phys.*, **118**, 1937, (2003).
387. (a) Thompson, W. H. *J. Chem. Phys.*, **117**, 6618, (2002). (b) Thompson, W. H. *J. Chem. Phys.*, **120**, 8125, (2004). (c) Gomez, J. A.; Thompson, W. H. *J. Phys. Chem. B*, **108**, 20144, (2004). (d) Michael, D.; Benjamin, I. *J. Chem. Phys.*, **114**, 2817, (2001).
388. Lewis, F. D.; Lauterbach, R. T.; Heine, H.-G.; Hartmann, W.; Rudolph, H. *J. Am. Chem. Soc.*, **97**, 1519–1525, (1975).
389. Frederick, B.; Johnston, L. J.; de Mayo, P.; Wong, S. K. *Can. J. Chem.*, **62**, 403–410, (1984).
390. Turro, N. J. *Proc. Natl. Acad. Sci. U.S.A.*, **80**, 609–621, (1983).
391. Gould, I. R.; Turro, N. J.; Zimmt, M. B. In *Adv. Phys. Org. Chem.*; Bethell, D., Ed.; Academic Press: London,; Vol. 20, 1-53, (1984).
392. Turro, N. J. *Chem. Commun.*, 2279–2292, (2002).
393. Syamala, M. S.; Ramamurthy, V. *J. Org. Chem.*, **51**, 3712–3715, (1986).
394. Hammond, G. S.; Saltiel, J.; Lamola, A. A.; Turro, N. J.; Bradshaw, J. S.; Cowan, D. O.; Counsell, R. C.; Vogt, V.; Christopher, D. *J. Am. Chem. Soc.*, **86**, 3197–3217, (1964).
395. Lewis, F. D.; Bedell, A. M.; Dykstra, R. E.; Elbert, J. E.; Gould, I. R.; Farid, S. *J. Am. Chem. Soc.*, **112**, 8055–8064, (1990).
396. Lakshminarasimhan, P. H.; Sunoj, R. B.; Karthikeyan, S.; Chandrashekar, J.; Johnston, L. J.; Ramamurthy, V. *J. Photochem. Photobiol. A*, **153**, 41–53, (2002).
397. Isak, S. J.; Eyring, E. M. *J. Phys. Chem.*, **96**, 1738–1742, (1992).
398. Kreller, D. I.; Kamat, P. V. *J. Phys. Chem.*, **95**, 4406–4410, (1991).

399. Copidas K. R., Leheny A. R., Caminati G., Turro N. J., Tomalia D. A. J., *J. Am. Chem. Soc.*, **113**, 1335-1342, (1991).
400. Camhati, G., Turro, N. J., Tomalia, D. A., *J. Am. Chem. Soc.*, **12**, 8515-8522, (1990).
401. Maria C., Orellana, G., Turro, N. J., Tomalia, D. A. *Macromolecules*, **23**, 910-912, (1990).
402. Jansen, J. F. G. A.; deBrabander, E. M. M.; Meijer, E. W. *Science*, **266**, 1226-1229, (1994).
403. Mattei, S.; Seiler, P.; Diederich, F. *Helv. Chem. Acta.*, **78**, 1904-1912, (1995).
404. Turro, C.; Niu, S., Bossman, S. H.; Tomalia, D. A.; Turro, N. J. *J. Phys. Chem.*, **99**, 5512-5517, (1995).
405. Ottaviani, M. F.; Cossu, E.; Turro, N. J.; Tomalia, D. A. *J. Am. Chem. Soc.*, **117**, 4387, (1995).
406. (a) Ottaviani, M. F.; Matteini, P.; Brustolon, M.; Turro, N. J.; Jockusch, S.; Tomalia, D. A. *J. Phys. Chem.*, **102**, 6029, (1998). (b) Ottaviani, M. F.; Daddi, R.; Brustolon, M.; Turro, N. J.; Tomalia, D. A. *Langmuir*, **15**, 1973, (1999).
407. Schneider, D. J.; Freed, J. H. Berliner, L. J., Reuben, J., Eds.; Plenum Press: New York, Vol. 8, p 1, (1989).
408. Ottaviani, M. F.; Martini, G.; Nuti, L. *Magn. Reson. Chem.*, **25**, 897-904, (1987).
409. Knauer, B. R.; Napier, J. J. *J. Am. Chem. Soc.*, **98**, 4395-4400, (1976).
410. Tauoin. C: Dvolaitokv. M. In *Surfactant Solutions. New Methods of Investigation*; Zana, R., Ed.: Surfactant" Science Series; Marcel Dekker: New York,; Vol. 22, p 359, (1987).
411. Hearing, G.; Luisi, P. L.; Hauser, H. *J. Phys. Chem.*, **92**, 3574, (1983).
412. Yoshioka, H., Kazama, S. *J. Colloid Interface Sci.*, **95**, 240, (1983).
413. Barelli, A.; Heicke, H. F. *Langmuir*, **2**, 780, (1986).
414. (a) Ottaviani, M. F.; Baglioni, P.; Martini, G. *J. Phys. Chem.*, **87**, 3146, (1983). (b) Baglioni, P.; Ferroni, E.; Martini, G.; Ottaviani, M. F. *J. Phys. Chem.*, **88**, 5187, (1984). (c) Baglioni, P.; Ottaviani, M. F.; Martini, G. *J. Phys. Chem.*, **90**, 5878, (1986).

415. Bratt, J. P.; Kevan, L. *J. Phys. Chem.*, **96**, 6849, (1992).
416. (a) Martini, G.; Ottaviani, M. F.; Ristori, S.; Lenti, D.; Sanguineti, A. *Colloids Surf*, **45**, 177, (1990). (b) Bonosi, F.; Gabrielli, G.; Margheri, E.; Martini, G. *Langmuir*, **6**, 1769, (1990). (c) Ristori, S.; Ottaviani, M. F.; Lenti, D.; Martini, G. *Langmuir*, **7**, 1958, (1991). (d) Ristori, S.; Martini, G. *Langmuir*, **8**, 1937, (1992). (e) Martini, G.; Ottaviani, M. F.; Ristori, S. *Croat. Chim. Acta*, **65**, 47, (1992) (f) Ottaviani, M. F.; Ghatlia, N. D.; Two, N. J. *J. Phys. Chem.*, **96**, 6075, (1992).
417. (a) Hayakawa, K.; Santerre, J. P.; Kwak, J. C. T. *Macromolecules*, **16**, 1642, (1983). (b) Hayakawa, K.; Santerre, J. P.; Kwak, J. C. T. *Biophys. Chem.*, **17**, 175, (1983).
418. Hiramoto K., Ojima N. and Kikugawa K., *Free Radical Res.*, **27**, 45–53, (1997).
419. Aliaga C., E. Lissi A., Augusto O. and Linares E., *Free Radical Res.*, **37**, 225–230, (2003).
420. Burton, G. W.; Ingold, K. U. *J. Am. Chem. Soc.*, **103**, 6472, (1981).
421. Rice-Evans, C. A.; Miller, N. J.; Paganda, G. *Free Rad. Biol. Med.*, **20**, 933, (1996).
422. Burton, G. W.; Ingold, K. U. *Acc. Chem. Res.*, **19**, 194, (1986).
423. Susan L. P. Changt and David I. Schuster\* *J. Phys. Chem.*, **91**, 3644-3649, (1987).